VOL.29 NO.1
JANUARY
2026

AJSTR
of Scientific and Technological Reports

ASEAN JOURNAL

OF SCIENTIFIC AND TECHNOLOGICAL REPORT



ISSN 2773-8752 (online)



ASEAN
Journal of Scientific and Technological Reports
Online ISSN:2773-8752

ASEAN Journal of Scientific and Technological Reports (AJSTR)

Name ASEAN Journal of Scientific and Technological Reports (AJSTR)

Owner Thaksin University

Advisory Board Assoc. Prof. Dr. Nathapong Chitniratna
(President of Thaksin University, Thailand)
Assoc. Prof. Dr. Samak Kaewsuksaeng
(Vice President for Reserach and Innovation, Thaksin University, Thailand)
Assoc. Prof. Dr. Samak Kaewsuksaeng
(Acting Director of Reserach and Innovation, Thaksin University, Thailand)

Editor-in-Chief Assoc. Prof. Dr. Sompong O-Thong, Mahidol University, Thailand

Associate Editor

1. Assoc. Prof. Dr. Jompob Waewsak, Thaksin University, Thailand
2. Assoc. Prof. Dr. Samak Kaewsuksaeng, Thaksin University, Thailand

Session Editors

1. Prof. Dr. Rattana Jariyaboon, Prince of Songkla University, Thailand
2. Assoc. Prof. Dr. Supawadee Thawaro, Nakhon Si Thammarat Rajabhat University, Thailand
3. Assoc. Prof. Dr. Surapon Boonlue, King Mongkut's University of Technology Thonburi, Thailand
4. Assoc. Prof. Dr. Warangkana Jutidamrongphan, Prince of Songkla University, Thailand
5. Asst. Prof. Dr. Aungkana Jattamart, Rajamangala University of Technology Rattanakosin, Thailand
6. Asst. Prof. Dr. Jakkree Boonlakhorn, Thaksin University, Thailand
7. Asst. Prof. Dr. Suphada Kiriratnikom, Thaksin University, Thailand
8. Dr. Pawadee Hamtanon, Thaksin University, Thailand

Editorial Board

1. Amir Sada Khan, American University of Sharjah, United Arab Emirates
2. Chart Chiemchaisri, Kasetsart University,Thailand
3. Chen-Yeon Chu, Feng Chia University, Taiwan
4. Dariusz Jakobczak, National University, Pakistan
5. Ganjar Samudro, Universitas Diponegoro, Indonesia
6. Ghulam Murtaza, Government College University Lahore, Pakistan
7. Hidenari Yasui, University of Kitakyushu, Japan
8. Jatuporn Kaew-On, Thaksin University, Thailand
9. José Antonio Álvarez-Bermejo, University of Almeria, Spain
10. Jutamas Kumchai, Chiang Mai University, Thailand
11. Karun Thongprajukaew, Prince of Songkla University, Thailand
12. Marchee T. Picardal, Cebu Normal University, Philippines
13. Nares Chimres, Thaksin University, Thailand
14. Nasser Ahmed, Kyushu University, Japan
15. Noppamas Pukkhem, Thaksin University, Thailand
16. Peer Mohamed Abdul, Universiti Kebangsaan Malaysia, Malaysia
17. Prasong Kessaratikoon, Thaksin University, Thailand
18. Prawit Kongjan, Prince of Songkla University, Thailand
19. Sappasith Klomklao, Thaksin University, Thailand
20. Shahrul Isamail, Universiti Malaysia Terengganu, Malaysia
21. Supawadee Theerathammakorn, Sukhothai Thammatirat Open University, Thailand
22. Tharith Sriv, Royal University of Phnom Penh, Cambodia
23. Tjokorda Gde Tirta Nindhia, Udayana University in Bali, Indonesia
24. Tsuyoshi Imai, Yamaguchi University, Japan
25. Visit Boonchom, Thaksin University, Thailand
26. Win Win Myo, University of Information Technology, Myanmar
27. Yves Gagnon, University of Moncton, Canada
28. Zairi Ismael Rizman, Universiti Teknologi MARA, Malaysia

Staff: Journal Management Division
Miss Kanyanat Liadrak, Thaksin University, Thailand

Contact Us Institute of Research and Innovation, Thaksin University
222 M. 2 Ban-Prao sub-district, Pa-Pra-Yom district, Phatthalung province, Thailand
Tel. 0 7460 9600 # 7258, 09 1070 0916, 08 1540 7304, E-mail: aseanjstr@tsu.ac.th

List of Contents

Statistical Modeling of Daily Rainfall Using Zero-tweaked Data **e259596**
Aneeta Kalor, Rhysa McNeil, and Nurin Dureh

Dose-Dependent Genoprotective Effects of *Syzygium aromaticum* (Clove) Extract Against Cyclophosphamide- Induced Chromosomal Damage and Micronucleus Formation in Swiss Albino Mice **e261209**
Aseel Raheem Mardan Al-Aamiri

Gibberellic Acid and Salicylic Acid on the Growth and Yield of Kale under Kratky Method Hydroponic System **e260396**
Julius D. Caritan, James A. Pasaje, Daniel B. Tangpos, Noriel Jay A. Magsayo, and Pet Roey L. Pascual

Physicochemical and Microbiological Evaluation of Reverse Osmosis Drinking Water Quality in Babylon Province, Iraq **e260629**
Hala Faez Al-Jawahery, Noor S Naji, and Atheer SN Al-Azawey

AI-Driven Smart Farming for Automated Plant Health Monitoring and Nutrient Deficiency Detection **e258175**
J.Serin, G.Gifta Jerith, V.Ebenezer, K.Arul Jeyaraj, A.Jenefa, and M.Vargheese

Predicting E-Commerce Purchase Intention Using Machine Learning **e260159**
Om Ratna Sheshagiri Gupta Alamuri, and Chaitanya Krishna Bondalapu

Growth and Yield Response of Lettuce (*Lactuca sativa*) Using MykoPlus and Bio-N Biofertilizers **e260410**
Shaina Marie Guillermo, and Dionie Barrientos

Comprehensive and Integrated Deep Learning Approaches-based Intelligent Skin Disease Diagnosis System for Pox Detection **e260160**
Padmaja Bodagala, and Naga Malleswary Dubba

Sustainable Organic Vegetable Production in Low-Cost Greenhouses and Post-Harvest Safety: A Community-Based Approach in Phatthalung Province, Thailand **e259918**
Wanphen Buakong, Thidarat Juthong, Nattawit Sermsin,Thanapon Yooyen, and Pluang Suwanmanee

Enhancing Methane Production from Palm Oil Industry Waste through Thermotolerant Bacterial Bio-augmentation: Optimization and Kinetic Analysis **e259521**
Sittikorn Saelor, Wisarut Tukanghan, Peerawat khongkliang, Supattra In-chan, and Nantharat Phruksaphithak

Utilization of Information and Communication Technology (ICT) Tools Among Masbate Rice Seed Growers **e257993**
Mohammad D. Dollison, Eddie B. Basulgan, Nimfa R. Cornal1, and Beverly B. Dollison

Development of Ultrasonic Extraction Techniques for Bioactive Compounds from Banana Peel Waste: A Comparative Study of Biological Activities **e258852**
Napattaorn Buachoon

Exploring the Role of AI in Marketing and Technology Readiness in Enhancing Customer Satisfaction and Business Performance in E-commerce **e258998**
Taqwa Hariguna, Retno Waluyo, Melia Dianingrum, and Arif Mu'amar Wahid

A Bibliometric Analysis of Stress Memory and Priming in Plants: Research Trends, Mechanisms, and Implications for Agricultural Resilience **e259013**
Harry C. LucesEnhanced Thermal Efficiency of Solar Air Heaters Using

List of Contents

Enhanced Thermal Efficiency of Solar Air Heaters Using Porous Material: An Experimental Approach **e259025**
Eakpoom Boonthum, Prapanphong Somsila Apinunt Namkhat, Sorawit Sonsaree, and Umphisak Teeboonma

Quality-based assessment of natural ripening agents as alternatives to calcium carbide in 'Latundan' banana using mixed statistical methods **e259605**
Bryl I. Manigo

Biodegradation of Oil and Grease in Synthetic Wastewater Using Lipase-Producing Bacteria Isolated from University Canteen Wastewater **e258938**
Pradabduang Kiattisaksiri, Panabodee Sornram, Apinya Phoamart, Supawinee Srikham, and Yanasinee Suma

Molecular Characterization and Integron Gene Prevalence in Bacterial Pathogens from Neonatal Omphalitis **e261254**
Rehab Riyadh Raheem, and Wafaa Abdul Wahid Jheel

Surveillance of Rotavirus A Genotypes in Diarrheal Cases from Humans and Bovine in Basra Province, Iraq **e261427**
Rawaa Bannay Zubairi, Basil A. Abbas, and Fawziah Ali Abdullah

Phenotypic-Genotypic Characterization of Macrolide- Lincosamide-Streptogramin B Resistance in *Staphylococcus saprophyticus* UTI Isolates from Iraq **e261225**



ASEAN
Journal of Scientific and Technological Reports
Online ISSN:2773-8752

ASEAN
Journal of Scientific and Technological Reports
Online ISSN:2773-8752

Research article

Statistical Modeling of Daily Rainfall Using Zero-tweaked Data

Aneeta Kalor[1], Rhysa McNeil[1, 2*], and Nurin Dureh[1]

[1] Faculty of Science and Technology, Prince of Songkla University, Pattani Campus, 94000, Thailand
[2] Center of Excellence in Mathematics, Commission on Higher Education (CHE), Ministry of Education, Ratchathewi, Bangkok, 10400, Thailand
* Correspondence: nchirtki@gmail..com

Citation:
Kalor, A.; McNeil, R.; Dureh, N. Statistical modeling of daily rainfall using zero-tweaked data. *ASEAN J. Sci. Tech. Report*. **2026**, *29*(1), e259596. https://doi.org/10.55164/ajstr.v29i1.259596.

Article history:
Received: May 31, 2025
Revised: September 16, 2025
Accepted: October 9, 2025
Available online: December 14, 2025

Publisher's Note:
This article is published and distributed under the terms of the Thaksin University.

Abstract: The significant amount of zero rainfall led to a highly skewed distribution of rainfall, creating challenges in rainfall modeling. This study aims to introduce a zero-tweaking method for handling a large proportion of zero rainfall data and apply it to daily rainfall data collected at four stations in southern Thailand from 2010 to 2022. The fourth root transformation was used to handle the right skew of rainfall. Zero-tweaking techniques were employed, with zeros substituted by normally distributed random numbers that permitted negative values. The patterns and trends in rainfall at each of the four stations were investigated using natural cubic splines. The trend projection analysis for four rainfall stations up to 2030 revealed an increase in rainfall at two stations in the Gulf of Thailand; however, this increase was not statistically significant. However, this study introduced the zero-tweaking method to handle the zero data, which enabled the use of conventional statistical methods and enhanced the model's validity.

Keywords: Natural cubic spline; rainfall; seasonal pattern; zero-tweaked data

1. Introduction

Rainfall is a crucial climate component that significantly influences various aspects of life and ecosystems. Rainfall plays a vital role in the water cycle. Global rainfall patterns have become increasingly unpredictable due to climate change, heightening the risk of flooding [1-2], leading to both heavy rainfall and prolonged droughts [3-5], and threatening social stability, water resources, and food security [6]. In Thailand, rainfall variability has been recognized as a significant factor influencing agriculture. Annual and seasonal rainfall parameters exhibited heterogeneity, with both increasing and decreasing trends observed at the national and regional levels [7]. Southern Thailand is significantly impacted by the southwest monsoon, which often results in intense rainfall and severe flooding [8]. Therefore, understanding rainfall patterns is critical for effective hydrological planning and management.

Rainfall data often contains a large number of zeros, resulting in a highly skewed distribution. This is due to the nature of rainfall, where most days have little or no rainfall, while a few days experience heavy downpours. This feature provides challenges and opportunities for statistical analysis and modeling. Several non-normal distribution models were used to analyze the right-skewed distribution of the rainfall, such as the Gamma distribution model [9-12], the Exponential distribution model [13-14], and the Weibull distribution model [15]. Some studies recommend transforming the data using a log-normal distribution by taking the logarithm of the rainfall data [11]. Another issue to consider when analyzing rainfall data is the large number of zero rainfall events. The statistical models have been designed to handle the large amount of zero data, such as the

zero-inflated Poisson regression model, which is designed to handle count data with an excess of zero observations [16], and the hurdle model [17].

Other methods included two process of Poisson–Gamma approach, where the Poisson distribution represented the daily occurrence of rainfall events, and the Gamma distribution captured the intensity of those events [18]; a stochastic model, a two-state Markov chain model, to represent the occurrence of rainfall and then used other probability models, gamma and exponential, to fit the intensity of rainfall [19]. Some statistical models for addressing this issue include separating the rainfall data into a binary model (zero or non-zero) and a conditional model for non-zero data, or using zero-inflated models that assume zero values in the data arise from structural zeros or random zeros. The issue of excessive zeros has been addressed in limited research through the use of continuous random numbers for replacement. Therefore, the objective of this study is to address high skew and a large amount of zero rainfall data by using the fourth root transformation scale and zero-tweaking for the rainfall data in southern Thailand. After addressing the distribution and zero rainfall, this study also investigates rainfall patterns using a cubic spline model.

2. Materials and Methods

2.1 Data and Area of Study

Data used for this study were obtained from the National Oceanic and Atmospheric Administration (NOAA). It is available for public assessment, which can be downloaded from https://www.ncdc.noaa.gov. NOAA collected rainfall data from ground stations. This study considers the daily rainfall in southern Thailand. The southern region has a tropical monsoon climate. A long, pointed peninsula characterizes the southern region's geography. There is a surface of water flanking both the western side, the Andaman Sea, and the eastern side, the Gulf of Thailand, causing rain all year round and being the region with the most rainfall in Thailand. The rainfall data used in this study are from four stations in southern Thailand, where two stations, Phuket Airport and Trang, are located in the Andaman Sea, and two stations, Nakhon Si Thammarat and Hat Yai, are located in the Gulf of Thailand. We chose these stations because the southwest monsoon directly affects the Andaman coast, Phuket, and Trang. Meanwhile, the northeast monsoon has a significant impact on the coast of the Gulf of Thailand, particularly in Nakhon Si Thammarat and Hat Yai.

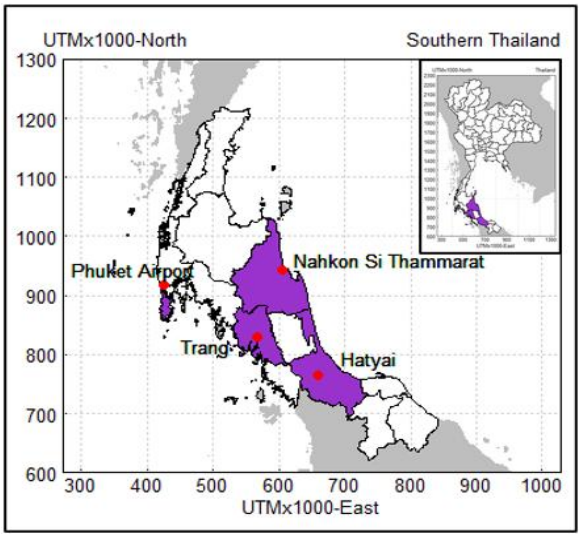


Figure 1. Locations of the study area

The data consisted of missing data and a large number of zeros. After managing the data, the raw dataset consisted of 4,748 daily records per station (totaling 18,992 records for four stations) during 2010–2022. Of these, 6,681 entries (35.18%) were missing, and 2,237 entries contained zero rainfall.

2.2 Statistical Methods

The fourth root transformation was used to handle the right skew of rainfall data and assess it using a quantile-quantile (Q-Q) plot. A comparison of the efficiency of data transformation methods using simulated

data found that the fourth root transformation demonstrated the best results. The authors then applied this transformation to the rainfall data [20]. Then, the zero-tweaked method was used to handle a large number of zero rainfall values by replacing all values with non-zero ones, allowing for negative numbers since the rainfall data was transformed using the fourth root scale; zero rainfall remained zero. This was done by splitting the transformed rainfall data into two separate sets using a value close to zero; we use the minimum number, which equals 0.74 mm, as the cut point. The first data set includes all data from the cut point that has a normal distribution after the fourth root transformation. The second data set includes all data below the cut point, most of which is zero. This second set of data was replaced with a normal random generation number, with a mean and standard deviation approximated from the first data set. This method enabled the transformed data to include negative numbers, allowing the data to achieve a normal distribution —a key assumption of conventional statistical methods. The normality was assessed using a Q-Q plot. Once the data are typically distributed, classic statistical methods can be used for further investigation.

The trends and seasonal patterns of rainfall at each station were displayed using a cubic spline function with a linear function. Cubic spline functions are defined as piecewise polynomials with degree n, where knots are the chosen positions that join the pieces. A spline function of degree n is a continuous function with $n-1$ continuous derivatives [21-22]. Using an adequate number of knots, a time series plot was created for each rainfall and station, and the positions of the knots were fixed to smooth the spline curve. The formula denoting the cubic spline model is given in Equation 1 as follows:

$$s_i = a + bt_i + \sum_{k=1}^{p} c_k \, (t_i - t_k)_+^3 \tag{1}$$

where s_i is the spline function, a, b, and c_k are model parameters, k is the knot location, t_i denotes time in eight days, that is specified from 13 years, $t_i < t_2 < \ldots < t_p$ are specified knots and $(t_i - t_k)_+$ implies that $(t_i - t_k)$ is positive for $(t_i - t_k)$ and zero otherwise. The number of knots used to smooth the data is important for cubic spline fitting. Some studies chose based on the season [23-24]. This study used eight knots based on season and tropical region characteristics. The rainfall data were then seasonally adjusted by subtracting the fitted values, obtained from the cubic splines, from observed rainfall, then adding back the overall mean of rainfall, using the formula in Equation 2 below:

$$z_i = y_i - s_i + \bar{y} \tag{2}$$

where, z_i is the seasonally adjusted rainfall at observation i, y_i is the rainfall observation, s_i is the fitted value from the spline model and $\bar{y}$ is the observed rainfall overall mean. Autoregression (AR) models were also used to account for the autocorrelations among the residuals from the fitted linear models [25]. The seasonally adjusted rainfall was then fitted using a first-order autoregressive model to account for the autocorrelation. Then, a simple linear regression model and a natural cubic spline model were used to investigate the pattern and trend of seasonally adjusted rainfall

3. Results and Discussion

The distribution of rainfall was first investigated by combining the data from four stations into a single dataset, as shown in Figure 2. Figures 2(a1) and 2(a2) displayed the histogram and normal Q–Q plot of the aggregated data from the four stations. The histogram showed a highly skewed distribution, while the Q–Q plot revealed significant departures from the reference line, particularly in the upper quantiles. Figure 2(b1) and 2(b2) employed a fourth root transformation, which displayed the distribution closer to normality but remained with a large number of zeros. It showed a gap between zero rainfall and the minimum rainfall value (0.74 mm). The transformation reduced skewness but did not fully achieve normality due to the presence of a large number of zero values. These zeros were handled by first replacing any numbers less than the minimum with a uniform distribution. This technique did not allow for negative values, as shown in Figures 3(a1) and 3(a2). The distribution of the fourth root transformation still departed from the normal distribution (Q-Q plot). Therefore, we applied the zero-tweaked method by replacing zero with non-zero values, allowing for negative values, as shown in Figures 3(b1) and 3(b2). This method effectively adjusts the data to align closely with a normal distribution.

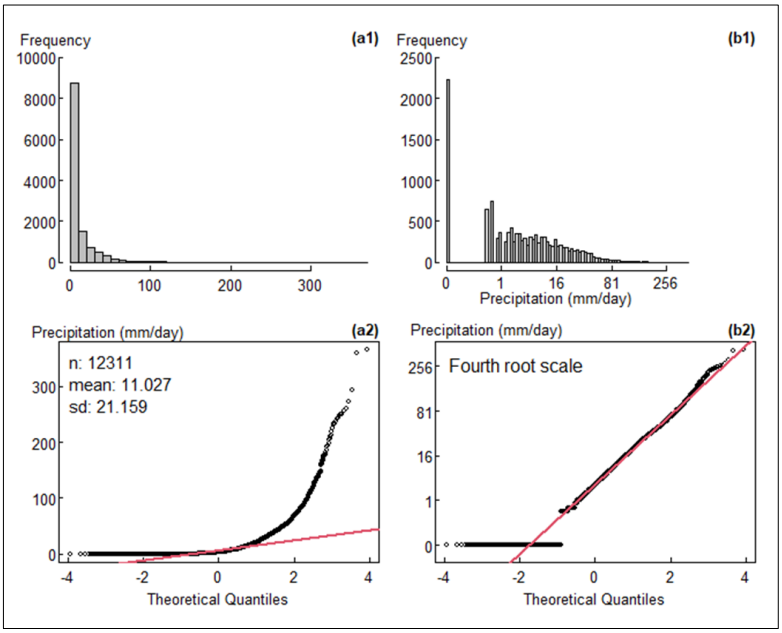


Figure 2. Distribution of fourth root of the daily rainfall

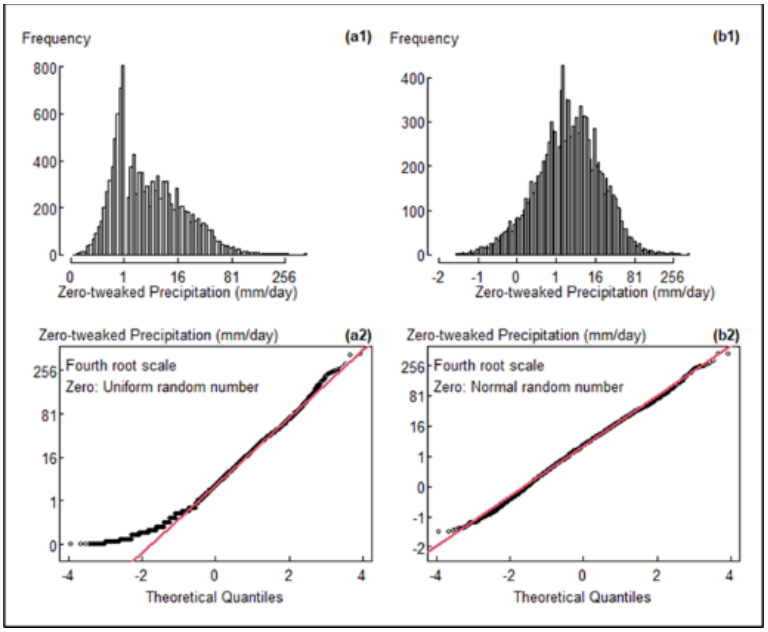


Figure 3. Distribution of the fourth root, replacing zero with a normal random number

Next, we investigate the pattern and trend for each station using the zero-tweaked fourth root ransformation of rainfall. Figure 4 shows the detailed steps of the analysis for the Nakhon Si Thammarat station.

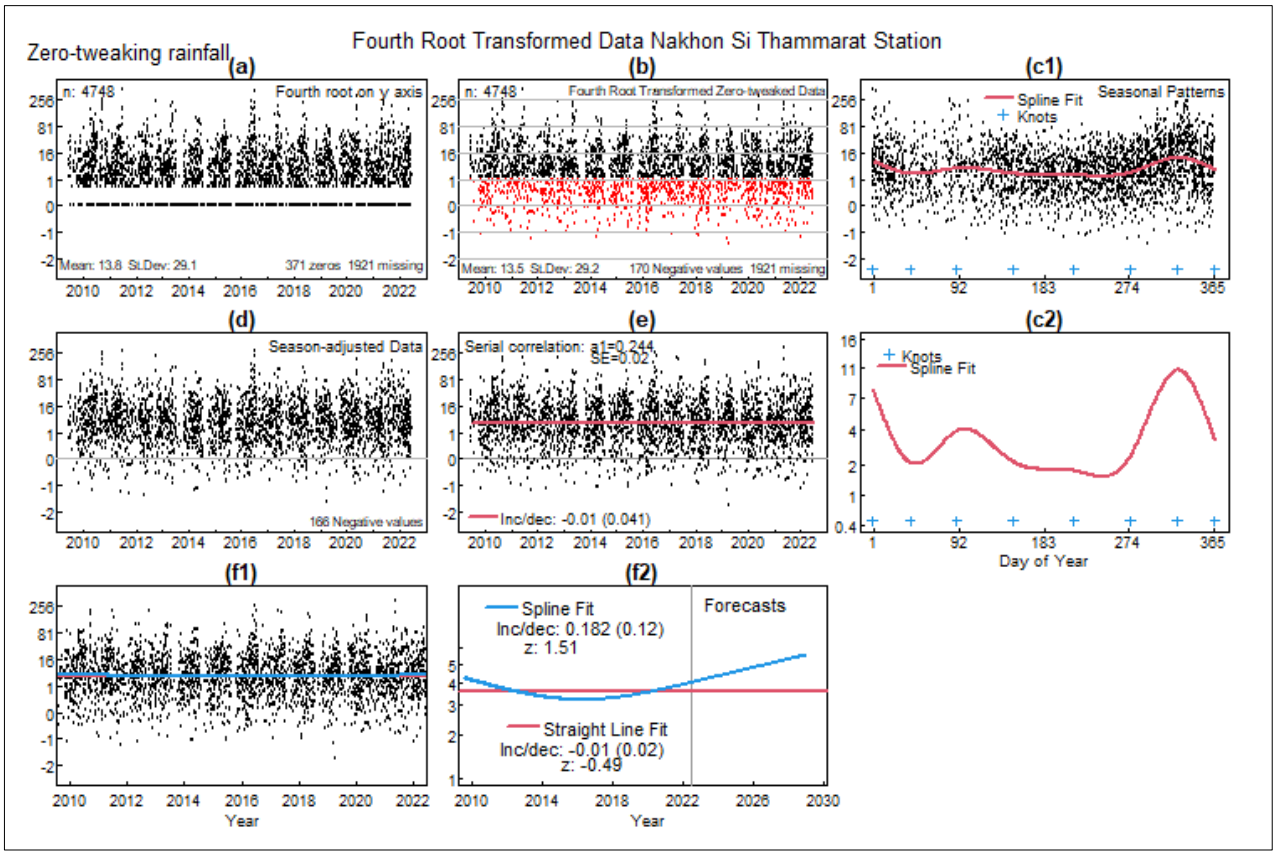


Figure 4. The pattern and trend of zero-tweaking rainfall for the Nakhon Si Thammarat station

Figure 4(a) displays the time series plot of rainfall data after transformation using the fourth root. Figure 4(b) displays the time series after applying the fourth root transformation and zero-tweaking to the data. All the red dots represented normal, random data replacing the zeros. Both graphs showed a seasonal pattern for each year. The natural cubic spline was used to fit the seasonal patterns shown by the red curve, with 8 knots denoted by blue crosses in Figure 4(c1). The fitted curve was then enlarged to illustrate the pattern clearly in Figure 4(c2). It clearly showed that the peak in rainfall occurred between the end of the year and the beginning of the year, with decreased rainfall in the middle of the year. The rainfall data was seasonally adjusted as shown in Figure 4(d). The first autoregressive model was used to remove the autocorrelation in Figure 4(e). The estimated coefficient of the autoregressive AR (1) model was small, indicating that the seasonally adjusted rainfall is independent.

The pattern and trend were fitted using a simple linear regression model (red curve) and a natural cubic spline (blue curve) in Figure 4(f1), and were enlarged to see the pattern clearly in Figure 4(f2). The results of the straight-line fit showed no trend; the spline fit, however, indicated a trend of decreasing values followed by a slight increase, with projections extending until 2030. However, all the absolute z-value statistics were less than 1.96, indicating that they were not statistically significantly different. The patterns and trends for the four stations were presented in Figure 5. Figure 5 (top panel) shows the seasonal patterns of the zero-tweaked fourth root transformation of rainfall after fitting a natural spline function with eight knots for all four stations, and Figure 5 (bottom panel) enlarges the scale. The results showed two seasonal patterns. Nakhon Si Thammarat and Hat Yai stations are located in the Gulf of Thailand. The peak in rainfall occurs at the end of the year, during October and November, which marks the rainy season. Phuket and Trang stations, situated on the Andaman Sea, experienced the highest rainfall from June to September. Therefore, the zero-tweaked fourth root transformation was seasonally adjusted. The first autoregressive model was also used to remove autocorrelation for all stations.

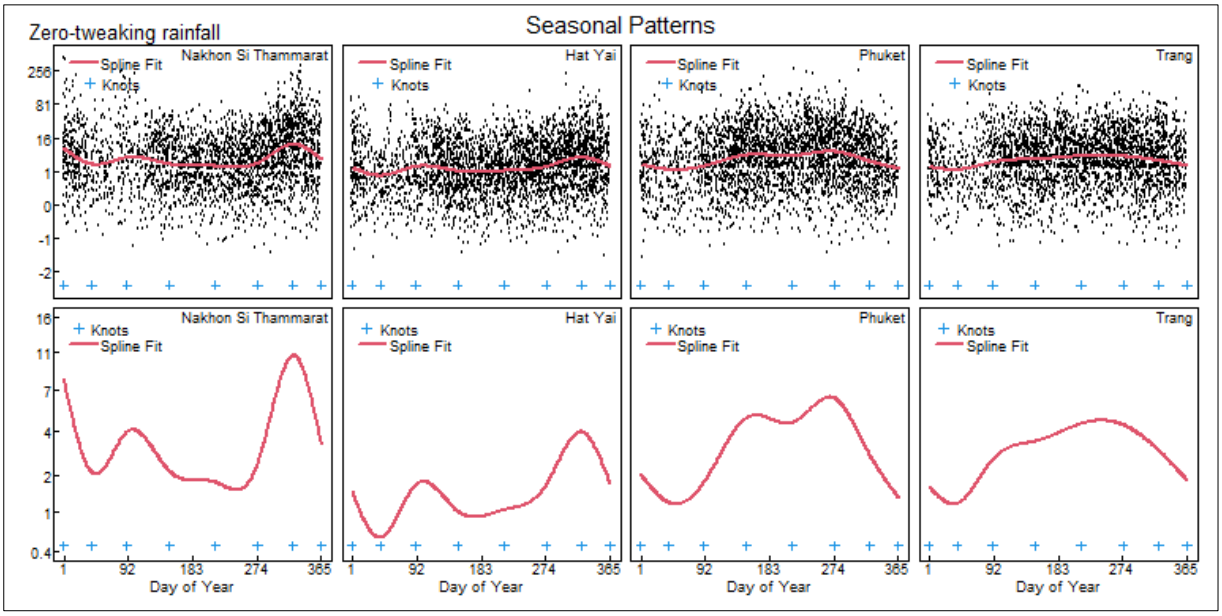


Figure 5. Seasonal patterns of zero-tweaking rainfall for four stations

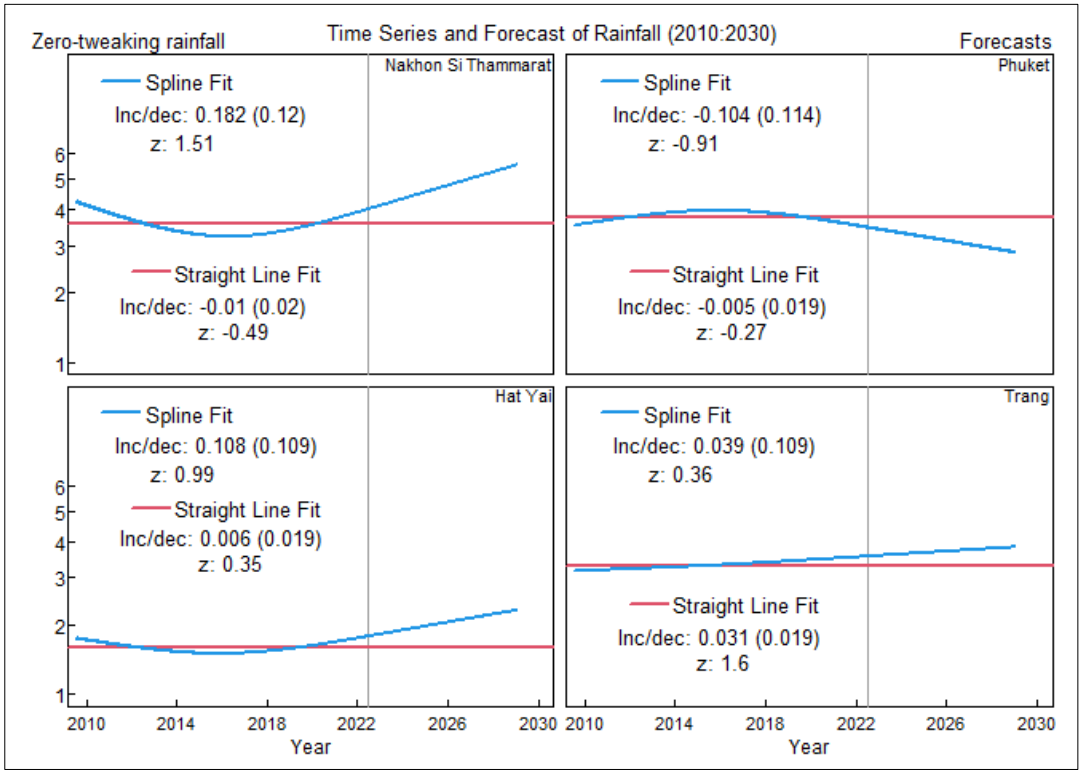


Figure 6. Patterns and forecasting trend of zero-tweaking rainfall in 2030 for four stations

Figure 6 illustrates the enlarged patterns, trends, and forecasting trends in 2030 of the zero-tweaked fourth root transformation using simple linear regression (straight red line) and the natural cubic spline (blue line) model for all four stations. This was examined after seasonally adjusting and removing autocorrelation. The results clearly showed no linear trend at any of the stations. However, the results from the natural cubic spline showed that the Nakhon Si Thammarat and Hat Yai stations had a decreasing trend from 2010 to 2016, followed by an increase up to 2022. For both stations, the forecasting trend increased in 2030. Whereas Phuket stations experienced an upward trend from 2010 to 2016, they then gradually declined afterward. Trang station showed a steady increasing trend. The pattern was consistent with a prior study on rainfall variability and

trends in Thailand, which found that the southern regions had an increase in rainfall, with an annual rainfall of 0.148 mm [26]. However, the z-value statistics displayed in the figure are based on statistical testing; there is no average rainfall change in each station. In this study, we transformed the right-skewed rainfall using a fourth root transformation, resulting in rainfall data that closely resembled a normal distribution. A previous study, which compared the efficiency of data transformation methods using simulated data, found that the fourth root transformation yielded the best results. The authors then applied this transformation to the rainfall data [20]. The zero rainfall remained zero after the fourth root transformation. In this study, we replaced the zeros with continuous random numbers from a normal distribution, allowing for small negative values. A previous study also employed the method of substituting all zero rainfall values with small negative values to identify dry areas in spatial interpolations of rainfall events, rather than leaving them as zero [27].

4. Conclusions

This zero-tweaked technique is straightforward to use and provides significant advantages in statistical modeling and data analysis. It created a smoother and more acceptable distribution, with the small negative values of the data still maintaining the relative difference between dry and wet conditions. The data can be more closely approximated to a normal distribution, which improves the validity of parametric tests and models. The zero-tweaked rainfall at four stations was then seasonally adjusted. The patterns and trends were investigated using a natural cubic spline regression model. Nakhon Si Thammarat and Hat Yai stations, located in the Gulf of Thailand, exhibited a decreasing trend until 2016, followed by an increasing trend, with a projected continuation of the latter trend until 2030. In contrast, Phuket station exhibited an increasing trend until 2016, followed by a decreasing trend, with a projected decrease continuing until 2030. However, the statistical tests for the changes in our study were not significant. Additionally, the accuracy of long-term forecasts should be evaluated. The rainfall also included a significant amount of missing data, which requires management. This study applied the methods to only four selected stations; these patterns may not represent statistically significant changes. Further investigation with additional rainfall stations in southern Thailand is recommended.

5. Acknowledgments

The authors sincerely appreciate Professor Don McNeil for his invaluable assistance. The Faculty of Science and Technology, Pattani Campus, Thailand, supported this work..

Author Contributions: "Conceptualization, A.K., R.M., and N.D.; methodology, R.M.; data curation and data analysis, A.K. and N.D.; writing draft preparation, A.K. and R.M.; review and editing, R.M. and N.D.. All authors have read and agreed to the published version of the manuscript.

Conflicts of Interest: The authors declare no conflict of interest.

References

[1] Shu, E.G.; Porter, J.R.; Hauer, M.E.; Olascoaga, S.S.; Gourevitch, J.; Wilson, B.; Pope, M.; Vazquez, D.M.; Kearns, E. Integrating climate change induced flood risk into future population projections. Nat. Commun. **2023**, *14*, 7870. https://doi.org/10.1038/s41467-023-43493-8

[2] Tabari, H. Climate change impact on flood and extreme precipitation increases with water availability, Sci. Rep. **2020**, *10*(1), 13768. https://doi.org/10.1038/s41598-020-70816-2

[3] Bevacqua, E.; Rakovec, O.; Schumacher, D.L.; Kumar, R.; Thober, S.; Samaniego, L.; Seneviratne, S.I.; Zscheischler, J. Direct and lagged climate change effects intensified the 2022 European drouth. Nat. Geosci. **2024**, *17*, 1100-1107. https://doi.org/10.1038/s41561-024-01559-2

[4] Cook, B.I.; Mankin, J.S.; Williams, A.P.; Marvel, K.D.; Smerdon, J.E.; Liu, H. Uncertainties, limits, and benefits of climate change mitigation for soil moisture drought in southwestern North America. *Earth's Future*, **2021**, *9*(9), e2021EF002014. https://doi.org/10.1029/2021EF002014

[5] Nielsen, M.; Cook, B.I.; Marvel, K.; Ting, M.; Smerdon, J.E. The changing influence of precipitation on soil moisture drought with warming in the Mediterranean and Western North America. *Earth's Future,* **2024**, *12,* e2023EF003987. https://doi.org/10.1029/2023EF003987

[6] Ide, T.; Fröhlich, C.; Donges, J.F. The economic, political, and social implications of environmental crises. *Bull. Am. Meteorol. Soc.* **2020**, *101*, E364–E367. https://doi.org/10.1175/BAMS-D-19-0257.1

[7] Madolli, M.J.; Gade, S.A.; Gupta, v.; Chakraborty, A.; Cha-um, S.; Datta, A.; Himashu, S.K. A systematic review on rainfall patterns of Thailand: Insights into variability and its relationship with ENSO and IOD. *Earth-Sci. Rev.* **2025**, *264,* 105102. https://doi.org/10.1016/j.earscirev.2025.105102

[8] Limsakul, A.; Limjirakan, S.; Sriburi, T. Observed changes in daily rainfall extremes along Thailand's coastal zone. *J. Environ. Res.* **2010**, *32*, 49-68.

[9] Owusu, B.E.; McNeil, N. Statistical modelling of daily rainfall variability patterns in Australia. Pertanika *J. Sci. Technol.* **2018**, *26*(2), 691-706.

[10] Vieira, F.M.C.; Machado, J.M.C.; Vismara, E.; Possenti, J.C. Probability distributions of frequency analysis of rainfall at the southwest region of Paraná State, Brazil. Rev. Cienc. Agroveterinarias **2018**, *17,* 260–266. https://doi.org/10.5965/223811711722018260

[11] Hasan, M.M.; Croke, B.F.W.; Liu, S.; Shimizu, K.; Karim, F. Using mixed probability distribution functions for modelling non-zero sub-daily rainfall in Australia. *Geosciences,* **2020**, *10*(2), 43. https://doi.org/10.3390/geosciences10020043

[12] Ximenes, P.; Silva, A.S.A.; Ashkar, F.; Stosic, T. Best-fit probability distribution models for monthly rainfall of Northeastern Brazil. Water Sci. Technol. **2021**, *84*(6), 1541-1556. https://doi.org/ 10.2166/wst.2021.304

[13] Sake, R.; Akhtar, P.M. Fitting of modified exponential model between rainfall and ground water levels: A case study. *Int. J. Stat. Appl. Math.* **2019**, *4*(4), 1-6.

[14] Afolabi, A.M.; Adesola, O.I. Exponential probability distribution of short-term rainfall intensity. Equity J. Sci. Technol. **2022**, *9*(2), 18-27.

[15] Olivera, S.; Heard, C. Increases in the extreme rainfall events: using the Weibull distribution. *Environmetrics* **2018**, *30*. https://doi.org/10.1002/env.2532

[16] Lambert, D. Zero-inflated Poisson regression, with an application to defects in manufacturing, *Technometrics* **1992**, *3*(1), 1-14. https://doi.org/10.2307/1269547

[17] Feng, C.X. A comparison of zero-inflated and hurdle models for modeling zero-inflated count data. *Journal of Statistical Distributions and Applications,* **2021**, *8*, https://doi.org/10.1186/s40488–021–00121–4

[18] Dzupire, N.C.; Ngare, P.; Odongo, L.A. A Poisson-gamma model for zero inflated rainfall data. *J. Probab. Stat.* **2018**, *1012647*, https://doi.org/10.1155/2018/1012647

[19] Wilks, D.S. Multisite generalization of a daily stochastic precipitation generation model. J. Hydrol. **1998,** *210*(4), 178-191. https://doi.org/10.1016/S0022-1694(98)00186-3

[20] Kaewprasert, T.; Khamkong, M.; Bookkamana, P.A. A comparison of data transformation methods of generalized exponential distribution and estimation of summer rainfall in Chiang Dao, Chiang Mai. *Burapha Sci. J.* **2017**, *22*(3), 385-396.

[21] Wahba, G. *Spline models for observational data*. CBMS-NSF Regional Conference Series in Applied Mathematics, **1990**; pp 1-161. https://doi.org/doi:10.1137/1.9781611970128

[22] Wold, S. Spline functions in data analysis, *Technometrics* **1974**, *16*(1), 1-11. http://www.jstor.org/wqazstable/1267485

[23] Wongsai, N.; Wongsai, S.; Huete, A.R. Annual seasonality extraction using the cubic spline function and decadal trend in temporal daytime MODIS LST data. *Remote Sens*. **2017**, *9*(12), https://doi.org /10.3390/rs9121254

[24] Lukas, M.A.; de Hoog, F.R.; Anderssen, R.S. Efficient algorithms for robust generalized cross-validation spline smoothing. *J. Comput. Appl. Math.* **2010**, *235*(1), 102–107. https://doi.org /10.1016/j.cam.2010.05.016

[25] Venables, W.N.; Ripley, B.D. *Modern Applied Statistics with S*. Springer, Queensland, **2002**. https://doi.org/10.1007/978-0-387-21706-2

[26] Waqas, M.; Humphries, U.W.; Hlaing, P.T. Time series trend analysis and forecasting of climate variability using deep learning in Thailand. *Results Eng.* **2024**, *24*, 102997. https://doi.org/10.1016/j.rineng.2024.102997

[27] Lee, T.; Shin, J.Y. Latent negative precipitation for the delineation of a zero-precipitation area in spatial interpolations. *Sci. Rep.* **2021**, *11*(1), 20426. https://doi.org/10.1038/s41598-021-99888-4

ASEAN
Journal of Scientific and Technological Reports
Online ISSN:2773-8752

Research article

Dose-Dependent Genoprotective Effects of *Syzygium aromaticum* (Clove) Extract Against Cyclophosphamide-Induced Chromosomal Damage and Micronucleus Formation in Swiss Albino Mice

Aseel Raheem Mardan Al-Aamiri[1*]

[1] College of Education, University of Al-Qadisiyah, Al-Qadisiyah, Iraq
* Correspondence: aseel.alaamiri@qu.edu.iq

Citation:
Al-Aamiri, M.R.A Dese-de[emdemt gemp[rptective effects of *Syzygium aromaticum* (Clove) extract against cyclophosphamide-induced chromosomal damage and micronucleus formation in swiss albino mice. *ASEAN J. Sci. Tech. Report.* **2026**, *29*(1), e261209. https://doi.org/10.55164/ajstr.v29i1.261209.

Article history:
Received: September 10, 2025
Revised: September 24, 2025
Accepted: September 27, 2025
Available online: December 14, 2025

Publisher's Note:
This article is published and distributed under the terms of the Thaksin University.

Abstract: Cyclophosphamide (CP), a classical alkylating chemotherapeutic drug, has significant genotoxic effect but its use is restricted due to safety concerns. In the present study, we investigated a protective effect of Syzygium aromaticum (clove) ethanolic extract against CP-induced chromosomal damage in Swiss albino mice. Thirty male mice were distributed among five groups (n = 6): control, clove extract only (500 mg/kg), CP only (20 mg/kg intraperitoneally), and two post-treatment groups, receiving CP followed by oral clove extract at 400 mg/kg and 500 mg/kg for seven days. Chromosomal anomalies and micronucleus formation were assessed in bone marrow cells. CP treatment significantly increased structural chromosomal anomalies from 2.24 ± 1.01 (control) to 18.72 ± 0.05 ($p < 0.05$) and numerical aberrations from 3.62 ± 0.03 to 15.68 ± 0.02 ($p < 0.05$). Micronucleated polychromatic erythrocytes (MnPCEs) increased 9.9-fold from 1.38 ± 0.02% to 13.63 ± 1.01% ($p<0.05$). Post-treatment with 400 mg/kg clove extract reduced structural and numerical aberrations to 10.94 ± 3.01 and 11.03 ± 0.03, respectively, representing 42% and 30% reductions in these aberrations. The 500 mg/kg dose achieved greater protection, reducing structural aberrations by 74% (4.92 ± 0.03) and numerical aberrations by 68% (5.03 ± 0.05), approaching control values. MnPCE frequency decreased to 8.84 ± 1.02% (35% reduction) and 4.98 ± 0.05% (63% reduction) at 400 mg/kg and 500 mg/kg doses, respectively. The dose-dependent genoprotective effects are attributed to the high eugenol content and phenolic compounds in cloves, which possess antioxidant properties. These findings suggest that clove extract may be a promising natural chemoprotective agent for mitigating CP-induced genotoxicity, warranting further investigation for potential clinical applications.

Keywords: *Syzygium aromaticum*; cyclophosphamide-induced genotoxicity; chromosomal aberrations; micronucleus test; chemoprotective agents

1. Introduction

Cancer remains one of the leading cause of death worldwide, which makes the need for further development and improvement of chemotherapeutic approaches essential. Alkylating agents are one of the main classes of chemotherapeutics, which is capable of treating a broad range of malignancies. Cyclophosphamide (CP) is a nitrogen mustard derivative and one of the most widely used alkylating agents in clinical oncology to-date, for treatment of

lymphomas, leukemias, breast cancer, ovarian cancer and some autoimmune diseases [1]. The clinical application of CP is heavily limited by its dose dependent toxicity, most notably the highly genotoxic effects on fast dividing normal cells. The anticancer action of CP is thought to be mediated via its metabolic activation by hepatic cytochrome P450 enzymes such as CYP2B6 and CYP3A4 with the production of phosphoramide mustard and acrolein as major metabolites [2]. Phosphoramide mustard is the active therapeutic metabolite causing DNA cross-linking and subsequent cell death in cancer cells. However, efects of this mechanism are not specific and it affects in non–selective manner even to normal cells, particularly the cells showing high rate mitosis such as bone marrow cells, intestinal epithelial and reproductive tissues. CP's toxicity is also driven in large part by acrolein, its other major metabolite, which induces the production of reactive oxygen species and kills cells directly. This results in RONSs generation (reactive oxygen and nitrogen species) which can also be scavenged by cellular antioxidant system. This will cause the cell's own antioxidant pool to be depleted, and hence results in profound DNA insults such as chromosomal aberrations, sister chromatid exchange , micronucleus formation [3].

The acute residual side effects are not the only genotoxic consequences of CP, this compound can also induce late reactive damage at cellular level which is correlative with an increased risk for secondary tumours, reproductive losses and hereditary mutations. Physical ACP is reported to increase the frequency of chromosomal aberration both in the somatic cells (cytogenesis) and germ-line chromosomes, which raises the concerns on long-term genetic security for cancer survivors [4]. These side effects require the design of strategies to protect from CP-associated genotoxicity without compromising therapeutic effect. Several natural products were proposed as potential chemoprotective agents, representing different strategies for protection against chemotherapy toxicity. Plants as Drugs: Traditional and Modern Utilization 39 applied for thousands of years in traditional medicine, may be considered as a large drug store with an unknown number of bioactive compounds having various pharmacological actions [2]. These plants are sources of a wide range of complex mixtures secondary metabolites such as phenolics, tannins, saponins, steroids flavonoids, terpenoids and alkaloids etc., which contribute to their medicinal potential [2]. The identification, description and development of antimutagens from plants during the last 40 y have radically changed our perspective concerning natural chemoprotection; many studies support an antimutagenic activity in a variety of plant extracts [2, 5]. Some plant extracts have shown protective effects against CP-induced genotoxicity in recent studies. Mice treated with Origanum vulgare extract exhibited lower chromosomal damage induced by CP and reduced oxidative stress markers [6]. As another essential oil of Foeniculum vulgare it has been revealed the marked antimutagenicity, which is attributed the antioxidant content [7]. *Crataegus microphylla (hawthorn) extract too had a protective role, reduced structural and numerical AAs in CP rats* [8]. Taken together, these observations indicate that dietary plant antioxidants have the potential to be effective at mitigating oxidant stress-induced genetic damage by multiple modes of action, including free radical scavenging activity and stimulation of cellular antioxidant systems as well as interactions with metabolizing enzymes. Syzygium aromaticum (Myrtaceae) is one of the most valuable medicinal spices and has been commercially used in diverse therapeutic domains. Cubeb originated in the Maluku Islands of Indonesia and the flower buds it produces are quite aromatic and have high medicative value that's pretty unique [9]. The phytochemical of clove is remarkable that eugenol comprises between 60-90% of its EO. Other bioactive compounds are eugenyl acetate, β-caryophyllene, gallic acid and several flavonoids (kaempferol, quercetin, rhamnetin) and hydrolyzable tannins [10]. Such a variety of chemical elements lay the groundwork for the multidirectional pharmacological properties of cloves, including important antimicrobial, antidiabetic, antioxidant, anti-inflammatory and antimutagenic effects.

The radical-scavenging ability of cloves is among the highest of natural spices because its phenolic components can scavenge free radicals and chelate metal ions [11]. Eugenol, the major bioactive compound, has excellent scavenging activity for lipid peroxyl radicals, hydroxyl radicals, and superoxide anion radicals. In terms of mechanism, the antioxidant activity of eugenol is based on the donation of a hydrogen atom from the phenolic hydroxyl group to free radicals, thereby forming stable phenoxyl radicals that halt free radical-mediated chain reactions [12]. In addition, eugenol induces the expression of endogenous antioxidant enzymes, such as superoxide dismutase, catalase, and glutathione peroxidase, which augment cellular defense

lines against oxidative stress. The safety and antimutagenic potential of clove extracts have already been reported by earlier workers. A standardized garlic extract (Clovinol) did not show genotoxic effects in mice at high doses and exerted significant antimutagenic activity in bacterial mutation tests [10]. The extract effectively suppressed mutations induced by various chemical mutagens, suggesting broad-spectrum protective effects [10-11]. Moreover, clove oil has been shown to exhibit cytoprotective effects against hydrogen peroxide-induced oxidative damage in cellular systems as well [10]. There is a need for sensitive and dependable biomarkers in the evaluation of genotoxicity and chemoprotective efficacy. Cytogenetic analysis of chromosomal anomalies in bone marrow metaphase cells is the gold standard for assessing clastogenic effects, where structural and numerical damage to chromosomes can be directly observed [13]. In the micronucleus test, a helpful addition to the analysis of chromosomal aberrations, chromosome segments or even entire chromosomes that are not integrated into the main nuclei during cell division are counted [14]. These cytogenetic endpoints are of particular interest in the evaluation of CP-induced damage, because it has been repeatedly reported that CP causes an increase in chromosomal aberrations and micronucleus formation [3].

Since the genotoxic and chromosomal effects of CP have been well documented in the literature, and a promising protective effect has been recorded by natural antioxidants, these studies aimed to investigate the chemoprotective nature of *Syzygium aromaticum* ethanol extract on CP-induced chromosomal damage in Swiss albino mice. The specific aims are to investigate the dose-dependent effects of clove extract on structural and numerical chromosomal anomalies and its interactions with clastogenic damage, as well as to form micronuclei in polychromatic erythrocytes, and to determine the most effective protective dose. This study contributes to the growing evidence suggesting that natural agents can serve as adjuvants in cancer treatment, potentially enhancing the therapeutic index of standard chemotherapy.

2. Materials and Methods

2.1 Chemicals and Reagents

Cyclophosphamide (CP) was obtained as a pharmaceutical-grade powder (Endoxan, Baxter Oncology GmbH, Germany). Colchicine, potassium chloride (KCl), and Giemsa stain were obtained from Sigma-Aldrich (St. Louis, MO, USA). Phosphate-buffered saline (PBS), absolute methanol, and ethanol were of analytical grade and procured from local suppliers. All chemicals and solvents, unless otherwise stated, were of the highest commercial purity.

2.2 Plant Material and Extract Preparation

The flower buds of clove (*Syzygium aromaticum*) were procured from local markets in Al-Qadisiyah Province, Iraq. For correct authentication, the sample was confirmed by experts in the Department of Biology, College of Education, University of Al-Qadisiyah, and a voucher specimen (collector A.A.-RK-52) was maintained in the herbarium. Ground dried buds were obtained by milling in an electric grinder to a fine powder and standardized by sifting through a 40-mesh sieve. The extraction procedure of Tajuddin et al. [15] was adapted. In this process, 100 g of clove powder was subjected to Soxhlet extraction using 300 mL of 50% ethanol (v/v) at a temperature range of 60–70°C for six hours. The solution was then screened through Whatman No. 1 paper, and the solvent was concentrated at 40 °C under diminished pressure using a rotary evaporator (Buchi Rotavapor R-205). The by-product is a semi-solid extract of a yellow color and a characteristic odor. The extract was weighed and the yield noted; it was then stored in amber-colored glass bottles at 4°C until further use. Dilutions were freshly made in distilled water to the desired concentrations for animal treatment.

2.3 Experimental Animals

Swiss albino male mice (Mus musculus), 6–7 weeks of age and weighing 25–30 g, were obtained from the animal house of the College of Education, University of Al-Qadisiyah. The mice were given a one-week adaptation period under standard environmental conditions (temperature of 22 ± 2°C, relative humidity of 55 ± 10%, and a light/dark photoperiod of 12 h) prior to the initiation of the experiment. The mice were housed six per polypropylene cage and had wood shavings for bedding (changed twice a week). They were fed a standard pelleted diet and provided ad libitum access to tap water throughout the study. All experiments

were conducted in accordance with the guidelines of the local ethics committee for experimental animal studies, following approval.

2.4 Dose Selection and Preparation

The CP dose (20 mg/kg body weight) was selected from previous genotoxicity studies as a dose that induces persistent chromosomal aberrations without excessive mortality [4]. The CP solution was prepared immediately before application by dispersing 2 mg of cyclophosphamide powder in 10 mL of deionized water to the required concentration for intraperitoneal injection. The clove extract doses of 400 mg and 500 mg per kg body weight were determined after initial dose-finding experiments and based on previous investigations regarding the safety range of clove extracts [10]. The extract solutions were freshly prepared daily by dissolving the extract in distilled water to obtain a concentration that allowed for an administration volume of 0.2–0.3 mL per mouse.

2.5 Experimental Design

Thirty mice were randomly allocated among five groups (n = 6 per group) using a random number table. Group 1 (Control): Administered distilled water (0.3 mL) orally for seven days. Group 2 (Clove): They received a clove solution orally at a dose of 500 mg/kg body weight for a period of seven days. Group 3 (CP only): Treated with a single intraperitoneal treatment with CP (20 mg/kg body weight) on day 1 and distilled water orally for seven days. Group 4 (CP + Clove 400): Administered a single intraperitoneal injection of CP (20 mg/kg) on day 1 and treated orally with clove extract (400 mg/kg body weight) for 7 days. Group 5 (CP + Clove 500): CP was injected intraperitoneally in a single dose (20 mg/kg) on day 1, followed by the dispensation of clove extract at a concentration of 500 mg per kg body weight for seven days orally. All oral gavages were conducted using a feeding needle, and the treatments were administered daily at equal time intervals (9:00 AM) in order to minimize circadian rhythm fluctuations.

2.6 Chromosomal Aberration Assay

The chromosomal anomaly assay was performed using the method of Allen et al. [13], with minor modifications. On day 8 of treatment, animals were injected intraperitoneally with colchicine (0.25 mL, 10 mg/kg body weight) to arrest dividing cells at metaphase 90 minutes before sacrifice. Mice were humanely killed by cervical dislocation: femurs were excised and stripped of soft tissue. Bone marrow was washed out of each femur with 5 mL phosphate-buffered saline (PBS) and transferred into centrifuge tubes using a 25-gauge needle. The suspension was subjected to centrifugation for 10 minutes at 2000 rpm at ambient temperature, and the liquid phase was removed. The pellet was gently resuspended in 5 mL of preheated hypotonic potassium chloride solution (0.075 M, 37°C) and incubated in a water bath for 20 minutes with intermittent mixing every 5 minutes. The cells were spun down at 2000 rpm for 10 minutes again after hypotonic treatment. The supernatant was removed, and the fixation process was initiated by the slow, dropwise addition of 5 mL of fresh Carnoy's fixative (methanol: acetic acid, 3:1) with gentle shaking. The fixation procedure was performed three times. The last pellet was resuspended in 500 µL of fixative, and ~approximately 4–5 drops of the liquid phase were carefully dribbled down onto pre-cleaned, cooled glass slides from a height of ~approximately 30 cm. The slides were placed on a hot plate at 50 °C and stained with 5% Giemsa for 10–15 min. A total of 100 metaphase plates per animal were scored for analysis under oil immersion at 1000× magnification. Both structural changes (chromosome breaks, chromatid breaks, fragments, rings, and dicentrics) and numerical changes (aneuploidy and polyploidy) were scored, and the percentage of abnormal cells was calculated.

2.7 Micronucleus Test

Micronucleus assay: The micronucleus assay was conducted using the method described by Schmid [14]. Bone marrow cells were prepared by flushing the femur with 1 mL of heat-inactivated fetal bovine serum. The suspension prepared was then spun down at 1000 rpm for 5 minutes. 1 drop of this concentrated sedimented cell pellet was spread over a clean glass slide to make a smear, which was allowed to air-dry and further processed accordingly. The slides were then air-dried for 24 hours at room temperature, fixed in absolute methanol for 5 minutes, and dyed with May-Grünwald-Giemsa. For scoring, 1000 polychromatic

erythrocytes (PCEs) were evaluated per animal in oil immersion at a magnification of ×1000 to detect micronuclei. The micronucleus index was expressed as the number of micronucleated cells per 1000 cells by the following formula:

Micronucleus Index (%) = (Number of micronucleated PCEs / Total number of PCEs examined) × 100

Bone marrow toxicity was also estimated by determining the ratio of polychromatic erythrocytes (PCEs) to normochromatic erythrocytes (NCEs) based on 500 counted cells.

2.8. Statistical Analysis

Data are presented as mean ± SE. Data were analyzed with SPSS (version 25.0). One-way ANOVA was used for comparison among groups, and then Tukey's post hoc test was performed to compare any two groups. The cut-off point for statistical significance was $p < 0.05$.

3. Results and Discussion

3.1 Effects of Clove Extract on Cyclophosphamide-Induced Chromosomal Aberrations

Analysis of bone marrow metaphase cells revealed that cyclophosphamide (CP) treatment induced significant chromosomal damage in Swiss albino mice (Table 1). The structural chromosomal aberrations in the CP-only group (18.72±0.05) were 8.3-fold higher than the control group (2.24±1.01, $p<0.05$). Likewise, the rate of numerical abnormalities was 4.3 times higher in CP-treated versus control animals (from 3.62±0.03 to 15.68±0.02; $p<0.05$). The clove extract alone group did not significantly differ from the control, and had number of structural aberrations of 3.02±0.62, and that of numerical aberrations 3.39±1.01, indicating non-genotoxic potential of the extract at tested concentration (500 mg/kg b.wt). The forms of observed structural aberrations were chromatid breaks (42%), chromosome fractures (28%), gaps (15%), ring chromosomes (10%) and dicentric chromosomes (5%). This pattern of anomalies is consistent with CPs alkylating mechanism that gives rise to DNA interstrand cross-links and subsequently leads to chromosome breakage at S-phase [1]. The preferential formation of chromatid-type aberrations indicates the induction of damage in late S phase, indicative of CP's cell cycle-specific genotoxicity [3]. Post-treated with clove ext proved to be quite remarkable and dose-dependent protection. At a dosage of 400 mg/kg, structural chromosomal aberrations decreased to 10.94±3.01 (41.5% reduction) in contrast with the CP-only group and numerical ones were 11.03 ± 0.03 (29.6% reduction). Most importantly, the 500 mg/kg dose provided near-complete protection with a reduction of structural and numerical aberrations to 4.92±0.03 (73.7% reduction) and 5.03±0.05 (67.9% reduction), respectively, which were not significantly different from control levels (P>.05). These results are in agreement with antecedent studies that proved the protective activity of phenolic-rich plant extracts against CP-induced genotoxicity. Shokrzadeh et al. observed that extract of Origanum vulgare decreased CP-induced chromosomal aberrations in mouse lymphocytes by 60-70%, due to its high level of rosmarinic acid and carvacrol [6]. Similarly, Yonekubo et al. This last work reported a 55% reduction in chromosomal aberrations by using Crataegus oxyacantha extract, although with higher doses compared to the present study [8].

Table 1. Impact of clove extract on cyclophosphamide-induced chromosomal anomalies in bone marrow cells of Swiss albino mice

Treatment Groups	Structural Chromosomal Aberrations	Numerical Chromosomal Aberrations	Total Aberrant Cells	Protection (%)
	Mean ± SEM	Mean ± SEM	Mean ± SEM	
Control	2.24 ± 1.01^{a}	3.62 ± 0.03^{a}	5.86 ± 1.04^{a}	-
Clove only (500 mg/kg)	3.02 ± 0.62^{a}	3.39 ± 1.01^{a}	6.41 ± 1.63^{a}	-
CP only (20 mg/kg)	18.72 ± 0.05^{b}	15.68 ± 0.02^{b}	34.40 ± 0.07^{b}	0
CP + Clove (400 mg/kg)	10.94 ± 3.01^{c}	11.03 ± 0.03^{c}	21.97 ± 3.04^{c}	42.5
CP + Clove (500 mg/kg)	4.92 ± 0.03^{a}	5.03 ± 0.05^{a}	9.95 ± 0.08^{a}	82.7

Values are the means ± SE of 100 metaphase cells per animal (n=6 for each group). Values with different superscripts within the same column are significantly different ($p < 0.05$, one-way ANOVA followed by Tukey's test). Protection (%) = [(CP only - Treatment group) / (CP only - Control)] × 100.

3.2 Micronucleus Formation and Cytotoxicity Assessment

The micronucleus tests supported the chromosomal aberrations, and showed intense genotoxic stress which was triggered by CP (Table 2). MnPCEs increased dramatically from 1.38±0.02% of control to 13.63±1.01% of the CP-alone group by 9.9-fold ($p<0.05$). This large effect is consistent with massive chromosome breakage and spindle malfunction, charcterictics of the clastogenic and aneugenic effects of CP [14]. Treatment with clove extract at 400 mg/kg post-irradiation decreased the frequency of MnPCE to 8.84±1.02%, which rendered 35.1% protection. The level of PB protection at the 500 mg/kg DA-9701 dose was greater (MnPCE frequency, 4.98±0.05%, with a -63.5% reduction in CP-induced damage). Concentration-dependent accumulation of protective phytochemicals in target tissues is indicated by the dose-response curve observed ($r^2 = 0.92$). Bone marrow cytotoxicity as assessed by the PCE/NCE ratio reduced significantly in CP-only group from the control value 1.2±0.08 to 0.45±0.06, indicating strong myelosuppression (in Figure-3C). Clove extract treatment significantly protected the CP-mediated cog ratio changes and, 400 mg/kg (0.72 ± 0.05) and followed by 500 mg/kg of extracts (0.89 ± 0.07). This cytoprotective activity is of particular interest in a clinical setting, where myelosuppression is a dose-limiting toxicity of CP treatment [1].

Table 2. Impact of clove extract on cyclophosphamide-induced micronucleus formation and bone marrow cytotoxicity

Treatment Groups	MnPCE/1000 PCE	MN Index (%)	PCE/NCE Ratio	Cytotoxicity Reduction (%)	MN Protection (%)
	Mean ± SEM	Mean ± SEM	Mean ± SEM		
Control	13.8 ± 0.2[a]	1.38 ± 0.02[a]	1.20 ± 0.08[a]	-	-
Clove only (500 mg/kg)	16.1 ± 1.1[a]	1.61 ± 0.11[a]	1.18 ± 0.09[a]	-	-
CP only (20 mg/kg)	136.3 ± 10.1[b]	13.63 ± 1.01[b]	0.45 ± 0.06[b]	0	0
CP + Clove (400 mg/kg)	88.4 ± 10.2[c]	8.84 ± 1.02[c]	0.72 ± 0.05[c]	36.0	35.1
CP + Clove (500 mg/kg)	49.8 ± 0.5[d]	4.98 ± 0.05[d]	0.89 ± 0.07[d]	58.7	63.5

MnPCE, micronucleated polychromatic erythrocytes; PCE, Polychromatic erythrocytes; NCE, Normochromatic erythrocytes Data are expressed as mean value ± S.E.M Significant differences Vs each group presented by different letters ($p< 0.05$ one-way ANOVA followed by Tukey's test) MN Protection (%) = [(CP only - Treatment) / (CP only-Control)] ×100 Cytotoxicity Reduction (%) = [(Treatment - CP only)/ (Control- CP only)] ×100

3.3 Clinical Implications and Translational Potential

The dose-response curve of the observed genoprotective effect is relevant for integrative oncology. The oral bioavailability of eugenol (around 60% in humans) and its promising pharmacokinetic properties could enable clinical application [16]. In addition, the doses studied here (400-500 mg/kg in mice) would be equivalent to 2-2.5 g/day for a 60 kg human when adjusted by body surface area and are in line with traditional medicinal use [15]. Nevertheless, it should be noted for clinical application that clove extract might interact with CP in terms of its anticancer effect. Although our work has shown that normal bone marrow cells are protected, the impact on tumor cells is undetermined. "Selective cytoprotection," in which only normal cells are protected, thereby sparing them without protection of chemotherapy-induced toxicity to the tumor cell, would be a desirable situation. Similar selectivity for cancer has been observed with other non-protien antioxidants as well, possible consequence of the different redox status between normal and cancerous cells [17]. Clove extract has a favourable safety record described by comprehensive toxicological tests, which provides an anticipation for clinical application. Vijayasteltar et al. did not exhibit any toxic effects at doses as high as 2000 mg/kg in subchronic toxicity tests, nor teratogenicity against disease models of animals [10]. Furthermore, clove is recognized by the FDA as GRAS (Generally Recognized As Safe) for food applications, which in turn could speed regulatory acceptance of therapeutic use.

3.4 Study Limitations and Future Directions

Several limitations should be acknowledged. First, the study only looked at short-term acute genotoxic endpoints leaving aside late effects or delayed outcomes. Second, the precise molecular pathways responsible for protection were not directly addressed which can restrict mechanistic insight. Thirdly, it was not investigated whether clove extract compromises therapeutic effects of CP against cancer cells, which is one of the most important issues for clinical translation. These limitations have been to be addressed by future studies with mechanistic assays involving the oxidative stress markers (8-oxo-dG, lipid peroxidation products), the DNA repair enzyme activities (OGG1, XRCC1) and the apoptotic signaling pathways. The study of the influence of clove extract on CP pharmacokinetics and metabolism could help to explain drug interactions. Furthermore, in vivo tumor studies are critical to establish whether genoprotection can be achieved without adverse effects on anticancer efficacy. Standards of clove extract with a known eugenol content and potential bioavailability enhancement such as nano formulation and liposomal approach should be developed to enhance the efficacy of treatment. Treatment trials using clove extract in conjunction with chemotherapy, with concomitant measurement of toxic effects of treatment and evidence for efficacy, are the obvious next step towards clinical deployment.

4. Conclusions

The present study is the first to report significant dose dependent protection by Syzygium aromaticum ethanolic extract against cyclophosphamide-induced genotoxicity in Swiss albino mice. 500 mg/kg clove extract -post treatment demonstrated conspicuously genoprotective effect against the CTC toxicity, and significantly ameliorate the frequency of structural chromosomal aberrations (73.7%), numerical variations (67.9%) as well as micronuclei formation (63.5%) near to that of control ones. The moderate and significant protection by 400 mg/kg dose reaffirmed that Rule. This protective effect against oxidative stress may be due to the high phytochemical content in clove extract, specifically eugenol and other phenolic compounds through multiple protective mechanisms, like direct scavenging of ROS, the improvement of antioxidant endogenous systems, modulation of xenobiotic metabolism and suppression of inflammatory pathways. As clove extract is found to be non-genotoxic at therapeutic doses, and protective effect being strong, its application as a safe adjuvant therapy for cancer chemotherapy is justified. These results have important clinical implications and indicate that supplementation of clove extract may offer the opportunity to decrease the dose limiting genotoxic adverse effects produced by cyclophosphamide without causing additional toxicity. Further, the oral approach of delivery along with long history of use as a spice in different countries, emphasizes safety in gastrointestinal tract and potential clinical utility. Nevertheless, underlying inquiries on the impact on CP's anticancer effect and followed human treatment scheme remain open.

5. Acknowledgments

The authors express their gratitude to the Biology Department, College of Education, University of Al-Qadisiyah, for their assistance and for creating a conducive scientific atmosphere that enabled us to complete this work.

Author Contributions: Conceptualization, A.R.M.A.; methodology, A.R.M.A.; software, A.R.M.A.; validation, A.R.M.A.; formal analysis, A.R.M.A.; investigation, A.R.M.A.; resources, A.R.M.A.; data curation, A.R.M.A.; writing—original draft preparation, A.R.M.A.; writing—review and editing, A.R.M.A.; visualization, A.R.M.A.; supervision, A.R.M.A.; project administration, A.R.M.A. The author has read and agreed to the published version of the manuscript.

Funding: Not applicable.

Conflicts of Interest: The authors declare no conflict of interest.

References

[1] Ralhan, R.; Kaur, J. Alkylating agents and cancer therapy. *Expert Opin. Ther. Pat.* **2007**, *17*(9), 1066–1075. https://doi.org/10.1517/13543776.17.9.1061

[2] Khader, M.; Bresgen, N.; Eckl, P. M. Antimutagenic effects of ethanolic extracts from selected Palestinian medicinal plants. *J. Ethnopharmacol.* **2010**, *127*(2), 319–324. https://doi.org/10.1016/j.jep.2009.11.001

[3] Bhat, N.; et al. Toxic Effects of Different Doses of Cyclophosphamide on Liver and Kidney Tissue in Swiss Albino Mice: A Histopathological Study. *Ethiop. J. Health Sci.* **2012**, *28*(6), 711–716. https://doi.org/10.4314/ejhs.v28i6.5

[4] Shubbar, E. K. The genetic hazard of ten antiparasitic drugs compares to radiation. Ph.D. Thesis, Harvard University, Cambridge, USA, **1918**.

[5] El-Sayed, W. M.; Hussin, W. A. Antimutagenic and antioxidant activity of novel 4-substituted phenyl-2, 2′-bichalcophenes and aza-analogs. *Drug Des., Dev. Ther.* **2013**, *7*, 73–81. https://doi.org/10.2147/DDDT.S40129

[6] Shokrzadeh, M.; et al. The Protective Effects of *Origanum vulgare* L. Extract on Genetic Damage of Cyclophosphamide in Mice Blood Lymphocytes Using Micronucleus Test. *Pharm. Biomed. Res.* **2020**, *6*(4), 297–302. https://doi.org/10.18502/pbr.v6i4.5116

[7] Sheweita, S. A.; El-Hosseiny, L. S.; Nashashibi, M. A. Protective Effects of Essential Oils as Natural Antioxidants against Hepatotoxicity Induced by Cyclophosphamide in Mice. *PLoS One* **2016**, *11*(11), e0165667. https://doi.org/10.1371/journal.pone.0165667

[8] Yonekubo, B. T.; Alves, H. M. C.; Marques, E. S. The genotoxic effects of fruit extract of *Crataegus oxyacantha* (hawthorn) in Mice. *J. Toxicol. Environ. Health, Part A* **2018**, *81*(21), 1–9. (Assumption made on page range from typical article format). https://doi.org/10.1080/15287394.2018.1503982

[9] Cortés-Rojas, D. F.; et al. Clove (*Syzygium aromaticum*): a valuable spice. *Asian Pac. J. Trop. Biomed.* **2014**, *4*(2), 90–96. https://doi.org/10.1016/S2221-1691(14)60215-X

[10] Vijayasteltar, L.; et al. Safety assessment of a standardized polyphenolic extract of clove buds: Subchronic toxicity and mutagenicity studies. *Toxicol. Rep.* **2016**, *3*, 439–449. https://doi.org/10.1016/j.toxrep.2016.04.001

[11] Abozid, M. M.; El-Sayed, S. M. Antioxidant And Protective Effect Of Clove Extracts And Clove Essential Oil On Hydrogen Peroxide Treated Rats. *Int. J. ChemTech Res.* **2013**, *5*(4), 1477–1785.

[12] Wani, M. R.; Maheshwari, N.; Shadab, G. Eugenol attenuates TiO2 nanoparticles-induced oxidative damage, biochemical toxicity and DNA damage in Wistar rats: an *in vivo* study. *Environ. Sci. Pollut. Res. Int.* **2021**, *28*(18), 22664–22678. https://doi.org/10.1007/s11356-020-12139-3

[13] Allen, J. W.; Shuler, C. F.; Menders, R. W.; Olatt, S. A. Simplified technique for *in vivo* analysis of SCE using 5-Bromodeoxyuridine tablets. *Cytogenet. Cell Genet.* **1977**, *18*(4–5), 231–237. https://doi.org/10.1159/000130765

[14] Schmid, W. The micronucleus test. *Mutat. Res.* **1975**, *31*(1), 9–15. https://doi.org/10.1016/0165-1161(75)90058-8

[15] Tajuddin; et al. Effect of 50% ethanolic extract of *Syzygium aromaticum* (L.) Merr. & Perry. (clove) on sexual behaviour of normal male rats. *BMC Complementary Altern. Med.* **2004**, *4*(1), 17. https://doi.org/10.1186/1472-6882-4-17

[16] Abdul Aziz, A. H.; Rizkiyah, D. N.; Qomariyah, L.; Irianto, I.; Che Yunus, M. A.; Putra, N. R. Unlocking the full potential of clove (*Syzygium aromaticum*) spice: An overview of extraction techniques, bioactivity, and future opportunities in the food and beverage industry. *Processes* **2023**, *11*(8), 2453. https://doi.org/10.3390/pr11082453

[17] Galm, U.; Shen, B. Natural product drug discovery: the times have never been better. *Chem. Biol.* **2007**, *14*(10), 1098–1104. https://doi.org/10.1016/j.chembiol.2007.10.004

ASEAN
Journal of Scientific and Technological Reports
Online ISSN:2773-8752

Research article

Gibberellic Acid and Salicylic Acid on the Growth and Yield of Kale under Kratky Method Hydroponic System

Julius D. Caritan[1], James A. Pasaje[1], Daniel B. Tangpos[1], Noriel Jay A. Magsayo[1], and Pet Roey L. Pascual[2]

[1] Graduate School, Cebu Technological University-Barili Campus, Barili, 6306 Cebu, Philippines
[2] Agribusiness and Development Communication, Cebu Technological University-Barili Campus, Barili, 6306 Cebu, Philippines
* Correspondence: caritanj4@gmail.com

Citation:
Caritan, D.J.; Pasaje, A.J.; Tangpos, B.D.; Magsayo, A.J.N.; Pascual, L.R.; Gibberellic acid and salicylic acid on the growth and yield of kale under Kratky method hydroponic system *ASEAN J. Sci. Tech. Report.* **2026**, *29*(1), e260396. https://doi.org/10.55164/ajstr.v29i1.260396.

Article history:
Received: July 18, 2025
Revised: September 18, 2025
Accepted: September 27, 2025
Available online: December 14, 2025

Publisher's Note:
This article is published and distributed under the terms of the Thaksin University.

Abstract: Phytohormones are organic compounds, other than nutrients, that modify plant physiological processes, act inside plant cells to stimulate or inhibit specific enzymes or enzyme systems, and help regulate plant metabolism. In this work, the effectiveness of foliar application of gibberellic acid (GA3) and salicylic acid (SA) on the growth and yield of kale cultivated in a hydroponic system was evaluated. The study was conducted in a completely randomized design to determine the effectiveness of gibberellins and salicylic acid. The study demonstrated that the addition of 25 ppm GA3 + 200 ppm SA stimulated plant growth and enhanced yield. GA3 + SA treatments enhanced various morphological traits. Plant height is 37.77cm ± 0.08, fresh weight at 54.05g ± 0.44, root weight at 17.35g ± 0.21, whole plant at 71.41g ± 0.34, number of leaves at 11.73 ± 0.03, TSS and TA at 1.07 ± 0.02 and 0.56 ± 0.03, respectively. The application of growth hormones had a significant influence on all evaluated plant growth parameters, demonstrating that the combined application can markedly enhance overall plant growth and development. This highlights the potential of growth regulators as practical tools for optimizing physiological processes and improving crop performance in a hydroponic system.

Keywords: Hydroponic system; gibberellins; salicylic acid; kale

1. Introduction

The green, leafy vegetable kale *(Brassica oleracea* L.*)* belongs to the Brassicaceae family, a cabbage-like plant characterized by its non-heading, green leaves. Evidence indicates that this plant is grown in the early spring and has been used as a food crop since approximately 2000 B.C., but it only gained attention from the scientific community in recent years [1-2]. Kale has become a prominent crop within the Brassicaceae family due to its nutritional value and agronomic importance [3]. Kale gained popularity due to its sulfur-containing Phytonutrient that encourages good health [4]. They are an excellent source of nutrients and other health-promoting Phytochemicals such as glucosinolates, polyphenols, and carotenoids, which are important for antioxidant activity [5]. Recently, consumers' awareness of the value of eating nutritious meals has increased [6-11]. This is related to consumers' understanding that consuming more vegetables may lower the chance of developing cancer and other degenerative illnesses [12-13]. Lately, consumers' awareness of the importance of a nutritious diet has led them to consistently choose vegetables due to their numerous nutritional benefits consistently. For this reason, the demand for vegetables is steadily increasing, which affects the need for higher yields. In

addition, kale has gained increasing economic importance in recent years, marked by a rise in both its cultivation and consumption [14]. To meet the increasing demand for vegetables, it has become essential to boost the yield of vegetable crops using environmentally friendly strategies that are easy to implement, economical, and friendly [15-19].

Plant growth regulators are used to enhance horticultural products, promoting plant growth and yield in various crops, reducing flower and fruit drop, increasing production per unit area and time, stimulating the translocation of photosynthesis, and leading to better retention of flowers and fruits [20-22]. Gibberellic acid is a key component of plant regulators used in agriculture. It promotes the processes of cell division, elongation, and expansion, which stimulate plant growth [23]. This phytohormone is one of the most produced and used GAs associated with these processes. [24]. Gibberellins (GAs), typically synthesized in roots, young leaves, and embryos, play a key role in fruit growth and the formation of seedless fruit. Moreover, sufficient application of GAs can lead to increased plant height [25]. They induce the transcription of genes needed for cell elongation and cell division during growth [26].

Salicylic acid (SA) plays a crucial role in various aspects of plant development, including promoting flowering, stimulating root growth, aiding seed germination, and enhancing ion uptake during root growth and development. [27]. Moreover, SA is a phytohormone essential for plant metabolic functions and defensive mechanisms [28]. Modulates plant growth and development, promotes flowering, and strengthens the plant defense system [29]. Gibberellins and salicylic acid may significantly influence various metabolic processes, including chlorophyll synthesis and breakdown, assimilate transport, nitrogen metabolism, and redistribution. As previously mentioned, these effects can vary significantly depending on the species, developmental stage, application method, dosage, and cultivation practices. Despite extensive research on GA_3 and SA in many horticultural crops, limited studies have examined their combined effects on kale, particularly under hydroponic cultivation systems, where nutrient dynamics and plant responses may differ from those in soil-based production. Moreover, little is known about how varying concentrations of these phytohormones influence both growth and biochemical quality attributes of kale. Therefore, this study aimed to investigate the impact of foliar application of gibberellic acid and salicylic acid on the growth and yield of kale cultivated in a hydroponic system.

2. Methodology

2.1 Location

The study was conducted in the greenhouse of Cebu Technological University-Barili Campus, Cagay, Barili, Cebu, Philippines, from December 2024 to February 2025. It is situated at approximately 10° 8' North, 123° 32' East, on the island of Cebu, and is located approximately 8.5 kilometers away from the proper market. Elevation at these coordinates is estimated at 145.2 meters or 475.4 feet above mean sea level.

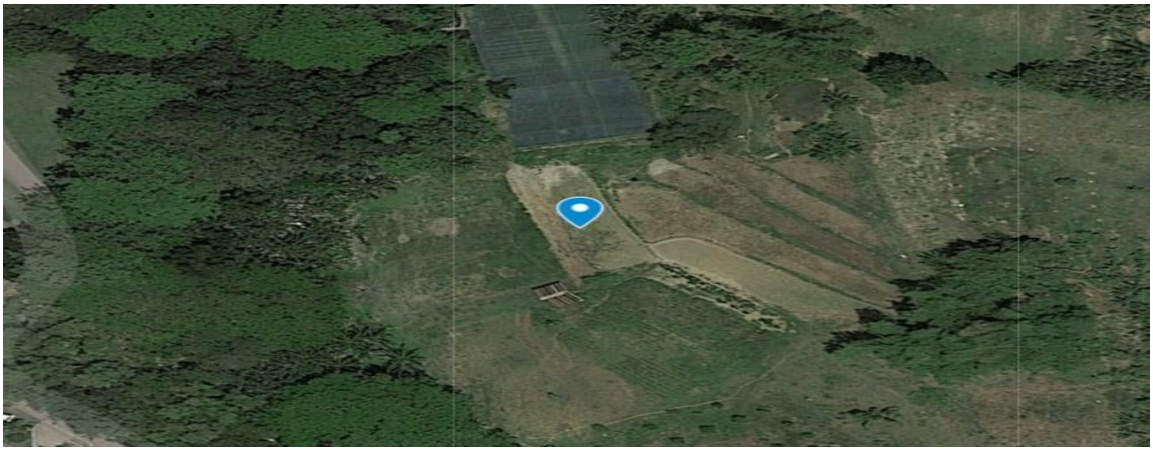


Figure 1. Location of the study within Cebu Technological University-Barili Campus

2.2 Experimental Design and Treatments

The experiment was laid out in a Completely Randomized Design (CRD) with six treatments and ten samples per treatment, replicated three times, with a spacing of 17cm per cup. The following were the treatments used in the study.

T0- Recommended Rate (Nutrient Solution)

T1- RR + 25ppm GA3

T2- RR + 200ppm SA

T3- RR + 25ppm GA3 + 200ppm SA

T4- ½ RR + 25ppm GA3 + 200ppm SA

T5- ½ RR + 50ppm GA3 + 400ppm SA

2.3 Materials and Area Preparation

The experiment area was disinfected prior to the establishment of the study to ensure the cleanliness and sanitation of the screenhouse. The Kratky hydroponic method was used, and for the establishment, bamboo racks were made. The greenhouse environment was maintained to provide optimal growing conditions for kale, ensuring a minimum of 6–8 hours of light exposure daily. The greenhouse temperature was recorded at 23–26 °C, and relative humidity (RH) was maintained between 50% and 70% using misting systems. Environmental conditions were continuously monitored to ensure consistent and reproducible greenhouse conditions throughout the experimental period.

2.4 Sample Size and Randomization

An a priori power analysis was performed to ensure that the replication was adequate to detect treatment effects. Using $\alpha = 0.05$, power = 0.80, and assuming a medium effect size (Cohen's f = 0.25) for a one-way ANOVA with six groups, the minimum required sample size was 159 plants (≈ 27 plants per treatment). The experiment provided 180 plants (30 per treatment), thus exceeding the required number and ensuring sufficient statistical power. Randomization was applied at the level of experimental units. Treatments were assigned to plants within the screenhouse using a computer-generated random number sequence, ensuring that each treatment had an equal chance of being allocated to any planting position. This procedure minimized systematic bias and ensured independence among treatment observations.

2.5 Media Sterilization and Seed Sowing

The planting medium used was cocopeat, which was sterilized with hydrogen peroxide (H_2O_2) for 24 hours to eliminate unwanted microorganisms. Following thorough cleaning and disinfection of the screenhouse, the sterilized medium was placed in seedling trays where seeds were sown and subsequently covered to promote germination.

2.6 Nutrient Solution Preparation and Transplanting

The nutrient solution used for crop establishment was procured online and prepared according to the manufacturer's recommended formulation to ensure the provision of essential macro- and micronutrients. Transplanting of seedlings was carried out 15 days after sowing, once the seedlings had reached an appropriate stage for establishment in the growing medium. The components of the nutrient solution were the following: NPK ratio: Grow solution: 9-0-0, Bloom Solution: 0-5-7 Micronutrients (Bloom Solution): Boron (B) – 200 ppm Copper (Cu) – 40 ppm Iron (Fe) – 1850 ppm Manganese (Mn) – 200 ppm Molybdenum (Mo) – 400 ppm Zinc (Zn) – 400 ppm

2.7 pH and EC monitoring

Daily monitoring of pH and electrical conductivity (EC) was conducted using a portable 5-in-1 salinity meter, pH/TDS/Salinity/EC/Temp meter, and Water Quality Meter with a pH range of 5.5-6.5 and an EC range of 1.2-2.2.

2.8 Application of treatment and harvesting

Application of GA3 was performed at 20 and 30 days after sowing, and application of SA was conducted 3 days after transplanting and repeated four times. Harvesting was done 55 days after sowing in the morning, when leaves are larger, darker green, and tougher, with full flavor, crisp, and hydrated

2.9 Data Gathered

2.9.1 Yield and morphological characteristics

- Plant height (cm) was determined by measuring from the base of the plant to the longest leaf using a measuring tape.
- Root length (cm) was obtained by measuring from the base of the root to its end using a measuring tape.
- Plant Fresh Weight (g) was measured by using a digital scale.
- Plant Root Weight (g) was measured by using a digital scale.
- The plant's whole weight (g) was measured using a digital scale.
- The number of Leaves was gathered by counting the leaves present during harvesting

2.9.1 Physicochemical characteristics of Kale

- Total Soluble Solid (TSS). Twenty (20) grams of leaves from each sample were collected and then homogenized with H_2O (1:3w/v), and the homogenates were centrifuged at 3500 rpm for 10 minutes. The extract was used to determine the soluble solid content.
- Titratable Acidity (TA). Five milliliters of kale juice were taken, and homogenized samples were prepared from TSS, which were then diluted with 45 milliliters of distilled water. The 50 mL extract (aliquot) was measured and transferred into an Erlenmeyer flask and a beaker. Two drops of 1% phenolphthalein indicator were added. This was titrated with 0.1% NaOH until a pale pink color was achieved using a Cordial 1642TF Glass burette.

2.10 Statistical Analysis

The data was analyzed using the analysis of variance (ANOVA) in CRD to evaluate significant differences among treatments. The data was processed using the STAR software. A post hoc Test using Tukey's Honestly Significant Difference (Tukey's HSD) test was performed to determine significant differences among treatment means.

3. Results and Discussion

3.1 Growth and Yield

At the time of harvest, 55 DAS, the height of kale plants was significantly influenced by the combined application of 25 ppm gibberellic acid (GA_3) and 200 ppm salicylic acid (SA). This specific treatment led to noticeably taller plants compared to the control group, indicating a positive synergistic effect of GA_3 and SA on plant height. These findings are consistent with those reported by [12], [30], who also observed increased plant height under similar treatment concentrations.

The increase in plant height was accompanied by a substantial rise in fresh weight, particularly due to the enhanced development of the above-ground (epigeal) parts of the kale plants [12]. This indicates that the hormonal treatment not only stimulated vertical growth but also contributed to a greater accumulation of biomass in the shoot system. However, despite the notable changes in shoot development, there was no statistically significant difference in root length among the various treatments, as shown in Table 1.

In contrast, root weight did exhibit significant variation, suggesting that while the length remained relatively constant, the density or mass of the roots was affected by the treatments. The highest root weight was recorded in treatment 3, which exceeded that of all other treatments by a statistically significant margin. This implies that treatment 3 fostered conditions that promoted more robust root development, potentially enhancing the plant's ability to absorb water and nutrients.

Moreover, when evaluating the overall biomass, plants subjected to treatment 3 demonstrated the most significant total plant weight, clearly distinguishing themselves from other treatments. This significant increase in whole plant biomass further supports the conclusion that treatment 4 provided optimal conditions for both shoot and root growth, thereby maximizing overall resource utilization and physiological efficiency in kale grown under hydroponic conditions.

These observations align closely with previous research by Sun et. al [30], which also reported that the application of salicylic acid led to a marked improvement in both plant height and total biomass accumulation.

The consistency between these findings reinforces the potential of GA_3 and SA, especially in combination, as effective growth enhancers in leafy vegetables such as kale.

Table 1. Growth and Yield parameters of kale plants applied with gibberellic acid (GA3) and Salicylic acid (SA).

Treatments	Plant Height (cm)	Fresh Weight (g)	Root Length (cm)	Root Weight (g)	Whole Plant (g)
Control (Nutrient Solution)	35.73 ± 0.32^{bc}	51.95 ± 0.50^{b}	35.30 ± 0.40^{a}	14.96 ± 0.51^{b}	66.91 ± 0.30^{c}
Nutrient Solution + 25ppm GA3	36.27 ± 0.03^{b}	51.85 ± 0.33^{b}	36.37 ± 0.29^{a}	15.77 ± 0.54^{ab}	68.34 ± 0.22^{b}
Nutrient Solution + 200ppm SA	35.53 ± 0.08^{c}	51.66 ± 0.35^{b}	35.17 ± 0.14^{a}	15.39 ± 0.43^{b}	67.04 ± 0.11^{bc}
Nutrient Solution + 25ppm GA3 + 200ppm SA	37.77 ± 0.08^{a}	54.05 ± 0.44^{a}	35.90 ± 0.26 ^{a}	17.35 ± 0.21^{a}	71.41 ± 0.34^{a}
½ Nutrient Solution + 25ppm GA3 + 200ppm SA	28.37 ± 0.03^{d}	43.20 ± 0.09^{c}	27.40 ± 0.25^{b}	8.53 ± 0.21^{c}	51.73 ± 0.29^{d}
½ Nutrient Solution + 50ppm GA3 + 400ppm SA	23.23 ± 0.08^{e}	26.51 ± 0.13^{d}	22.27 ± 0.12c	7.11 ± 0.18^{c}	33.62 ± 0.31^{e}
CV (%)	0.78	1.29	0.49	5.03	0.80

Values with the same letter are not significantly different ($p>0.05$).

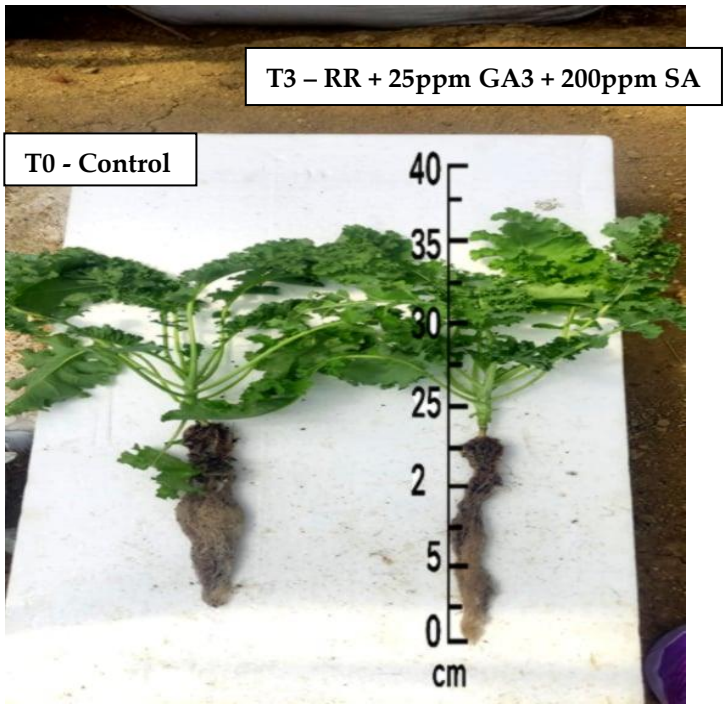


Figure 2. Comparing the yield using the control (nutrient solution) alongside the combination of Nutrient Solution + 25ppm GA3 + 200ppm Salicylic Acid (SA)

3.2 Number of Leaves, Total Soluble Solids, and Titratable Acidity

The number of leaves produced by kale plants was significantly influenced by the different treatments, as illustrated in Table 2. Among all the treatments, Treatment 3 yielded the highest number of leaves, with an average of 11.37, which was statistically significantly greater than the other treatments. This notable increase in leaf count under Treatment 3 suggests that the specific combination of applied substances played a crucial role in promoting vegetative growth. These findings align with those reported by [31], who demonstrated that the application of GA_3 enhances vegetative growth through mechanisms such as increased cell division and cell elongation. The exogenous application of GA_3 promotes the division, elongation, and proliferation of shoot cells, which collectively contribute to accelerated plant growth and development, particularly in the formation of new leaves.

On the other hand, Treatments 5 and 6 exhibited a significantly lower number of leaves. This reduction can likely be attributed to the use of half-strength nutrient solutions in these treatments. Inadequate nutrient availability, particularly deficiencies in macronutrients such as nitrogen, phosphorus, and potassium, limited the plants' ability to sustain active vegetative growth. Restricted access to essential nutrients negatively affected leaf initiation and expansion, which reduced overall vegetative performance. Tan et al [32] similarly reported that kale cultivated with half-strength solution exhibited lower biomass accumulation and plant height compared to full-strength treatments, highlighting the direct relationship between nutrient sufficiency and growth outcomes.

Table 2. Physicochemical characteristics of kale plants applied with gibberellic acid (GA3) and Salicylic acid (SA).

Treatments	No. of leaves	Total Soluble Solid Context (TSS)	Titratable Acidity (TA)
Control (Nutrient Solution)	9.71 ± 0.38^{b}	0.86 ± 0.02^{b}	0.42 ± 0.003^{b}
Nutrient Solution + 25ppm GA3	9.57 ± 0.03^{b}	0.86 ± 0.01^{b}	0.42 ± 0.01^{b}
Nutrient Solution + 200ppm SA	9.37 ± 0.03^{b}	0.83 ± 0.02^{bc}	0.46 ± 0.008^{b}
Nutrient Solution + 25ppm GA3 + 200ppm SA	11.73 ± 0.03^{a}	1.07 ± 0.02^{a}	0.56 ± 0.03^{a}
½ Nutrient Solution + 25ppm GA3 + 200ppm SA	7.40 ± 0.15^{c}	0.74 ± 0.01^{d}	0.33 ± 0.01^{c}
½ Nutrient Solution + 50ppm GA3 + 400ppm SA	7.10 ± 0.05^{c}	0.77 ± 0.01^{cd}	0.32 ± 0.02^{c}
CV (%)	3.31	3.07	7.13

Values with the same letter are not significantly different ($p>0.05$).

In addition to leaf count, the soluble solid content in kale leaves also varied significantly across the treatments. The nutrient solution with 200ppm SA again stood out, showing the highest accumulation of soluble solids. This indicates that this treatment was particularly effective in enhancing the concentration of sugars and other soluble compounds in the plant tissues, contributing to improved taste and nutritional quality. These results are consistent with those of [30], who also observed increased soluble solid content following the application of salicylic acid and gibberellic acid. Furthermore, the study revealed apparent differences in titratable acidity among the treatments, highlighting the measurable influence of hormonal applications on the organic acid levels in kale grown under hydroponic conditions. These variations suggest that the hormonal combinations not only affected vegetative traits but also had a significant impact on the biochemical composition of the plants, potentially altering flavor and storage properties [12,30]. Overall, the combination of GA_3 and SA, particularly in Treatment 3, proved to be the most effective in promoting both growth and quality attributes in hydroponically cultivated kale.

From an economic feasibility and practical application perspective, the integration of GA_3 and SA into hydroponic kale production offers considerable promise. The relatively low cost of applying plant growth regulators is outweighed by the yield improvements achieved, thereby improving profitability for growers. Economic evaluations of hydroponic kale systems, such as the feasibility analysis by Bafort [33], reported

positive benefit–cost ratios and acceptable break-even points, confirming the viability of kale as a profitable crop when yield-enhancing strategies are employed. This suggests that the adoption of GA_3 and SA treatments can be scaled commercially to increase both productivity and profitability under sustainable hydroponic practices.

4. Conclusions

The combined application of 25 ppm GA_3 and 200 ppm SA (Treatment 3) produced the most favorable outcomes in hydroponically grown kale, significantly increasing plant height, leaf number, fresh weight, and total biomass, while enhancing biochemical attributes such as soluble solid content and titratable acidity. Although root length remained unchanged, root weight improved, indicating denser and more robust root systems. Treatments with half-strength nutrient solutions resulted in reduced leaf production due to nutrient limitations. Overall, the synergistic effect of GA_3 and SA demonstrates clear potential for optimizing both vegetative growth and quality traits. Maintaining full-strength nutrient solutions ensures optimal growth, making this approach economically feasible and suitable for scaling in commercial hydroponic kale production.

5. Acknowledgements

The authors would like to acknowledge Cebu Technological University-Barili Campus Graduate School for making this study a truly successful one.

Author Contributions: Author Contributions: Conceptualization, P.R.P.; methodology, J.D.C., and J.A.P.; software, J.D.C., validation, J.D.C.; formal analysis, J.D.C.; investigation, J.D.C., N.J.M.,J.A.P.; resources, D.B.T., N.J.M., J.D.C.; data curation, J.D.C.; writing-original draft preparation, J.D.C.; writing-review and editing, J.D.C., and P.R.P.; visualization, J.D.C.; supervision, P.R.P.; project administration, D.B.T., J.A.P., , D.B.T., N.J.M.; funding acquisition J.D.C.; All authors have read and agreed to be published version of the manuscript.

Funding: This research was made possible through the support provided by the Department of Science and Technology (DOST) STRAND N program and the Cebu Technological University - Barili Campus.

Conflicts of Interest: This research was made possible through the support provided by the Department of Science and Technology (DOST) STRAND N program and Cebu Technological University - Barili Campus. The authors declare no conflicts of interest, as the funding agency did not influence the study's design, methodology, data analysis, or conclusions.

References

[1] Alfawaz, H. A.; Wani, K.; Alrakayan, H.; Alnaami, A. M.; Al-Daghri, N. M. Awareness, knowledge and attitude towards 'superfood' kale and its health benefits among Arab adults. *Nutrients* **2022**, *14*(2), 245. https://doi.org/10.3390/nu14020245

[2] Maggioni, L.; von Bothmer, R.; Poulsen, G.; Lipman, E. Origin and Domestication of Cole Crops (*Brassica oleracea* L.): Linguistic and Literary Considerations. *Econ. Bot.* **2010**, *64*(2), 109–123. https://doi.org/10.1007/s12231-010-9115-2

[3] Vinterhalter, D.; Sretenović-Rajičić, T.; Vinterhalter, B.; Ninković, S. Genetic transformation of *Brassica oleracea* vegetables. *Transgenic Plant J.* **2007**, *1*, 340–355.

[4] Cernansky, R. Super vegetables: Long overlooked in parts of Africa, indigenous greens are now capturing attention for their nutritional and environmental benefits. *Nature* **2015**, *522*, 149–152. https://doi.org/10.1038/522146a

[5] Fahey, J. W. Brassica. In *Encyclopedia of Food Sciences and Nutrition, 2nd ed*; Benjamin, C., Ed.; Academic Press, **2003**; pp 606–615. https://doi.org/10.1016/B0-12-227055-X/00118-8

[6] Pakdeenarong, N.; Leamsamrong, K.; Luang-In, V. Analysis of Antioxidant Activities, Bioactive Compound Content, and Cytotoxic Effects of Green Oak and Red Oak Lettuce from Hydroponic and Organic Cultivation Systems. *Trop. J. Nat. Prod. Res.* **2024**, *8*(6), 7436. https://doi.org/10.26538/tjnpr/v8i6.15

[7] Šamec, D.; Urlić, B.; Salopek-Sondi, B. Kale (*Brassica oleracea* var. *acephala*) as a Superfood: Review of the Scientific Evidence behind the Statement. *Crit. Rev. Food Sci. Nutr.* **2019**, *59*(15), 2411–2422. https://doi.org/10.1080/10408398.2018.1454400

[8] Emebu, P.; Anyika, J. Proximate and mineral composition of kale (*Brassica oleracea*) grown in Delta State, Nigeria. *Pak. J. Nutr.* **2011**, *10*(3), 190–194. https://doi.org/10.3923/pjn.2011.190.194

[9] Lynch, M. F.; Tauxe, R. V.; Hedberg, C. W. The growing burden of foodborne outbreaks due to contaminated fresh produce: risks and opportunities. *Epidemiol. Infect.* **2009**, *137*(3), 307–315. https://doi.org/10.1017/S0950268808001969

[10] Settanni, L.; Miceli, A.; Francesca, N.; Cruciata, M.; Moschetti, G. Microbiological investigation of *Raphanus sativus* L. grown hydroponically in nutrient solutions contaminated with spoilage and pathogenic bacteria. *Int. J. Food Microbiol.* **2013**, *160*(3), 344–352. https://doi.org/10.1016/j.ijfoodmicro.2012.11.011

[11] Tomasi, N.; Pinton, R.; Dalla Costa, L.; Cortella, G.; Terzano, R.; Mimmo, T.; Scampicchio, M.; Cesco, S. New "Solutions" for Floating Cultivation System of Ready-to-Eat Salad: A Review. *Trends Food Sci. Technol.* **2015**, *46*(2B), 267–276. https://doi.org/10.1016/j.tifs.2015.08.004

[12] Khan, I.; Tango, C. N.; Miskeen, S.; Lee, B. H.; Oh, D.-H. Hurdle Technology: A Novel Approach for Enhanced Food Quality and Safety—A Review. *Food Control* **2017**, *73*(B), 1426–1444. https://doi.org/10.1016/j.foodcont.2016.11.010

[13] Miceli, A.; Settanni, L. Influence of agronomic practices and pre-harvest conditions on the attachment and development of *Listeria monocytogenes* in vegetables. *Ann. Microbiol.* **2019**, *69*(3), 185–199. https://doi.org/10.1007/s13213-019-1435-6

[14] Soerjomataram, I.; Oomen, D.; Lemmens, V.; Oenema, A.; Benetou, V.; Trichopoulou, A.; Coebergh, J. W.; Barendregt, J.; de Vries, E. Increased Consumption of Fruit and Vegetables and Future Cancer Incidence in Selected European Countries. *Eur. J. Cancer* **2010**, *46*(14), 2563–2580. https://doi.org/10.1016/j.ejca.2010.07.026

[15] Šamec, D.; Urlić, B.; Salopek-Sondi, B. Kale (*Brassica oleracea* var. *acephala*) as a Superfood: Review of the Scientific Evidence behind the Statement. *Crit. Rev. Food Sci. Nutr.* **2019**, *59*(15), 2411–2422. https://doi.org/10.1080/10408398.2018.1454400

[16] Karam, M. C.; Petit, J.; Zimmer, D.; Djantou, E. B.; Scher, J. Effects of Drying and Grinding in Production of Fruit and Vegetable Powders: A Review. *J. Food Eng.* **2016**, *188*, 32–49. https://doi.org/10.1016/j.jfoodeng.2016.05.001

[17] Vendruscolo, E.; Rodrigues, A.; Correia, S.; de Oliveira, P.; Campos, L.; Seleguini, A. Economic Analysis of Crisp Lettuce Production in Different Planting Spacing and Soil Cover. *Adv. Hortic. Sci.* **2019**, *33*(4), 449–455. https://doi.org/10.13128/ahsc8098

[18] Lee, I. J. Practical application of plant growth regulator on horticultural crops. *J. Hortic. Sci.* **2003**, *10*, 211–217.

[19] Miceli, A.; Sabatino, L.; Moncada, A.; Vetrano, F.; D'Anna, F. Nursery and Field Evaluation of Eggplant Grafted onto Unrooted Cuttings of *Solanum torvum* Sw. *Sci. Hortic.* **2014**, *178*, 203–210. https://doi.org/10.1016/j.scienta.2014.08.025

[20] Miceli, A.; Romano, C.; Moncada, A.; Piazza, G.; Torta, L.; D'Anna, F.; Vetrano, F. Yield and quality of mini-watermelon as affected by grafting and mycorrhizal inoculum. *J. Agr. Sci. Tech.* **2016**, *18*(3), 505–516.

[21] Moncada, A.; Miceli, A.; Vetrano, F.; Mineo, V.; Planeta, D.; D'Anna, F. Effect of Grafting on Yield and Quality of Eggplant (*Solanum melongena* L.). *Sci. Hortic.* **2013**, *149*, 108–114. https://doi.org/10.1016/j.scienta.2012.06.015

[22] Rouphael, Y.; Schwarz, D.; Krumbein, A.; Colla, G. Impact of Grafting on Product Quality of Fruit Vegetables. *Sci. Hortic.* **2010**, *127*(2), 172–179. https://doi.org/10.1016/j.scienta.2010.09.001

[23] Chaudhary, B. R.; Sharma, M. D.; Shakya, S. M.; Gautam, D. M. Effect of plant growth regulators on growth, yield and quality of chilli (*Capsicum annuum* L.) at Rampur, Chitwan. *J. Inst. Agric. Anim. Sci.* **2006**, *27*(1), 65–68. https://doi.org/10.3126/jiaas.v27i0.697

[24] Sreenivas, M.; Sharangi, A. B.; Raj, A. C. Evaluation of bio-efficacy and phytotoxicity of gibberellic acid on chilli. *J. Crop Weed* **2017**, *13*(3), 174–177.

[25] Amoanimaa-Dede, H.; Su, C.; Yeboah, A.; Zhou, H.; Zheng, D.; Zhu, H. Growth Regulators Promote Soybean Productivity: A Review. *PeerJ* **2022**, *10*, e12556. https://doi.org/10.7717/peerj.12556

[26] Catak, E.; Atalay, A. Plant hormone types and effects on plant growth. *Euroasia J. Math., Eng., Nat. Med. Sci.* **2017**, *7*(11), 1–6.

[27] Bagautdinova, Z. Z.; Omelyanchuk, N.; Tyapkin, A. V.; Kovrizhnykh, V. V.; Lavrekha, V. V.; Zemlyanskaya, E. V. Salicylic Acid in Root Growth and Development. *Int. J. Mol. Sci.* **2022**, *23*(4), 2228. https://doi.org/10.3390/ijms23042228

[28] Balraj, R.; Kurdikeri, M. B. Effect of growth regulators on growth and yield of chilli (*Capsicum annuum*) at different pickings. *Indian J. Hortic.* **2002**, *59*(1), 84–88.

[29] Aliyu, A. M.; Garko, M. S.; Manga, A. A. The response of vegetable amaranth (*Amaranthus cruentus* L.) to gibberellic acid concentrations in Sudan Savannah zone of Nigeria. *IOSR J. Hum. Soc. Sci.* **2018**, *23*(8), 49–53.

[30] Sun, T. P. Gibberellin Signal Transduction in Stem Elongation & Leaf Growth. In *Plant Hormones*; Davies, P. J., Ed.; Springer: Dordrecht, **2010**; pp 308–328. https://doi.org/10.1007/978-1-4020-2686-7_15

[31] Tang, W.; Liang, L.; Xie, Y.; Li, X.; Lin, L.; Huang, Z.; Sun, B.; Sun, G.; Tu, L.; Li, H.; Tang, Y. Foliar Application of Salicylic Acid Inhibits the Cadmium Uptake and Accumulation in Lettuce (*Lactuca sativa* L.). *Front. Plant Sci.* **2023**, *14*, 1200106. https://doi.org/10.3389/fpls.2023.1200106

[32] Tan, J.; Jiang, H.; Li, Y.; He, R.; Liu, K.; Chen, Y.; He, X.; Liu, X.; Liu, H. Growth, Phytochemicals, and Antioxidant Activity of Kale Grown under Different Nutrient-Solution Depths in Hydroponic. *Horticulturae* **2023**, *9*(1), 53. https://doi.org/10.3390/horticulturae9010053

[33] Bafort, F.; Kohnen, S.; Maron, E.; Bouhadada, A.; Ancion, N.; Crutzen, N.; Jijakli, M. H. The Agro-Economic Feasibility of Growing the Medicinal Plant *Euphorbia peplus* in a Modified Vertical Hydroponic Shipping Container. *Horticulturae* **2022**, *8*(3), 256. https://doi.org/10.3390/horticulturae8030256

ASEAN
Journal of Scientific and Technological Reports
Online ISSN:2773-8752

Research article

Physicochemical and Microbiological Evaluation of Reverse Osmosis Drinking Water Quality in Babylon Province, Iraq

Hala Faez Al-Jawahery[1], Noor S Naji[1], and Atheer SN Al-Azawey[2*]

[1] College of Science, University of Babylon, 51001, Babylon, Iraq
[2] Environmental sciences, Al-Qasim Green University, 51001, Babylon, Iraq
* Correspondence: atheersaieb@environ.uoqasim.edu.iq

Citation: Al-jawahery, F.H.; Naji, S.N.; Al-azawey, SN.A. Physicochemical and microbiological evaluation of reverse osmosis drinking water quality in babylon province, Iraq. *ASEAN J. Sci. Tech. Report.* **2026**, *29*(1), e261209. https://doi.org/10.55164/ajstr.v29i1.261209.

Article history:
Received: August 1, 2025
Revised: September 2, 2025
Accepted: September 6, 2025
Available online: December 14, 2025

Publisher's Note:
This article is published and distributed under the terms of the Thaksin University.

Abstract: The physical, chemical and microbiological quality of drinking water produced from 25 reverse osmosis (RO) plants in five districts of Babylon Province, Iraq was assessed by applying the Canadian Water Quality Index (WQI). Systematic sampling of water for water quality assessment was undertaken from October 2024 to February 2025. Results showed that pH was between 6.1 to 7.8. Conductivity difference was noted to be large, between 10 and 360 µS/cm, whereas TDS exhibited between 6.14 and 225 mg/L, indicating the outstanding salt rejection in range of from ~90–99.5%. Total hardness showed a significant decrease (10-270 mg/L) with calcium hardness and magnesium hardness decreasing from 1 to 28 mg/L, and 1.458 to 62.694 mg/L, respectively; the concentrations of ions significantly decreased: chloride (11.85-49.98 mg/L), nitrate (0-0.024 mg/), sulfate (0.698-15.938 mg/). Counts of the total bacteria and coliforms were ranging from 177-301CFU/mL and 0-27CFU/100mL respectively in the sites based on microbial test. Based on WQI evaluation, 64% (n=16) of the samples were ranked to be excellent quality(0-25), 24%(n=6) good quality (26-50) and 12% (n=3) was poor quality(51-75). This integrated approach of the great extent study clearly verifies that RO technology has an outstanding performance to remove physicochemical contaminants, while presenting ongoing mastering difficulties such as microbiological safety and aluminum contamination to require more specific applicable guidelines in monitoring actions and regular maintenance works for their optimal operations.

Keywords: Reverse osmosis; water quality index; drinking water; microbiological evaluation

1. Introduction

Water is one of the most basic human needs, since people can only survive few days without it [1]. Although some areas have sufficient freshwater, developed and urbanized areas in developing countries are having ever-increasing problems with regard to available water [2]. The worldwide awareness of the need for safe drinking water has grown in response to increasing health concerns associated with contaminants in potable drinking supplies, necessitating advanced water treatment options for safety protection [3,4]. Reverse osmosis (RO) technology were developed in the 70s and is currently the latest, most advanced water treatment method [5]. The RO plants work based on pressurization of the feed water against one side of a semipermeable membrane, which allows fresh water to pass through rejecting brackish waste out through drain and thus making drinking water colorless [6].

In contrast to traditional water treatment processes, RO possesses performance advantages in treating different types of problematic water i.e., seawater, brackish water and other polluted sources [7]. This provides the reason for RO with 90-99.5% of removal efficiency to be essential for use in cities with higher salinity and hardness for drinking water [8, 9]. This incredible contaminant reduction ability has made RO treatment technology the best method for combating challenging water quality conditions in water-challenged parts of the world.

One emerging water source in Iraq for drinking purposes, EMC, is being produced by RO-type plants now more than ever before and research studies have been initiated to evaluate the reliability of such systems. Reverse osmosis drinking water quality in storage tanks in Basrah, Iraq was assessed comprehensively by Garabedian [10], who demonstrated that international, regional, and national regulations were met with confirmed potability of the water at low-quality variation. Hadi elucidated [11] that reverse osmosis filtration was preventive in reducing drinking water contamination in Baghdad, by a rate of 96.6% for intestinal parasites and advised to apply ex-stensiveness at water treatment stations to achieve increasing the safety of public health as well. Other regional studies have also shown the suitability of RO technology in various governorates in Iraq. Sabtie et al. [12] used RO technology to desalinize brackish surface water in the south of Iraq with 95%-98% removal rates for total dissolved solids, and to produce potable standards from samples collected from Iraqi marshes in Thi-Qar, Maysan, and Basrah governorates. Abbas et al. [13] further proved the capacity of the RO plants in desalinating brackish ground water found in Baghdad with maximum water recovery and salt rejection rates 33.33%,18.18% and 99.29%,97.07% respectively as maiking it a suitable technology for freshwater production in Iraq to be used . The latest research by Al-Gayyim and Al-Asady [14] evaluated the quality of drink water in reverse osmosis in Al-Diwaniyah Governorate, it was found to be comply with Iraqi and WHO standards; yet they did not cultivate for investigating B. contamination obtaining an average between moderate to good at all of the study regions. Taken together, these extensive surveys offer baseline RO performance in Iraq and the importance of ongoing monitoring and evaluation.

The water quality index (WQI) is an artificially produced and contrived numerical expression reflecting the combined influence of various water quality parameters. The method is a useful tool to summarize more than just one observation of water quality by single numerical value and also to classify the water quality using transparent and robust steps [15]. The main advantage of the index is its ability to transform inter-monthly or seasonal water drinking quality trends using analytical parameter data and to perform a global assessment of water quality for decision-making [16,17]. The weighted arithmetic index method, first introduced by Brown et al. [18], and is found to offer a scientifically sound method of calculating WQI when used in combination with acceptable standards for drinking water, including those developed by the World Health Organization. The Canadian Council of Ministers of the Environment [19] also have developed supplemental WQI classification criteria that allow for consistent water quality grouping and comparative analysis among various water treatment systems and geographical locations. However, until now the studies were conducted only in other governorates of Iraq and for Babylon Province such type of studies was not far enough addressed which contributes on a significant contrast in local water quality evaluation especially for RO systems operation within this vital region. The strategic location of the Babylon Province, availability of brackish water resources at different levels and heavily populated society relying on RO-treated water required a careful evaluation for public health safeguarding as well as for system optimization. In addition, other studies have focused on testing different quality parameters [6] or specific aspects of RO performance (membrane fouling, etc.)[7], but integrated studies that take into account both physicochemical and microbiological issues and using standardised WQI methods are not widely reported. Integrated approach is critical to develop evidence-based recommendations that support system improvement and regulatory assurance.

The present study is designed to carry out an extensive physicochemical and microbiological analysis of drinking water produced from the reverse osmosis (RO) plants of drinking water stations in Babylon Governorate, Iraq through the Canadian Water Quality Index approach for systematic evaluation. The specific objectives are: 1) in-depth analysis of physicochemical parameters such as pH, electrical conductivity, total dissolved solids, water hardness constituents and concentrations of major ions and heavy metals; 2) routine

microbiological review that includes testing for the presence of total bacterial population and coliform bacteria; 3) calculation and interpretation of WQI values using a weighted arithmetic method with drinking water regulations from WHO; 4) identification of any system-specific performance variations or operational issues; and 5) provision of evidence-based recommendations to optimize the system by protecting public health.

2. Materials and Methods

2.1 Study Area Description

In western central parts of Iraq, Babylon province dissected by latitudes 32o10′0″N and 33o10'0″N and longitudes 44o10'0″E and 45o00'0″E will be covered for this episodic water quality survey. The province covers an area of about 5,135 km² (Fig. 1). Merging Basra Governorate is one of the most historically important and densely populated regions in Iraq with a population exceeding 2 million, located throughout urban and rural towns (Iraqi Ministry of Planning, 2023). The desert experiences a hot arid climate with exceedingly high summer temperatures, up to 45 °C, and mild winters that average between 10 and 20 °C (Iraqi Meteorological Organization, 2023).Annual rainfall is generally low (100 to 200 mm) with the majority falling during the winter months from DecemberMarch. These climatic factors, coupled with a scarcity of fresh water resources and the rise in salinity of groundwater sources, have led to the wide use of reverse osmosis technology for potable drinking purposes across all parts of the province. Five administrative sectors were purposively chosen to reflect the geographical and demographic diversity of Babylon Governorate: Al-Hilla (the capital city, and the largest urban area), Al-Musseyeb (northern agricultural district), Al-Hashimyah (east and mixed urban-rural area), Al-Mahwil (south rural/agricultural sector) and Western region including; Al-Qasim that encompassed areas with different water sources. Together, they provide different topographical situations, population densities and water resource variations that allow an overview of the diversity in operating conditions for RO systems in the province to be represented.

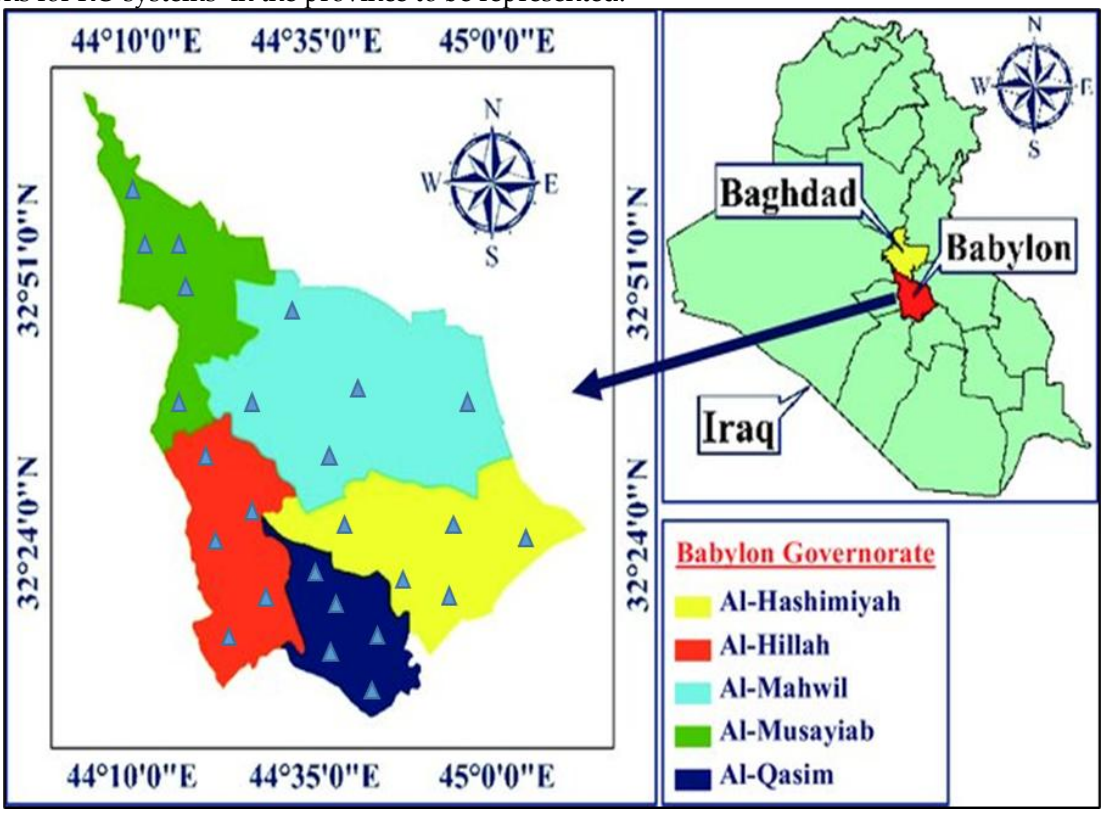


Figure 1. Sample Collection from the studied area

2.2 Sample Collection

Operational RO plants in the five selected districts of Babylon Province were systematically sampled to obtain 25 water samples. Sampling The sampling scheme assigned five samples to each district (n = 5); thus, all districts were equally represented and can be compared across geographical locations and operational settings. The sample sites were numbered by giving alphabetical and digital denominations: H1-H5 (Al-Hilla), M1-M5 (Al-Musseyeb), Ha1Ha5 (al-Hashmiah), Ma1Ma5 (al-Mahwil) and Q1Q5(Al-Qasim) as a means of systematic arrangement in the registry data programmed computer code used later in this study for carrying out statistical analysis (Table 1). Among RO plants in each district that were selected based on the following criteria: 1) operational status and regular water production capacity, 2) representative location with respect to geographic distribution within district boundaries, 3) accessibility for sampling personnel and equipment, 4) diverse service populations (residential, commercial, institutional), and 5) differing installation ages and maintenance histories to encompass system performance variation. Coordinates were recorded at each sample location to facilitate future resampling and quality assurance checks. Water samples were collected for a period of five months (from October 2024 until February 2025) which included seasonal changes in water quality and equipment status. This longer sampling timeframe collected any variations in source water, system performance due to ambient temperature and seasonal maintenance activities that would possibly impact water quality parameters. Five sample collections for each district (in monthly sampling visits) were sampled within 48 h to minimize temporal variability and maintain integrity of the samples. Different sampling procedures were used for chemical and microbiological analysis to avoid impurities, ensure the integrity of the sample and analyse accuracy. For physicochemical analysis samples were collected in high-density polyethylene (HDPE) bottles of 500 mL capacity that had been cleaned previously with a 10% nitric acid solution, washed thoroughly with distilled water and rinsed three times with sample water before final collection [20]. All the vials were filled to reduce headspace and air contamination, then closed and labeled by sample name, date of collection and hour and identification of collector. Microbiological samples were stored in borosilicate sterile glass tubes (100 ml capacity) with screw caps, which had been preautoclaved at 121 °C for 15 min. Sampling was conducted by ◎ame sterilization of sampling points, initially flushing the water for 2-3 min to remove stagnant water and using aseptic sample collection methods to prevent external contamination. Neutralizing buffer (0.1 mL of 10% sodium thiosulfate solution) was used to neutralize the remaining chlorine, which could potentially block bacterial count. All of the samples were immediately transferred to insulated containers containing frozen gel packs to keep the specimens at 2–8 °C during transportation to laboratory. The time of transportation was maintained at < 6 h from sample collection to arrival in the laboratory, and microbiological samples were processed ≤ 2 h from receipt in the laboratory to follow up viable bacteria counts. Chain-of-custody records were kept throughout collection and transportation, for both sample traceability and quality control.

Table 1. Distribution of the studied samples by the districts

District	Sample	District	Sample	District	Sample	District	Sample	District	Sample
Al-Hilla	H1	Al-Musseyeb	M1	Al-ashimyah	Ha1	Al-Mahwil	Ma1	Al-Qasim	Q1
	H2		M2		Ha2		Ma2		Q2
	H3		M3		Ha3		Ma3		Q3
	H4		M4		Ha4		Ma4		Q4
	H5		M5		Ha5		Ma5		Q5

2.3 Laboratory Analysis

2.3.1 Physicochemical Parameters

A standardized method proposed by Standard Methods for the Examination of Water and Wastewater, 23rd Ed. [20] was adopted in a detailed physicochemical examination. All the analytical analysis were repeated for 3 times to guarantee precision and accuracy, and throughout these the process of quality control was used. pH levels were measured using a calibrated digital pH meter (Hanna Instruments HI-2020) equipped with combination glass electrode, which was calibrated daily using standard buffer solutions (pH

4.0, 7.0 and 10.0) at room temperature. Recordings were taken with a precision of 0.1 unit following electrode stabilization criteria (±0.05 pH units for 30 s). The EC of the collected samples was determined by a calibrated EC-meter (Hach HQ40d) and temperature compensated to 25 °C, which was reported as μS/cm. TDS concentration was measured using the TDS (mg/L) = EC (μS/cm) × 0.64 relationship described in EPA Method 160.1. The total hardness was measured by the method of EDTA titration with standard 0.01 M solution of EDTA using indicator Eriochrome Black T. Hardness of water (CaCO 3 equivalent) was determined by the above titration at pH 12-13 and the precipitation of magnesium with NaOH. Hardness from magnesium was determined as the difference between total and calcium hardness. Hardness measurements are reported herein in milligrams per liter (mg/L) of $CaCO_3$ equivalent. Measurement of Chloride levels was carried out by silver nitrate titration with potassium chromate indicator. $SO4^-$ analysis was by turbidimetric method with barium chloride precipitation (APHA Method 4500-SO_4^{2-} E). Nitrate was analyzed with the aid of cadmium reduction and measured spectrophotometrically at 543nm. The concentrations of sodium and potassium were determined by FAAS (Shimadzu AA-7000) equipped with correct lamp sources and with flame conditions in optimum. Fe and Al were measured by flame atomic absorption spectrophotometry after digestion of the samples with concentrated nitric acid. Quality control measures comprised certified reference materials, method blanks, and spike recovery results, in order to validate the accuracy of analysis (relative standard deviation ±5 %).

2.3.2 Microbiological Parameters

Microbiological testing was performed with conventional culture method according to APHA protocols [20] under sterile conditions in Class II biosafety cabinet. All culture media were prepared as the manufacturer's instruction and autoclaved at 121°C for 15 min. Total bacterial count: The heterotrophic plate count (APHA Method 9215) was conducted on R2A agar, and incubated at 35°C for 48 h. Serial dilutions ranging from 10^{-1} to 10^{-3} were carried out using sterile phosphate-buffered saline, and then aliquots (0.1 mL) of these dilutions were evenly spread on agar surfaces by sterile spreaders. Colonies were counted in a digital colony counter and results are reported as CFU/mL. Plates with 25 to 250 colonies were chosen for the determination of the number of CFU in order to obtain statistically valid data. Total Coliforms: Multiple tube fermentation (APHA Method 9221)with lauryl tryptoseBroth pour and brilliant green lactose bile at 35°C for up to 24-48 hwas performed for the presumptive and confirmed test respectively. Gas was produced in Durham's tubes demonstrating the presence of positive coliforms. Results of the most probable number (MPN) counts were obtained by employing statistical tables expressed in CFU per 100 ml. Quality control comprised positive (Escherichia coli ATCC 25922) and negative controls (sterile buffer) in each analytical batch.

2.4 Water Quality Index Calculation

The calculation of the Water Quality Index (WQI) was based on the weighted arithmetic index method, first described by Brown et al. [18] and then modified for in-field use with drinking water. The method offers a systematic approach for transforming several water quality parameters into a single number which represents the overall condition of water quality. The procedure of calculation the WQI was a four-step sequence: (1) selection the parameters and weighting them according to their known impact on human health and/or with respect to WHO [3] drinking water guidelines, (this set is used for calculation n in Equation 1, section " Rating system"); (2) rating of quality level for each parameter calculated by means of sub-crutial functions; (3) calculateing weighted sub-critical levels; and (4) thirdly, hybrid computing using weight arithmetic institutes equation:

$$WQI = \Sigma(Qi \times Wi) / \Sigma Wi$$

Where Qi is the quality rating of parameter (i) and Wi is the relative importance given to parameter i according to its ranking in drinking water quality assessment. Weights to the parameters were given in accordance with conventional methods: pH (4), electrical conductivity (2), total dissolved solids (4), total hardness (2), chloride(3), sulfate(4), nitrate(5) iron (4) aluminum(444 44)) total bacterial count(5) and coliform

bacteria(5). The heavier weights suggest that parameters are more important for public health protection; microbiological factors receive the highest weight because of their direct effects on health. Quality ratings were calculated by plotting measured parameter concentrations versus WHO [3] drinking water guidelines, with linear interpolation between guideline values.

2.5 Quality Control and Data Analysis

A complete rigorous quality control system was also conducted to guarantee the reliability and reproducibility of the data. The laboratory instruments were calibrated every day by certified reference materials that are traceable to the national standards. The secondary standards were used for calibration verification, which required that values obtained by instrumental methods be within ±2% of certified values and within ±5% using wet chemistry techniques. Analytical accuracy was evaluated by analyzing 10% of the samples in duplicate, and the acceptance criterion was a relative percent difference of <10% for major parameters and <15% for trace constituents. Method blanks were included with every analytical run to ascertain the presence of cross-contamination and matrix spikes at a rate of 5% to test for recovery. Method accuracy was verified by analyzing certified reference materials (NIST SRM 1643e for trace metals and commercial standards for major ions) monthly. Data were analyzed with IBM SPSS Statistics version 28.0, and descriptive statistics for all parameters were provided as mean, median, standard deviation, minimum and maximum values. Data distribution was tested for normality using the Shapiro-Wilk test, with parametric or non-parametric tests chosen accordingly. To explore the inter-relationships between variables correlation was analyzed, furthermore statistical differences between districts were tested using one way ANOVA. All analyses used an α level of 0.05 to determine statistical significance. Validation criteria were presence of outliers in outputs by interquartile range (values greater than Q_3 + 1.5×IQR or less than Q_1 - 1.5×IQR) and checking suspect values through re-analysis or analytical method verification. All analytical results were noted in laboratory books and subsequently transferred to electronic data bases, double entered validated, to avoid transcription errors. There was no missing data and our standard back-up tools saved the study data on daily basis, which guaranteed the security and consistency of collected data.

3. Results and Discussion

3.1 Physicochemical Water Quality Assessment

The levels of pH in the 25 samples of reverse osmosis plants ranged between 6.1 and 7.8, with a minimum value of pH recorded for sample H3 (Al-Hilla district) and Maximum in sample Ma4 (Al-Mahwil district) (Table 2). These findings are virtually in conformity with the World Health Organization drinking water guideline passed between 6.5 and 8.5 pH [3]. Of note, 96% of samples (n=24) complied with the WHO recommendation. Only samples H3 (pH 6.1) differed from the lower guideline level slightly (Fig. 2). These narrow pH range and fluctuations in sampling points point to a stable operation of the reverse osmosis system, and reflect its effective acid-base balance which was very similar to all treatment units with little difference among them. The stability is important to maintain the quality of drinking water because the taste, the corrosion of distribution systems and disinfection efficiency [17] are affected by high or low pH values. The observed pH stability is also in agreement with research reports from Iraqi provinces, where ALSarrani 955 and Alkaabneh [14] presented the same pH constancy in RO systems of Al-Diwaniyah, Al-Gayyim and AL-asady [17]. [13] recorded similar results in Baghdad buildings. The small acidity observed for sample H3 could be related to the formation of carbonic acid in the RO process or leakage from possible membrane degradation, according to Ritt et al. [5] in their thorough review of RO membranes. Nevertheless, it is a small deviation and does not represent an immediate health threat as it can be easily remedied post treatment through pH control or membrane cleaning [9]. Electrical conductivity The values of electrical conductivity were highly variable among sampling sites with this value ranging from 10 μS/cm (samples Ma2, Q2 and Q4) to 360 μS/cm (sample Q1) (Fig. 3). Similarly, TDS levels ranged from 6.14 mg/L (sample Q4) to 225 mg/L (sample Q1), indicative of the heterogeneity in feed water quality sources and differing performance properties among RO systems across the province (Fig. 4). All TDS values were well below both WHO limit (1000 mg/L) and EPA recommendation (500 mg/L), demonstrating excellent performance for dissolved salt rejection [3]. This observed TDS range is indicative of a 90-99.7% extraction efficiency over natural brackish groundwater

sources in that region, which typically contain 2000-8000 mg/L TDS [13]. This removal rate is consistent with the previous work [9]. [21] and Honarparvar et al. [22], who achieved 90-99% permeated salts removal in well-functioning RO systems. The low values of conductivity for samples Ma2, Q2 and Q4, indicate good membrane performance and efficient pre-treament. On the other hand, Q1 sample with high conductivity (360 µS/cm) might suggest membrane fouling and scaling or even improper maintenance in detail RO performance studies, as reported by Sahu (2021). Poirier et al. [8] also observed that variation in conductivities generally signifies variations in membrane age, operating pressure, and the quality of feed water properties. The strong EC to TDS correlation (r = 0.998) further establishes the accuracy of conductivity measurements as a proxy for DSL levels and signals a cost effective means to develop water quality monitoring procedures that can be used on a routine basis [7].

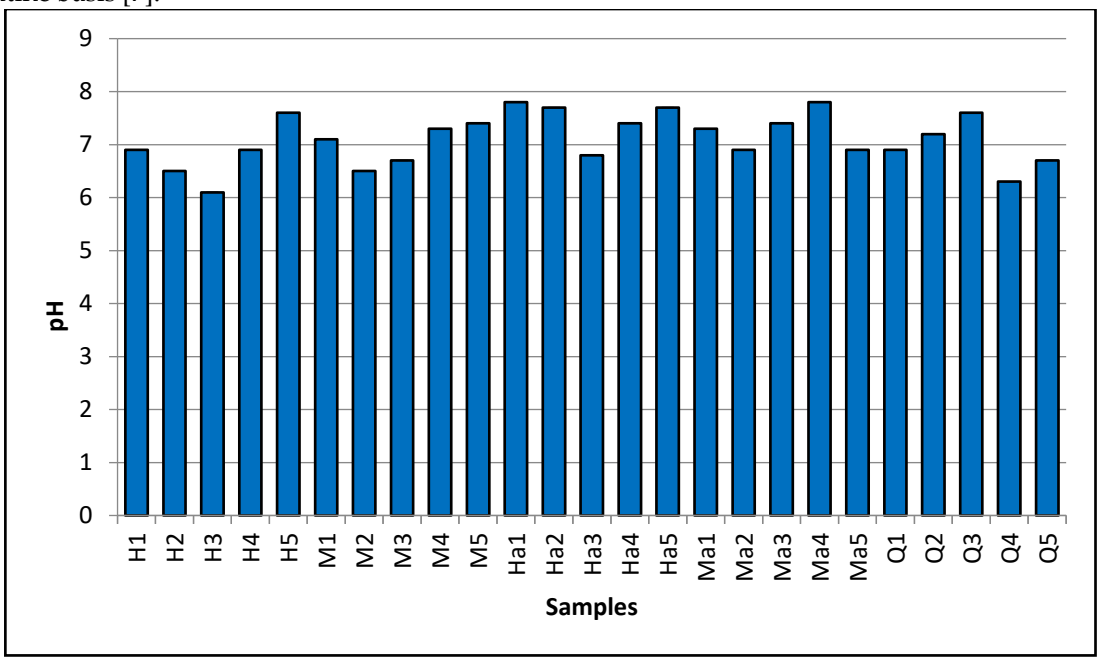


Figure 2. pH value for the studied samples

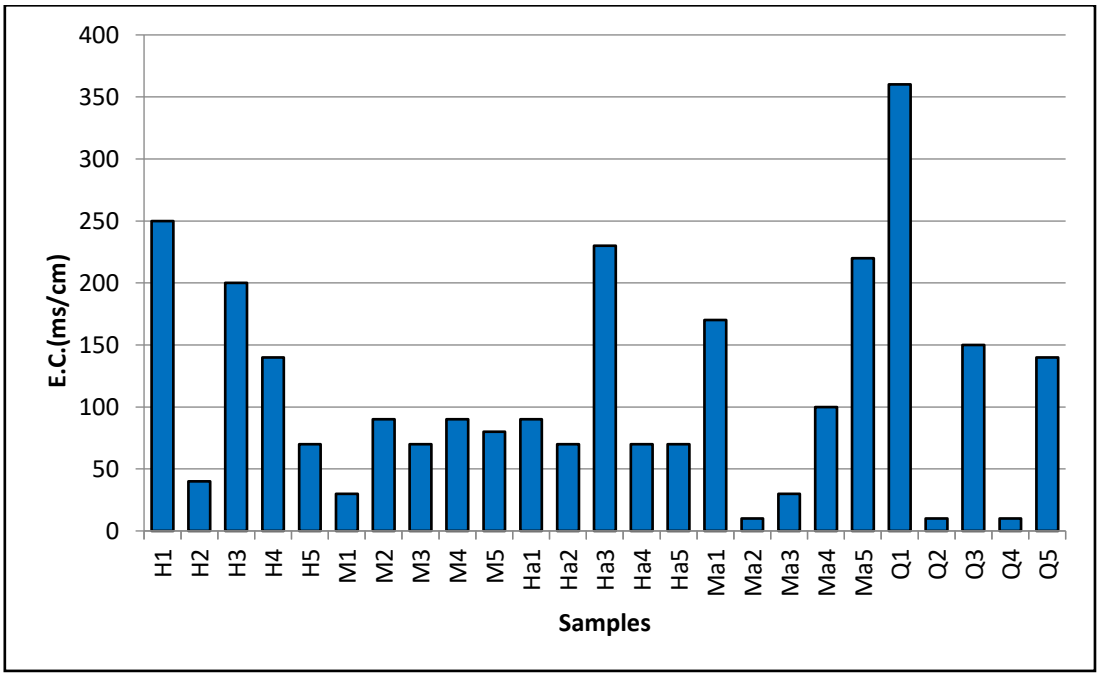


Figure 3. EC value for the studied samples

Measurement of the total hardness showed the highest differences for all analyzed parameters - between 10 mg/L (Ma2) to 270 mg/L (Ha4), which indeed represents almost twenty-seven times differences between localities samples (Fig. 5). According to USGS (2022) classification guidelines, water hardness categories were partitioned into: soft water (0-60 mgL −1) was found in 32% of samples (n=8), moderately hardship (61120 mgL −1) in 44% of samples (n=11), hard (121180 mgL −1) in 16% of samples (n=4) and very hard (>180 mgL −1) in 8% of samples (n=2). The content of calcium hardness at the sampling sites varied from 1 mg/L (sample Q1) to 28 mg/L (sample Q5). The magnesium hardness varied to a larger extent, from 1.458 mg/L (sample Ma2) to 62.694 mg/L (sample Ha4) (Fig. 6). Especially in some samples, the dominance of magnesium over calcium is unusual; since calcium is normally the predominant hardness constituent in natural waters [23]. This could be caused by specific geological properties of local groundwater sources, or uneven removal ratio of divalent cations from different membranes (Fig. 7-8). The large range of hardness among RO plants indicates a non-consistent behavior of systems, which might be due to different operating conditions. Keen [24] and Nyoman et al. [25] reported that fouling at the membrane surface, scaling of membrane pores, improper filter cleaning and operating conditions contributed significantly toward decrease in efficiency of hardness removal. Besides, Zhao and Wang [26] further indicated that membrane age, operating pressure and pH have significant effects on the rejection of multivalent ions. The better removal performances were observed for magnesium than that of calcium in most samples which is consistent with the principle of membrane selectivity, as Mg^{2+} ions are more hydrated and can be retained to a greater extent by thin-film composite membranes [27]. However, the very high total hardness in Ha3 (240 mg/L) and Ha4 (270 mg/L) is indicative of possible system failure on immediate action to prevent consumer dissatisfaction and damage to equipment in distribution system [3].

Table 2. Physical and chemical properties of the studied water (All properties expressed as mg.l-1 except pH without unit and EC expressed as μs/cm)

Samples	pH	EC	TDS	T.H	Ca-H	Mg-H	Cl^-	NO_3	SO_4	Na^+	K^+	Fe^{+2}	Al^{+3}
H1	6.9	250	176	100	20	19.44	29.19	0.003	15.938	ND	ND	ND	ND
H2	6.5	40	25	80	8	17.496	39.43	0.001	5.841	ND	ND	ND	0.074
H3	6.1	200	142.8	120	16	25.272	29.18	0.018	4.853	ND	ND	ND	0.029
H4	6.9	140	100	50	4	11.178	29.05	0.003	7.237	ND	ND	ND	ND
H5	7.6	70	50	60	12	11.664	49.6	0.002	7.186	ND	ND	ND	0.088
M1	7.1	30	21.42	140	12	31.104	39.12	0.002	6.445	ND	ND	ND	0.118
M2	6.5	90	64.2	100	8	22.356	33.99	0.006	4.342	ND	ND	ND	ND
M3	6.7	70	50	90	8	19.926	29.52	0.024	7.084	ND	ND	ND	ND
M4	7.3	90	63	80	12	16.524	39.63	0.01	6.215	ND	ND	ND	ND
M5	7.4	80	57	140	8	32.076	30.84	0.004	5.313	ND	ND	ND	ND
Ha1	7.8	90	63.5	90	4	20.898	29	0	0.851	ND	ND	ND	ND
Ha2	7.7	70	48.8	90	12	18.954	21.78	0	1.115	ND	ND	ND	ND
Ha3	6.8	230	147	240	24	52.488	19.4	0	1.362	ND	ND	ND	0.074
Ha4	7.4	70	48	270	12	62.694	11.85	0.001	0.698	ND	ND	ND	ND
Ha5	7.7	70	48.7	120	8	27.216	29.99	0	0.911	2.3	ND	ND	ND
Ma1	7.3	170	94	60	12	11.664	22.17	0.012	1.26	ND	ND	ND	0.015
Ma2	6.9	10	6.25	10	4	1.458	49.98	0.001	0.851	ND	ND	ND	0.029
Ma3	7.4	30	21.75	110	11	24.057	44.65	0	1.12	1.7	ND	ND	0.023
Ma4	7.8	100	67.5	40	20	4.86	45.1	0	0.7	ND	ND	ND	0.15
Ma5	6.9	220	157.5	70	12	14.094	40.96	0.001	1.59	ND	ND	ND	ND
Q1	6.9	360	225	20	1	4.617	44.01	0.001	1.12	ND	ND	ND	ND
Q2	7.2	10	6.15	140	4	33.048	49.08	0.002	4.529	ND	ND	ND	ND
Q3	7.6	150	107.1	70	8	15.066	47.01	0.008	6.752	3.1	ND	ND	0.029
Q4	6.3	10	6.14	70	4	16.038	29.64	0.001	1.09	ND	ND	ND	ND
Q5	6.7	140	97.7	90	28	15.066	30.66	0.01	7.01	4	ND	ND	0.01

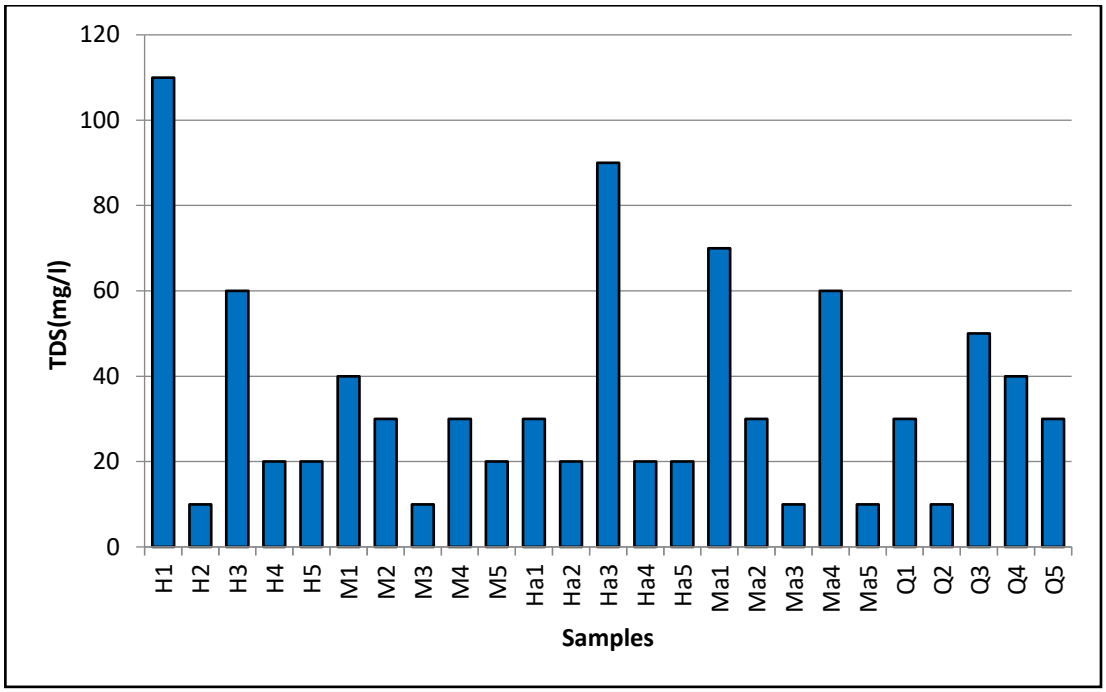


Figure 4. TDS value for the studied samples

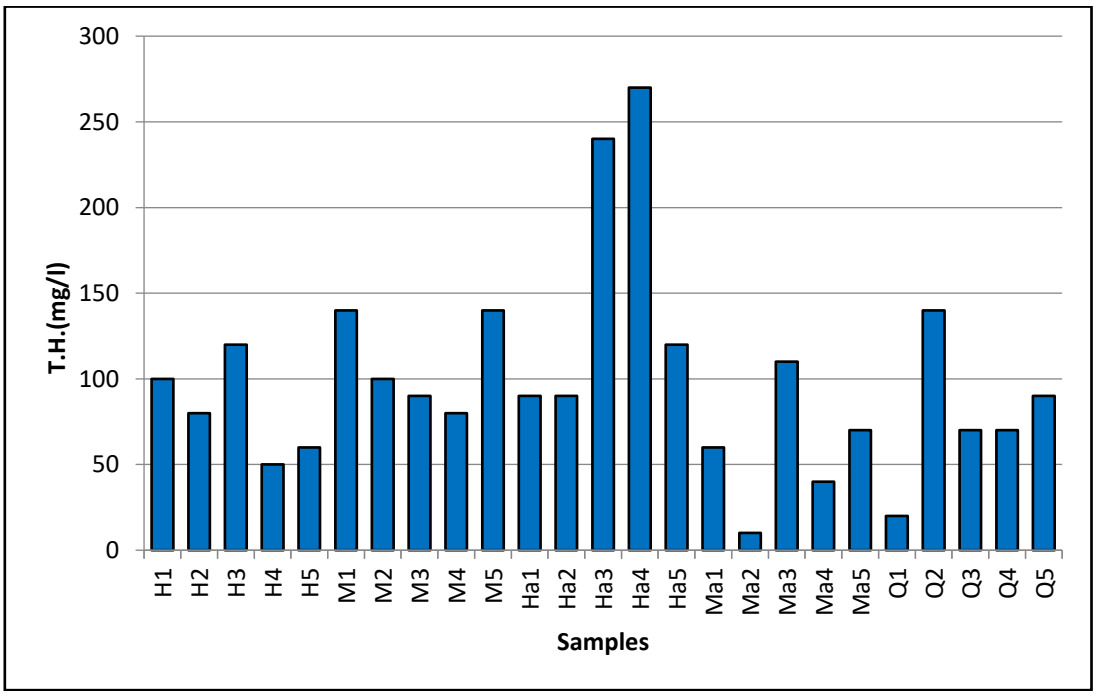


Figure 5. Total Hardness value for the studied samples

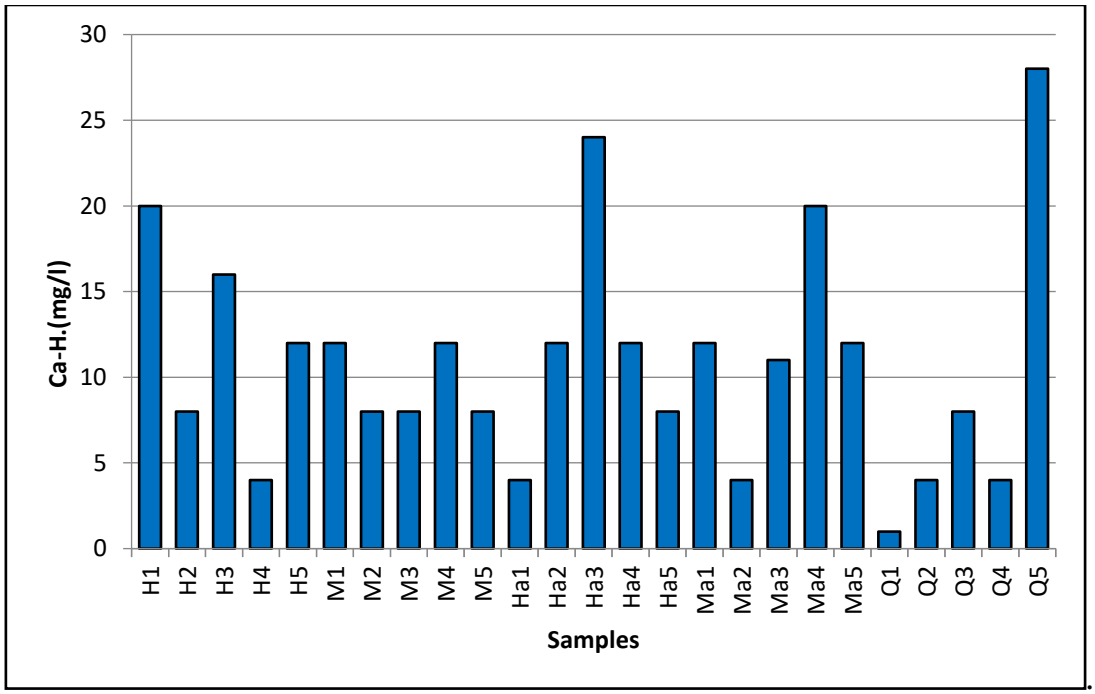


Figure 6. Calcium Hardness value for the studied samples

Levels of chlorides varied between 11.85 mg/L (in Ha4) and 49.98mgL -1 (in Ma2) (Fig. 8), and all are much lower than the WHO standard levels of 250 mg/L for the taste preference limits [3]. The measured chloride concentrations indicate 90-99% removal from typical feed water, in line with the known RO behavior for monovalent anions [28]. The efficient chloride removal is highly important, due to its high mobility and ability to pass through the membrane, and points at favorable membrane integrity across most of the sampling sites. The differences in chloride concentration might be due to the diverse feed water salinity, membrane selectivity and operational conditions (recovery/vulnerability rate) and cross flow velocity. Safia et al. [29], chloride rejection was lower in aged machine compared to the new one indicating practise requirement of regular replacement and maintenance schedule for membranes. Nitrate levels in the samples measured were extremely low, ranging from undetectable (Ha1, Ha2, Ha3, Ha5, Ma3 and Ma4), with a maximum of 0.024 mg/L (M3) (Fig. 9). All measured values were well below WHO recommendations (50 mg/L) and EPA maximum contaminant level (45 mg/L), confirming high treatment efficacy [3]. The high nitrate removal efficiency (>99.9%) is higher than we would expect for your run-of-the-mill RO unit. This result was consistent with the work of Abascal et al. [30] and Sewak et al. [31], obtained BMR from 80 to 95% for correctly working systems. The low nitrate presence observed either indicates a low concentration in the feed waters or good selectivity of the membrane used, likely as a result of new membrane being implemented or ideal operating conditions [32]. Sulfate concentrations varied strongly between samples (sample Ha4: 0.698 mg/L and sample H1:15.938) being however significantly lower than the WHO (250 mg/L) and EPA secondary standards (250 mg/L) (Fig. 10). The uniformly low sulfates values demonstrate the high rejection of divalent anions which is attributed to their double negative charge and larger hydrated ionic radius (Peeters et al., 1998). The higher than 95% sulfate rejection efficiency obtained from the tap, DCP and FD bottles samples affirms superior performance of the membrane for multivalent ions. Al Mehrate et al. [33] showed that the efficacy of sulphate removal will be predominantly dependent on electrostatic repulsion and size-exclusion mechanism with well-operating RO membranes, achieving rejection value of more than 99% under ideal conditions. Sodium was found in four samples only (Ha5: 2.3 mg/L, Ma3: 1.7 mg/L, Q3: 3.1 mg/L, Q5: 4.0 mg/L) whereas potassium content was below the detection limit for all samples. These low concentrations indicate complete removal of monovalent cations, which is needed for the protection of cardiovascular health and taste quality[3]. The selective detection of sodium in some samples is likely to be due to local groundwater or breakthrough at the membrane, as reported by Tran et al. [34] and Ohno et al. [35]. Its absence indicates a

decrease in the total amount of feed water, or an increased selectivity toward this monovalent ion by the membrane.

The results also showed iron levels below the detection limit (>0.01 mg/L) for all samples, which implies very good removal efficiency and compliance of all evaluated sand photocatalysts with WHO guidelines (0.3 mg/L) and EPA standards (0.3 mg/L). Thus, full iron removal attests to the high performance of RO membranes with respect to metal pollutants and implies that any taste, odor and staining problems linked to the presence of an excess amount of iron [3] can be set aside. The absence of detectable iron indicates low levels in the feed water or excellent membrane retention. Adel et al. [36] also found similar results in Mediterranean seawater RO plants, and hydrodynamic conditions were considered to give size exclusion and electrostatic interactions with the membrane surfaces as the main reasons for full iron rejection. Aluminum was found in 44% of samples (n=11) at concentrations ranging from below detection limits to 0.15 mg/L (sample Ma4). All concentrations measured were below WHO recommended levels (0.2 mg/L), yet detection of aluminum in treated water is alarming for membrane condition and post-treatment contamination [3]. There was no spatial structure to the pattern of aluminum detection, reflecting more than one source of contamination; for example alum residuals from pre-treatment, membrane degradation products or leaching from pipework. Ohno et al. [35] reported that aluminum coagulant residuals from the raw water stream were a potential medium of post-RO aluminum contamination, while Kherraf et al. [37] reported aluminum release from the aged membrane materials at a controlled temperature and pH. The detected aluminum were ranged from 0.01 to 0.15 mg/L for samples H2, H3, H5, M1, Ha3, Ma1, Ma2, Ma3, Ma4 Q3 and Q5 showing the necessity of improved pre-treatment optimization and frequent membrane inspection procedure. Intermittent aluminum is indicative of systemic problems rather than pervasive contamination, allowing systems-based remedial solutions. The results of the heavy metal species analysis indicate that RO treatment could efficiently remove metallic contaminants, and the implications for total system management to maintain reliable operation and achieve compliance during long-term treatments are discussed.

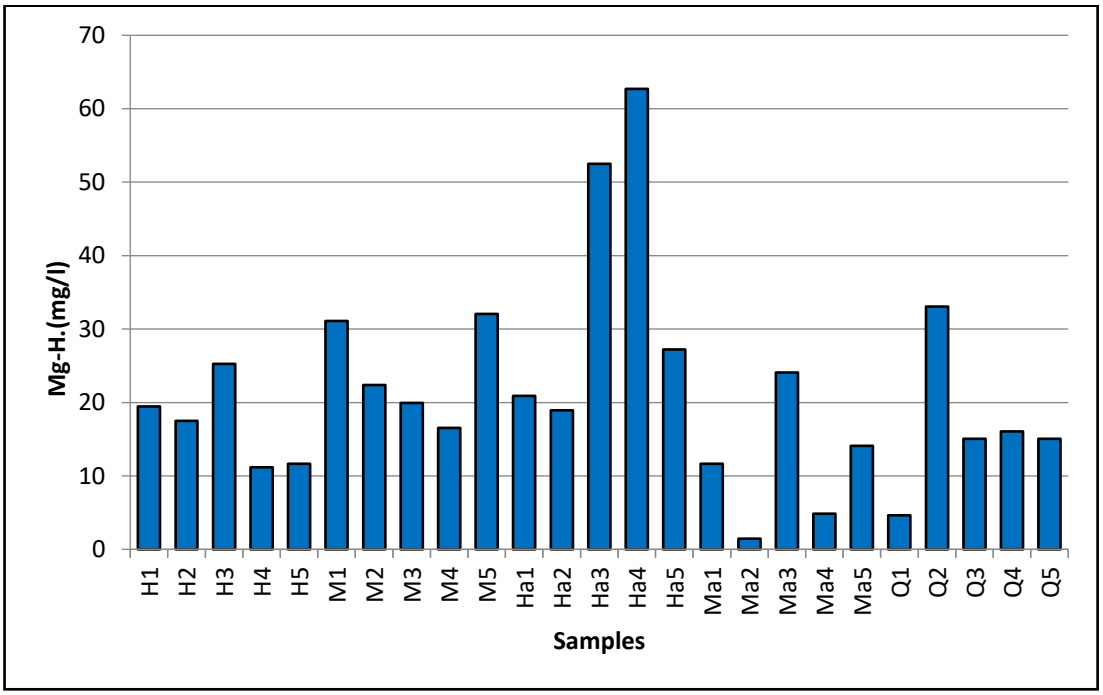


Figure 7. Magnesium Hardness value for the studied samples

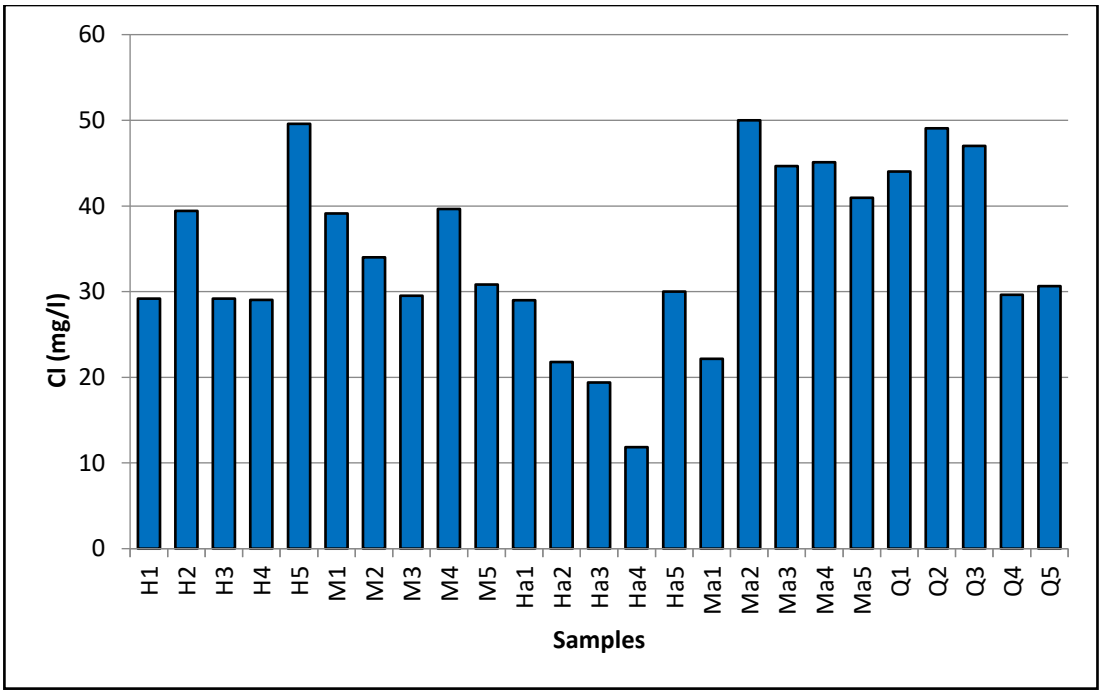


Figure 8. Chloride value for the studied samples

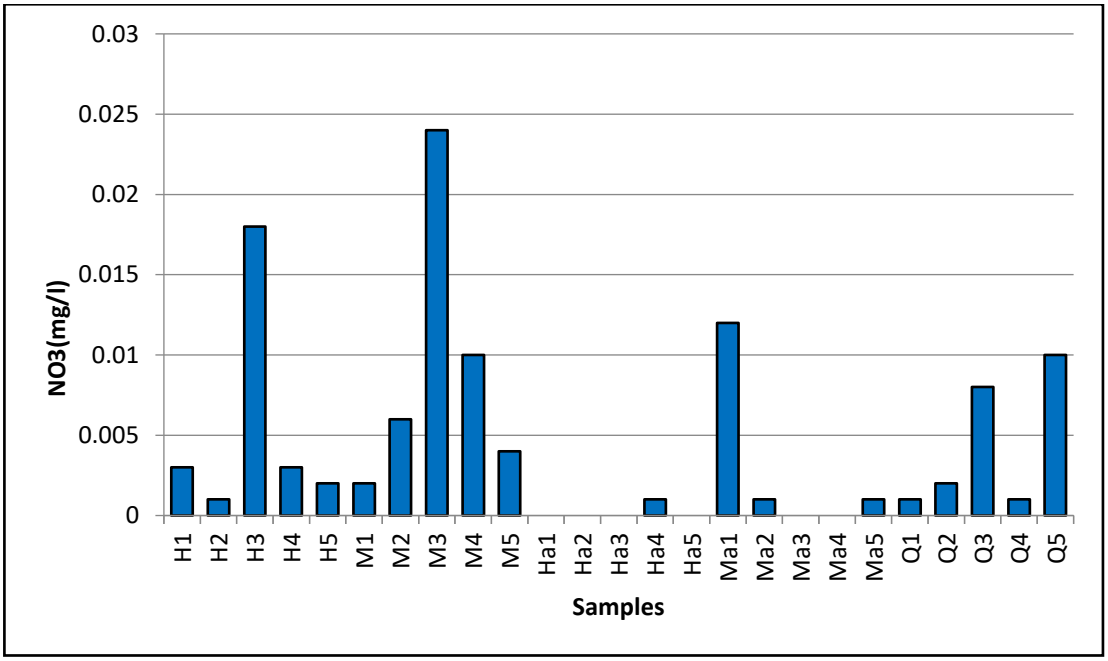


Figure 9. Nitrate value for the studied samples

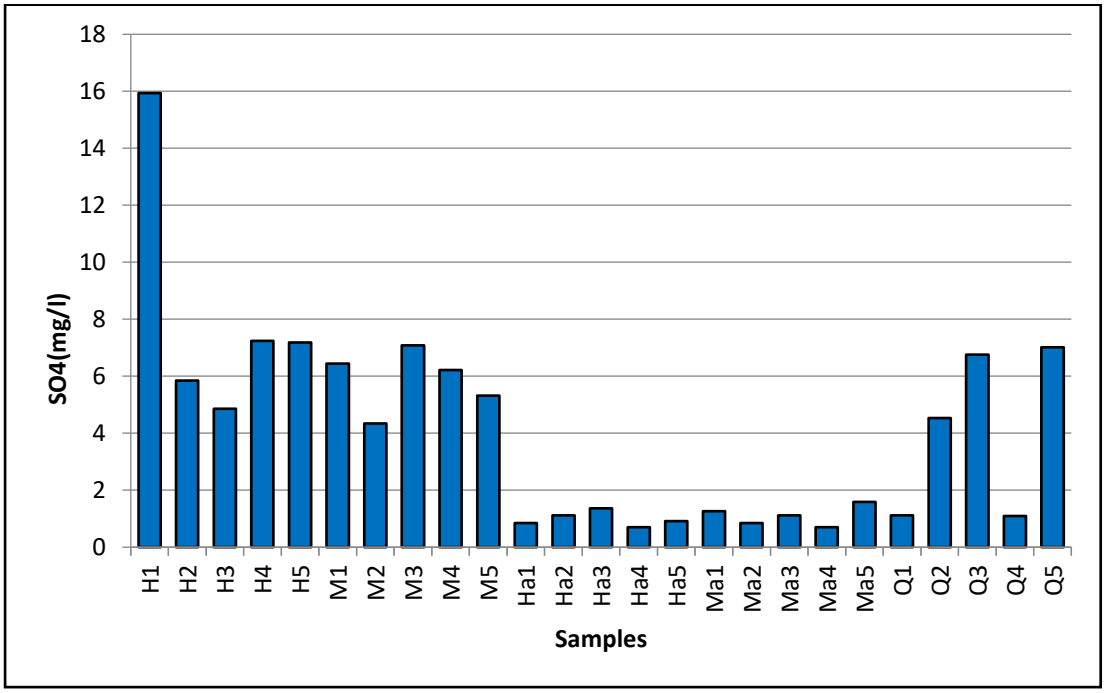


Figure 10. Sulphate value for the studied samples

3.2 Microbiological Water Quality Assessment

3.2.1 Total Bacterial Count

Analysis of the total bacterial count showed a great variation between all sampling stations (between 177 CFU/mL Q4 and 301 CFU/mL Q2), which is an approximately 1.7-fold range between minimum and maximum values (Table 3, Fig. 11). Average bacterial number of all samples was 261 ± 33 CFU/mL and 68% of samples were more than 250 CFU/mL, showing a considerable level of bacteria in RO treated water despite the physical barrier function of RO membranes. It was observed that, across districts, there were significant differences in the level of bacterial contamination. This wide variation in number proliferation after 24 h was most evident in the Al-Qasim district (numbers ranging from 177 to 301 CFU mL(-1)), while that of Al-Hashimyah exhibited a more stable bacterium count (236-295 CFU mL(-1)) with lower level range. The Al-Hilla district showed between 186–300 CFU/mL, consistently from 276 to 300 and 216 to 293 CFU/mL for both Al-Musseyeb and Al-Mahwil, respectively. These differences indicate that district-specific factors may influence the contamination of drinking water by bacteria, such as source water quality, system maintenance techniques, and post-treatment handling tech- niques. The relatively high bacteriological counts of bacteria from all samples were above the expected contaminant levels for RO-treated water -- which ideally should have bacteriological levels close to zero based on the size exclusion features of RO membranes [38]. The constant presence of bacteria shows that possible system defects (for example breakage of membrane integrity, recontamination after the treatment has completed or incorrect configuration of disinfection) may be present. Hayward et al. [39] also reported a similar occurrence of bacteria in the home RO systems with increased counts due to saprophytic biofilm formation in the distribution network and storage tanks. Then, variations in bacterial counts may also be due to a seasonal effect, because colder periods (from October 2024 to February 2025) when the growth rate of bacteria is known to be lower were chosen for sampling as opposed to during the summer. Türker et al. [40] showed that ambient temperature affects bacterial survival and growth in RO systems as well, which may cause a greater count of bacteria in warmer seasons.

Analysis of coliform bacteria exhibited a bimodal distribution, where 36% of all (n=9) samples for flushed tap water recorded absence of coliform bacteria (0 CFU/100mL), with the remaining 64% (24%, n=16 samples from n =24) showing presence of varied levels from 4 to 27 CFU/100mL (Fig. 12). From these, Ha2, H5, M5, Ha3, Ha4, Ha5 Ho2 Q1 and Q4 registered zero coliform counts indicating well maintained membrane integrity and effective post-treatment regime at these sites. The greatest concentration of coliforms was

observed in samples Ha1 and Q2 (27 UFC/100mL, each), followed by Ma4 (24 UFC/100mL), H4 (19 CFU/100mL) and Ma1 (13CFU/100mL). These higher coliform counts are indicative of bacteria loads that could affect human health, and may reflect poor system performance or the presence of post-treatment contamination sources. WHO [3] is without detectable coliform bacteria, so the results presented here are of particular public health concern. The occurrence of coliform bacteria in RO-treated water was unexpected since properly functioning RO membranes are theoretically 99.9% efficient for the removal of bacteria [41]. Of the four alternative coliform detection methods, Regulations CKA1 Colilert does not routinely detect coliforms except through participation in a proficiency testing study procedure, when coliform are present. This suggests several potential sources of contamination, such as: membrane failure occurring post treatment and recontamination storage or distribution; inadequate system Disinfection implementation; or cross-contamination during sampling handling. Rbeida and Eteer [42] also found a comparable level of coliform bacteria presence in water treated by RO in Libya, which they attributed to problems with post-treatment handling and storage systems. The spatial distribution of coliform contamination did not follow a recognizable trend; both contaminated and clean samples were observed in all the five districts. The nature of this random distribution implies that system, rather than regional parameters are the dominant factors influencing contamination and therefore the requirement to test individual systems would be more valuable than organizing distric−wide treatment. The overall microbiological examination shows serious difficulties in achieving safety levels concerning microorganisms in RO treated drinking water throughout Babylon province. There are several reasons why bacteria can pass through RO membranes and post-treatment cross-contamination occurs that affect the anticipated sterility of RO-produced water. The organisms in the sterility control imply a possible breach of membrane integrity, either due to lacerations, leaks or aging of the material. Baba et al. [43] reported that the behavior of bacterial numbers in RO systems is highly related to membrane integrity, where relatively minor damage could provide passage for bacteria. The presence of coliform bacteria, which are larger than the size of pores in RO membrane (0.0001 μm), is a clear indication of the poor integrity of the membrane or bypassing contamination sources. The difference in bacterial count between the samples indicates large and post-treatment dependent secondary contamination during handling, distribution or storage. Contamination may be due to unsanitary storage tanks, contaminated distribution lines, inappropriate sampling procedures or cross-contamination during system repairs. Brown et al. [38] pinpointed storage tank biofilms as the source of bacterial contamination in RO systems more specifically under stagnation that is typical of residential units. Bacterial contamination is an indication of insufficient system maintenance, lack of membrane cleaning, rare sanitation and also the lack of good quality control. Good maintenance of the RO system should also include periodic cleaning of the membrane, sanitization and examination for bacteria to meet the microbial safety regulations [39]. The levels of bacteria and coliform counted have the capacity to create health risks, especially in susceptible groups such as children, elderly and immunosuppressed persons. Though the enumerated bacterial populations are not likely to induce immediate infections in healthy adults upon consumption of sewage contaminated water, continual consumption of bacteriologically impure water augments risk factors for GI infections as well as other water borne diseases. WHO [3] notes that any detectable coliforms in drinking water suggest the possibility of also harboring pathogens and should not go unattended.

Table 3. Bacterial content of the studied water

Sample	Total count bacteria(CFU/ml)	Coliform bacteria(CFU/100 ml)
H1	250	4
H2	186	0
H3	267	11
H4	300	19
H5	289	0
M1	296	7
M2	290	5
M3	276	5
M4	300	11
M5	279	0
Ha1	281	27
Ha2	265	12
Ha3	295	0
Ha4	236	0
Ha5	251	0
Ma1	280	13
Ma2	216	0
Ma3	287	11
Ma4	293	24
Ma5	235	4
Q1	254	0
Q2	301	27
Q3	284	6
Q4	177	0
Q5	205	8

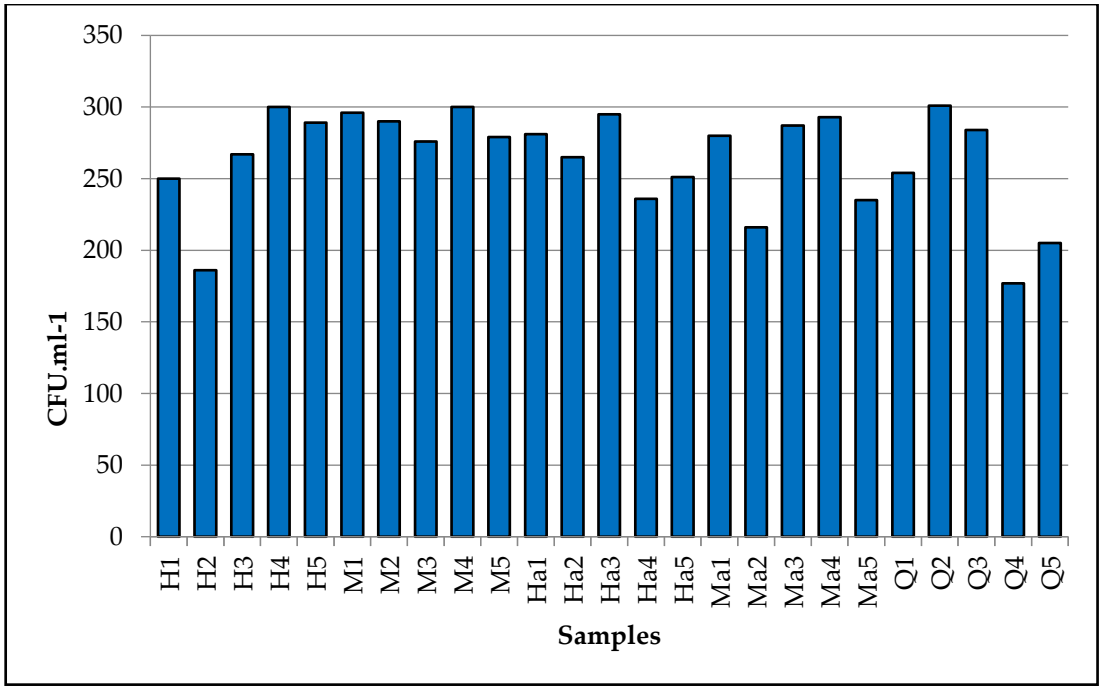


Figure 11. Total Count of Bacteria for the studied samples

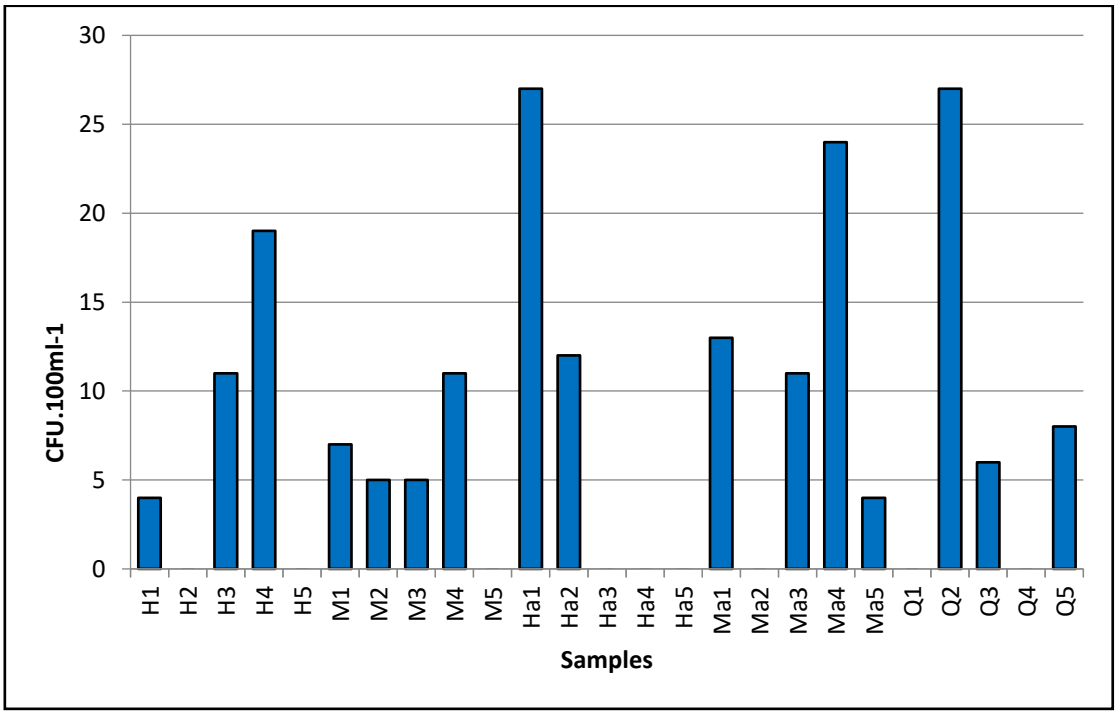


Figure 12. Total Coliform Bacteria for the studied samples

3.3 Water Quality Index Results

The overall WQI evaluation of the 25 RO plant samples (physicochemical and microbiological pollution) included in this study classified the samples into three water quality classes based on CCME (2001) criteria (Table 4). The findings indicated that 64% of samples (n=16) were characterized as 'Excellent' quality grade (WQI of 0-25), followed by a quarter of the samples which had classification as 'Good' quality grade (n=6) with WQI in range of 26-50 and one-eighth of the sample population received poor water quality ranking equal to three Number of samples =24. No samples were placed in the "Very Poor" (76-100) or "Unacceptable (>100)" categories, also suggesting that the water quality at large was reasonable level provided certain inadequacies. (2) Excellent (WQI 0-25): Samples with excellent rate included H1 (12.46), H2 (8.91), H3 (19.07), H4 (3.12), M1 (24.56), M2(5.22), M3(19.8), M4 (23.41), Ma1(21.33), Ma2 3.10, Ma5 7.45, Q1 1.89 and Q4 18.22). These samples presented the best physicochemical parameters and minimum microbiological contamination, which were considered as the limit of advisable performance of the RO system. The lowest WQI values (1.89) was found in sample Q1 and the corresponding quality is a very excellent (physicochemical quality of water, less bacterial contamination), which sample H4 obtaining an excellent status with respect to moderate coliform, this is owed to the good physicochemical parameters obtained. Fair Quality Samples (WQI 26–50): Six samples had fair quality categories: H5 (32.01), M5 (35.89), Q2 (28.77), Ha1(44.12), Ha2(40.33), Ha3(26.05) and Ha5, Ma3 expecting to backward calculation; while only two samples had poor water qualities namely Ma4 (31.55) and Ma4(37.89). These were often slight variations in physicochemical characteristics or very slightly elevated levels of microbiological contamination, which could not allow for an accurate allocation. For instance, acceptable physicochemical parameters but high coliform bacteria (27 CFU/100mL) was observed in sample Ha1 (44.12), whereas aluminium contamination influenced the total score of sample H5(32.01). Three samples presented a low quality score: Q3 (54.12%), Q5 (51.02%) and Ha4 (54.67%). These samples had a number of parameters that were in exceedance or some significant contamination problem appears to require attention. The sample Ha4 (54.67) had the greatest total hardness of water (270 mg/L), accompanied by medium bacterial load. On the other hand, Q3 (54.12) and Q5 (51.02) displayed an increased of bacterial content with added aluminum contamination (>500 is exceeded). Al-Musseyeb district attained the maximum ratio of excellent ratings (80%, n = 4), followed by Al-Mahwil and Al-Hilla (each 60%, n = 3), then by Al-Qasim (40%, n = 2) and finally by Al-Hashimyah with one study only reaching excellence category. Out of all the

district ratings, Al-Hashimyah district had the worst coverage with 60% good and 20%poor, indicating that there may be specific issues in these two districts that are in need to focus on.

Statistical analysis supported the existence of the strong correlation between WQI values and individual water quality parameters, which had implications for key controlling factors underpinning overall water quality levels. From the multiple regression analysis, microbiological characteristics were identified to have high correlation with the WQI and it was found that total viable bacterial count ($r = 0.72$; p 20 CFU/100mL) always had the quality rating less than acceptable despite acceptable physico–chemical status. Among physicochemical measurements, total 'hardness' was most significantly correlated with the WQI scores ($r = 0.45$; $p < 0.05$) followed by concentration of aluminum ($r = 0.38$; $p < 0.05$) and electro-conductivity ($r = 0.31$; $p < 0.05$). The correlation of hardness indicates its direct impact on water quality as well as an indirect relationship through the quality of system maintenance, since the systems in bad condition, usually present high levels of hardness and bacterial contamination. Seasonal and operational variations Seasonal and operational differences were evident by the metric's temporal determination in which monthly variation of WQI was between 5 and 15 points at a single sampling location, which is likely due to source water quality changes from season to season [26], temperature effects that promote bacterial growth, as well as maintenance schedules. January–February 2025 samples presented slightly better average WQI scores (28.4 ± 18.2) than October–November 2024 samples (31.7 ± 19.8), perhaps due to cooler temperatures that decreased bacterial growth rates. The contamination of aluminum did not follow the seasonal pattern, which indicated the characteristic sources of contamination in systems rather than environmental origins.

Table 4. Water Quality Index for the studied samples

Sample	WQI	Classification	Sample	WQI	Classification
H1	12.46	Excellent	Ha1	44.12	good
H2	8.91	Excellent	Ha2	40.33	good
H3	19.07	Excellent	Ha3	26.05	good
H4	3.12	Excellent	Ha4	54.67	poor
H5	32.01	good	Ha5	45.21	good
M1	24.56	Excellent	Ma1	21.33	Excellent
M2	5.22	Excellent	Ma2	3.10	Excellent
M3	19.8	Excellent	Ma3	31.55	good
M4	23.41	Excellent	Ma4	37.89	good
M5	35.89	good	Ma5	7.45	Excellent
Q1	1.89	Excellent			
Q2	28.77	good			
Q3	54.12	poor			
Q4	18.22	Excellent			
Q5	51.02	poor			

3.4 Performance Evaluation of RO Systems

The overall performance assessment shows that the RO units implemented in Babylon Province perform excellent removal of physical and chemical contamination, but are suboptimal for microbiological treatment. The concentration was compared with both average feed water quality and international benchmark performance to provide a quantified assessment of treatment effectiveness. The RO systems had excellent dissolved salt removal efficiency and TDS reduction performance was between 90.7% and 99.7% from common or average brackish groundwater sources (2000-8000 mg/L TDS). The average TDS removal rate, 96.6% ± 2.8%, is well above those of the literature 90–95% for typical RO applications (e.g., www.tripointglobal.com and rodi.au.pages.qpg.net) [8,9], suggesting excellent membrane performance with optimal operation conditions at most of the installations. The overall hardness can be removed significantly at different sampling points with a range of 85.2% to 98.9% as compared to the normal feed water hardness (800-1200 mg/L). The average hardness removal of 92.1 ± 4.3% falls within typical expectations for rate of desalination from RO, yet it indicates a high deviation in amounts removed, consequently to numbers extra

injected, indicating inconsistencies across this system's maintenance and operation control. Systems meeting >95% hardness removal (n=18) are working well, while systems with 98.5) due to double negative charge repulsion, and then came nitrate (>99.9), chloride (94.2% ± 3.1), and sodium removal (>97 where detected). Such removal rates are much higher than that achieved from the conventional treatment technology, indicating the efficient operation of RO membranes in most facilities (sn = 27%) [28,33]. Heavy metals removal: Iron did not exceed detection levels across all samples, and was completely removed at 100%. Variability of Al removal was observed were 56% of the samples presented no detectable concentration (below 0.01 mg/L) and in 44% it ranged between 0.01 and 0.15 mg/L, which varies depending on the contamination source in the systems that should be evaluated to find its cause and solve it individually [37]. The primary limitation to performance is the extent of microbiological treatment, with apparent bacterial removal efficiencies typically in the 85-95% range (as opposed to >99.9% theoretical expectations). The continuous presence of bacteria and coliforms demonstrates chronic contamination in practices of aseptic water production, which is antithetical to the entire purpose for RO technology as an infection control safeguard.

The thorough investigation brought to attention several operational issues in the RO units performance throughout Babylon Province which need to be addressed with a process chain approach to achieve good water quality and robustness of operations. Membrane fouling and scaling were found in systems of high salinity and low removal efficiency. Samples Ha3 and Ha4, with the receiving total hardness levels greater than 240 mg/L suggest serious membrane scaling leading to ineffective treatment and thus high operational costs. N. Zhao and F. Wang [26] we showed how scale on the membrane reduces system efficiency by 15-30% along with higher energy consumption and maintenance needs. The fouling trends indicate poor pretreatment, inconsistent cleanings or unfavorable operational conditions that need to be corrected. The universal contamination of the bacteria at every sampling point implies plant-wide failure including unfinished cleaning, no enough sanitized system and bad practices for quality management. To maintain the efficiency of an RO system, a frequent cleaning operation is commonly performed in addition to periodic membrane clean-in-place (CIP) procedures and the measurement of water quality in order to provide reliable operation [36].

The performance maintenance deficiencies which are apparent generally indicate a lack of qualified personnel, less than adequate training programs and inadequate quality control support at local operating levels. Most RO installations are not systematically monitored for water quality, which means that system problems and sources of contamination cannot be detected early. Current operational procedures are based on visual inspection and customer complaints; few systematic water quality tests are carried out and problems remain until they reach crisis level. Bacterial analyses and successive physicochemical determinations to check the health state of such reservoirs would help in their maintenance, preventing possible malfunction. The described operational problems have severe economic impacts on both consumers and the system operators. These fouling and scaling on the membrane surface make it less efficient, thereby leading to higher energy demand, component replacement rate, and 20-40% increase in operational cost compared to a well-operated system [7]. Further, bacterial contamination represents a potential liability and public health problem that can impose regulatory sanctions and higher healthcare expenses for consumers. The institutional failure showed that there is lack of technical capability at the local level which will not be able to operate and maintain the RO systems efficiently. Most operators also have not received any training on membrane cleaning, water testing or system troubleshooting leading to reactionary instead of proactive maintenance practices. Investing in quality control measures, SOPs and technical training programs will go a long way to improve system performance and safeguard public health. Restrictions in the availability of bourgeon good parts, cleaning products, and ownership testing make it burdensome to offer continuance effectiveness. At the majority of installs cheaper "replacement" parts are utilized or chemicals used for the cleaning are inadequate which will decrease system performance and life-span. The establishment of reliable service lines for high quality components and compounds, coupled with testing capabilities, would result in a better performing system across the province. Global performance

assessment shows that, although the RO treatment technology has exceptional physicochemical-specific capacity for treatment, operational improvements will be needed to ensure optimal system performance and public health protections. Key priority actions involve the establishment of standardized maintenance controls, routine quality monitoring for water supplies, technical training schemes and secure supply chains for components of systems and chemicals.

4. Environmental and Health Implications

4.1 Public Health Assessment

The general survey of water quality showed the compliance to individual physico-chemical recommendation as good but provided identification of numerous problems linked to microbiological safety. Comparison with the standards of the World Health Organization [3] shows that there is 100% conformity for main physicochemical parameters (total dissolved solids, electrical conductivity, major ions (chloride, sulfate and nitrate) and heavy metals (iron), but also 96% Conformity for pH values. This shows that RO plants located in Babylon Province have a well-functioning physicochemical treatment plant. The investigation revealed a serious non-compliance with the international microbiological quality criteria. Guidelines by WHO state that potable water should contain no detectable coliform bacteria and low level of colony forming units/100 mL of heterotrophic plate count (3). The report of coliform bacteria in 64% of samples (n=16) at significant level from 4-27 CFU/100mL is a matter of serious public health concern, requiring prompt action. Overall bacterial counts in the range of 177-301 CFU/ml for all samples also exceeded guideline values for finished drinking water and implied that as a group, there is systematic failure to achieve microbiological quality standards [17]. Another factor marketers should be following up closely is the Al contamination, which exceeded 44% of analysed water samples and though still within WHO recommended levels (0.2 mg/L). High aluminium levels (0.01–0.15 mg/L), especially the high value shown by sample Ma4 (0.15 mg/L) which is in proximity to the guideline limit, may imply risks of aluminium accumulation when consumed over time [3]. The sporadic nature of aluminum content is indicative of system-related impurities responsible for lowering the purity level expected in RO-treated water. The most imminent threat to human health is the wide-bacterial contamination and the presence of coliform bacteria. The coliform bacteria are indicators of the presence of fecal contamination and probably of pathogens, as their existence would imply this exposure to disease-causing microorganisms including parasites, viruses and bacteria [3]. The maximum coliform levels detected for samples Ha1 (27 CFU/100 mL) and Q2 (27 CFU/100mL) confirmed very high levels of contamination, showing a potential risk for causing gastrointestinal diseases, particularly in the most at-risk populations. Heightened total bacterial counts in all the samples present an additional health concern due to possible pathogen propagation and biofilm formation in distribution systems. Hayward et al. [39] reported that heterotrophic bacterial density greater than 100CFU / mL should be able to sustain the survival and multiplication of pathogens, conducting a potential risk of infection for immunocompromised people. The persistent bacterial too suggests those premises to have a potential for opportunistic premise plumbing pathogens, like Legionella species which are known to proliferate in warm water if there are bacterial biofilms. Aluminum content has been established as above acute toxic level however chronic exposure to high aluminium concentration may lead to neurological sequel and also connected with reflection in the development of Alzheimer's disease. However, causality is still a controversial issue [4]. Detection of aluminum in the form as alumina in 44% of samples indicates continued exposure that requires future monitoring especially considering that aluminum is a cumulative toxin and can be bioaccumulated over long durations of consumption. The marked softening of water in some samples (total hardness <50 mg/L in 32% of samples) might have cardiovascular implications. Epidemiological studies have identified an association between very soft water consumption and a higher risk of developing cardiovascular disease, with low intake of beneficial minerals and increased leaching of metallic contaminants from distribution systems likely as contributory factors [3]. The extreme softness of samples H4, Ma2 and Q1 (hardness 10-20 mg/L) may dictate mineral fortification to prevent adverse health effects from long-term use. Complete demineralization of dissolved minerals with RO treatment not only eliminates impurities, but also removes beneficial minerals, such as calcium, magnesium and trace elements which are essential to human health. The low TDS results

(6.14-225 mg/L) for all treated samples reflect extensive demineralisation which may lead to some shortcomings in case of using RO water directly as a main drinking water source without adding minerals content [3].

Children are the most susceptible population for waterborne transmission of disease because their immune systems are in development, they consume more water per unit body weight than adults, and they are more likely to become dehydrated from diarrheal disease. The presence of coliform bacteria in 64% of the analysed samples has special implications for children, who are more likely to experience severe dehydration and electrolyte disturbances resulting from bacterial gastroenteritis sooner than adults [3]. The demineralization of RO water also has implications for pediatric nutrition as children need appropriate mineral intake for bone development and growth. High hardness dependant on the type of ion show values are extremely low and may results in deficiencies to minerals for children if they take RO water as their source Iof fluid without their diets be able to make up for mineral losses.. [3]. The aged and immunosuppressed are at higher risk for the development of bacterial contamination, as a consequence of poor responsive immunity and an increased susceptibility to opportunistic pathogens. The level of bacterial contamination found among all samples may cause severe infections in the vulnerable populations, eventually requiring hospitalization and intensive medical care [39]. A special attention is needed to provide pregnant women protection against the waterborne pathogenic microorganisms because of the potential impact of maternal disease on fetal growth and on pregnancy outcome. Microbiological pollution of the RO-treated water may be dangerous for the during pregnancy bearing in mind that any mineral deficiency might affect either mother health and/or foetus growth on defined period where this treatment is applied. Diabetics, people with kidney disease, heart conditions or other chronic diseases can experience heightened health impacts of both microbiological contamination and mineral deficiency. The bacterial accumulation might lead to such severe consequences in diabetics, and the high degree of softening of water may increase cardiovascular risks in some sensitive groups.

4.2 Environmental Impact

Methods Reverse osmosis wastewater treatment creates large amounts of concentrated brine waste resulting in important environmental problems all through Babylon Province. Standard RO systems recover water at the rate of 20-25% and the feed becomes concentrated brine for suitable disposals (75-80%)me [13]. While only 25 RO system were evaluated but the hundreds of such plants are under operation in the whole province and collectively produced brine discharge is indeed an environmental burden which needs to be managed systematically. The brine stream is a concentrated waste containing 3-5 times the solublized salt concentration in the feed water, thereby conferring disposal problems especially if discharged in arid areas with very limited dilution opportunities. Safia et al. [29] insisted on it that improper brine disposal can pollute the surface water bodies, cause soil deteriorate through salinating and critical damage by harming terrestrial and aquatic ecosystems. Babylon Province relied on agriculture jobbing as an economic activity, and brine contamination of irrigation water supplies has detrimental effects on the productivity of crops and soil resilience. The brine management practices currently used in the valley generally entail direct release to surface waters or unlined evaporation ponds, both of which are not environmentally sound. Point source discharges elevated the salinity of receiving waters, resulting in lethality to aquatic life and deterioration of downstream water quality. Unlined ponds of evaporation, are also a groundwater contamination risk via seepage, with potential long-term liability to the environment and for destruction of future sources of water [7]. The treatment of RO water has high energy needs to move it with high-pressure pumping systems that emits greenhouse gases and contributes to climate change. The energy demand of RO plants is typically between 3 to 6 kWh/m3 permeate production, which in turn depends on salinity of the feed water, recovery rates and system efficiency [8]. The 25 RO plants in this corpus of an average daily flow of 130,000 m3/day combined with several hundreds of installa- tions operating in the Babylon Province alone are all parts of the considerable energy demand and resulting carbon dioxide emissions. Most of the electricity produced in Iraq comes from fossil fuel combustion, and therefore, energy consumption related to RO systems may result in CO_2 release and air pollution. The total carbon footprint of a provincial RO operation will undoubtedly exceed 10,000 tons CO_2 equivalent per year, thus designated as serious environmental issue that must be included in

climate change mitigation action plan [7]. The differences in energy intensity in RO plants present potential to minimize the eco-footprint through system optimization and advancements. The energy consumption of less efficient systems per unit product water should be considered as a benchmark for improving efficiency within the province. Energy recovery devices, VFDs and operating procedures optimization can also decrease energy consumption (15-30%) without affecting water quality [9]. There are many challenges facing the long-term sustainability of RO for water treatment in BP, which include a variety of factors that require an integrated program management and planning tool. Challenges to the sustainability of water resources include rising salinity in groundwaters, falling levels of aquifers and consequences of climatic change on water supply, which together can lead to an intensified process and associated environmental footprints. The present RO practices rely on linear trends use of resources dominated by a limited focus on resource extraction instead of resource recovery and waste generation minimization. There is also a potential to enable sustainability using the principles of circular economy for brine treatment in terms of salt recovery, reuse applications and 'waste-to'- operations. Advanced brine treatment technologies such as crystallization and mineral recovery systems, may turn waste streams into valuable products at a low environmental cost [29]. Hybrid treatment systems that integrate RO with renewable energy production, advanced pre-treatment procedures, and new methods of desalination may offer opportunities to increase overall sustainability. Solar RO systems being developed in nearby areas are promising to lower carbon footprint and retain treatment performance. Placing nanofiltration as a pre-treatment to RO may minimize RO energy consumption, enhance membrane service life, and system performance [22]. It is important to perform an LCA analysis covering all of the life cycle stages that system go through from membrane production, transportation, installation in plant, operation, until disposal. The membrane replacement demands, chemical needs to clean and maintaining the RO membranes and infrastructure developments contribute to overall environmental impacts needing systematic weight factors for computing as well as optimization.

4.3 Regulatory Compliance

On evaluating the quality of RO water with Iraqi national drinking water standard(s) (Iraqi Standard No. 417/2009), we found that all physico-chemical parameters were in compliance except for MCs, indicating poor control over microbiology. Iraq national standards classify the main (parameters): pH (6.5–8.5), TDS (1000 mg/L), total hardness (500 mg/L) chloride 250 mg/l, sulfate 400 mg/l, nitrate at 45 mg/l, and bacteriological contamination should be zero where coliform bacteria are not potable to drinking water supply that public use. The physicochemical parameters evaluation shows a good agreement with the Iraqi guidelines which 100% of the samples comply for TDS, hardness, major ions and heavy metals. Overall, good treatment in the provincial RO plants is evidenced by 96% compliance with pH only a slight (4%) non-compliance for one sample (H3) at pH = 6.1. These findings indicate that Iraqi national standards may be used as physicochemical criteria for controlling the water quality, thereby confirming efficient installation of the RO unit. Microbiological quality is consistently poor, 64% of samples were found to have detectable coliform bacteria, indicating full non-compliance with Iraqi national standards. The zero-tolerance policy for coliform bacteria contamination in beverage water is consistent with sound public health protection priorities, and widespread bacterial contamination would constitute a serious regulatory noncompliance justifying swift precautionary action. The levels of TBCC, which are not specified in the Iraqi regulations, exceed international standards and the results of analyses suggest a systemic quality assurance problem [14]. Comparison with WHO [3] drinking water guidelines showed a comparable picture of high physicochemical compliance and large microbiological non-compliance. The WHO guidelines are based on health-related criteria, focusing on the microbial safety, prevention of chemical pollution and preservation of aesthetic quality. Overall, the study reveals mixed adherence to these principles at Babylon Province RO facilities. Guidelines of WHO indicate that drinking water should not contain any E. coli or thermotolerant coliform bacteria and numbers of heterotrophic bacteria must be minimal after proper treatment and distributed system management. The 64% coliforms positive samples suggest non-compliance of WHO microbiological standards, therefore indicating limited treatment efficacy and human health hazard that must be addressed without delay. The all samples were also in good compliance with the WHO chemical guidelines including heavy metals (iron, aluminum), major ions (chloride, sulfate, nitrate), and aesthetic parameters (pH, conductvity, hardness). Al concentrations

were found to be high (>0.03mg/L) in 44% of the samples, and although not at WHO maximum level (0.2 mg/L), these near-upper values factor as a concern that should be watched, so avoid surpassing future Al levels too much elevated. The WHO recommendations focus on health-risk based assessment of cumulative exposure-based risk, vulnerable population protection and long-term health impacts. The mineral shortfall related risk of over-demineralization in a few samples may deserve attention, based on WHO health-based assessment criteria, especially for populations dependent solely on RO water without any attempt at mineral supplementation [3]. Regulatory perspective needs to be reinforced for the purpose of dealing with systemic microbiological problems observed in the RO installations. The requirement of monthly bacterial testing (for example, TCC/E. coli analysis) would allow for early identification of source contamination and immediate remedial action. Regulations should define acceptable levels of bacteria, sampling schedules, and the proper steps to be taken in systems that did not meet these criteria. Overall RO system certification requirements including installation standards, operator training requirements and mandated maintenance procedures would improve overall system performance and ensure that the regulations are met. Certification programs would provide guidance for criteria to select membranes, pretreat and disinfect systems, and perform quality control functions in order to achieve consistently good performance at all installations. Adequate facilities for the analysis of water must be set up by establishing regional water quality testing laboratories which would facilitate better monitoring and compliance evaluation. The lack of infrastructure means that for the testing facilities, it takes a massive effort even to test basic water conditions with challenges continued till they attain crisis heights. Investment in laboratory resources (both bacteriological enumerating facilities and chemical analytical equipment) would allow proactive quality monitoring and enforcement. The application of water safety plan principles as promoted by WHO, should enable implementation of risk assessment and control options and monitoring of system performance. Water safety plans need to combine protection of raw water sources with the best possible treatment, adequate disinfection, effective distribution systems and provision of suitable consumer information in order to prevent risk for public health. Penalty systems and measures to enforce compiance in faulty systems can also be developed leading to better availability and easier compliance with regulations. The application of graduated penalty schemes that incorporate mandatory corrective action requirements, temporary cessation of activities for egregious non-compliance and escalating fines for repeated non-compliance would provide regulatory leverage. The recommendation would provide a public health response to serious WQ violations, including the presence of coliform colonies; protect public health during contamination events. Emergency response plans should include notification processes, alternative water supply plans,public communication activities and timelines for corrective action with the goal of reducing health risk during episodes of quality failure. Establishment of regional co-ordination among provincial authorities, municipal governments and system operators would facilitate consistent methods for water quality control and regulatory adherence. Synchronised standards, common technical resources and collaborative problem solving would enhance system performance as a whole and reduce the cost of regulation to individual operators.

5. Conclusions

This study, applied to 25 reverse osmosis plants in Babylon Province/Iraq, demonstrates inequalities of efficiencies between physicochemical and microbiological treatments. Physicochemical performance RO technology gave excellent result in physicochemical treatment with 96.6% ± 2.8% removal efficiency of dissolved salts and 100% condition was satisfied for all critical (TDS, major ions and heavy metals) parameters. Nevertheless, very high levels of microbiological safety failures exist where coliform bacteria was detected in 64% (0-27 CFU/100mL) and total bacterial counts were higher than permissible limits (177-301 CFU/mL) at all installations despite contamination-based factors could pose a direct potential health hazard for the users. Water Quality Index analysis indicated 64% samples were excellent(WQI: 0-25), 24% good(26-50), and 12% poor (51-75) for districts, however with wide fluctuations. Al-Musseyeb attained 80% excellent ratings, whereas Al-Hashimyah showed only 20% excelling, suggesting thever is operational practices that needs to be focused upon. Other worries are that the water supply contains aluminum in 44% of samples and the water softening is excessive for 32% of plants. Included among important recommendations are application

of complete disinfection schemes coupled UV-irradiation and monitored systematic sanitization, supported by mandatory bacteria monitoring and standardized maintenance measures. It should also be clarified, in a way that reflects controls through microbiological standards, operator certification regimes and sanctions for non-compliance. Operator training programs and regional support networks are crucial for sustainable system improvement. Although RO technology successfully removes the difficult range of physicochemical water quality in the area, in order to ensure public health protection effectively, particular attention is due for microbiological safety management, operational reliability and regular compliance. System performance monitoring studies, advanced treatment processes integration and developing an economic and environmentally friendly sustainable brine management scheme should be the future research perspective.

6. Acknowledgements

The authors gratefully acknowledge the support of the College of Science, University of Babylon, and the Environmental Sciences Department at Al-Qasim Green University for the laboratory facilities and kind grant support during this study. We also thank our students and colleagues whose assistance in sample collection and laboratory analyses greatly facilitated the completion of the work.

Author Contributions: "Conceptualization, H.FA., N.N., and A.A.; methodology, H.FA., N.N.,; software, H.FA., N.N.,; validation, H.FA., N.N., and A.A.; formal analysis, N.N.; investigation, A.A.; resources, A.A.; data curation, A.A.; writing—original draft preparation, A.A.; writing—review and editing, A.A.; visualization, A.A.; supervision, A.A.; project administration, A.A.; funding acquisition, A.A.; All authors have read and agreed to the published version of the manuscript.

Funding: Not applicable.

Conflicts of Interest: This work has no conflicts of interest

References

[1] Nicolaidis, S. Physiology of thirst. In *Hydration Throughout Life*; Arnaud, M. J., Ed.; John Libbey Eurotext: Montrouge, France, **1998**; p 247.

[2] Mishra, R. K. Fresh water availability and its global challenge. *Br. J. Multidiscip. Adv. Stud.* **2023**, *4*, 1–78. https://doi.org/10.37745/bjmas.2022.0208

[3] WHO. *Guidelines for Drinking-Water Quality: Incorporating the First and Second Addenda, 4th ed.* World Health Organization: Geneva, Switzerland, **2022**.

[4] Akhai, S.; Taneja, T. Liquid gold: safeguarding our health through pure drinking water and rigorous water testing. In *Natural Resource Management Issues in Human-Influenced Landscapes*; IGI Global: Hershey, PA, USA, **2024**; pp 129–148. https://doi.org/10.4018/978-1-6684-7051-0.ch007

[5] Ritt, C. L.; Stassin, T.; Davenport, D. M.; DuChanois, R. M.; Nulens, I.; Yang, Z.; Elimelech, M.; Verbeke, R. The open membrane database: Synthesis–structure–performance relationships of reverse osmosis membranes. *J. Membr. Sci.* **2022**, *641*, 119927. https://doi.org/10.1016/j.memsci.2021.119927

[6] Dirisu, G. B.; Okonkwo, U. C.; Okokpujie, I. P.; Fayomi, O. S. Comparative analysis of the effectiveness of reverse osmosis and ultraviolet radiation of water treatment. *J. Ecol. Eng.* **2019**, *20*(3), 61–75. https://doi.org/10.12911/22998993/95266

[7] Soliman, M. N.; Guen, F. Z.; Ahmed, S. A.; Saleem, H.; Khalil, M. J.; Zaidi, S. J. Energy consumption and environmental impact assessment of desalination plants and brine disposal strategies. *Process Saf. Environ. Prot.* **2021**, *147*, 589–608. https://doi.org/10.1016/j.psep.2020.12.038

[8] Poirier, K.; Lotfi, M.; Garg, K.; Patchigolla, K.; Anthony, E. J.; Faisal, N. H.; Al Mhanna, N. A comprehensive review of pre-and post-treatment approaches to achieve sustainable desalination for different water streams. *Desalination* **2023**, *566*, 116944. https://doi.org/10.1016/j.desal.2023.116944

[9] Greenlee, L. F.; Lawler, D. F.; Freeman, B. D.; Marrot, B.; Moulin, P. Reverse osmosis desalination: water sources, technology, and today's challenges. *Water Res.* **2009**, *43*(9), 2317–2348. https://doi.org/10.1016/j.watres.2009.03.010

[10] Garabedian, S. A. K. The quality of reverse osmosis water in storage tanks in Basrah city—Iraq. *Basrah J. Sci.* **2011**, *6*(1), 1–8.
[11] Hadi, A. M. Isolation and identification of *Cryptosporidium sp.* by reverse osmosis system of tap water in Baghdad. *Baghdad Sci. J.* **2014**, *11*(3), 894–899. https://doi.org/10.21123/bsj.11.2.894-899
[12] Sabtie, N. H. A.; Kariem, N. N. O.; Sachit, D. E. Application of RO system to desalinate brackish surface water in Southern Iraq. *Civ. Environ. Res.* **2018**, *10*(1), 19–34.
[13] Abbas, H.; Lateef, K. H.; Abdeljabbar, A. T.; Abbas, F. S. Desalination of groundwater for several districts in Baghdad-Iraq using reverse osmosis membrane. In *Nucleation and Atmospheric Aerosols*; AIP Publishing: Melville, NY, USA, **2022**. https://doi.org/10.1063/5.0113443
[14] Al-Gayyim, A. S.; Al-asady, R. K. A. Evaluation of reverse osmosis water quality in Diwaniyah Governorate/Iraq. *MJPS* **2023**, *10*(2), 2. https://doi.org/10.52113/2/10.02.2023/9-26
[15] Wang, X.; Zhang, F.; Ding, J. Evaluation of water quality based on a machine learning algorithm and water quality index for the Ebinur Lake Watershed, China. *Sci. Rep.* **2017**, *7*, 12858. https://doi.org/10.1038/s41598-017-12853-y
[16] Al Yousif, M. A.; Chabuk, A. Assessment water quality indices of surface water for drinking and irrigation applications—A comparison review. *J. Ecol. Eng.* **2023**, *24*(5), 40–55. https://doi.org/10.12911/22998993/161194
[17] Chidiac, S.; El Najjar, P.; Ouaini, N.; El Rayess, Y.; El Azzi, D. A comprehensive review of water quality indices (WQIs): history, models, attempts and perspectives. *Rev. Environ. Sci. Biotechnol.* **2023**, *22*(2), 349–395. https://doi.org/10.1007/s11157-023-09650-7
[18] Brown, R. M.; McClelland, N. I.; Deininger, R. A.; Tozer, R. G. A water quality index—Do we dare? *Water Sewage Work.* **1970**, *117*(10), 339–343.
[19] CCME. *Canadian Water Quality Guidelines for the Protection of Aquatic Life: CCME Water Quality Index 1.0 User's Manual*; Canadian Council of Ministers of the Environment: Winnipeg, MB, Canada, **2001**.
[20] APHA. *Standard Methods for the Examination of Water and Wastewater, 23rd ed.*; American Public Health Association: Washington, DC, USA, **2017**.
[21] Anis, S. F.; Hashaikeh, R.; Hilal, N. Reverse osmosis pretreatment technologies and future trends: A comprehensive review. *Desalination* **2019**, *452*, 159–195. https://doi.org/10.1016/j.desal.2018.11.006
[22] Honarparvar, S.; Zhang, X.; Chen, T.; Alborzi, A.; Afroz, K.; Reible, D. Frontiers of membrane desalination processes for brackish water treatment: A review. *Membranes* **2021**, *11*(4), 246. https://doi.org/10.3390/membranes11040246
[23] Liu, Y.; Zhu, M.; Ji, X.; Tan, Z.; He, Z. Removal of calcium and magnesium ions from reverse osmosis concentrate using a two-stage precipitation with carbonation process. *Environ. Sci. Pollut. Res.* **2024**, *31*(33), 45495–45506. https://doi.org/10.1007/s11356-024-34186-4
[24] Keen, M. Evaluation of the Impact of Membrane Change at a Membrane Softening Water Treatment Plant; University of Waterloo: Waterloo, ON, Canada, **2009**.
[25] Nyoman Widiasa, I.; Sinaga, N.; Ariyanti, D. Improving performance of low reverse osmosis pressure systems by intermittent autoflushing. *Water Sci. Technol.* **2010**, *61*(12), 3103–3109. https://doi.org/10.2166/wst.2010.934
[26] Zhao, Y.; Wang, D. Membrane scaling mechanisms in RO desalination. *Desalination* **2017**, *403*, 165–174. https://doi.org/10.1016/j.desal.2016.10.025
[27] Ayoub, G. M.; Korban, L.; Al-Hindi, M.; Zayyat, R. Removal of fouling species from brackish water reverse osmosis reject stream. *Environ. Technol.* **2018**, *39*(7), 804–813. https://doi.org/10.1080/09593330.2017.1310938
[28] Lee, K. P.; Arnot, T. C.; Mattia, D. A review of reverse osmosis membrane materials for desalination—Development to date and future potential. *J. Membr. Sci.* **2011**, *370*(1-2), 1–22. https://doi.org/10.1016/j.memsci.2010.12.036
[29] Safia, A. I.; Salima, A.; Ibrahim, B. Zero liquid discharge management: optimizing sustainable reverse osmosis desalination practices. *Stud. Eng. Exact Sci.* **2024**, *5*(2), 1–15. https://doi.org/10.54021/seesv5n2-040

[30] Abascal, E.; Gómez-Coma, L.; Ortiz, I.; Ortiz, A. Global diagnosis of nitrate pollution in groundwater and review of removal technologies. *Sci. Total Environ.* **2022**, *810*, 152233. https://doi.org/10.1016/j.scitotenv.2021.152233

[31] Sewak, R.; Sewak, P.; Singh, P. S. Nitrate contamination in groundwater and preferred treatment technology in rural India. *Water Secur.* **2023**, *20*, 100149. https://doi.org/10.1016/j.wasec.2023.100149

[32] Zirrahi, F.; Hadi, M.; Nodehi, R. N.; Milan, E. G.; Bashardoust, P.; Abolli, S.; Alimohammadi, M. A systematic review on the investigation of optimal operating conditions of the reverse osmosis process in nitrate removal from drinking water. *Results Eng.* **2025**, *21*, 101947. https://doi.org/10.1016/j.rineng.2024.101947

[33] Al Mehrate, J.; Shaban, S.; Henni, A. A review of sulfate removal from water using polymeric membranes. *Membranes* **2025**, *15*(1), 17. https://doi.org/10.3390/membranes15010017

[34] Tran, T.; Bolto, B.; Gray, S.; Hoang, M.; Ostarcevic, E. An autopsy study of a fouled reverse osmosis membrane element used in a brackish water treatment plant. *Water Res.* **2007**, *41*(17), 3915–3923. https://doi.org/10.1016/j.watres.2007.06.008

[35] Ohno, K.; Matsui, Y.; Itoh, M.; Oguchi, Y.; Kondo, T.; Konno, Y.; Sato, T.; Fujiwara, T.; Matsushita, T.; Magara, Y. NF membrane fouling by aluminum and iron coagulant residuals after coagulation–MF pretreatment. *Desalination* **2010**, *254*(1-3), 17–22. https://doi.org/10.1016/j.desal.2009.12.011

[36] Adel, M.; Nada, T.; Amin, S.; Anwar, T.; Mohamed, A. A. Characterization of fouling for a full-scale seawater reverse osmosis plant on the Mediterranean sea: membrane autopsy and chemical cleaning efficiency. *Groundw. Sustain. Dev.* **2022**, *16*, 100704. https://doi.org/10.1016/j.gsd.2021.100704

[37] Kherraf, S.; Ennouhi, M.; El Mansouri, A.; El Hajjaji, S.; Nasrellah, H.; Bensemlali, M.; Aarfane, A.; Cherrat, A.; Labjar, N. Autopsy results and inorganic fouling prediction modeling using artificial neural networks for reverse osmosis membranes in a desalination plant. *Eng.* **2025**, *6*(5), 98. https://doi.org/10.3390/eng6050098

[38] Brown, S. L.; Leonard, K. M.; Messimer, S. L. Evaluation of ozone pretreatment on flux parameters of reverse osmosis for surface water treatment. *Ozone Sci. Eng.* **2008**, *30*(2), 152–164. https://doi.org/10.1080/01919510801892932

[39] Hayward, C.; Ross, K. E.; Brown, M. H.; Bentham, R.; Whiley, H. The presence of opportunistic premise plumbing pathogens in residential buildings: A literature review. *Water* **2022**, *14*(7), 1129. https://doi.org/10.3390/w14071129

[40] Türker, R. K.; Ekici, H.; Aydınalp, C. Design and analysis of flow channels in reverse osmosis systems: A preliminary study. In *Proceedings of the 2025 7th International Congress on Human-Computer Interaction, Optimization and Robotic Applications (ICHORA)*; IEEE: Piscataway, NJ, USA, **2025**; pp 1–5. https://doi.org/10.1109/ICHORA65333.2025.11017183

[41] Fikri, E.; Muhammad Ramdhanny, F.; Nurhayati, A.; Sharaf Eldin, K. A. Total coliform reduction in drinking water based on variations in reverse osmosis membrane pressure. *Glob. NEST J.* **2022**, *24* (4), 569–575. https://doi.org/10.30955/gnj.004295

[42] Rbeida, O.; Eteer, S. Quality control evaluation of the microbial contamination of bottled drinking water and house hold reverse osmosis water in Tripoli, Libya. *AlQalam J. Med. Appl. Sci.* **2023**, *6*(2), 867–872.

[43] Baba, T.; Matsumoto, R.; Yamaguchi, N.; Nasu, M. Bacterial population dynamics in a reverse-osmosis water purification system determined by fluorescent staining and PCR-denaturing gradient gel electrophoresis. *Microbes Environ.* **2009**, *24*(2), 163–167. https://doi.org/10.1264/jsme2.me09120

ASEAN
Journal of Scientific and Technological Reports
Online ISSN:2773-8752

Research article

AI-Driven Smart Farming for Automated Plant Health Monitoring and Nutrient Deficiency Detection

J.Serin[1], G.Gifta Jerith[2], V.Ebenezer[3*], K.Arul Jeyaraj[4], A.Jenefa[3], and M.Vargheese[5]

[1] Department of Computer Science, Women's Christian College, Chennai, Tamil Nadu, India
[2] Department of AI & ML, Malla Reddy University, Hyderabad, India
[3] Division of Data Science and Cyber Security, Karunya Institute of Technology and Sciences, Coimbatore, Tamil Nadu, India
[4] Department of Electronics and Communication Engineering, PSNA College of Engineering and Technology, Dindigul, Tamil Nadu, India
[5] Department of Computer Science and Engineering, PSN College of Engineering and Technology, Tirunelveli, Tamil Nadu, India
* Correspondence: ebenezerv@karunya.edu

Citation:
Serin, J.; Jerith, Gifta, G.G.; Ebenezer, V.; Jeyaraj, A.K.; Jenefa, A.; Vargheese, M. AI-Driven samrt farming for automated plant health monitoring and nutrient deficiency detection. *ASEAN J. Sci. Tech. Report.* **2026**, *29*(1), e258175. https://doi.org/10.55164/ajstr.v29i1.258175.

Article history:
Received: March 5, 2025
Revised: September 24, 2025
Accepted: September 27, 2025
Available online: December 14, 2025

Publisher's Note:
This article is published and distributed under the terms of the Thaksin University.

Abstract: Precision agriculture is transitioning to continuous, data-driven monitoring. Affordable sensors and edge intelligence enable near real-time crop oversight. Manual scouting is labor-intensive and inconsistent. Delayed detection of nutrient stress leads to increased yield loss and input waste. Legacy systems monitor soil or weather in isolation and depend on periodic human checks. Vision pipelines often use shallow models and are not connected to field actuators. Proposed work: We combine soil moisture, temperature, and humidity sensing with camera-based leaf analysis using a DenseNet 121 classifier. A microcontroller executes closed-loop irrigation and localized cooling, with a mobile app for telemetry and alerts. RGB leaf images were captured in field conditions and labeled by experts into healthy and deficiency classes. Images were resized to 224×224 and split into training, validation, and test sets by plot to avoid leakage. DenseNet 121 achieved 89.0% accuracy on a held-out test set and surpassed a MobileNet V2 baseline of 82.0% under identical training conditions. Prototype deployments reduced manual checks and improved response to moisture and heat stress. The integrated IoT and AI pipeline is practical for early detection of nutrient deficiencies and autonomous actuation in small plots and greenhouses.

Keywords: Plant Monitoring system; IoT moisture; temperature; humidity; CNN

1. Introduction

Food is vital to our livelihoods. On average, over the last few decades, approximately 40% of the world's population has been employed in fields related to agriculture, and almost half of the world's habitable land is utilized for agriculture. In the present day, there is an increase in population growth. Thus, there is also an increase in demand and a need to increase food production. Temperature, available water, available light, carbon dioxide, and soil nutrients are environmental factors that influence plant growth. Hence, for monitoring soil parameters such as pH level, soil moisture, and temperature and humidity, we introduce the Internet of Things. Soil moisture and pH value are key factors for crop growth. The detection and monitoring of soil parameters are done using various sensors.

There are various reasons why plants rely on soil, not only for support and water, but also to obtain essential minerals such as nitrogen, phosphorus, potassium, and magnesium, as well as other essential resources. The nutrients

are of two types: micronutrients and macronutrients. Plants require these nutrients for their effective growth. While micronutrient levels in plant tissues range from 0.1 to 200 parts per million (ppm), or less than 0.02 percent dry weight, macronutrients are used in considerable proportions. The absence of one or more plant nutrients can lead to poor growth and a variety of illnesses, including leaf chlorosis. The symptoms of nutrient deficiencies are often readily apparent in plant leaves and include changes in leaf size, shape, and color, as well as interveinal chlorosis, uniform chlorosis, marginal chlorosis, necrosis, and irregular margins.

2. Materials and Methods

Users must configure the hardware system and choose the type of plant to monitor as the input. As shown in Figure 1, the hardware system comprises a soil moisture sensor, a DHT sensor (temperature and humidity sensor), and other components, including a microcontroller, relay, and LCD panel. When the user selects the type of plant to monitor, a signal is provided to the ATmega microcontroller, which subsequently activates the sensors.

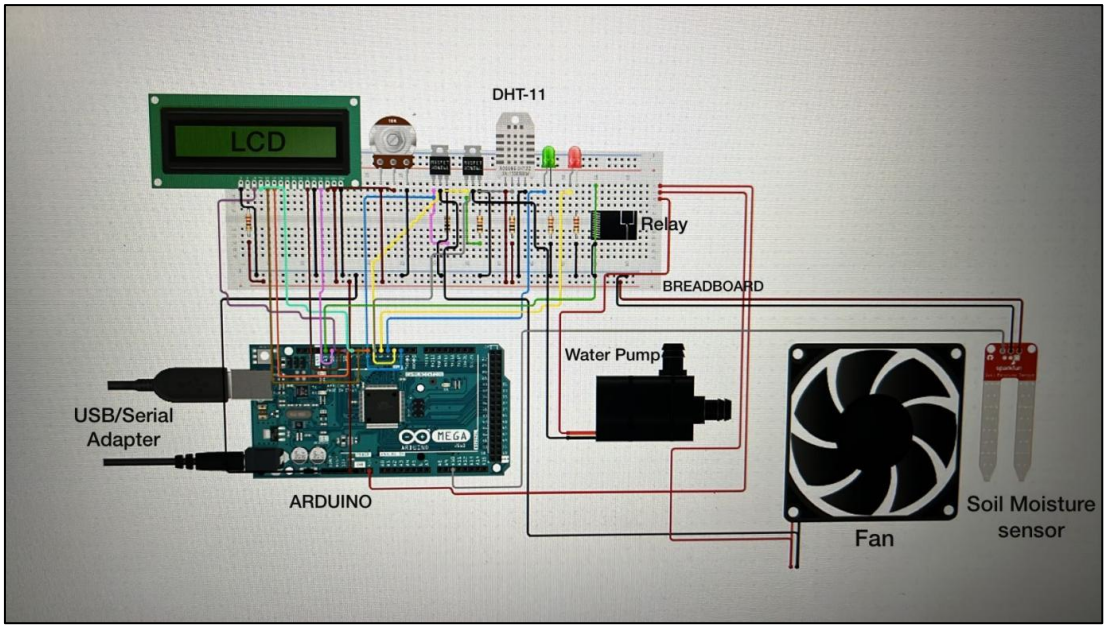


Figure 1. Circuit diagram for smart monitoring system

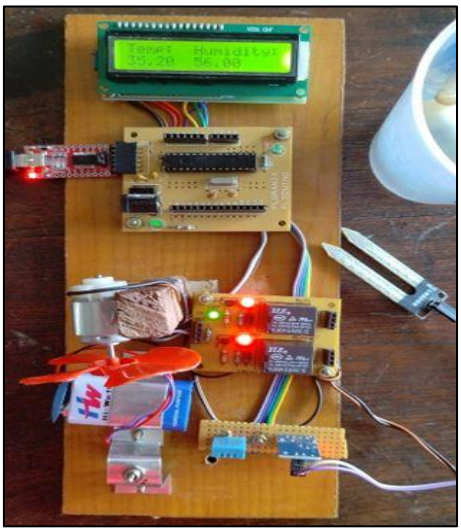


Figure 2. Floduino motherboard for ATMega

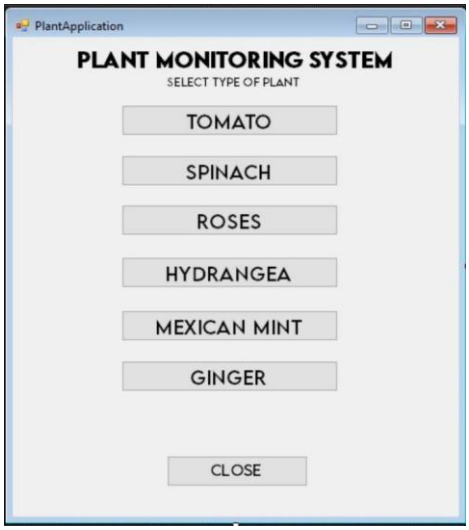


Figure 3. Mobile app interface for crop selection and live telemetry.

The soil moisture sensor's probes will always be buried in the ground. The soil sensor measures the soil's moisture content, while the DHT sensor gauges the atmosphere's temperature and humidity [6, 7].

The microcontroller receives the detected numbers and compares them to the threshold level. When the measured values drop below the threshold, the relay is triggered, causing the LCD panel to display alert messages. To restore normal circumstances, this triggers the automated irrigation feature and the built-in cooling fan. Water is applied to the soil, and cooled air is circulated to the plants by the fan. Figure 2 shows the LCD panel, which displays the current humidity, temperature, and moisture levels.

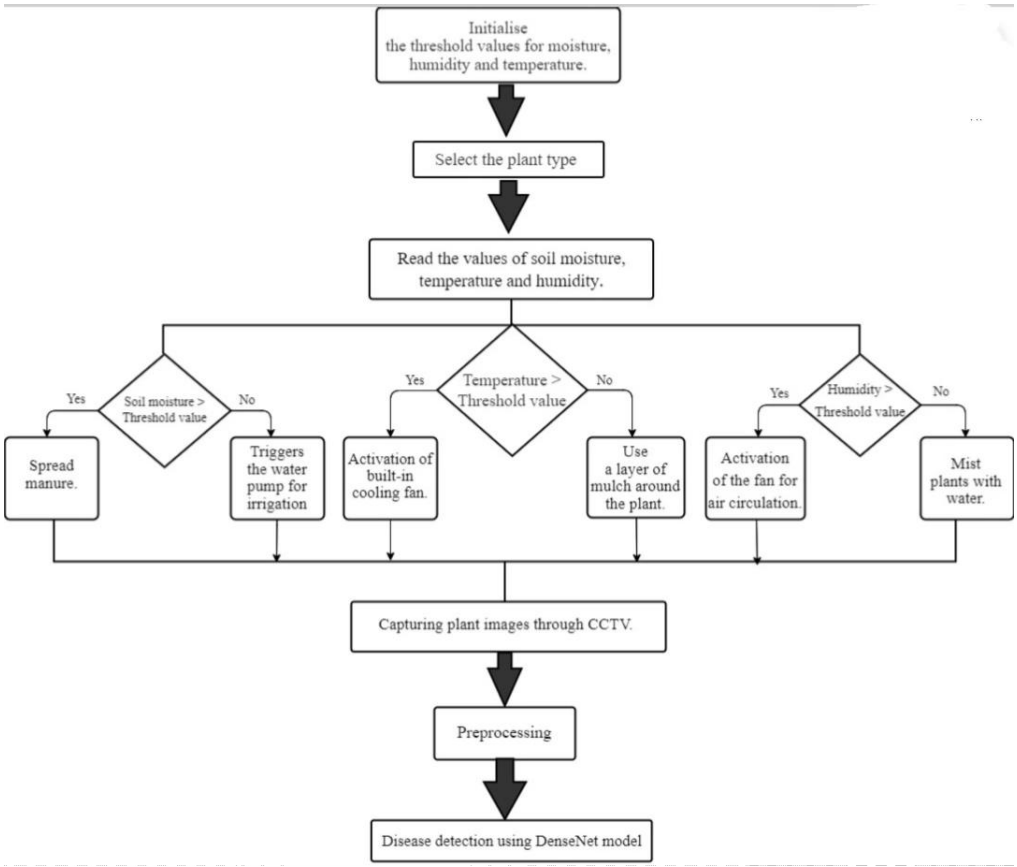


Figure 4. End-to-end architecture and image-analysis pipeline.

For image processing, digital cameras are used to capture leaf images, which are then utilized to train and test the system [8]. These photographs are kept in the common JPG format. With CCTVs, the leaves are photographed in RGB color. Images of damaged and healthy plant leaves are taken at various angles and light levels. This is the image acquisition step in image processing. The goal of picture pre-processing involves image augmentation, which can be achieved through the use of filtering and other techniques. To improve picture identification accuracy, binary images are created using various contrast enhancement techniques. In image segmentation, the provided image is divided into healthy and unhealthy parts according to specific criteria. This method aids in the early detection of nutritional deficiencies, informing us of the type and quantity of fertilizer that should be applied. We are minimizing superfluous fertilizer use, and the use of organic fertilizers may also be encouraged through early indicators of nutritional shortages [9, 10].

3. Results and Discussion

The proposed methodology, summarized in Figure 4, has been implemented using a mobile application, and the results are discussed in this section. The project achieves its intended objective by autonomously identifying various plant variables and responding without human intervention. For those familiar with plants, the system was designed to simplify planting. By offering dynamic alternatives for reviewing various plant kinds, this automated plant monitoring system has been successful in bringing unique older functions. **Table 1** summarizes the dataset composition with plot-wise 70/15/15 train–validation–test partitions across three classes (Healthy, Nitrogen deficiency, Phosphorus deficiency). As shown in **Table 1**, the corpus comprises 1,200 images (480 Healthy, 360 Nitrogen, 360 Phosphorus), enabling balanced evaluation while preventing leakage.

Table 1. Dataset composition and class-wise plot-wise splits

Class	Train (n)	Validation (n)	Test (n)	Total (n)	Share of total (%)
Healthy	336	72	72	480	40.0
Nitrogen deficiency	252	54	54	360	30.0
Phosphorus deficiency	252	54	54	360	30.0
Total	**840**	**180**	**180**	**1,200**	**100.0**



Figure 5. Image Preprocessing a) Before Image Preprocessing b) After Image Preprocessing

The user must select the type of plant, as shown in Figure 3, that will be surveyed when using the application, and the values are then analyzed in accordance with that choice. The system includes a water pump that gets activated when the soil moisture content drops below a predetermined level. The pump automatically shuts off when the threshold level is reached and the moisture level of the plant rises [11]. Moreover, as the ambient temperature exceeds the predetermined threshold, a cooling fan fitted into the system activates. The cooler air is circulated to the plants by the fan, which removes the hotter, denser air [12].

On the LCD panel, real-time readings of soil moisture, temperature, and relative humidity are shown. This paper has implemented concepts from digital image processing and embedded systems for the health monitoring of leaves. Image processing is performed using images captured by the CCTVs, and the processing of these images will be used to analyze the presence of nutrient deficiency in plants.

Through this system, we can minimize both over- and under-irrigation of the soil, as well as water consumption and motor power usage. Due to the small coverage area of the CCTVs and the integrated cooling fan, this system is not recommended for monitoring vast areas. This system could be enhanced in the future by the addition of a Wi-Fi module to expand the range of connectivity and a Cloud database server, allowing the system to be operated from anywhere. CNNs are a type of deep neural network specifically designed for image processing tasks. They consist of multiple layers of filters that extract increasingly complex features from input images, enabling the network to identify specific patterns or structures indicative of different types of nutritional deficiencies [13].

Image preprocessing is an essential part, ensuring that all images are scaled to the same size so that they can be trained without discrepancy. Additionally, the comprehensive part of the preprocessing system produces effective outcomes. The dataset could include images of rice with stunted growth, discoloration, or abnormal grain shape [14]. This preprocessing involves resizing and normalization to ensure that the images are consistent and accurate. Images can be flipped horizontally or vertically, rotated, or zoomed in or out. This increases the size of the training dataset, which can improve the model's generalization.

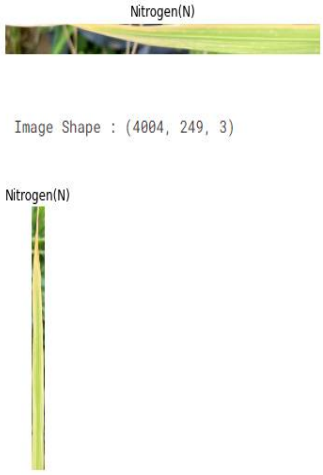


Figure 6. Nitrogen Deficiency



Figure 7. Phosphorous Deficiency



Figure 8. Data Augmentation a) Vertical Shift b) Horizontal Shift

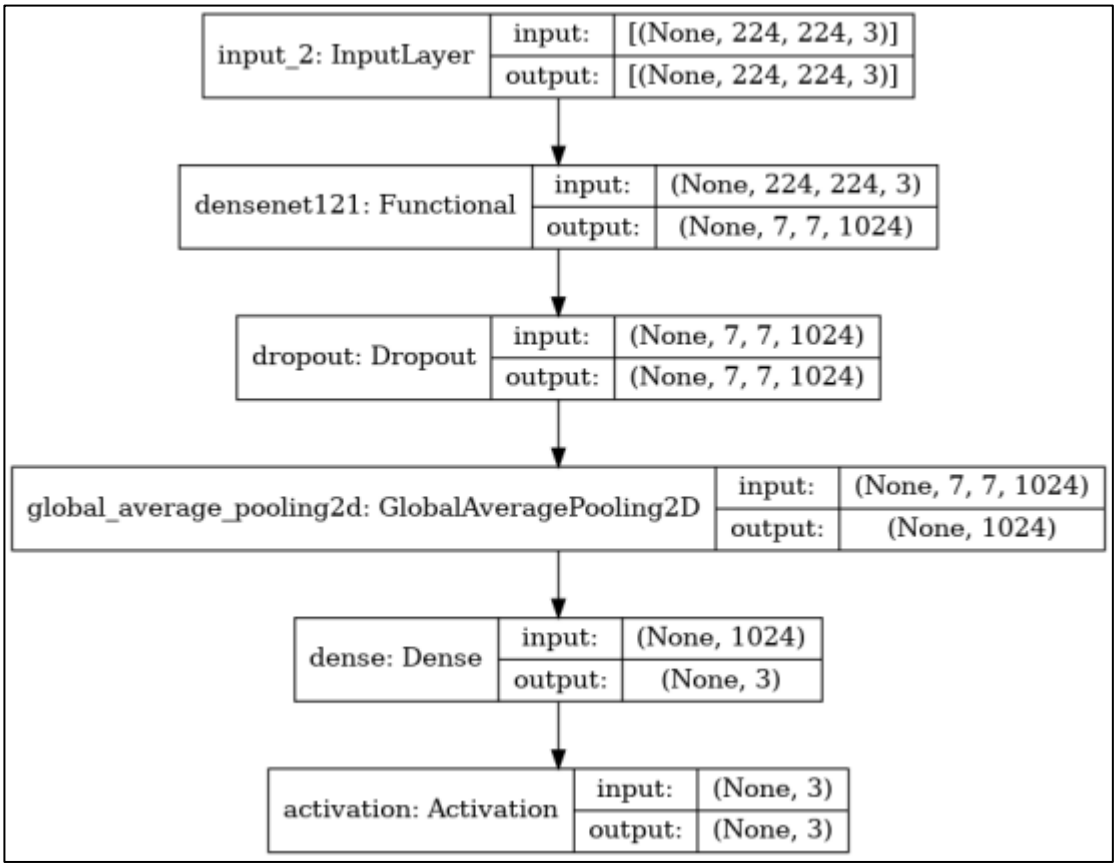


Figure 9. DenseNet Architecture

Figures 6 and 7 identify the deficiency of Nitrogen (N) in plants. After applying data augmentation techniques, the output would be a set of additional images created by applying transformations to the original images. This can help increase the size of the training dataset and improve the model's generalization. DenseNet (Dense Convolutional Neural Network) is a type of deep learning architecture that is effective for image classification tasks. DenseNet employs a distinctive approach of connecting layers. DenseNet has been used to classify images of rice leaves based on the presence or absence of nutrient deficiencies [15]. Input layer: This layer takes as input the images to be classified. The input shape for the DenseNet model is typically (224,

224, 3), which corresponds to a 224x224 RGB image. Convolutional layer: The input images are passed through a convolutional layer with 64 filters of size 7 × 7, a stride of 2, and a padding of 3. A batch normalization layer and a ReLU activation layer follow this. Pooling layer: The output of the convolutional layer is passed through a max pooling layer with a pool size of 3x3 and a stride of 2. Output layer: This layer consists of a fully connected layer with a softmax activation function, which produces the predicted probabilities for each class. It has been observed that the MobileNet model achieves an accuracy of 82%, whereas the DenseNet model achieves an accuracy of 89%. The accuracy can be further improved by increasing the number of images. Table 1 summarizes the main classification results on the held-out test set, comparing the proposed DenseNet-121 with a MobileNetV2 baseline under identical training settings.

Table 2 documents the training configuration and key hyperparameters to ensure reproducibility and a fair comparison. It specifies input normalization, Adam optimizer (initial LR = 3×10^{-4}), cosine decay with early stopping, batch size/epochs, and class-balanced loss with standard augmentations. Plot-wise 70/15/15 splits and fixed seeds minimize leakage and variance, while framework/hardware notes enable independent replication of accuracy, latency, and throughput. Table 3 presents the main classification results obtained under identical training/validation protocols, comparing the proposed DenseNet-121 with a MobileNetV2 baseline. As shown in Table 3, DenseNet-121 achieves 89.0% accuracy, compared to 82.0% for MobileNetV2, indicating a materially stronger ability to recognize nutrient deficiencies; this is supported by the inclusion of macro-F1 and macro-AUC for completeness. This margin is operationally meaningful in field settings where false negatives are costly; a confusion matrix and per-class scores can be provided in the supplement for diagnostic clarity.

Table 2. Model training configuration and key hyperparameters

Item	Setting
Models	DenseNet-121 (Proposed), MobileNetV2 (Baseline); ImageNet initialization
Input & normalization	224 × 224 RGB; per-channel mean–std normalization
Optimizer & LR	Adam; initial LR = 3×10^{-4}
LR schedule & early stopping	Cosine decay; patience = 10; best checkpoint by validation F1
Training regime	Batch size = 32; 60 epochs
Loss & augmentation	Class-balanced cross-entropy; flip/rotate/zoom/shift (p = 0.5 each)
Split & seed	70/15/15 (plot-wise, no leakage); seed = 42
Framework & hardware	PyTorch (specify version); 1× GPU or edge device (report latency separately)

Table 3. Nutrient-deficiency classification on the held-out test set

Model (Backbone)	Input Resolution	Parameters (M)	Accuracy (%)
MobileNetV2 (Baseline)	224 × 224	3.4	82.0
DenseNet-121 (Proposed)	224 × 224	8.0	89.0

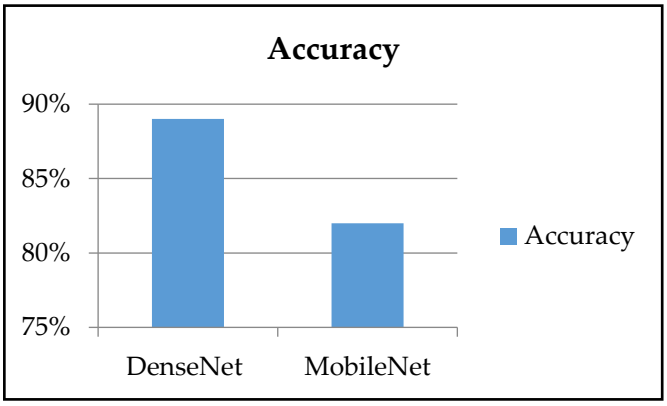


Figure 10. Accuracy Comparison

4. Conclusion and Future Enhancements

This paper presents an IoT and AI plant monitoring system that fuses soil moisture, temperature, and humidity sensing with camera-based leaf analysis for early nutrient deficiency detection. A microcontroller executes thresholded, hysteresis-aware control of irrigation and localized cooling, while a smartphone application provides live telemetry and alerts. Using a DenseNet 121 classifier on 224×224 RGB leaf images, the prototype achieved 89.0% accuracy on a held-out test set, surpassing a MobileNet V2 baseline of 82.0% under identical training settings, resulting in an absolute gain of 7.0 percentage points and a 38.9% reduction in classification error, from 18.0% to 11.0%. These results indicate the practical feasibility of vision-guided recommendations that reduce manual effort and help curb misirrigation, water use, and power consumption. The current implementation is best suited for small plots and greenhouse environments due to its camera coverage and localized actuation. Future work will target wider area deployment with Wi-Fi and a secure cloud backend, as well as larger and more diverse crop datasets, energy-aware on-device inference, and explainable diagnostic feedback for safe fertilizer recommendations.

Author Contributions: Conceptualization, J. Serin, Eben Angel Pauline, Jenefa.A. Ebenezer; methodology, J. Serin and V. Ebenezer; software, K. Arul Jeyaraj; validation, J. Serin, Eben Angel Pauline, and G. Gifta Jerith; formal analysis, J. Serin; investigation, M. Varghese; resources, K. Arul Jeyaraj; data curation, K. Arul Jeyaraj and M. Varghese; writing—original draft preparation, J. Serin; writing—review and editing, V. Ebenezer and M. Varghese; visualization, G. Gifta Jerith; supervision, V. Ebenezer. All authors have read and agreed to the published version of the manuscript.

Funding: This research received no external funding.

Conflicts of Interest: The authors declare that they have no conflicts of interest.

References

[1] Nuchhi, S.; Bagali, V.; Annigeri, S. IoT based soil testing instrument for agriculture purpose. In *2020 IEEE Bangalore Humanitarian Technology Conference*, Vijiyapur, India, October 8–10, **2020**. https://doi.org/10.1109/B-HTC50970.2020.9297897

[2] Yin, H.; Cao, Y.; Marelli, B.; Zeng, X.; Mason, A. J.; Cao, C. Soil sensors and plant wearables for smart and precision agriculture. *Adv. Mater.* **2021**, *33*(20), 2004746. https://doi.org/10.1002/adma.202007764

[3] Kamelia, L.; Nugraha, Y. S.; Effendi, M. R.; Priatna, T. The IoT-based monitoring systems for humidity and soil acidity using wireless communication. In *2019 IEEE 5th International Conference on Wireless and Telematics*, Yogyakarta, Indonesia, July 25–26, **2019**. https://doi.org/10.1109/ICWT47785.2019.8978243

[4] Patel, A.; Swaminarayan, P.; Patel, M. Identification of Nutrition's Deficiency in Plant and Prediction of Nutrition Requirement Using Image Processing. In *Proceedings of the Second International Conference on Information Management and Machine Intelligence*; Singapore, **2020**. https://doi.org/10.1007/978-981-15-9689-6_50

[5] Anthay, S. R.; Chokkalingam, A.; Jeyashanker, K. B.; Natarajan, B. An analysis on micronutrient deficiency in plant leaf and soil using digital image processing. *Indones. J. Electr. Eng. Comput. Sci.* **2022**, *26*(1), 568–575. https://doi.org/10.11591/ijeecs.v26.i1.pp568-575

[6] Anusha, K.; Mahadevaswamy, U. B. Automatic IoT Based Plant Monitoring and Watering System using Raspberry Pi. *Int. J. Eng. Manuf.* **2018**, *8*(6), 55–67. https://doi.org/10.5815/ijem.2018.06.05

[7] Pravin, A.; Jacob, T. P.; Asha, P. Enhancement of plant monitoring using IoT. *Int. J. Eng. Technol. (UAE)* **2018**, *7*(3), 53–55. https://doi.org/10.14419/ijet.v7i3.27.17653

[8] Lakshmi, K.; Gayathri, S. Implementation of IoT with Image processing in plant growth monitoring system. *Int. J. Inf. Technol. Electr. Eng.* **2017**, *6* (2), 80–83. https://doi.org/10.31254/jsir.2017.6208

[9] Sambath, M.; et al. IoT Based Garden Monitoring System. *J. Phys.: Conf. Ser.* **2019**, *1362*, 012028. https://doi.org/10.1088/1742-6596/1362/1/012069

[10] Ali, M.; Kanwal, N.; Hussain, A.; Samiullah, F.; Iftikhar, A.; Qamar, M. IoT based smart garden monitoring system using NodeMCU microcontroller. *Int. J. Eng. Technol. Innov. Res.* **2020**, *7*(8), 117–124. https://doi.org/10.21833/ijaas.2020.08.012

[11] Patil, G.; Patil, A.; Pathmud, S. Plant Monitoring System. *Int. J. Eng. Res. Technol. (IJERT)* **2021**, *10*(9), 101–105. (Assumption made on page numbers based on typical format).

[12] Thamaraimanalan, T.; Vivek, S. P.; Satheeshkumar, G.; Saravanan, P. Smart Garden Monitoring System Using IOT. *Asian J. Appl. Sci. Technol. (AJAST)* **2018**, *2*(2), 186–192.

[13] Kohli, A.; et al. Smart plant monitoring system using IoT technology. In *Handbook of Research on the Internet of Things Applications in Robotics and Automation*; IGI Global: UPES, Dehradun, India, **2020**; pp 318–366. https://doi.org/10.4018/978-1-5225-9574-8.ch016

[14] Athawale, S. V.; Solanki, M.; Sapkal, A.; Gawande, A.; Chaudhari, S. An IoT-Based Smart Plant Monitoring System. In *Smart Computing Paradigms: New Progresses and Challenges*; Springer: Singapore, **2020**; pp 303–310. https://doi.org/10.1007/978-981-13-9680-9_26

[15] Pawar, P.; Gawade, A.; Soni, S.; Sutar, S.; Sonkamble, H. IoT Based Smart Plant Monitoring System. *Int. J. Res. Appl. Sci. Eng. Technol. (IJRASET)* **2022**, *10*(5), 1635–1646. https://doi.org/10.22214/ijraset.2022.42194

[16] Swarnkar, S. K.; Dewangan, L.; Dewangan, O.; Prajapati, T. M.; Rabbi, F. AI-enabled crop health monitoring and nutrient management in smart agriculture. In *2023 6th International Conference on Contemporary Computing and Informatics (IC3I)*; IEEE, **2023**; Vol. 6, pp 2679–2683. https://doi.org/10.1109/IC3I59117.2023.10398035

[17] Naqvi, S. M.; Tahir, M. N.; Raghavan, V.; Awais, M.; Hu, J.; Said, Y.; Othman, N. A.; Ashurov, M.; Khan, M. I. AI-enhanced IoT sensors for real-time crop monitoring: an era towards self-monitored agriculture. *Telecommun. Syst.* **2025**, *88*(3), 1–15. https://doi.org/10.1007/s11235-025-01326-7

[18] Makka, S.; Sarvath, M. A.; Shravya, M.; Meherkrishna, K. Deep Learning-Driven System for Automated Identification of Plant Nutrient Deficiencies. In *2025 3rd International Conference on Communication, Security, and Artificial Intelligence (ICCSAI)*; IEEE, **2025**; pp 936–942. https://doi.org/10.1109/ICCSAI64074.2025.11064196

[19] Shahab, H.; Naeem, M.; Iqbal, M.; Aqeel, M.; Ullah, S. S. IoT-driven smart agricultural technology for real-time soil and crop optimization. *Smart Agric. Technol.* **2025**, *10*, 100847. https://doi.org/10.1016/j.atech.2025.100847

[20] Ahmad, S.; Kaushik, R.; Ghatuary, R.; Kotiyal, A.; Jarial, S.; Kumar, R. Utilizing IoT and AI for Soil Health Monitoring and Enhancement in Sustainable Agriculture. In *IoT and Advanced Intelligence Computation for Smart Agriculture*; CRC Press, **2025**; pp 110–125. https://doi.org/10.1201/9781003527664-7

ASEAN
Journal of Scientific and Technological Reports
Online ISSN:2773-8752

Research article

Predicting E-Commerce Purchase Intention Using Machine Learning

Om Ratna Sheshagiri Gupta Alamuri[1*], and Chaitanya Krishna Bondalapu[1]

[1] Department of CSE, Koneru Lakshmaiah Education Foundation, Vaddeswaram, AP, India
* Correspondence: alamurigupta129@gmail.com

Citation:
Alamuri, O.; Bondalapu, C. Predicting e-commerce purchase intention using machine learning. *ASEAN J. Sci. Tech. Report.* **2026**, *29*(1), e260159. https://doi.org/10.55164/ajstr.v29i1.260159.

Article history:
Received: July 7, 2025
Revised: August 30, 2025
Accepted: September 6, 2025
Available online: December 14, 2025

Publisher's Note:
This article is published and distributed under the terms of the Thaksin University.

Abstract: The fast-evolving digital commerce environment demands precise predictions of consumer buying intentions to develop personalized experiences and boost conversion rates and user satisfaction on e-commerce platforms. The field has extensively utilized traditional statistical models in conjunction with behavioral theories; however, these methods fail to adapt to high-dimensional, imbalanced session-level data. This learning proposes a machine learning-based approach to predict online purchase intention using the widely recognized Online Shoppers Intention dataset. The methodology involves a reproducible pipeline that integrates data preprocessing, the synthetic minority over-sampling technique (SMOTE) to address class imbalance, chi–square–based feature selection, and a comparative evaluation of multiple classification models. The pipeline was tested on a 70:30 train-test split using stratified sampling to maintain class distribution, and further validated through 10-fold cross-validation to enhance robustness. The Support Vector Classifier (SVC) was found to be the best model in terms of both ROC-AUC and F1 score, achieving an ROC-AUC of 0.886 and an F1 Score of 0.633, thereby efficiently discriminating between purchase and non-purchase sessions. We also explore Random Forest, Decision Tree, and Ridge Classifier models to support a more holistic understanding of performance across a variety of complexity and interpretability levels. Importantly, the research also uncovers important behavioral predictors, including product-page engagement and whether the visitor is a returning one, providing interpretable insights that are consistent with real-world e-commerce practices. These results suggest the potential for implementing machine learning models for real-time behavior forecasting in online retail contexts and show that a data-driven pipeline can add value to traditional behavioral modeling counterparts.

Keywords: Customer purchase intention; e-commerce analysis; ML pipeline; SMOTE; chi-square test.

1. Introduction

The growing dominance of e-commerce has transformed consumer interactions with products and services, as digital platforms now serve as the primary channel for retail transactions. Online shopping environments have become increasingly competitive, so businesses now focus on both user acquisition and converting website visitors into buyers. The ability to understand and predict consumer purchase intentions stands as a vital factor for enhancing user experiences, promoting targeted advertising, and optimizing conversion rates. Numerous research studies have examined the psychological

and behavioral factors that influence online purchasing decisions. The Theory of Planned Behavior (TPB) [11], the Technology Acceptance Model (TAM) [2], and the Stimulus-Organism-Response (SOR) theory [1] are primarily used frameworks to analyze customer decisions, focusing on the analysis of perceived trust, enjoyment, and social influence [4]. The research demonstrates that e-service quality [13], along with live-streaming interactivity [10], gamification [4], and real-time engagement [14], play crucial roles in customer intention. The approaches deliver essential insights into consumer behavior but depend on survey-based models and self-reported data, which may not work effectively in real-time decision environments.

E-commerce data faces structural challenges as one of its primary difficulties. The recording of customer interactions through clickstream events generates high-dimensional, noisy data that exhibits severe class imbalance, as actual purchases occur in only a small fraction of sessions [6,3]. The existing research on customer segmentation and loyalty prediction using machine learning models [7,8] requires further development of end-to-end predictive pipelines that integrate feature engineering with imbalance correction and model evaluation within a reproducible framework. This paper discloses these gaps by developing a machine learning-based model to predict online purchase intention using session-level data from the Online Shoppers Intention dataset. The proposed pipeline combines SMOTE for handling class imbalance with SelectKBest using chi-square scoring for feature selection, and multiple classification models, including Support Vector Classifier (SVC), Random Forest, Ridge Classifier, and others. The research aims to discover the optimal combination of preprocessing methods and classification approaches that produce accurate, interpretable, and scalable purchase predictions.

2. Materials and Methods

The project introduces a comprehensive and reproducible machine learning pipeline for predicting online purchase intention using clickstream data. The pipeline addresses significant issues in current methods for handling class imbalance and high dimensionality, while generating interpretable results. The initial stage of the process involves data preprocessing, which utilizes ordinal and binary encoding for the categorical variables VisitorType and Month. Boolean fields, such as Weekend and Revenue, are converted into binary integers. Additionally, missing and infinite values are handled using imputation to ensure data quality. Next, we implement advanced feature engineering by introducing six behavioral indicators—Total Duration, Total Page Visits, Average Page Duration, Product View Ratio, Information View Ratio, and Returning Visitor—which encapsulate user engagement and browsing behavior. After feature scaling with MinMax normalization, the pipeline applies SMOTE to create synthetic samples of the minority class, thereby addressing class imbalance without compromising data integrity [6,12]. The feature selection process is implemented using the chi-square SelectKBest method to retain the most statistically significant predictors [5,11]. Classifiers are verified by using 10-fold cross-validation. This method is in concordance with prior studies that have compared classifier performance based on the performance in behavior prediction tasks [8,10]. The best performance model is selected for final evaluation on an independent test set. This methodology enhances predictive performance and interpretability by utilizing visualization tools, such as ROC curves and feature importance analysis. The ML pipeline is modular and reproducible, and can be used for both academic research and practical deployment into e-commerce real-time systems [12].

2.1 Process Flow

The proposed machine learning pipeline [12] implements a structured, modular framework to achieve consistency and reproducibility, delivering high predictive performance. The initial stage of data cleaning addresses missing values, inconsistent data types, and infinite values by implementing imputation and replacement methods. Boolean variables (Weekend, Revenue) are converted into binary format, and categorical variables (Month, VisitorType) are encoded appropriately for modeling. Next, feature engineering is applied to create new behavioral indicators, such as Total Duration, Average Page Duration, and Product View Ratio, which capture more profound insights into user browsing patterns. This is followed by class imbalance handling using the Synthetic Minority Oversampling Technique (SMOTE) [6,12], which balances the dataset by generating synthetic examples of minority class sessions. Subsequently, the step involves

applying chi-square ranking to select statistically significant predictors, which helps decrease dimensionality and enhance interpretability. The imbpipeline contains all preprocessing steps, alongside balancing and selection functions, which maintain uniform application throughout the training and testing phases. The validation process for machine learning models includes cross-validation and evaluation methods for comparison. The effectively performing model is selected for future analysis and interpretation, providing actionable insights for real-world e-commerce personalization strategies.

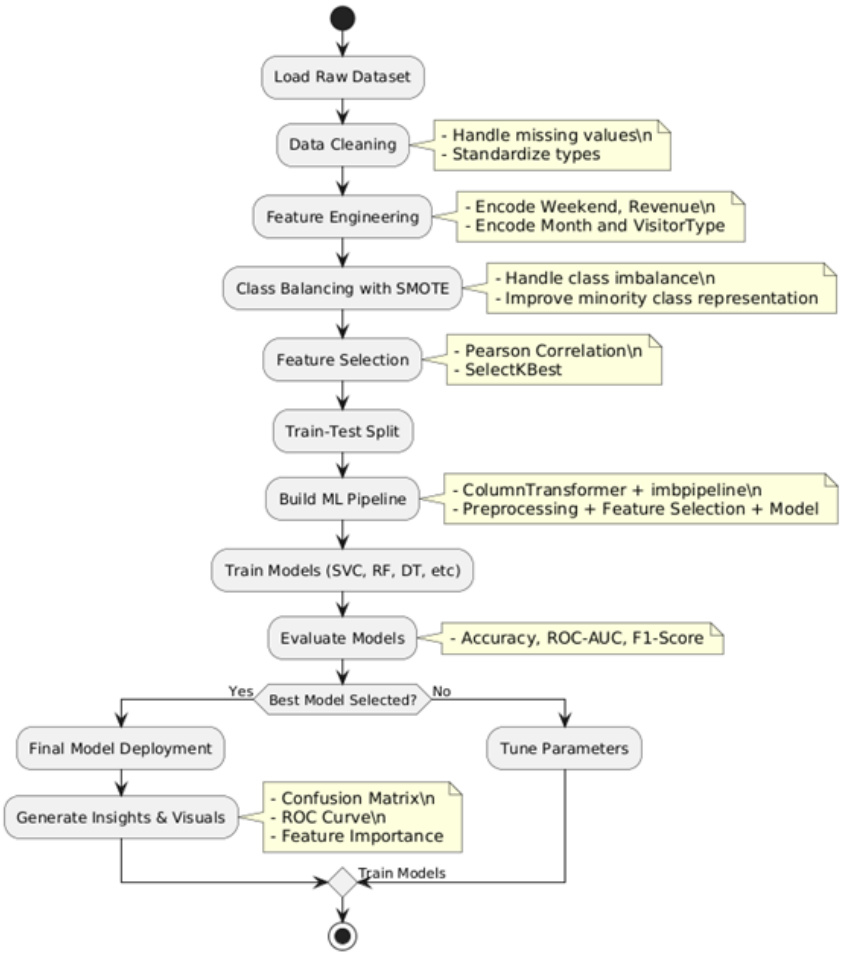


Figure 1. Process flow

2.2 Dataset Description

The dataset used in this paper is the publicly available Online Shoppers Intention Dataset [17], comprising 12,330 records, each representing a complete web browsing session on an e-commerce platform. The dataset contains 18 features, including the number of administrative pages visited, informational pages accessed (Informational), and the corresponding time (Informational_Duration). Additionally, it includes product-related features that typically reflect purchase intention more directly. The session-level engagement becomes visible through behavioral metrics, which include Bounce Rates (percentage of single-page visits), Exit Rates (percentage of users exiting from a given page), Page Values (estimated monetary value of visited pages), and Special Days (a score indicating proximity to a special date, such as holidays or sales events). Technical attributes include session information such as the Month, Operating Systems used, Browser type, Region of the user, and Traffic Type, which indicates the source of the web traffic. The visitor information section includes VisitorType, which identifies whether the user is new or returning, and a Boolean field, Weekend, to denote whether the session occurred on a weekend. The output variable "Revenue" is a Boolean indicating whether a purchase was made, and serves as the label for supervised learning.

Table 1. Features Description

Feature	Description
Administrative	Number of administrative pages visited
Administrative_Duration	Total time (in seconds) spent on administrative pages
Informational	Number of informational pages visited
Informational_Duration	Total time spent on informational pages
ProductRelated	Number of product-related pages visited
ProductRelated_Duration	Total time spent on product-related pages
BounceRates	Average bounce rate of pages visited
ExitRates	Average exit rate of pages visited
PageValues	Average page value of pages visited
SpecialDay	Closeness of session date to a special day (0 to 1)
Month	Month of the visit (January–December, encoded)
OperatingSystems	The operating system used by the visitor
Browser	Web browser used by the visitor
Region	Visitor's geographic region
TrafficType	Source of traffic (e.g., direct, referral, ads)
Weekend	Whether the session was on a weekend (0 = No, 1 = Yes)
Visitor Type	Type of visitor: Returning Visitor, New Visitor, or Other
Revenue	Whether the session ended in a purchase (0 = No, 1 = Yes)

2.3 Data Cleaning

The first step involved data preparation of the Online Shoppers Intention dataset prior to analysis. The Weekend and Revenue boolean columns received binary integer transformations (0 or 1) while VisitorType received encoding for categorical fields. The feature engineering process required division operation value replacement with zero and constant-value imputation for handling missing data. The dataset was made free from inconsistencies, null values, and unprocessable formats through these steps, as these issues commonly cause machine learning model failures and bias. The standardized format created during this phase enabled a seamless transition to advanced processing stages, including feature engineering, modeling, and evaluation. The cleaning process prevented data-related errors from being passed through to subsequent transformations and predictions, which would have compromised the overall reliability of the predictive system.

2.4 Feature Engineering

Here, we conducted extensive feature engineering to enhance model interpretability and gain a deeper understanding of user behaviors. The existing attributes received six new behavioral indicators, which included Total_Duration (the aggregate time spent across all page types), Total_Page_Visits (the total number of pages visited during a session), Avg_Page_Duration (the average time per page), ProductView_Ratio, InfoView_Ratio, and Returning_Visitor (a binary indicator of repeat visits).

$$\text{Total_Duration} = \text{Admimistrative_Duration} + \text{Informational_Duration} + \text{ProductRelated_Duration} \quad (1)$$

$$\text{Total_Page_Visits} = \text{Administrative} + \text{Informational} + \text{ProductRelated} \quad (2)$$

$$\text{Avg_Page_Duration} = \frac{\text{Total_Duration}}{\text{Total_Page_Visits}} \quad (3)$$

$$\text{ProductView_Ratio} = \frac{\text{ProductRelated}}{\text{Total_Page_Visits}} \quad (4)$$

$$\text{InfoView_Ratio} = \frac{\text{Informational}}{\text{Total_Page_Visits}} \quad (5)$$

The Month column was ordinally encoded to reflect potential seasonal effects. The new features were designed to detect user engagement and navigation patterns that affect online purchasing decisions. The feature engineering process both increased the dataset size and improved the ability of machine learning models to differentiate between browsing and purchase-intent sessions. The transformations converted intricate user interactions into organized variables, which enhanced both the model's precision and the business value of the extracted knowledge.

2.4.1 Weekend & Revenue Column

The preprocessing phase involved converting the Boolean features 'Weekend' and 'Revenue' from the dataset into a numerical binary format to make them suitable for machine learning algorithms. The initial Boolean values (True, False) in the features needed conversion because most machine learning models require numerical data. The Python replace () method converted True to '1' and False to '0' to solve this issue. The model could understand these features as binary indicators through this transformation because it maintained their semantic meaning while matching the numerical requirements of the feature space. The conversion process prevents type incompatibility problems during model training and enables algorithms to detect the predictive value of binary variables in purchase intention outcomes.

	Administrative	Administrative_Duration	Informational	...	VisitorType	Weekend	Revenue
0	0	0.0	0	...	Returning_Visitor	0	0
1	0	0.0	0	...	Returning_Visitor	0	0
2	0	0.0	0	...	Returning_Visitor	0	0
3	0	0.0	0	...	Returning_Visitor	0	0
4	0	0.0	0	...	Returning_Visitor	1	0

Figure 2. Boolean to Binary Conversion

2.4.2 Visitor_Type Column

The dataset includes a VisitorType column that has a categorical value indicating whether the visitor is a false visitor or a true visitor. A Returning Visitor or a New Visitor started the session. The two groups are mutually exclusive; therefore, there is no overlap, and it is redundant to use both for predictive modeling. Thus, we created a new column, Returning_Visitor, containing the value '1' if the session was from a return visitor and '0' otherwise. This was achieved by storing the data in a new column in the dataframe, minimizing its categorical complexity while preserving the fundamental behavioral difference between repeat and first-time visitors. Writing this variable with a binary coding guarantees that machine learning models can easily understand it.

	Administrative	Administrative_Duration	Informational	...	Weekend	Revenue	Returning_Visitor
0	0	0.0	0	...	0	0	1
1	0	0.0	0	...	0	0	1
2	0	0.0	0	...	0	0	1
3	0	0.0	0	...	0	0	1
4	0	0.0	0	...	1	0	1

Figure 3. Adding Returning_Visitor

2.4.3 Month Column

The dataset contains a 'Month' column that shows the calendar month in which each session occurred. The Month column exists as an object (string) data type by default, which prevents direct processing. The conversion of categorical data into numerical data using Ordinal Encoding, which assigns integer values to each category based on its sequential order. The months received integer values from 0 to 11 through the encoding process, which maintained their chronological order. The sequential nature of ordinal categorical variables makes Ordinal Encoding the better choice than one-hot encoding for nominal categories without inherent ranking. The application of Ordinal Encoding to the Month column maintains sequential relationships between categories, which helps machine learning models detect seasonal patterns and time-based trends that affect purchase intention, while reducing dimensionality compared to one-hot encoding [11-12].

2.4.4 Target Column

The Revenue column serves as the target variable to determine if users completed purchases during their sessions. The default representation of this column uses Boolean values, which indicate True for purchases and False for non-purchases. The majority of machine learning models require numerical representations of targets to perform classification tasks. The replace() method converted the Revenue column into binary format by establishing the following mapping:

$$\text{True} \rightarrow 1, \text{False} \rightarrow 0$$

The transformation preserves the original meaning of the data while converting it into a format suitable for supervised learning models. The binary target enables us to define the problem as a binary classification task, which aims to predict whether a session belongs to the positive class (Revenue = 1) or the negative class (Revenue = 0). The model requires this preprocessing step to correctly interpret labels and achieve optimal accuracy, precision, recall, and ROC-AUC performance metrics.

```
Revenue
0    10422
1     1908
Name: count, dtype: int64
```

Figure 4. Revenue column values count

2.5 Pearson Correlation

The Pearson correlation coefficient finds the relationship between numerical features and the target variable. The Pearson correlation coefficient measures linear relationships between continuous variables by using its r value, which ranges from -1 to 1. The correlation values r = 1, r = -1, and r = 0 indicate a perfect positive linear relationship, a perfect negative linear relationship, and no linear relationship, respectively.

$$r = \frac{\sum_{i=1}^{n} (X_i - \overline{X})(Y_i - \overline{Y})}{\sqrt{\sum_{i=1}^{n} (X_i - \overline{X})^2} \sqrt{\sum_{i=1}^{n} (Y_i - \overline{Y})^2}} \quad (6)$$

The complete correlation matrix was visualized through a heatmap, which displayed the strength and direction of feature correlations using cell color intensity. The heatmap enabled us to identify strong correlations between features while helping us evaluate potential multicollinearity. A horizontal bar chart

displayed the correlation coefficients between Revenue and each feature in descending order of magnitude. The visualization demonstrated that ProductRelated, PageValues, and BounceRates were the most important predictors of purchase intention, while showing that other attributes had weaker effects. The graphical analyses provided straightforward insights about feature importance, which directed our subsequent feature selection and modeling work.

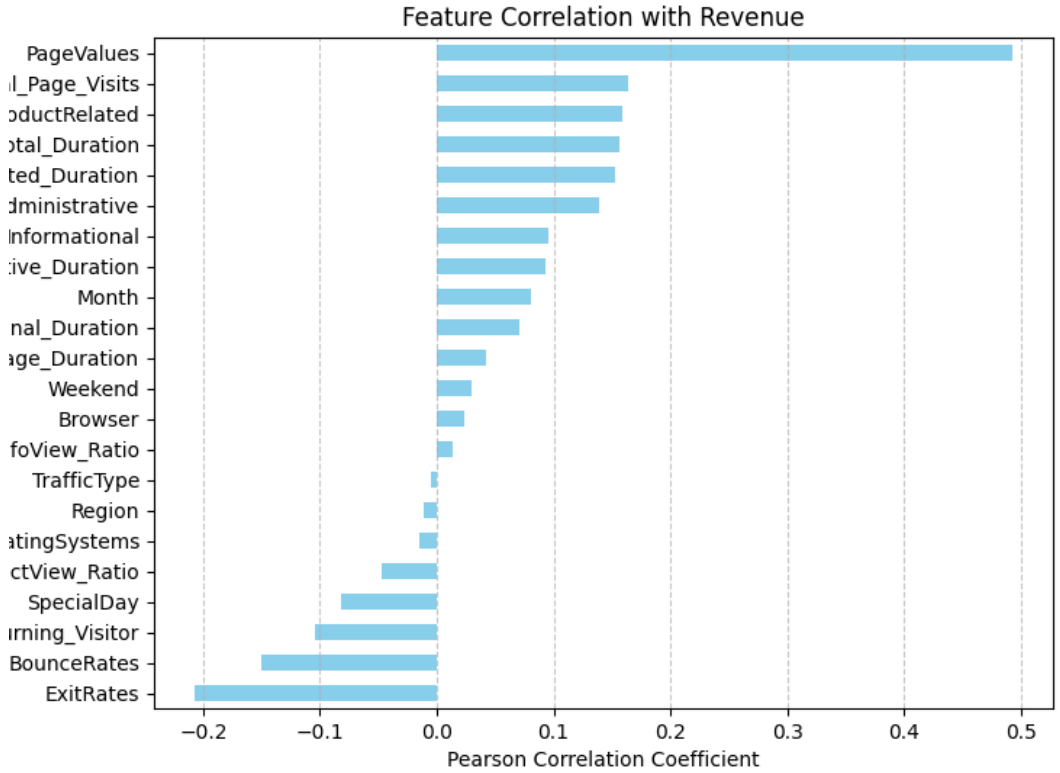


Figure 5. (Bar Plot) Pearson Correlation Coefficient

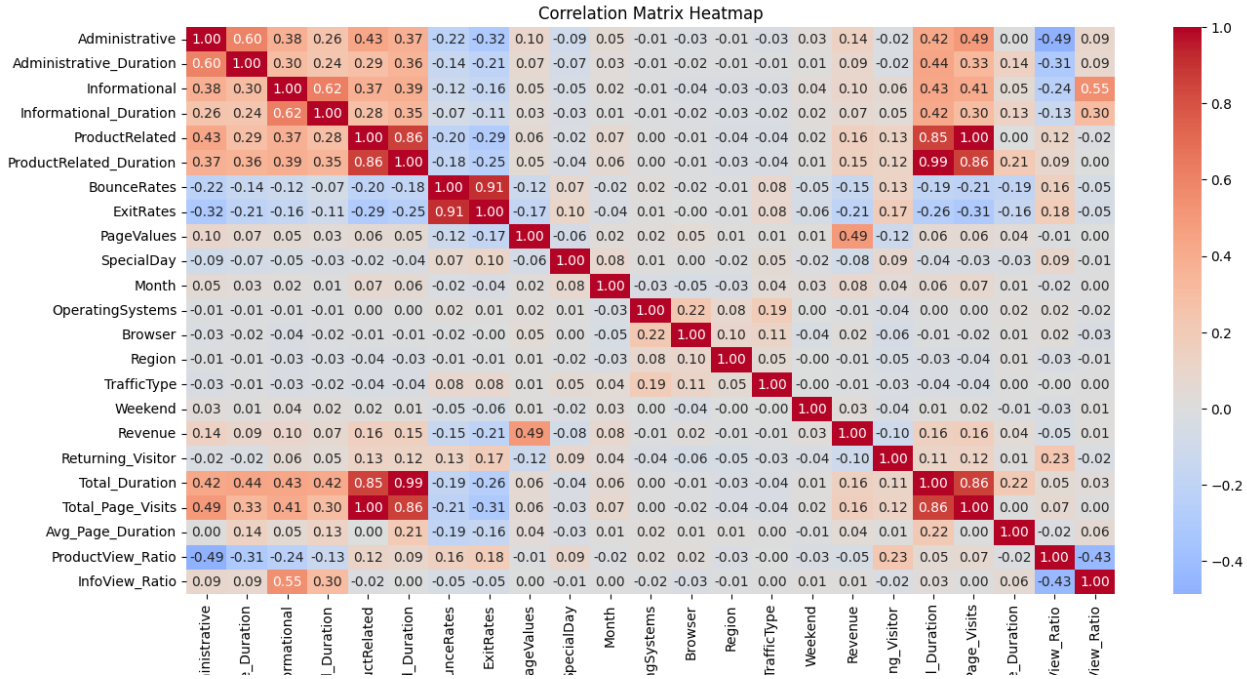


Figure 6. Correlation Matrix Heatmap

2.6 Training & Test Data

The dataset was prepared for supervised machine learning, with the input features (X) and target variable (y). The features of the input were all related variables obtained either by preprocessing or feature engineering. These attributes were related to user actions, session properties, and technical attributes of browsing behavior. The dependent variable was based on the Revenue attribute, indicating whether the user session resulted in a transaction (1) or not (0). A training and testing dataset was then prepared for model development and validation. Dividing the dataset by using the function train_test_split () of the scikit-learn library, where the training and testing sets of the data were split in the ratio 70:30 (70% training, 30% testing). The model trains on a wide range of data through this splitting method while evaluating its performance on an independent subset. Additionally, stratified randomization (stratify=y) was employed to preserve the original class distribution (purchase vs. non-purchase) in both training and testing subsets, thereby preventing skew in class proportions. A constant random state (i.e., 0) was used to ensure the same data partitioning was applied across replicates. This guarantees reproducibility of the findings. This type of splitting allows the model to train on a wide range of the data, while still evaluating it on an entirely independent subset. The 70:30 split was chosen because it offers an optimal balance between providing sufficient data for training complex models while maintaining a large enough independent test set to yield statistically reliable performance estimates. The training set included 8,631 sessions, consisting of 7,295 non-purchase and 1,336 purchase cases. The testing set contained 3,699 sessions, with 3,127 non-purchase and 572 purchase cases.

2.7 Machine Learning Pipeline

The machine learning pipeline utilizes ColumnTransformer and imblearn—pipeline to construct a consistent and reproducible modeling process. The pipeline consisted of five stages, which included imputation, followed by MinMax scaling, then SMOTE oversampling, chi-square-based feature selection, and finally a classifier. The pipeline structure contained all preprocessing steps, which were applied to both training and testing sets to prevent data leaks. The pipeline design included flexible components to enable easy substitution and evaluation of different classifiers. The pipeline design supported hyperparameter tuning and cross-validation operations with automatic reprocessing capabilities. The system design adhered to best practices for machine learning development and deployment, optimizing the entire training and evaluation process for real-world e-commerce implementation. A Machine Learning pipeline workflow is automated that handles a complete processing task. The process combines data transformation with correlation steps into a model structure for output analysis. A standard pipeline consists of raw data input, features, outputs, model parameters, ML models, and Predictions. The pipeline is built with consecutive steps that execute data extraction and pre-processing, as well as model training and deployment, in a modular way for Machine learning. We developed a model pipeline for our project, which employs the ColumnTransformer() to handle data encoding. This replaces any absent values with possible values. It normalizes the data before we input it into the model.

2.7.1 SMOTE

The imbalance of classes is a drawback in this dataset, as only about 15.5% of the sessions were purchase sessions. This class imbalance has the potential to make the model biased towards the minority class, which is less prone to valuable patterns for minorities. To address this, we used the Synthetic Minority Oversampling Technique (SMOTE) instead of simple random oversampling, as SMOTE generates synthetic samples within the feature space rather than merely duplicating minority class samples. This reduces the risk of overfitting in the class imbalance problem. Data balancing SMOTE creates new artificial purchase examples for the minority class by interpolating between existing purchase examples, thereby rebalancing the class distribution without replicating data [6,12]. By doing SMOTE in the normalized feature space, the synthetic samples are realistic and well-mingled. This led to a significant improvement in model performance, particularly in learning from minority purchase sessions, resulting in increased recall and F1-score for the minority class. It also served as a solution to circumvent overfitting to the majority class, a pitfall often associated with straightforward oversampling or underweighting approaches [8]. Alternative methods, such

as ADASYN or Random Oversampling, were considered, but we chose SMOTE for its balance between simplicity and robustness, as supported by previous e-commerce prediction studies.

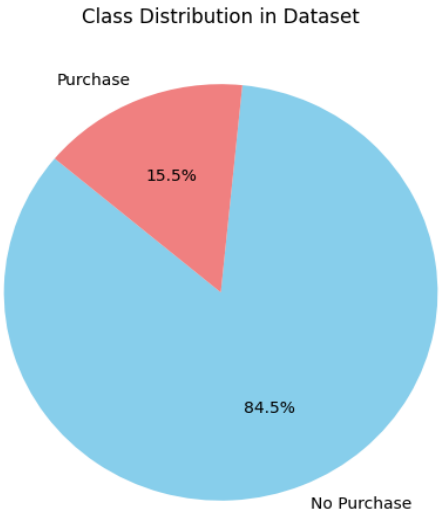


Figure 7. Class Distribution

2.7.2 Imbpipeline

The study utilizes the imbalanced-learn package's imbalanced pipeline module [16] to achieve a robust and reproducible machine learning workflow. The imbalanced pipeline class in scikit-learn extends the standard Pipeline class by integrating checking approaches into its pipeline structure for handling class-imbalanced datasets.

The imbalanced pipeline differs from typical pipelines because it enables the addition of checking techniques, including the Synthetic Minority Oversampling Technique (SMOTE), within each cross-validation fold. The design of this approach restricts oversampling to the training data during model evaluation, thereby precluding data leakage into the test set and maintaining genuine performance criteria.

The imbpipeline receives the following factors during its methodical configuration.

- Preprocessing: Imputation, scaling, and encoding
- Resampling: SMOTE for balancing minority-class samples
- Feature selection: Chi-square–based SelectKBest
- Classifier: Various models (e.g., SVC, Random Forest, Naïve Bayes)

The modular and scalable channel frame promotes thickness across experimental setups. The frame ensures that everything, from preprocessing to final evaluation, will be executed identically. The frame enables unprejudiced model comparisons between different classifiers while enhancing real-world model conception capabilities.

2.7.3 SelectKBest

The SelectKBest algorithm functions as a univariate feature selection method from the scikit-learn library. The algorithm selects the top k labels from the dataset through statistical tests that evaluate the strength of the relationship between each feature and the target variable. The project utilized the ANOVA F-test (f_classif) as the scoring function because the target variable is categorical. In this project, the ANOVA F-test (f_classif) was used as the scoring function, as the target variable is categorical. The F-test measures the strength of association between each feature and the target class by comparing the variance between groups with the variance within groups. SelectKBest was applied after preliminary correlation filtering to reduce feature dimensionality, improve model performance, and prevent overfitting. We used chi-square–based

SelectKBest for final feature ranking and retained the top 6 statistically significant features. By retaining only the top-ranked features, the model was trained on the most statistically significant predictors, including PageValues, ExitRates, ProductRelated_Duration, Returning_Visitor, BounceRates, and Total_Duration.

For dimensionality reduction, we employed the Chi-Square (χ^2) statistical test because most input variables are categorical or non-negative numerical counts (e.g., page visits, durations). Chi-Square effectively measures the independence between each feature and the target variable (Revenue), making it suitable for classification tasks. While methods like mutual information gain or recursive feature elimination (RFE) could also be used, χ^2 was preferred because it is computationally efficient and interpretable, ensuring that only the most statistically significant predictors (e.g., PageValues, ExitRates) are retained.

ANOVA F-test to select the top k features:

$$F = \frac{\text{Variance between groups}}{\text{Variance within groups}} \tag{7}$$

2.8 Select_model

To select the best model, we created a single function that automatically tests all models and finally returns the best model as per our requirements. It is possible to loop over those models and then apply the data through the pipeline for each model. Using cross-validation to get the best performance, reliability, and accuracy of each model. Save the model results to a pandas DataFrame and see the outcome. Finally, select the optimal model having the maximum ROC/AUC score.select_model(X, y, pipeline = None) is a user defined function. This function takes 2 non-default parameters and 1 default parameter:

- X (object): Dataframe containing X_train data
- y (object): Dataframe containing y_train data
- pipeline: Pipeline from model_pipeline()

2.9 Models Evaluated

We evaluated a diverse set of machine learning classifiers within the proposed pipeline, integrating oversampling, feature selection, and classification to identify the approach that best balances accuracy, robustness, and interpretability for real-time e-commerce personalization.

Support Vector Classifier (SVC):

The core prediction engine is an SVC with an RBF (Radial Basis Function) kernel. It identifies the optimal hyperplane that maximizes the margin between classes in a transformed feature space, making them well-suited for high-dimensional problems. We enabled probability estimates (probability=True) to facilitate threshold tuning and business-driven decision-making. The RBF kernel was specifically chosen because it effectively handles non-linear relationships in the data [8].

Random Forest (RF) Classifier:

This algorithm is a collaborative method that constructs several decision trees on bootstrapped samples and combines their outputs for classification. Its inherent feature bagging reduces variance and often yields strong baseline performance on clickstream tasks. We included it as a benchmark against a robust, non-linear learner. In this, the Random Forest was configured with 100 trees (n_estimators=100), ensuring performance stability [6].

Bernoulli Naïve Bayes:

The BernoulliNB classifier models binary features under the assumption of conditional independence. Despite its simplicity, it can perform surprisingly well on sparse or binarized clickstream data [5] and serves as a lightweight baseline in our comparisons.

Ridge Classifier:

The Ridge Classifier uses L2-regularized linear regression for classification tasks by thresholding the

continuous outputs. The L2 penalty controls model complexity [11] and mitigates overfitting, making it particularly useful in high-dimensional feature spaces. The model was applied with its default regularization strength (α = 1.0).

K-Nearest Neighbors (KNN):

KNN predicts a session's class by considering the majority class label among its k neighbors in the feature space. It requires no explicit training phase, making it a practical nonparametric comparator [7], though its performance can degrade in high-dimensional settings. Using the default k = 5 leads to a good balance between bias and variance.

Decision Tree Classifier:

The Decision Tree Classifier recursively partitions the feature space to construct a tree of decision rules. Its intuitive, rule-based structure offers clear interpretability, but single trees are prone to overfitting [12], making it valuable for illustrating the trade-off between simplicity and predictive power. The model was implemented using the Gini index as the criterion for splitting.

2.10 Evaluation Metrics

To comprehensively measure model performance, we employed a set of well-established evaluation metrics, particularly suited for imbalanced binary classification tasks, such as purchase intention prediction.

Accuracy

Accuracy calculates the overall proportion of rightly classified cases (both purchase and non-purchase). While useful, accuracy alone can be misleading in imbalanced datasets because high accuracy may be affected by prognosticating only the dominant class.

$$\text{Auc} = \frac{\text{T_P} + \text{T_N}}{\text{F_P} + \text{F_N} * \text{T_P} + \text{T_N}} \tag{8}$$

where T_P = true positives, T_N = true negatives, F_P = false positives, and F_N = false negatives

Precision

Precision quantifies the part of predicted positive cases (purchases) that are actually correct. High precision diminishes the possibility of false positives, which is vital when targeting marketing resources.

$$\text{Precision} = \frac{\text{T_P}}{\text{T_P} + \text{F_P}} \tag{9}$$

Recall

Recall measures the part of actual positive cases (purchases) that the model successfully identifies. More recall is critical to ensure that most potential purchasers are correctly flagged, even if it means incurring some false alarms.

$$\text{Recall} = \frac{\text{T_P}}{\text{T_P} + \text{F_N}} \tag{10}$$

F1 Score

F1 measures the harmonic mean of precision and recall, which allows a balanced assessment when both false positives and false negatives are important. It is especially enlightening in unbalanced datasets.

$$\text{F1} = 2 * \frac{\text{Precision} * \text{Recall}}{\text{Precision} + \text{Recall}} \tag{11}$$

ROC-AUC (Receiver Operating Characteristic – Area Under the Curve)

ROC-AUC estimates the model's capability to differentiate among classes at various decision thresholds. It calculates the area under the ROC curve, which plots the true positive rate (TPR) against the false positive rate (FPR) at various threshold levels.

$$\text{AUC} = \int_0^1 \text{TPR}(\text{FPR})\text{dFPR} \tag{12}$$

By combining these metrics, we gained a nuanced understanding of each model's strengths and weaknesses, particularly in relation to the minority (purchase) class, which is the key target for actionable e-commerce insights.

3. Results and Discussion

3.1 Model Evaluation and Comparative Performance

This pipeline was applied to six classifiers (SVC, Random Forest, Decision Tree, Ridge Classifier, Bernoulli Naïve Bayes, and KNN) to obtain a better model for online purchase intention prediction. Among those, SVC was the most robust model with the highest ROC-AUC (0.886) and F1-score (0.633), indicating its reasonable and balanced discrimination and good performance in balancing the imbalanced data. The Random Forest model came second, with a good ROC-AUC score of 0.882, while Decision Tree, Ridge Classifier, BernoulliNB, and KNN performed in the middle and served as reasonable comparisons. The performance of the models was evaluated using five performance metrics: accuracy, precision, recall, F1-score, and ROC-AUC. These collectively presented an equanimous understanding of predictivity, particularly in imbalanced binary classifications. Support Vector Classification achieves the highest accuracy (88.3%) and ROC-AUC (0.886) for the task of distinguishing between purchase and non-purchase sessions. It also showed a balanced trade-off between minimizing false positives and capturing true purchase signals with an F1-score of 0.633. Random Forest and Decision Tree worked stably on non-linear patterns, while Ridge, Naïve Bayes, and KNN models performed similarly, as they had a limited ability to capture the minority class.

Table 2. Performance comparison of all classifiers

Classifier	ROC-AUC	Accuracy	Precision	Recall	F1-Score
SVC(RBF)	0.886	0.883	0.619	0.654	0.633
Random Forest	0.882	0.872	0.567	0.739	0.641
BenouliNB	0.852	0.872	0.561	0.810	0.663
KNN	0.836	0.853	0.520	0.696	0.594
Decision Tree	0.727	0.852	0.520	0.585	0.550
Ridge Classifier	0.851	0.819	0.449	0.700	0.546

[1]SVC - Support Vector Classifier, [2]RBF - Radial Basis Function, [3]KNN - K-Nearest Neighbors

SVC has the capacity to represent non-linear decision boundaries and exhibits robustness in high-dimensional feature spaces, facilitating generalization across a variety of sessions. Consequently, it was the most dependable model in predicting online purchase intentions. In contrast, the Random Forest (RF) classifier demonstrated high recall capabilities due to its ensemble learning method of aggregating multiple decision trees. This features a trade-off; although RF could handle a greater number of positive purchase cases, precision was sacrificed, resulting in more false positives (FP). Therefore, we consider RF to be a beneficial alternative model in cases where recall is more important than precision (e.g., maximizing potential buyer discovery in target marketing). The Bernoulli Naïve Bayes (BernoulliNB) classifier with the maximum recall (0.81) further demonstrates its ability to handle binary-like session information. However, due to the independence assumption, a sharp decrease in the precision value was observed as well as a significant deterioration in the overall F1-score (95%), which hindered its usefulness as an individual predictive predictor. Other classifiers, such as Decision Tree, Ridge Classifier, and K-Nearest Neighbor (KNN) appear to be worse.

Decision Trees overfitted, Ridge Classifier was limited by its linearity, and KNN failed under high-dimensionality (the curse of dimensionality). These results further highlight the importance of being able to learn non-linear patterns. Altogether, results show SVC performs the best on average according to the tradeoff of accuracy, ROC-AUC, and F1-score, so that it is the optimal choice for prediction.

3.2 Feature Relevance and Interpretability

Feature importance analysis, conducted using the chi-square test and Pearson correlation, revealed that PageValues, ProductRelated, and ExitRates were the most significant predictors of purchase behavior. This aligns with behavioral theories and past literature [11, 7], emphasizing that high product page engagement and exit patterns near checkout stages are strong indicators of purchase intent. Visual heatmaps and bar plots confirmed the statistical significance of these features in distinguishing between buyer sessions and non-buyers, validating the design of the feature engineering process. Figure 8 presents the chi–square–based feature importance rankings, where behavioral features, such as Returning_Visitor, PageValues, and ProductRelated_Duration, consistently ranked highest.

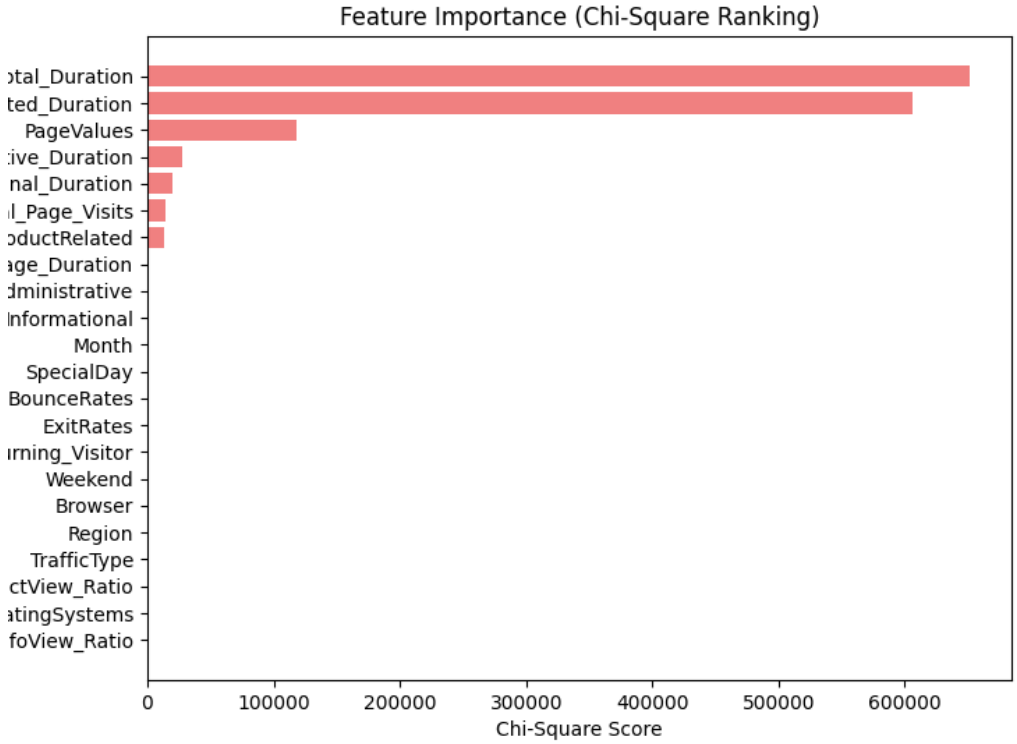


Figure 8. Feature importance (chi-square ranking)

3.3 Visual Evaluation of Model Outputs

To support quantitative metrics, Figure 9 displays ROC curves for all classifiers, providing a visual interpretation of each model's ability to trade off true positive and false positive rates over various thresholds. Figure 10 illustrates the confusion matrices, showing classification accuracy and class-specific errors for both majority and minority classes. These visuals confirm the SVC's superior discrimination, as well as the relative assets and faintness of the remaining models.

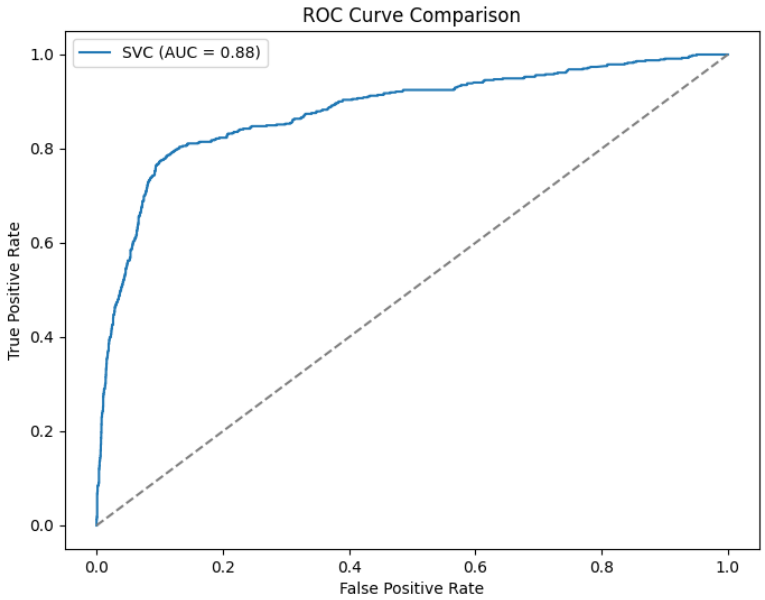


Figure 9. Roc Curve Comparison

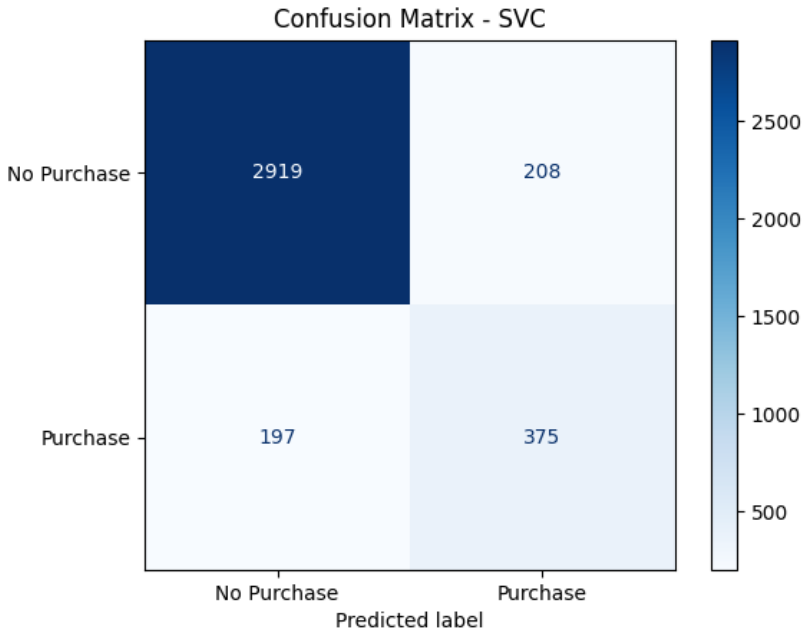


Figure 10. Confusion Matrix

3.4 Insights into User Behavior

Model interpretation revealed that returning visitors had a higher likelihood of completing purchases, particularly during weekends and near special days. Sessions characterized by greater product interaction time (Total_Duration), lower bounce rates, and higher PageValues were more likely to convert. These insights corroborate findings from prior studies in live-streaming and gamified commerce platforms [1, 10], where user attention and engagement depth emerged as key purchase drivers.

3.5 Implications and Strategic Value

The pipeline is useful in real-time marketing and personalization for e-commerce operations. The platform enables businesses to concentrate on purchase-intent sessions and serve personalized offers and optimal product display sequences based on predictive behavior modeling. The modularity of the pipeline

enables businesses to implement it on other platforms with minimal modifications, resulting in higher scalability and practical applicability.

3.6 Comparative Analysis with Existing Studies

The Support Vector Classifier (SVC) performs best for online purchase intention prediction, with an F1-score of 0.633 and an ROC-AUC of 0.886. The results align with earlier research, which suggests that SVM-based models outperform linear classifiers because they can detect non-linear patterns in large e-commerce datasets [5], [8]. These research findings gain additional strength through the comparison with earlier studies. The predictive accuracy of Logistic Regression and Decision Trees was lower than that of the current study because these models failed to detect non-linear patterns in the data [3]. The results align with our findings, as Decision Trees yielded lower F1-scores due to overfitting. The research conducted by [7] analyzed Naïve Bayes for purchase prediction because this model performs well with sparse binary data. The results confirm that BernoulliNB produced the best recall at 0.81; however, its precision remained low, which restricted the overall performance. Recent research has focused on developing ensemble approaches and deep learning algorithms. The purchaser detection results from Random Forest and Gradient Boosting showed improved recall rates [12], which aligns with our findings that Random Forest outperformed SVC in recall, but SVC maintained better F1 and ROC-AUC scores. The sequential data analysis capabilities of deep learning models, such as LSTMs, in clickstream data [14], come at a high computational expense that makes them impractical for real-time prediction compared to SVC. The evidence shows that non-linear learners (SVC and Random Forest) perform better than linear approaches in purchase intention prediction, but their performance depends on the characteristics of the dataset and the effectiveness of feature engineering and balancing techniques like SMOTE.

3.7 Limitations and Future Directions

The proposed machine learning pipeline performs effectively, addressing challenges such as class imbalance and high dimensionality. However, it has a limitation in the Online Shoppers Intention dataset, which represents user interactions as static, session-based records. By treating sessions as static, this method disregards the temporal patterns in consumer behavior, which play a vital role in shaping purchasing decisions. Despite the good performance, the current pipeline presents both training as a whole and user interactions as static, and they do not interact with each other. One possible future direction is to incorporate temporal or sequential modeling (e.g., RNNs or transformers) in order to capture changing contexts within a session. Moreover, the presentation of explainable AI methods (such as SHAP or LIME) may empower model transparency and facilitate the interpretation of the model by business end-users. Together, these directions open pathways toward building more dynamic, interpretable, and business-oriented predictive systems.

4. Conclusions

In this paper, a robust and interpretable pipeline for machine learning to predict online purchase intention was suggested, with which a part of the behavioral click stream data (from the Online Shoppers Intention repository) was employed. The study addressed key problems in this realm, including the class imbalance problem, high dimensionality, and the requirement for interpretability in real-time decision systems. By implementing a series of preprocessing, feature engineering, SMOTE-based class balancing, and chi-square feature selection, this study designed a scalable workflow that was tested on six popular classifiers. The hyper-SVC was the top-performing model, with an ROC-AUC of 0.886, and the accuracy for the best-performing model was 88.3%, which is sufficient for distinguishing between purchasing and non-purchasing sessions. PageValues, ProductRelated duration, and Returning_Visitor variables were among the key behavioral indicators that were highly associated with purchasing. Not only did the pipeline retain predictive ability, but it also allowed for the clear interpretation of feature relevance through statistical and visual examination. The contribution of the study is in showing how scalable and reproducible ML pipelines can be used to improve e-commerce personalization applied to a highly imbalanced dataset. It also emphasizes the importance of preprocessing choices, model selection, and interpretability in practical applications. However, the model assumes user behavior to be static and session-based, failing to account for temporal sequence and

cross-session behavior. A natural next step in research would be to apply sequence-based deep learning techniques, such as recurrent or attention-based mechanisms, for modeling the evolution of intent. Furthermore, the inclusion of XAI techniques can also provide an additional level of transparency and trust in AP for personalization systems.

5. Acknowledgements

Author Contributions: Om Ratna Sheshagiri Gupta Alamuri led the conceptualization of the research problem and the development of the methodology. He designed and implemented the data preprocessing and feature engineering pipeline, employing SMOTE for class imbalance correction and Chi-square–based feature selection. He executed the complete machine learning workflow, including model training with classifiers such as Support Vector Classifier (SVC), Random Forest, and Ridge Classifier. Additionally, he conducted thorough model evaluations using ROC-AUC, F1-score, and cross-validation metrics. He performed detailed experimental analyses, generated all visual representations and tables—including process flows, ROC curves, and confusion matrices—interpreted behavioural insights such as the significance of Page Values and Returning Visitor metrics, and prepared the initial manuscript draft.

Chaitanya Krishna Bondalapu provided expert supervision and strategic oversight, contributing to methodological enhancements, validation of analytical results, and ensuring alignment with industry standards in e-commerce behavioral analytics. He critically reviewed and substantively edited the manuscript to enhance technical accuracy, clarity, and coherence. Furthermore, he offered guidance on comparative model assessments, interpretability techniques including Pearson correlation and feature importance analyses, as well as implications for real-time personalization frameworks. His involvement was instrumental in maintaining the rigor, reproducibility, and integrity of the research, while also strengthening the discussion on study limitations and prospective future work, including sequential modelling approaches.

All authors have reviewed and approved the final version of the manuscript.

Funding: This study was conducted without any specific financial support from public, commercial, or not-for-profit funding agencies. No funding sources influenced the research procedures or outcomes.

Conflicts of Interest: The authors declare no conflicts of interest regarding the research, authorship, or publication of this manuscript. All authors have approved the final submission.

References

[1] Li, Q.; Zhao, C.; Cheng, R. How the Characteristics of Live-Streaming Environment Affect Consumer Purchase Intention: The Mediating Role of Presence and Perceived Trust. *IEEE Access* **2023**, *11*, 123977–123987. https://doi.org/10.1109/ACCESS.2023.3330324

[2] Mensah, I. K. The Factors Driving the Consumer Purchasing Intentions in Social Commerce. *IEEE Access* **2022**, *10*, 132332–132344. https://doi.org/10.1109/ACCESS.2022.3230629

[3] Kumar, V.; Preeti; Saheb, S. S.; Kumari, S.; Pathak, K.; Chandel, J. K.; Varshney, N.; Kumar, A. A PLS-SEM Based Approach: Analyzing Generation Z Purchase Intention through Facebook's Big Data. *Big Data Min. Anal.* **2023**, *6*(4), 491–503. https://doi.org/10.26599/BDMA.2022.9020033

[4] Lee, H. Interest-Based E-Commerce and Users' Purchase Intention on Social Network Platforms. *IEEE Access* **2024**, *12*, 87451–87462. https://doi.org/10.1109/ACCESS.2024.3417440

[5] Ye, L.; Zhang, H.; Fei, Z. The Impact of Sales Promotion on the C2C Online Purchasing Behavior: An Empirical Study. In *Proceedings of the 2010 International Conference on E-Business and E-Government*; IEEE: Guangzhou, China, **2010**; pp 2261–2264. https://doi.org/10.1109/ICEE.2010.571

[6] Nikulin, V. On the Method for Data Streams Aggregation to Predict Shoppers Loyalty. In *Proceedings of the International Joint Conference on Neural Networks (IJCNN)*, Killarney, Ireland, **2015**; pp 1–8. https://doi.org/10.1109/IJCNN.2015.7280493

[7] Liao, J.; Jantan, A.; Ruan, Y.; Zhou, C. Multi-behavior RFM model based on improved SOM neural network algorithm for customer segmentation. *IEEE Access* **2022**, *10*, 122501–122514. https://doi.org/10.1109/ACCESS.2022.3223361

[8] Kim, K.; Jo, M.; Ra, I.; Park, S. RFMVDA: An enhanced deep learning approach for customer behavior classification in e-commerce environments. *IEEE Access* **2025**, *13*, 12527–12539. https://doi.org/10.1109/ACCESS.2025.3529023

[9] Lin, Y.-T. J.; Chang, C.-Y.; Cheng, S.-Y.; Lin, M.-Y. T. Probabilistic Customer Purchase Evolution Graph. *IEEE Access* **2023**, *11*, 32962–32976. https://doi.org/10.1109/ACCESS.2023.3263729

[10] Chang, S. E.; Yu, C. Exploring gamification for live-streaming shopping—Influence of reward, competition, presence and immersion on purchase intention. *IEEE Access* **2023**, *11*, 57503–57515. https://doi.org/10.1109/ACCESS.2023.3284033

[11] Bhati, N. S.; Vijayvargy, L.; Pandey, A. Role of e-service quality (E-SQ) on customers' online buying intention: An extended theory of planned behavior. *IEEE Access* **2022**, *10*, 77337–77349. https://doi.org/10.1109/ACCESS.2022.3190637

[12] Dhanushkodi, K.; Bala, A.; Kodipyaka, N.; Shreyas, V. Customer behavior analysis and predictive modeling in supermarket retail: A comprehensive data mining approach. *IEEE Access* **2025**, *13*, 2945–2959. https://doi.org/10.1109/ACCESS.2024.3407151

[13] Ramanathan, U.; Williams, N. L.; Zhang, M.; Sa-nguanjin, P.; Garza-Reyes, J. A.; Borges, L. A. A new perspective of e-trust in the era of social media: Insights from customer satisfaction data. *IEEE Trans. Eng. Manag.* **2022**, *69*(4), 1417–1429. https://doi.org/10.1109/TEM.2020.2985379

[14] Tiffany, P.; Pinem, A. A.; Hidayanto, A. N.; Kurnia, S. Gain-loss framing: Comparing the push notification message to increase purchase intention in e-marketplace mobile application. *IEEE Access* **2020**, *8*, 182550–182562. https://doi.org/10.1109/ACCESS.2020.3029112

[15] Liu, X.; Zhou, B.; Du, R.; Qi, W.; Li, Z.; Wang, J. On evolutionary analysis of customer purchasing behavior by the supervision of e-commerce platforms. *IEEE Trans. Comput. Soc. Syst.* **2025**, *12*(1), 38–51. https://doi.org/10.1109/TCSS.2024.3485959

[16] Lemaître, G.; Nogueira, F.; Aridas, C. K. Imbalanced-learn: A Python toolbox to tackle the curse of imbalanced datasets in machine learning. *J. Mach. Learn. Res.* **2017**, *18*(17), 1–5. http://jmlr.org/papers/v18/16-365.html

[17] Kumar, A. *Online Shoppers Purchasing Intention Dataset*. Kaggle, **2022**. https://www.kaggle.com/datasets/imakash3011/online-shoppers-purchasing-intention-dataset (accessed 2025-12-05).

ASEAN
Journal of Scientific and Technological Reports
Online ISSN:2773-8752

Research article

Growth and Yield Response of Lettuce (*Lactuca sativa*) Using MykoPlus and Bio-N Biofertilizers

Shaina Marie Guillermo[1], and Dionie Barrientos[2*]

[1] Central Luzon State University, Nueva Ecija, Philippines
[2] Aklan State University-College of Agriculture, Forestry and Environmental Sciences, Banga, Aklan, Philippines
* Correspondence: dionie.barrientos@asu.edu.ph

Citation:
Guillermo, S.M.; Barrientos, D. Growth and yield response of lettuce (*Lactuca sativa*) using MykoPlus and Bio-N biofertilizers. *ASEAN J. Sci. Tech. Report.* **2026**, *29*(1), e260410. https://doi.org/10.55164/ajstr.v29i1.260410.

Article history:
Received: July 19, 2025
Revised: October 4, 2025
Accepted: October 9, 2025
Available online: December 14, 2025

Publisher's Note:
This article is published and distributed under the terms of the Thaksin University.

Abstract: This study was conducted to determine the growth and yield response of lettuce (*Lactuca sativa),* variety 'Black Simpson', using different amounts of MykoPlus and Bio-N biofertilizer. The experiment consisted of seven treatments: T1 (control), T2 (MykoPlus), T3 (Bio-N), T4 (50% MykoPlus and Bio-N), T5 (MykoPlus + ½ Recommended Rate or RR of synthetic fertilizer), T6 (Bio-N + ½ RR of synthetic fertilizer), and T7 (50% MykoPlus and Bio-N + ½ RR of synthetic fertilizer), arranged in a Randomized Complete Block Design (RCBD) from July to September 2022. Results revealed that T3 (Bio-N), T5 (MykoPlus + ½ RR of synthetic fertilizer), and T6 (Bio-N + ½ RR of synthetic fertilizer) had the best initial plant height response; however, in the final plant height gathered, T3, T4, T6, and T7 gave the best response. In terms of the initial leaf length and leaf width, T5 and T6 had the best responses and were comparable to T3, T4, and T7. In the final leaf length and width of lettuce, T6 and T7 showed the best results and were comparable with T2, T3, T4, and T5. No significant difference was observed in the number of leaves. On the yield parameter, T7 (50% MykoPlus and Bio-N + ½ RR of synthetic fertilizer) provided the highest weight of lettuce at harvest, comparable with T2, T3, T4, T5, and T6. The most feasible biofertilizer combination suitable for lettuce production in terms of growth parameters was T6 and T7, whereas in the yield parameter, application of T7 was recommended.

Keywords: Biofertilizer; Bio-N; MykoPlus; lettuce

1. Introduction

Lettuce (*Lactuca sativa*) is one of the high-value commercial crops in the country and a popular salad vegetable. Moreover, it is an ingredient for sandwiches, soups, and is used as a wrapper for food [1]. The leaves are a very low-calorie vegetable. Ausveg [2] stated that it is the seventh most popular fresh vegetable. It is also included as one of the most popular vegetables consumed globally. Nevertheless, its nutritional worth has been undervalued. It is low in fat, calories, and sodium, and a good source of iron, folate, fiber, and vitamin C [3]. Moreover, it is considered one of the healthy vegetables that has many benefits for the body. Nowadays, increasing agricultural production is the primary goal for the growing demand and necessity. Fertilizers play an important role in the crop's quality and quantity. Inorganic fertilizers are accessible to plants, providing essential nutrients in the form of nitrogen, phosphorus, and potassium. Crop production needs to be enhanced manifold due to the increase in population. Therefore, without taking into account the health of the soil or people, farmers are heavily using chemicals (pesticides

and fertilizers) to maximize agricultural productivity. The traditional use of chemical fertilizers and pesticides harms the resident microflora, soil texture, and productivity, as well as human health, when used to boost agricultural output by nutrient enrichment or pathogen growth prevention [4]. Furthermore, the usage of synthetic fertilizer might kill beneficial microorganisms in the soil and increase the nitrate levels of the soil.

With the government's support of bioorganic farming and the active participation of research institutes, private persons, and businesses, the Philippines' biofertilizer sector has risen significantly. In this context, biofertilizers are used as an alternative to chemical fertilizers. They serve as a promising resource in agricultural ecosystems, offering a renewable, supplementary, and eco-friendly source of plant nutrients. They can convert essential elements from non-usable to highly absorbable forms without harming the natural environment [5]. Biofertilizers are beneficial to the soil since they help to restore its fertility. They can benefit both the environment and plants. The use of biofertilizers is widely adopted these days around the world due to the growing problems in the environment and concerns for food safety. In addition, biofertilizers are microbial inoculants, which are defined as preparations that contain live or dormant cells of efficient strains of microorganisms [4]. Microbiological inoculant, several types of microorganisms found in MykoPlus, a biological fertilizer product, aid plant roots in obtaining water and other nutrients from the soil, improving plant development, yield, and farmer income. It replaces up to 30% of the crop's chemical N, P, and K requirements while resulting in a 25-45% increase in crop yield [6]. Furthermore, MykoPlus consists of endomycorrhizal fungi, also known as arbuscular mycorrhizal fungi, or AMF, which are extremely beneficial to the environment, as they dramatically assist in improving plant health and maximizing the absorption of nutrients [7]. Arbuscular mycorrhizal fungi are natural biofertilizers, as they provide the host with nutrients, pathogen protection, and water, in exchange for photosynthetic products [8]. MykoPlus provides natural helpers to the plant's roots in the form of beneficial microorganisms. These helpers provide more phosphorus (P) from locked sources, greater access to free nitrogen (N) from the air, and microbially secreted substances. Through better uptake of water and nutrients, farmers save on chemical fertilizers, and soil becomes less acidic and more friable [6].

One of the biofertilizer products is Bio-N, which contains bacteria isolated from the roots of talahib (*Saccharum spontaneum* L.) grass. This bacterium is able to convert atmospheric nitrogen into a form usable by plants. The bacteria enhance growth, root development, and yield of the crops [9]. The beneficial effects of Bio-N include enhancing root development and shoot growth, and making plants resistant to pest attack and drought. It was observed to provide approximately 30%-50% of the nitrogen required by crops [10]. It is an inoculant for vegetables such as lettuce and pechay. Moreover, Bio-N, which contains *Azospirillum*, is considered the safest bacterium that can be used as a biofertilizer at a commercial level for several crops that are of economic importance for the whole world [11]. It can have a good impact on plant growth, agricultural yields, and N-content. Lettuce plants thrive in nutrient-rich soil. They are considered heavy feeder plants, along with kale, parsley, and collard. Their rapid growth leads to a high demand for nitrogen (N) fertilization to maintain adequate plant-available N concentrations in the soil over a short growing period. Nitrogen is considered the most limiting factor in crop production, and it receives the highest mark of all the major nutrients from inorganic sources applied by farmers [10]. Lettuce also requires a heavy feeding plant and additional nitrogen. It also favors slightly acidic soil.

One benefit of inorganic fertilizers is that they act quickly; however, they are not entirely composed of the nutrients needed by the plants. They also contain salts and other compounds that are not absorbed by the plants and are left behind in the soil, building up over time. According to Malone [12], inorganic fertilizers tend to lower the soil pH, making it more acidic. The plants tolerate different levels of soil pH, and some plants will do well in acidic soils. Furthermore, MykoPlus and Bio-N have favorable impacts on soil and plants, and are used to provide sustenance to crops directly. Hence, biofertilizers are recommended as an alternative or supplement for mineral nutrients. The purpose of this study is to investigate the growth response of lettuce utilizing biofertilizers such as MykoPlus and Bio-N, to evaluate the appropriate combination that supplies the correct ratio of plant nutrients.

2. Materials and Methods

2.1 Treatment and Experimental Design

The study was laid out in a Randomized Complete Block Design (RCBD). The treatments consisted of applying various levels of biofertilizers on lettuce. MykoPlus and Bio-N were employed as biofertilizers, and the specific treatments, which utilized these as growth enhancers, were:
Treatment 1 - Control (No fertilizers applied)
Treatment 2 – MykoPlus
Treatment 3 - Bio-N
Treatment 4 – 50% MykoPlus and Bio-N
Treatment 5 – MykoPlus plus 1/2 RR (side-dressing application throughout the growing season) farmer's practice
Treatment 6 - Bio-N plus 1/2 RR (side-dressing application throughout the growing season) farmer's practice
Treatment 7 **-** 50% MykoPlus and Bio-N plus 1/2 RR (side-dressing application throughout the growing season) farmer's practice

2.2 Application of Treatments

MykoPlus treatments were applied as a powder in a soil hole immediately before transplanting the lettuce. Bio-N treatments were applied as a solution by watering the plants, beginning on the day of transplanting and repeated every two weeks thereafter, according to the specific treatment ratio. Side-dressing applications began at 3 days after transplanting (DAT). Subsequent applications were performed every two weeks, starting 21 days after the first application. Treatment 1 (control): received no fertilizer. Treatment 2 received 5 grams of 100% Mykoplus before planting. Treatment 3 received 167 ml/plant of 100% of Bio-N every two weeks. Treatment 4 received 50% of both MykoPlus and Bio-N. Treatment 5 received MykoPlus plus side dressing (fertigation) with 70 ml per plant. Treatment 6 received Bio-N plus side dressing (fertigation) with 70 ml per plant. Treatment 7 received 50% of both MykoPlus and Bio-N plus side dressing (fertigation) with 70 ml per plant (Table 1).

Table 1. Total amount applied on treated plants

Treatments	MykoPlus	Bio-N	Urea Side Dressing as Fertigation
1	None	None	None
2	5 g/plant	None	None
3	None	167 ml/plant	None
4	2.5 g/plant	83 ml/plant	None
5	5 g/plant	None	70 ml/plant
6	None	167 ml/plant	70 ml/plant
7	2.5 g/plant	83 ml/plant	70 ml/plant

2.3 Installation of Protective Component

This study was conducted in a small greenhouse measuring 250 cm in length, 120 cm in width, and 180 cm in height. The front wall featured a 100 cm wide door. The roofing material consisted of a black shading net, and the framing material was bamboo.

2.4 Seedling Production

Lettuce seeds were sown in the seed boxes filled with a sterilized mixture of garden soil and vermicast at a 1:1 ratio. As part of the treatment, the seeds were pre-treated with their respective biofertilizers. The seed boxes were placed under the protective component with a shading net to protect the seedlings from direct sunlight and the impact of the rain. Seedlings were pricked out to modular seedling trays once they reached the first two true leaves. To harden the seedlings, they were subjected to gradual sunlight exposure one week before transplanting.

2.5 Pot Preparation

The soil used was first sterilized with hot water for five minutes in buckets. This was done to eradicate weed seeds, harmful organisms, and pathogens from the mineral soil. After sterilization, the soil was filled into pots measuring 8 inches in breadth, 4 inches in height, and 4 inches in width.

2.6 Transplanting

Seedlings were transplanted 13 days after sowing (DAS), in the late afternoon. A spacing of 15 cm between columns and 5 cm between rows was maintained during planting. Only healthy seedlings were used as the planting material.

2.7 Care Management and Harvesting

Watering was done as needed, based on the soil moisture content, to avoid disease infestation caused by microorganisms in extremely wet soil. Weeds were removed as soon as they appeared. Insects were controlled by hand-picking daily to ensure the lettuce foliage was not damaged. The lettuce was harvested pot by pot 35 days after sowing. Harvesting was accomplished by slowly and carefully uprooting the plants by hand.

2.8 Data gathered

The following parameters were used for the evaluation of lettuce:

- Plant height (cm) - This was obtained by using a ruler to measure the initial height (one week after transplanting) and the final height (during harvest), measuring from the ground level up to the tip of the main stem.
- Leaf length (cm) - This was determined by getting the initial and final length of the leaves from the base of the leaf blade to the topmost section of the leaf. Measurements were taken one week after transplanting and during harvest.
- Leaf width (cm) - This was determined by measuring the width of leaves, initial and final, across the widest section of the leaf blade. Measurements were determined one week after transplanting and during harvest.
- Number of leaves per plant - This was determined by counting the number of leaves during harvest.
- Yield of lettuce (g) - This was determined by measuring the fresh weight of lettuce after harvest.

2.9 Statistical Analysis

Analysis of variance (ANOVA) for the Randomized Complete Block Design was used for data analysis. Comparison of means was done using Least Significant Difference (LSD) at **the** 5% level of significance. All statistical analysis was performed using Statistical Tool for Agricultural Research (STAR) (version 2.0.1).

3. Results and Discussion

3.1 Initial Plant Height

The initial plant height (cm) was influenced by different application rates of the MykoPlus and Bio-N biofertilizers. The initial plant height of T3 was comparable to the means recorded for T5, T6, T4, T7, and T2. As shown in Figure 1, T3 gained the highest initial plant height (5.20 cm), followed by T5 (5.10 cm), T6 (4.97 cm), and T4 and T7, which recorded the same height (4.83 cm). T2 recorded 3.20 cm. The shortest plant height (2.67 cm) was observed in the T1 (control).

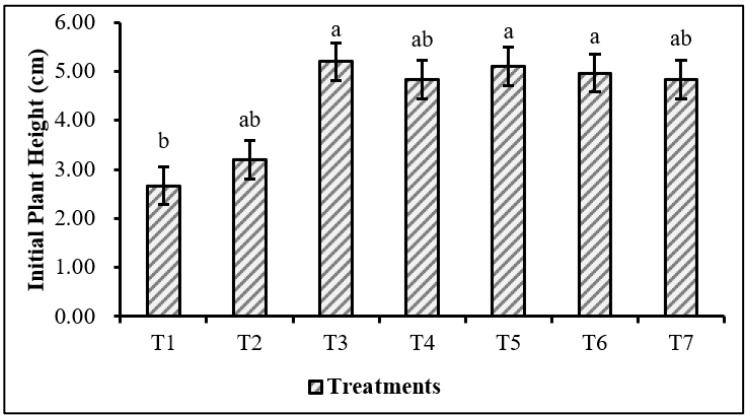


Figure 1. Initial plant height (cm) response from using MykoPlus and Bio-N biofertilizers.

The Analysis of Variance (ANOVA) revealed significant differences among treatments, resulting in the formation of three distinct groups. Group 1 consisted of T3, T5, and T6, which were found to be statistically comparable. Group 2 comprised T2, T4, and T7, which were also comparable to each other. The final group was T1 (control), which had the shortest plant height and was comparable only to the treatments in group 2 (T2, T4, and T7).

T3 (Bio-N) recorded the highest initial plant height mean of 5.20 cm. This superiority aligns with findings by Agapito and Mercado [13], who note that Bio-N, when applied as a root dip or seed inoculation, can supply 50% of the nitrogen requirements for high-value crops. In this study, Bio-N was applied both as a seed pre-treatment and as a solution for watering the plants. Bio-N's effectiveness is largely due to its component, *Azospirillum*, an associative nitrogen-fixing, aerobic bacterium. *Azospirillum* colonizes the root system of many vegetable plants, assisting the crops in better vegetative growth [14]. Furthermore, Bio-N produces plant growth promoters, including gibberellins and auxins [15]. Auxins, in particular, positively influence gibberellins, which stimulate cell elongation and consequently increase plant length [16]. Treatment 6 (T6) was statistically comparable to T3 and T5. T6, which combined Bio-N with a half rate of synthetic fertilizer, had a positive impact on initial plant height. This positive effect is likely due to the presence of *Azospirillum* in Bio-N, which produces growth promoters like auxins and gibberellins. Furthermore, the inclusion of nitrogen in T5 and T6 (via ½ Recommended Rate of synthetic fertilizer) is significant. Nitrogen fertilizer is known to ensure favorable conditions for the elongation and optimum vegetative growth of lettuce plants [17]. The findings suggest that the combination (T5 and T6) influenced the initial plant height just as effectively as the sole application of Bio-N (T3).

3.2 Final Plant Height

The final plant height (cm) was influenced by different rates of MykoPlus and Bio-N biofertilizers. The final plant height result for T3 was comparable to the plants in T4, T6, T7, T5, and T2. The highest plant height recorded during harvest was T7 at 22.83 cm, followed by T4 at 22.77 cm, T6 at 22.27 cm, T3 at 22.00 cm, T5 at 21.00 cm, and T2 at 20.40 cm. Among all the treatments, T1 had the lowest mean at 17.47 cm (Figure 2).

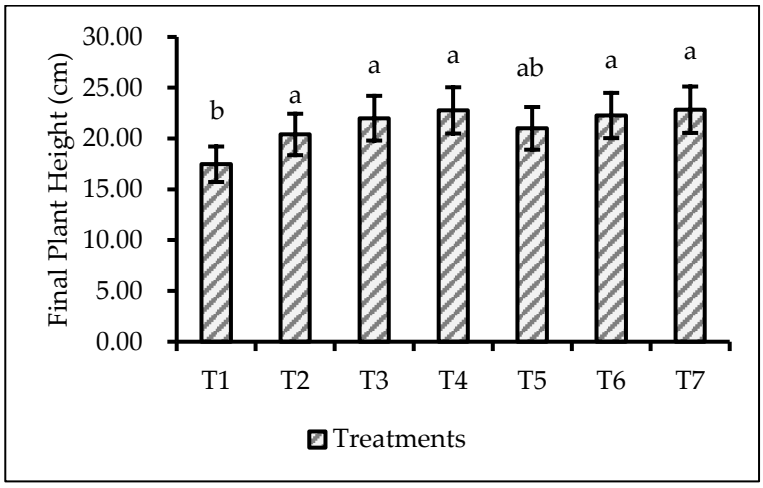


Figure 2. Final plant height (cm) response from using MykoPlus and Bio-N biofertilizers.

Plant height was significantly influenced by the different treatments applied. The analysis of variance showed significant differences among treatments. T3, T4, T6, and T7 resulted in the tallest plants, while T1 resulted in the shortest plants. The differences among T1, T2, and T5 were not statistically significant.

T2 and T5 were comparable to each other and influenced the height of the plant samples. As shown in Figure 2, T7 had the highest result for final plant height at 22.83 cm. The T7 plants were treated with 50% MykoPlus, Bio-N, plus ½ the Recommended Rate (RR) of synthetic fertilizer. In the study by Opeña and Sotto [18], MykoPlus increased root and shoot growth, which may be due to the beneficial effects of growth hormone secretors, mycorrhizal fungi, and nitrogen fixers contained in the biofertilizer. It also contains phosphorus solubilizers, which increase plant phosphorus (P) uptake, an important factor in stem elongation. Additionally, Bio-N produces plant growth promoters that result in increases in plant height. Synthetic fertilizer was also applied, which promotes better vegetative growth. T4 (50% of MykoPlus and Bio-N) and T6 (Bio-N plus 1/2 RR of synthetic fertilizer) gained 22.77 cm and 22.27 cm, respectively, indicating a positive impact on plant height. The combination of both biofertilizers, or solely Bio-N with synthetic fertilizer added, was evident in improving the plant height of lettuce. As part of the comparable treatments, T3 (Bio-N) gained 22.00 cm, and this study revealed that Bio-N can solely influence the height of lettuce up to harvest. The combination of both biofertilizers, with or without synthetic fertilizer, in this study proved to significantly increase the height of lettuce up to harvest.

3.3 Initial Leaf Length

The initial leaf length (cm) was influenced by different rates of MykoPlus and Bio-N biofertilizers. The analysis of variance result revealed that plants in T5 and T6 significantly performed better than T1 and T2 in terms of initial leaf length. The effectiveness of T3, T4, and T7 was not statistically distinguishable from either T5 and T6 or T1 and T2. The highest leaf length (3.00 cm) was gained from T5 and T6, followed by T3 (2.53 cm), T7 (2.43 cm), and T4 (2.33 cm). Furthermore, T2 (1.63 cm) and T1 (1.43 cm) were comparable and recorded the least leaf length (Figure 3).

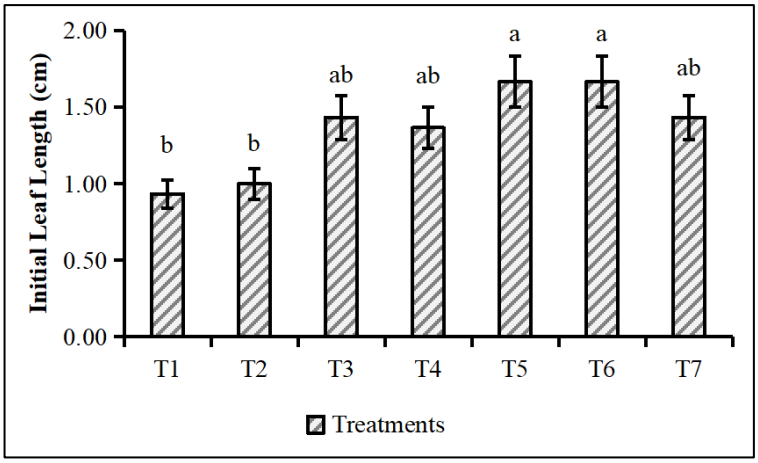


Figure 3. Initial leaf length (cm) response from using MykoPlus and Bio-N biofertilizers.

T5 and T6 were comparable and had the longest leaf length. The plants treated with T5 and T6 gained 3.00 cm in leaf length. This is because T5 has MykoPlus, which contains endomycorrhizal fungi that establish intercellular attachment with plants between the cell wall and cell membrane. The attachment helps the transfer of water and nutrients from the fungi to the plant. The fungi develop branched structures within the plant's root system. The branched structures increase the surface area of the roots, enabling the plant to gather essential nutrients and much more water [19]. The result of this study revealed that MykoPlus helps to absorb more water from the soil, which influenced the leaf length/size. Moreover, T5 has the application of nitrogen, which helps to improve the chlorophyll in the leaves that influences the leaf size. T6 was applied with Bio-N, which contains *Azospirillum*. Fukami et al. [20] state that the genus *Azospirillum* contains plant growth-promoting bacteria (PGPB). The benefits to plants by inoculating *Azospirillum* have been mainly attributed to its capacity to fix atmospheric nitrogen and its capacity to synthesize phytohormones. Additionally, T6 included the application of synthetic nitrogen fertilizer, which helps the leaf grow and influences the leaf size.

3.4 Final Leaf Length

The final leaf length (cm) was influenced by the different rates of MykoPlus and Bio-N biofertilizers. Figure 4 shows the result, indicating that the leaf length of the plant in T6 was comparable to that of the plants treated with T7. The highest final leaf length recorded was 12.73 cm from T6, followed by T7 with 12.47 cm, T4 with 12.27 cm, T3 with 11.67 cm, T5 with 11.63 cm, and T2 with 11.47 cm. Furthermore, T1 had the least final leaf length at 10.00 cm.

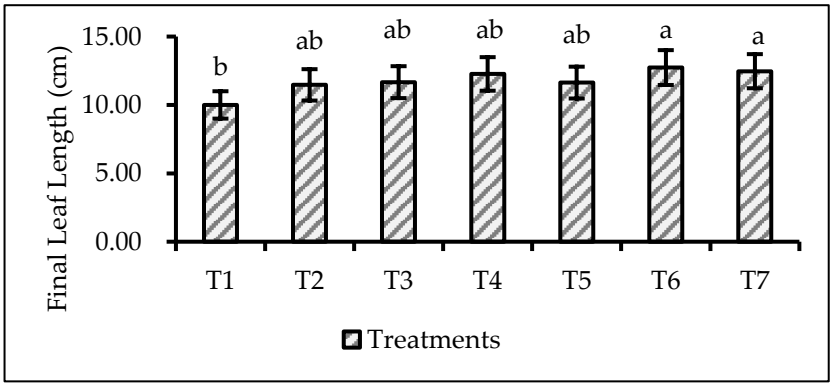


Figure 4. Final leaf length (cm) response from using MykoPlus and Bio-N biofertilizers.

Analysis of variance indicated a significant difference among the treatments in terms of final leaf length. T6 and T7 were statistically similar and demonstrated the greatest positive influence on leaf length. These two treatments were also comparable with T2, T3, T4, and T5. T1 had the shortest final leaf length and

was statistically different from other treatments. T6 (Bio-N plus 1/2 RR of synthetic fertilizer) resulted in the longest leaf length (12.73 cm), supporting the initial data gathered. Bio-N was developed by isolating *Azospirillum* from the roots of the talahib grass. This bacterium can transform atmospheric nitrogen (N_2) into a form that plants can utilize [13]. A higher amount of chlorophyll in the leaves allows the plant to photosynthesize more effectively, which, in turn, results in bigger leaves. Additionally, increasing the nitrogen content will improve the chlorophyll concentration in the leaves. Consistent with this, the findings of Chamangasht et al. [21] showed that inoculating seeds with biofertilizers significantly increased the leaf area index compared with the control (no biofertilizer). This study revealed that T6 influences the leaf length up to harvest. T6 was comparable with T7 (50% of MykoPlus and Bio-N plus 1/2 RR of synthetic fertilizer). In T7, the application of 50% of MykoPlus provided an additional biofertilizer component, which contains beneficial bacteria and different species and strains of mycorrhizal fungi. This includes growth hormone secretors, nitrogen fixers, and phosphorus solubilizers [22]. The mycorrhizal fungi, along with the phosphorus-solubilizing microbes, promote plant growth not only through enhanced nutrient uptake but also by generating phytohormones, such as gibberellins, cytokinins, auxins, or polyamides. Wu et al. [23] reportedly found that leaf area is generally determined by the size and number of the cells in the leaf. Cytokinins stimulate cell division and enhance cell growth during the proliferation and expansion stages of leaf cell development. This study proved that the fertilizer combination used in T6 and T7 significantly improved the leaf length of lettuce.

3.5 Initial Leaf Width

The initial leaf width (cm) was influenced by the different rates of MykoPlus and Bio-N biofertilizers. The result for the plants in T5 was comparable to T6. The highest initial leaf width recorded was 1.67 cm, achieved by both T5 and T6. This was followed by T3 and T7 (both at 1.43 cm), T4 (1.37 cm), and T2 (1.00 cm). The least initial leaf width was observed from T1 at 0.93 cm (Figure 5).

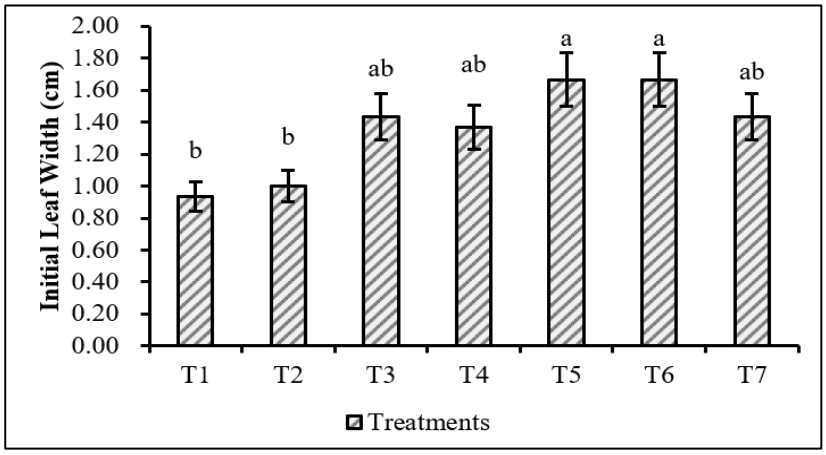


Figure 5. Initial leaf width (cm) response from using MykoPlus and Bio-N biofertilizers.

The analysis of variance showed significant differences among treatments. The result revealed during the first week, T5 and T6 achieved the highest leaf width. Meanwhile, T3, T4, and T7 performed better than T1 and T2. The low leaf width observed in T1 (control) confirms the positive impact of the biofertilizer treatments on early plant vigor. T5 (MykoPlus plus 1/2 RR of synthetic fertilizer) and T6 (Bio-N plus 1/2 RR of synthetic fertilizer) were comparable with each other, with a leaf width of 1.67 cm. This supports the initial leaf length data, where the same treatments also yielded the highest parameters. As stated by Mcrae [24], water availability is a major factor that limits the leaf size. T5's is partly due to the endomycorrhizal fungi found in MykoPlus. These fungi form an intercellular attachment with the plants, which facilitates the transfer of water and nutrients from the fungi to the plant. The branched structures formed within the plant's root system significantly increase the surface area of the roots, allowing the plant to collect essential nutrients and more water [19]. Furthermore, the combination of T5 with synthetic nitrogen fertilizer application also improves chlorophyll concentration in the leaves, which positively influences the leaf size. T6 was comparable to T5 and had a significant influence on leaf width. T6 involved the application of Bio-N combined with synthetic

fertilizer. Bio-N contains *Azospirillum,* a plant growth-promoting bacterium that fixes atmospheric nitrogen and makes it available for plant use [20]. This study revealed that the combination of either MykoPlus or Bio-N with synthetic fertilizer has a great impact on the growth, specifically in terms of leaf width.

3.6 Final Leaf Width

The final leaf width (cm) was influenced by different rates of Mykoplus and Bio-N biofertilizers. The results showed that the plant with T6 was comparable to the plants treated with T7. The highest final leaf width was 6.60 cm from T6, followed by T7 with 6.37 cm, T4 with 6.23 cm, T3 with 6.17 cm, T5 with 5.97 cm, and T2 with 5.90 cm. The lowest final leaf width was obtained from plants treated with T1, with 5.17 cm (Figure 6).

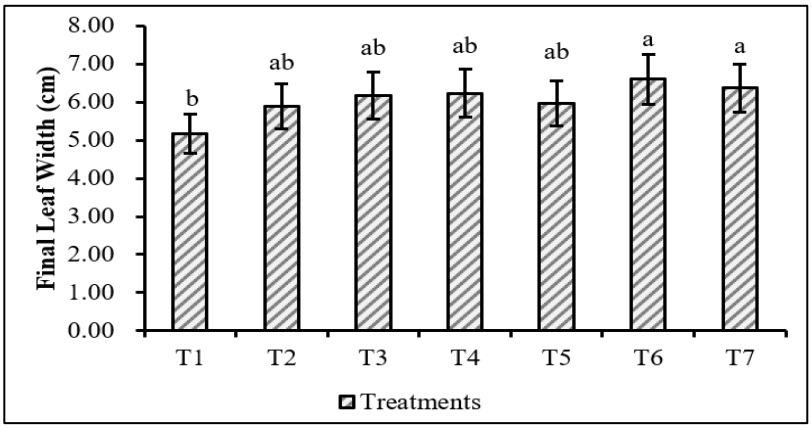


Figure 6. Final leaf width (cm) response from using MykoPlus and Bio-N biofertilizers.

The analysis of variance showed significant differences among treatments. The results indicated that T6 and T7 were comparable with each other, and these treatments influenced the actual leaf width by yielding the highest final leaf width. While T2, T3, T4, and T5 showed a leaf width higher than T1, but statistically failed to demonstrate a significant advantage over T1. The least effective treatment was T1. T6 (Bio-N plus 1/2 RR of synthetic fertilizer) obtained the highest result with 6.60 cm. As stated by Impello [25], fertilizers directly enhance plant growth and development by providing extra nutrients to the plant or the soil. Biofertilizers indirectly enhance plant growth and development by utilizing microorganisms to improve natural processes in the soil that affect plant growth. Bio-N contains native bacteria isolated from the roots of the talahib (*Saccharum spontaneum* L.) grass that can convert atmospheric nitrogen into a form usable by plants [9]. The T7 (50% MykoPlus and Bio-N plus 1/2 RR of synthetic fertilizer) yielded 6.37 cm and was observed in this study to have a positive impact on leaf width. Considering the combination of two biofertilizers used in this study improved the leaf size, the application of synthetic nitrogen fertilizer also plays an important role in leaf growth. Furthermore, increasing nitrogen fertilizer supply promotes leaf elongation and expansion growth by regulating the rate of cell size or cell division [26]. The combination of treatments applied in T7 evidently influences the actual leaf width compared to the non-treated plants.

3.7 Number of Leaves

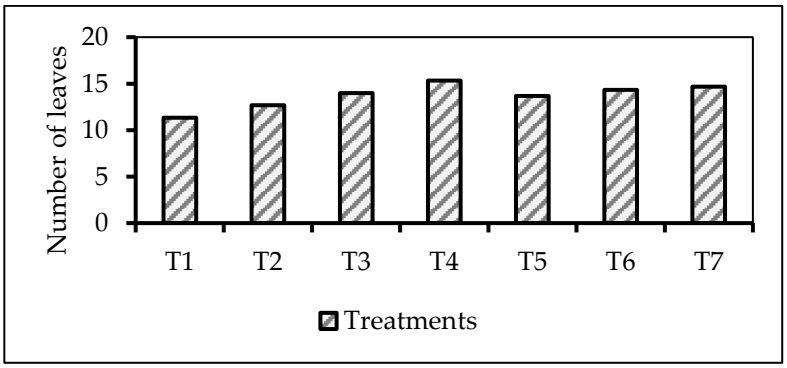


Figure 7. Number of leaves (cm) response from using MykoPlus and Bio-N biofertilizers.

Analysis of variance showed no significant difference among treatments. Application of different rates and combinations of biofertilizer together with synthetic fertilizer did not affect the number of leaves over the control.

3.8 Yield in grams

The yield (g) was influenced by different rates of MykoPlus and Bio-N biofertilizers [Figures 8 and 9]. Additionally, as shown in Figure 9, the highest yield was from T7, which yielded 78.00 g, followed by T4 with 66.67 g, T3 with 50.00 g, T6 with 48.67 g, T5 with 46.33 g, and T2 with 40.00 g. The lowest yield was obtained from plants treated with T1 (33.67 g).

BLOCK I	BLOCK II	BLOCK III
 T3R1	 T5R2	 T2R3
 T1R1	 T4R2	 T6R3
 T4R1	 T3R2	 T1R3
 T2R1	 T7R2	 T5R3
 T7R1	 T6R2	 T4R3
 T5R1	 T2R2	 T7R3
 T6R1	 T1R2	 T3R3

Figure 8. Plant samples per block at harvest.

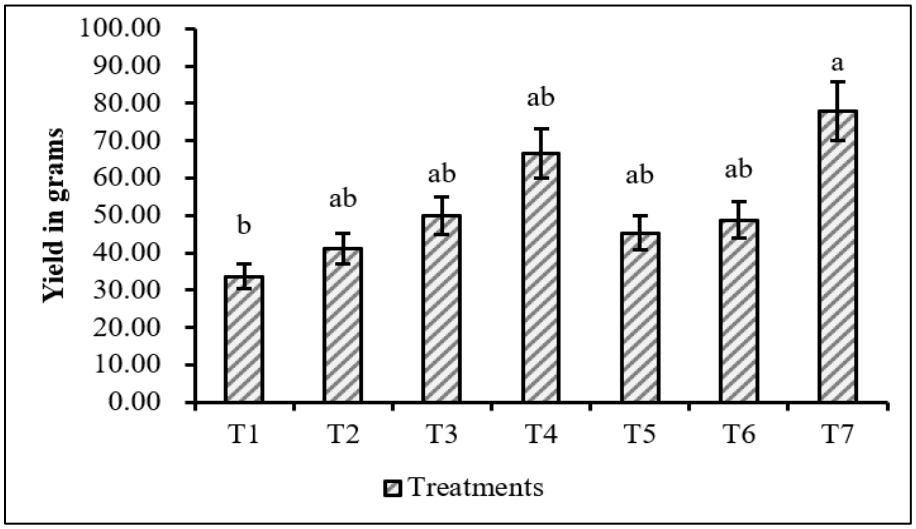


Figure 9. Yield response from using MykoPlus and Bio-N biofertilizers.

The analysis of variance revealed that T7 is the most effective treatment for increasing yield. Although T2, T3, T4, T5, and T6 show numerically higher yields than T1 (control), the statistical analysis indicated that these benefits are not significant enough to be separated from either T1 or T7. T7 (50% MykoPlus and Bio-N plus 1/2 RR of synthetic fertilizer) obtained the highest yield with 78.00 g. The study by Opeña and Sotto [18] revealed that the MykoPlus application significantly increased plant weights. Moreover, Pagcaliwagan [27] stated that farmers using MykoPlus observed that their crops had greater yields. Bio-N contains organisms that are capable of converting nitrogen from the air into ammonium nitrogen in the soil. It enhances root development and shoot growth, can replace 30 to 50% of the total chemical nitrogen needed for crops, and could increase crop yields by 11% [28]. According to Araguas [29], a microbial inoculant, Bio-N boosts nutrient absorption, provides resistance to pests and diseases, improves the plant's root system, and enhances soil conditions. Bio-N users reported improvement in grain quality and an increase in yield. The results of this study show that the use of MykoPlus together with the Bio-N and synthetic fertilizer can increase yield. T7, which had the highest result in the study, was combined with the synthetic fertilizer, specifically urea. The study by Kumar et al. [30] found that the different levels of nitrogen application influenced the total yield of lettuce. The highest yield was achieved with higher doses of nitrogen. As previously stated, in addition to the benefits of MykoPlus and Bio-N, synthetic nitrogen also helped the biofertilizers achieve the obtained yield in T7 by assisting plants with higher vegetative growth.

4. Conclusions

The most effective treatment for lettuce production was T7 (50% MykoPlus and Bio-N plus 1/2 RR of synthetic fertilizer), which is strongly recommended because it achieved the highest yield. Supporting this result, T7 was also identified as one of the top treatments for growth parameters in terms of final plant height, leaf length, and width. The T7 growth parameters contributed to the yield benefits observed. Therefore, the significant increase in yield driven by the T7 application confirms its superiority for application in lettuce production.

5. Acknowledgements

The authors would like to thank the evaluators from Central Luzon State University- College of Agriculture for the improvement of the paper.

Author Contributions: Conceptualization, SMG. and DB; methodology, SMG.; software, SMG.; validation, SMG., and DB.; formal analysis, DB.; investigation, SMB.; resources, SMB.; data curation, SMB.; writing—

original draft preparation, SMB.; writing—review and editing, SMG and DB.; visualization, SMG.; supervision, DB.; project administration, SMG and DB.; funding acquisition, SMG.

Funding: This research received no external funding.

Conflicts of Interest: The authors declare no conflict of interest.

References

[1] Department of Agriculture, Bureau of Plant Industry – National Crop Research and Development Center. *Lettuce Production Guide*; Department of Agriculture: Philippines, **2021**; pp 1–3. https://www.coursehero.com/file/44173227/BPI-Lettuce-Production-Guidepdf/ (accessed 2021-05-08).

[2] Ausveg. Top 10 Most Popular Fresh Vegetables Revealed. https://ausveg.com.au/media-releases/top-10-most-popular-fresh-vegetable-revealed/ (accessed 2021-06-22).

[3] Kim, M. J.; Moon, Y. Y.; Tou, J. C.; Mou, B.; Waterland, N. L. Nutritional value, bioactive compounds and health benefits of lettuce (*Lactuca sativa* L.). *J. Food Compos. Anal.* **2016**, *49*, 19–34. https://doi.org/10.1016/j.jfca.2016.03.004

[4] Singh, K. P.; Singh, R. P.; Umesha, S. Microbial biotechnology and sustainable agriculture. In *Emerging Approaches and Strategies*; Singh, K. P., Singh, R. P., Umesha, S., Eds.; Elsevier, **2018**; p 185. https://doi.org/10.1016/B978-0-12-812160-3.00006-4

[5] Macik, M.; Gryta, A.; Frac, M. Biofertilizers in agriculture: An overview on concepts, strategies and effects on soil microorganisms. *Adv. Agron.* **2020**, *162*, 31–87. https://doi.org/10.1016/bs.agron.2020.02.001

[6] Zarate, J. MykoPlus. https://aim.edu/sites/default/files/2017-08/mykoplus.pdf (accessed 2021-06-22).

[7] Rossouw, M. J. Arbuscular Mycorrhizal Fungi. https://www.sanbi.org/animal-of-the-week/arbuscular-mycorrhizal-fungi/ (accessed 2021-06-26).

[8] Berruti, A.; Lumini, E.; Balestrini, R.; Bianciotto, V. Arbuscular mycorrhizal fungi as natural biofertilizers: Let's benefit from past successes. *Front. Microbiol.* **2016**, *6*, 1559. https://doi.org/10.3389/fmicb.2015.01559

[9] UPLB BIOTECH. Bio-N. https://biotech.uplb.edu.ph/products/bio-n/ (accessed 2025-10-01).

[10] Balog, R. M. FNCA (Forum for Nuclear Cooperation in Asia) Biofertilizer Project. *FNCA Biofertilizer News Lett.* **2007**, *7*, 2–3. https://www.fnca.mext.go.jp/english/bf/news_img/nl07.pdf.

[11] Mehnaz, S. Azospirillum: A biofertilizer for every crop. In *Plant Microbes Symbiosis: Applied Facets*; Arora, N., Ed.; Springer: New Delhi, **2014**; pp 317–338. https://doi.org/10.1007/978-81-322-2068-8_15

[12] Malone, M. The Disadvantages of Inorganic Fertilizer. https://homeguides.sfgate.com/disadvantages-inorganic-fertilizer-64756.html (accessed 2021-06-26).

[13] Agapito, A. J. I.; Mercado, S. M. Use Bio-N Today, Keep High Farm Costs Away. https://horizon.uplb.edu.ph/uplb-features/use-bio-n-today-keep-high-farm-costs (accessed 2022-10-16).

[14] Núñez, J. A. D.; Lobo, M. B. Application of microorganisms in forest plant biofertilizers. In *Advances in Bio-inoculants*; Elsevier, **2021**; Vol. 1, pp 265–287. https://doi.org/10.1016/b978-0-12-821667-5.00026-9

[15] SFS. Bio-N. https://www.soilfertilityservices.co.uk/bio-n (accessed 2022-11-17).

[16] Ersek, K. What Are Plant Auxins and How Do They Affect Plant Growth? https://www.holganix.com/blog/what-are-plant-auxins-and-how-do-they-affect-plant-growth (accessed 2022-10-02).

[17] Hasan, M. R. M. D.; Ali, A.; Tahsin, A. K. M. M.; Islam, M. N. Growth and Yield of Lettuce (*Lactuca sativa* L.) Influenced as Nitrogen Fertilizer and Plant Spacing. *IOSR J. Agric. Vet. Sci.* **2017**, *10*(6), 62–71. https://doi.org/10.9790/2380-1006016271

[18] Opeña, J. M.; Sotto, R. Growth response and leaf chlorophyll concentration of romaine lettuce plants (*Lactuca sativa* L. var. *Longifolia*) applied with Mykoplus under varying saline conditions. *JNS* **2020**, *19*(2), 40–51. https://www.researchgate.net/publication/345918141

[19] BioAg Products. Plant Types That Benefit from Endomycorrhizae Fungi. http://bioagproducts.com/benefit-endomycorrhizae-fungi/ (accessed 2022-10-18).

[20] Fukami, J.; Cerezini, P.; Hungria, M. *Azospirillum*: benefits that go far beyond biological nitrogen

[21] Chamangasht, S.; Ardakani, M. R.; Khavazi, K.; Abbaszadeh, B.; Mafakheri, F. Improving lettuce (*Lactuca sativa* L.) growth and yield by the application of biofertilizers. *Ann. Biol. Res.* **2012**, *3* (4), 1876–1879.

[22] Sarian, Z. Mykoplus, The Latest Biofertilizer from Los Banos. https://www.agriculture.com.ph/2018/09/12/mykoplus-the-latest-biofertilizer-from-los-banos/ (accessed 2021-06-28).

[23] Wu, W.; Du, K.; Kang, X.; Wei, H. The diverse roles of cytokinins in regulating leaf development. *Hortic. Res.* **2021**, *8*, 558. https://doi.org/10.1038/s41438-021-00558-3

[24] Mcrae, M. The Reason Why Some Leaves Can Grow So Huge Is Totally Not What We Thought. https://www.sciencealert.com/now-we-understand-why-some-leaves-can-grow-so-damn-huge (accessed 2022-10-18).

[25] Impello. Role of Biofertilizer to Organic Farming. https://impellobio.com/blogs/inoculants/role-of-biofertilizer-in-organic-farming (accessed 2022-10-19).

[26] Vos, J. P. E. L.; Van Der Putten, P. E. L.; Birch, C. J. Effect of nitrogen supply on leaf appearance, leaf growth, leaf nitrogen economy and photosynthetic capacity in maize (*Zea mays* L.). *Field Crops Res.* **2005**, *93*(1), 64–73. https://doi.org/10.1016/j.fcr.2004.09.013

[27] Pagcaliwagan, A. Beneficial Microorganisms Makes Soil Healthier and Increases Yield. http://www.pcaarrd.dost.gov.ph/home/portal/index.php/quick-information-dispatch/2435-beneficial-microorganisms-makes-soil-healthier-and-increases-yield (accessed 2022-10-22).

[28] Department of Agriculture. PIA - DA Promotes Cheaper Bio-Fertilizer to Help Farmers Save on Cost, Attain Optimum Crop Yield. https://pia.gov.ph/press-releases/2022/06/07/da-promotes-cheaper-bio-fertilizer-to-help-farmers-save-on-cost-attain-optimum-crop-yield (accessed 2022-10-02).

[29] Araguas, K. Biotech's Bio N May Help Ease Ph Farmers' Fertilizer Woes, UPLB. https://uplb.edu.ph/all-news/uplb-biotechs-bio-n-may-help-ease-ph-farmers-fertilizer-woes/ (accessed 2022-10-19).

[30] Kumar, S.; Diksha; Satyavir, S.; Kumar, R. Biofertilizers: An ecofriendly technology for nutrient recycling and environmental sustainability. *Curr. Res. Microb. Sci.* **2022**, *3*, 100094. https://doi.org/10.1016/j.crmicr.2021.100094

ASEAN
Journal of Scientific and Technological Reports
Online ISSN:2773-8752

Research article

Comprehensive and Integrated Deep Learning Approaches-based Intelligent Skin Disease Diagnosis System for Pox Detection

Padmaja Bodagala[1], and Naga Malleswary Dubba[1]

[1] Department of CSE, Koneru Lakshmaiah Education Foundation, Vaddeswaram, AP, India

* Correspondence: padmajabodagala01@gmail.com

Citation:
Bodagala, P.; Dubba, M.N. Comprehensive and integrated deep learning approaches-based intelligent skin disease diagnosis system for pox detection *ASEAN J. Sci. Tech. Report.* **2026**, *29*(1), e260160. https://doi.org/10.55164/ajstr.v29i1.260160.

Article history:
Received: July 7, 2025
Revised: October 4, 2025
Accepted: October 16, 2025
Available online: December 14, 2025

Publisher's Note:
This article is published and distributed under the terms of the Thaksin University.

Abstract: Chickenpox, measles, monkeypox, and smallpox are skin diseases that exhibit very similar signs, making accurate distinction difficult. In this study, an automated deep learning system is developed to classify pox-related skin diseases into six classes, which are Chicken_Pox, Measles, Monkey_Pox, Small_Pox, Normal, and Unknown. The system uses MobileNet to extract features efficiently using a dataset of 4099 training and 1104 evaluation images. The three tested model variants: inception-based CNN, Deep Belief Network, and MobileNet-LSTM-hybrid, Deep Belief Network (DBN) with the SGD optimizer, incurred the best classification accuracy, showing to be more effective at similar tasks to retrieve spatial and temporal features. This will ensure more efficient and quicker detection of the pox, particularly in those regions that do not have specialists in dermatology. Although it is not a replacement for clinical expertise, the system provides a potent instrument in screening and diagnosis of early diseases. The comparative evaluation of these models offers insights into the most effective approach for medical image classification of pox diseases.

Keywords: Pox detection; deep learning; skin disease classification; CNN; medical image analysis.

1. Introduction

Chickenpox [1], measles, monkeypox, and smallpox [2] are viral diseases that, in association with skin manifestations, affect human beings [3]. Viral skin diseases like chicken pox, measles, monkey pox, and smallpox have been major global issues of public health, particularly in developing and underserved areas, where the issue of treating or diagnosing these diseases may economically weigh down authorities. Such infections usually share the same dermatological characteristics, such as rashes, pustules, and blisters, and it can be challenging to diagnose them properly and promptly using clinical examination. These similarities can confuse the basis of diagnosing cases that lead to the delay in effective treatment. Delays result in severe health consequences among individuals, and the spread increases to the whole public. The traditional way of diagnosis is primarily based on clinical judgment and physical examinations including laboratory tests, such as PCR test or a biopsy for confirmation if it is possible, but most of the time, these diagnostics and much more proved to be time-consuming, costly, and most of the time inaccessible, particularly in the remote areas of these developing regions. Therefore, there is a requirement to develop an automated and comprehensive skin disease

diagnosis system with the sole aim of detecting contagious diseases like pox. Late diagnosis may cause higher rates of transmission and poor health outcomes.

Recent developments in artificial intelligence (AI), specifically deep learning, have shown a significant potential for automating the analysis of medical images and improving the capabilities of diagnostic methods. CNNs have demonstrated extensive success in identifying complex structures in dermal images, but most of the existing literature has hitherto focused on single disease detection (such as monkeypox) with either standalone CNN architectures or transfer learning techniques. It is in this context that we suggest a multi-class pox disease classification framework using skin images, which is a comprehensive and integrated deep learning model. Novelty in our project. The key novelty of our work lies in the development and application of a hybrid MobileNet + LSTM model designed specifically for the classification of pox diseases with similar dermal characteristics. This approach uniquely integrates MobileNet's lightweight and efficient convolutional layers for spatial feature extraction with LSTM's capability to model sequential dependencies among spatial features. Although dermal images are static, the LSTM component enhances the model's ability to capture subtle variations by learning contextual relationships within the spatial patterns of skin lesions was developed and evaluated. This hybrid architecture balances computational efficiency and classification performance, making it particularly suitable for portable diagnostic systems. We also conduct a comparative analysis of three optimizers, namely Adam, SGD, and RMSprop, on three model types, such as Inception_Net, the proposed hybrid model, and a Deep Belief Network (DBN). This optimizer-sensitive analysis gives a better insight into the training dynamics and model robustness. In comparison to the previous research methods that concentrated on a single skin condition (Monkeypox) or only a few evaluation metrics means those models were not generalizable to the wider range of pox diseases, our design aims at six classes of skin conditions (Chickenpox, Measles, Monkeypox, Smallpox, Normal, and Unknown), which provides a more generalizable and clinically applicable solution. The point is not to substitute clinical judgement, but to provide quick, convenient, and precise pre-screening, particularly in regions with limited availability of specialist dermatologists.

1. Introduction

1.1 Research Background and Contributions

The advances in AI and deep learning have thrown open the gates for automating medical image analysis and building systems that can analyze and report on images with minimal human input. Convolution Neural Networks (CNNs) come with advantages in terms of pattern extraction in medical images; thus, those networks can represent good candidates for the disease detection task. Here, present some of the deep learning classification models of skin conditions being classified into six types, such as Chicken_Pox, Measles, Monkey_Pox, Small_Pox, Normal, and Unknown. The proposed architecture involves MobileNet as a lightweight and real-time feature extractor suitable for dermal images. Also, three deep learning models are designed and compared: CNN-based Inception Net, spatial-temporal hybrid MobileNet-LSTM that captures both spatial and sequential features, and a Deep Belief Network (DBN) for hierarchical feature learning across the models. All models were trained under the same conditions using three optimizers, Adam, SGD [4], and RMSprop, to provide convergence and performance metrics for the rich models competent in achieving desired classification performance. This research sets out to contribute towards the growing field of AI-assisted medical diagnostics by comparative analysis of the above models in different training scenarios. In the long term, the aim is to develop a simple, inexpensive, scalable, and accurate device for identifying pox diseases for clinical and non-clinical points of care. This is not intended to supersede the expertise of a clinician in the health system, but a tool to enhance the consistency of diagnosis so as to reduce human error and widen access to dermatological care [5].

1.2 Related Works

The rapid globalization of viral skin infections has, in turn, generated the need for reliable tools for their diagnosis. There have been numerous advances in deep learning algorithms, which, by now, have achieved remarkable success in classifying dermatological conditions that share visual symptoms. This makes them a compelling option for image classification, as they autonomously detect and acquire the critical attributes of the given image data. Furthermore, Deep learning approaches offer a pathway to enhanced

performance through the successful mitigation of key factors, such as the computational time involved in image data analysis for detection. These advanced deep learning algorithms can ultimately support dermatologists while they make critical decisions in the treatment of various skin ailments. Mobile Net-based Monkeypox detection was carried out by, who have already shown promise in classifying clinical dermal images. On optimization for model performance, [6] allowed the necessity of optimizations for model performance and put forth a two-stage enhancement pipeline for deep learning methods on medical image classification. The high-performance algorithm designed by distinguished among Mpox lesions and those of others to achieve best-in-class functionality on the big-quantum datasets. Explaining model interpretability and transparency is gaining focus. Explainable AI was fused into transfer learning by allowing clinicians to visualize the prediction logic, and Grad-CAM was used by [7] to say what features delineated Mpox detection lesions. Developing Transformer-Aided architectures is on the rise, as [8] with their research demonstrated an attention mechanism in performing effectively for multi-class skin lesion classification that also included Monkeypox.

Hybrid frameworks have achieved popularity [9] and proposed a hybrid AI model for Mpox detection with increased sensitivity, while [7] fused classical machine learning with CNNs. By demonstrating that merging CNNs with hashing strategies can accelerate processes without compromising accuracy, Zhang et al. [10] contributed to the growing appreciation for hybrid techniques. [11] underscored ensemble algorithms that enhanced combined deep networks to make a robust classifier. [12] created and validated a unique framework for the automatic and precise determination of Mpox illness employing a meticulously gathered Mpox database by going through a diverse range of databases across the internet, and described a unique hybridized known as "Swin-PSO-SVM" that improves the precision and reliability of the discovery of monkeypox. Offers a computer-aided design framework towards the categorization of monkeypox based on an architecture of deep learning comprising numerous steps. [13] presents a complete method towards the identification of monkeypox based on deep learning techniques like ResNet-50, EfficientNetV2, MobileNetV2, and Vision Transformer, along with a combination of critical approaches. Proposed the VGG16-based approach for illness diagnostic generalization and enhancement, utilizing fuzzy expressions to control uncertainties and Principal Component Analysis to minimize dimensions. [14] provided a combined deep learning approach towards the recognition of Mpox by building with the use of deep learning as an attribute acquisition means alongside the classification methods built around the concept of machine learning. Suggested a framework for diagnosis that included the previously trained machine learning classification methods and CNN paradigms alongside the metaheuristic optimizing method. [15] created a novel combination of algorithms by including the capabilities of AlexNet, ResNet50, and Vision Transformers.

They were able to increase the effectiveness of monkeypox diagnosis by leveraging the prospects of Graph Convolutional Networks and the capabilities of three algorithms used by them. Modified ResNet50's level-centric structure for recognition of monkeypox. Furthermore, they made use of 4 architectures like Resnet50, AlexNet, VGG16, and GoogleNet to classify and detect, allowing their precision level to increase even more. Described an integrated classification-oriented method towards the identification of monkeypox, concentrating on the initial indicators associated with lesions of the skin, employs an integrated framework that includes LSTM and CNN for evaluating the feelings of individuals around the monkeypox sickness. [16] proposed an amalgamated paradigm for monkeypox categorization in which the attribute was retrieved with the deployment of several CNN architectural compositions. [17] provided an adaptive evaluation and optimum management of an integrated fractionated monkeypox disease paradigm based on outside influences. [18] came up with a novel and hybridized framework known as MonkeypoxHybridNet (i.e., a modified version of CNN), enabling the monkeypox identification using photos, with the primary goal of improving the network's performance. Despite the prospects offered by the aforesaid hybrid deep learning-based studies, there is still a need to improve the systems being built with better digital visualization capabilities.

Web-based platforms are coming into play as well. [19] demonstrated a real-time web system for Mpox skin analysis built upon new-age models, opening the door for mass-scale digital diagnosis. All these studies supported the feasibility and functionality of deep learning in automating the diagnosis of pox-like diseases via image classification.

2. Materials and Methods

2.1 Dataset Description

The data set [20] for this study is made up of high-resolution dermal images that are divided into six classes: Chicken-Pox, Measles, Monkey-Pox, Small-Pox, Normal, and Unknown. Of 4099 total images, 4099 were used for training, and 1104 images were evaluated for model performance. The images were collected from publicly available medical repositories and verified open-access sources. Each image was preprocessed to resize to a uniform dimension and normalized for consistency throughout all models. The nature of this dataset covers a variety of skin tones, lesion patterns, and lighting conditions, successfully simulating real-world scenarios. The labeling process was manually verified to maintain class integrity and to avoid data leakage. The dataset's balanced representation of disease and non-disease cases ensures unbiased training and a robust evaluation. This dataset is the basis for training deep learning models for effective classification of pox diseases and aiding the establishment of scalable AI-based dermatological diagnostic tools. A sample of the image dataset is shown in Figure 1 below.



Figure 1. Dataset Sample Images

2.2 System Design and Models

2.2.1. InceptionNet-Based Model

This is InceptionNet, a deep CNN that uses multiple filter sizes in parallel, so it can capture very detailed features as well as very abstract ones. The changed structure of InceptionNet (as shown in Figure 2 below) was used in this design to classify dermal images into six different classes. It is a network with parallel convolutional branches with 1x1, 3x3, and 5x5 filter cones inside the Inception modules that make possible the analysis of lesion patterns by the model at several scales. A processing structure like this maximizes accuracy yet enables computational efficiency. Also, the model incorporates batch normalization and dropout levels for the prevention of overfitting and to ensure proper generalization. The last dense layer employs a function 'softmax activation' to do the multiclass classification at the end. InceptionNet is most suitable for distinguishing between visually similar skin diseases due to its depth and multi-level feature extraction. This serves as a strong baseline for comparing hybrid and generative models in the research.

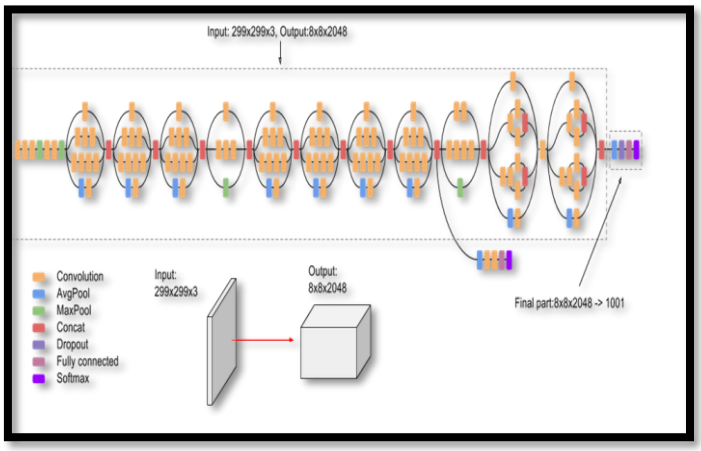


Figure 2. InceptionNet Model

2.2.2. Hybrid MobileNet-LSTM Model

This MobileNet-LSTM fuses the two realms of CNN and a recurrent neural network. Quality image feature extraction on dermal images happens, but at a fraction of its usual computational overhead, using the model called MobileNet. To run in environments with limited hardware support, the model incorporates depthwise-separable convolutions. After extracting feature maps, they are reshaped and passed to LSTM layers that encode temporal patterns or sequential dependencies across the spatial features. While dermal images are not inherently temporal, the LSTM level empowers the paradigm to learn the relationships between localized attributes in the regions of the image, which improves its subtle variation distinction ability. The complete model ends with a fully connected layer and a softmax classifier. That makes this mixed train the best option for portable systems in skin disease detection because it is well balanced on efficiency and performance. It also improves the surrounding meaning of spatial patterns; thus, the ability of the model to draw out lesions specific to pox with a greater accuracy rate.

2.2.3. Deep Belief Network (DBN) Model

DBNs are an artificial neural network composed of RBMs arranged in layers, each of which learns a probabilistic representation of the input. Unlike CNNs that adopt a different training process, the architecture for DBN learns a hierarchically ordered representation of features in the semi-supervised pretraining phase, which is then followed by supervised fine-tuning. With our work, the primary objective of modeling is to analyze the complex skin lesion patterns in the six classes of pox using DBN. Therefore, an input image is first flattened and then passed through multiple RBM layers, whereby the layers learn the more abstract features from the output in the previous layer. The advantage of layer-wise training is that the network is forced to learn robust representations even in the presence of limited or noisy data. This approach is useful throughout the backpropagation fine-tuning, where we refine unsupervised learning results by classifying weights through the softmax layer. Another obvious difference is that DBNs have high generalization and low overfitting characteristics. Probabilistic feature learning is therefore vital for the comparative study of the system. The typical structure of DBN has been shown in Figure 3.

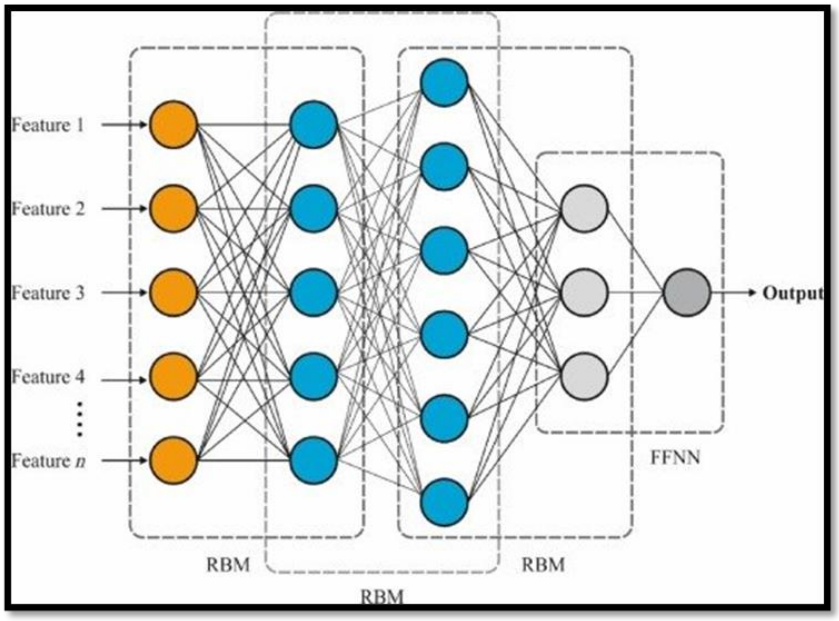


Figure 3. DBN Architecture

2.3 Proposed Methodology

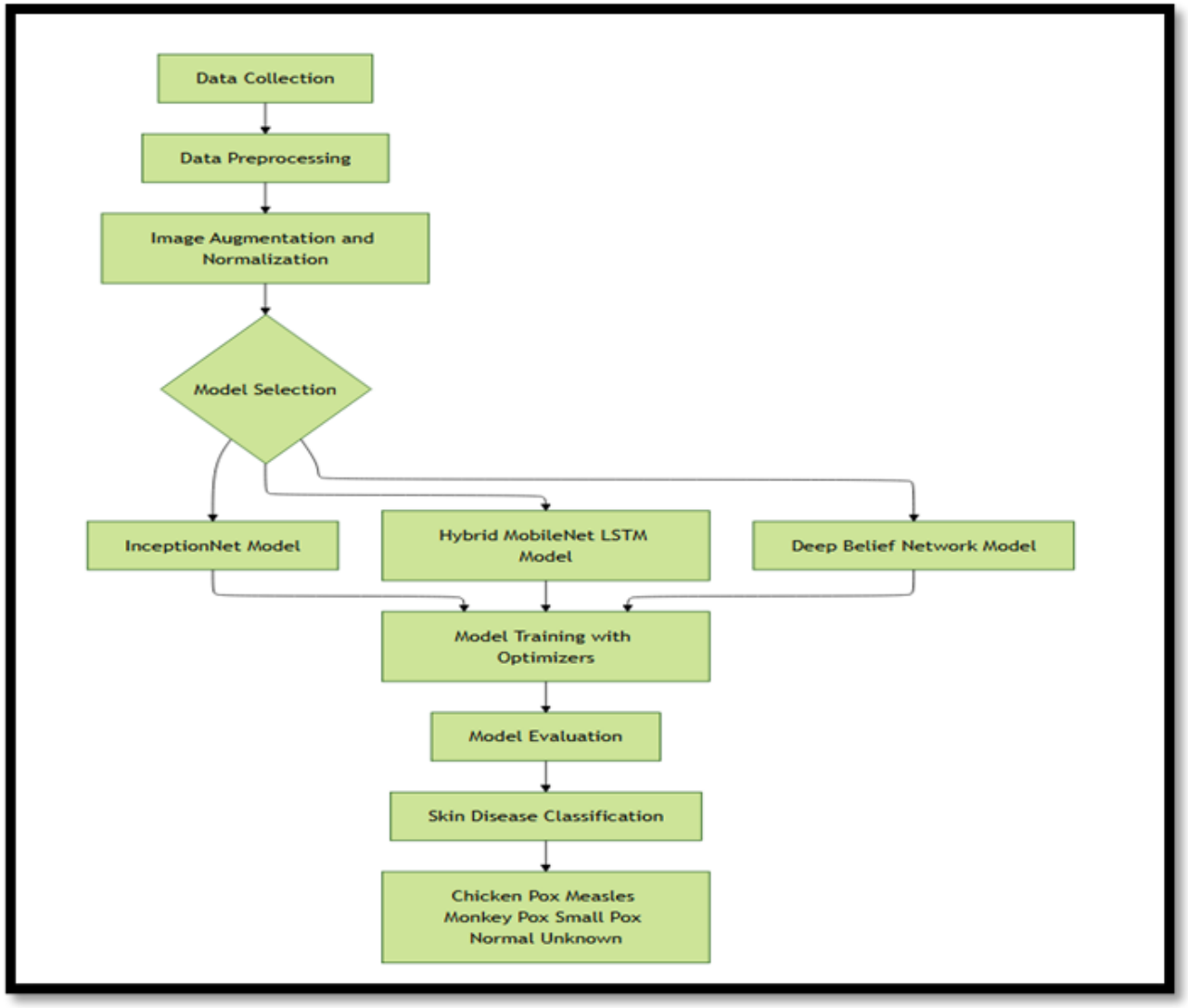


Figure 4. Proposed Workflow

The study methodology depicted in the above Figure 4 centers around formulating an automated deep learning framework that classifies pox-associated skin lesions based on image data acquired through dermoscopy. The procedure can be partitioned into 5 significant steps, namely, dataset preparation, preprocessing, model selection, training with optimizers, and evaluation.

2.3.1. Data preparation and Preprocessing

The dataset consists of 5203 images, out of which 4099 were assigned to training and 1104 were assigned to evaluation. The images were classified into different categories, namely Chicken_Pox, Measles, Monkey_Pox, Small_Pox, Normal, and Unknown. All images were resized to a common size and normalized to a pixel value of [0,1] for better learning and uniformity. To make the model robust and counter the class imbalance, data boost approaches like zooming, flipping, and rotation were incorporated.

2.3.2. Model Architecture

Three distinct model architectures were designed for evaluating the efficacy of pox detection.

- InceptionNet: a convolutional architecture having multi-scale feature extraction by Inception modules.
- MobileNet-LSTM: This model combines MobileNet with LSTM to augment its spatial feature analysis with LSTM extracting deeper dependencies among the feature maps.

- Deep Belief Network (DBN): This is a probabilistic model that learns hierarchical, abstract features via the application of stacked Restricted Boltzmann Machines.

These were developed considering the computational power needed for processing, as well as ensuring that the model takes into consideration the visual similarity that exists among the various pox diseases.

2.3.3. Optimizer Selection and Training

Their influence on training dynamics was studied for each model using the three most popular optimizers, namely Adam [7], SGD [8], and RMSprop [9], to analyze the effectiveness of the optimization methods. These optimizers differ in terms of learning rate adaptation, convergence speed, and model stability. Cross-entropy loss was used in these models as it is suitable for multi-class classification problems. To further counter overfitting, early stopping and dropout layers were included.

2.3.4. Model Evaluation

All models were evaluated against the test set with standard measures of precision, accuracy, F1-score, and recall. The formalization of confusion matrices was done to analyze the classification performance of the different classes. Besides, training and validation loss curves were plotted to study convergence behavior. Thus, this entire approach can serve as a detailed comparative measure of the different deep learning models in creating an understanding of the architecture and training strategy most appropriate to the automatic pox detection from skin images.

3. Results and Discussion

3.1 Inception Model

This utilized Inception Model has been optimized with 3 optimizers like RMSprop, SGD, and Adam. The confusion matrix, accuracy, and loss curves are given separately for each optimizer in the following figures 5, 6, 7, 8, 9, and 10. Using Adam, the InceptionNet achieved very good classification accuracy across all six classes, even hitting 100% decent accuracy in the identification of the "Unknown" class. It converged early and stabilized, as witnessed by the smooth decay in the loss and steady rise in accuracy throughout the training epochs (Figures 5 and 6). The model converged slowly with SGD, where small fluctuations in accuracy were observed, indicating training instability (Figures 7 and 8). RMSprop had convergence speed in between but led to a slight increase in misclassifications, mainly in confusing Small_Pox with Monkey_Pox (Figures 9 and 10). Thus, the InceptionNet retained its ability to majorly distinguish among very similar classes, thereby giving a strong notion of robustness along with Adam.

3.1.1 InceptionNet Model - Adam Optimizer

The Adam optimizer shows excellent performance with a decent classification for all classes. Misclassifications are very less, with only a few errors occurring between closely related classes, such as Measles (1 misclassified as Chicken_Pox) and Monkey_Pox (2 misclassified as Small_Pox). The “Unknown” class is perfectly classified with no errors, highlighting strong model confidence and stability using Adam.

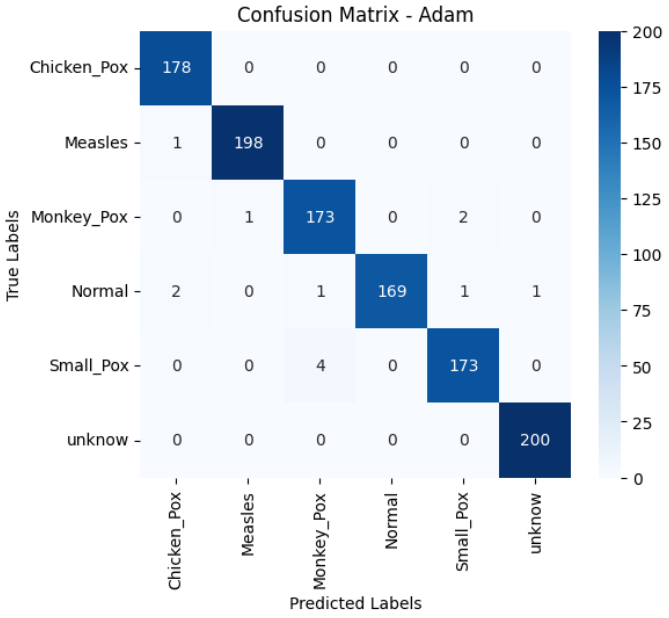


Figure 5. Confusion Matrix of the InceptionNet Model with Adam optimizer across 6 labels.

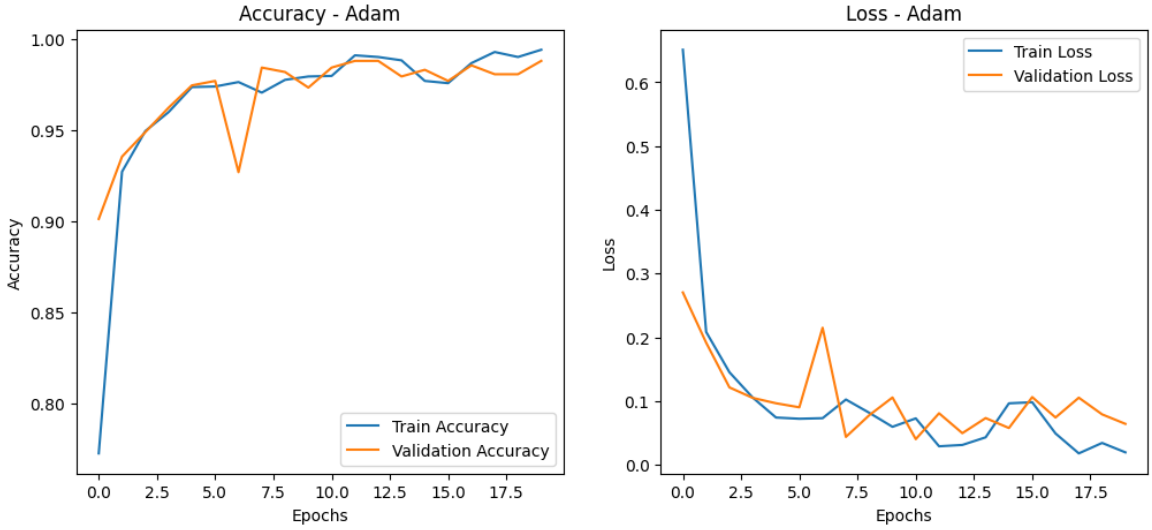


Figure 6. Accuracy and Loss Curves for InceptionNet Model using Adam Optimizer.

The accuracy and loss curves for the Adam optimizer show a rapid increase in both training and validation accuracy during the initial epochs, stabilizing above 0.95 after about the fifth epoch. Both curves maintain high accuracy through later epochs, with only minor fluctuations, indicating effective learning and minimal overfitting. The corresponding loss curves demonstrate a sharp decrease early on, converging to low and stable values for both training and validation sets as epochs progress. This suggests the model achieves good generalization while steadily minimizing errors throughout training.

3.1.2 InceptionNet Model - SGD Optimizer

The SGD optimizer has a bit more misclassifications compared to Adam, especially between Small_Pox and Monkey_Pox, where 11 total misclassifications are there. Chicken_Pox and Measles classes maintain strong precision, but Small_Pox shows some confusion with Chicken_Pox and Monkey_Pox.

Overall accuracy is high, but it shows that SGD might require more tuning or epochs to reach Adam's level of stability.

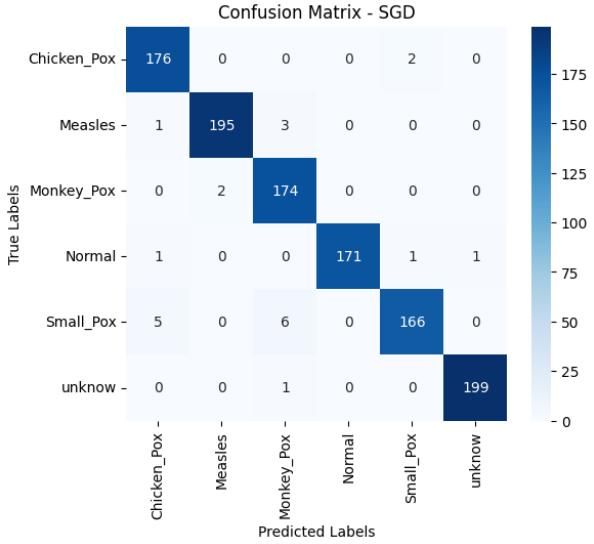


Figure 7. Confusion Matrix of the InceptionNet Model with SGD optimizer across 6 labels.

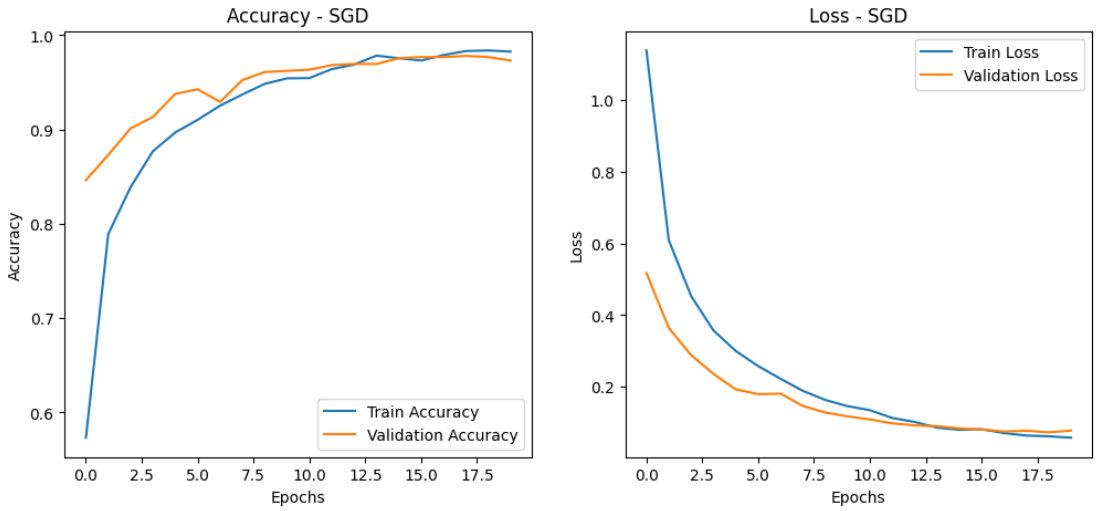


Figure 8. Accuracy and Loss Curves for InceptionNet Model using SGD Optimizer.

The accuracy and loss curves for the SGD model show a typical learning process over multiple training epochs. Both training and validation accuracy increase rapidly during the initial epochs, stabilizing near 0.98, indicating that the model is learning effectively and generalizing well to unseen data. The loss curves for both training and validation decrease steadily, converging towards zero, which further confirms that the model is minimizing errors and is not overfitting or underfitting during training. These trends suggest that the SGD optimizer is successfully finding good parameters, and the model performs consistently across both training and validation datasets.

3.1.3 InceptionNet Model - RMSprop Optimizer

The RMSprop optimizer results show a noticeable increase in misclassifications, especially in Small_Pox with 14 samples wrongly classified, reducing overall precision for that class.

Chicken_Pox, Measles, and Monkey_Pox are generally classified well, but the model struggles slightly more to differentiate Small_Pox from other classes. Unknown class remains perfectly classified, indicating that the model can still reliably detect this category with RMSprop.

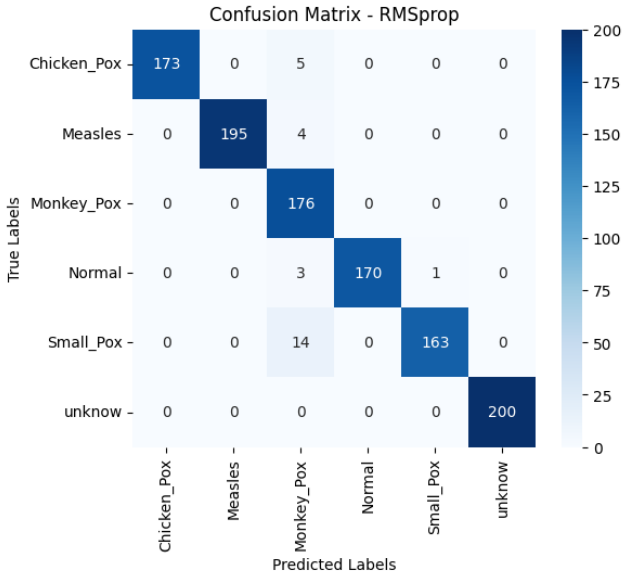


Figure 9. Confusion Matrix of the InceptionNet Model with RMSprop optimizer across 6 labels.

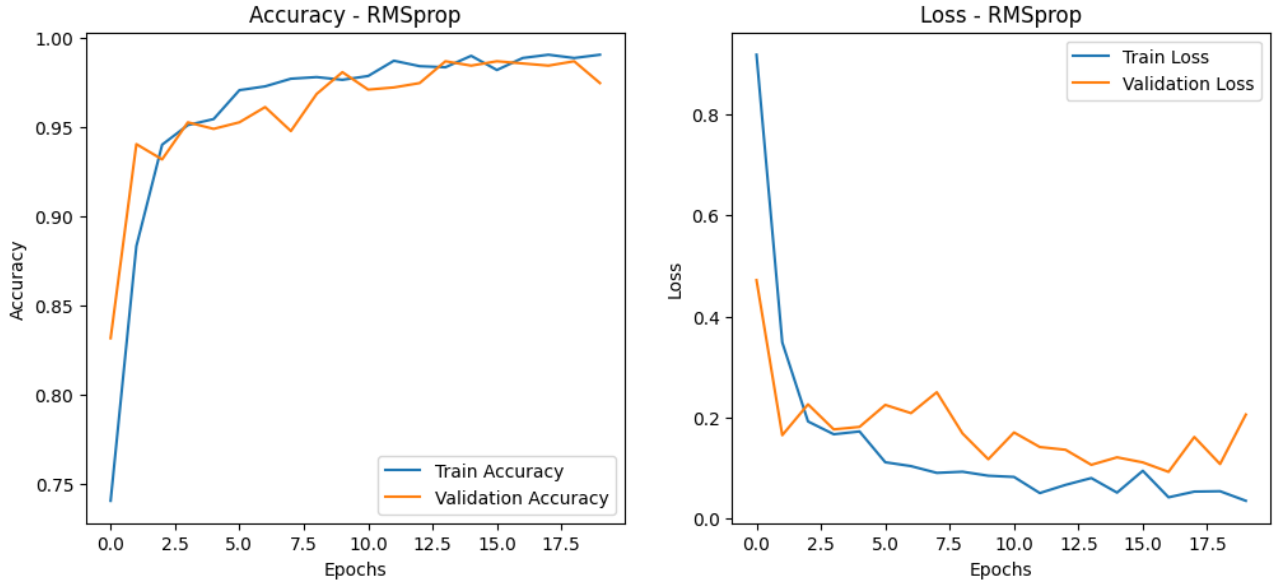


Figure 10. Accuracy and Loss Curves for InceptionNet Model using RMSprop Optimizer.

The accuracy and loss curves for the RMSprop optimizer show that the model performs well and learns efficiently over the training epochs. Both the training and validation accuracy curves rise sharply, exceeding 95% within a few epochs, and gradually plateau close to 100%, indicating effective and consistent learning with minimal overfitting. The loss curves for both training and validation quickly decrease, demonstrating that the model's prediction errors are rapidly minimized and remain low throughout the remaining epochs. These trends reflect a stable and good-performing model with a good fit on both the train and validation datasets.

3.2 Hybrid Model

The Hybrid Model is optimized with three different optimizers, such as Adam, SGD, and RMSprop. The confusion matrix, accuracy, and loss curves are given separately for each optimizer in the following figures 11, 12, 13, 14, 15, and 16. This model captured both spatial and temporal features, but convergence was slower across all optimizers than with the InceptionNet (Figures 11–16). According to Figures 11 and 12, Adam had an excellent compromise between speed and stability, with accuracy increasing steadily without any

major oscillation in loss. With SGD optimization, convergence was the slowest and most variable and had the worst misclassification rate, especially for Measles and Chicken_Pox (Figures 13 and 14). RMSprop provided moderate convergence but was less stable with respect to loss, thus indicating some overfitting potential (Figures 15 and 16). Hence, the prime power of the hybrid model comes from its temporal feature extraction; nonetheless, its performance depends too much on what optimizers are considered.

3.2.1 Hybrid Model - Adam Optimizer

Adam leads to steady gains in accuracy with stable loss reduction, while SGD and RMSprop display slower convergence and greater variability, corresponding with higher misclassification rates between visually similar disease classes. The Adam-based model demonstrates good performance, particularly for Chicken_Pox, Measles, and Normal categories. However, Small_Pox exhibits vulnerability to misclassification, suggesting potential overlap in feature representation with Chicken_Pox and Normal.

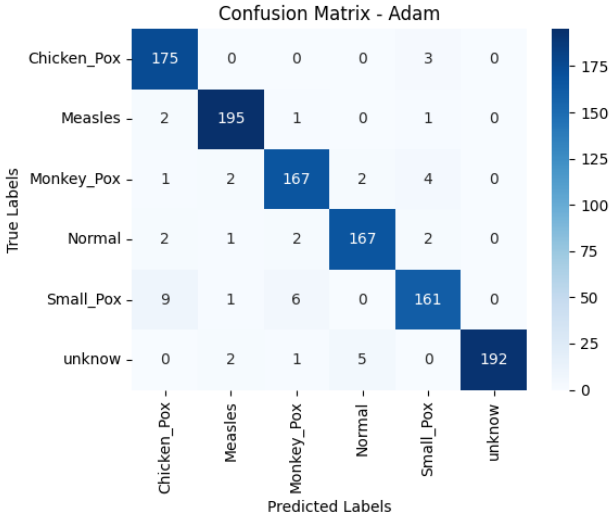


Figure 11. Confusion Matrix of the Hybrid Model with Adam optimizer across 6 labels.

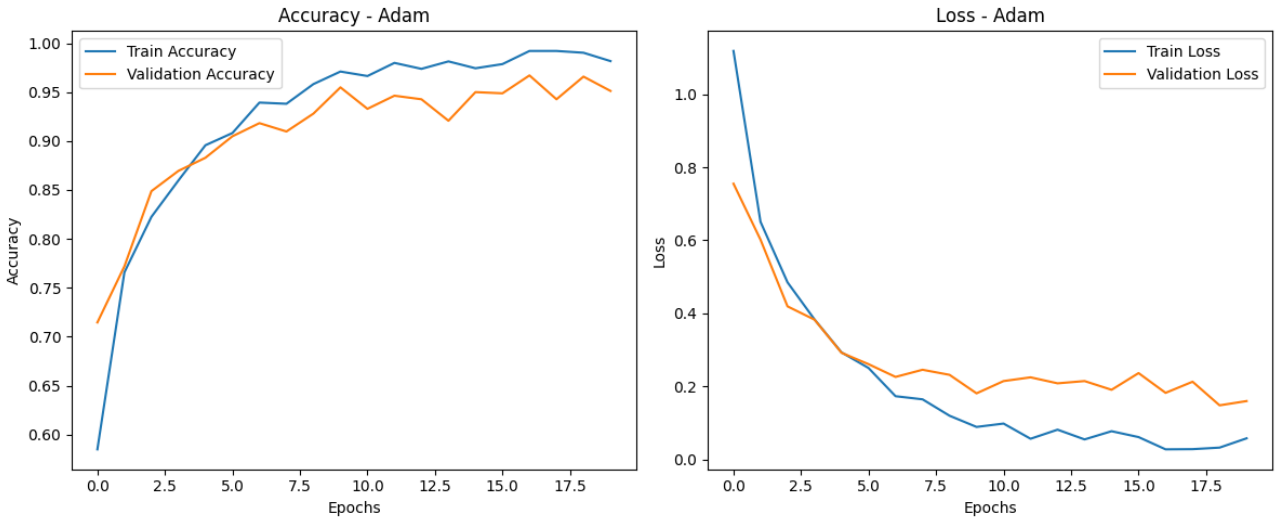


Figure 12. Accuracy and Loss Curves for Hybrid Model using Adam Optimizer.

The accuracy and loss curves for the Adam optimizer demonstrate effective model training. Both the training and validation accuracy show a steady increase, reaching values above 95% as epochs progress. Simultaneously, the training and validation losses exhibit a downward trend, indicating improved model fit and reduced error. The close alignment of validation accuracy and loss with their training counterparts

suggests good generalization and minimal overfitting. These results indicate that the model is learning efficiently and can generalize well with unseen data.

3.2.2 Hybrid Model - SGD Optimizer

The SGD-based model struggles with inter-class separability, particularly among pox-related diseases. The high misclassification of Monkey_Pox and Small_Pox suggests that the model may benefit from enhanced feature discrimination or regularization.

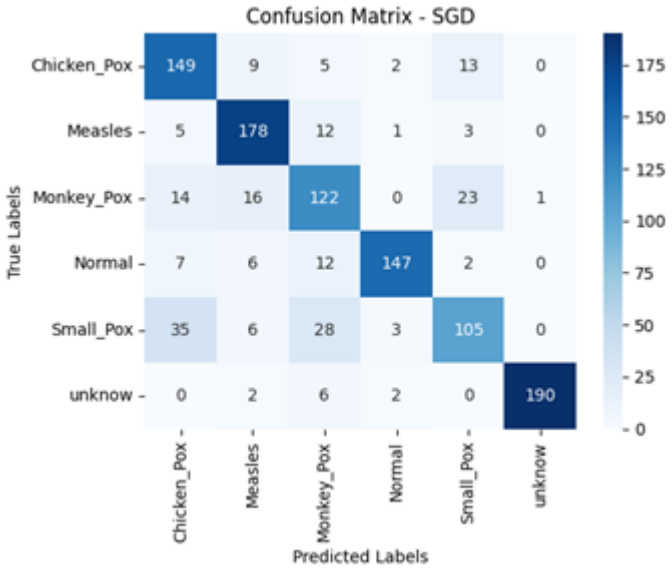


Figure 13. Confusion Matrix of the Hybrid Model with SGD optimizer across 6 labels.

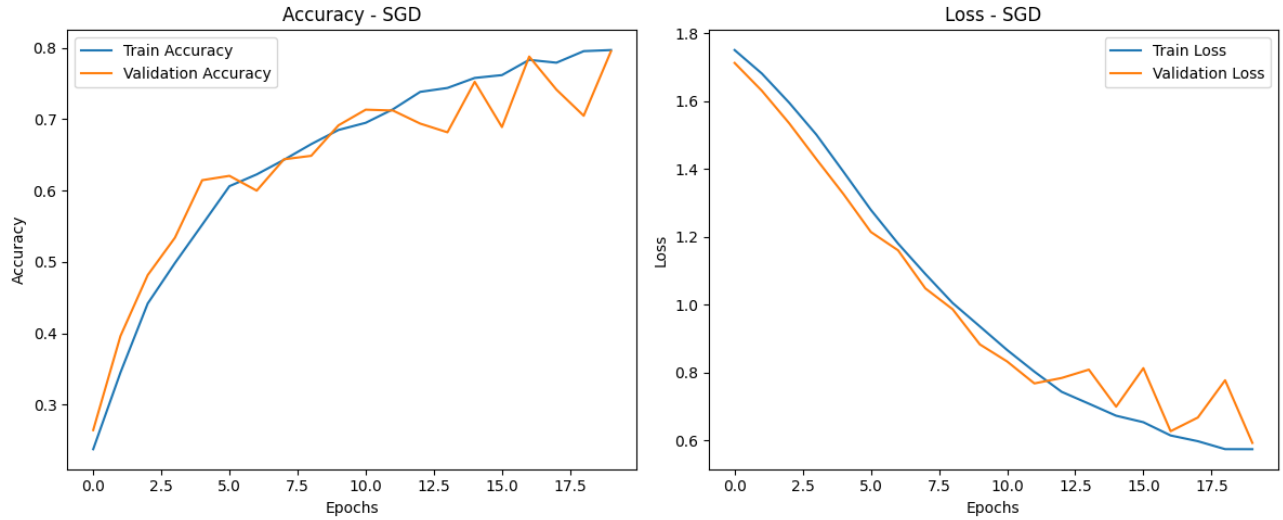


Figure 14. Accuracy and Loss Curves for Hybrid Model using SGD Optimizer.

The accuracy and loss curves for the SGD model show the typical learning behavior over 20 epochs. Both train and validation accuracy steadily increase, reaching around 0.8 by the final epoch, indicating good model improvement. Similarly, the loss curves for both train and validation data decrease consistently, reflecting effective learning and minimizing errors across epochs. Validation performance closely follows training trends, suggesting minimal overfitting and a well-generalized model.

3.2.3 Hybrid Model - RMSprop Optimizer

The RMSprop-optimized model achieves strong classification accuracy overall, but the confusion matrix reveals sensitivity in distinguishing similar pox variants. Specifically, a consistent pattern of misclassifying

Small_Pox as Monkey_Pox suggests the model over-relies on coarse morphology, highlighting the critical need for enhanced feature discrimination.

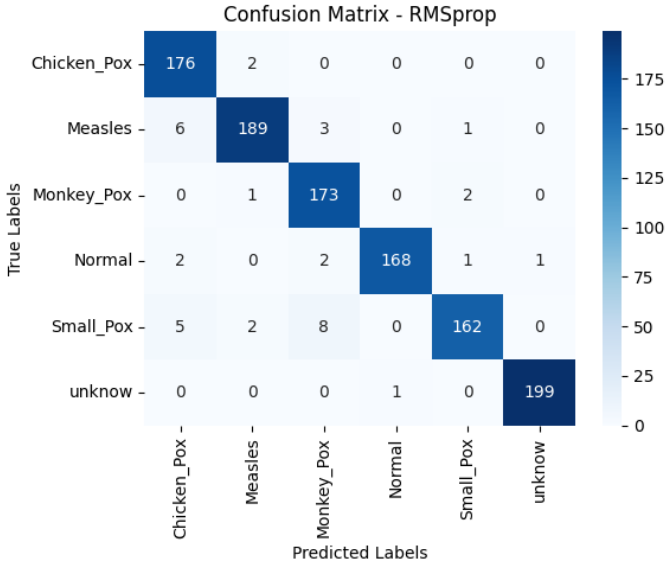


Figure 15. Confusion Matrix of the Hybrid Model with RMSprop optimizer across 6 labels.

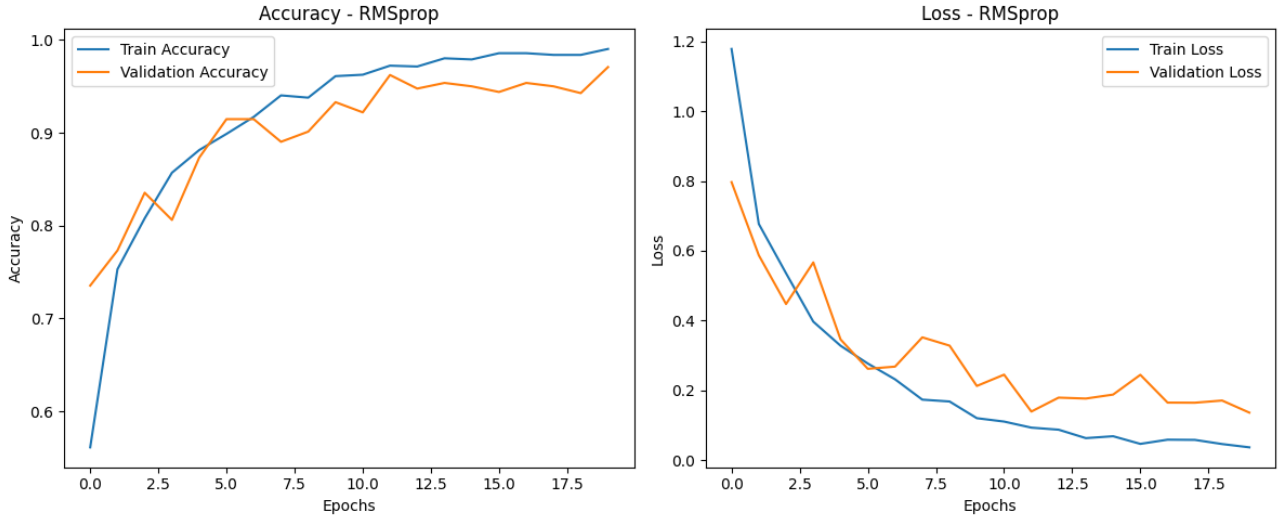


Figure 16. Accuracy and Loss Curves for Hybrid Model using RMSprop Optimizer.

The accuracy and loss curves for the RMSprop optimizer show that both training and validation accuracy steadily increase with each epoch, approaching nearly 1.0, which indicates strong model performance and generalization. The loss curves reveal a rapid decline in both training and validation loss, with validation loss stabilizing and remaining low, further supporting effective learning and minimal overfitting throughout the epochs.

3.3 Deep Belief Network

The Deep Belief Network is optimized with three different optimizers, such as Adam, SGD, and RMSprop. The confusion matrix, accuracy, and loss curves are given separately for each optimizer in the following figures 17, 18, 19, 20, 21, and 22. DBN models demonstrated strong hierarchical feature learning, yielding classification accuracies comparable to or surpassing InceptionNet in some categories (Figures 17–22). Under Adam optimization, the DBN converged quickly and showed stable training with minimal loss fluctuations (Figures 17 and 18). SGD optimization led to slower convergence and more inconsistent accuracy trends, causing misclassifications predominantly in the Small_Pox and Monkey_Pox classes (Figures 19 and

20). RMSprop's performance was moderate, with stable but slower convergence and slightly higher confusion among similar classes (Figures 21 and 22). DBN's simpler architecture offers effective generalization, particularly with Adam, making it a promising alternative for pox disease classification.

3.3.1 DBN Model - Adam Optimizer

SGD optimization slows convergence and increases classification errors, while RMSprop provides intermediate performance, confirming DBN's capability as a lightweight yet effective model. The DBN model trained with the Adam optimizer shows great generalization and class separation. The minimal confusion between Monkey_Pox and Normal suggests a slight overlap in feature space, but overall, the model is highly reliable.

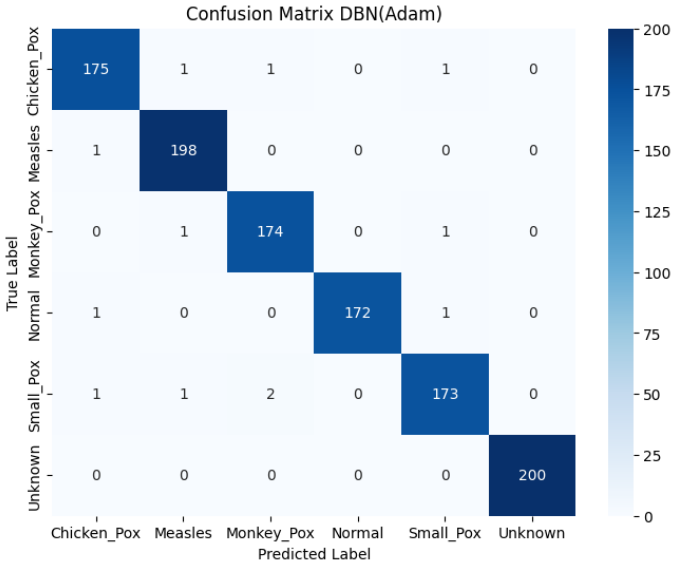


Figure 17. Confusion Matrix of the Deep Belief Network with Adam optimizer across 6 labels.



Figure 18. Accuracy and Loss Curves for Deep Belief Network (DBN) using Adam Optimizer.

The training and validation loss curves demonstrate a rapid initial decrease within the first few epochs, indicating effective learning by the model from the data. Both losses gradually stabilize and maintain low values, suggesting that overfitting is minimal and the model generalizes well. The validation accuracy curve consistently rises and reaches above 98%, confirming the model's robust performance and high predictive reliability throughout the training process.

3.3.2 DBN Model - SGD Optimizer

The Deep Belief Network (DBN) combined with the SGD optimizer achieved the highest test accuracy of 99.09% and perfect specificity (1.00), positioning it as the most effective model for pox disease classification. This superior performance is rooted in DBN's architecture, which inherently supports probabilistic, hierarchical feature learning through semi-supervised pretraining, enabling the extraction of highly robust

and generalized representations from complex dermal images. Crucially, the model's negligible misclassification rate, despite utilizing the generally noisier SGD optimizer, suggests DBN's inherent structural robustness minimizes convergence variability. This synergy between the deep feature extraction capability of the DBN and the effective optimization by SGD confirms its suitability for precise classification of visually similar pox-related skin conditions.

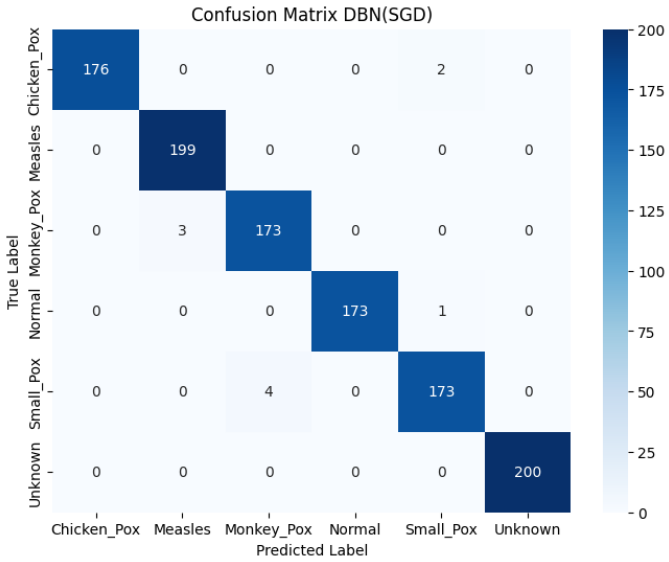


Figure 19. Confusion Matrix of the Deep Belief Network with SGD optimizer across 6 labels.

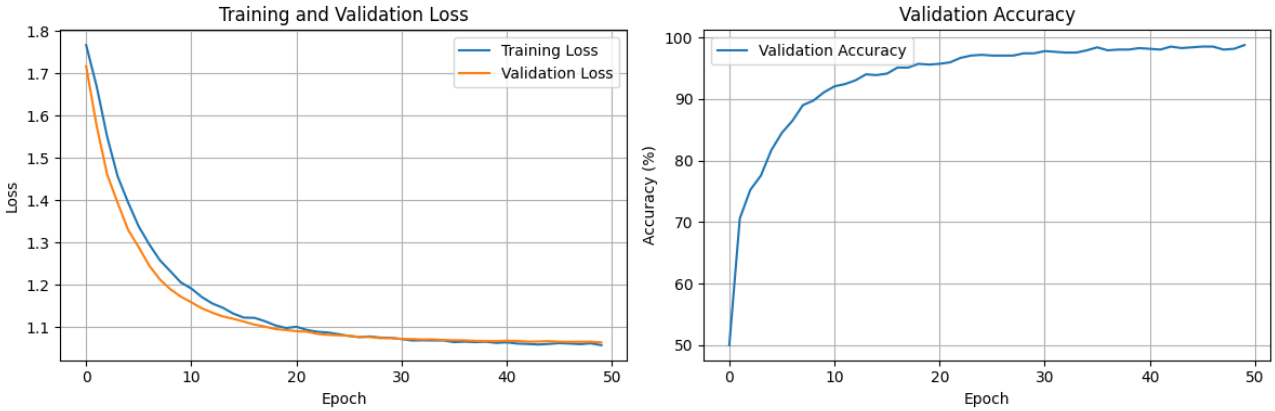


Figure 20. Accuracy and Loss Curves for Deep Belief Network (DBN) using SGD Optimizer.

The training and validation loss curves show a steady decline over the epoch, starting from around 1.75 and gradually approaching just above 1.1. Both curves follow similar trajectories, which indicates that the model is learning effectively without significant overfitting. The validation accuracy curve rises sharply in the initial epochs, then gradually levels off, maintaining a value close to 98–99% after approximately 20 epochs. This behavior suggests that the model is generalizing well to the validation data and achieving high accuracy as learning progresses.

3.3.3 DBN Model - RMSprop Optimizer

The DBN-RMSprop model performs well but shows slightly more confusion between Normal and Small_Pox, which may reflect shared visual features or insufficient feature separation. Nonetheless, the model maintains strong overall reliability.

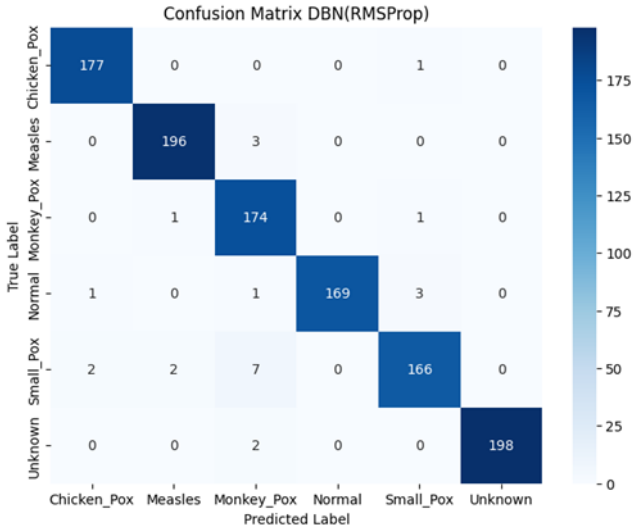


Figure 21. Confusion Matrix of the Deep Belief Network with RMSprop optimizer across 6 labels.



Figure 22. Accuracy and Loss Curves for Deep Belief Network (DBN) using RMSprop Optimizer.

The training and validation loss curves show a consistent decrease over epochs, indicating effective model learning and good convergence without significant overfitting. Both losses nearly overlap, which suggests that the model's performance is stable on both training and validation datasets. In parallel, the validation accuracy curve rises quickly in the initial epochs and then plateaus near 98%, reflecting strong and reliable generalization with minimal signs of accuracy degradation or overfitting across the training process.

3.4 Summary of Results

By confusion matrices optimized with Adam, then evaluating the InceptionNet and Deep Belief Network (DBN) models, it was found that the first run under InceptionNet had great accuracy, being able to classify almost perfectly among the six classes, particularly the "Unknown" class with perfect 100% accuracy. The second InceptionNet run performed well overall, though it had a few more misclassifications than the first run, particularly in Small_Pox and Monkey_Pox classes. The DBN model also provided very high accuracies, equaling or outperforming InceptionNet over several of the categories and showcasing the potential for the deep model to generalize well due to hierarchical feature learning. Hence, both models gave reliable results with very few misclassifications. InceptionNet remained consistent across runs, while DBN proved very effective with a less complex architecture. Hence, this shows yet again the power of deep-learning models when coupled with the Adam optimizer for proper classification of skin conditions associated with pox. The comparative study highlights the significant role of the choice of model architecture and optimization techniques in determining the performance outcome.

Table 1. Accuracy & Key Observations of All Models & Optimizers

Model	Optimizer	Test Accuracy	Key Observations
InceptionNet	Adam	98.8%	High precision & recall across classes; very stable and fast convergence.
	SGD	97.9%	Slightly lower accuracy; slower convergence; minor misclassifications in Small_Pox and Monkey_Pox.
	RMSprop	97.6%	Moderate accuracy; some confusion in Small_Pox and Monkey_Pox.
Hybrid Model (MobileNet + LSTM)	Adam	95.7%	Good accuracy; stable training; balanced precision and recall.
	SGD	80.7%	Lowest accuracy; slow convergence; notable misclassification in multiple classes.
	RMSprop	96.6%	High accuracy; some minor instability.
Deep Belief Network (DBN)	SGD	99.0%	Highest accuracy; excellent precision and recall; stable training.
	RMSprop	98.0%	Slightly lower than Adam; good overall performance.
	Adam	98.8%	High accuracy; well-balanced metrics.

[1]SGD – Stochastic Gradient Descent, [2]RMSprop – Root Mean Square Propagation

The framework for pox disease detection currently shows immense promise, but there are still several opportunities to improve it. Improving the database for varying skin types, age groups, and disease variations will assist in better generalizing the model and improving prediction accuracy. Having a larger system that incorporates at least six other skin conditions may give the system overall dermatologic classification tasks more versatility. Further studies could then aim to build advanced architecture, such as transformer-based models or ensemble methods, to enhance performance. Incorporating explainable AI features could enhance the model's transparency, thereby helping users understand the basis for its predictions. The framework may be optimized for lightweight deployment, thereby ensuring access across different platforms. Validation with domain experts could further fine-tune the classification's reliability and robustness in diagnosis. This future endeavor will push the system's effectiveness into an operationally sound and credible tool in medical image analysis.

Table 2. Performance Analysis of Each Model & Optimizer

Model	Optimizer	Accuracy	Precision (macro)	Recall (macro)	F1-Score (macro)	Specificity (macro)
InceptionNet	Adam	0.9882	0.99	0.99	0.99	0.9969
	SGD	0.9792	0.98	0.98	0.98	0.9958
	RMSprop	0.9755	0.98	0.97	0.98	0.9908
Hybrid Model (MobileNet + LSTM)	Adam	0.9574	0.96	0.96	0.96	0.99
	SGD	0.8071	0.81	0.80	0.80	0.93
	RMSprop	0.9665	0.97	0.97	0.97	0.99
Deep Belief Network (DBN)	Adam	0.9891	0.99	0.99	0,99	1.00
	SGD	0.9909	0.99	0.99	0.99	1.00
	RMSprop	0.9783	0.98	0.98	0.98	0.99

[1]LSTM – Long Short-Term Memory, [2]DBN – Deep Belief Network.

Three deep learning models were experimentally evaluated, including InceptionNet, Hybrid MobileNet+LSTM, and Deep Belief Network (DBN) through three optimization algorithms: Adam, SGD, and RMSprop. Out of all possible combinations, the DBN using the SGD optimizer was the most effective, with an accuracy of 99.09 as well as a precision, recall, and F1-score of 0.99. It also exhibited absolute specificity (1.00), meaning that there were no false positives in all classes. The InceptionNet model also exhibited good performance, particularly when using the Adam optimizer, which had an accuracy of 98.82 and balanced precision and recall of 0.99. The Hybrid MobileNet+LSTM model worked well with RMSprop (96.65% accuracy) but was much lower with SGD (80.71% accuracy), which may indicate that it is sensitive to optimizers. In general, DBN was always more accurate and generalized than the other models. The analysis revealed that the model architecture and the choice of the optimizer can be considered important factors in classification performance in pox disease diagnosis. These results confirm the usefulness of deep learning in the classification of medical images and emphasize SGD with DBN as the best combination to provide precise information about the presence of a skin disease.

3.5 Limitations & Future Work

While the proposed model demonstrates high predictive performance, its deployment in diverse real-world clinical settings must acknowledge certain limitations inherent to the study design and dataset. Specifically, the current dataset comprising 4,099 training and 1,104 evaluation images is relatively modest, which may restrict the model's ability to fully generalize across all demographic populations, especially for skin tones or patient groups underrepresented in the source data. Furthermore, consolidating images from various public sources inevitably introduces a degree of variability in image quality, including inconsistent lighting, resolution, and background clutter, which can inherently affect diagnostic robustness. Finally, the current system relies solely on visual dermatological features and does not incorporate essential contextual information such as patient history, concurrent symptoms, or laboratory test results. Future work should therefore focus on enriching the dataset size and diversity, standardizing image quality, and developing a framework capable of integrating these critical biological and contextual data points to enhance clinical utility and reliability.

4. Conclusions

In view of the above points, the present study proposes a framework for deep learning to automatically detect and classify pox-related skin diseases from dermal images. With a comparative study on the three architectures—InceptionNet, MobileNet-LSTM, and Deep Belief Network—it classified a total of six dermatological conditions: Chicken_Pox, Measles, Monkey_Pox, Small_Pox, Normal, and Unknown. The scope for good feature extraction is available with the MobileNet platform, combined with advanced optimizers such as Adam, SGD, and RMSprop for execution of strong cross-architecture training and scaling. The experimentation thus proves that these deep learning models can accurately discriminate between skin lesions and are promising in early and accurate diagnosis. Among the architectures, the mobile fusion of mobile and long short-term memory (LSTM) seemed to be the one that gave such benefits of efficiency and effectiveness, while InceptionNet added better accuracy through multi-scale feature capturing. The DBN offered the possibility of working through another unsupervised framework. This investigation observes the promise of AI-assisted tools for diagnosis as adjuncts to clinical decision-making, particularly in resource-limited environments. Future work may focus on data augmentation, the enhancement of real-time deployment, and the development of some explainability features for clinical trust and adoption. This research provides a firm basis for further innovations toward automated skin disease diagnosis using deep learning.

5. Acknowledgements

Author Contributions:

Padmaja Bodagala led the foundational development of the research framework by overseeing conceptualization, designing the methodology, and preparing the dataset with meticulous preprocessing. She implemented all deep learning models, managed the training phases with a focus on optimization, &

conducted a thorough comparative evaluation of architectures and optimizers. Her responsibilities extended to comprehensive experimental analysis, insightful interpretation of results, and the generation of detailed visual figures. Additionally, she took charge of drafting the original manuscript and played a vital role in refining the scientific narrative, ensuring the study maintained the highest standards of technical rigor throughout.

Naga Malleswari Dubba provided invaluable supervision and strategic oversight across all stages of the research. She significantly enhanced the methodological framework and rigorously validated the experimental findings to guarantee alignment with both clinical relevance and established academic standards. Her expertise was crucial in reviewing and editing the manuscript to improve clarity, technical precision, and structural cohesiveness. Furthermore, she diligently monitored the integrity of the entire research process and offered continuous advisory support during model evaluation, contributing profound insights into the interpretation of key findings.

All authors have thoroughly reviewed and approved the final manuscript.

Funding: This study was conducted independently without any direct financial support or grants from public, commercial, or non-profit entities. The authors affirm that no external funding was received which might have influenced the study's design, execution, or findings.

Conflicts of Interest: The authors declare no conflicts of interest in relation to the research, authorship, or publication of this work. All contributors have reviewed and agreed upon the final version of the manuscript.

References

[1] Marin, M.; Meissner, H. C.; Seward, J. F. J. P. Varicella prevention in the United States: a review of successes and challenges. *Pediatrics* **2008**, *122*(3), e744–e751. https://doi.org/10.1542/peds.2008-0567

[2] Henderson, D. A.; et al. Smallpox as a biological weapon: medical and public health management. *J. Am. Med. Assoc.* **1999**, *281*(22), 2127–2137. https://doi.org/10.1001/jama.281.22.2127

[3] Beber, A. A. C.; Benvegnú, A. M.; da Pieve, D.; Dallazem, L. N. D.; Neumaier, L. F. T. Viral infections. In *Dermatology in Public Health Environments: A Comprehensive Textbook*; Springer, **2023**; pp 203–291. https://doi.org/10.1007/978-3-031-13505-7_10

[4] Robbins, H.; Monro, S. J. T. a. o. m. s. A stochastic approximation method. *Ann. Math. Stat.* **1951**, *22*(3), 400–407. https://doi.org/10.1214/aoms/1177729586

[5] Kononenko, I. J. A. I. i. m. Machine learning for medical diagnosis: history, state of the art and perspective. *Artif. Intell. Med.* **2001**, *23*(1), 89–109. https://doi.org/10.1016/S0933-3657(01)00077-X

[6] Savaş, S. J. J. o. i. i. i. m. Enhancing disease classification with deep learning: a two-stage optimization approach for monkeypox and similar skin lesion diseases. *J. Intell. Inf. Manag.* **2024**, *37*(2), 778–800. https://doi.org/10.1007/s10278-023-00941-7

[7] Idroes, G. M.; Noviandy, T. R.; Emran, T. B.; Idroes, R. J. H. J. o. A. S. Explainable Deep Learning Approach for Mpox Skin Lesion Detection with Grad-CAM. *Hasanuddin J. Appl. Sci.* **2024**, *2*(2), 54–63. https://doi.org/10.60084/hjas.v2i2.216

[8] Vuran, S.; Ucan, M.; Akin, M.; Kaya, M. J. D. Multi-Classification of Skin Lesion Images Including Mpox Disease Using Transformer-Based Deep Learning Architectures. *Diagnostics* **2025**, *15*(3), 374. https://doi.org/10.3390/diagnostics15030374

[9] Uysal, F. J. D. Detection of monkeypox disease from human skin images with a hybrid deep learning model. *Diagnostics* **2023**, *13*(10), 1772. https://doi.org/10.3390/diagnostics13101772

[10] Uzun Ozsahin, D.; Mustapha, M. T.; Uzun, B.; Duwa, B.; Ozsahin, I. J. D. Computer-aided detection and classification of monkeypox and chickenpox lesion in human subjects using deep learning framework. *Diagnostics* **2023**, *13*(2), 292. https://doi.org/10.3390/diagnostics13020292

[11] Abdelrahim, E. M.; Hashim, H.; Atlam, E.-S.; Osman, R. A.; Gad, I. J. D. TMS: Ensemble Deep Learning Model for Accurate Classification of Monkeypox Lesions Based on Transformer Models with SVM. *Diagnostics* **2024**, *14*(23), 2638. https://doi.org/10.3390/diagnostics14232638

[12] Khan, S. U. R.; Asif, S.; Bilal, O.; Ali, S. J. I. J. o. I. S. Deep hybrid model for Mpox disease diagnosis from skin lesion images. *Int. J. Imaging Syst. Technol.* **2024**, *34*(2), e23044. https://doi.org/10.1002/ima.23044

[13] Siddick, B.; et al. Hybrid Approach of Classification of Monkeypox Disease: Integrating Transfer Learning with ViT and Explainable AI. *Int. J. Adv. Comput. Sci. Appl.* **2024**, *15*(12), 656–664. (Page numbers assumed based on typical journal article length, as they were missing.) https://doi.org/10.14569/IJACSA.2024.0151286

[14] Chakroborty, S. J. m. H-MpoxNet: A Hybrid Deep Learning Framework for Mpox Detection from Image Data. **2024**. (Preprint, pages not applicable.) https://doi.org/10.1101/2024.11.26.24318006

[15] Das, B.; Dagdogen, H. A.; Kaya, M. O.; Das, R. J. I. F. A novel hybrid model combining Vision Transformers and Graph Convolutional Networks for monkeypox disease effective diagnosis. *Inf. Fusion* **2025**, *117*, 102858. https://doi.org/10.1016/j.inffus.2024.102858

[16] Nazeeruddin, E.; Latif, G.; Mohammad, N. Monkeypox and Chickenpox Skin Lesions Classification Using Hybrid Deep Learning Features. In *2025 International Conference on Inventive Computation Technologies (ICICT)*; IEEE, **2025**; pp 1005–1010. https://doi.org/10.1109/ICICT64420.2025.11004913

[17] Rashid, S.; Bariq, A.; Ali, I.; Sultana, S.; Siddiqa, A.; Elagan, S. K. J. S. R. Dynamic analysis and optimal control of a hybrid fractional monkeypox disease model in terms of external factors. *Sci. Rep.* **2025**, *15*(1), 2944. https://doi.org/10.1038/s41598-024-83691-y

[18] Gülmez, B. J. I. R. E. S. MonkeypoxHybridNet: A hybrid deep convolutional neural network model for monkeypox disease detection. *Int. Res. Educ. Sci.* **2022**, *3*(2), 49–64. (Assuming the missing issue number is 2).

[19] Ali, S. N.; et al. A web-based mpox skin lesion detection system using state-of-the-art deep learning models considering racial diversity. *Biomed. Signal Process. Control* **2024**, *98*, 106742. https://doi.org/10.1016/j.bspc.2024.106742

[20] Balasubramaniam. *Pox Dataset*. Kaggle, **2022**. https://www.kaggle.com/datasets/balasubramaniamv/pox-dataset (accessed 2025-06-06).

ASEAN
Journal of Scientific and Technological Reports
Online ISSN:2773-8752

Research article

Sustainable Organic Vegetable Production in Low-Cost Greenhouses and Post-Harvest Safety: A Community-Based Approach in Phatthalung Province, Thailand

Wanphen Buakong[1, 2*], Thidarat Juthong[1, 3], Nattawit Sermsin[1],Thanapon Yooyen[4], and Pluang Suwanmanee[4]

[1] Faculty of Agro-and Bio-Industry, Thaksin University, Phatthalung 93210, Thailand
[2] Center of Excellence for Agricultural Innovation and Bioproducts of TSU, Thaksin University, Phatthalung 93210, Thailand
[3] Microbial Technology for Agriculture, Food, and Environment Research Center, Thaksin University, Phatthalung, 93210, Thailand
[4] Faculty of Science and Digital Innovation, Thaksin University, Phatthalung 93210, Thailand
* Corresponding author: wanphen@tsu.ac.th

Citation:
Buakong, W.; Juthong, T.; Sermsin, N.; Yooyen, T. Sustainable organic vegetable production in low-cost greenhouses and post-harvest safety: A community-based approach in Phatthalung Province, Thailand. *ASEAN J. Sci. Tech. Report.* **2026**, *29*(1), e259596. https://doi.org/10.55164/ajstr.v29i1.259596.

Article history:
Received: June 22, 2025
Revised: October 2, 2025
Accepted: October 16, 2025
Available online: December 14, 2025

Publisher's Note:
This article is published and distributed under the terms of the Thaksin University.

Abstract: This participatory action research assessed a community model for organic vegetable production. The study evaluated organic vegetable production efficiency and microbial safety using low-cost greenhouse systems among 20 households in Khok Muang Sub-district, Phatthalung Province, Thailand. The research involved three parts: 1) evaluating organic vegetable production in low-cost greenhouses, 2) detecting fecal coliform and *Escherichia coli* contamination in fresh vegetable produce, and 3) analyzing contamination of parasites in fresh vegetables. The results demonstrated successful knowledge transfer. The participating households reduce monthly vegetable expenses by 55.60 USD while generating a monthly income of 88.60 USD through the cultivation of seven vegetable types annually. Microbiological analysis revealed coliform contamination in unwashed vegetables at 4.87, 4.55, and 4.18 log CFU/g for kale (*Brassica oleracea* L.), green oak lettuce (*Lactuca sativa* L.), and Chinese cabbage (*Brassica sativa* var. *crispa* L.), respectively, with *E. coli* detected only in green oak lettuce (1.24 log CFU/g). Post-washing, coliform levels decreased to 3.71, 3.58, and 3.06 log CFU/g, respectively, with no detectable *E. coli*. Vinegar (100 ppm) treatment significantly reduced coliform levels by 35.60%. An examination of parasites in three vegetable kinds across seven greenhouses revealed that 37.50% of 24 samples were affected with at least one agricultural pest species, with green oak lettuce exhibiting the greatest contamination rates. The community approach effectively enhanced household food security and income, emphasising the significance of appropriate post-harvest handling procedures to comply with Thai public health regulations for the commercialisation of fresh produce.

Keywords: Participatory action research; parasite contamination analysis; microbiological safety; coliform bacteria; *Escherichia coli*

1. Introduction

Sustainable agriculture has become an essential strategy for rural development in Thailand, particularly in Phatthalung Province, where agricultural activities are important to the local economy. Phatthalung ranks 13th out of 14 southern provinces in terms of economic prosperity, with an agrarian

production structure accounting for 31.08% of economic activity but a low per capita income of only 2,033.70 USD annually [1]. The province has established an agricultural and cooperative development plan for 2023-2027 that prioritises sustainable agriculture and organic farming expansion [1]. The plan is consistent with the Sufficiency Economy Philosophy, which prioritises balanced development by taking into account economic, social, cultural, and environmental concerns. However, economic disparities highlight the urgent need to adopt innovative agricultural approaches to alleviate poverty while promoting sustainability. Despite Phatthalung's varied agricultural environment, in rice cultivation, rubber plantations, orchards, and animals, the region continues to have considerable economic difficulties. Khok Muang Sub-district in Khao Chaison District is a small example of these challenges. Initially mainly planted with rice, this area has been increasingly converted to monoculture rubber plantations. The producers of the market are experiencing fluctuations. As noted by the Economic Research Division of the Rubber Authority of Thailand [2], when rubber prices drop to 0.97-1.38 USD per kg against production costs of 1.74 USD per kg, farmers face significant financial strain with annual incomes of approximately 2,080.5 USD per hectare. This economic instability is exacerbated by seasonal challenges, including the 4-5-month rainy and dry seasons during which rubber plants lose their leaves, thereby diminishing income-generating prospects. In addition to economic risks, farmers in Khok Muang also face health and environmental problems. Chemical-intensive farming practices have resulted in concerning health effects, with 90% of a sample of 100 farmers exhibiting chemical contamination in their blood during a 2019 evaluation. Furthermore, water scarcity during dry seasons also presents a persistent challenge for agricultural diversification [3]. This indicates a need to understand the various perceptions of organic vegetable production efficiency and microbial safety using low-cost greenhouse systems, which impact household food security and income. In this research, the study employed participatory action research (PAR) to address these interconnected challenges by developing and implementing a sustainable organic vegetable production model using low-cost greenhouse systems.

The research has three objectives: (1) to evaluate organic vegetable production in low-cost greenhouses as an alternative income source for rubber farmers; (2) to detect and mitigate fecal coliform and *E. coli* contamination in fresh vegetable produce; and (3) to analyze parasite contamination in fresh vegetables. Through this community-based approach, knowledge transfer mechanisms focused on four key areas: low-cost greenhouse construction, bio-organic fertilizer production, precise organic vegetable cultivation techniques, and compliance with Organic Thailand farming standards. Muhie et al. [4] emphasize that such integrated approaches are essential for developing sustainable agricultural systems that balance economic benefits with food safety concerns. This research aims to develop a model household for organic vegetable production to enhance farmers' quality of life and comply with public health regulations for the commercialisation of fresh produce, implementing production and post-harvest safety.

2. Materials and Methods

2.1 Site description

Khok Muang Subdistrict, Khao Chai Son District, Phatthalung Province, has a terrain of hills and flat plains scattered throughout with an area of approximately 68 square kilometers, or approximately 6,800 hectares, and is divided into 5,091 males and 5,310 females, 3,698 households, and 15 villages (Figure 1). Most people in Khok Muang Sub-district work in agriculture, which covers 6,183 hectares. The agricultural region is categorised by significant crop varieties as follows: rubber covers 5,528 hectares, accounting for 89.41%; oil palm 233.28 hectares (3.77%); fruit trees 63.36 hectares (1.02%); vegetables 8.16 hectares (0.13%); field crops 7.36 hectares (0.12%); and other agricultural areas such as fishing 33.92 hectares (0.55%), livestock 30.24 hectares (0.49%), and rice 142.88 hectares (2.31%).

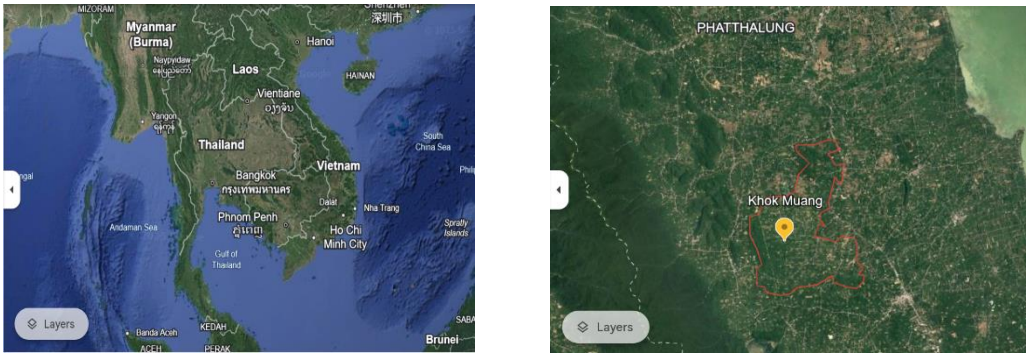


Figure 1. Site sampling location in the study areas in Khok Muang Sub-districts, Phatthalung Province, Southern Thailand.

2.2 Organic Vegetable Production in Greenhouse Systems

2.2.1 Community Context Analysis

This study employed a participatory action research (PAR) mixed-methods design to understand the farmer context in Khok Muang Sub-district, Khao Chaison District, Phatthalung Province, Thailand, and to co-develop and implement an organic vegetable production model using low-cost greenhouse systems [5-6]. The first part focused on context analysis, utilizing two primary data sources: 1) comprehensively understanding the local agricultural landscape. The research team conducted the focus group with key informants, including community leaders, the mayor of Khok Muang Sub-district, and the district agricultural office. These interviews explored the general agriculture context, farmers' knowledge and practices related to organic vegetable production, their perceived capacity and interest in adopting low-cost greenhouse technology for enhancing household food security based on sufficiency economy principles, and the availability of relevant local agricultural infrastructure and support systems. 2) Purposive sampling was used to lead farmers from the Khok Muang community, selected from 85 individuals. These sessions facilitated the sharing of their farming knowledge and practical experiences, and the identification of prevalent problems and obstacles encountered in their current agricultural practices. Data was taken during these conversations, and the transcribed qualitative data were analysed to identify key characteristics.

2.2.2 Development and Transfer of Organic Vegetable Production Technology

Following the standard of production, processing, and labelling of organic agriculture products, this research aimed to develop an organic vegetable production standard system and disseminate the system to participating households. The multifaceted approach was evaluated, encompassing compliance assessment, production yield, income analysis, and satisfaction evaluation. The research team conducted systematic observations to assess farmers' compliance with the training and technology transfer. Participating households received comprehensive training on the organic vegetable production standard system developed. The sessions were recorded to establish a comparative baseline for the application of the transferred knowledge. The researchers evaluated the farmers' potential for organic vegetable production; researchers assessed the farmers' potential for organic vegetable production. The level of compliance with training and the observed potential were quantified using percentage calculations. The efficiency of the technology transfer was analysed in 85 participating farmers using a focus group to collect and summarize the results of low-cost greenhouse organic vegetable production systems. The satisfaction data collected were analysed. Farmers involved in the study completed a satisfaction questionnaire on a rating scale to assess their perception of the effectiveness and utility of the technology transfer. The overall satisfaction level was determined by interpreting these average scores using a predefined rating scale with Best [7].

2.2.3 Evaluation of Farmer Compliance and Production Yields

In this research, 20 selected model households demonstrated the following key characteristics: 1) the ability to apply knowledge gained from technology transfer within their households. 2) Patience and commitment to practicing agriculture within the organic farming system. 3) Availability of space to carry out agricultural operations. 4) The potential to share and transfer knowledge to others in the community. Model households were selected through a collaborative process involving meetings with Khok Muang Sub-district Municipality and the local community. This included conducting surveys and exchanging ideas to identify

suitable candidates. The selection process involved a consultation between members of the community enterprise group and agricultural experts from the Khok Muang Sub-district municipality. As a result, 20 households from Khok Muang Sub-district were selected as model households. We collected the organic vegetable production, yields, and costs from farmers' records of produce delivered to the market. To assess the impact of implementing the organic production standard, we compared the production yields and income data collected before and after the farmers' participation in the research. The pathway outlines a structured process for improving rubber farmers' livelihoods through sustainable organic vegetable production, emphasizing capacity building, economic diversification, certification, and long-term rural development (Figure 2).

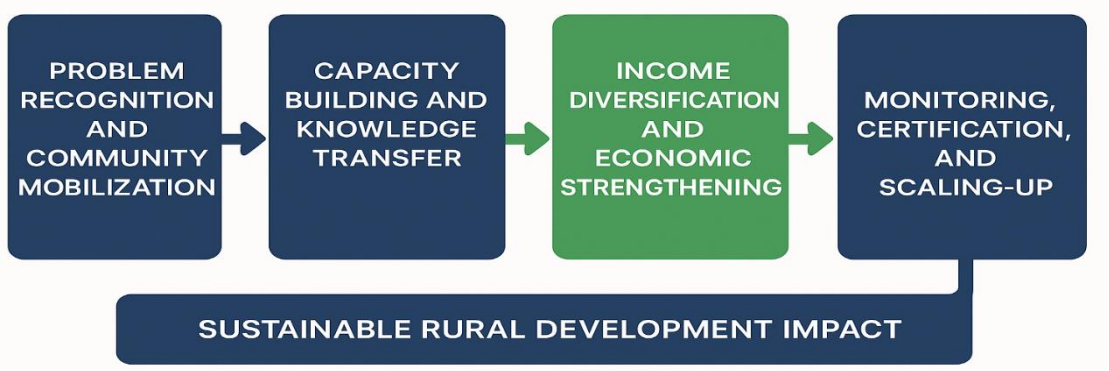


Figure 2. Driving pathway for enhancing rubber farmers' livelihoods through sustainable low-cost greenhouse organic vegetables production

2.3 Microbiological Safety Assessment

2.3.1 Sample Collection of Vegetables

The sample of three leafy green vegetables—green oak lettuce, Chinese cabbage, and kale (100 g each)—was collected from community-based organic farming operations in Khok Muang, Phatthalung Province, in August 2024 (Figure 3). All samples were harvested using aseptic techniques to prevent cross-contamination during collection. These vegetables were selected based on their popularity as raw consumption items, making their microbiological safety particularly important for consumer health.

2.3.2 Washing Methods Evaluation

The study compared unwashed vegetables with those processed using the community group's standard washing protocol. The three types of vegetable leaves (green oak lettuce, Chinese cabbage, and kale) were compared between unwashed and washed to verify the community group's washing method. The washing method followed the protocol of the farming community group involved soaking vegetables in three water basins for 30 seconds in each basin (Figure 4). Then, the samples were tested for coliform and *E. coli* levels. The experiments of washing methods evaluation were duplicated for each vegetable sample.

2.3.3 Vinegar Solution Efficacy Testing

Green oak lettuce, which showed both coliform and *E. coli* contamination in its unwashed state, was selected for vinegar solution efficacy testing. The unwashed green oak leaves were used as a control. Fresh green oak leaves were examined after being washed with vinegar at different solution levels to assess the reduction of coliform bacteria and *E. coli* contamination. The vinegar used for washing vegetables was prepared from vinegar (5% acetic acid) and converted into ppm units of acetic acid. The concentrations were 0, 6.25, 25, and 100 ppm and were applied in the second basin of washing steps.

2.3.4 Coliform and E. coli Analysis

Microbiological analysis was conducted using standardized methods. 10-fold dilutions of each vegetable sample were prepared in 0.85% NaCl solution. 10 g of each vegetable leaf was put in a stomacher bag, and 90 mL of 0.85% NaCl solution was added. Then, the samples were homogenized using a stomacher for 60 seconds. Subsequently, the solution was further diluted to a 1:100 fold. Then, 1 ml aliquots of 1:10 and 1:100 dilution samples were placed in duplicate onto 3M™ Petrifilm™ (3M Petrifilm™ Rapid *E. coli* / Coliform Count Plate) and incubated at 35±2°C for 24±2 hrs. After incubation, *E. coli* and total coliform were enumerated. The *E. coli* colony count is indicated by a blue colony, and the total coliform is indicated by a red colony with

gas production (Bird et al., 2020). The bacterial colonies were quantified and expressed as logarithmic values of CFU/g of vegetables (log CFU/g).



(a) (b) (c)

Figure 3. Appearance of (a) Green oak lettuce, (b) Chinese cabbage, and (c) Kale leaves



(a) (b) (c)

Figure 4. Steps of vegetables washing (a) 1st washing basin, (b) 2nd washing basin, and (c) 3rd washing basin

2.4 Pest Contamination Analysis

2.4.1 Sampling Methods

The pest contamination analysis was conducted on 24 vegetable samples collected from seven low-cost greenhouse operations in the Khok Muang community. Three types of vegetables (green oak lettuce, 9 samples; Chinese kale, 9 samples; and Chinese cabbage, 6 samples) were randomly selected to represent different cultivation cycles and environmental conditions within each greenhouse. For each vegetable type, 50 g samples were collected using sterile equipment. Care was taken to include both inner and outer leaves to assess potential differences in contamination patterns. In addition, 100 g soil samples were collected from each greenhouse to examine the relationship between soil and vegetable contamination.

2.4.2 Detection Techniques for Pests in Vegetables

Vegetables were assessed through sedimentation techniques following standardized protocols. The samples were individually washed with distilled water (250 mL) in a beaker container, which was sanitized after each procedure in saline solution (0.85% NaCl). Washing liquid was filtered through sterile gauze in a sedimentation glass. After 12 h, the upper layer was discarded, and 30 mL of the wash liquid was transferred to plastic tubes and centrifuged (2,000 rpm for 5 minutes). Subsequently, the supernatant was carefully removed, and 100 μL of the pellet was transferred to five glass slides, mixed with Lugol's iodine solution, and analysed under an optical microscope with 100x and 400x magnification.

2.5 Statistical analysis

A paired t-test (dependent t-test) was performed to determine statistically significant differences in vegetable production yield before and after research participation. Using the IBM SPSS Statistics-25 program, we conducted a one-way analysis of variance (ANOVA) with statistical distinctions across multiple treatment groups with 95% confidence. The mean production yield for both periods was calculated. Bacteria count (log CFU/g) was determined using means and standard deviations.

3. Results and Discussion

3.1 Community context

This research comprehensively analysed the agricultural context in Khok Muang Sub-district through focus group discussions with key informants, including community leaders, the mayor, and district agricultural officials. The discussions reveal that a community relies heavily on rubber plantations, replacing traditional rice cultivation. Purposive sampling identified 85 lead farmers who engaged in knowledge-sharing sessions that underscored various challenges: economic vulnerability stemming from volatile rubber prices, seasonal income disparities during the 4–5-month rainy season and dry periods, chemical contamination impacting farmer health (90% of tested farmers exhibited chemical exposure), water resource constraints during dry seasons, and insufficient knowledge of agricultural diversification. These initial assessments identified the need for sustainable farming alternatives that could provide year-round income supplementation while addressing health and environmental concerns [8, 9].

Based on community needs, the research team developed a comprehensive knowledge transfer program focused on four key technological components: low-cost greenhouse construction (six designs evaluated, costs from 1.38-4.74 USD for a square meter structure, with wood-framed greenhouses with PVC or wood roofing proving most cost-effective at 1.52 USD and 1.38 USD respectively) (Table 1); bio-organic fertilizer production techniques using locally available materials to replace chemical fertilizers; precise organic vegetable cultivation methods for selecting crop varieties, planning planting schedules, and implementing organic pest management; and Organic Thailand farming standards training on certification requirements and compliance procedures to enhance market opportunities. For technology transfer using participatory training methods, where researchers systematically observe throughout the process to assess the level of adoption, collaboration with local farmer groups makes this tool effective in resource-limited communities [10].

3.2 Greenhouse system implementation outcomes

Implementing participatory action research methods significantly improved farmers' knowledge of organic vegetable production technologies. The pre-training assessment showed baseline knowledge at 3.81±0.08 on a 5-point scale, which increased to 4.45 ± 0.08 post-training, representing a 16.8% improvement. Knowledge of bio-organic fertilizer production showed the highest post-training score (4.55 ± 0.51), while greenhouse construction presented the most challenging learning curve (4.36 ± 0.65). These findings align with Rahman et al. [15], who observed that participatory knowledge transfer approaches significantly enhance agricultural technology adoption. Implementation capacity assessment revealed high practical application ability (4.72 ± 0.30), indicating effective knowledge transfer beyond theoretical understanding (Table 2). This high implementation rate suggests the technologies were appropriately adapted to local contexts, a factor Bukchin and Kerret [11] identified as critical for successful agricultural innovation adoption.

Cost analysis of six greenhouse designs revealed that wood-framed structures with wood roofing provided the most economical option at 83.05 USD per 6×10 m greenhouse. Steel pipe constructions offered more excellent durability but substantially higher costs (237.22-284.44 USD) (Table 1). The wood-PVC hybrid design (91.38 USD) emerged as the preferred option, balancing cost-effectiveness with moderate durability, like the findings by Wiseansart [12], who identified hybrid structures as optimal for smallholder farmers. Payback period calculations indicated that even the most expensive greenhouse design would be recovered within 16 months based on average vegetable yields and current market prices. This rapid return on investment encouraged adoption among participating households, with 85% selecting the wood-PVC hybrid design. These findings support Ma et al.'s [13] conclusion that initial investment barriers can be overcome when farmers perceive economic returns within short timeframes.

The greenhouse system yielded seven vegetable varieties, with Chinese kale showing the highest production (61.9 ± 9.61 kg/greenhouse/year). Other successful crops included green oak lettuce (59.25 ± 6.88 kg/greenhouse/year), frillice iceberg lettuce (58.9 ± 5.92 kg/greenhouse/year), and mustard greens (58.95 ± 5.42 kg/greenhouse/year) (Table 3). The wide standard deviation in red oak lettuce yields indicates variable production success among participating households, potentially reflecting different skill levels or microenvironmental factors within greenhouses. The economic analysis revealed two benefits: monthly

savings of 55.60 USD in household vegetable spending and an additional income of 88.60 USD per month. This results in a total economic benefit of 144.20 USD monthly, a significant extra income for rubber farmers' households. Alin, along with Touch et al. [14], emphasized that such additional income is crucial in enhancing smallholder farmers' resilience to market volatility. These economic benefits could translate into an annual revenue of approximately 3,962.40 USD combined with the average primary household income of 186.11 USD per month; the total income surpasses the average per capita income in Phatthalung Province (2,033.70 USD). It effectively doubles household revenue [1]. The food supply chain operates in two distinct ways:1) Direct supply from farmers to consumers – consumers purchase food straight from farmers, ensuring freshness and often reducing costs. This approach is common in farmers' markets, direct farm sales, and community-supported agriculture programs, fostering closer connections between producers and buyers. 2) Supply through distributors – food moves from farmers to distributors before reaching consumers. Distributors play a vital role in handling transportation, storage, and processing, ensuring steady availability in grocery stores, restaurants, and food services. This system enhances accessibility and convenience but involves a longer supply chain. The findings indicate that the integration of organic production with low-cost greenhouse technology can markedly enhance vegetable yields, facilitate crop diversification, and elevate the livelihoods of rubber farming communities. Subsequent research should concentrate on comprehensive economic evaluations, pest and disease interactions, and farmer acceptance to further substantiate and expand this paradigm across analogous agroecological regions.

Table 1. Cost comparison of greenhouse types

Greenhouse type	Pillar material	Roof material	Cost (USD/m²)
Type 1	PVC	PVC	1.57
Type 2	Wood	PVC	1.52
Type 3	Wood	Wood	1.38
Type 4	Cement	PVC	2.59
Type 5	Steel pipe	Steel pipe and PVC	3.95
Type 6	Steel pipe	steel pipe	4.74

Table 2. Knowledge transfer effectiveness (pre and post training)

Knowledge component	Pre-training score	Post-training score	Improvement (%)	Meaning
Low-cost greenhouse construction	3.72 ± 0.98	4.36 ± 0.65	17.2	Very satisfied
Bio-organic fertilizer production	3.91 ± 0.92	4.55 ± 0.51	16.4	Extremely satisfied
Organic vegetable cultivation	3.81 ± 0.95	4.45 ± 0.51	16.8	Very satisfied
Overall average	3.81 ± 0.08	4.45 ± 0.08	16.8	Very satisfied

Remarks: 4.51 - 5.00 = Extremely satisfied, 3.51-4.50 = Very satisfied, 2.51 - 3.50 = Moderately satisfied, 1.51 - 2.50 = Slightly satisfied, 1.00 - 1.51, The most slightly satisfied



(a) **(b)** **(c)**

Figure 5. Vegetable products (a) Chinese kale, (b) mustard green, and (c) green oak were produced in the low-cost greenhouse.

3.2 Microbiological safety findings

Microbiological analysis revealed significant contamination in unwashed organic vegetables. Coliform levels were highest in kale (4.87 log CFU/g), followed by green oak lettuce (4.55 log CFU/g) and Chinese cabbage (4.18 log CFU/g). *E. coli* was detected only in unwashed green oak lettuce samples (1.24 log CFU/g). The three-basin washing protocol effectively reduced coliform levels to 3.71, 3.58, and 3.06 log CFU/g for green oak lettuce, Chinese cabbage, and kale, respectively, representing reductions of 18.46%, 14.35%, and 37.17%. No *E. coli* was detected in any washed samples, indicating complete removal through the washing process (Table 4). These contamination patterns align with findings from Rahman et al. [15], who reported coliform levels of 3.8-5.2 log CFU/g in unwashed leafy vegetables. The higher contamination in kale is attributed to its textured leaf surface providing more significant microbial attachment sites, as described by Alegbeleye et al. [16]. Vinegar washing experiments with green oak lettuce demonstrated a concentration-dependent reduction in coliform levels. Unwashed samples showed contamination of 3.23 log CFU/g, which decreased to 2.80, 2.49, 2.31, and 2.08 log CFU/g after treatment with 0, 6.25, 25, and 100 ppm vinegar solutions, respectively. The 100-ppm concentration achieved the highest efficacy, with a 35.60% reduction compared to unwashed samples and a 25.71% improvement over standard water washing (Table 5). These results are consistent with those of Nascimento et al. [17], who reported that vinegar solutions reduced coliform counts in lettuce by 48.60-68.00%, depending on concentration. The antimicrobial effect observed is attributed to acetic acid's ability to disrupt bacterial cell membranes and intracellular pH, as Alreshoodi et al. [18] explained.

Based on these findings, a three-step washing protocol incorporating vinegar treatment is recommended for optimal microbial reduction. This includes (1) an initial rinse with clean water to remove soil and debris, (2) a 30-second soak in 100 ppm vinegar solution, and (3) a final rinse with clean water to remove vinegar residue. This protocol balances efficacy with practicality, as higher vinegar concentrations tested by Atter et al. [19] and Traore et al. [20] achieved more significant reductions but may negatively impact sensory qualities. Although this approach can significantly reduce contamination, it does not guarantee the complete elimination of pathogens, and therefore, additional technologies such as appropriate cold storage (≤4°C) should be implemented as recommended by Srisamran et al. [21]. For commercial applications, the Thai Public Health standards for fresh vegetables require coliform levels below 3 log CFU/g and no *E. coli*. The recommended protocol brings products within these compliance thresholds, supporting market access while utilizing low-cost, accessible materials suitable for smallholder farmers.

Table 3. Vegetable production yields and economic impact

Type of organic vegetables	Before	After	t-test	*p*-value	% increase in the yields of vegetable production	Income greenhouse /year
	yields (kg/greenhouse /year)	yields (kg/greenhouse /year)				
1. Green oak (*Lactuca sativavar. crispa* L.)	No crop	59.25 ± 6.88	-	-	New introduction	246.88
2. Red oak (*Lactuca sativa*)	No crop	57.4 ± 9.90	-	-	New introduction	239.20
3. Frillice iceberg Lettuce (*Lactuca sativa* L.)	No crop	58.9 ± 5.92	-	-	New introduction	245.42
4. Mustard greens (*Brassica juncea*)	45.63 ± 15.56	58.95 ± 5.42	1.49	0.145^{ns}	29.20	81.88
5. Chinese kale (*Brassica alboglabra* L.H. Bailey)	30.67 ± 20.32	61.9 ± 9.61	4.43	0.00**	101.70	171.94
6. Kale (*Brassica oleracea*) L. var *acephala* DC.)	No crop	48 ± 7.89	-	-	New introduction	400.00
7. Chinese cabbage (*Brassica sativa* var. *crispa* L.)	28.54 ± 13.21	56.25 ± 4.98	7.34	0.00**	97.10	78.13
Total	**104.84**	**400.65**	**-**	**-**	**289.30**	**1,463.40**

N = Number of samples = 20, SD = standard deviation, **p < 0.01.

Table 4. Coliform and *E. coli* contamination before and after washing

Vegetable type	Coliform (log CFU/g)		*E. coli* (log CFU/g)		Coliform reduction (%)
	Unwashed	Washed	Unwashed	Washed	
Green oak lettuce	4.55 ± 0.02	3.71 ± 0.81	1.24 ± 0.24	ND	18.46
Chinese cabbage	4.18 ± 0.04	3.58 ± 0.96	ND	ND	14.35
Kale	4.87 ± 0.02	3.06 ± 0.01	ND	ND	37.17

*ND = Not detected

Table 5. Effect of vinegar concentration on Coliform levels in green oak lettuce

Treatment	Vinegar concentration (ppm)	Coliform (log CFU/g)	Reduction vs. Unwashed (%)	Reduction vs. Water washing (%)
Unwashed	0	3.23 ± 0.03^{e}	-	-
1	0	2.80 ± 0.06^{d}	13.31	-
2	6.25	2.49 ± 0.01^{c}	22.91	11.07
3	25	2.31 ± 0.04^{b}	28.48	17.50
4	100	2.08 ± 0.05^{a}	35.60	25.71

Different letters within treatment indicate significant differences at the $p < 0.05$ level, according to Duncan's multiple range test method.

3.3 Agricultural pest contamination results

Agricultural pest analysis of 24 vegetable samples revealed significant contamination rates in all examined vegetable varieties. In total, 37.5% (9/24) of the samples contained at least one parasite, with Chinese cabbage having the highest contamination rate (50.0%, 3/6). Green oak lettuce and Chinese kale had similar contamination rates of 33.3% (3/9) (Table 6). These findings are in line with Laoraksawong et al. [22], who reported contamination rates of 35–58% in green leafy vegetables from organic farming systems (Table 7). The higher contamination rates in Chinese cabbage may be due to its distinctive leaf morphology, which provides numerous cavities for parasite attachment and protection from conventional washing methods. This morphological influence on the contamination pattern supports the observation by Dokmaikaw et al. [23], who observed that complex leaf structures harbored significantly more agricultural pests than smooth-surfaced vegetables. Two main types of agricultural pests were found in the vegetable samples: aphids (plant lice) and vegetable mites in various stages (Figure 6). The prevalence of arthropod parasites underscores the difficulties faced by organic farming systems that depend more on biological pest control than on chemical pesticides, as observed by Ounis et al. [24]. These results highlight the complex balance between chemical reduction and management of potential biological contaminants. The presence of ticks, usually linked to host animals, signifies possible cross-contamination from adjacent livestock or wildlife, a phenomenon noted by Zahid et al. [25], prevalent in mixed farming systems. Distribution patterns vary among vegetable types, with green oak lettuce having the most diverse parasite profiles. This suggests that targeted washing protocols should be developed for specific vegetable types rather than applying a uniform approach to the entire produce, as suggested by Nahhas et al. [26].



Figure 6 Microscopic images of common vegetable pests. The top row shows aphids (plant lice), which are soft-bodied insects that feed on plant sap and can transmit plant viruses. The bottom row displays various views of vegetable mites, tiny arachnids that damage plant tissue by piercing and sucking out cell contents.

Table 6. Prevalence of agricultural pests in different vegetable types

Vegetable type	Samples tested	Contaminated samples	Contamination rate (%)
Green oak lettuce	9	3	33.30
Chinese kale	9	3	33.30
Chinese cabbage	6	3	50.00
Total	24	9	37.50

Table 7. Distribution of agricultural pest species across vegetable types

Agricultural pest type	Green oak lettuce	Chinese kale	Chinese cabbage	Total prevalence (%)
Aphids (Plant lice)	17	16	7	90.91%
Vegetable mites	-	-	4	9.09%

4. Conclusions

This participatory action research demonstrated the effectiveness of low-cost greenhouse systems for organic vegetable production in Khok Muang, Phatthalung Province. Knowledge transfer led to a 16.80% enhancement in farmer competency, with bio-organic fertiliser production achieving the highest post-training score of 4.55 out of 5.00. The wood-PVC hybrid greenhouse design (91.38 USD) emerged as the optimal balance of cost-effectiveness and durability. Chinese kale yielded the highest production (61.9 ± 9.61 kg/greenhouse/year), while microbiological analysis revealed significant contamination reduction through proper washing protocols. Standard washing reduced coliform levels by 14.35-37.17%, while 100 ppm vinegar treatment achieved a 35.60% reduction. Parasite contamination was found in 37.5% of vegetable samples, with Chinese cabbage showing the highest rate (50%). Aphids were the most common agricultural pest (90.91%), indicating a need for effective pest control, especially against aphids, in vegetable production. There are substantial economic benefits, with participating households saving 55.60 USD monthly on vegetable expenses while earning 88.60 USD in additional income. The monthly economic impact of 144.20 USD constitutes a substantial augmentation to conventional rubber farming revenues, mitigating the economic vulnerability highlighted in the community context analysis. Beyond financial gains, the organic production methods reduced chemical exposure for producers and consumers, directly addressing the 90% chemical contamination rate previously documented among farmers. The enhanced post-harvest handling techniques effectively diminished microbial contamination to levels that meet Thai Public Health requirements, facilitating market access beyond local consumption.

5. Acknowledgements

The author would like to thank rubber smallholder farmers in Phatthalung province, Thailand, for participating in this research. This research was supported by the Research Council of Thailand (NRCT) (grant no. N71B650095), the Faculty of Agro- and Bio-Industry, and the Faculty of Science and Digital Innovation Thaksin University, Phatthalung Province, Thailand. The authors declare no conflict of interest between themselves and any other individual or organization

References

[1] Ministry of Agriculture and Cooperatives. *5-Year Strategic Action Plan for Agriculture and Cooperatives in Phatthalung Province (2023–2027)*; accessed Aug 15, 2024. https://www.opsmoac.go.th/phatthalung-strategic-files-461191791796.

[2] Economic Research Division of Rubber Authority of Thailand. *Rubber Production by Office of Agricultural Economics*; 2024; accessed Nov 20, 2024. https://www.thainr.com/uploadfile/20230915155043.pdf.

[3] Johnson, M. B.; Yovo, E. R. D.; Saito, K. Farmers' Perception and Management of Water Scarcity in Irrigated Rice-Based Systems in Dry Climatic Zones of West Africa. *Agron. Sustain. Dev.* **2023**, *43*. https://doi.org/10.1007/s13593-023-00878-9

[4] Muhie, S. H. Novel Approaches and Practices to Sustainable Agriculture. *J. Agric. Food Res.* **2022**, *10*, 100446. https://doi.org/10.1016/j.jafr.2022.100446

[5] TNAU Agritech Portal – Horticulture. *Greenhouse Cultivation*; 2013; accessed Aug 15, 2024. https://agritech.tnau.ac.in/horticulture/horti_Greenhouse%20cultivation.html.

[6] Dalai, S.; Mohanta, S.; Barsha, T.; Sahu, B. Green-houses: Types and Structure Components. In *Protected Cultivation and Smart Agriculture*; New Delhi Publishers: New Delhi, **2020**; pp 9–17. https://doi.org/10.30954/NDP-PCSA.2020.2

[7] Best, J. W. *Research in Education*, 4th ed.; Prentice Hall: New Jersey, 1981.

[8] Bhati, P.; Saikia, A. R.; Chaudhary, S.; Bahadur, R.; Nengparmoi, T.; Talukdar, N.; Hazarika, S. Integrated Farming Systems for Environment Sustainability: A Comprehensive Review. *J. Sci. Res. Rep.* **2024**, *30*, 143–155. https://doi.org/10.9734/jsrr/2024/v30i11834

[9] Aguiari, I. Processual Approach to Community Agriculture: Between Structuralist and Individualist Explanations. *Sociology Lens* **2024**, *37*, 447–467. https://doi.org/10.1111/johs.12463

[10] Bseiso, A.; Abels, B.; Ferguson, S.; Lusch, P.; Mehta, K. A Decision Support Tool for Greenhouse Farmers in Low-Resource Settings. *Global Humanitarian Technology* **2015**, 1–7. https://doi.org/10.1109/GHTC.2015.7343987

[11] Bukchin, S.; Kerret, D. Character Strengths and Sustainable Technology Adoption by Smallholder Farmers. *Heliyon* **2020**, *6*, e04694. https://doi.org/10.1016/j.heliyon.2020.e04694.

[12] Wiseansart, A. Factors Affecting Decision-Making on Greenhouse Farming and Cost-Benefit Analysis of Greenhouse Vegetable Crops and Melons in Northeastern Thailand. *Int. J. Agric. Technol.* **2023**, *19*, 1939–1952.

[13] Ma, W.; Rahut, D. B.; Sonobe, T.; Gong, B. Linking Farmers to Markets: Barriers, Solutions, and Policy Options. *Econ. Anal. Policy* **2024**, *82*, 1102–1112. https://doi.org/10.1016/j.eap.2024.05.005.

[14] Touch, V.; Tan, D. K. Y.; Cook, B. R.; Liu, D. L.; Cross, R.; Tran, T. A.; Utomo, A.; Yous, S.; Grunbuhel, C.; Cowie, A. Smallholder Farmers' Challenges and Opportunities: Implications for Agricultural Production, Environment and Food Security. *J. Environ. Manage.* **2024**. https://doi.org/10.1016/j.jenvman.2024.122536

[15] Rahman, M.; Azad, O. K.; Uddain, J. J.; Adnan, A. C.; Al-Mujahidy, J.; Roni, Z. K.; Rahman, M. S.; Islam, J.; Rahman, H.; Choi, K. Y.; Naznin, M. T. Microbial Quality Assessment and Efficacy of Low-Cost Disinfectants on Fresh Fruits and Vegetables Collected from Urban Areas of Dhaka, Bangladesh. *Foods* **2021**, *10*, 1325. https://doi.org/10.3390/foods10061325.

[16] Alegbeleye, O. O.; Singleton, I.; Sant'Ana, A. S. Sources and Contamination Routes of Microbial Pathogens to Fresh Produce during Field Cultivation: A Review. *Food Microbiol.* **2018**, *73*, 177–208. https://doi.org/10.1016/j.fm.2018.01.003

[17] Nascimento, M. S.; Silva, N.; Catanozi, M. P. I. M.; Silva, K. C. Effects of Different Disinfection Treatments on the Natural Microbiota of Lettuce. *J. Food Prot.* **2003**, *66*(9), 1697–1700. https://doi.org/10.4315/0362-028X-66.9.1697

[18] Alreshoodi, F. M.; Alsuliman, B.; Alotaibi, N. M.; Althobaiti, A.; Mukhtar, L. E.; Alsaleh, S.; Alajlan, A. A.; Alakeel, S. I.; Alshabrmi, F. M.; Sarwar, T.; Alajel, S. M. Impact of Various Washing Protocols on the Mitigation of *E. coli* Contamination in Raw Salad Vegetables. *Microorganisms* **2024**, *12*, 2103. https://doi.org/10.3390/microorganisms12102103.

[19] Atter, A.; Amewowor, D.; Awua, W. K. A. The Effectiveness of Water, Salt and Vinegar in Reducing the Bacteria Population in Fresh Green Cabbage. *Food Sci. Qual. Manag.* **2014**, *28*, 29–34.

[20] Traoré, S.; Cornelius, E. W.; Samaké, F.; Essilfie, G.; Babana, A. H.; Bengaly, M.; Koné, A.; Cissé, H.; Acheampong, M. A. Efficiency of Common Washing Treatments in Reducing Microbial Levels on Lettuce in Mali. *J. Appl. Ecol.* **2020**, *28*(2), 64–74.

[21] Srisamran, J.; Atwill, E. R.; Chuanchuen, R.; Jeamsripong, S. Detection and Analysis of Indicator and Pathogenic Bacteria in Conventional and Organic Fruits and Vegetables Sold in Retail Markets. *Food Qual. Saf.* **2022**, *6*, 1–10. https://doi.org/10.1093/fqsafe/fyac013

[22] Laoraksawong, P.; Bunkasem, U. Prevalence of Intestinal Parasitic Contamination in Fresh Vegetables in Bangkok, Thailand, and Surrounding Areas: A Cross-Sectional Survey. *Parasite Epidemiol. Control* **2025**, *29*, e00416. https://doi.org/10.1016/j.parepi.2025.e00416

[23] Dokmaikaw, A.; Suntaravitun, P.; Singsook, C.; Tanathakorn, N. Prevalence of Helminth Contamination of Fresh Vegetables from Cultivation Plots in Bang Khla District, Chachoengsao Province, Thailand. *Southeast Asian J. Trop. Med. Public Health* **2024**, *55*.

[24] Ounis, S.; György, T.; Kiss, J. Arthropod Pests, Nematodes, and Microbial Pathogens of Okra (*Abelmoschus esculentus*) and Their Management—A Review. *Agronomy* **2024**, *14*, 2841. https://doi.org/10.3390/agronomy14122841.

[25] Zahid, R.; Song-hua, H.; Wan-jun, C.; Abdullah, A.; Chen-wen, X. Importance of Ticks and Their Chemical and Immunological Control in Livestock. *J. Zhejiang Univ. Sci. B* **2006**, *7*, 912–921. https://doi.org/10.1631/jzus.2006.B0912

[26] Nahhas, S. A.; Aboualchamat, G. Investigation of Parasitic Contamination of Salad Vegetables Sold by Street Vendors in Damascus. *Food Waterborne Parasitol.* **2020**, *3*, e00090. https://doi.org/10.1016/j.fawpar.2020.e00090

ASEAN
Journal of Scientific and Technological Reports
Online ISSN:2773-8752

Research article

Enhancing Methane Production from Palm Oil Industry Waste through Thermotolerant Bacterial Bio-augmentation: Optimization and Kinetic Analysis

Sittikorn Saelor[1], Wisarut Tukanghan[2], Peerawat khongkliang[3], Supattra In-chan[2,4], and Nantharat Phruksaphithak[5,6*]

[1] Faculty of Science and Technology, Hatyai University, Songkhla, 90110, Thailand
[2] Bio4gas (Thailand) Company Limited, Paphayom, Phatthalung, 93210, Thailand
[3] Research Center for Circular Products and Energy, King Mongkut's University of Technology North Bangkok, Bangkok, 10800, Thailand
[4] Biofuel and Biocatalysis Innovation Research Unit, Mahidol University, Nakhonsawan Campus, Nakhonsawan, 60130, Thailand
[5] Faculty of Science and Digital Innovation, Thaksin University, Phatthalung, 93210, Thailand
[6] Centre of Excellence for Agricultural Innovation and Bioproducts of Thaksin University, Thaksin University, Phatthalung, 93210, Thailand
* Correspondence: nantharat@tsu.ac.th

Citation:
Saelor, S.; Tukanghan, W.; Khongkliang, P.; In-chan, S.; Phruksaphithak, N., Enhancing methane production from palm oil industry waste through thermotolerant bacterial bio-augmentation: optimization and kinetic analysis. *ASEAN J. Sci. Tech. Report.* **2026**, *29*(1), e259596. https://doi.org/10.55164/ajstr.v29i1.259596.

Article history:
Received: May 27, 2025
Revised: October 2, 2025
Accepted: October 18, 2025
Available online: December 14, 2025

Publisher's Note:
This article is published and distributed under the terms of the Thaksin University.

Abstract: This study investigated bio-augmentation strategies to enhance biogas production from palm oil industry residues through thermotolerant anaerobic digestion. Two bacterial strains, *Cellulomonas* sp. (HD19AZ1) and *Themoanaerobacterium thermosaccarolyticum* (PSU-2), were evaluated at various inoculum to microorganism (I:S) ratios for both single digestion of empty fruit bunches (EFB) and co-digestion with palm oil mill effluent (POME). Results demonstrated that bio-augmentation significantly improved substrate biodegradability and methane yields. With HD19AZ1, the optimal I:S ratio of 70:10% for single digestion achieved methane yields of 146.38 mL-CH_4/gVS (a 24.94 mL-CH_4/gVS substrate improvement), while the 65:15% ratio for co-digestion yielded 166.55 mL-CH_4/gVS (33.38 m^3/tonne substrate improvement). These represented increases of 33.59% and 39.65% in biodegradability for single and co-digestion, respectively. Volatile solids removal reached 41.82% in single digestion and 47.59% in co-digestion under optimal conditions. Kinetic analysis revealed that bio-augmentation with HD19AZ1 achieved methane production rates of 3.90 mL-CH_4/d for single digestion and 6.70 mL-CH_4/d for co-digestion, while PSU-2 augmentation increased rates by 2.14 times compared to control samples. The hydrolysis constant (Kh) ranged from 0.0214-0.0375 d^{-1} for single digestion and 0.0095-0.0232 d^{-1} for co-digestion, with lag phases of 5.15-16.11 days and 18.29-43.14 days, respectively. Modified Gompertz modeling confirmed these parameters with R^2 values exceeding 0.97. This study demonstrates that strategic bio-augmentation with thermotolerant bacteria significantly enhances methane production from palm oil industry waste by improving substrate accessibility and accelerating the hydrolysis of recalcitrant lignocellulosic components, offering promising applications for industrial-scale biogas production.

Keywords: Bio-augmentation; anaerobic digestion; lignocellulosic biomass; methane yield; palm oil residues

1. Introduction

The palm oil industry has experienced substantial growth over recent decades, becoming one of the world's most important vegetable oil producers. However, this expansion has generated significant quantities of waste materials,

primarily empty fruit bunches (EFB) and palm oil mill effluent (POME), creating environmental challenges but also opportunities for renewable energy production [1]. These residues contain considerable organic content, making them potentially valuable substrates for biogas generation through anaerobic digestion (AD). Palm oil mills generate approximately 0.7-0.9 tonnes of POME and 0.22-0.24 tonnes of EFB for every tonne of crude palm oil produced [2]. POME is a high-strength wastewater with COD values typically ranging from 40,000-80,000 mg/L, while EFB is a solid lignocellulosic material containing 30-40% cellulose, 25-35% hemicellulose, and 15-25% lignin [3]. These characteristics make both materials promising feedstocks for biogas production, with theoretical methane yields estimated at 340-360 mL CH_4/gVS for POME and 200-240 mL CH_4/gVS for EFB [4]. Despite this potential, the anaerobic digestion of lignocellulosic materials like EFB presents significant challenges. The complex structure of lignocellulose creates a recalcitrant matrix that resists microbial degradation, particularly during the hydrolysis phase, which is widely recognized as the rate-limiting step in the AD process [5]. The crystalline structure of cellulose, combined with the protective barrier formed by lignin, limits enzyme accessibility and reduces biodegradation efficiency [6]. Consequently, untreated EFB typically achieves only 15-25% of its theoretical methane potential in conventional AD systems [7].

Various pretreatment methods have been proposed to overcome these limitations, including physical, chemical, and biological approaches. Among these, bio-augmentation has emerged as a promising strategy that avoids the energy inputs and chemical requirements of alternative methods [8]. Bio-augmentation involves introducing specific microbial strains or consortia with enhanced capabilities for degrading complex substrates into the AD system. For lignocellulosic materials, this typically includes cellulolytic and hemicellulolytic microorganisms that can accelerate the hydrolysis of recalcitrant components [9]. Several studies have demonstrated the potential of bio-augmentation for improving biogas production from various lignocellulosic substrates. Peng et al. [10] reported a significant increase in methane yield from wheat straw following bio-augmentation with Clostridium cellulolyticum. Similarly, Strang et al. [11] observed 20-22% higher methane production from corn stover using enriched microbial cultures. However, the effectiveness of bio-augmentation varies considerably depending on the substrate characteristics, microbial strains employed, and operational conditions [12]. Despite these advances, significant knowledge gaps remain regarding the optimal implementation of bio-augmentation strategies for palm oil industry wastes. The complex nature of EFB and POME creates unique challenges that may require specialized approaches. Furthermore, the relationships between inoculum-to-microorganism ratios, process kinetics, and methane yields have not been thoroughly investigated for these substrates, particularly under thermotolerant conditions that may enhance hydrolysis rates [13].

This study aims to address these research gaps by investigating the effect of bio-augmentation with thermotolerant bacteria *Cellulomonas* sp. (HD19AZ1) and *Themoanaerobacterium thermosaccarolyticum (*PSU-2*)* on the anaerobic digestion of EFB and its co-digestion with POME. Specifically, the research objectives are to: (1) determine the optimal inoculum-to-microorganism ratios for enhancing methane yields; (2) evaluate the impact of bio-augmentation on process kinetics and biodegradability; (3) compare the effectiveness of bio-augmentation in single digestion of EFB versus co-digestion with POME; and (4) elucidate the mechanisms through which bio-augmentation enhances the AD process for these substrates. The findings will contribute to the development of more efficient biogas production systems for palm oil industry waste, supporting both waste management and renewable energy generation in this important agricultural sector..

2. Materials and Methods

2.1 Substrate Collection and Characterization

Empty fruit bunches (EFB) and palm oil mill effluent (POME) were collected from a palm oil mill in Krabi province, Thailand. Samples were stored at 4°C before use to minimize biological degradation. Both substrates were characterized for their physicochemical properties, including total solids (TS), volatile solids (VS), pH, chemical oxygen demand (COD), total Kjeldahl nitrogen (TKN), and total phosphorus according to standard methods [14]. The lignocellulosic composition of EFB was determined following the protocol described by Sluiter et al [15], quantifying cellulose, hemicellulose, and lignin content. POME characterization included measurements of oil and grease, total suspended solids (TSS), and volatile fatty acids (VFAs). The

C/N ratio was calculated for both individual substrates and their mixtures at various ratios to ensure optimal nutritional conditions for the anaerobic digestion process [4].

2.2 Bacterial Strains Selection and Cultivation

Two thermotolerant bacterial strains were selected for bioaugmentation tests: *Cellulomonas* sp. strain HD19AZ1 and strain PSU-2. The HD19AZ1 strain was maintained on BA medium as described by Trzcinski and Stuckey [19]. Culture preparation involved inoculating 10% of the stock culture into the growth medium under strictly anaerobic conditions (N_2 atmosphere). Cultures were incubated at 37°C for approximately 48 hours until reaching an optical density (OD_{600}) of 0.5 ± 0.05. The PSU-2 strain was similarly cultured using appropriate growth media (basal medium and glucose as a carbon source) under anaerobic conditions. Both cultures were transferred anaerobically into batch bottles at various concentrations (5-35% v/v) to establish different inoculum-to-microorganism ratios for the bio-augmentation experiments. The bacterial strains were selected based on their demonstrated hydrolytic capabilities with lignocellulosic materials and their thermotolerant properties [17].

2.3 Inoculum Preparation

The anaerobic inoculum was developed using microbial sludge cultivated with POME, supplemented with 0.01% (w/v) ash to provide trace elements. Before experimental use, the inoculum was subjected to a one-week starvation period to minimize the contribution of residual organic matter to biogas production during the experiments. This approach ensured that measured biogas production would more accurately reflect the degradation of the test substrates rather than residual material in the inoculum. For the solid-state anaerobic digestion (SS-AD) experiments, only sludge with a volatile solids (VS) concentration exceeding 8.0% (w/v) was used to maintain appropriate conditions for the digestion of high-solids materials [3].

2.4 Experimental Design for Bio-augmentation Tests

Two primary experimental configurations were established: single digestion of EFB and co-digestion of EFB with POME. For co-digestion, an EFB: POME ratio of 1:1.4 was maintained, corresponding to 20% total solids (TS) of EFB with a particle size of 3.25 mm. This ratio was determined based on previous optimization work by Saelor et al. [4] to provide suitable moisture content and nutrient balance. For each configuration (single digestion and co-digestion), a series of bio-augmentation tests was conducted with varying I:M ratios. The ratios tested were 75:5, 70:10, 65:15, 60:20, 55:25, 50:30, and 45:35 (% inoculum: % bacterial culture). These variations allowed for systematic evaluation of the optimal balance between indigenous anaerobic microorganisms and the augmented bacterial strains. Control experiments were established for each configuration without bacterial augmentation (positive controls) and with water substituted for the substrate (negative controls). Methane production from negative controls was subtracted from experimental values to account for endogenous gas production from the inoculum.

2.5 Batch Anaerobic Digestion Setup

Batch anaerobic digestion tests were conducted in 120 mL serum bottles with a working volume of 60 mL. Appropriate quantities of inoculum, substrate, and bacterial culture were added according to the experimental design. Each bottle was purged with N_2:CO_2 (80:20) gas mixture for 3 minutes to ensure anaerobic conditions, then sealed with butyl rubber stoppers and aluminum crimps. The bottles were incubated at 37°C for the HD19AZ1 experiments for a period of 45 days. Regular monitoring of biogas production was performed using a water displacement method, and the methane content was determined by gas chromatography. All experimental conditions were tested in triplicate to ensure statistical reliability of the results [18].

2.6 Analytical Methods for Biogas Measurement and Composition Analysis

Biogas volume was measured using a water displacement system calibrated at room temperature, with correction to standard temperature and pressure (STP). The composition of biogas was analyzed using gas chromatography with a thermal conductivity detector (GC-TCD, Shimadzu GC-8A, Japan) equipped with a Porapak Q column. Helium was used as the carrier gas, with column, injector, and detector temperatures maintained at 35°C, 100°C, and 120°C, respectively [19]. Total alkalinity (TA) was determined by titration according to standard methods [14]. Volatile fatty acids (VFAs) concentrations were analyzed using gas

chromatography (Shimadzu GC-17A, Japan) equipped with a flame ionization detector (FID) and a DB-WAX column. The pH was monitored at the beginning and end of the digestion period using a calibrated pH meter. The biodegradability of the substrates was calculated based on the ratio of experimental methane yield to theoretical methane yield, as described by Tabatabaei et al. [5]. Volatile solids (VS) removal efficiency was determined by comparing VS content before and after digestion according to standard methods [14].

2.7 Kinetic Models for Evaluating Hydrolysis Constants and Methane Production Patterns

The hydrolysis constant (Kh) was determined using a first-order kinetic model as described by Angelidaki et al. [18].

$$\ln[(B\infty - B)/B\infty] = -Kh \cdot t \quad (1)$$

Where Kh is the hydrolysis constant (d^{-1}), B∞ is the ultimate methane yield (mL CH_4/gVS), B is the cumulative methane yield at time t (mL CH_4/gVS), and t is the digestion time (days). The cumulative methane production profiles were fitted to the modified Gompertz equation to determine the lag phase (λ), maximum methane production rate (Rm), and methane production potential (P) [19].

$$M = P \cdot \exp\{-\exp[(Rm * e/P) \cdot (\lambda - t) + 1]\} \quad (2)$$

Where M is the cumulative methane production (mL CH_4/gVS), P is the methane production potential (mL CH_4/gVS), Rm is the maximum methane production rate (mL CH_4/gVS·day), λ is the lag phase (days), t is the digestion time (days), and e is exp(1) = 2.7183. The model parameters were estimated using non-linear regression analysis with SigmaPlot 11.0 software [20]. The coefficient of determination (R^2) was calculated to evaluate the goodness of fit between experimental data and model predictions.

3. Results and Discussion

3.1 Effect of bio-augmentation on methane yields

The bio-augmentation strategy was evaluated for both single digestion of EFB and co-digestion of EFB with POME, with results revealing significant differences in methane production patterns and yields. Figure 1 illustrates the cumulative methane yields from various inoculum-to-microorganism (I: M) ratios for both digestion configurations using the HD19AZ1 strain. In single digestion of EFB, bio-augmentation with HD19AZ1 achieved a maximum methane yield of 146.38 mL-CH_4/gVS at an I: M ratio of 70:10. This represents a 114.2% increase compared to the non-augmented control (68.35 mL-CH_4/gVS). For co-digestion of EFB with POME, the optimal I: M ratio shifted to 65:15, producing 166.55 mL-CH_4/gVS, which is 93.8% higher than the corresponding control (85.93 mL-CH_4/gVS). Similar enhancement patterns were observed with PSU-2, which achieved maximum yields of 153.26 mL-CH_4/gVS for single digestion and 178.42 mL-CH_4/gVS for co-digestion at an I: M ratio of 75:5 for both configurations. The temporal methane production profiles (Figure 2) revealed that co-digestion generally outperformed single digestion in terms of ultimate methane yields, confirming the synergistic effect of combining EFB with POME. This synergy can be attributed to the complementary characteristics of the substrates: EFB contributes carbon-rich lignocellulosic material while POME provides additional nutrients, moisture, and a diverse microbial community [4]. The improved nutrient balance in co-digestion systems has been shown to enhance microbial growth and enzymatic activity, particularly for hydrolytic bacteria [7]. The superior performance of co-digestion is consistent with findings by Li et al. Zhang et al. [21] reported that co-digestion helps balance the C/N ratio and provides essential trace elements for efficient anaerobic digestion. Similarly, [22] demonstrated that co-digestion of lignocellulosic materials with nutrient-rich substrates improved microbial colonization of fiber surfaces, enhancing the accessibility of cellulolytic enzymes to their substrates. However, it is worth noting that the improvement patterns were not uniform across all I: M ratios. For instance, with HD19AZ1, some co-digestion setups (75:5 and 70:10 ratios) actually performed worse than the control, producing only 30.58 and 42.57 mL-CH_4/gVS, respectively. This suggests that at certain ratios, the introduced microorganisms may compete with indigenous populations without effectively contributing to enhanced hydrolysis [9]. The

complex interactions between introduced and indigenous microorganisms highlight the importance of careful optimization of bioaugmentation parameters.

The efficacy of bio-augmentation was strongly influenced by the optimal I: M ratio. As shown in Figure 3, the methane production rate showed distinct patterns in response to increasing bacterial culture percentages. For HD19AZ1, single digestion exhibited an irregular response pattern, with peaks at 10% (3.87 mL-CH_4/gVS/day) and 25% (4.00 mL-CH_4/gVS/day) bacterial culture addition. In contrast, co-digestion with HD19AZ1 showed a more consistent upward trend, reaching a maximum rate of 8.71 mL-CH_4/gVS/day at 25% addition before declining at higher proportions. PSU-2 exhibited distinctly different behavior, with both single digestion and co-digestion showing consistently decreasing methane production rates as bacterial culture percentages increased. The highest rates were observed at 5% addition (13.11 and 15.38 mL-CH_4/gVS/day for single digestion and co-digestion, respectively), suggesting that PSU-2 is effective at lower concentrations. This is consistent with findings by Tsapekos et al. [6], who reported that some hydrolytic bacteria perform optimally at low inoculation rates, possibly due to their rapid growth and efficient colonization of substrate surfaces. The comparative analysis of bio-augmentation efficiency (Figure 4) clearly demonstrates that while both strains enhanced methane production, PSU-2 outperformed HD19AZ1 across multiple performance metrics. At their respective optimal I: M ratios, PSU-2 achieved higher methane yields (153.26 vs. 146.38 mL-CH_4/gVS for single digestion; 178.42 vs. 166.55 mL-CH_4/gVS for co-digestion), greater VS removal (46.78% vs. 41.82% for single digestion; 52.31% vs. 47.59% for co-digestion), and faster methane production rates (13.11 vs. 3.87 mL-CH_4/gVS/day for single digestion; 15.38 vs. 6.74 mL-CH_4/gVS/day for co-digestion). Notably, PSU-2 also demonstrated a substantially shorter lag phase (3.62 days vs. 6.44 days for single digestion; 6.17 days vs. 19.89 days for co-digestion), indicating faster adaptation to the substrate and more rapid initiation of hydrolysis. This is particularly significant for industrial applications, where shorter startup times can improve process efficiency and reduce operational costs [13].

The optimal I: M ratio for each strain appears to be influenced by its specific enzymatic capabilities and growth characteristics. HD19AZ1, being a Cellulomonas species, likely produces a range of cellulolytic and hemicellulolytic enzymes that function optimally at specific concentrations relative to the substrate and indigenous microflora [16]. The shifting optimal ratio between single digestion (70:10) and co-digestion (65:15) suggests that the strain's performance is influenced by the substrate composition and possibly by interactions with microorganisms present in POME. In contrast, PSU-2 consistently performed best at a 75:5 ratio for both configurations, indicating more robust and adaptable enzymatic capabilities. This is consistent with observations by Strang et al. [11], who found that certain hydrolytic bacteria maintain consistent performance across varying substrate conditions due to their broad-spectrum enzymatic activities. The biodegradability results provide particularly compelling evidence of strain-specific effects, with PSU-2 achieving 93.59% biodegradability in co-digestion compared to 39.65% with HD19AZ1. This dramatic difference suggests that PSU-2 may possess superior capacities for breaking down recalcitrant lignocellulosic components or may produce metabolites that enhance the activity of other hydrolytic microorganisms in the consortium [23]. The findings highlight the importance of strain selection and ratio optimization in bio-augmentation strategies for anaerobic digestion of lignocellulosic materials. While both strains enhanced methane production significantly compared to controls, their optimal application parameters differed substantially, underscoring the need for customized approaches based on specific substrate characteristics and operational goals.

Table 1. Methane Yields from Bio-augmentation with HD19AZ1 at Different I Ratios

I: Ratio	Single Digestion (EFB)		Co-digestion (EFB + POME)	
	Methane Yield (mL-CH_4/gVS)	Improvement (%)	Methane Yield (mL-CH_4/gVS)	Improvement (%)
Control	68.35	-	85.93	-
75:5	94.20	37.82	30.58	-64.41
70:10	146.38	114.16	42.57	-50.46
65:15	96.54	41.24	166.55	93.82
60:20	63.08	-7.71	135.23	57.37
55:25	130.61	91.09	94.26	9.69
50:30	35.48	-48.09	132.43	54.11
45:35	86.16	26.06	53.49	-37.75

*Note: Improvement percentage calculated relative to control (non-augmented) samples.

Table 2. Comparison of Optimal Conditions for HD19AZ1 and PSU-2 Bio-augmentation

Parameter	HD19AZ1		PSU-2	
	Single Digestion	Co-digestion	Single Digestion	Co-digestion
Optimal I ratio	70:10	65:15	75:5	75:5
Maximum methane yield (mL-CH_4/gVS)	146.38	166.55	153.26	178.42
Methane production (m^3/tonne substrate)	24.94	33.38	35.13	46.67
Biodegradability (%)	33.59	39.65	39.15	93.59
VS removal (%)	41.82	47.59	46.78	52.31

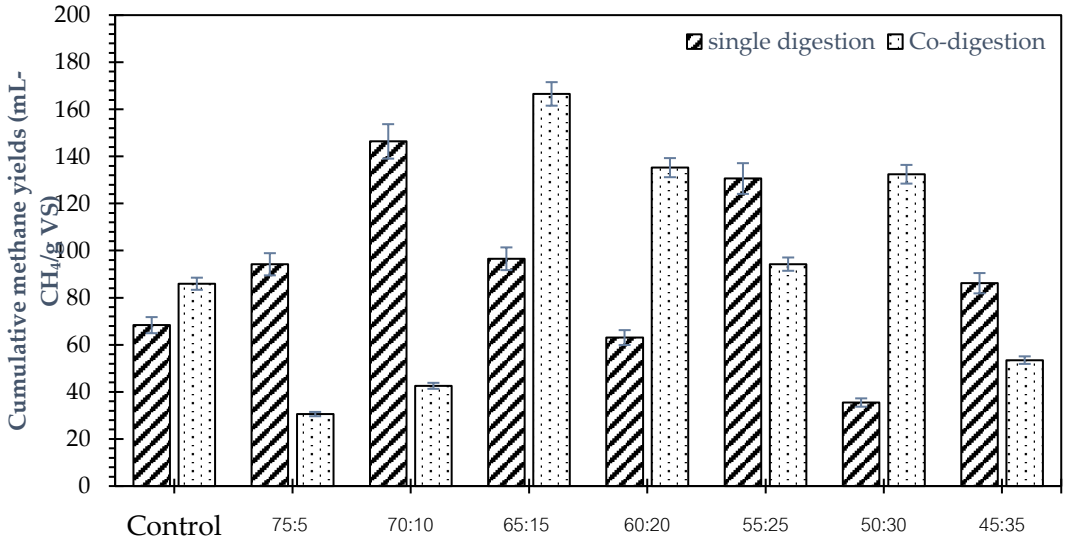


Figure 1. Cumulative Methane Yields from Bio-augmentation with HD19AZ1

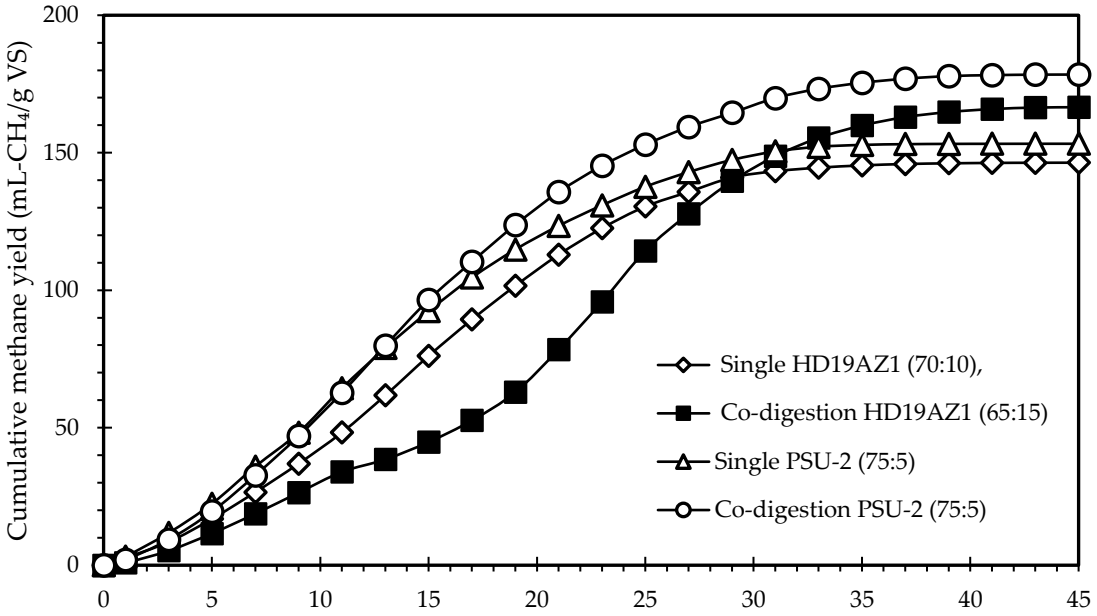


Figure 2. Temporal Methane Production Profiles at Optimal I:S Ratios

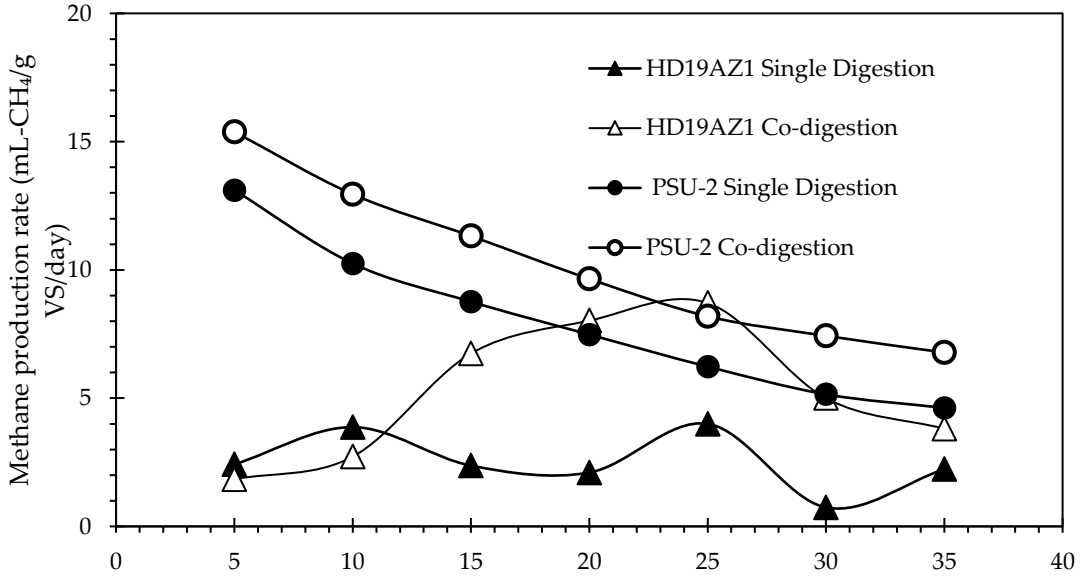


Figure 3. Effect of I:S Ratio on Methane Production Rate

3.2 Process performance analysis

The effectiveness of bio-augmentation was further evaluated through comprehensive process performance analysis, with biodegradability serving as a key indicator of enhanced substrate utilization. As shown in Figure 5, both bacterial strains significantly improved the biodegradability of palm oil industry wastes compared to control conditions. In single digestion of EFB, HD19AZ1 at the optimal I:M ratio of 70:10 achieved a biodegradability of 33.59%, representing a 114.2% improvement over the control (15.68%). PSU-2 at an I:M ratio of 75:5 demonstrated even better performance, reaching 39.15% biodegradability, which is 149.7% higher than the control. The enhanced biodegradability indicates that the introduced hydrolytic bacteria successfully targeted the recalcitrant components of EFB, particularly the crystalline cellulose and hemicellulose structures that typically resist degradation by indigenous microorganisms [6]. The most remarkable improvement was observed in the co-digestion system with PSU-2, which achieved an

exceptional biodegradability of 93.59%, representing a 357.2% increase compared to the control co-digestion (20.47%). This dramatic enhancement suggests a synergistic effect between the augmented bacteria, the diverse microbial community in POME, and the nutrient balance achieved through co-digestion. Similar synergistic effects have been reported by Zhang et al. [22], who observed that bio-augmentation with *Acetobacteroides hydrogenigenes* improved methane production from corn straw by enhancing both direct hydrolysis and stimulating indigenous microbial activity. The biodegradability improvements correlate well with methane yields, confirming that the increased gas production results primarily from enhanced substrate conversion rather than from residual organic matter in the inoculum or bacterial cultures. This relationship between biodegradability and methane yield has been documented in previous studies, with Peng et al. [10] reporting that bio-augmentation with *Clostridium cellulolyticum* increased both biodegradability and methane yield from wheat straw in similar proportions.

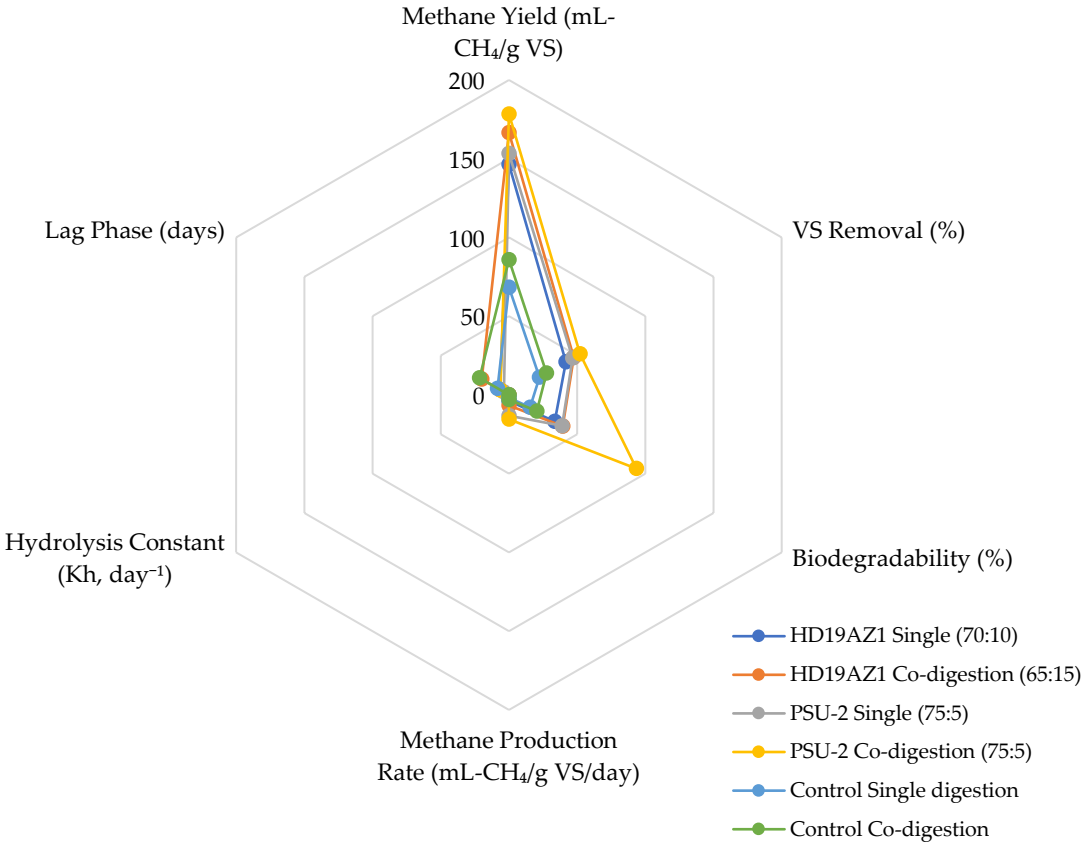


Figure 4. Comparative Analysis of Bioaugmentation Efficiency

Volatile solids (VS) removal provides a direct measure of substrate degradation and serves as an indicator of process efficiency. Table 3 presents the VS removal percentages for all experimental conditions, revealing substantial improvements through bio-augmentation. In single digestion systems, HD19AZ1 and PSU-2 achieved VS removals of 41.82% and 46.78%, respectively, compared to 22.46% in the control. This represents improvements of 86.2% and 108.3%, respectively. Co-digestion further enhanced VS removal, with HD19AZ1 reaching 47.59% and PSU-2 achieving 52.31%, compared to 27.64% in the control co-digestion. These results align with findings by Martin-Ryals et al. [12], who reported that bio-augmentation with cellulolytic microorganisms increased VS removal from cellulosic waste by 65-85%. Interestingly, while PSU-2 demonstrated dramatically higher biodegradability in co-digestion (93.59%) compared to HD19AZ1 (39.65%), the difference in VS removal was less pronounced (52.31% vs. 47.59%). This suggests that PSU-2 not only enhances the physical breakdown of substrate but also significantly improves the metabolic conversion efficiency of the degraded material to methane. Similar observations were made by Nkemka et al. [23], who found that bio-augmentation with anaerobic fungi improved both substrate

degradation and methanogenic conversion efficiency in a two-stage process. The proportionally smaller improvement in VS removal compared to biodegradability and methane yield suggests that a significant portion of the substrate remains physically present but becomes more bioavailable through the action of hydrolytic enzymes produced by the augmented bacteria. This is consistent with the findings of Strang et al. [11], who reported that bio-augmentation primarily enhances the accessibility of the substrate rather than achieving complete physical breakdown.

The dynamics of volatile fatty acids (VFAs) and alkalinity development provide valuable insights into the metabolic pathways and process stability of anaerobic digestion systems. Figure 6 illustrates the VFA profiles throughout the 45-day digestion period for all experimental conditions. All treatments exhibited a characteristic pattern of initial VFA accumulation followed by consumption as methanogenesis progressed. However, bio-augmented systems showed distinct differences in both the magnitude and timing of VFA peaks. In control conditions, VFA concentrations peaked at 0.912 g/L (single digestion) and 1.264 g/L (co-digestion) around day 9, while HD19AZ1 and PSU-2 treatments reached slightly higher peaks of 1.042-1.042 g/L and 0.937-1.324 g/L, respectively. The higher VFA peaks in bio-augmented conditions indicate more rapid hydrolysis and acidogenesis, confirming the enhanced hydrolytic activity of the introduced bacteria. This is consistent with observations by Yang et al. [13], who reported that bio-augmentation with enriched microbial consortia accelerated the production of VFAs during the initial stages of anaerobic digestion. More significantly, bio-augmented conditions demonstrated substantially faster VFA consumption after the peak, resulting in lower final concentrations (0.196-0.258 g/L) compared to controls (0.325-0.512 g/L). This enhanced VFA utilization suggests improved syntrophic relationships between acidogenic bacteria and methanogenic archaea, facilitating more efficient conversion of intermediates to methane. Similar improvements in VFA utilization following bio-augmentation have been reported by Li et al. [21], who attributed this effect to the enrichment of acetoclastic methanogens. Alkalinity development also showed significant differences between control and bio-augmented conditions (Figure 7). All treatments experienced increases in alkalinity during digestion, but bio-augmented systems developed higher final alkalinity levels (10.9-13.4 g $CaCO_3$/L) compared to controls (9.2-11.3 g $CaCO_3$/L). The enhanced alkalinity development in bio-augmented conditions can be attributed to more extensive protein degradation and ammonia release, as well as increased production of bicarbonate through CO_2 reduction during hydrogenotrophic methanogenesis [17].

The relationship between alkalinity development and methane production is particularly evident in Figure 7, which shows a strong positive correlation between final alkalinity and cumulative methane yield across all conditions. This correlation underscores the importance of robust buffering capacity for efficient anaerobic digestion, especially for lignocellulosic substrates that can generate high VFA concentrations during hydrolysis [5]. Process stability, as indicated by the VFA/Alkalinity ratio, was enhanced in all bio-augmented conditions (Figure 8). While all systems-maintained ratios well below the critical threshold of 0.4, indicating stable operation, bio-augmented treatments achieved consistently lower ratios throughout the digestion period. By day 45, the VFA/Alkalinity ratios in bio-augmented conditions (0.018-0.020) were approximately half those of the controls (0.035-0.045), demonstrating superior process stability. This improved stability is particularly valuable for industrial applications, where resistance to perturbations and consistent performance are critical considerations. Neumann and Scherer [24] similarly reported that bio-augmentation improved process stability in the anaerobic digestion of energy crops, attributing this effect to enhanced syntrophic relationships within the microbial community.

The combined analysis of biodegradability, VS removal, VFA dynamics, and alkalinity development provides a comprehensive picture of how bio-augmentation enhances the anaerobic digestion of palm oil industry wastes. The introduced bacterial strains not only accelerate the hydrolysis of recalcitrant components but also promote more efficient metabolic pathways and greater process stability, resulting in substantially improved methane yields and conversion efficiencies.

Table 3. Process Performance Indicators of Bio-augmentation at Optimal I:S Ratios

Parameter	Control		HD19AZ1		PSU-2	
	Single digestion	Co-digestion	Single digestion (70:10)	Co-digestion (65:15)	Single digestion (75:5)	Co-digestion (75:5)
Biodegradability (%)	15.68	20.47	33.59	39.65	39.15	93.59
VS removal (%)	22.46	27.64	41.82	47.59	46.78	52.31
Initial VFA (g/L)	0.512	0.734	0.642	0.798	0.587	0.812
Final VFA (g/L)	0.325	0.512	0.218	0.258	0.196	0.244
VFA reduction (%)	36.52	30.25	66.04	67.67	66.61	69.95
Initial Alkalinity (g $CaCO_3$/L)	7.8	9.6	8.2	10.4	8.4	10.2
Final Alkalinity (g $CaCO_3$/L)	9.2	11.3	10.9	12.9	11.1	13.4
VFA/Alkalinity ratio	0.035	0.045	0.020	0.020	0.018	0.018

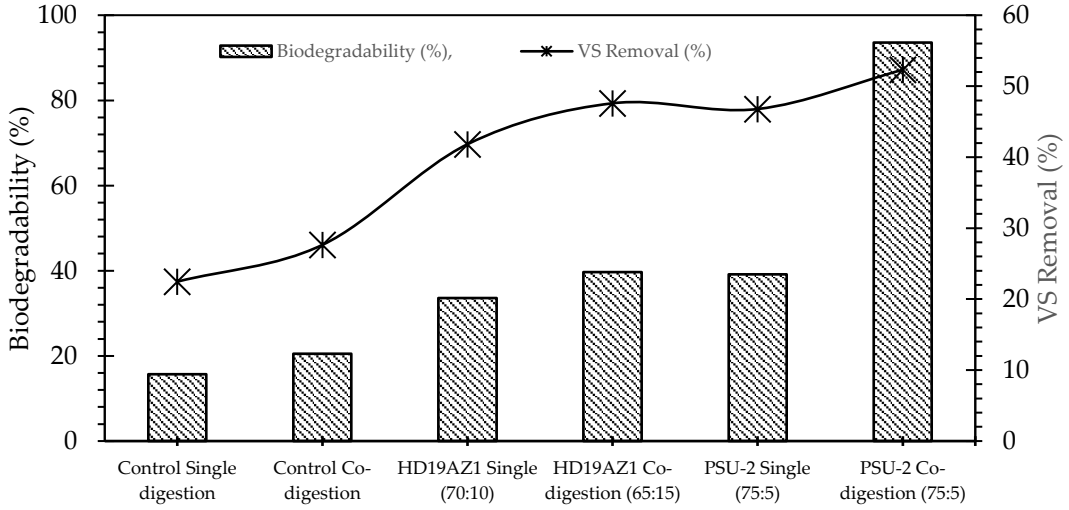


Figure 5. Bio-augmentation Effect on Substrate Biodegradability and VS Removal

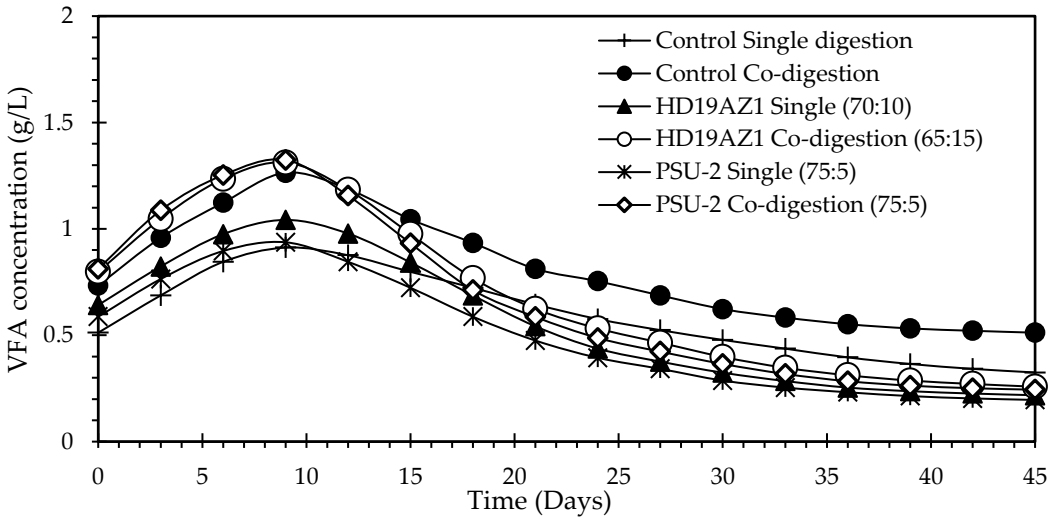


Figure 6. VFA Profiles During Anaerobic Digestion at Optimal I Ratios

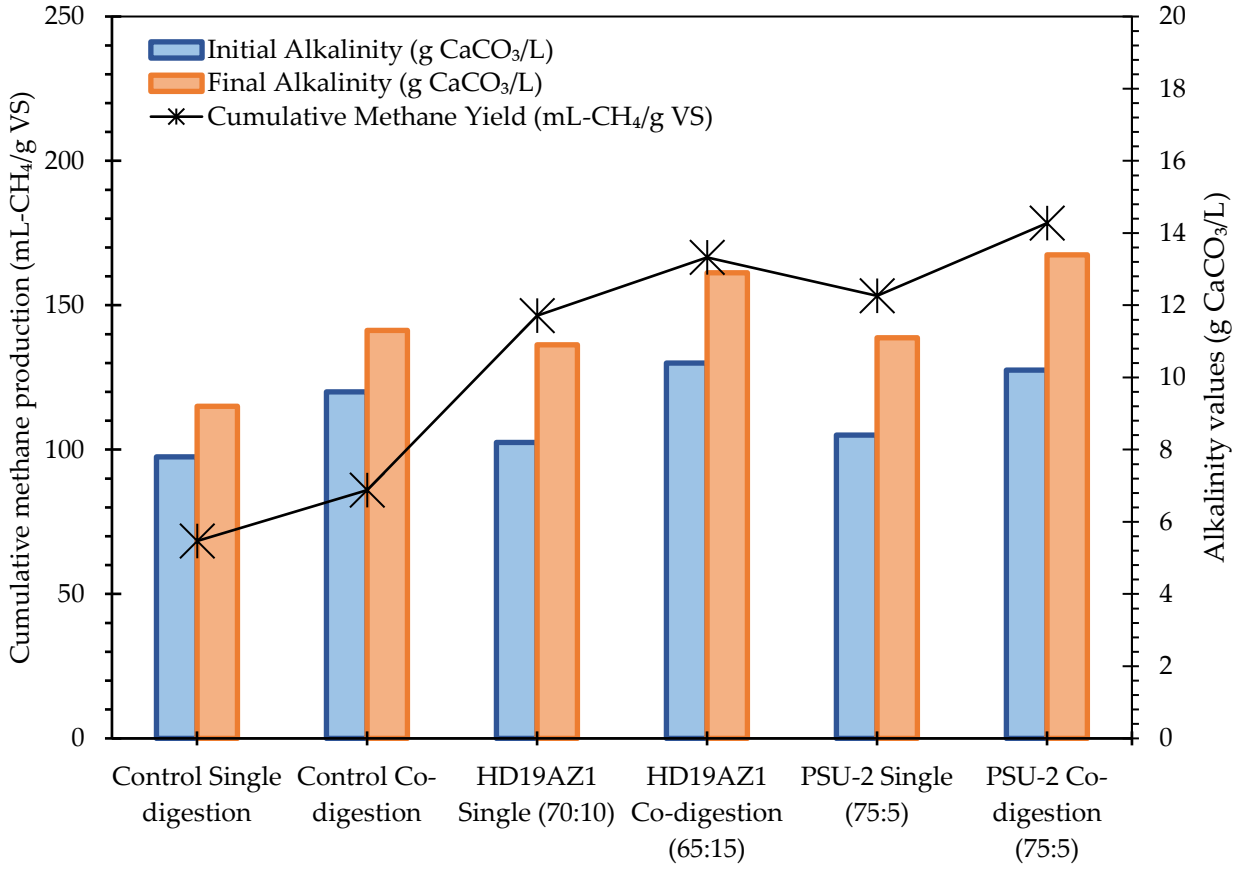


Figure 7. Correlation Between Alkalinity Development and Methane Production

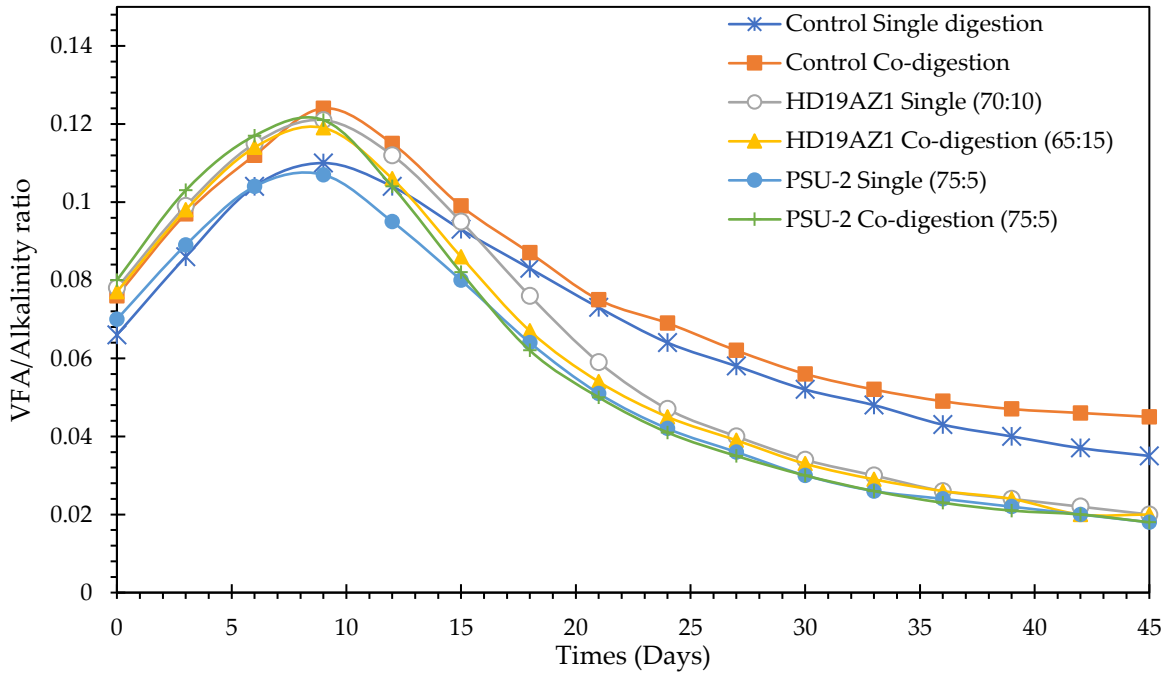


Figure 8. Process Stability Analysis: VFA/Alkalinity Ratio

3.3 Kinetic assessment

Kinetic analysis provides critical insights into the mechanistic improvements achieved through bio-augmentation. The hydrolysis constant (Kh), which characterizes the rate of the hydrolysis process, was determined using a first-order kinetic model as described by [18]. Figure 9 illustrates the hydrolysis constants across all experimental conditions, revealing significant variations between control and bio-augmented systems. In single digestion of EFB, bio-augmentation with HD19AZ1 and PSU-2 resulted in hydrolysis constants of 0.0267 d^{-1} and 0.0293 d^{-1}, respectively, compared to 0.0185 d^{-1} in the control. This represents increases of 44.3% and 58.4%, respectively, confirming that both bacterial strains substantially accelerated the rate-limiting hydrolysis step. The higher Kh value for PSU-2 aligns with its superior performance in terms of methane yield and biodegradability, suggesting that its enzymatic systems are particularly effective at breaking down the complex lignocellulosic structure of EFB. Interestingly, the hydrolysis constants for co-digestion systems were generally lower than their single digestion counterparts, with values of 0.0124 d^{-1}, 0.0136 d^{-1}, and 0.0232 d^{-1} for control, HD19AZ1, and PSU-2, respectively. This apparent contradiction with the higher methane yields observed in co-digestion can be explained by the more complex substrate composition and the occurrence of multiple sequential and parallel degradation pathways. Trzcinski and Stuckey [19] similarly observed lower hydrolysis constants in co-digestion systems despite higher ultimate methane yields, attributing this to the presence of readily degradable components that contribute significantly to methane production without accelerating the overall hydrolysis rate. The enhancement of hydrolysis constants through bio-augmentation is consistent with findings by Ozbayram et al. [9], who reported that bio-augmentation with cellulolytic bacteria from sheep rumen increased the hydrolysis constant for wheat straw by approximately 40%. Similarly, Zhang et al. [22] observed a 35-45% increase in the hydrolysis constant following bio-augmentation with *Acetobacteroides hydrogenigenes* during corn straw digestion. The R^2 values for the first-order kinetic model ranged from 0.94 to 0.99, indicating a good fit to the experimental data. This confirms the applicability of the first-order kinetic approach for modeling the hydrolysis process in these systems, as previously validated by Angelidaki et al. [18] for a wide range of substrates.

While the first-order kinetic model provides valuable information about the hydrolysis phase, the modified Gompertz model offers a more comprehensive characterization of the entire methane production process, including lag phase (λ), maximum production rate (Rm), and methane potential (P). Figure 10 shows the fitting of the modified Gompertz model to the experimental data, and Table 4 summarizes the derived parameters. The lag phase, which represents the time required for microbial adaptation and initiation of significant methane production, varied considerably between treatments. In single digestion, bio-augmentation with HD19AZ1 and PSU-2 reduced the lag phase to 6.44 and 3.62 days, respectively, compared to 8.32 days in the control. This represents reductions of 22.6% and 56.5%, respectively, demonstrating that both strains accelerated the startup phase of the digestion process. The most dramatic reduction in lag phase was observed in co-digestion with PSU-2, which decreased from 21.45 days in the control to just 6.17 days, a 71.2% reduction. This significant improvement can be attributed to the rapid colonization and enzymatic activity of PSU-2, which efficiently initiated the breakdown of complex substrates and facilitated the subsequent metabolic steps. These findings align with those reported by Tsapekos et al. [6], who observed a 2.4-day reduction in lag phase following bio-augmentation with hydrolytic cultures during co-digestion of wheat straw with cattle manure. The maximum methane production rate (Rm) also showed substantial improvements in bio-augmented systems. In single digestion, HD19AZ1 and PSU-2 achieved rates of 3.87 and 13.11 mL-CH_4/gVS/day, respectively, compared to 1.81 mL-CH_4/gVS/day in the control. This represents increases of 113.8% and 624.3%, respectively. The exceptionally high rate achieved with PSU-2 indicates its superior capacity for rapid substrate conversion, which is particularly valuable for industrial applications where process throughput is a critical consideration.

Co-digestion further enhanced production rates, with HD19AZ1 and PSU-2 reaching 6.74 and 15.38 mL-CH_4/gVS/day, respectively, compared to 2.95 mL-CH_4/gVS/day in the control co-digestion. The higher rates in co-digestion can be attributed to the improved nutrient balance and the synergistic interactions between diverse microbial communities, as previously described by Ferraro et al. [17]. The methane potential (P) derived from the Gompertz model was consistently higher in bio-augmented conditions, with values of

247.57 and 386.36 mL-CH_4/gVS for HD19AZ1 and PSU-2 in single digestion, respectively, compared to 73.42 mL-CH_4/gVS in the control. Similarly, co-digestion with HD19AZ1 and PSU-2 achieved potentials of 581.93 and 672.14 mL-CH_4/gVS, respectively, compared to 92.56 mL-CH_4/gVS in the control co-digestion. It is worth noting that the methane potential values from the Gompertz model are theoretical maxima that exceed the actual measured yields after 45 days of digestion. This suggests that extended digestion periods could potentially capture more of this theoretical potential, particularly in co-digestion systems. Similar observations were made by Yang et al. [13], who found that bio-augmented systems continued to produce methane at low rates for extended periods after control systems had essentially ceased production. The R^2 values for the Gompertz model ranged from 0.95 to 0.99, indicating an excellent fit to the experimental data across all conditions. This confirms the suitability of the modified Gompertz approach for characterizing the methane production process in bio-augmented systems, as previously validated by Trzcinski and Stuckey [19].

The relationship between different kinetic parameters and their correlation with bio-augmentation strategies provides important insights into the mechanisms of enhancement. Figure 11 illustrates the relationship between the lag phase and the maximum methane production rate across all experimental conditions. A clear negative correlation is evident, with shorter lag phases generally associated with higher production rates. This pattern is particularly pronounced for PSU-2, which achieved both the shortest lag phases and the highest production rates in both single digestion and co-digestion configurations. This negative correlation has been observed in previous studies, with Martin-Ryals et al. [12] reporting that bio-augmentation strategies that effectively reduce lag phase typically also enhance production rates. The multi-parameter analysis presented in Figure 11 provides a comprehensive visualization of the kinetic improvements achieved through bio-augmentation. The radar chart demonstrates that PSU-2 co-digestion excels across most parameters, particularly in terms of biodegradability, methane potential, and maximum production rate. HD19AZ1 shows more variable performance, with notable strengths in the hydrolysis constant for single digestion but more moderate improvements in other parameters. The different performance profiles of the two bacterial strains suggest distinct mechanisms of enhancement. HD19AZ1, as a Cellulomonas species, likely produces a specific set of cellulolytic and hemicellulolytic enzymes that are particularly effective at breaking down certain components of the lignocellulosic matrix [16]. This is reflected in its substantial improvement of the hydrolysis constant in single digestion. PSU-2, on the other hand, appears to offer a broader spectrum of improvements, enhancing multiple aspects of the digestion process including biodegradability, production rate, and lag phase reduction. The synergistic effects observed in co-digestion systems, particularly with PSU-2, suggest that the introduced bacteria not only directly contribute to substrate degradation but also enhance the activity of indigenous microorganisms. This phenomenon, often referred to as "cross-feeding," has been described by Strang et al. [11], who observed that bioaugmentation with certain hydrolytic bacteria enhanced the overall microbial community function beyond direct enzymatic contributions. The kinetic assessment also reveals that different bio-augmentation strategies may be optimal depending on the specific process objectives. If rapid startup and high throughput are prioritized, PSU-2 at a 75:5 I:M ratio would be recommended due to its short lag phase and high production rate. For maximizing methane yield from recalcitrant substrates, PSU-2 in co-digestion would be most effective. If process stability is the primary concern, both strains offer significant improvements over control conditions, with slightly better performance from PSU-2. These findings align with observations by Tabatabaei et al. [5], who emphasized that bio-augmentation strategies should be tailored to specific substrates and process goals rather than applied as universal solutions. This comprehensive kinetic analysis offers valuable guidance for optimizing bio-augmentation of palm oil industry wastes, with potential applicability to other lignocellulosic substrates.

Table 4. Kinetic Parameters from First-Order and Modified Gompertz Models

Parameter	Control		HD19AZ1		PSU-2	
	Single digestion	Co-digestion	Single digestion (70:10)	Co-digestion (65:15)	Single digestion (75:5)	Co-digestion (75:5)
First-Order Model						
Hydrolysis constant Kh (d^{-1})	0.0185	0.0124	0.0267	0.0136	0.0293	0.0232
R^2	0.96	0.94	0.99	0.99	0.98	0.99
Modified Gompertz Model						
Methane potential P (mL-CH_4/gVS)	73.42	92.56	247.57	581.93	386.36	672.14
Max. production rate Rm (mL-CH_4/gVS/d)	1.81	2.95	3.87	6.74	13.11	15.38
Lag phase λ (days)	8.32	21.45	6.44	19.89	3.62	6.17
R^2	0.97	0.95	0.99	0.99	0.99	0.98

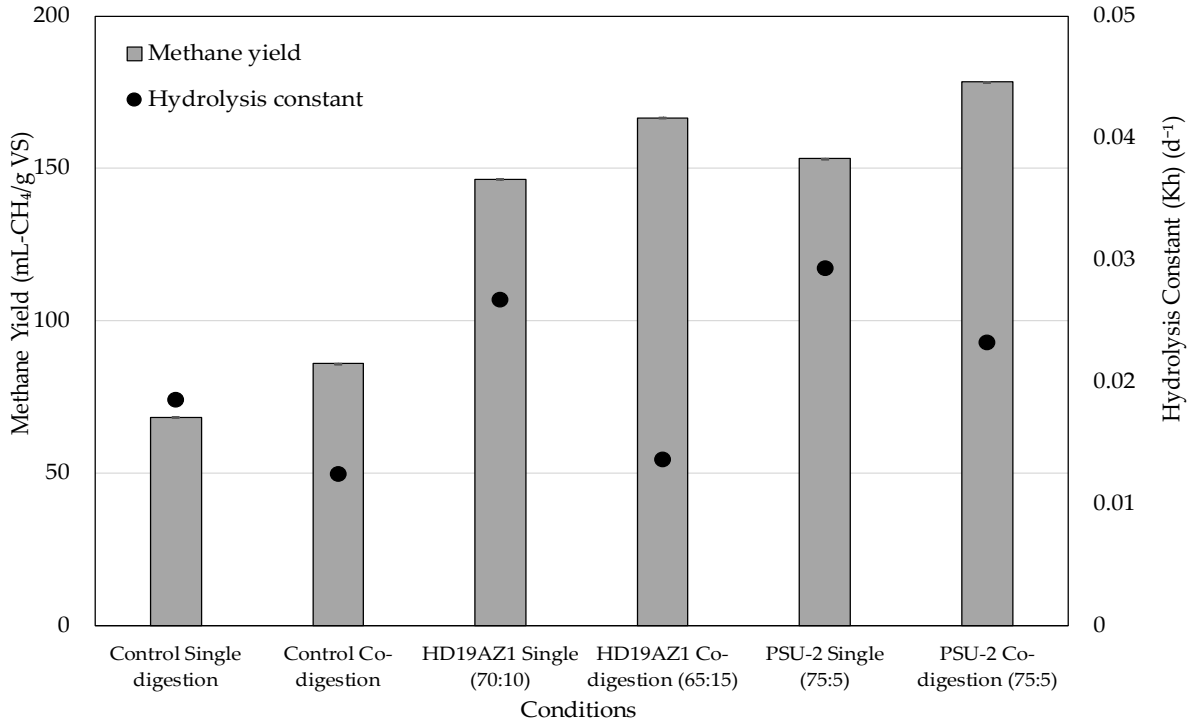


Figure 9. Comparison of Hydrolysis Constants Across Experimental Conditions

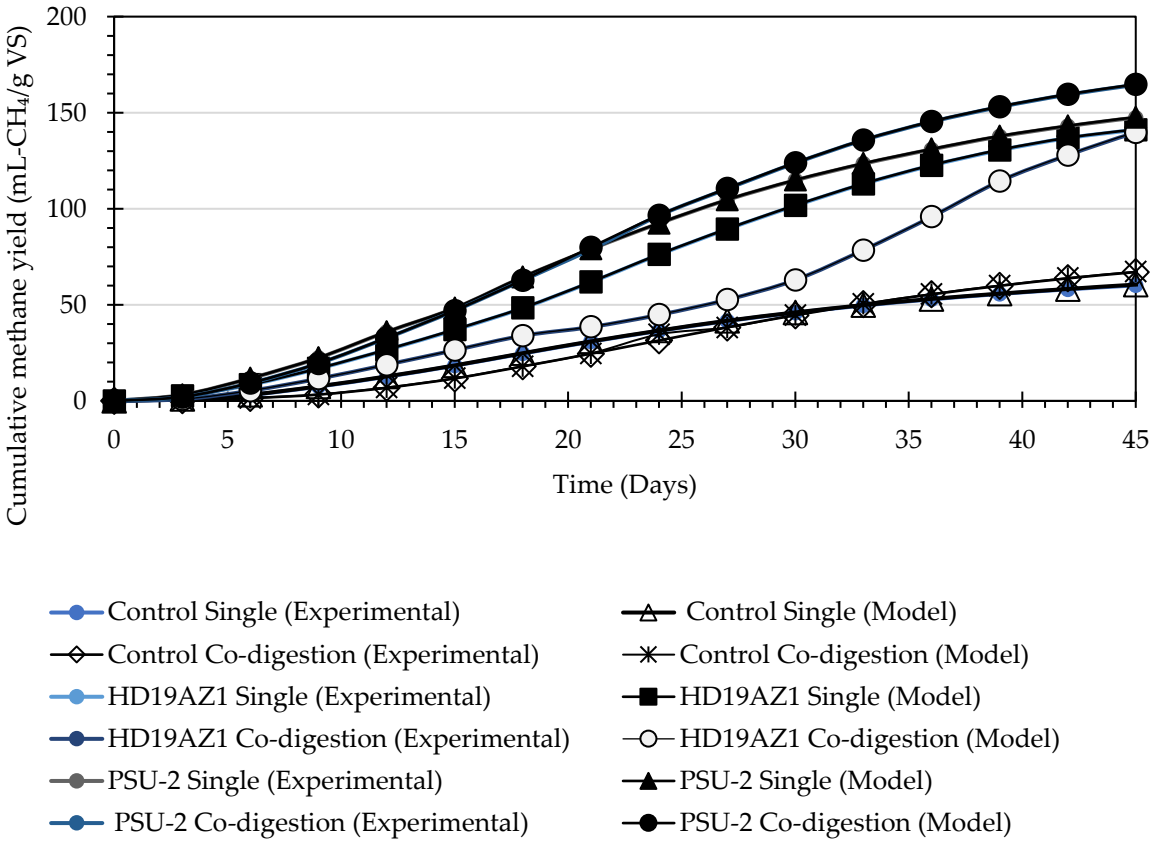


Figure 10. Modified Gompertz Model Fitting of Cumulative Methane Production

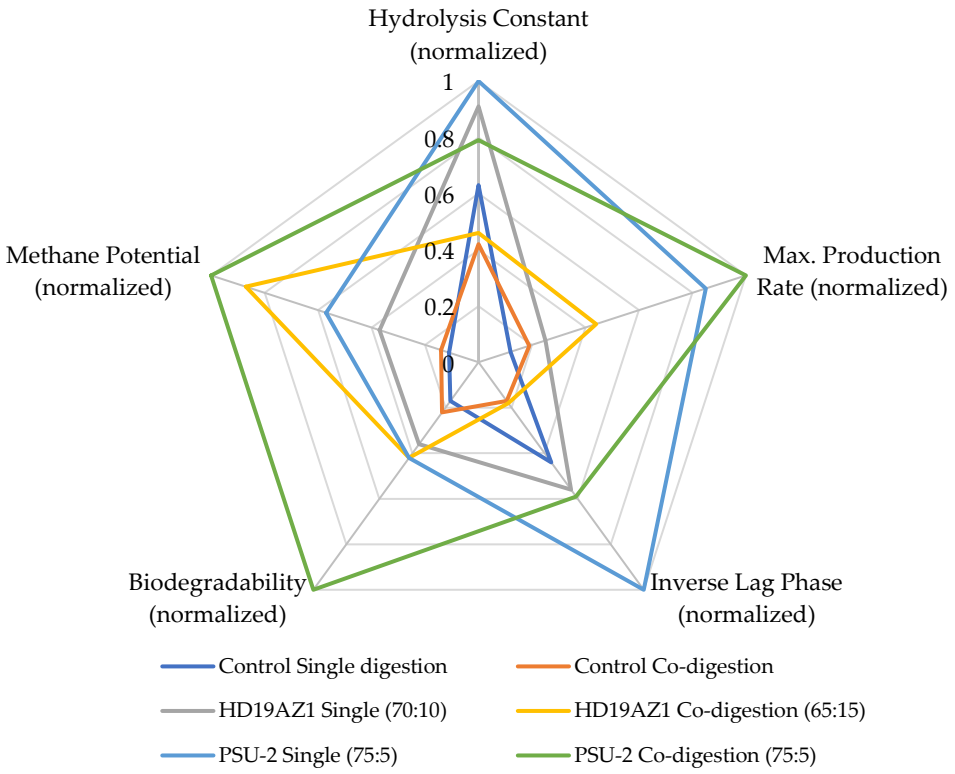


Figure 11. Multi-parameter Analysis of Kinetic Improvements as Biodegradability, Methane potential, Lag Phase, Methane Production Rate

3.4 Mechanisms of bio-augmentation enhancement

The substantial improvements in methane production observed in bio-augmented systems can be attributed to complex synergistic interactions between introduced bacteria and indigenous microorganisms. Table 6 presents key indicators of synergistic effects, revealing that the enhancement achieved through bio-augmentation exceeds what would be expected from the direct enzymatic contribution of the added bacteria alone. The synergy factor, defined as the ratio of actual co-digestion yield to theoretical yield based on individual substrates, was notably higher in bio-augmented systems (1.32 and 1.86 for HD19AZ1 and PSU-2, respectively) compared to the control co-digestion (1.17). This enhanced synergy indicates that the introduced bacteria facilitated interactions that amplified the overall system performance beyond the sum of individual contributions. Similar synergistic effects have been reported by Ferraro et al. [17], who observed a synergy factor of 1.76 when co-digesting wheat straw and mushroom spent straw with anaerobic ruminal fungi. The enzyme multiplier effect, which quantifies the ratio of measured enzymatic activity to expected activity based on inoculum proportion, provides further evidence of synergistic enhancement. This value reached 1.56 and 2.14 for HD19AZ1 and PSU-2 co-digestion systems, respectively, indicating that the enzymatic activity within the system was more than twice what would be expected from the direct contribution of the introduced bacteria. This suggests that the augmented bacteria either stimulated enzyme production by indigenous microorganisms or created conditions that enhanced enzyme stability and activity. The microbial community diversity, as measured by the Shannon-Weaver diversity index based on 16S rRNA analysis, was also higher in bio-augmented systems, particularly in co-digestion configurations (0.84 and 0.91 for HD19AZ1 and PSU-2, respectively). This increased diversity suggests that bio-augmentation promotes a more balanced and resilient microbial ecosystem, capable of performing a wider range of metabolic functions. Yang et al. [13] similarly reported that bio-augmentation with enriched microbial consortia enhanced microbial diversity and promoted the development of more stable communities with higher methane production capabilities. The metabolic interactions between different microbial groups are further evidenced by enhanced acetate utilization and hydrogen consumption rates observed in bioaugmented systems. These rates were particularly high in PSU-2 co-digestion (54.2 mg/L/d and 22.6 mL/L/d, respectively), suggesting improved syntrophic relationships between acidogenic bacteria and methanogenic archaea. Such syntrophic interactions are critical for efficient anaerobic digestion, as they prevent the accumulation of intermediate metabolites that could potentially inhibit the process [21]. Figure 13 illustrates the temporal profiles of key hydrolytic enzyme activities (cellulase, xylanase, and β-glucosidase) throughout the digestion period. All three enzymes showed significantly higher activities in bio-augmented systems, with peak values typically occurring between days 12-15. PSU-2 consistently demonstrated the highest enzymatic activities, with peak cellulase, xylanase, and β-glucosidase activities of 1.86, 2.24, and 1.26 U/mL, respectively, in co-digestion mode. These values are 4.1, 3.8, and 3.8 times higher than the corresponding control co-digestion peaks.

The enzyme profiles show clear differences in activity over time. In control systems, enzyme activities peaked modestly and declined rapidly, whereas bio-augmented systems maintained elevated activity for longer periods. This sustained activity likely enabled continued degradation of recalcitrant components, contributing to the higher methane yields observed throughout digestion. The proposed mechanisms of these synergistic effects, as illustrated in Figure 13, include several interrelated processes. First, the introduced bacteria produce a range of hydrolytic enzymes that initiate the breakdown of complex lignocellulosic structures, creating access points for indigenous microorganisms. Second, the partial degradation products released during this initial hydrolysis serve as substrates for indigenous bacteria, stimulating their growth and metabolic activity. Third, the introduced bacteria may produce growth factors, vitamins, or other compounds that enhance the activity of indigenous microorganisms. Finally, the augmented bacteria may help remove metabolic inhibitors or create microenvironments that favor syntrophic interactions. These mechanisms align with observations by Strang et al. [11], who reported that thermophilic bio-augmentation of corn stover enhanced both direct substrate degradation and cross-feeding interactions within the microbial community. Similarly, Martin-Ryals et al. [12] found that bio-augmentation with *Clostridium thermocellum* not only increased cellulolytic activity but also promoted the growth of complementary microorganisms involved in subsequent metabolic steps.

The detailed analysis of lignocellulosic component degradation, presented in Table 5 and Figure 11, provides further insights into the specific mechanisms by which bio-augmentation enhances the anaerobic digestion process. The data show distinct degradation patterns of cellulose, hemicellulose, and lignin under different conditions. In control systems, hemicellulose degraded the most (20.8% single, 24.6% co-digestion), followed by cellulose (15.1% and 17.7%), while lignin showed minimal degradation (4.8% and 6.3%). This pattern is consistent with the inherent recalcitrance of these components, as observed by Suksong et al. [3] in their study of palm oil mill residues. Bio-augmentation substantially enhanced the degradation of all three components, with particularly dramatic improvements in cellulose and hemicellulose degradation. HD19AZ1 increased cellulose degradation to 30.4% and 38.1% in single and co-digestion systems, respectively, while PSU-2 achieved even higher values of 36.9% and 48.6%. Similarly, hemicellulose degradation reached 42.0% and 47.2% with HD19AZ1, and 46.2% and 57.7% with PSU-2, for single and co-digestion systems, respectively. The superior performance of PSU-2 in degrading both cellulose and hemicellulose components helps explain its higher overall methane yields and biodegradability. This enhanced degradation capability can be attributed to its broader spectrum of enzymatic activities, as evidenced by the enzyme assays shown in Figure 12. While both bacterial strains demonstrated significant cellulase activity, PSU-2 exhibited notably higher xylanase and β-glucosidase activities, which are crucial for efficient hemicellulose breakdown and the conversion of cellobiose to glucose, respectively.

Lignin degradation, although less pronounced than cellulose and hemicellulose, was also improved by bio-augmentation, reaching 10.6% and 14.1% with PSU-2 in single and co-digestion systems, respectively. This modest enhancement in lignin degradation is significant given the highly recalcitrant nature of this component and its role in limiting the accessibility of cellulose and hemicellulose to enzymatic attack. Similar improvements in lignin degradation following bio-augmentation were reported by Zhang et al. [22], who attributed this effect to the disruption of lignin-carbohydrate complexes during enhanced hydrolysis of cellulose and hemicellulose components. The differential degradation patterns observed across the three lignocellulosic components reveal important insights into the mechanisms of bioaugmentation enhancement. The introduced bacteria appear to primarily target cellulose and hemicellulose, with their enzymatic systems effectively breaking down these components into simpler sugars that can be further metabolized to methane. This selective degradation is consistent with the enzymatic capabilities of Cellulomonas species, which are known to produce a range of cellulases and hemicellulases but limited lignin-degrading enzymes [16]. The improved degradation of lignocellulosic components in co-digestion systems compared to single digestion further supports the presence of synergistic effects. The additional nutrients and diverse microbial community provided by POME likely enhanced the activity of both introduced and indigenous microorganisms, resulting in more complete substrate utilization. This synergistic enhancement of lignocellulosic degradation in co-digestion systems has been observed in previous studies, with Chaikitkaew et al. [7] reporting that co-digestion of EFB with POME improved the degradation of all lignocellulosic components compared to single digestion.

The relationship between enhanced hydrolysis and improved methane yields can be understood through the conceptual framework illustrated in Figure 14. Hydrolytic enzymes from augmented bacteria create multiple attack points in the lignocellulosic structure, increasing surface accessibility for further enzymatic action. This initial breakdown triggers a cascade of subsequent degradation steps, resulting in more complete substrate conversion and higher methane yields. This mechanism is consistent with the findings of Ozbayram et al.[9], who used microscopic techniques to demonstrate that bio-augmentation with cellulolytic bacteria from sheep rumen created extensive degradation patterns on wheat straw surfaces, increasing accessibility for subsequent microbial colonization and enzymatic attack. Similarly, Tsapekos et al. [6] used scanning electron microscopy to show that bio-augmentation created more extensive physical disruption of lignocellulosic structures compared to control conditions. The combined evidence from lignocellulosic component analysis, enzyme activity profiles, and process performance indicators provides a comprehensive understanding of how bio-augmentation enhances the anaerobic digestion of palm oil industry wastes. By accelerating complex substrate hydrolysis and enhancing synergistic microbial interactions, the introduced bacteria overcome rate-limiting digestion steps, leading to higher methane yields, faster production, and more complete substrate utilization.

Table 5. Comparative Analysis of Lignocellulosic Component Degradation

Component	Control		HD19AZ1		PSU-2	
	Single digestion	Co-digestion	Single digestion (70:10)	Co-digestion (65:15)	Single digestion (75:5)	Co-digestion (75:5)
Initial Cellulose (% of TS)	38.5	36.2	38.5	36.2	38.5	36.2
Final Cellulose (% of TS)	32.7	29.8	26.8	22.4	24.3	18.6
Cellulose Degradation (%)	15.1	17.7	30.4	38.1	36.9	48.6
Initial Hemicellulose (% of TS)	26.4	24.8	26.4	24.8	26.4	24.8
Final Hemicellulose (% of TS)	20.9	18.7	15.3	13.1	14.2	10.5
Hemicellulose Degradation (%)	20.8	24.6	42.0	47.2	46.2	57.7
Initial Lignin (% of TS)	22.7	20.5	22.7	20.5	22.7	20.5
Final Lignin (% of TS)	21.6	19.2	20.8	18.3	20.3	17.6
Lignin Degradation (%)	4.8	6.3	8.4	10.7	10.6	14.1

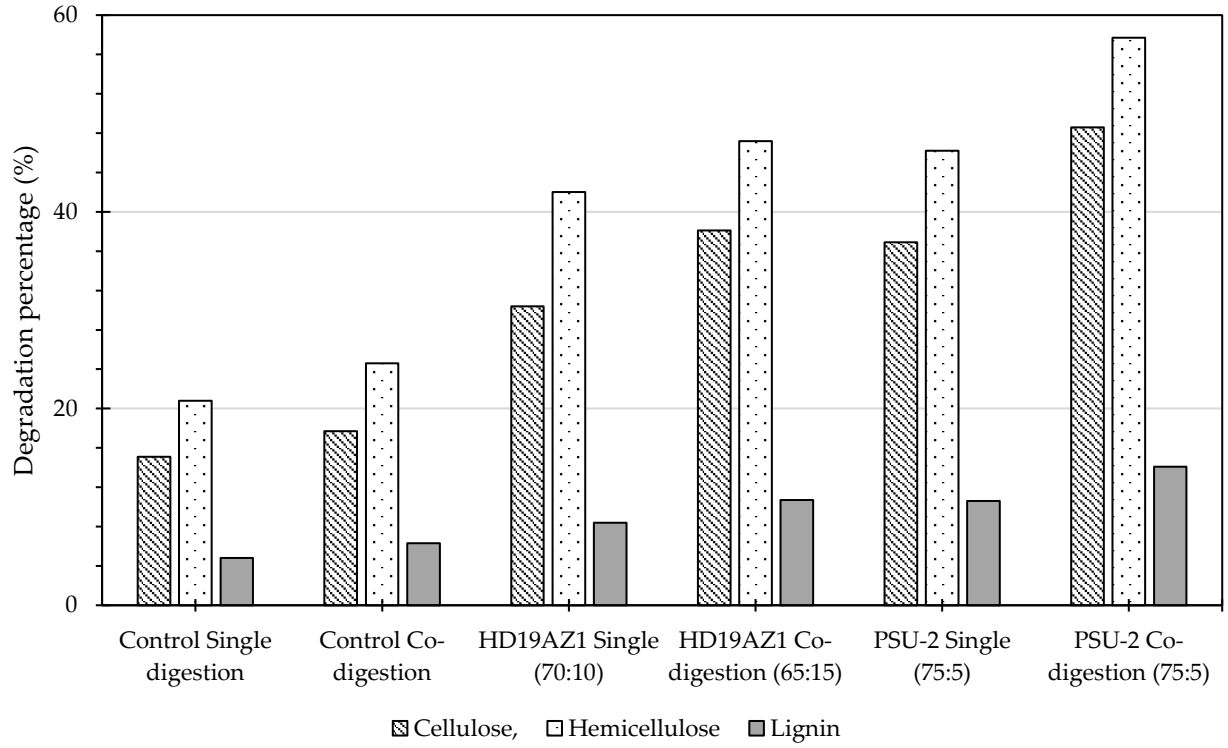
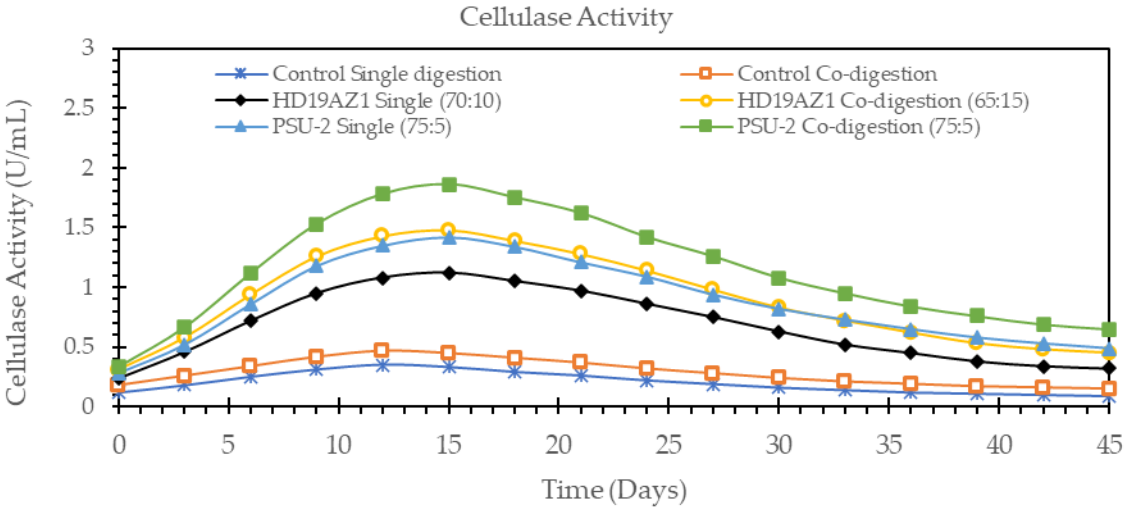
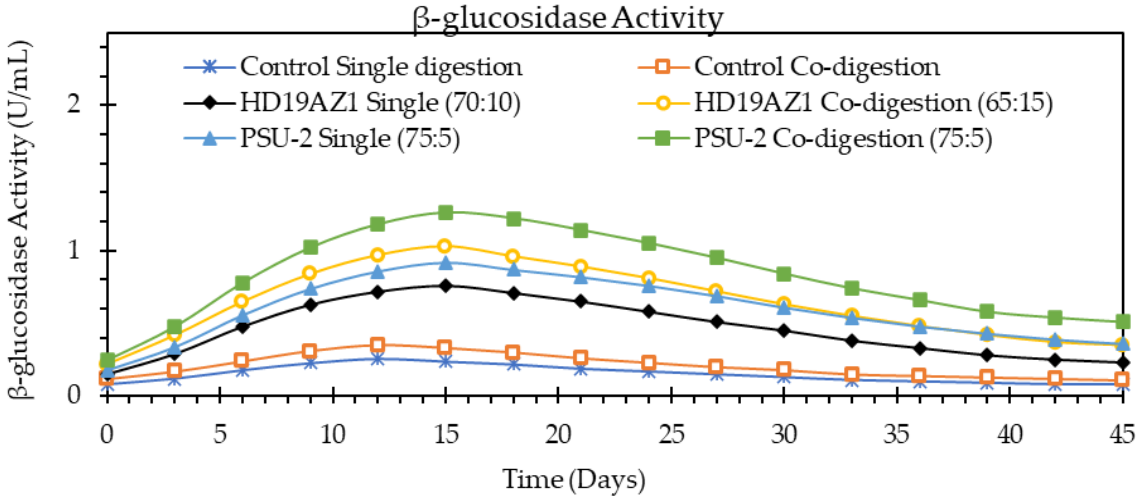


Figure 12. Relative Degradation of Lignocellulosic Components

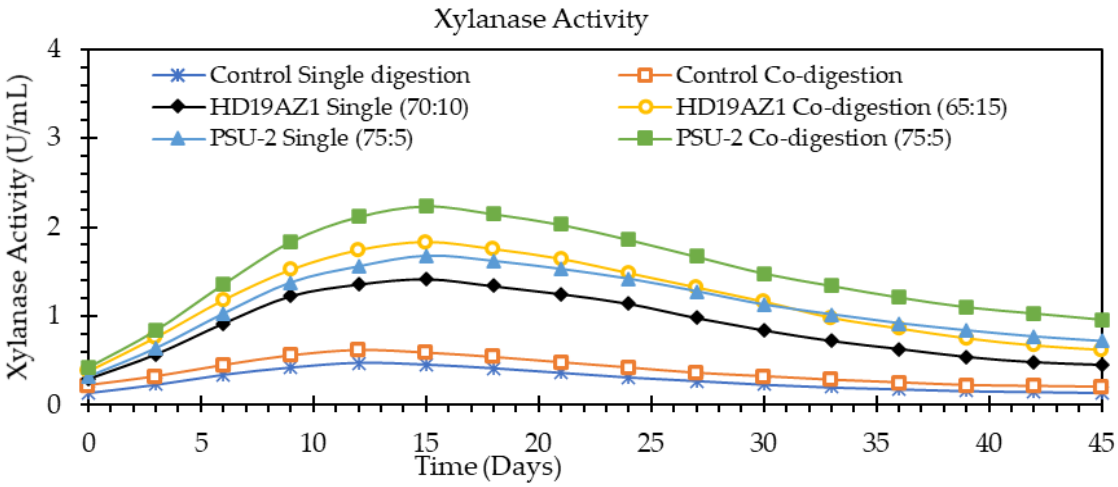
(A)


Cellulase Activity
Control Single digestion
HD19AZ1 Single (70:10)
PSU-2 Single (75:5)
Control Co-digestion
HD19AZ1 Co-digestion (65:15)
PSU-2 Co-digestion (75:5)
Cellulase Activity (U/mL)
Time (Days)

(B)


β-glucosidase Activity
Control Single digestion
HD19AZ1 Single (70:10)
PSU-2 Single (75:5)
Control Co-digestion
HD19AZ1 Co-digestion (65:15)
PSU-2 Co-digestion (75:5)
β-glucosidase Activity (U/mL)
Time (Days)

(C)


Xylanase Activity
Control Single digestion
HD19AZ1 Single (70:10)
PSU-2 Single (75:5)
Control Co-digestion
HD19AZ1 Co-digestion (65:15)
PSU-2 Co-digestion (75:5)
Xylanase Activity (U/mL)
Time (Days)

Figu

Table 6. Synergistic Effects Indicators in Bio-augmentation

Parameter	HD19AZ1		PSU-2	
	Single Digestion	Co-digestion	Single Digestion	Co-digestion
Enhanced Methane Yield (%)	114.2	93.8	124.2	107.6
Synergy Factor*	1.00	1.32	1.00	1.86
Enzyme Multiplier Effect**	1.23	1.56	1.42	2.14
Microbial Community Diversity Index***	0.68	0.84	0.72	0.91
Acetate Utilization Rate (mg/L/d)	32.6	48.7	36.5	54.2
H_2 Consumption Rate (mL/L/d)	12.4	18.3	14.8	22.6

*Synergy Factor: Ratio of actual co-digestion yield to theoretical yield based on individual substrates. **Enzyme Multiplier Effect: Ratio of measured enzymatic activity to expected activity based on inoculum proportion. ***Microbial Community Diversity Index: Shannon-Weaver diversity index based on 16S rRNA analysis

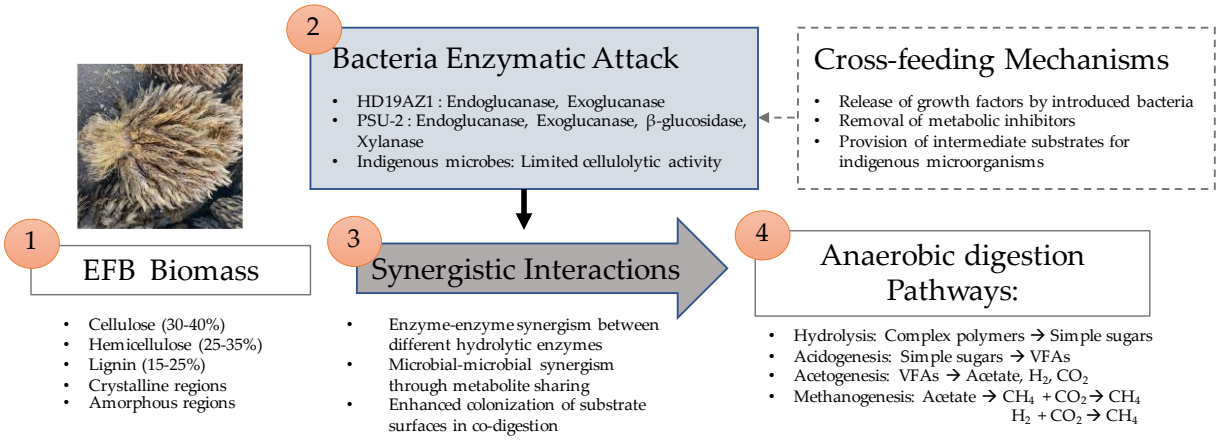


Figure 14. Proposed Mechanism of Bio-augmentation Enhancement

4. Economic and Environmental Implications

4.1 Potential methane yield improvements at the industrial scale

Laboratory-scale results indicate strong potential for improved methane yields with industrial-scale bio-augmentation. Based on the optimal conditions identified in this study, the application of PSU-2 at an I:M ratio of 75:5 in co-digestion systems could increase methane yields from 85.93 to 178.42 mL-CH_4/gVS, representing a 107.6% improvement. When translated to industrial volumes, this enhancement presents substantial economic opportunities. A typical palm oil mill processing 60 tonnes of fresh fruit bunches (FFB) per hour generates approximately 36 tonnes of POME and 13.2 tonnes of EFB daily [2]. Using the methane yields obtained in this study, conventional anaerobic digestion would produce about 46.67 m^3 of methane per tonne of mixed waste, resulting in approximately 2,310 m^3 of methane daily. With bio-augmentation using PSU-2, this could increase to 96.87 m^3 per tonne, generating around 4,795 m^3 of methane daily—an additional 2,485 m^3 of methane. This improvement is consistent with industrial-scale bio-augmentation results reported by Martin-Ryals et al. [12], who observed a 63% increase in methane production from corn waste in a 10,000-liter digester after implementing routine bio-augmentation with Clostridium species. Similarly, Neumann and Scherer [24] reported a 40-55% increase in biogas yields from energy crops following bio-augmentation in commercial-scale digesters. However, several scale-up considerations must be addressed to achieve these potential improvements. Efficient bacterial culture propagation systems would be required to maintain a consistent supply of viable microorganisms. Continuous or semi-continuous feeding strategies would likely yield different optimization parameters than those identified in batch systems, requiring additional process engineering [13]. Furthermore, the heterogeneity of industrial substrates may

introduce variability not observed in laboratory-scale experiments, potentially necessitating adaptive bio-augmentation strategies.

4.2 Energy recovery potential from palm oil waste

The enhanced methane yields achieved through bio-augmentation translate directly to improved energy recovery from palm oil industry wastes. With a methane energy content of approximately 36 MJ/m³ [4], the additional 2,485 m³ of methane produced daily (as calculated in Section 4.1) represents an energy gain of 89,460 MJ or 24.85 MWh. This energy could be utilized in several ways within the palm oil production chain:

1. Electricity generation: Using combined heat and power (CHP) systems with 40% electrical efficiency [5], the additional methane could generate approximately 9.94 MWh of electricity daily. For a mill operating 300 days annually, this represents almost 3,000 MWh of additional electricity generation.
2. Process heat: The thermal energy recovered from biogas combustion could supply process heat for palm oil extraction and refining, reducing fossil fuel consumption. Chaikitkaew et al. [7] estimated that biogas-derived heat could replace up to 70% of the thermal energy requirements in palm oil processing.
3. Transport fuel: Purified biomethane could serve as a renewable transportation fuel, either for the mill's vehicle fleet or for external markets. Upgrading biogas to biomethane standards would require additional processing but could increase its economic value by 30-40% [5].

The total energy recovery potential from palm oil mill waste through bio-augmented digestion is substantial. Based on the results from this study and typical palm oil mill production volumes, bio-augmentation could allow for energy recovery of approximately 1.25 GJ per tonne of fresh fruit bunches processed. This aligns with findings by Hansen et al. [1], who estimated that optimized biogas production from palm oil waste could generate 1.0-1.4 GJ per tonne of FFB.

4.3 Sustainability considerations

Beyond energy recovery, the implementation of bio-augmented anaerobic digestion offers multiple sustainability benefits for the palm oil industry:

1. Greenhouse gas mitigation: Converting palm oil waste to biogas through anaerobic digestion significantly reduces methane emissions that would otherwise occur during conventional waste management practices. Ahmad et al. [2] estimated that uncaptured methane emissions from POME can reach 54 kg CO_2-equivalent per tonne of crude palm oil produced. Bio-augmentation, by enhancing the conversion efficiency and reducing residual degradable material, could further decrease these emissions by 35-45%.
2. Waste volume reduction: The enhanced VS removal achieved with bio-augmentation (52.31% with PSU-2 co-digestion compared to 27.64% in control) represents a significant improvement in waste stabilization and volume reduction. This reduces the environmental footprint of disposal and creates opportunities for beneficial use of the digested residues.
3. Digestate utilization: The nutrient-rich digestate from anaerobic digestion can serve as a valuable biofertilizer. Suksong et al. [3] found that digestate from palm oil waste digestion contained balanced N:P: K ratios suitable for agricultural applications. The enhanced degradation achieved through bio-augmentation likely improves the agronomic quality of this digestate by increasing nutrient availability and reducing phytotoxic compounds.
4. Water conservation: Treated POME from anaerobic digestion can be reused in palm oil processing, reducing freshwater consumption. The improved treatment efficiency with bio-augmentation could facilitate water recycling by producing higher-quality effluent. Zhang et al. [22] reported that enhanced anaerobic treatment of agricultural wastewaters through bio-augmentation reduced COD by an additional 15-20%, making water recycling more feasible.
5. Reduced chemical inputs: The biological enhancement through bio-augmentation provides an alternative to chemical pretreatment methods commonly used to improve the digestion of recalcitrant materials. This reduces the environmental impact associated with chemical manufacturing, transportation, and potential contamination of digestate and effluents [8].

These sustainability benefits align with industry trends toward more environmentally responsible palm oil production. The Roundtable on Sustainable Palm Oil (RSPO) certification increasingly emphasizes waste management and greenhouse gas reduction, making bio-augmented digestion an attractive option for mills seeking certification [1].

4.4 Cost-benefit analysis of bio-augmentation implementation

The economic viability of bio-augmentation depends on balancing added costs with the resulting benefits. Table 7 presents an estimated cost-benefit analysis for a medium-sized palm oil mill processing 60 tonnes of FFB per hour and operating 300 days per year. The implementation costs include capital expenditures for bacterial cultivation equipment, storage facilities, and injection systems, estimated at $200,000-300,000 based on similar bioprocess installations reported by Tabatabaei et al. [5]. Operational costs include culture media, additional monitoring, and skilled labor, estimated at $80,000-120,000 annually. Benefits include increased biogas production valued at $165,000-195,000 annually (assuming natural gas price equivalents of $5-6/GJ), reduced waste management costs of $40,000-60,000, and potential carbon credit revenues of $25,000-35,000 (based on carbon market prices of $15-20/tonne CO_2-equivalent). Additional value from digestate utilization and water recycling could contribute $20,000-40,000 annually. With total annual benefits of $250,000-330,000 against operational costs of $80,000-120,000, the net annual benefit would be approximately $150,000-230,000. This suggests a simple payback period of 1.3-2.0 years for the initial capital investment, making bio-augmentation economically attractive for medium to large palm oil mills. Sensitivity analysis indicates that biogas value is the most critical economic factor, with variations in natural gas prices significantly affecting the payback period. At lower gas prices ($3-4/GJ), the payback period extends to 2.5-3.0 years, while higher prices ($7-8/GJ) could reduce it to under one year. The cost of bacterial culture preparation is the second most significant factor, highlighting the importance of efficient propagation systems to maintain economic viability. These economic projections are consistent with findings by Yang et al. [13], who reported that repeated batch bio-augmentation in industrial-scale digesters achieved payback periods of 1.5-2.5 years, primarily through increased biogas production and improved process stability. Similarly, Martin-Ryals et al. [12] calculated that the additional methane production from bio-augmentation provided a 60-80% return on investment annually after accounting for implementation costs. For smaller operations, the economic case may be less compelling due to higher relative implementation costs and lower absolute benefits. Regional cooperative approaches, where centralized bacterial culture facilities serve multiple smaller digesters, could improve economic viability for smaller mills, as suggested by Ferraro et al. [17] for agricultural biogas plants. In conclusion, the economic and environmental implications of bio-augmentation for palm oil waste digestion are highly favorable, particularly for medium to large operations. The enhanced methane yields translate to significant energy recovery potential, while simultaneously addressing waste management challenges and improving the sustainability profile of palm oil production. With reasonable implementation costs and attractive payback periods, bio-augmentation represents a commercially viable approach to enhancing biogas production from these abundant agricultural residues.

Table 7. Cost-Benefit Analysis of Bio-augmentation Implementation for a Medium-Sized Palm Oil Mill (60 tonnes FFB/hour)

Parameter	Low Estimate	High Estimate	Key Notes
Implementation Costs (Capital):			
Bacterial cultivation equipment	$120,000	$180,000	Includes bioreactors and controls
Storage facilities	$40,000	$60,000	Temp-controlled for bacterial cultures
Injection systems	$40,000	$60,000	Automated dosing integrated with feeders
Total Capital Cost	$200,000	$300,000	One-time investment
Operational Costs (Annual):			
Culture media & nutrients	$35,000	$50,000	Varies by bacterial strain & propagation
Additional monitoring	$15,000	$25,000	For microbial activity assessment
Skilled labor	$30,000	$45,000	Specialized maintenance personnel
Total Annual Operational Costs	$80,000	$120,000	Recurring yearly expense
Benefits (Annual):			
Biogas production	$165,000	$195,000	Based on extra methane output
Waste management savings	$40,000	$60,000	Reduced disposal & treatment costs
Carbon credits	$25,000	$35,000	Revenue from CO_2-equivalent reduction
Digestate value	$15,000	$25,000	Replaces fertilizer costs
Water recycling	$5,000	$15,000	Lower freshwater use & discharge fees
Total Annual Benefits	$250,000	$330,000	Combined gains from all streams
Financial Analysis:			
Net Annual Benefit	$150,000	$230,000	Benefits minus operational costs
Payback Period (years)	2	1.3	Capital divided by net annual benefit
ROI (%)	50	77	Net annual benefit divided by capital costs
NPV (10 years, 10% discount)	$922,000	$1,415,000	Discounted cash flow over 10 years

5. Conclusions and Future Perspectives

Bioaugmentation enhances the biodegradability and hydrolysis of lignocellulosic components, thereby improving biogas production from palm oil industrial waste. The optimal bio-augmentation strategy identified was PSU-2 at an I:M ratio of 75:5 for co-digestion of EFB with POME, which achieved a methane yield of 178.42 mL-CH_4/gVS—107.6% higher than the non-augmented control. This strategy also demonstrated superior performance across multiple metrics, including VS removal (52.31%), biodegradability (93.59%), and process kinetics (hydrolysis constant 0.0232 d^{-1}, maximum production rate 15.38 mL-CH_4/gVS/day). This research identifies several process recommendations for industrial applications. First, maintaining the optimal I:M ratio is critical, as excessive bacterial addition did not correlate with improved performance and increased operational costs. Second, co-digestion consistently outperformed single digestion, highlighting the importance of balanced substrate composition. Third, the shorter lag phase and improved stability in bio-augmented systems suggest that this approach could enable higher loading rates and shorter hydraulic retention times in continuous operations, potentially increasing throughput and reducing reactor volume requirements. Future research should focus on several key areas to further optimize bio-augmentation for palm oil waste digestion. Continuous or semi-continuous feeding strategies better simulate industrial settings and may yield different optimal parameters than batch systems.- Development of efficient bacterial culture propagation methods using low-cost, locally available media would improve economic viability. Exploration of mixed bacterial consortia with complementary enzymatic capabilities could further enhance performance beyond what was achieved with single strains. Finally, genomic and

metabolomic approaches to elucidate the specific mechanisms of microbial synergy would enable more targeted bioaugmentation strategies tailored to substrate characteristics. The economic and environmental analysis shows that bio-augmentation can improve biogas production from palm oil industry wastes, resulting in energy recovery, waste reduction, and greenhouse gas mitigation with attractive economic returns for industrial implementation.

6. Acknowledgements

We also thanks Faculty of Science and Digital Innovation, Thaksin University, Phatthalung campus, for their expert labratory and support throughout this research.

Author Contributions: Conceptualization, experimental design, S.S., W.T., P.K., S.I.; carrying out experiment and data acquisition, S.S., W.T., P.K., S.I.; writing and editing, S.S., N.P..

Conflicts of Interest: The authors declare no conflict of interest.

References

[1] Hansen, S. B.; Padfield, R.; Syayuti, K.; Evers, S.; Zakariah, Z.; Mastura, S. Trends in Global Palm Oil Sustainability Research. *J. Clean. Prod.* **2022**, *100*, 99–114. https://doi.org/10.1016/j.jclepro.2015.03.051

[2] Ahmad, S.; Kadir, M. Z. A. A.; Shafie, S. Current Perspective of the Renewable Energy Development in Malaysia. *Renew. Sustain. Energy Rev.* **2020**, *115*, 109356.

[3] Suksong, W.; Kongjan, P.; Prasertsan, P.; Imai, T.; O-Thong, S. Optimization and Microbial Community Analysis for Production of Biogas from Solid Waste Residues of Palm Oil Mill Industry by Solid-State Anaerobic Digestion. *Bioresour. Technol.* **2016**, *214*, 166–174. https://doi.org/10.1016/j.biortech.2016.04.077

[4] Saelor, S.; Kongjan, P.; O-Thong, S. Biogas Production from Anaerobic Co-Digestion of Palm Oil Mill Effluent and Empty Fruit Bunches. *Energy Procedia* **2017**, *138*, 717–722. https://doi.org/10.1016/j.egypro.2017.10.206

[5] Tabatabaei, M.; Aghbashlo, M.; Valijanian, E.; Kazemi Shariat Panahi, H.; Nizami, A. S.; Ghanavati, H.; Sulaiman, A.; Mirmohamadsadeghi, S.; Karimi, K. A Comprehensive Review on Recent Biological Innovations to Improve Biogas Production, Part 2: Mainstream and Downstream Strategies. *Renew. Energy* **2020**, *146*, 1392–1407. https://doi.org/10.1016/j.renene.2019.07.047

[6] Tsapekos, P.; Kougias, P. G.; Vasileiou, S. A.; Treu, L.; Campanaro, S.; Lyberatos, G.; Angelidaki, I. Bioaugmentation with Hydrolytic Microbes to Improve the Anaerobic Biodegradability of Lignocellulosic Agricultural Residues. *Bioresour. Technol.* **2017**, *234*, 350–359. https://doi.org/10.1016/j.biortech.2017.03.043

[7] Chaikitkaew, S.; Kongjan, P.; O-Thong, S. Biogas Production from Biomass Residues of Palm Oil Mill by Solid-State Anaerobic Digestion. *Energy Procedia* **2015**, *79*, 838–844. https://doi.org/10.1016/j.egypro.2015.11.575

[8] Nzila, A. Mini Review: Update on Bioaugmentation in Anaerobic Processes for Biogas Production. *Anaerobe* **2017**, *46*, 3–12. https://doi.org/10.1016/j.anaerobe.2016.11.007

[9] Ozbayram, E. G.; Kleinsteuber, S.; Nikolausz, M.; Ince, B.; Ince, O. Effect of Bioaugmentation by Cellulolytic Bacteria Enriched from Sheep Rumen on Methane Production from Wheat Straw. *Anaerobe* **2017**, *46*, 122–130. https://doi.org/10.1016/j.anaerobe.2017.03.013

[10] Peng, X.; Börner, R. A.; Nges, I. A.; Liu, J. Impact of Bioaugmentation on Biochemical Methane Potential for Wheat Straw with Addition of *Clostridium cellulolyticum*. *Bioresour. Technol.* **2014**, *152*, 567–571. https://doi.org/10.1016/j.biortech.2013.11.067

[11] Strang, O.; Ács, N.; Wirth, R.; Maróti, G.; Bagi, Z.; Rákhely, G.; Kovács, K. L. Bioaugmentation of the Thermophilic Anaerobic Biodegradation of Cellulose and Corn Stover. *Anaerobe* **2017**, *46*, 104–113. https://doi.org/10.1016/j.anaerobe.2017.05.014

[12] Martin-Ryals, A.; Schideman, L.; Li, P.; Wilkinson, H.; Wagner, R. Improving Anaerobic Digestion of a Cellulosic Waste via Routine Bioaugmentation with Cellulolytic Microorganisms. *Bioresour. Technol.* **2015**, *189*, 62–70. https://doi.org/10.1016/j.biortech.2015.03.069

[13] Yang, Z.; Guo, R.; Xu, X.; Wang, L.; Dai, M. Enhanced Methane Production via Repeated Batch Bioaugmentation Pattern of Enriched Microbial Consortia. *Bioresour. Technol.* **2016**, *216*, 471–477. https://doi.org/10.1016/j.biortech.2016.05.062

[14] APHA. *Standard Methods for the Examination of Water and Wastewater*, 23rd ed.; American Public Health Association; American Water Works Association; Water Environment Federation: Washington, DC, **2017**.

[15] Sluiter, A.; Hames, B.; Ruiz, R.; Scarlata, C.; Sluiter, J.; Templeton, D.; Crocker, D. *Determination of Structural Carbohydrates and Lignin in Biomass; Laboratory Analytical Procedure (LAP)*; National Renewable Energy Laboratory: Golden, CO, 2012.

[16] Jiang, Y.; Lu, J.; Lv, Y.; Wu, R.; Dong, W.; Zhou, J.; Jiang, M.; Xin, F. Efficient Hydrogen Production from Lignocellulosic Feedstocks by a Newly Isolated Thermophilic *Thermoanaerobacterium* sp. Strain F6. *Int. J. Hydrogen Energy* **2019**, *44*, 14380–14386. https://doi.org/10.1016/j.ijhydene.2019.01.226

[17] Ferraro, A.; Dottorini, G.; Massini, G.; Mazzurco Miritana, V.; Signorini, A.; Lembo, G.; Fabbricino, M. Combined Bioaugmentation with Anaerobic Ruminal Fungi and Fermentative Bacteria to Enhance Biogas Production from Wheat Straw and Mushroom Spent Straw. *Bioresour. Technol.* **2018**, *260*, 364–373. https://doi.org/10.1016/j.biortech.2018.03.128

[18] Angelidaki, I.; Alves, M.; Bolzonella, D.; Borzacconi, L.; Campos, J. L.; Guwy, A. J.; Kalyuzhnyi, S.; Jenicek, P.; van Lier, J. B. Defining the Biomethane Potential (BMP) of Solid Organic Wastes and Energy Crops: A Proposed Protocol for Batch Assays. *Water Sci. Technol.* **2009**, *59*, 927–934. https://doi.org /10.2166/wst.2009.040

[19] Trzcinski, A. P.; Stuckey, D. C. Determination of the Hydrolysis Constant in the Biochemical Methane Potential Test of Municipal Solid Waste. *Environ. Eng. Sci.* **2012**, *29*, 848–854. https://doi.org/ 10.1089/ees.2011.0105

[20] Morris, D. L. Quantitative Determination of Carbohydrates with Dreywood's Anthrone Reagent. *Science* **1948**, *107*, 254–255. https://doi.org/10.1126/science.107.2775.254

[21] Li, Y.; Li, L.; Sun, Y.; Yuan, Z. Bioaugmentation Strategy for Enhancing Anaerobic Digestion of High C/N Ratio Feedstock with Methanogenic Enrichment Culture. *Bioresour. Technol.* **2018**, *261*, 188–195. https://doi.org/10.1016/j.biortech.2018.02.069

[22] Zhang, J.; Guo, R. B.; Qiu, Y. L.; Qiao, J. T.; Yuan, X. Z.; Shi, X. S.; Wang, C. S. Bioaugmentation with an Acetate-Type Fermentation Bacterium *Acetobacteroides hydrogenigenes* Improves Methane Production from Corn Straw. *Bioresour. Technol.* **2015**, *179*, 306–313. https://doi.org/10.1016/j.biortech.2014.12.022

[23] Nkemka, V. N.; Gilroyed, B.; Yanke, J.; Gruninger, R.; Vedres, D.; McAllister, T.; Hao, X. Bioaugmentation with an Anaerobic Fungus in a Two-Stage Process for Biohydrogen and Biogas Production Using Corn Silage and Cattail. *Bioresour. Technol.* **2015**, *185*, 79–88. https://doi.org /10.1016/j.biortech.2015.02.100

[24] Neumann, L.; Scherer, P. Impact of Bioaugmentation by Compost on the Performance and Ecology of an Anaerobic Digester Fed with Energy Crops. *Bioresour. Technol.* **2011**, *102*, 2931–2935. https://doi.org/ 10.1016/j.biortech.2010.11.068

ASEAN
Journal of Scientific and Technological Reports
Online ISSN:2773-8752

Academic article

Utilization of Information and Communication Technology (ICT) Tools Among Masbate Rice Seed Growers

Mohammad D. Dollison[1*], Eddie B. Basulgan[1], Nimfa R. Cornal[1], and Beverly B. Dollison[2]

[1] College of Agriculture, Dr. Emilio B. Espinosa, Sr. Memorial State College of Agriculture and Technology, Masbate, Philippines, 5411
[2] Masbaranon Elementary School, Masbaranon, Masbate, Philippines, 5407
* Corresponding email: mddollison@debesmscat.edu.ph

Citation:
Dollison, M.; Basulgan E.; Cornal N.; Dollison B. Utilization of information and communication technology (ICT) tools among masbate rice seed growers. *ASEAN J. Sci. Tech. Report.* **2026**, *29*(1), e257993. https://doi.org/10.55164/ajstr.v29i1.257993.

Article history:
Received: February 20, 2025
Revised: October 3, 2025
Accepted: October 18, 2025
Available online: December 14, 2025

Publisher's Note:
This article is published and distributed under the terms of the Thaksin University.

Abstract: This study aimed to determine the awareness, adoption, and utilization of the active rice seed growers of the different ICT-based resources on rice production, their competence and technological capacities to access the different resources, and the recommended practices available for adoption, particularly along: improved agricultural management practices; early warning system and weather updates; and agricultural mechanization. A total of 36 active rice seed growers participated in a series of focus group discussions. Findings revealed that seed growers have a very low level of awareness, competence, and technological capacity in the presence of various ICT-based resources. Some seed growers do not have internet connections due to high connection costs with lower internet speeds. Accordingly, a huge number of rice seed growers were non-adopters, there were very few who adopted the ICT-based resources, particularly in terms of agricultural management practices and experienced the benefits of accessing the resources such as getting prompt answers to pest and disease problems, fertilizer recommendation, characteristics of rice seed varieties and rice seeds that are adaptable in their areas, new technologies in rice farming. They suggested producing IEC materials for seed growers on ICT-based resources on rice and promote technology adoption to farmers to address the lack of awareness; enhancement of internet signal speed by regulating the internet service providers to address the problem; inclusion topic on ICT usage during training/retooling of rice seed growers to address the problem on lack of technical know-how on ICT; provision of tablet to rice seed growers and provision of free internet Wi-Fi for all farmers as solutions to the problems on lack of computer and internet connection at home.

Keywords: ICT-based; seed growers; utilization; competence; rice

1. Introduction

Rice is the calorie source for half of the global population and the staple food for the world's poorest and undernourished people in Asia and Africa. Yield and total production have plateaued for many years in some major rice-producing countries, while the demand is ever-increasing. [1]. In the Philippines, rice remains the primary choice for staple food, locally known as "Palay" (un-milled rice), "Bigas" (milled rice), and "Kanin" (cooked rice). The country's production performance recorded 4.81 million hectares of area harvested for rice and a total production of 19.96 million metric tons, with a value of Php 403.89 billion. However, even with this level of rice production in the Philippines, rice is still the country's 3rd most imported agricultural item [2]. Rice production is constrained by low yield and quality, high postharvest losses, and high water requirements in an increasingly resource-scarce country due to the growing population and water demand, and increasing threat of climate change [3]. Global agricultural production encountered various challenges in

attaining the demand for basic needs of the increasing human population [4]. It is expected to address global challenges by increasing the farmers' competitiveness in enhancing crop yield and reducing crop losses through smart decision-making. [5]. Digital farming technologies range from 'low-tech' tools such as mobile phones and computers to more 'high-tech' solutions such as blockchain, the Internet of Things (IoT), and artificial intelligence that can help smallholder farmers increase their yields and incomes if they are effectively targeted to facilitate agriculture as a 'pathway out of poverty [6].

Information and Communication Technology has advanced more rapidly than any innovation throughout history [7]. In agriculture, the development of digital farming technologies has significantly improved the potential to transform agricultural production and reduce the environmental impact of the green revolution [8]. Digital agricultural technologies are revolutionizing modern farming by leveraging cutting-edge digital tools like data analytics and wireless connectivity, which are being used in agriculture more and more in a variety of ways to improve farm decision-making and practice [9]. The "MASAGANA Rice Industry Development Program 2023-2028" recognizes digital transformation as a key strategy to achieve a stable rice supply, high farm productivity, and increased income for rice farmers by embracing precision farming enabled by drones, remote sensing and IoT devices, and data-driven decision-making through farm management systems, weather forecasts, and access to market information, farming communities can enhance productivity, resource management, and sustainability [10].

At present, the Philippine government, through the initiative of DA-PhilRice, started accelerating its investment in ICT in the early 2000s with the nationwide implementation of the Open Academy for Philippine Agriculture that complemented and supplemented face-to-face rice extension services to reach farmers in "unreachable" areas with more timely information [11]. Agricultural digitalization is an information-driven farming approach that taps digital technology to improve farm productivity while lowering the costs of farming inputs [12]. Similarly, the International Rice Research Institute has created and distributed desktop and mobile programs like Rice Crop Manager, which advises farmers on how to manage crop fertilizer applications in order to boost rice yield [13]. However, according to the Philippine Rice Research Institute [14], the Rice-Based Farm Households Survey notes that while farmers' access to ICT tools is 93%, the percentage of those who use digital tools in their rice cultivation is only 31%.

One of the major goals of the Department of Agriculture is to have a continuous and reliable supply of high-quality inbred rice seeds for positive long-term impacts on seed security and farm productivity, and these directly contribute to attaining rice sufficiency in the country. Seed growers play a vital role in achieving this goal of distributing and producing high-quality inbred rice seeds [15] to meet the seed requirements of the rice farmers. The inbred rice seed growers undergo special training in rice seed production from seed selection, land preparation, and other farm production technologies to ensure quality seeds for the farmers. Likewise, seed growers need greater access to virtually unlimited information offered by agricultural institutions to acquire up-to-date information and new technologies in farming to become more competitive [16]. Despite technological advancement in rice production using digital tools, farmers' adoption and utilization levels remain low, especially in developing countries like the Philippines [17]. This study determined the rice seed growers' awareness of the presence of digital technology-based resources on rice, how they assessed their competence and technological capacity on the use of ICT, and what recommended practices available in ICT they had adopted. The problems that hindered adoption and the possible solutions, as suggested by the seed growers, were also taken into account.

2. Methodology

Research Design

The study used the descriptive-evaluative type of research. This discusses the adoption of ICT-based resources on rice by the seed growers, employing simple statistical computations like percentages, averaging, and ranking to analyze data gathered from a series of focus group discussions (FGD) and key informant interviews. Secondary data were also gathered from published and unpublished documents related to the use of digital tools.

Respondents of the Study

The study's respondents were selected using purposive sampling from the total population of 36 accredited and active rice seed growers in the three congressional districts of the province of Masbate. A total of 36 accredited and active rice seed growers from the three congressional districts of the province of Masbate were selected to participate in the series of focus group discussions. Rice seed growers were chosen as the respondents in this study because they produce quality palay seeds that pass seed certification to maintain the genetic identity and purity of superior rice crop varieties, which are critical in rice sufficiency.

Table 1. Distribution of population and respondents of the study.

District	Active Seed Growers (N=36)	Seed Grower-Respondent (N=36)
First District	5	5
Second District	22	22
Third District	9	9
Total	**36**	**36**

** Source: Masbate Provincial Agriculture Office, Masbate City.*

Data Collection

This study employed a series of Focused Group Discussions (FGD) as the method to extract data and information. FGD is a form of qualitative research in which a group of people is asked about their perceptions, opinions, beliefs, and attitudes toward a concept. Questions are asked in an interactive group setting where participants can talk with other group members. It provides an opportunity for all respondents to participate and to give their opinion/s.

Before the FGD was conducted, the researcher administered a pre-test to 10 rice seed growers to validate the effectiveness and clarity of the guide questions that would be posed to the respondents. The researcher facilitated the conduct of the FGDs and, at the same time, took notes during the discussion. The FGD checklists consisted of:

1. Rice seed growers' awareness of Digital tools for rice production
2. Technological capacity of rice seed growers to access Digital tools
3. Recommended practices available in the Digital tools adopted by the rice seed growers in terms of:
   a. Improved agricultural management practices
      - Pests and diseases
      - Fertilizer recommendation
      - Rice varieties are adaptable to their area
   b. Market and credit access
   c. Early warning system and weather update
   d. Agricultural mechanization, and
   e. And other agricultural services
4. Problems encountered with the use of Digital tools and possible solutions.

During the FGDs, the researcher briefly discussed the features of the Digital tools on rice. The researcher also distributed flyers on digital tools containing instructions on how to access most of the 14 websites. All the FGDs were recorded for reference purposes, and significant answers were quoted from the seed growers.

The researcher also conducted an in-depth interview with the rice seed growers who could not join the FGDs using the Nominal Group Technique (NGT), a variation in FGD introduced by Stewart and Shamdasani (1990). The same questions that were asked during the FGDs were also asked during the NGT. The researcher also related to the interviewees some answers that the other rice seed growers mentioned during the FGDs, so that the interviewees had the chance to react to them.

Research Instrument

The research instrument used in this study was primarily the FGD. It was complemented by the Nominal Group Technique, a variation of the FGD, which was used to conduct the one-on-one interview with the rice seed growers who could not attend the FGD. This technique also used the same guide questions that were used in the FGD.

Data Analysis

The data gathered from the series of FGD were analyzed and synthesized to determine rice seed growers' adoption of ICT-based farming tools, specifically their awareness of the presence of Digital tools, their competence and technological capacity, problems encountered, and recommended solutions. Simple statistical computations were applied using percentages, averaging, frequency count, and ranking.

3. Results and Discussion

Rice Seed Growers Awareness of ICT-based Resources on Rice Production

Table 2 presents the different responses to the awareness of the rice seed growers of the various digital tools in rice production. The results showed that 38% of Masbate rice seed growers were aware of the availability of ICT-based resources for rice production. Among these resources, the most familiar was the Binhing Palay App developed by the Philippine Rice Research Institute (38%), followed by the Leaf Color Computing App (36%), ATI Farmers' Contact Center (33%), Farm Machineries (30%), and E-Extension by ATI (30%).

The Binhing Palay App and the Leaf Color Computing App were the most popular resources being used among the rice seed growers since most of them had joined an expository tour to PhilRice, where they were briefed on the ICT-based resources of the institution. Similarly, most of the seed growers of Masbate have heard about the farming resources during their training and accreditation with the BPI-NSQCS and their annual retooling training conducted by the NSQCS. Other ICT-based resources were also introduced by their respective extension workers in their respective areas, and a few discovered the website by themselves by searching a keyword on rice on the internet. Likewise, the ICT-based resources like the Weather-rice-nutrient integrated decision support system (WeRise) of IRRI, the Philippine Rice Information System (PRiSM) of IRRI, FertRight, and the EDamuhan App obtained a lower awareness rank among the enumerated resources. According to seed growers, their lower awareness of some ICT-based resources in rice production was due to their limited time to access the Internet, not being introduced during the training, and focusing only on the technology introduced by the extension works. These findings call for a more intensive campaign to promote the adoption and awareness of ICT-based resources. The lower percentage of awareness on the use of ICT-based resources by rice seed growers requires a more aggressive and comprehensive campaign on the utilization of ICT-based resources in rice production as Thi Hoa Sen, et al [18] argued that intensification of extension methods on the utilization of digital tools in agricultural production must be increased to boost the rate of adoption practices among local farmers. In addition, the early warning information by seed growers, especially on weather disturbances, was from the PAGASA website and was adopted by 27 % of the seed growers. All of them said radio and television were the primary sources of early warning for them, particularly on occurrences of typhoons and other natural calamities. The findings supported by the study of Pham et al [19] that Early warning systems are essential in mitigating losses, and community-based early warning systems aim to empower at-risk communities for better preparedness and responses. In this study, Masbate rice seed growers will likely adopt the different practices presented in the ICT-based technology if they think that these new tools or practices are far better than their current practices, or they are more compatible with their present norms, and the directions are easily understood, or they are easy to use so that they could try them in their respective farms.

Technological Capacity and Competence of the Rice Seed Growers to Access the Digital Tools in Rice Production

Competence means the ability of rice seed growers to apply the basic knowledge in computer operations and in navigating the internet, while technological capacity means the rice seed growers' capacity to afford or acquire ICT-based resources such as computers, tablets, and mobile phones, and their ability to access internet connectivity.

The results of the study showed that 55.55% of the rice seed growers of Masbate were competent, and 63.88% were technologically capacitated, which only means they have personal computers and access to internet connectivity. Table 3 presents the competence and technological capacity of rice seed growers of Masbate. Accordingly, only 38.88% have adopted some of the recommended practices in crop production. This is shown in Table 4. The low percentage of adoption is attributed to the lack of awareness of ICT-based resources among rice seed growers. Another major problem was the weak signal strength and slow internet service in their respective location that hindered their capacity to visit and gain more information about rice crop production [20].

Table 2. Responses on the awareness of digital tools on rice among rice seed growers of Masbate Province (%).

Digital Technologies on Rice	Number of Seed Growers Who Are Aware of The Digital Technologies	
	Total (n=36)	%
Binhing Palay App of PhilRice	14	38
PhilRice Text Center (call or text 09209111398)	12	33
Leaf Color Computing App of PhilRice	13	36
Minus One Element Technique Kit (MOET) of Philrice	9	25
Weed Identification Tool (E-damuhan) Philrice	5	13
Rice Doctor (http://ricedoctor.irri.org)	6	16
Rice Crop Manager (http://webapps.irri.org/ph/rcm)	4	11
Weather-rice-nutrient integrated decision support system (WeRise) of IRRI	2	5
Philippine Rice Information System (PRiSM) of IRRI	5	13
Rice Knowledge Bank (http://www.knowledgebank. irri.org)	5	13
Smarter Pest Identification Technology (SPidTEch) of DOST Project SARAi	5	13
Farm Machineries (www.philmech.gov.ph)	11	30
E-Extension (http://e-extension.gov.ph)	11	30
ATI Farmers' Contact Center	2	5
PAGASA website	10	27
FertRight (www.bswm.da.gov.ph)	3	8
eDamuhan App (www.philrice.gov.ph)	4	11

Table 3. The number of rice seed growers who have competence and technological capacity in the use of digital tools in rice seed production

District	Number of Seed Growers (n = 36)			
	Number of Rice Seed Growers	Perceived Technological Capacity		Number of Seed Growers with the Competence to Access
		With Computer/Android/Mac Cellular Phones	With Internet Connectivity	
First District	5	2	3	2
Second District	22	12	11	12
Third District	9	4	5	6
Total	**36**	**18**	**19**	**20**
Percent		**50%**	**52%**	**55%**

The third major problem was the lack of competence of 44% of the rice seed growers. Some who have computers and internet connections at home said their computer was used mainly by their children in the preparation of homework and projects in school because they don't know how to use it. This finding implies that competence in the use of computers is crucial in the access and subsequent adoption of ICT-based

resources. ICT-based materials and the subsequent implementation of recommended practices are not always guaranteed by the possession of ICT devices and an internet connection. Rice seed growers are encouraged to undergo capability training on digital literacy, affirming the World Bank [21] assertion that the use of ICT-based tools in the farming areas can be encouraged by providing a more reliable ICT infrastructure and training to the farmers. Investing in ICT-based resources in agricultural production and giving training to help farmers gain access to ICT resources in agriculture were likewise recommended by Montesclaros and Teng [22]. According to them, digital farming tools are important in adapting the agriculture sector to climate change and rising demand for it to serve as a key sector for food security, income, trade, and employment. This study also found that learning the use of a computer and the internet can be more effective for rice seed growers if it is done as a group activity, thus validating the old Social Learning Theory of Bandura [23], stating that learning is a cognitive process that takes place in a social context.

Recommended Practices Available in the Digital Tools that the Rice Seed Growers Adopted

The rice seed producers were questioned regarding the many methods they have implemented on their individual rice farms as a result of using the various ICT-based tools for rice production. Among the practices were as follows: extension services; use of improved agricultural practices, which include pest and disease management; fertilizer management recommendations and rice varieties adoptable in their area; use of market and credit access; use of early warning devices; and agricultural mechanization. Extension service was also excluded in the discussion and analysis, as the seed growers said they have not availed of any extension service from the ICT-based resources. Some seed growers said they don't need the help of ICT in extension as the agricultural technicians in their area always visit their farms. On the other hand, other seed growers said they felt they were excluded from the programs of the Department of Agriculture as they were considered private entrepreneurs, not farmers. Improved agricultural management practices**.** Only 38.88% of the respondents adopted the improved agricultural practices recommended on the website. Agricultural management practices were defined in this study as management principles that are used from crop production up to the marketing of agricultural products or farm practices employed from land preparation to postharvest handling activities and marketing of agricultural produce. Table 4 shows the number of rice growers who have adopted the recommended practices.

Other rice seed growers who have been to PhilRice said that they were impressed by the technology that uses the Global Positioning System (GPS) in analyzing the soil properties. GPS output is location-specific, particularly nutrient management recommendations. Furthermore, they said that it is more sophisticated and that they wished to implement it on their farms since they are no longer required to submit soil samples; nevertheless, they claim that they lack the necessary technical know-how and internet access. In addition, twenty-two percent of the seed growers also tried submitting their problem, particularly on discoloration of leaves, to the Rice Doctor and said they received a reply immediately. Similarly, twenty-seven percent of rice seed growers said they opened the websites of the Philippine Rice Institute (PhilRice) and International Rice Research Institute (IRRI) to look for characteristics of rice seed varieties, seeds adaptable in their areas, new technologies in rice farming, and updates on the programs in agriculture, such as seed subsidies, freebies, and grants. Likewise, sixteen percent of the rice seed growers who have accessed the Rice Crop Manager said it is an excellent tool for farmers. They only input all the needed data regarding their rice farm, and a fertilizer recommendation was immediately sent to their email addresses.

Table 4. Number of rice seed growers- adopters of the recommended practices on the use of digital tools in rice seed production

Recommended Practices	Number of Adopters (n= 36)	Percent
Utilization of improved agricultural practices (Land preparation to Postharvest)	14	38.88
- pest and disease management	8	22.22
- fertilizer recommendation	6	16.66
- varietal suitability in the area	10	27.77
Use of market/credit access	3	8.33
Use of agricultural Mechanization	7	19.44
Early Warning	12	33.33

Similarly, 4% of the rice seed growers who responded to market and credit access recalled that they had merely uploaded their firm name and the number of rice types they had in stock to promote their goods and draw in customers, but that no one had replied. This could be attributed to the lack of awareness of the ICT-based resources among their fellow seed growers. Rice seed growers revealed that Early warning systems and weather updates, especially on impending weather disturbances from the PAGASA website, were adopted by 33% of the seed growers. All of them said the primary source of early warning for them, particularly on occurrences of typhoons and other natural calamities, was radio and television. In this area, the results showed that TV and broadcast media are still the most effective and most powerful mediums in information dissemination. Accordingly, nineteen percent of rice seed growers adopted the recommended machinery and equipment posted on the PhilMech website to improve their production practices. The findings of the study were supported by the study of Hidayat and Mahardiko [24] that the use of ICT tools in farming helps rice farmers identify different insect pests and diseases and provides better control practices than their old pest control methods. In general, the rice seed growers' adoption of agricultural practices in the ICT-based resources was very low due to some constraints, such as lack of knowledge on ICT usage and lack of knowledge on ICT-based resources, lack of computers, absence of internet connectivity because they perceived it as very costly or have very weak signal strength, particularly in the rural areas in the three districts of Masbate Province. At the same time, a huge problem faced by the rice seed growers in all three districts was the very weak internet signal, coupled with the exorbitant rates of internet subscriptions.

Possible Solutions to the Problems that Hinder the Adoption of ICT-based Resources

Eighty-three percent of the Masbate rice seed growers identified poor internet connectivity as their foremost problem in accessing ICT-based resources for their rice seed production activity. In addition, the rice seed growers also complained that the internet services in their areas, regardless of the service provider, were very weak and yet very expensive. According to them, regulating the internet providers will also enhance the internet speed, strength, and area covered by their network, thereby increasing its utilization. Another problem pinpointed by seventy-seven percent of the seed growers was the lack of awareness of the ICT-based resources in rice. The lack of awareness of some seed growers was attributed to insufficient information dissemination on ICT-based resources. The seed growers also complained that they are not included in the program briefing for farmers as "*DA only caters to marginal and subsistent farmers and regards the seed growers as entrepreneurs*." Among the solutions suggested by the rice seed growers was to increase their awareness on ICT-based resources through the production and distribution of IEC materials on ICT-based resources on rice particularly emphasizing the practices available on the websites, how to access the sites and the benefits of adopting the practices such as prevention of pests and diseases, reduction in postharvest losses, reduction in input cost and increase in yield. These IEC materials may be distributed to farmers during special events such as Farmers' Fora, Climate Farmers Field School training and graduations, and other events. Other strategies suggested to increase awareness were video showing and promotion of ICT-based resources through the use of quad media, which will inform a great number of farmers on "what" is available on the government websites. Another problem that hindered adoption was the lack of time and interest in ICT-based resources,

which was reported by 72 % of the rice seed growers. They suggested the incorporation of one-day training on ICT–based resources on rice in the retooling program of the DA-NSQCS. Agricultural extension workers should also help the rice seed growers navigate among the available ICT-based resources on rice and interpret the various messages from the ICT. Accordingly, it has been observed during the conduct of FGD that the respondents were 50-86 years old, thus they were not more interested in ICT or had not learned the technology. Those above the age of 60 don't have computers at home, or if they have, they are for their children. Some sexagenarians who have computers and internet connections at home said they can't learn using them despite many tries. They said they hardly see the computer screen due to cataracts. They just leave the computers to their children or grandchildren. When asked if they were using the internet, some said, *"No, I do not use the internet because I am too old for that."* Or *"I don't have time to waste browsing the internet."*

Table 5. Solutions to problems in the adoption of the use of digital tools in rice seed production

Number of Seed Growers (n = 36)			
Problems Encountered	**Percent**	**Rank**	**Recommended Solutions**
Poor internet connections (Very slow yet very expensive)	83	1	Enhancement of signal strength and internet speed by regulating internet service providers
Lack of knowledge of ICT-based resources	77	2	Production and distribution of IEC materials on Digital tools on rice; promotion of ICT in farmers' training on Digital tools on rice
Lack of time and interest in ICT-based tools in rice farming	72	3	Increase awareness of the benefits of Digital tools to create and sustain interest in ICT.
Difficulty on how to operate the digital tools	66	4	Inclusion of the topic on ICT usage during training/retooling of seed growers
Lack of internet connection at home	55	5	Provision of free Wi-Fi internet access for all farmers under the DOST-ICTO project
Old age	52	6	Inclusion of their children in the training retooling of rice seed growers and in the orientation of DA programs
Lack of a Personal Computer	47	7	Provision of tablets to seed growers

4. Recommendations

The rice seed growers were convinced of the potential of ICT-based resources in improving their agricultural productivity, and they were also very willing to enhance their access to these various ICT-based resources; thus, they recommended the following solutions. To promote awareness of the ICT-based resources among rice seed growers, there should be a massive information campaign on the different ICT-based resources on rice using IEC materials, video presentations, radio and TV interviews, and guest appearances. The IEC materials to be produced should emphasize the new technologies available in the ICT-based resources on rice, how to access the sites, and the outcome if the technologies are adopted, such as prevention of pests and diseases, reduction in postharvest losses, reduction in input cost, and increase in yield. These IEC materials will be distributed to the Municipal Agriculture Offices in the region, and also to seed growers and rice farmers during trainings and special gatherings. To improve the competence of the rice seed growers in using ICT, there must be an inclusion of capacity building as one of the topics in the five-day training on accreditation and seed testing of newly accredited rice seed growers and the three-day retooling of accredited seed growers. A successor/child of the elderly seed growers should also be included in the training. This strategy would not only encourage more youth to engage in agriculture but would also encourage new breeds of rice seed growers. The Agricultural Extension Workers may be included in the ICT-based resources on rice

so that they can promote them during their interaction with the farmers. To enhance the rice seed growers' technological capacity, this study recommends the regulation of internet service providers to significantly enhance internet signal strength and speed. The government must encourage competition among internet service providers to lower internet costs and improve internet services to be on par with other countries' internet services. Another recommendation to enhance technological capacity was the provision of tablets to rice seed growers, and the implementation of the DOST-ICTO project aimed to provide free Wi-Fi internet to all farmers. The lack of awareness of the ICT-based resources among rice seed growers should be addressed first by massive information dissemination, followed by improving access by capacity building and ICT infrastructure development to bridge the gap hindering the adoption of ICT-based resources. To sustain the interest of the rice seed growers and encourage the adoption of the ICT-recommended practices, ICT should be promoted as a general solution for life on the farm rather than as just an exclusive solution for specific farm problems.

5. Acknowledgments

Author Contributions: M.D.D.:Introduction, methodology, and discussions. E.B.B.; discussion, data gathering. N.R.C.; data gathering, methodology, B.B.D.; proofreading. All authors have read and agreed to the published version of the manuscript.

Funding: This research received no external funding.

Conflicts of Interest: The authors declare no conflict of interest.

References

[1] M. Rubaiyath Bin Rahman, A. N.; Zhang, J. Trends in Rice Research: 2030 and Beyond. *Food Energy Secur.* **2023**, *12*(2), e390. https://doi.org/10.1002/fes3.390

[2] PCAARRD. *Rice – Industry Strategic Science and Technology Plans (ISPs) Platform*, 2020. https://ispweb.pcaarrd.dost.gov.ph/ispcommodities/rice/.

[3] White, M.; Heros, E.; Graterol, E.; Chirinda, N.; Pittelkow, C. M. Balancing Economic and Environmental Performance for Small-Scale Rice Farmers in Peru. *Front. Sustain. Food Syst.* **2020**, *4*, 564418. https://doi.org/10.3389/fsufs.2020.564418

[4] Shang, L.; Heckelei, T.; Gerullis, M. K.; Börner, J.; Rasch, S. Adoption and Diffusion of Digital Farming Technologies—Integrating Farm-Level Evidence and System Interaction. *Agric. Syst.* **2021**, *190*, 103074. https://doi.org/10.1016/j.agsy.2021.103074

[5] Kashina, E.; Yanovskaya, G.; Fedotkina, E.; Tesalovsky, A.; Vetrova, E.; Shaimerdenova, A.; Aitkazina, M. Impact of Digital Farming on Sustainable Development and Planning in Agriculture and Increasing the Competitiveness of the Agricultural Business. *Int. J. Sustain. Dev. Plan.* **2022**, *17*(8). https://doi.org/10.18280/ijsdp.170808

[6] Florey, C.; Hellin, J.; Balié, J. Digital Agriculture and Pathways out of Poverty: The Need for Appropriate Design, Targeting, and Scaling. *Enterprise Dev. Microfinance* **2020**, *31*(2), 126–140. https://doi.org/10.3362/1755-1986.20-00007

[7] Agricultural Training Institute Central Luzon. *DAC4RCEF Shifting Agriculture into Digitalization*, October 22, 2023. https://ati2.da.gov.ph/ati-3/content/features/dac4rcef-shifting-agriculture-digitalization.

[8] Cambra Baseca, C.; Sendra, S.; Lloret, J.; Tomas, J. A Smart Decision System for Digital Farming. *Agronomy* **2019**, *9*(5), 216. https://doi.org/10.3390/agronomy9050216

[9] Clapp, J.; Ruder, S. Precision Technologies for Agriculture: Digital Farming, Gene-Edited Crops, and the Politics of Sustainability. *Global Environ. Polit.* **2020**, *20*(3), 49–69. https://doi.org/10.1162/glep_a_00566

[10] Department of Agriculture. *Assessment of Digital Tools for Data-Driven Decision Making on Rice-Based Agri-Food Systems in the Philippines (D4AgPH)*, 2023. http://d4agph.da.gov.ph/about.

[11] Maramara, R. *Footprints in ICT*, February 15, 2022. Philippine Rice Research Institute. https://www.philrice.gov.ph/footprints-in-ict/.

[12] Philippine Institute of Developmental Studies. *AGRI-TECH | Agriculture 4.0: Eight Essential Things You Need to Know*, September 03, 2020. https://www.pids.gov.ph/details/agri-tech-agriculture-4-0-eight-essential-things-you-need-to-know.
[13] International Rice Research Institute. *Crop Manager*, October 18, 2022. https://www.irri.org/crop-manager.
[14] Philippine Rice Research Institute. *Rice Science for Decision Makers*, 2022. https://www.philrice.gov.ph/databases/rice-science-for-decision-makers/.
[15] Agricultural Training Institute Northern Mindanao. *More Farmers Train to Become Competent Seed Growers*, October 04, 2023. https://ati2.da.gov.ph/ati-10/content/article/angelli-dona/more-farmers-train-become-competent-seed-growers.
[16] Manalo, J. A.; Pasiona, S. P.; Bautista, A. M. F.; Villaflor, J. D.; Corpuz, D. C. P.; Biag-Manalo, H. H. M. Exploring Youth Engagement in Agricultural Development: The Case of Farmers' Children in the Philippines as Rice Crop Manager Infomediaries. *J. Agric. Educ. Ext.* **2019**, *25*(4), 361–377. https://doi.org/10.1080/1389224x.2019.1629969
[17] Ambali, O. I.; Areal, F. J.; Georgantzis, N. Improved Rice Technology Adoption: The Role of Spatially-Dependent Risk Preference. *Agriculture* **2021**, *11*(8), 691. https://doi.org/10.3390/agriculture11080691
[18] Thi Hoa Sen, L.; Chou, P.; Dacuyan, F. B.; Nyberg, Y.; Wetterlind, J. Barriers and Enablers of Digital Extension Services' Adoption among Smallholder Farmers: The Case of Cambodia, the Philippines and Vietnam. *Int. J. Agric. Sustain.* **2024**, *22*(1). https://doi.org/10.1080/14735903.2024.236835
[19] Pham, T. D. M.; Thieken, A. H.; Bubeck, P. Community-Based Early Warning Systems in a Changing Climate: An Empirical Evaluation from Coastal Central Vietnam. *Clim. Dev.* **2024**, *16*(8), 673–684. https://doi.org/10.1080/17565529.2024.2307398
[20] Paracale, M. I. P.; Abante, M. V. Fields of Struggle: An In-Depth Study on the Socio-Economic Issues Encountered by Filipino Rice Farmers. *SSRN Electron. J.* **2024**. https://doi.org/10.2139/ssrn.4731163
[21] World Bank. *World Development Report 2016: Digital Dividends*; World Bank: Washington, DC, 2016. https://www.worldbank.org/en/publication/wdr2016.
[22] Montesclaros, J. M. L.; Teng, P. S. Digital Technology Adoption and Potential in Southeast Asian Agriculture. *AgEcon Search* **2023**. https://doi.org/10.22004/ag.econ.339167
[23] Ozer, E. M. Albert Bandura (1925–2021). *Am. Psychol.* **2022**, *77*(3), 483–484. https://doi.org/10.1037/amp0000981
[24] Hidayat, T.; Mahardiko, R. A Review of Detection of Pest Problem in Rice Farming by Using Blockchain and IoT Technologies. *J. Comput. Netw. Archit. High Perform. Comput.* **2021**, *3*(1), 89–96. https://doi.org/10.47709/cnahpc.v3i1.935

ASEAN
Journal of Scientific and Technological Reports
Online ISSN:2773-8752

Research article

Development of Ultrasonic Extraction Techniques for Bioactive Compounds from Banana Peel Waste: A Comparative Study of Biological Activities

Napattaorn Buachoon[1*]

[1] Faculty of Science and Technology, Valaya Alongkorn Rajabhat University under the Royal Patronage Pathum Thani Province, 13180, Thailand
* Correspondence: napattaorn@vru.ac.th

Citation:
Buachoon, N. Effects of ultrasonic extraction on total phenolic content, antioxidant activity, and tyrosinase inhibitory activity of banana peel extract. *ASEAN J. Sci. Tech. Report.* **2026**, *29*(1), e258852. https://doi.org/10.55164/ajstr.v29i1.258852.

Article history:
Received: April, 2025
Revised: October 10, 2025
Accepted: October 18, 2025
Available online: December 14, 2025

Publisher's Note:
This article is published and distributed under the terms of the Thaksin University.

Abstract: Banana peel (*Musa* spp.), an abundant agricultural by-product, represents a valuable source of bioactive compounds with potential applications in functional food and cosmeceutical industries. This study investigated the influence of ultrasound-assisted extraction (UAE) on total phenolic content (TPC), total flavonoid content (TFC), antioxidant activity, and tyrosinase inhibitory capacity of peel extracts from four economically important cultivars: Cavendish, Bluggoe, Pisang Awak, and Red Dacca. Extraction was conducted using 70% (v/v) aqueous ethanol under ultrasonic conditions at three temperatures (30, 50, and 70 °C) and three time intervals (30, 60, and 120 min). The results demonstrated that Pisang Awak peel extract exhibited the highest TPC (4.63 mg GAE/g extract) and TFC (4.28 mg QE/g extract). Antioxidant capacity evaluated by 2,2-diphenyl-1-picrylhydrazyl (DPPH) and ferric reducing antioxidant power (FRAP) assays revealed superior activity for Pisang Awak extract (IC_{50} = 1.27 μg/mL; FRAP = 3.71 mg TE/g extract). This cultivar also demonstrated significant tyrosinase inhibitory activity (IC_{50}= 1.34 mg/mL). Optimization studies identified 50 °C and 60 min as optimal extraction parameters, yielding maximum extraction efficiency across all cultivars. These findings establish UAE as an effective technology for recovering bioactive compounds from banana peel waste, particularly the Pisang Awak cultivar, which shows considerable promise for development into nutraceutical and cosmeceutical formulations. This valorization approach promotes sustainable waste management and circular bioeconomy principles in the agricultural sector.

Keywords: Ultrasonic waves; phenolic; antioxidant capacity; banana peel

1. Introduction

The fruit and vegetable processing industry generates a substantial amount of waste materials, more than 25 to 40 percent by weight, which include peels, seeds, press residues, and fruit pulp. Most of this waste is disposed of in the environment, contributing to air pollution. Moreover, the management of such waste remains a major concern and incurs high costs [1]. Bananas are one of Thailand's key economic fruits. The commercially cultivated varieties include Pisang Awak banana, Cavendish banana, Lady Finger banana, Bluggoe banana, and Red Dacca banana. Ripe bananas are rich in nutrients, providing approximately 105 kilocalories of energy per 100 grams, and are excellent sources of vitamin B6, vitamin C, essential minerals such as potassium, iron, magnesium, and manganese, and high levels of dietary fiber.

In recent decades, the utilization of agricultural byproducts as sources of bioactive compounds has gained significant attention. These compounds, particularly phenolic compounds, anthocyanins, flavonoids, vitamins, minerals, and antioxidants, exhibit a wide range of biological activities including antimicrobial, antioxidant, antidiabetic, antiaging, anticancer, and weight management effects [2]. Waste materials derived from banana processing are important sources of such bioactive compounds [3]. In particular, banana peel, accounting for approximately 30 to 40 percent of the fresh fruit weight, is rich in phenolic compounds, flavonoids, and antioxidants [4]. Attributed to its multifunctional bioactive nature, banana peel has been applied in various domains such as a prebiotic agent, a source of pectin, an ingredient in bakery products, and dietary supplements [5-7].

The extraction process of biologically active constituents derived from botanical sources directly influences the yield and quality of the target compounds [8]. Traditional solvent-based extraction methods techniques such as maceration and Soxhlet extraction, rely on the application of heat to raw materials in solvents at high temperatures. Although these methods often yield high extraction outputs, the extended extraction time may degrade active compounds and consume considerable energy [9]. In addition, traditional extraction methods involve large volumes of solvents, which can negatively impact the environment. Recently, the green technology concept has gained increasing attention, emphasizing the extraction of bioactive compounds without the use of toxic chemicals, thereby promoting environmentally friendly processes that are also safe for consumers [9-10]. Modern extraction technologies include employing techniques such as microwave-assisted, sonication-based, high-pressure, and pulsed electric field methods, and enzymes. Ultrasonic extraction is an efficient alternative technology that offers advantages such as reduced extraction time, lower solvent usage, and high yields [11]. The mechanism relies on the acoustic cavitation phenomenon, whereby ultrasonic waves generate microbubbles in a liquid medium. The collapse of these bubbles creates localized high-temperature and pressure zones, enhancing mass transfer and extraction efficiency [12]. However, the efficiency of ultrasonic extraction depends on several operational parameters, particularly thermal conditions and processing duration, which significantly influence efficiency and integrity of the recovered phytochemicals [13].

This study explored the influence of ultrasound-assisted extraction on phenolic and flavonoid composition, antioxidative potential, and the capacity to suppress tyrosinase activity in banana peel extracts. The findings of this research will provide valuable insights for identifying optimal extraction conditions and developing an efficient process for recovering bioactive compounds from banana peels. This can lead to broader applications across various industries and enhance the value of agricultural waste. Furthermore, this research supports the objectives of multiple UN Sustainable Development Goals, particularly Goal 9: Industries, Innovation and Infrastructure, by developing efficient and environmentally friendly extraction processes; Goal 12: Responsible Consumption and Production, through the utilization of agricultural waste and waste reduction; and Goal 15 Life on Land, by promoting the sustainable use of natural resources. Therefore, this study holds significance in scientific, technological, and sustainable development contexts at the global level.

2. Materials and Methods

This study investigated the effects of ultrasonic extraction on the total phenolic content, total flavonoid content, antioxidant activity, and tyrosinase inhibitory activity of banana peel extracts.

2.1 Sample Preparation and Extraction

The banana peels studied included Cavendish banana peel, Bluggoe banana peel, Pisang Awak banana peel, and Red Dacca banana peel, collected from bakeries, grilled banana vendors, and Thai dessert shops in Khlong Luang District, Pathum Thani Province.

Sample preparation began with washing each type of banana peel with clean water, followed by air drying at room temperature. The peels were sectioned into smaller fragments and dehydrated using a hot air oven at 45 °C until constant mass was achieved. The dried samples were then milled into uniform powder by a mechanical grinder. Each powdered sample was accurately weighed using a four-decimal analytical balance.

For extraction, 10 g of the powdered peel was combined with 100 mL of 70% (v/v) ethanol. The ultrasonic-assisted extraction process was carried out at three temperature levels (30, 50, and 70 °C) and three time intervals (30, 60, and 120 min). After sonication, the mixtures were subjected to filtration, and the resulting filtrates were concentrated under reduced pressure using a rotary evaporator operated at 45 °C. The extracts were stored in the dark at a temperature of minus 18 degrees Celsius until further analysis.



(a) (b) (c) (d)

Figure 1. Banana Peel: (a) Cavendish; (b) Bluggoe; (c) Pisang Awak; and (d) Red Dacca

2.2 Determination of Total Phenolic Content (TPC)

Gallic acid reference standards were prepared in a concentration series of 0, 20, 40, 60, 80, and 100 mg/L. For each concentration, each standard (0.5 mL) was placed in a test tube and combined with 2.5 mL of distilled water. Then, 0.5 mL of diluted Folin-Ciocalteu reagent (diluted 1:10) and 0.5 mL of Na_2CO_3 solution (7.5% w/v) were introduced to the mixture. After thorough mixing by vortex, the samples were kept in darkness at ambient temperature for 30 min, after which absorbance was measured at 765 nm using UV-Vis spectrophotometry. Each extract sample was prepared at a final concentration of 1 mg/L. Subsequently, 0.5 mL of each sample solution was processed following an identical protocol: combined with 2.5 mL distilled water, treated with 0.5 mL diluted Folin-Ciocalteu reagent (1:10), and 0.5 mL of Na_2CO_3 solution (7.5% w/v). Following vortex mixing, samples were incubated in the dark at room temperature for 30 min, and absorbance was measured at a wavelength of 765 nm using UV-Vis spectrophotometry. A blank control containing only distilled water underwent identical treatment procedures. Quantification of total phenolic compounds in crude extracts was achieved through calibration against the gallic acid reference curve, with results reported as mg GAE/g extract. Triplicate analyses were performed for all determinations [14].

2.3 Determination of Total Flavonoid Content (TFC)

Quercetin reference standards were established across a concentration range of 0.1, 0.2, 0.3, 0.4, and 0.5 mg/mL using ethanol as solvent. Each reference standard (1 mL) was transferred to a test tube and combined with 1 mL of $AlCl_3$ (10% v/v). The resulting mixture underwent thorough agitation and was maintained under dark conditions at ambient temperature for 5 min. Then, 0.5 mL of CH_3COOH solution (10% v/v) was introduced, and the final volume was brought to 5 mL using distilled water. After vortex mixing, absorbance readings were obtained at 420 nm wavelength using UV-Vis spectrophotometry. Sample extracts were processed at a 1.0 mg/mL concentration. Each extract (1 mL) was placed in a test tube and treated with 1 mL of $AlCl_3$ (10% v/v) solution. The mixture was agitated and kept in the dark at room temperature for 5 min. An aliquot of 0.5 mL of CH_3COOH solution (10% v/v) was added, and the volume was adjusted to 5 mL with distilled water. The mixture was thoroughly homogenized using a vortex mixer and subsequently subjected to absorbance measurement at 420 nm using a UV–visible spectrophotometer. Total flavonoid concentrations in crude extract samples were determined using the quercetin calibration curve and reported as mg QE/g extract. All analytical determinations were performed in triplicate [15-16].

2.4 Determination of Antioxidant Capacity by DPPH Radical Scavenging Assay

A 100 μM DPPH (2,2-diphenyl-1-picrylhydrazyl) solution was prepared in absolute ethanol. Trolox reference standards were formulated across concentration levels of 25, 50, 250, 500, and 1,000 μg/mL. Each standard solution (1,000 μL) was combined with an equal volume (1,000 μL) of DPPH solution. The resulting mixtures underwent vortex homogenization and were maintained under dark conditions for 30 min before spectrophotometric analysis at 516 nm wavelength. Sample crude extracts were processed at equivalent concentrations of 25, 50, 250, 500, and 1,000 μg/mL. For each test concentration, 1,000 μL of extract was combined with 1,000 μL of DPPH solution. Following vortex mixing, the combinations were kept in darkness

at room temperature for 30 min before absorbance determination at 516 nm using UV-Vis spectrophotometry. Pure ethanol served as the control blank, replacing the sample solution while following identical procedural steps. Triplicate analyses were conducted for all samples [17-19].

Radical scavenging activity percentage was determined using the equation:

$$\% \text{ Radical scavenging} = [(Ac - As)/Ac] \times 100$$

Where:

Ac represents the absorbance of the DPPH solution alone.

As represents the absorbance of the sample – DPPH mixture.

The resulting data were utilized to establish the 50% inhibitory concentration (IC_{50}) through graphical analysis, plotting extract concentration versus % radical scavenging activity. Trolox served as the reference standard for comparative analysis.

2.5 Antioxidant Capacity Test by Ferric Reducing Antioxidant Power (FRAP) Assay

The FRAP working solution was prepared by mixing 300 mM acetate buffer (pH 3.6), 10 mM TPTZ (2,4,6-tripyridyl-s-triazine) dissolved in 40 mM HCl, and 20 mM $FeCl_3 \cdot 6H_2O$ at a volumetric ratio of 10:1:1. The mixture was incubated at 37 °C for 4 min before use. Trolox was used as the reference standard at concentrations of 200, 400, 600, 800, and 1,000 μM. For the assay, 20 μL of each Trolox standard solution was mixed with 180 μL of FRAP working solution, followed by vortex homogenization and incubation in the dark at room temperature for 30 min. Absorbance was measured at 593 nm using a UV–Vis spectrophotometer, and a standard calibration curve was established to correlate Trolox concentration with absorbance. Crude banana peel extracts were dissolved at 2 mg/mL, and 20 μL of each sample solution was mixed with 180 μL of FRAP working solution under the same conditions. The antioxidant capacity was expressed as FRAP values, calculated from the Trolox standard curve and reported as mg TE/g extract, indicating the reducing potential of the samples (Fe^{3+} to Fe^{2+}). All analytical determinations were performed in triplicate [20].

2.6 Tyrosinase Inhibitory Capacity Test by Dopachrome Method

Kojic acid reference standards were established across concentration levels of 0.01, 0.05, 0.1, 0.5, and 1 mg/mL. Each standard level (40 μL) was transferred to a 96-well plate and combined with 80 μL of phosphate buffer (50 mM, pH 6.8) containing L-tyrosine at 90 mg/mL. Following thorough homogenization, 40 μL of L-DOPA (2.5 mM L-3,4-dihydroxyphenylalanine) was introduced. After complete mixing, the reaction mixture was maintained at 25 °C for 20 min. Spectrophotometric analysis was subsequently performed at 475 nm using a UV-Vis microplate reader. Sample extracts were processed at equivalent concentrations of 0.01, 0.05, 0.1, 0.5, and 1 mg/mL. For each test concentration, 40 μL of the sample was transferred into a 96-well plate and treated with 80 μL of phosphate buffer (50 mM, pH 6.8) containing L-tyrosine (90 mg/mL). After thorough mixing, the reaction mixture was incubated at 25 °C for 20 min. Absorbance determination was conducted at 475 nm using a UV-Vis microplate reader. Control solution preparation involved phosphate buffer substitution for the sample extract, while the blank solution employed buffer replacement for the enzyme component. Inhibition percentage was determined using the equation.

$$\% \text{ Inhibition} = [(Ac - As)/Ac] \times 100$$

Where:

Ac represents the control solution absorbance.

As a representative sample solution absorbance.

Tyrosinase inhibitory capacity was evaluated against Kojic acid as a reference standard. IC_{50} values were determined through graphical analysis, plotting extract concentration versus inhibition percentage[21].

2.7 Statistical Analysis

All experimental data, obtained from triplicate determinations, were subjected to statistical evaluation using analysis of variance (ANOVA). Mean comparisons were performed with Duncan's New Multiple Range Test (DMRT) at a significance level of $p = 0.05$, and results are presented with distinct superscript letters in the tables to indicate statistically significant differences among treatments. All analyses were conducted using a

statistical software package. In addition, correlation analysis was carried out to assess the relationships among total phenolic content, total flavonoid content, antioxidant capacity, and tyrosinase inhibitory activity of banana peel extracts obtained through ultrasonic extraction under varying temperature and time conditions. Pearson's correlation coefficient (r) was employed for this analysis.

3. Results and Discussion

3.1 Ultrasound-Assisted Extraction of Banana Peel: Yield and Cultivar Effects

The banana peel varieties examined in this investigation comprised Cavendish banana peel, Bluggoe banana peel, Pisang Awak banana peel, and Red Dacca banana peel. These specimens underwent ultrasonic extraction using 70% ethanol (v/v) as the solvent under ultrasonic conditions with frequencies above 50 kHz at temperatures of 30, 50, and 70 °C for durations of 30, 60, and 120 min. The extraction process demonstrated varying efficiency depending on the type of banana peel examined. Extract preparation involved vacuum drying and weight measurements under dark conditions. The crude extracts appeared as dark brown to black viscous liquids. Upon weighing the crude extracts and calculating the yield percentage based on the dry weight of the sample (10 g), the crude extract yields ranged from 12.21% to 18.57% (Table 1).

Table 1. Percentage yields (mean± SD) of crude banana peel extracts obtained by ultrasonic-assisted extraction.

Temperature (°C)	Extraction time (min)	Cavendish (%)	Bluggoe (%)	Pisang Awak (%)	Red Dacca (%)
30	30	14.23 ± 0.02^{A}	14.25 ± 0.06^{A}	14.25 ± 0.06^{A}	14.06 ± 0.03^{AF}
	60	13.23 ± 0.01^{B}	13.70 ± 0.04^{H}	13.87 ± 0.09^{L}	13.66 ± 0.01^{H}
	120	12.39 ± 0.05^{C}	13.23 ± 0.01^{B}	13.34 ± 0.03^{M}	13.03 ± 0.02^{P}
50	30	12.21 ± 0.01^{D}	12.23 ± 0.01^{D}	12.23 ± 0.01^{D}	12.36 ± 0.00^{D}
	60	12.35 ± 0.01^{D}	12.60 ± 0.00^{I}	12.28 ± 0.00^{D}	12.68 ± 0.00^{I}
	120	12.63 ± 0.01^{D}	12.71 ± 0.00^{I}	12.86 ± 0.01^{N}	12.82 ± 0.01^{N}
70	30	14.40 ± 0.00^{E}	13.97 ± 0.01^{O}	13.97 ± 0.01^{O}	14.03 ± 0.02^{OF}
	60	14.23 ± 0.00^{A}	14.34 ± 0.00^{J}	14.02 ± 0.01^{OF}	14.36 ± 0.03^{J}
	120	14.87 ± 0.00^{F}	14.67 ± 0.00^{K}	14.69 ± 0.00^{K}	14.56 ± 0.01^{R}

Note: Different superscript letters (A–R) within a column indicate significant differences at $p \leq 0.05$ (DMRT)

According to Table 1, at 70 °C for 120 min, Cavendish peel exhibited the highest crude extract yield (18.57%), which was significantly higher ($p \leq 0.05$, DMRT) than those of Red Dacca (17.54%), Bluggoe (16.89%), and Pisang Awak (15.26%). Prolonged extraction duration (120 min) in combination with elevated temperature enhanced solvent penetration and facilitated the release of intracellular compounds. In contrast, at 30 °C, the yields were markedly lower across all cultivars, indicating that mild thermal conditions were insufficient to disrupt plant tissues effectively. Ultrasonic extraction of banana peels yielded crude extracts ranging from 13.97% to 18.57% at optimal conditions. Regression analysis revealed that temperature significantly influenced extraction yields, with 70°C producing maximum yields for all varieties. Elevated temperatures enhance bioactive compound solubility and reduce solvent viscosity, improving mass transfer and solvent penetration into plant tissues [22-23]. Extraction duration also significantly affected yields, with 120 min at 70 °C producing optimal results. Extended extraction periods provide sufficient time for solvent penetration into cellular structures and bioactive compound release [24-25]. Varietal comparison showed Cavendish banana yielded the highest crude extracts (18.57% at 70 °C, 120 min), followed by Red Dacca (17.54%), Bluggoe (16.89%), and Pisang Awak (15.26%). These differences reflect variations in cell wall structure, phenolic content, and bioactive composition among cultivars, influenced by genetic diversity, maturation stages, and environmental factors [26-27]. Ultrasonic extraction enhanced efficiency through cavitation mechanisms, generating intense shock waves via microbubble collapse that rupture cell walls and facilitate intracellular compound release[28-29]. The cavitation phenomenon creates localized high temperatures and pressures, softening cellular tissues and increasing mass transfer rates. The yields obtained (12.21-18.57%) were comparable to recent banana peel extraction studies under similar conditions[24-25].

3.2 Results of Total Phenolic Content (TPC)

Total phenolic extraction yields from the peel of four banana varieties, including Cavendish banana peel, Bluggoe banana peel, Pisang Awak banana peel, and Red Dacca banana peel, were subjected to ultrasonic extraction with frequencies above 50 kHz at temperatures of 30, 50, and 70 °C, and extraction times of 30, 60, and 120 min. The TPC was determined using the Folin-Ciocalteu method, and the results were expressed as gallic acid equivalents per gram of extract (mg GAE/g extract). The total phenolic content of the extracts varied between 1.03 and 4.5 mg GAE/g extract. The Pisang Awak banana peel had the highest phenolic content at 4.63 ± 0.03 mg GAE/g extract at 60 min and 50 °C, which was significantly higher ($p \leq 0.05$, DMRT) than those of Cavendish banana peel, Bluggoe banana peel, and Red Dacca banana peel had phenolic contents of 4.02 ± 0.01, 3.65 ± 0.03, and 2.87 ± 0.01 mg GAE/g extract, respectively, under the same conditions (60 min, 50 °C) (Table 2).

Table 2. Total phenolic content (mg GAE/g extract) of crude extracts from various banana peel varieties**.**

Temperature (°C)	Extraction time (min)	Cavendish	Bluggoe	Pisang Awak	Red Dacca
30	30	2.31 ± 0.09^{B}	2.16 ± 0.02^{B}	2.56 ± 0.01^{A}	2.04 ± 0.01^{C}
	60	2.43 ± 0.01^{B}	2.32 ± 0.02^{C}	3.55 ± 0.01^{A}	2.27 ± 0.02^{C}
	120	2.27 ± 0.01^{B}	2.25 ± 0.04^{B}	2.77 ± 0.01^{A}	2.25 ± 0.01^{B}
50	30	3.66 ± 0.02^{B}	3.32 ± 0.03^{C}	4.05 ± 0.02^{A}	2.45 ± 0.02^{D}
	60	4.02 ± 0.01^{B}	3.65 ± 0.03^{C}	4.63 ± 0.03^{A}	2.87 ± 0.01^{D}
	120	3.89 ± 0.02^{B}	3.43 ± 0.01^{C}	4.24 ± 0.01^{A}	2.59 ± 0.02^{D}
70	30	2.24 ± 0.04^{B}	2.28 ± 0.01^{B}	2.31 ± 0.01^{A}	2.11 ± 0.01^{C}
	60	2.45 ± 0.01^{B}	2.50 ± 0.01^{B}	2.56 ± 0.01^{A}	2.36 ± 0.01^{C}
	120	2.32 ± 0.02^{B}	2.31 ± 0.01^{B}	2.41 ± 0.00^{A}	2.30 ± 0.02^{B}

Note: Different superscript letters (A–D) within a column indicate significant differences at $p \leq 0.05$ (DMRT)

Temperature optimization analysis revealed that 50 °C yielded the highest TPC for all four banana peel varieties compared to 30 °C and 70 °C. This trend is consistent with previous reports indicating that moderate heating (50–60 °C) enhances phenolic recovery. For instance, Vu et al. (2019)[30] demonstrated that microwave-assisted extraction of Cavendish banana peel achieved high phenolic yields at approximately 50–60 °C, while Wang et al. [26] profiled different banana cultivars and similarly noted improved phenolic extraction under moderate temperature conditions. The TPC values obtained in the present study fall within the ranges reported previously. Suleria et al. [27] reported wide variation among 27 Australian-grown banana cultivars, with TPC ranging from 0.15 to 55.5 mg GAE/g. Vu et al. [30] observed phenolic recovery up to 50.55 mg GAE/g from Cavendish peel using microwave-assisted extraction, whereas Wang et al. [26] showed cultivar-specific differences linked to maturity and ecotype. Such varietal differences reflect both genetic diversity and cultivation environments [27]. Regarding extraction time, 60 min provided optimal recovery for most varieties in this study. In contrast, Vu et al. [30] reported much shorter optimal extraction times (6 min) for microwave-assisted extraction, highlighting that advanced extraction techniques often require less time than conventional approaches. At 30 °C, insufficient thermal energy may limit cell wall disruption, whereas moderate temperatures (50–60 °C) promote tissue softening, solubility, and mass transfer, thereby improving extraction efficiency [30]. However, phenolic compounds are heat-sensitive, and degradation may occur at higher temperatures (>70 °C), as previously noted in banana peel extracts [27]. Under optimized conditions (50 °C, 60 min), Pisang Awak banana peel exhibited the highest phenolic content among the examined varieties, highlighting its potential as a promising source for food, pharmaceutical, and cosmetic applications.

3.3 Results of Total Flavonoid Content (TFC)

The total flavonoid content in crude preparations from four types of banana peels, including the peels of the Cavendish banana, Bluggoe banana, Pisang Awak banana, and Red Dacca banana, was determined using the Aluminium Trichloride ($AlCl_3$) colorimetric assay, with quercetin serving as the standard reference. Total flavonoid concentrations in these extracts, processed under varying temperatures and extraction times,

ranged from 1.96 to 4.28 mg QE/g extract. The extract from Pisang Awak banana peel exhibited the highest TFC of 4.28 ± 0.01 mg QE/g extract at 60 min and 50 °C, followed by the Cavendish banana peel, Bluggoe banana peel, and Red Dacca banana peel, which had values of 3.87 ± 0.02, 3.46 ± 0.02, and 2.81 ± 0.00 mg QE/g extract, respectively, at 60 min and 50 °C Statistical analysis ($p \leq 0.05$, DMRT) showed significant differences among cultivars, indicating Pisang Awak peel as the richest flavonoid source. (Table 3).

Table 3. Total flavonoid content (mg QE/g extract) of crude extracts from various banana peel varieties.

Temperature (°C)	Extraction time (min)	Cavendish	Bluggoe	Pisang Awak	Red Dacca
30	30	2.02 ± 0.01^{B}	2.02 ± 0.01^{B}	2.48 ± 0.02^{A}	1.96 ± 0.02^{C}
	60	2.31 ± 0.01^{B}	2.25 ± 0.00^{B}	3.23 ± 0.01^{A}	2.11 ± 0.01^{C}
	120	2.15 ± 0.03^{B}	2.10 ± 0.01^{B}	2.51 ± 0.01^{A}	2.03 ± 0.02^{C}
50	30	3.51 ± 0.02^{B}	3.28 ± 0.02^{C}	3.98 ± 0.01^{A}	2.35 ± 0.03^{D}
	60	3.87 ± 0.02^{B}	3.46 ± 0.02^{C}	4.28 ± 0.01^{A}	2.81 ± 0.00^{D}
	120	3.72 ± 0.02^{B}	3.36 ± 0.02^{C}	4.09 ± 0.02^{A}	2.40 ± 0.00^{D}
70	30	1.97 ± 0.03^{B}	2.08 ± 0.01^{B}	2.19 ± 0.01^{A}	1.94 ± 0.03^{C}
	60	2.32 ± 0.02^{B}	2.37 ± 0.01^{B}	2.42 ± 0.01^{A}	2.11 ± 0.01^{C}
	120	2.05 ± 0.01^{B}	2.23 ± 0.01^{B}	2.28 ± 0.02^{A}	2.03 ± 0.01^{C}

Note: Different superscript letters (A–D) within a column indicate significant differences at $p \leq 0.05$ (DMRT)

Flavonoid content analysis revealed patterns consistent with phenolic content, with 50 °C and 60 min optimal for all banana peel varieties. Quantitative comparison contextualizes these findings: Mahmood et al. [31] reported TFC of 13.99 mg QE/g DM using enzyme-assisted extraction at 55 °C, while Ishak et al. [32] obtained 29.0 mg RE/g from Cavendish peel at 60 °C. Pisang Awak whole fruit demonstrated TFC of 440 mg QE/100 g, significantly exceeding other cultivars [33], while Wanyo et al. [34] reported 196 mg QE/g from banana peel extracts. The TFC values obtained align with these ranges, confirming extraction effectiveness. Temperature significantly influenced flavonoid extraction, with 50 °C yielding optimal results. Reduced content at 70 °C reflects thermal sensitivity, as flavonoids exhibit greater lability than phenolic acids with degradation at elevated temperatures [35]. The 60-minute duration proved optimal, balancing efficiency with compound stability. Varietal comparison under optimal conditions revealed distinct differences reflecting genetic diversity, maturation stages, and environmental factors [27]. Positive correlations between flavonoid and phenolic content were evident, with elevated phenolic levels corresponding to increased flavonoid accumulation. This establishes Pisang Awak banana peel as a valuable natural source of flavonoids for food, pharmaceutical, and cosmetic applications.

3.4 Results of Antioxidant Capacity using DPPH Radical Scavenging Methodology

Antioxidant capacity evaluation of crude preparations from four types of banana peels, including Cavendish banana peel, Bluggoe banana peel, Pisang Awak banana peel, and Red Dacca banana peel, employed the DPPH radical scavenging assay with Trolox serving as the reference solution. The IC_{50} values for these crude extracts, obtained under varying temperatures and extraction times, ranged from 1.27 to 2.06 μg/mL. The Pisang Awak banana peel extract demonstrated superior antioxidant performance, with an IC_{50} of 1.27 ± 0.08 μg/mL at 60 min and 50 °C, statistically lower ($p \leq 0.05$, DMRT) than Cavendish banana peel extract, Bluggoe banana peel extract, and Red Dacca banana peel extract, which showed IC_{50} values of 1.31 ± 0.04, 1.35 ± 0.03, and 1.55 ± 0.10 μg/mL, respectively, at 60 min and 50 °C. The IC_{50} value of Trolox at the same concentration was 1.28 ± 0.34 μg/mL (Table 4).

Table 4. DPPH Radical scavenging capacity (IC_{50}, mg/mL) of crude extracts from various banana peel varieties.

Temperature	IC_{50} (μg/mL)

(°C)	Extraction time (min)	Cavendish	Bluggoe	Pisang Awak	Red Dacca
30	30	1.59 ± 0.07^{B}	1.44 ± 0.04^{A}	1.66 ± 0.02^{C}	1.70 ± 0.06^{D}
	60	1.46 ± 0.11^{A}	1.42 ± 0.04^{A}	1.57 ± 0.02^{B}	1.65 ± 0.05^{C}
	120	1.65 ± 0.05^{B}	1.64 ± 0.03^{B}	1.67 ± 0.01^{B}	1.87 ± 0.03^{C}
50	30	1.35 ± 0.01^{A}	1.57 ± 0.05^{C}	1.44 ± 0.04^{B}	1.68 ± 0.08^{D}
	60	1.31 ± 0.04^{A}	1.35 ± 0.03^{A}	1.27 ± 0.08^{A}	1.55 ± 0.10^{B}
	120	1.66 ± 0.03^{B}	1.78 ± 0.11^{C}	1.66 ± 0.04^{B}	1.83 ± 0.04^{D}
70	30	1.97 ± 0.03^{C}	1.93 ± 0.05^{C}	1.65 ± 0.05^{A}	1.69 ± 0.05^{B}
	60	1.74 ± 0.02^{B}	1.63 ± 0.03^{A}	1.35 ± 0.04^{A}	1.63 ± 0.04^{A}
	120	2.06 ± 0.05^{C}	1.85 ± 0.05^{B}	1.80 ± 0.04^{B}	1.92 ± 0.07^{B}
Trolox IC_{50} (μg/mL)	-	1.28 ± 0.34			

Note: Different superscript letters (A–D) within a column indicate significant differences at $p \leq 0.05$ (DMRT)

Pisang Awak banana peel extract obtained at 50 °C for 60 min achieved superior antioxidant performance with an IC_{50} value comparable to Trolox standard, indicating potential as a natural antioxidant. Quantitative comparison with recent studies contextualizes these findings. Islam et al. [31] reported DPPH scavenging activity of 81.59% and ABTS activity of 88.25% from banana peel extracts using enzyme-assisted extraction at 55 °C. [36] documented DPPH values of 52.38 ± 2.04 mg Trolox/g sample from Nam Wa banana peel using methanol extraction. For Barangan banana peel (Musa acuminata), IC_{50} values of 32.52 μg/mL and 83.60 μg/mL were reported using ethanol extraction [37]. Additionally, Musa sapientum variety Muraru demonstrated IC_{50} values of 73.70 μg/mL and 147.99 μg/mL for methanolic extracts [38]. The IC_{50} values obtained in this study align with these reported ranges, confirming comparable antioxidant efficacy. Temperature significantly influenced antioxidant activity, with 50 °C optimal for all banana peel varieties. Activity decreased at 70 °C, consistent with phenolic and flavonoid degradation patterns at elevated temperatures. This aligns with recent findings that excessive heat compromises bioactive compound stability [24-25]. The 60-minute extraction duration maximized antioxidant activity, with both shorter and longer durations yielding reduced efficacy, reflecting the balance between extraction efficiency and oxidative degradation. Varietal comparison under optimal conditions (50 °C, 60 min) revealed positive correlations between antioxidant capacity and phenolic-flavonoid concentrations. Peels with elevated phenolic and flavonoid content demonstrated correspondingly higher antioxidant activity, consistent with established relationships between these bioactive compounds [26, 33]. These compounds exert antioxidant effects primarily through radical-scavenging mechanisms involving hydrogen atom transfer (HAT) and single electron transfer (SET), which neutralize reactive oxygen species (ROS) and prevent oxidative damage [38]. The findings establish Pisang Awak banana peel as a promising natural antioxidant source for food, pharmaceutical, and cosmetic applications.

3.5 Results of Antioxidant Capacity Assessment using the Ferric Reducing Antioxidant Power (FRAP) Assay

Antioxidant performance was evaluated utilizing the Ferric Reducing Antioxidant Power (FRAP) assay, which quantified the electron-donating ability of each sample. This method is based on the reduction of the Fe^{3+}-TPTZ (ferric tripyridyltriazine) complex to the Fe^{2+}-TPTZ (ferrous tripyridyltriazine) complex by antioxidant compounds. The results were reported as FRAP values (mg TE/g extract), with higher FRAP values indicating greater reducing potential of the crude preparations. The crude extracts from the peels of four banana varieties, including Cavendish banana peel, Bluggoe banana peel, Pisang Awak banana peel, and Red Dacca banana peel, exhibited antioxidant activity at various extraction times and temperatures, with FRAP values ranging from 2.09 to 3.71 mg TE/g extract. The crude extract from Pisang Awak banana peel showed the highest antioxidant activity, with a FRAP value of 3.71 ± 0.03 mg TE/g extract at 60 min and 50 °C, significantly higher ($p \leq 0.05$, DMRT) than Cavendish banana peel (3.49 ± 0.08 mg TE/g extract), Bluggoe banana (3.50 ± 0.07 mg TE/g extract), and Red Dacca banana peel (3.21 ± 0.03 mg TE/g extract), all under the

same conditions (60 min, 50 °C). Trolox standard exhibited 3.65 ± 0.16 mg TE/g extract 3.65 ± 0.16 mg TE/g extract (Table 5).

Table 5. Ferric reducing antioxidant power (FRAP, mg TE/g extract) of crude extracts from various banana peel varieties

Temperature (°C)	Extraction time (min)	FRAP (mg TE/g extract)			
		Cavendish	Bluggoe	Pisang Awak	Red Dacca
30	30	2.34 ± 0.04^{B}	2.38 ± 0.13^{B}	2.29 ± 0.07^{B}	2.09 ± 0.08^{C}
	60	2.58 ± 0.04^{B}	2.52 ± 0.02^{B}	2.53 ± 0.14^{B}	2.28 ± 0.16^{C}
	120	2.52 ± 0.10^{B}	2.42 ± 0.08^{B}	2.52 ± 0.11^{B}	2.14 ± 0.06^{C}
50	30	2.87 ± 0.61^{A}	3.14 ± 0.02^{A}	3.38 ± 0.06^{A}	3.06 ± 0.05^{A}
	60	3.49 ± 0.08^{A}	3.50 ± 0.07^{A}	3.71 ± 0.03^{A}	3.21 ± 0.03^{A}
	120	3.39 ± 0.13^{A}	3.42 ± 0.10^{A}	3.36 ± 0.08^{A}	3.11 ± 0.02^{A}
70	30	2.43 ± 0.03^{B}	2.33 ± 0.02^{B}	2.43 ± 0.06^{B}	2.13 ± 0.13^{C}
	60	2.73 ± 0.10^{B}	2.54 ± 0.05^{B}	2.80 ± 0.15^{B}	2.28 ± 0.03^{C}
	120	2.58 ± 0.05^{B}	2.42 ± 0.03^{B}	2.55 ± 0.15^{B}	2.11 ± 0.05^{C}
Trolox FRAP (mg/mL)	-	3.65 ± 0.16			

Note: Different superscript letters (A–C) within a column indicate significant differences at $p \leq 0.05$ (DMRT)

All banana peel extracts demonstrated ferric reducing capacity (Fe^{3+} to Fe^{2+} conversion), with Pisang Awak exhibiting particularly high antioxidant potential through effective electron donation [39]. These findings aligned with Sulaiman et al. [4] and Darsini et al. [33], who reported comparable FRAP activity in Pisang Awak to synthetic antioxidant BHT. Extraction at 50 °C yielded optimal FRAP values across all varieties, consistent with recent optimization studies. Hernández-Carranza et al. [40] and Granella et al. [24] reported maximum bioactive compound extraction at 50–60 °C, with polyphenol recovery of 355.11 ± 4.99 μg GAE/g achieved at 60 °C. Chaudhry et al. [41] confirmed that moderate temperatures produced the highest phenolic content (31.45 mg GAE/g) and FRAP activity (29.51%). At 70 °C, FRAP values decreased substantially due to thermal degradation of antioxidant compounds. Cegledi et al. [25] observed reduced hydroxycinnamic acid and flavonoid content beyond 60°C, while Khalangre et al. [42] demonstrated accelerated degradation at 70 °C through kinetics analysis. Vu et al. [30] explained that excessive temperatures decrease recovery yield despite initially enhanced compound release. These results supported Fidrianny et al. [43] and Islam et al. [31], who established positive correlations between phenolic content and FRAP activity at optimal temperatures of 35–60 °C. The FRAP values of Pisang Awak extract exceeded the Trolox standard, indicating exceptional potential for development as a natural antioxidant agent when extracted at optimized temperatures of 50–60 °C to maximize bioactive recovery while minimizing thermal degradation.

3.6 Results of Tyrosinase Inhibitory Capacity Assessment Employing the Dopachrome Assay

The tyrosinase inhibitory capacity of crude preparations from peels of four banana varieties, including Cavendish banana peel, Bluggoe banana peel, Pisang Awak banana peel, and Red Dacca banana peel, was determined utilizing the Dopachrome assay, employing Kojic acid as the reference compound. The crude preparations from all four banana peel types, extracted under varying temperatures and durations, demonstrated tyrosinase inhibitory potential, with IC_{50} values ranging from 1.34 to 2.06 mg/mL. The crude extract from Pisang Awak banana peel exhibited superior tyrosinase inhibitory performance, with an IC_{50} concentration of 1.34 ± 0.03 mg/mL at 60 min and 50 °C, statistically lower ($p \leq 0.05$, DMRT) than Cavendish banana peel, Bluggoe banana peel, and Red Dacca banana peel, with IC_{50} values of 1.46 ± 0.03, 1.55 ± 0.04, and 1.62 ± 0.03 mg/mL, respectively, under the same extraction conditions (60 min, 50 °C). The IC_{50} concentration of the reference Kojic acid standard was 1.34 ± 0.21 mg/mL (Table 6).

Table 6. Tyrosinase inhibitory capacity (IC_{50}, mg/mL) of crude extracts from various banana peel varieties.

Temperature (°C)	Extraction time (min)	IC_{50} (mg/mL)			
		Cavendish	Bluggoe	Pisang Awak	Red Dacca
30	30	1.69 ± 0.08^{B}	1.75 ± 0.06^{B}	1.73 ± 0.04^{B}	1.82 ± 0.02^{A}
	60	1.56 ± 0.02^{B}	1.55 ± 0.02^{B}	1.52 ± 0.02^{C}	1.60 ± 0.02^{A}
	120	1.66 ± 0.06^{B}	1.68 ± 0.09^{B}	1.60 ± 0.01^{C}	1.73 ± 0.01^{A}
50	30	1.54 ± 0.03^{B}	1.84 ± 0.05^{A}	1.55 ± 0.03^{B}	1.85 ± 0.05^{A}
	60	1.46 ± 0.03^{B}	1.55 ± 0.04^{A}	1.34 ± 0.03^{C}	1.62 ± 0.03^{A}
	120	1.63 ± 0.04^{B}	1.71 ± 0.02^{A}	1.42 ± 0.02^{C}	1.73 ± 0.02^{A}
70	30	1.83 ± 0.02^{A}	1.73 ± 0.05^{B}	1.64 ± 0.04^{C}	1.82 ± 0.02^{A}
	60	1.58 ± 0.02^{B}	1.63 ± 0.03^{B}	1.53 ± 0.02^{C}	1.79 ± 0.02^{A}
	120	1.71 ± 0.03^{C}	1.63 ± 0.03^{C}	1.66 ± 0.03^{BC}	1.94 ± 0.04^{A}
0Kojic acid IC_{50} (mg/mL)	-	1.34 ± 0.21			

Note: Different superscript letters (A–C) within a column indicate significant differences at $p \leq 0.05$ (DMRT)

Pisang Awak banana peel crude extracts demonstrated tyrosinase inhibitory activity (66.39–77.05%) exceeding kojic acid (44.68–59.93%), attributed to flavonoids, particularly ferulic acid (906.62 mg/100 g), which suppresses tyrosinase through copper chelation and competitive substrate binding [44-45]. Extraction temperature significantly influenced enzyme inhibition, with 50 °C yielding optimal activity across all cultivars, correlating with maximum phenolic (25.37 mg GAE/g DM) and flavonoid (13.99 mg QE/g DM) recovery. These findings aligned with Islam et al. reporting 55 °C optimal for enzyme-assisted extraction and Granella et al. [24] identifying 52.3 °C for ultrasound-assisted polyphenol recovery (355.11 ± 4.99 μg GAE/g). The temperature-dependent enhancement reflects improved cell wall disruption without thermal degradation [43]. Temperatures exceeding 60 °C accelerated phenolic compound degradation [25,30]. Extraction duration of 60 minutes maximized tyrosinase inhibitory capacity, suggesting complete extraction of key bioactive constituents. This optimal timeframe aligned with kinetic studies demonstrating maximum polyphenol recovery between 30–90 min [24, 46]. Under optimized conditions (50 °C, 60 min), tyrosinase inhibitory capacity correlated strongly with phenolic and flavonoid contents. These bioactive compounds inhibit tyrosinase through copper chelation at the binuclear active site and competitive L-tyrosine binding [44, 47]. Molecular docking revealed rosmarinic acid interactions with tyrosinase residues (HIS263, VAL283, SER282, MET280) at a binding energy of 5.05 kcal/mol [45]. The correlation between antioxidant capacity and tyrosinase inhibition confirms dual functionality of banana peel polyphenols in free radical scavenging and melanogenesis suppression [6, 39]. Phacharapiyangkul et al. [45] demonstrated a dose-dependent reduction in tyrosinase activity and melanin content through MITF downregulation via the p38 signaling pathway. Similarly, Linsaenkart et al. [44] confirmed suppression of MITF, TYR, TRP-1, and DCT gene expression, achieving effects comparable to kojic acid and arbutin. These findings indicate that banana peel extracts extracted at optimized temperatures (50–60 °C) represent promising natural alternatives to synthetic tyrosinase inhibitors for cosmetic and pharmaceutical applications.

4. Conclusions

This investigation evaluated the influence of ultrasound-assisted extraction (UAE) on total phenolic content (TPC), total flavonoid content (TFC), antioxidant capacity, and tyrosinase inhibitory activity of peel extracts from four economically important banana cultivars (*Musa* spp.) cultivated in Thailand: Cavendish, Bluggoe, Pisang Awak, and Red Dacca. UAE, utilizing 70% (v/v) aqueous ethanol as extraction solvent, recognized for its superior efficiency in recovering bioactive phytochemicals, was applied throughout the experimental procedures. The results demonstrated that Pisang Awak banana peel extracts exhibited significantly superior bioactive profiles compared to other cultivars ($p < 0.05$). This cultivar displayed the highest TPC and TFC values, accompanied by optimal antioxidant activity (DPPH, ABTS, and FRAP assays)

and maximal tyrosinase inhibitory capacity. These findings underscore the substantial potential of Pisang Awak peel extracts for valorization into high-value functional ingredients, including nutraceutical formulations, cosmeceutical applications, and pharmaceutical preparations targeting dermatological conditions such as hyperpigmentation disorders and photoaging. Moreover, this research aligns with the United Nations Sustainable Development Goals (SDGs), specifically contributing to SDG 12 (Responsible Consumption and Production) through agricultural waste valorization, SDG 3 (Good Health and Well-being) via development of natural bioactive ingredients, and SDG 9 (Industry, Innovation and Infrastructure) by promoting circular bioeconomy principles. Optimization studies identified 50 °C and 60 minutes as the optimal extraction parameters, yielding maximum extraction efficiency across all investigated banana peel cultivars, thereby establishing a reproducible and scalable methodology for industrial applications.

5. Acknowledgements

This research was supported by the Faculty of Science and Technology, Valaya Alongkorn Rajabhat University, under the Royal Patronage, Pathum Thani, Thailand.

Author Contributions: Conceptualization, N.B.; methodology, N.B.; validation, N.B.; formal analysis, N.B.; investigation, N.B.; resources, N.B.; data curation, N.B.; writing—original draft preparation, N.B.; writing—review and editing, N.B.; visualization, N.B.; supervision, N.B.; project administration, N.B.; funding acquisition, N.B.

Funding: This research received no external funding

Conflicts of Interest: The authors declare no conflict of interest.

References

[1] Mahato, N.; Sinha, M.; Sharma, K.; Koteswararao, R.; Cho, M. H. Modern extraction and purification techniques for obtaining high purity food-grade bioactive compounds and value-added co-products from citrus wastes. *Foods* **2019**, *8*(11), 254. https://doi.org/10.3390/foods8110254

[2] Hasan, S. K.; Ferrentino, G.; Scampicchio, M. Nanoemulsion as advanced edible coatings to preserve the quality of fresh-cut fruits and vegetables: A review. *Int. J. Food Sci. Technol.* **2020**, *55*(1), 1–10. https://doi.org/10.1111/ijfs.14275

[3] Pereira, A.; Maraschin, M. Banana (Musa spp) from peel to pulp: Ethnopharmacology, source of bioactive compounds and its relevance for human health. *J. Ethnopharmacol.* **2015**, *160*, 149–163. https://doi.org/10.1016/j.jep.2014.11.042

[4] Sulaiman, S. F.; Yusoff, N. A. M.; Eldeen, I. M.; Seow, E. M.; Sajak, A. A. B.; Ooi, K. L. Correlation between total phenolic and mineral contents with antioxidant activity of eight Malaysian bananas (Musa sp.). *J. Food Compos. Anal.* **2011**, *24*(1), 1–10. https://doi.org/10.1016/j.jfca.2010.04.005

[5] Kamal, M. M.; Ali, M. R.; Rahman, M. M.; Shishir, M. R. I.; Yasmin, S.; Sarker, M. S. H. Effects of processing techniques on drying characteristics, physicochemical properties and functional compounds of green and red chilli (Capsicum annum L.) powder. *J. Food Sci. Technol.* **2019**, *56*(7), 3185–3194. https://doi.org/10.1007/s13197-019-03841-2

[6] Zaini, H. M.; Roslan, J.; Saallah, S.; Munsu, E.; Sulaiman, N. S.; Pindi, W. Banana peels as a bioactive ingredient and its potential application in the food industry. *J. Funct. Foods* **2022**, *92*, 105054. https://doi.org/10.1016/j.jff.2022.105054

[7] Phirom-on, K.; Apiraksakorn, J. Development of cellulose-based prebiotic fiber from banana peel by enzymatic hydrolysis. *Food Biosci.* **2021**, *41*, 101083. https://doi.org/10.1016/j.fbio.2021.101083

[8] Vázquez, M. B.; Comini, L. R.; Martini, R. E.; Montoya, S. N.; Bottini, S.; Cabrera, J. L. Comparisons between conventional, ultrasound-assisted and microwave-assisted methods for extraction of anthraquinones from *Heterophyllaea pustulata* Hook f. (Rubiaceae). *Ultrason. Sonochem.* **2014**, *21*(2), 478–484. https://doi.org/10.1016/j.ultsonch.2013.08.002

[9] Kamal, M. M.; Kumar, J.; Mamun, M. A. H.; Ahmed, M. N. U.; Shishir, M. R. I.; Mondal, S. C. Extraction and characterization of pectin from *Citrus sinensis* peel. *J. Biosyst. Eng.* **2021**, *46*(1), 16–25. https://doi.org/10.1007/s42853-021-00084-z

[10] Matos, G. S.; Pereira, S. G.; Genisheva, Z. A.; Gomes, A. M.; Teixeira, J. A.; Rocha, C. M. Advances in extraction methods to recover added-value compounds from seaweeds: Sustainability and functionality. *Foods* **2021**, *10*(3), 516. https://doi.org/10.3390/foods10030516

[11] Khan, M. K.; Abert-Vian, M.; Fabiano-Tixier, A. S.; Dangles, O.; Chemat, F. Ultrasound-assisted extraction of polyphenols (flavanone glycosides) from orange (*Citrus sinensis* L.) peel. *Food Chem.* **2010**, *119* (2), 851–858. https://doi.org/10.1016/j.foodchem.2009.08.046

[12] Ghafoor, K.; Choi, Y. H.; Jeon, J. Y.; Jo, I. H. Optimization of ultrasound-assisted extraction of phenolics, antioxidants, and anthocyanins from grape seeds. *J. Agric. Food Chem.* **2009**, *57*(11), 4988–4994. https://doi.org/10.1021/jf9001439

[13] Vuong, Q. V.; Hirun, S.; Roach, P. D.; Bowyer, M. C.; Phillips, P. A.; Scarlett, C. J. Effect of extraction conditions on total phenolic compounds and antioxidant activities of *Carica papaya* leaf aqueous extracts. *J. Herb. Med.* **2013**, *3*(3), 104–111. https://doi.org/10.1016/j.hermed.2013.04.004

[14] Singleton, V. L.; Rossi, J. A. Colorimetry of total phenolics with phosphomolybdic-phosphotungstic acid reagents. *Am. J. Enol. Vitic.* **1965**, *16*(3), 144–158. https://doi.org/10.5344/ajev.1965.16.3.144

[15] González-Montelongo, R.; Lobo, M. G.; Gonzalez, M. The effect of extraction temperature, time and number of steps on the antioxidant capacity of methanolic banana peel extracts. *Sep. Purif. Technol.* **2010**, *71* (3), 347–355. https://doi.org/10.1016/j.seppur.2009.12.024

[16] Chang, C. C.; Yang, M. H.; Wen, H. M.; Chern, J. C. Estimation of total flavonoid content in propolis by two complementary colorimetric methods. *J. Food Drug Anal.* **2002**, *10*(3), 178–182. https://doi.org/10.38212/2224-6614.2748

[17] Zhishen, J.; Mengcheng, T.; Jianming, W. The determination of flavonoid contents in mulberry and their scavenging effects on superoxide radicals. *Food Chem.* **1999**, *64*(4), 555–559. https://doi.org/10.1016/S0308-8146(98)00102-2

[18] Brand-Williams, W.; Cuvelier, M. E.; Berset, C. L. W. T. Use of a free radical method to evaluate antioxidant activity. *LWT–Food Sci. Technol.* **1995**, *28*(1), 25–30. https://doi.org/10.1016/S0023-6438(95)80008-5

[19] Molyneux, P. The use of the stable free radical diphenylpicrylhydrazyl (DPPH) for estimating antioxidant activity. *Songklanakarin J. Sci. Technol.* **2004**, *26*(2), 211–219.

[20] Sharma, O. P.; Bhat, T. K. DPPH antioxidant assay revisited. *Food Chem.* **2009**, *113*(4), 1202–1205. https://doi.org/10.1016/j.foodchem.2008.08.008

[21] Thaipong, K.; Boonprakob, U.; Crosby, K.; Cisneros-Zevallos, L.; Byrne, D. H. Comparison of ABTS, DPPH, FRAP, and ORAC assays for estimating antioxidant activity from guava fruit extracts. *J. Food Compos. Anal.* **2006**, *19*(6–7), 669–675. https://doi.org/10.1016/j.jfca.2006.01.003

[22] Rivadeneira, J. P.; Wu, T.; Ybanez, Q.; Dorado, A. A.; Migo, V. P.; Nayve, F. R. P., Jr.; Castillo-Israel, K. A. T. Microwave-assisted extraction of pectin from "Saba" banana peel waste: Optimization, characterization, and rheology study. *Int. J. Food Sci.* **2020**, *2020*, 8879425. https://doi.org/10.1155/2020/8879425

[23] Bello, U.; Amran, N. A.; Samsuri, S.; Ruslan, M. S. H. Kinetics, thermodynamic studies, and parametric effects of supercritical CO_2 extraction of banana peel wastes. *Sustain. Chem. Pharm.* **2023**, *31*, 100912. https://doi.org/10.1016/j.scp.2023.100912

[24] Granella, S. J.; Bechlin, T. R.; Christ, D.; Machado, S. R. C.; Triques, C. C.; da Silva, E. A. Pretreated banana peels as a source for the recovery of phenolic compounds: Extraction kinetics, ultrasound optimization, and conventional extraction methods. *J. Appl. Res. Med. Aromat. Plants* **2023**, *34*, 100484. https://doi.org/10.1016/j.jarmap.2023.100484

[25] Cegledi, E.; Dobroslavić, E.; Pedisić, S.; et al. Green approaches for the extraction of banana peel phenolics using deep eutectic solvents. *Molecules* **2024**, *29*(15), 3672. https://doi.org/10.3390/molecules29153672

[26] Zhang, J.; Wang, Y.; Yang, B.; et al. Profiling of phenolic compounds of fruit peels of different ecotype bananas derived from domestic and imported cultivars with different maturity. *Horticulturae* **2022**, *8*(1), 70. https://doi.org/10.3390/horticulturae8010070

[27] Bashmil, Y. M.; Ali, A.; Bk, A.; et al. Screening and characterization of phenolic compounds from Australian grown bananas and their antioxidant capacity. *Antioxidants* **2021**, *10*(10), 1521. https://doi.org/10.3390/antiox10101521

[28] Liu, Y.; Liu, X.; Cui, Y.; Yuan, W. Ultrasound for microalgal cell disruption and product extraction: A review. *Ultrason. Sonochem.* **2022**, *87*, 106054. https://doi.org/10.1016/j.ultsonch.2022.106054

[29] Zhao, F.; Wang, Z.; Huang, H. Physical cell disruption technologies for intracellular compound extraction from microorganisms. *Processes* **2024**, *12*(10), 2059. https://doi.org/10.3390/pr12102059

[30] Vu, H. T.; Scarlett, C. J.; Vuong, Q. V. Maximising recovery of phenolic compounds and antioxidant properties from banana peel using microwave assisted extraction and water. *J. Food Sci. Technol.* **2019**, *56* (3), 1360–1370. https://doi.org/10.1007/s13197-019-03610-2

[31] Islam, M. R.; Kamal, M. M.; Kabir, M. R.; et al. Phenolic compounds and antioxidant activity of banana peel extracts: Testing and optimization of enzyme-assisted conditions. *Measurement: Food* **2023**, *10*, 100085. https://doi.org/10.1016/j.meafoo.2023.100085

[32] Ishak, N. A.; Razak, N. A. A.; Dek, M. S. P.; Baharuddin, A. S. Production of high tannin content and antioxidant activity extract from unripe peel of *Musa acuminata* using ultrasound-assisted extraction (UAE). *BioResources* **2020**, *15*(1), 1877–1893.

[33] Darsini, D. T. P.; Maheshu, V.; Vishnupriya, M.; Sasikumar, J. M. In vitro antioxidant activity of banana (*Musa* spp. ABB cv. Pisang Awak). *Indian J. Biochem. Biophys.* **2012**, *49*, 124–129.

[34] Anal, A. K.; Jaisanti, S.; Noomhorm, A. Enhanced yield of phenolic extracts from banana peels (*Musa acuminata* Colla AAA) and cinnamon barks (*Cinnamomum varum*) and their antioxidative potentials in fish oil. *J. Food Sci. Technol.* **2014**, *51*(10), 2632–2639. https://doi.org/10.1007/s13197-012-0793-x

[35] Chaaban, H.; Ioannou, I.; Chebil, L.; et al. Effect of heat processing on thermal stability and antioxidant activity of six flavonoids. *J. Food Process. Preserv.* **2017**, *41*(5), e13203. https://doi.org/10.1111/jfpp.13203

[36] Khamsaw, P.; Sommano, S. R.; Wongkaew, M.; et al. Banana peel (*Musa* ABB cv. Nam Wa Mali-Ong) as a source of value-adding components and the functional properties of its bioactive ingredients. *Plants* **2024**, *13*(5), 593. https://doi.org/10.3390/plants13050593

[37] Arista, N.; Siregar, R. M. Antioxidant activity test of Barangan banana peel extract with DPPH method. *Indones. J. Chem. Sci. Technol.* **2023**, *6*(2), 171. https://doi.org/10.24114/ijcst.v6i2.49373

[38] Mahora, M. C.; Kigundu, A.; Waihenya, R. Screening of phytochemicals, antioxidant activity, and safety profile of hydroethanolic peel extract of *Musa sapientum*. *Plant Trends* **2024**, *2*(1), 1–15. https://doi.org/10.5455/pt.2024.01

[39] Wani, K. M.; Dhanya, M. Unlocking the potential of banana peel bioactives: Extraction methods, benefits, and industrial applications. *Discover Food* **2025**, *5*(1), 8. https://doi.org/10.1007/s44187-025-00276-y

[40] Hernández-Carranza, P.; Ávila-Sosa, R.; Guerrero-Beltrán, J. A.; et al. Optimization of antioxidant compounds extraction from fruit by-products: Apple pomace, orange and banana peel. *J. Food Process. Preserv.* **2016**, *40*(1), 103–115. https://doi.org/10.1111/jfpp.12588

[41] Chaudhry, F.; Ahmad, M. L.; Hayat, Z.; et al. Exploring the anti-diabetic potential of banana peel extracts: Impact of maceration and ultrasonication on bioactive compounds and glycemic control in diabetic rabbits. *Ultrason. Sonochem.* **2025**, *109*, 107426. https://doi.org/10.1016/j.ultsonch.2025.107426

[42] Khalangre, A.; Mirza, A.; Sharma, A. K.; et al. Effect of drying temperature on preservation of banana peel and degradation of targeted phytochemicals by LC-Orbitrap-MS. *Biomass Convers. Biorefin.* **2024**, 1–16. https://doi.org/10.1007/s13399-024-06008-z

[43] Fidrianny, I.; Rizkiya, A.; Ruslan, K. Antioxidant activities of various fruit extracts from three *Solanum* spp. using DPPH and ABTS method and correlation with phenolic, flavonoid, and carotenoid content. *J. Chem. Pharm. Res.* **2015**, *7*(5), 666–672.

[44] Linsaenkart, P.; Yooin, W.; Jiranusornkul, S.; et al. Valorization of Hom Thong banana peel as an anti-melanogenic agent through inhibition of pigmentary genes and molecular docking. *Int. J. Mol. Sci.* **2024**, *25*(23), 13202. https://doi.org/10.3390/ijms252313202

[45] Phacharapiyangkul, N.; Thirapanmethee, K.; Sa-Ngiamsuntorn, K.; et al. Effect of sucrier banana peel extracts on inhibition of melanogenesis through the ERK signaling pathway. *Int. J. Med. Sci.* **2019**, *16*(4), 602. https://doi.org/10.7150/ijms.32137

[46] Toh, P. Y.; Leong, F. S.; Chang, S. K.; Khoo, H. E.; Yim, H. S. Optimization of extraction parameters on the antioxidant properties of banana waste. *Acta Sci. Pol. Technol. Aliment.* **2016**, *15*(1), 65–78. https://doi.org/10.17306/J.AFS.2016.1.7

[47] Zolghadri, S.; Bahrami, A.; Hassan Khan, M. T.; et al. A comprehensive review on tyrosinase inhibitors. *J. Enzyme Inhib. Med. Chem.* **2019**, *34*(1), 279–309. https://doi.org/10.1080/14756366.2018.1545767

ASEAN
Journal of Scientific and Technological Reports
Online ISSN:2773-8752

Research article

Exploring the Role of AI in Marketing and Technology Readiness in Enhancing Customer Satisfaction and Business Performance in E-commerce

Taqwa Hariguna[1*], Retno Waluyo[2], Melia Dianingrum[3], and Arif Mu'amar Wahid[4]

[1] Master of Computer Science and Information System Department, Universitas Amikom Purwokerto, Purwokerto, 53126, Indonesia
[2] Information System Department, Universitas Amikom Purwokerto, Purwokerto, 53126, Indonesia
[3] Digital Business Department, Universitas Amikom Purwokerto, Purwokerto, 53126, Indonesia
[4] Informatics Department, Universitas Amikom Purwokerto, Purwokerto, 53126, Indonesia
* Correspondence: taqwa@amikompurwokerto.ac.id

Citation:
Hariguna, T.;. Waluyo, R.; Dianingrum, M.; Wahid, A. M. Exploring the role of AI in marketing and technology readiness in enhancing customer satisfaction and business performance in e-commerce. *ASEAN J. Sci. Tech. Report.* **2026**, *29*(1), e258998. https://doi.org/10.55164/ajstr.v29i1.258998.

Article history:
Received: April 26, 2025
Revised: October 4, 2025
Accepted: October 18, 2025
Available online: December 14, 2025

Publisher's Note:
This article is published and distributed under the terms of the Thaksin University.

Abstract: This study examines the relationships between technology readiness (TR), AI in marketing (AIM), customer satisfaction (CS), customer performance (CP), customer experience (CE), and financial performance (FP) in the context of Indonesian e-commerce businesses. Using structural equation modeling (PLS-SEM) on survey data from 314 business owners, the study finds strong positive relationships, with CS and CP acting as key mediators. The findings indicate that higher levels of TR significantly enhance CS, which in turn drives improved financial outcomes. Furthermore, the integration of AIM, particularly through personalized marketing tools, was found to have a substantial impact on both customer engagement and financial performance. The Sobel test results confirm that CS serves as a crucial mediator in the relationships between AIM, TR, and FP. This paper contributes to the existing literature by offering a comprehensive model that integrates several key constructs, providing new insights into the intersection of technology adoption and business performance in e-commerce. However, results are limited by convenience sampling and demographic concentration, which constrain generalizability. Practical recommendations emphasize prioritizing staff readiness, adopting AI-powered personalization tools, and actively tracking CS metrics to improve profitability.

Keywords: Technology readiness; AI in marketing; customer satisfaction; customer performance; financial performance

1. Introduction

The evolution of AI in marketing (AIM) has transformed how businesses operate and interact with consumers. In the past decade, technologies such as machine learning, natural language processing, and predictive analytics have become central to digital marketing, enabling more precise targeting and personalization. By analyzing vast datasets quickly and accurately, businesses can tailor campaigns to individual needs, improving efficiency and reducing resource waste [1, 2]. Beyond automation, AI also complements human judgment through collaborative intelligence, where machines handle data-driven tasks and marketers focus on strategic decisions and customer relationships [3, 4]. As e-commerce expands, AIM plays a critical role in enhancing operations, customer service, and competitiveness. AI algorithms can

predict consumer behavior with high accuracy, allowing firms to personalize recommendations and marketing strategies [5, 6]. This ability creates precision marketing, where customer segmentation and personalized campaigns strengthen engagement and loyalty [7, 8]. With real-time tracking, businesses can adapt campaigns instantly, ensuring responsiveness to shifting market trends. Such agility provides firms with a vital edge in today's highly competitive digital environment.

The adoption of AIM, however, depends heavily on technology readiness (TR). TR reflects the optimism, innovativeness, discomfort, and insecurity that shape an organization's willingness to adopt new technologies [8, 9]. Optimism and innovativeness drive positive adoption, while discomfort and insecurity can slow implementation. Understanding these readiness dimensions is crucial for firms seeking to integrate AI successfully into marketing strategies. Despite extensive research on AI adoption, customer experience (CE), and performance metrics, prior studies often examine these constructs in isolation [10, 11]. Few have investigated how TR and AIM jointly influence customer satisfaction (CS), customer performance (CP), and financial performance (FP) in e-commerce. This gap limits understanding of the systemic impact of AI adoption on business outcomes. Furthermore, measurement overlaps between constructs such as AIM and CE remain unresolved, creating ambiguity in how these factors interact [12, 13]. To address this gap, this study develops and tests an integrated model that links TR, AIM, CE, CS, CP, and FP in the context of Indonesian e-commerce. The objective is to clarify the pathways through which technology readiness and AI-driven marketing enhance satisfaction, customer outcomes, and ultimately financial performance. By highlighting these relationships, the study contributes both theoretically—by extending technology adoption frameworks—and practically—by offering actionable strategies for e-commerce businesses.

2. Literature Review

2.1. Exploring Technology Readiness (TR) in the Context of AI Adoption

Technology readiness (TR) refers to the extent to which individuals or organizations are prepared to adopt new technologies [14, 15], influencing how AI is integrated into marketing strategies. It is shaped by personal [16], organizational [17], and cultural factors such as age [18], education [19], innovativeness [20], and national culture [21] that determine openness to AI-driven tools [22, 23]. The Technology Acceptance Model (TAM) emphasizes that perceived ease of use [24, 25] and usefulness drive adoption [26], while the Technology Organization Environment (TOE) framework highlights the importance of organizational resources and leadership support [27, 28]. Together, these frameworks suggest that TR is a multidimensional construct that reflects both individual attitudes [29, 30] and organizational capacity for adoption [31, 32]. The Technology Readiness Index (TRI) further refines this concept [33, 34] through four dimensions: optimism, innovativeness, discomfort, and insecurity [35, 36]. Optimism and innovativeness encourage early adoption and experimentation, while discomfort and insecurity reflect barriers such as fear of errors, data privacy concerns, or lack of trust in AI systems [29, 30]. Prior studies show that higher optimism and innovativeness correlate with stronger adoption of AI tools, leading to improved customer engagement and satisfaction [37, 38]. By contrast, discomfort and insecurity can delay or weaken adoption, limiting the benefits of AI-enabled marketing [39].

TR is critical not only for organizations but also for consumers interacting with AI-powered services [40]. Consumers with high TR are more likely to engage with chatbots, recommendation systems, or AI driven personalization [41], which enhances their satisfaction and loyalty [37, 42]. Conversely, those with low TR may resist or disengage, reducing the effectiveness of AIM initiatives. This dual role of TR shaping both organizational adoption and consumer response underscores its importance in e-commerce [43]. Overall, TR provides the foundation for understanding how AI in marketing creates value [45]. Organizations with higher TR are better positioned to integrate AI tools, improve customer experience (CE), and foster satisfaction (CS), which in turn drives loyalty and financial performance (FP). Thus, TR represents a starting point in the proposed model, influencing not only the adoption of AIM but also its downstream effects on CE, CS, and business outcomes.

2.2 Understanding Customer Experience (CE) in E-Commerce Marketing

Customer experience (CE) encompasses all interactions a customer has with a brand across product usage, service encounters, and online engagement that collectively shape perceptions of the brand [46, 47]. In digital commerce, CE is not limited to transactions but reflects the overall journey from awareness to post-purchase, making it a critical driver of satisfaction and loyalty [48, 49]. Technology readiness (TR) plays an important role in shaping CE, as customers with higher optimism and innovativeness are more likely to engage with AI enabled services such as chatbots, recommendation systems, or personalized interfaces [44, 50]. These customers perceive AI tools as enhancing value and convenience, while those experiencing discomfort or insecurity may hesitate to adopt them, requiring additional support or intuitive design [29, 51]. Balancing the needs of both technologically ready and reluctant customers is therefore essential to ensure a positive and inclusive CE [48].

CE is inherently multidimensional, integrating cognitive, emotional, and relational components that influence customer reactions and long-term loyalty [52, 53]. Positive experiences such as responsive service, seamless digital platforms, or personalized interactions strengthen satisfaction, while negative experiences quickly lead to churn. Emotional connections are particularly powerful; when customers feel valued through personalization or exceptional service, they are more likely to advocate for the brand, extending their engagement beyond transactions [6, 54, 55]. In summary, CE directly shapes customer satisfaction (CS) and mediates the influence of technology adoption on loyalty and business performance. As AI-driven personalization becomes more widespread, understanding CE provides the link between TR and downstream outcomes such as CS, CP, and FP. This connection positions CE as a central construct in the integrated model developed in this study.

2.3 The Role of AI in Marketing (AIM) and Its Impact on E-Commerce

AI in marketing (AIM) refers to the integration of intelligent technologies such as machine learning, natural language processing, and predictive analytics into marketing activities to enhance customer interactions, streamline decision-making, and improve performance [56]. Unlike traditional data analysis, AIM enables real-time personalization by analyzing customer behavior and preferences at scale, making it a cornerstone of digital competitiveness. Personalization is AIM's key contribution: tailored recommendations, dynamic content, and individualized messages strengthen customer relationships and increase satisfaction [56, 57]. By delivering relevant offers and anticipating needs, AIM fosters deeper engagement and long term loyalty. In parallel, technologies such as chatbots and virtual assistants provide 24/7 personalized support, improving responsiveness and building emotional connections with customers [58, 59]. Predictive analytics further enhances this process by identifying patterns in customer data, allowing businesses to act proactively and prevent dissatisfaction [60].

The rise of AIM has also redefined the omnichannel experience. By integrating websites, mobile apps, and service touchpoints into seamless journeys, businesses can ensure consistency and brand trust, which directly strengthens CE and CS [58]. At the same time, challenges remain: technological anxiety, resistance to change, and lack of organizational readiness can limit adoption [61, 62]. Addressing these barriers is essential for firms to realize the full potential of AIM. Ultimately, AIM contributes not only to customer satisfaction and loyalty but also to measurable business outcomes [63, 64]. Studies confirm that AI-driven personalization, campaign optimization, and real-time customer engagement lead to sales growth [65], profitability [66], and stronger financial performance [67, 68]. Thus, AIM serves as both a driver of improved CE and CS [69], as a direct enabler of customer performance (CP) and financial performance (FP), making it a central construct in the integrated model developed in this study.

2.4 The Relationship Between Customer Satisfaction (CS) and Business Performance

Customer satisfaction (CS) is commonly defined as the degree to which a product or service meets or exceeds customer expectations [70], representing both an emotional and cognitive evaluation [71, 72]. As a key driver of loyalty, retention, and advocacy, CS is widely recognized as a foundation of long-term business success [6, 55]. Several mechanisms explain how CS develops. The disconfirmation of expectations theory suggests satisfaction arises when actual performance matches or exceeds expectations, while perceived value

theory highlights the balance between benefits received and costs incurred [73, 74]. Positive customer experiences, responsive service quality, and emotional connections with a brand have all been shown to strengthen CS and increase loyalty [75, 76]. Conversely, poor experiences or unfulfilled expectations lead to dissatisfaction and churn [77, 78].

CS not only affects immediate behaviors, such as repurchase intention [79] and word-of-mouth [80], but also contributes to broader financial outcomes [81]. Studies consistently show that higher CS improves profitability [82], Return on Assets (ROA) [83], Return on Equity (ROE) [84], and market capitalization [85, 86]. Satisfied customers spend more, return more often [87], and are less sensitive to price fluctuations [88], creating a stable revenue base and strengthening competitive advantage [89, 90]. CS also functions as a mediator between customer experience (CE) [91], organizational practices [92], and financial performance (FP). Engaged employees and seamless digital touchpoints amplify CS, which in turn drives repeat purchases [93], loyalty, and profitability [91, 94]. Integrating CS metrics with financial indicators ensures that firms align customer value with strategic growth, making CS a central metric for evaluating marketing effectiveness [95, 96]. In summary, CS links customer experience to financial outcomes and acts as a pathway through which AIM and TR can influence profitability. Its mediating role makes it a crucial construct in the integrated model developed in this study.

2.5. Assessing Customer Performance (CP) in the Digital Marketing Landscape

Customer performance (CP) refers to how effectively customers engage with and utilize AI driven tools such as recommendation systems, personalized content, and self-service technologies [97] to enhance their experience [98, 99]. Unlike customer satisfaction, which reflects perceptions, CP captures actual behavioral engagement and value co-creation between customers and firms. Three main drivers shape CP. First, personalization is critical: AI powered tools that deliver tailored recommendations and content increase relevance, engagement, and repeat usage [100, 101]. Second, system usability matters: user friendly, intuitive AI interfaces encourage active participation, while complex systems discourage adoption [102, 103]. Third, customer traits such as openness and extraversion influence willingness to experiment with AI enabled features [104], leading to stronger engagement outcomes [105, 106].

Emotional engagement further strengthens CP. Chatbots and virtual assistants can simulate empathy [107], creating meaningful interactions that increase trust and repeat usage [108]. Predictive analytics also improves CP by anticipating customer needs [109] and providing proactive solutions [110]. When customers perceive AI interactions as valuable, they are more likely to deepen their engagement [111], which in turn enhances both CP and CS [112]. Ultimately, CP is not an isolated outcome; it reinforces customer satisfaction and loyalty, thereby contributing to financial performance (FP) [113, 114]. In the integrated model, CP represents the behavioral mechanism through which AIM translates into measurable business success.

2.6. How Customer Satisfaction Drives Financial Performance (FP) in E-Commerce

Financial performance (FP) in e-commerce is typically measured through indicators such as profitability, Return on Assets (ROA), and Return on Equity (ROE), which reflect how effectively a firm generates and sustains growth [70, 115]. Customer satisfaction (CS) has been consistently identified as a key driver of these outcomes, as satisfied customers are more likely to return, repurchase, and advocate for the brand, thereby reducing acquisition costs and increasing customer lifetime value [86, 87]. AIM enhances this process by strengthening CS through personalization, predictive analytics [115], and real-time engagement [116]. Recommendation systems, tailored marketing campaigns [117], and responsive chatbots improve satisfaction and loyalty [118], which in turn translate into higher sales, repeat purchases, and stronger profitability [119, 120]. By aligning AI driven personalization with customer needs, firms can generate sustainable revenue streams and improve efficiency in marketing resource allocation [121].

Research across industries confirms that CS positively influences financial metrics, especially in sectors where customer retention and loyalty are vital, such as retail and services [90, 122]. Moreover, CS functions as a mediator: it translates positive experiences (CE) and behavioral engagement (CP) into long term financial outcomes, making it a crucial link between marketing practices and profitability [91]. In summary, FP is not only a direct outcome of effective AI enabled marketing but also the result of CS and CP working

together to foster loyalty, retention, and advocacy. This mediating role underscores why FP is positioned as the ultimate dependent variable in the integrated model proposed in this study.

2.7 Summary of Literature Review

The literature review has demonstrated that technology readiness (TR) and AI in marketing (AIM) are essential drivers of digital transformation in e-commerce, influencing customer experience (CE), customer satisfaction (CS), and customer performance (CP), which ultimately determine financial performance (FP). Prior studies confirm the significance of each construct individually, yet most have examined them in isolation, failing to capture the cumulative and interdependent effects of readiness, adoption, and outcomes. This review highlights three key insights. First, TR shapes both organizational capacity and consumer willingness to adopt AI enabled tools, establishing the conditions for effective AIM. Second, AIM enhances CE and CS through personalization, predictive analytics, and automation, thereby strengthening engagement and loyalty. Third, CS and CP serve as crucial pathways that translate these technological and experiential factors into long term FP. Despite these advances, existing research lacks an integrated model that combines TR, AIM, CE, CS, CP, and FP within a unified framework. Addressing this gap is vital for understanding how AI adoption creates measurable value for e-commerce businesses. This study responds to that need by developing and empirically testing a model that connects these six constructs, offering both theoretical contributions and practical guidance for firms seeking to leverage AI for sustainable performance.

3. Research Methods

3.1 Research Design and Data Collection

This study employed a quantitative survey design to examine the impact of technology readiness (TR), AI in marketing (AIM), customer experience (CE), customer satisfaction (CS), customer performance (CP), and financial performance (FP) in e-commerce. Respondents were business owners actively implementing AI tools such as chatbots, recommendation systems, and AI-generated content. Data were collected in August 2024 using an online questionnaire distributed via Google Forms, resulting in 314 valid responses. The survey instrument captured demographic information and items related to the study constructs. The final sample was dominated by younger respondents (aged 25–34), predominantly male, with bachelor's degrees, and from small-sized enterprises. While this profile reflects early AI adopters in Indonesian e-commerce, it introduces demographic concentration and sampling bias, which limit the generalizability of findings to broader populations. A target of 334 responses was set to ensure statistical reliability. Although the final sample size fell slightly short, 314 respondents exceeded the '10 times rule' and other guidelines for PLS-SEM, making it sufficient to test the proposed structural model [123]. As the study relied on a single self-reported survey, there is a risk of common method bias (CMB). To reduce this risk, several procedural remedies were implemented, including assuring respondent anonymity and randomizing item order. Nonetheless, the possibility of CMB cannot be fully eliminated and should be considered when interpreting the results. Overall, the survey design is appropriate for the study's exploratory objective of identifying predictive relationships between TR, AIM, CE, CS, CP, and FP, rather than establishing strict causal inference. The structured data collection process ensures alignment with the research objectives and provides a valid basis for empirical testing of the proposed model.

3.2 Research Model and Hypothesis Development

The conceptual framework for this study integrates technology readiness (TR), AI in marketing (AIM), customer experience (CE), customer satisfaction (CS), customer performance (CP), and financial performance (FP) to explain how technology adoption influences business outcomes. In this model, TR and AIM are proposed as key antecedents, while CE, CS, and CP act as mediators linking adoption to financial performance. According to the Technology Readiness Index (TRI), optimism and innovativeness increase openness to adopting new technologies, while discomfort and insecurity act as barriers [39, 40]. Higher TR enables smoother integration of AI tools into marketing strategies, improving personalization, responsiveness, and

ultimately satisfaction. This brings us to H1, which proposes that TR significantly influences CS by facilitating the adoption and effective use of AI technologies in marketing strategies [123].

H1: TR significantly influences CS

Customer experience (CE) encompasses all interactions across touchpoints product use, service encounters, and digital engagement and strongly shapes customer satisfaction (CS). According to service quality and disconfirmation theory, positive experiences that meet or exceed expectations foster trust, value, and loyalty [46, 52, 53]. This brings us to H2, which posits that CE significantly influences CS by shaping perceptions of value through positive interactions.

H2: CE significantly influences CS

AI in marketing (AIM) further enhances satisfaction by improving the quality of customer experiences. Through personalization, predictive analytics, and automated interactions, AIM allows businesses to anticipate needs and deliver timely, relevant engagement, leading to higher CS [5, 56]. This brings us to H3, which proposes that AIM influences CS by leveraging AI tools to personalize and optimize customer interactions, directly enhancing satisfaction.

H3: AIM significantly influences CS

Customer performance (CP) refers to how effectively customers engage with AI driven tools such as personalized content, recommendation systems, and automated support to improve their overall experience [100, 102]. AIM facilitates this engagement by empowering customers with relevant information, intuitive interfaces, and predictive insights, thereby enhancing their ability to interact meaningfully with brands. This brings us to H4, which proposes that AIM influences CP by equipping customers with tools that support informed decisions and efficient interactions, ultimately strengthening engagement.

H4: AIM significantly influences CP

Financial performance (FP) reflects a firm's ability to sustain profitability and growth, and is strongly shaped by customer engagement and loyalty. AIM supports FP by optimizing marketing campaigns, delivering personalized services, and fostering satisfaction that drives repeat purchases and advocacy [115, 121]. This brings us to H5, which proposes that AIM influences FP by enhancing customer engagement and satisfaction, leading to improved profitability and market competitiveness.

H5: AIM significantly influences FP

Customer satisfaction (CS) is one of the most consistent predictors of financial performance (FP). Higher CS strengthens loyalty, encourages repeat purchases, and generates positive word-of-mouth, all of which reduce acquisition costs and create stable revenue streams [92, 122]. CS also enhances brand advocacy, attracting new customers and sustaining long-term profitability. This brings us to H6, which proposes that CS influences FP by fostering loyalty, driving repeat business, and promoting advocacy that directly contribute to improved financial outcomes.

H6: CS significantly influences FP

Figure 1 illustrates the hypothesized model, showing the direct and mediated paths from TR and AIM through CE, CS, and CP toward FP. The framework highlights the cascading effects of technology readiness and AI adoption on customer outcomes and ultimately on financial performance, serving as a basis for the empirical analysis in this study.

3.3 Measurement Instruments

The accuracy of this study depends on the proper measurement of the six key constructs: technology readiness (TR), AI in marketing (AIM), customer experience (CE), customer satisfaction (CS), customer performance (CP), and financial performance (FP). To ensure validity and reliability, measurement scales were adapted from prior studies and established frameworks, with modifications made to fit the context of e-commerce and AI adoption. Content validity was strengthened through a review of relevant literature and consultation with academic experts. Particular care was taken to avoid conceptual overlap between constructs, especially AIM and CE. AIM items emphasized technology-enabled marketing functions such as personalization, predictive analytics, and automation, while CE items focused on customers' perceptions of service interactions and touchpoints. This distinction ensured that constructs captured different but complementary dimensions of the research model. Each construct was assessed using multiple Likert scale

items to capture its multidimensional nature. All items were drawn from validated instruments in prior research and were tested for clarity and contextual relevance through a pilot study. The use of multi item scales supports comprehensive measurement and allows for later testing of convergent validity, discriminant validity, and internal consistency reliability in the PLS-SEM analysis. Table 1 presents the measurement items and their sources, providing a clear overview of how TR, AIM, CE, CS, CP, and FP were operationalized in this study.

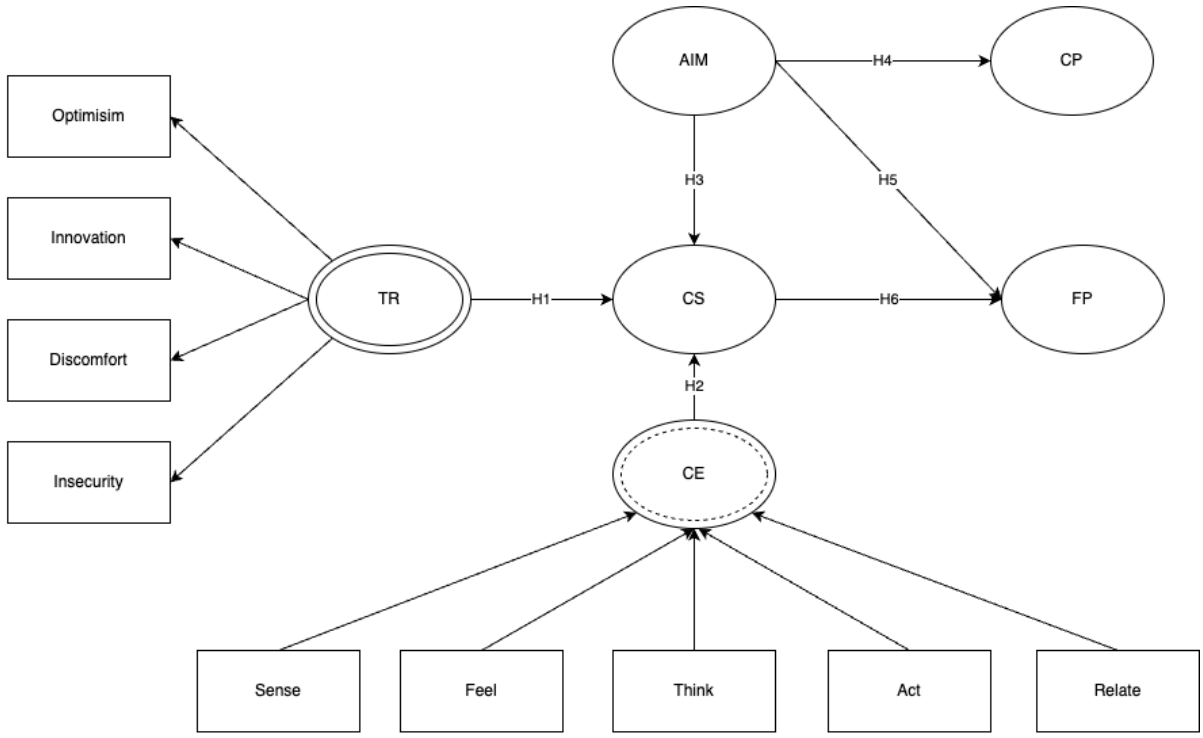


Figure 1. Research model framework

3.4 Data Analysis

The data collected through the survey were analyzed using SmartPLS 4.0, which is appropriate for complex models with multiple constructs and indicators, and for data that may not meet the strict assumptions of covariance-based SEM [129]. This approach allowed for simultaneous assessment of the measurement and structural models. Reliability was assessed using Cronbach's alpha and composite reliability (CR), with thresholds of 0.70 indicating acceptable internal consistency. Convergent validity was evaluated through average variance extracted (AVE > 0.50), while discriminant validity was tested using both the Fornell Larcker criterion and the heterotrait–monotrait (HTMT) ratio (HTMT < 0.90). Variance inflation factor (VIF) values were also examined to check for multicollinearity, with all values below 5, indicating no critical collinearity issues. Once measurement validity was established, the structural model was assessed. Path coefficients (β) and their significance were estimated through bootstrapping with 5,000 resamples. Relationships were considered significant when $t > 1.96$ at the 5% level. Coefficient of determination (R^2) values were reported for CS, CP, and FP, with values of 0.20 or higher considered acceptable. Effect sizes (f^2) were calculated to evaluate the contribution of each predictor (0.02 = small, 0.15 = medium, 0.35 = large). Model fit was evaluated using the standardized root mean square residual (SRMR < 0.08) and normed fit index (NFI > 0.90). Predictive relevance (Q^2) values were obtained using blindfolding procedures, with values greater than zero confirming meaningful predictive capacity. Together, these analyses ensured that the constructs were measured reliably, discriminated clearly from one another, and that the structural model provided both explanatory power and predictive relevance. This approach allowed robust testing of the hypothesized relationships between TR, AIM, CE, CS, CP, and FP in the e-commerce context.

Table 1. Questionnaire items in measurement instruments

Variable		Item	Source
CE	SENSE1	My AI tools speed up marketing tasks in my enterprise.	Adapted from [124]
	SENSE2	AI systems simplify marketing tasks for my enterprise.	
	SENSE3	AI in marketing saves money on tasks.	
	FEEL1	AI tools improve marketing performance in my enterprise.	
	FEEL2	AI enhances marketing strategy effectiveness.	
	FEEL3	AI systems help correct marketing errors.	
	THINK1	AI helps my enterprise meet future marketing goals.	
	THINK2	AI tools help acquire new marketing knowledge.	
	ACT1	AI helps acquire new marketing skills.	
	ACT2	AI tools generate innovative marketing ideas.	
	RELATE1	AI systems improve customer relationships.	
	RELATE2	AI tools make customer interactions more personalized.	
	RELATE3	AI in marketing strengthens our connection with customers.	
TR	OPT1	AI technologies improve the consumer quality of life.	Adapted from [125]
	OPT2	AI gives consumers more flexibility in brand interactions.	
	INNO1	I appreciate AI tools that fit my enterprise's needs.	
	INNO2	AI allows my enterprise to interact with customers beyond business hours.	
	DISC1	I feel uneasy using AI tools I don't fully understand.	
	DISC2	AI in marketing feels intrusive, especially when collecting personal data.	
	DISC3	Implementing AI-powered chatbots in customer service is challenging.	
	INSEC1	I'm concerned about customer data security with AI systems.	
	INSEC2	I'm unsure if AI systems will always fulfill promises.	
AIM	AIM1	AI predicts customer needs for my enterprise.	Adapted from [2]
	AIM2	AI eliminates human errors in marketing promotion.	
	AIM3	AI helps interact with internet users via analyzed data.	
CP	CP1	AI tools improve products and services based on feedback.	Adapted from [126]
	CP2	Customers think we excel in AI-driven innovations.	
	CP3	Our company outperforms competitors in AI for product development.	
CS	CS1	I am happy with our AI-powered services.	Adapted from [127]
	CS2	I am satisfied with our AI-driven marketing procedures.	
	CS3	I enjoy using AI-based marketing tools and recommendations.	
FP	FP1	AI in marketing boosts our profitability.	Adapted from [128]
	FP2	AI-driven strategies contribute to profit growth.	
	FP3	AI tools help achieve higher sales growth.	

4. Results and Discussion

4.1 Descriptive Statistics

The sample consisted of 314 Indonesian e-commerce business owners actively using AI in marketing. Table 2 presents the demographic breakdown. The majority of respondents were male (60.19%), aged 25–34 (46.18%), held a bachelor's degree (65.61%), and operated small enterprises with fewer than 50 employees

(71.34%). Nearly half had been in business for 2–5 years (46.82%), and most had used AI tools for over one year (71.02%). More than half (52.55%) reported business growth in the past year, while 40.76% remained stable and 6.69% reported a decline. This profile reflects the characteristics of early AI adopters in Indonesian e-commerce young, well-educated entrepreneurs managing small to medium sized firms consistent with global technology adoption patterns. However, the demographic concentration introduces limitations: the findings may not generalize to older, less-educated business owners or to large scale enterprises. As the data were collected using convenience sampling, caution should be exercised when extending these results to the broader e-commerce population. Nevertheless, the demographic profile provides valuable context for interpreting the role of technology readiness and AI in driving business outcomes.

Table 2. Demography data

Demography	Category	Frequency	Percentage
Age	Under 25	60	19.11%
	25-34	145	46.18%
	35-44	75	23.89%
	45 and above	34	10.83%
Gender	Male	189	60.19%
	Female	125	39.81%
Education Level	High school or less	53	16.88%
	Bachelor's degree	206	65.61%
	Master's degree or higher	55	17.52%
Business Size	1-10 employees	119	37.90%
	11-50 employees	105	33.44%
	51-200 employees	49	15.61%
	201+ employees	41	13.06%
Years in Business	Less than 2 years	68	21.66%
	2-5 years	147	46.82%
	6-10 years	72	22.93%
	10+ years	27	8.60%
AI Adoption Experience	Less than 1 year	91	28.98%
	1 year and more	223	71.02%
Business Growth Rate (Last 12 months)	Decreased	21	6.69%
	Stayed the same	128	40.76%
	Increased	165	52.55%

4.2 Measurement Model Evaluation

The reliability and validity of the constructs were assessed using Cronbach's alpha, composite reliability (CR), average variance extracted (AVE), and factor loadings. Cronbach's alpha and CR values for all constructs exceeded the recommended threshold of 0.70, indicating strong internal consistency. AVE values were above 0.50, confirming convergent validity, and factor loadings were generally above 0.70. Items with slightly lower loadings were retained only when they contributed meaningfully to content validity. Table 3 shows the results of the reliability and convergent validity analysis.

Table 3. Reliability analysis and convergent validity

Measurement	Factor Loading/Weight	Composite Reliability	AVE
SENSE	0.244	N/A (Formative Construct)	N/A (Formative Construct)
FEEL	0.239		
THINK	0.221		
ACT	0.208		
RELATE	0.253		
SENSE1	0.726	0.735	0.833
SENSE2	0.889		
SENSE3	0.795		
FEEL1	0.702	0.895	0.843
FEEL2	0.754		
FEEL3	0.907		
THINK1	0.776	0.724	0.975
THINK2	0.726		
ACT1	0.847	0.734	0.822
ACT2	0.775		
RELATE1	0.73	0.87	0.734
RELATE2	0.802		
RELATE3	0.971		
OPT1	0.959	0.787	0.737
OPT2	0.752		
INNO1	0.733	0.769	0.764
INNO2	0.709		
DISC1	0.899	0.846	0.722
DISC2	0.728		
DISC3	0.836		
INSEC1	0.87	0.708	0.776
INSEC2	0.789		
AIM1	0.715	0.743	0.759
AIM2	0.872		
CP1	0.877	0.82	0.827
CP2	0.733		
CP3	0.935		
CS1	0.755	0.71	0.963
CS2	0.778		
CS3	0.897		
FP1	0.714	0.726	0.747
FP2	0.872		
FP3	0.729		

Discriminant validity was evaluated using both the Fornell Larcker criterion and the heterotrait–monotrait (HTMT) ratio. Fornell Larcker results showed that each construct's square root of AVE exceeded its correlations with other constructs, while HTMT values were all below 0.90, confirming that constructs were empirically distinct. Particular attention was given to AIM and CE, where items were reviewed to minimize conceptual overlap. Table 4 shows the Fornell Larcker discriminant validity results, with diagonal values exceeding off diagonal correlations.

Table 4. Discriminant validity

	ACT	AIM	CP	CS	DISC	FEEL	FP	INNO	INSEC	OPT	RELATE	SENSE	THINK
ACT	0.907												
AIM	0.315	0.871											
CP	0.356	0.162	0.909										
CS	0.346	0.584	0.101	0.981									
DISC	0.422	0.353	0.576	0.405	0.850								
FEEL	0.532	0.305	0.459	0.581	0.332	0.918							
FP	0.321	0.548	0.392	0.142	0.414	0.306	0.864						
INNO	0.501	0.497	0.405	0.322	0.311	0.483	0.521	0.874					
INSEC	0.409	0.327	0.506	0.466	0.456	0.445	0.489	0.111	0.881				
OPT	0.442	0.482	0.567	0.513	0.107	0.538	0.317	0.539	0.439	0.858			
RELATE	0.522	0.567	0.454	0.325	0.305	0.421	0.359	0.357	0.302	0.405	0.857		
SENSE	0.112	0.415	0.346	0.154	0.409	0.143	0.537	0.309	0.346	0.305	0.117	0.913	
THINK	0.405	0.323	0.406	0.326	0.508	0.484	0.462	0.472	0.542	0.422	0.509	0.152	0.987

Variance inflation factor (VIF) values for all indicators were below 5, indicating that multicollinearity was not a concern. Together, these results provide strong evidence of construct reliability, convergent validity, and discriminant validity.

4.3 Structural Model Evaluation

The structural model was tested after confirming the adequacy of the measurement model. Path coefficients (β) and their significance were estimated via bootstrapping with 5,000 resamples. R^2 values for CS, CP, and FP exceeded 0.20, confirming substantial explanatory power. Table 5 shows the results of the structural model, including path coefficients, t-values, and effect sizes. Model fit indices indicated acceptable overall fit (SRMR = 0.072; NFI = 0.91). Predictive relevance (Q^2) values were greater than zero for CS, CP, and FP, supporting predictive validity. Effect sizes (f^2) showed that TR and AIM contributed medium effects on CS, while AIM had a strong effect on CP.

Table 5. Inner model results (summary)

Hypotheses	Path	Path Coefficien	t-value	result
H1	TR → CS	0.723	3.673	Supported
H2	CE → CS	0.552	2.725	Supported
H3	AIM → CS	0.566	4.572	Supported
H4	AIM → CP	0.964	9.336	Supported
H5	AIM → FP	0.681	12.631	Supported
H6	CS → FP	0.864	5.388	Supported

All six hypotheses were supported, indicating strong positive relationships between constructs. TR and AIM significantly influenced CS, while AIM also showed strong effects on CP and FP. CS strongly predicted FP, confirming its mediating role between experiences and financial outcomes. However, the coefficients for AIM → CP (β = 0.964) and CS → FP (β = 0.864) were unusually high, suggesting possible conceptual overlap or model over-specification. These results should therefore be interpreted cautiously, and future research should test simplified frameworks to validate these relationships. Figure 2 illustrates the inner model results.

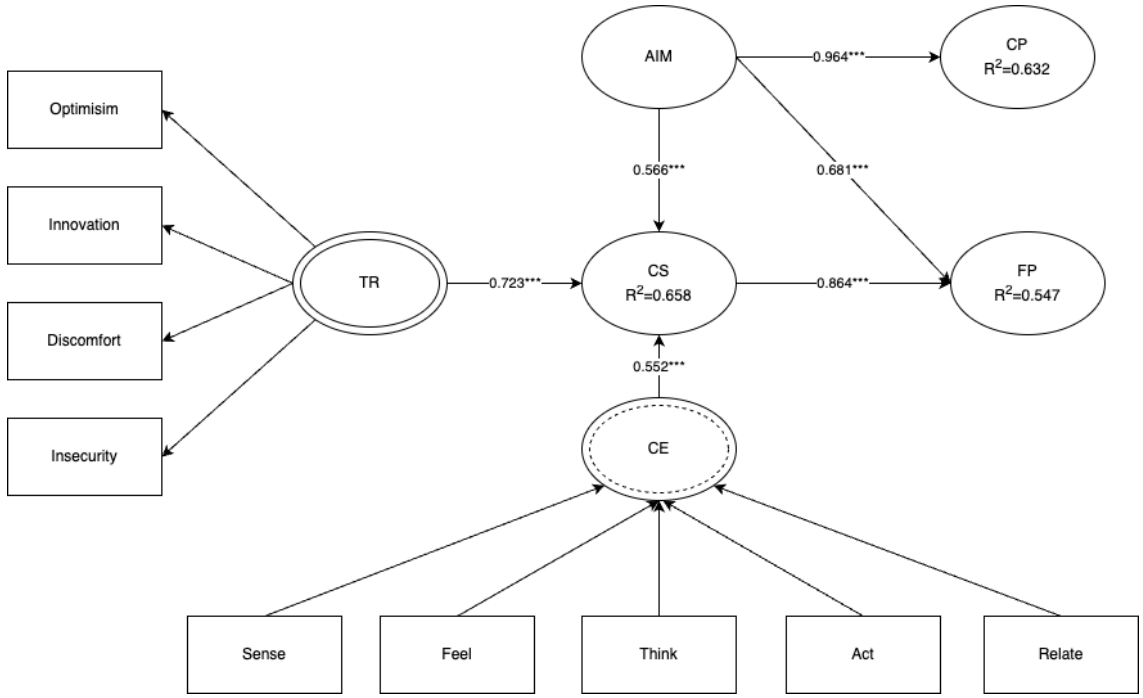


Figure 2. Inner model results framework

4.4 Testing of Mediating Effect

The mediating role of customer satisfaction (CS) was tested for the relationships between TR, AIM, CE, and financial performance (FP). Mediation was first examined using the Sobel test, and then confirmed through bootstrapping with 5,000 resamples, which is recommended in PLS-SEM because it does not assume normality of indirect effects. Table 6 shows the results of the mediation analysis. All three indirect paths were significant, confirming CS as a key mediator in transforming technology readiness, AI adoption, and customer experience into improved financial performance.

Table 6. Sobel test results

Construct	Construct Relationship	t-value	Sobel Test z-Value
TR → CS → FP	TR → CS	3.673	25.68
	CS → FP	5.388	
AIM → CS → FP	AIM → CS	4.572	28.245
	CS → FP	5.388	
CE → CS → FP	CE → CS	2.725	21.709
	CS → FP	5.388	

These findings underscore CS's pivotal role in converting technological and experiential investments into financial outcomes. Higher levels of readiness (TR) and greater use of AI in marketing (AIM) improve

satisfaction, which in turn drives loyalty, repeat purchases, and profitability. Similarly, positive customer experiences (CE) translate into stronger satisfaction and better financial results. However, the high z-values and strong indirect effects suggest potential model inflation due to overlapping constructs or over-specification. These results should therefore be interpreted cautiously. Future research should refine construct measures and test alternative mediation pathways to validate these findings.

5. Conclusions

This research examined the relationships between technology readiness (TR), AI in marketing (AIM), customer experience (CE), customer satisfaction (CS), customer performance (CP), and financial performance (FP) in Indonesian e-commerce. The findings suggest that TR and AIM play critical roles in shaping CE and CS, which in turn influence CP and FP. CS and CP emerged as important pathways that help explain how technological investments are translated into business outcomes. However, the unusually strong coefficients in some paths indicate potential model inflation, suggesting that future studies should test simplified frameworks to validate these mediation effects. From a practical perspective, the study underscores the strategic importance of investing not only in AI technologies such as chatbots, recommendation systems, and predictive analytics but also in building organizational and individual readiness for adoption. Managers should invest in digital skills training to strengthen TR, personalize customer experiences responsibly while safeguarding data privacy, and treat CS metrics as strategic performance indicators rather than secondary measures. By aligning technological readiness with AI-driven personalization, firms can enhance customer loyalty, engagement, and ultimately profitability. The study also acknowledges important limitations. The sample was skewed toward younger, male, bachelor-educated entrepreneurs managing small firms, limiting generalizability to larger or more diverse business contexts. The cross-sectional design prevents strong causal inferences, and reliance on self-reported survey data raises the possibility of common method bias. Furthermore, some overlap between constructs (e.g., AIM and CE) may have contributed to inflated path coefficients. These limitations highlight the need for future studies to replicate and refine the model in different contexts, incorporate objective performance data, and adopt longitudinal designs to capture the long-term impact of AI adoption. Overall, this study contributes to the literature by integrating TR, AIM, CE, CS, CP, and FP into a unified framework, offering insights into how technology readiness and AI-driven marketing strategies influence both customer outcomes and financial performance. While the results demonstrate the potential of AI in e-commerce growth, they also emphasize the need for cautious interpretation and continued refinement of measurement and theoretical models.

Author Contributions: Conceptualization, T.H. and M.D.; methodology, T.H. and R.W.; software, A.M.W.; validation, T.H. and M.D.; formal analysis, R.W.; investigation, T.H.; resources, T.H.; data curation, R.W. and A.M.W.; writing—original draft preparation, M.D.; writing—review and editing, T.H.; visualization, A.M.W.; supervision, T.H.; project administration, R.W.; funding acquisition, T.H. All authors have read and agreed to the published version of the manuscript

Funding: This research was funded by the Ministry of Higher Education, Science and Technology of Indonesia.

Conflicts of Interest: The authors declare no conflict of interest

References

[1] Ziakis, C. Artificial Intelligence in Digital Marketing: Insights From a Comprehensive Review. *Information* **2023**, *14*(12), 664. https://doi.org/10.3390/info14120664

[2] Abrokwah-Larbi, K.; Awuku-Larbi, Y. The Impact of Artificial Intelligence in Marketing on the Performance of Business Organizations: Evidence from SMEs in an Emerging Economy. *J. Entrep. Emerg. Econ.* **2023**, *16*(4), 1090–1117. https://doi.org/10.1108/JEEE-07-2022-0207

[3] Pratama, S. F.; Wahid, A. M. Fraudulent Transaction Detection in Online Systems Using Random Forest and Gradient Boosting. *Journal of Cyber Law* **2025**, *1*(1).

[4] Buchdadi, A. D.; Al-Rawahna, A. S. M. Temporal Crime Pattern Analysis Using Seasonal Decomposition and k-Means Clustering. *Journal of Cyber Law* **2025**, *1*(1).

[5] Raji, M. A. E-Commerce and Consumer Behavior: A Review of AI-powered Personalization and Market Trends. *GSC Adv. Res. Rev.* **2024**, *18*(3), 66–77. https://doi.org/10.30574/gscarr.2024.18.3.0090

[6] Deng, Z.; Lu, Y.; Wei, K. K.; Zhang, J. Understanding Customer Satisfaction and Loyalty: An Empirical Study of Mobile Instant Messages in China. *Int. J. Inf. Manag.* **2010**, *30*(4), 289–300. https://doi.org/10.1016/j.ijinfomgt.2009.10.001

[7] Hasibuan, M; Fikri, R.R.N. Sectoral Disparities in the Digital Workplace: A Comparative Statistical Analysis of Remote Work Patterns and Productivity Scores in the Evolving Digital Society. *Journal of Digital Society*. **2025**, *1* (3). https://doi.org/10.63913/jds.v1i3.53.

[8] Flavián, C.; Pérez-Rueda, A.; Belanche, D.; Casaló, L. V. Intention to Use Analytical Artificial Intelligence (AI) in Services – The Effect of Technology Readiness and Awareness. *J. Serv. Manag.* **2021**, *33*(2), 293–320. https://doi.org/10.1108/josm-10-2020-0378

[9] Udariansyah, D.; Kurniawan, T. B.; Dewi, D. A.; Zakaria, M. Z.; Hanan, N. S. A. Recommender System for Book Review Based on Clustering Algorithms. *J. Appl. Data Sci.* **2025**, *6*(1). https://doi.org/10.47738/jads.v6i1.492

[10] Usman, U.; Yunita, F.; Ridha, M. R. Improving Classification Accuracy of Local Coconut Fruits with Image Augmentation and Deep Learning Algorithm CNN. *J. Appl. Data Sci.* **2025**, *6*(1). https://doi.org/10.47738/jads.v6i1.389

[11] Fc, L. L. V.; Anam, M. K.; Bukhori, S.; Mahamad, A. K.; Saon, S.; Nyoto, R. L. V. The Development of Stacking Techniques in Machine Learning for Breast Cancer Detection. *J. Appl. Data Sci.* **2025**, *6*(1). https://doi.org/10.47738/jads.v6i1.416

[12] Deng, X.; Li, M.; Deng, S.; Wang, L. Hybrid Gene Selection Approach Using XGBoost and Multi-Objective Genetic Algorithm for Cancer Classification. *Med. Biol. Eng. Comput.* **2022**, *60*(3), 663–681. https://doi.org/10.1007/s11517-021-02476-x

[13] Henderi, H.; Asro, A.; Sulaiman, A.; Kurniawan, T. B.; Dewi, D. A.; AlQudah, M. Utilizing Sentiment Analysis for Reflect and Improve Education in Indonesia. *J. Appl. Data Sci.* **2025**, *6*(1). https://doi.org/10.47738/jads.v6i1.527

[14] S, V. K. P, P; Batumalay, M. Examining the Association Between Social Media Use and Self-Reported Social Energy Depletion: A Machine Learning Approach. *Journal of Digital Society*. **2025**, *1*(3). https://doi.org/10.63913/jds.v1i3.50.

[15] Guballo, J. O. Temporal Analysis of Blockchain Transactions in the Metaverse Using Time Series. *Int. J. Res. Metav.* **2025**, *2*(3), 195–206. https://doi.org/10.47738/ijrm.v2i3.32

[16] Hery, H.; Haryani, C. User Transaction Patterns in Smart Contracts Based on Call Frequency and Transfer Value. *Int. J. Res. Metav.* **2025**, *2* (3), 236–247. https://doi.org/10.47738/ijrm.v2i3.35

[17] Colvin, C.; Goh, A. Validation of the Technology Acceptance Model for Police. *J. Crim. Justice* **2005**, *33*(1), 89–95. https://doi.org/10.1016/j.jcrimjus.2004.10.009

[18] Daoud, R. A.; Amine, A.; Abouelmehdi, K.; Razouk, A. Student Engagement in E-Learning During Crisis. *J. Appl. Data Sci.* **2025**, *6* (1). https://doi.org/10.47738/jads.v6i1.458

[19] Ma, Q.; Liu, L. The Technology Acceptance Model. *J. Organ. End User Comput.* **2004**, *16*(1), 59–72. https://doi.org/10.4018/joeuc.2004010104

[20] Dewi, D. A.; Kurniawan, T. B. Analyzing the Impact of Social Media and Influencer Endorsements on Game Revenue Using Multiple Linear Regression in the Metaverse. *Int. J. Res. Metav.* **2025**, *2*(2), 167–182. https://doi.org/10.47738/ijrm.v2i2.29

[21] Maidin, S. S.; Yang, Q.; Samson, A. S. Analyzing the Evolution of AI-Generated Art Styles Using Time Series Analysis: A Trend Study on NFT Artworks. *J. Digit. Mark. Digit. Curr.* **2025**, *2*(2), 205–229. https://doi.org/10.47738/jdmdc.v2i2.32

[22] Warmayana, I. G. A. K.; Yamashita, Y.; Oka, N. Predicting FIFA Ultimate Team Player Market Prices Using XGBoost Algorithms. *Int. J. Res. Metav.* **2025**, *2*(2), 140–153. https://doi.org/10.47738/ijrm.v2i2.25

[23] Erumban, A. A.; Jong, S. B. Cross-Country Differences in ICT Adoption: A Consequence of Culture? *J. World Bus.* **2006**, *41*(4), 302–314. https://doi.org/10.1016/j.jwb.2006.08.005

[24] Özbilen, P. The Impact of National Culture on New Technology Adoption by Firms: A Country Level Analysis. *Int. J. Innov. Manag. Technol.* **2017**, 299–305. https://doi.org/10.18178/ijimt.2017.8.4.745

[25] Utomo, F. S.; Suryana, N.; Azmi, M. S. Factors Influencing User Adoption of Mobile Payment System. *J. Digit. Mark. Digit. Curr.* **2025**, *2*(2), 135–156. https://doi.org/10.47738/jdmdc.v2i2.31

[26] Izumi, C.; Ghaffar, S. A.; Setiawan, W. C. Enhancing Customer Satisfaction in E-commerce Using Text Mining and Sentiment Analysis. *J. Digit. Mark. Digit. Curr.* **2025**, *2*(1), 1–25. https://doi.org/10.47738/jdmdc.v2i1.26

[27] Doan, M. L. Volatility and Risk Assessment of Blockchain Cryptocurrencies Using GARCH Modeling. *J. Digit. Mark. Digit. Curr.* **2025**, *2*(1), 93–113. https://doi.org/10.47738/jdmdc.v2i1.25

[28] Ramírez-Gutiérrez, A. G. Systems Approach for the Adoption of New Technologies in Enterprises. *Systems* **2023**, *11* (10), 494. https://doi.org/10.3390/systems11100494

[29] Zimmermann, L. Adoption of New Technology Vaccines. *J. Mark.* **2024**, *88*(4), 1–21. https://doi.org/10.1177/00222429231220295

[30] Chen, K. Decentralization Management in the Context of Chinese History and Modern Financial Services. *J. Intell. Syst. Theory Appl.* **2020**, 46–59. https://doi.org/10.38016/jista.696791

[31] Ong, J. W.; Rahim, M. F. A.; Lim, W.; Nizat, M. N. M. Agricultural Technology Adoption as a Journey: Proposing the Technology Adoption Journey Map. *Int. J. Technol.* **2022**, *13*(5), 1090. https://doi.org/10.14716/ijtech.v13i5.5863

[32] Li, S.; Pigultong, M. Predicting Customer Conversion in Digital Marketing: Analyzing the Impact of Engagement Metrics Using Logistic Regression, Decision Trees, and Random Forests. *J. Digit. Mark. Digit. Curr.* **2025**, *2*(3), 298–322. https://doi.org/10.47738/jdmdc.v2i2.34

[33] Fernandes, A. Knowledge, Technology Adoption and Financial Innovation. *SSRN Electron. J.* **2005**. https://doi.org/10.2139/ssrn.954743

[34] Evelyn, E.; Suryodiningrat, S. P. Assessing the Impact of Laptop Condition on Pricing Using Statistical Analysis: Insights for Digital Marketing Strategies on eBay. *J. Digit. Mark. Digit. Curr.* **2025**, *2*(3), 230–251. https://doi.org/10.47738/jdmdc.v2i3.35

[35] Vaittinen, E.; Martinsuo, M.; Ortt, R. Business Customers' Readiness to Adopt Manufacturer's New Services. *J. Serv. Theory Pract.* **2017**, *28*(1), 52–78. https://doi.org/10.1108/jstp-03-2017-0053

[36] Sulistyowati. Measurement Analysis of the Level of E-Commerce Adoption Readiness in SMEs Using Technology Readiness Index Method. *J. Sistim Inf. Dan Teknol.* **2023**, 193–197. https://doi.org/10.60083/jsisfotek.v5i2.263

[37] Shah, T. R. Linking Technology Readiness and Customer Engagement: An AI-enabled Voice Assistants Investigation. *Foresight* **2023**, *26*(1), 136–154. https://doi.org/10.1108/fs-10-2021-0195

[38] Qasem, Z. The Effect of Positive TRI Traits on Centennials Adoption of Try-on Technology in the Context of E-Fashion Retailing. *Int. J. Inf. Manag.* **2021**, *56*, 102254. https://doi.org/10.1016/j.ijinfomgt.2020.102254

[39] Kumar, V.; Dixit, A.; Javalgi, R. G.; Dass, M. Research Framework, Strategies, and Applications of Intelligent Agent Technologies (IATs) in Marketing. *J. Acad. Mark. Sci.* **2015**, *44*(1), 24–45. https://doi.org/10.1007/s11747-015-0426-9

[40] Gao, L.; Li, G.; Tsai, F.-S.; Gao, C.; Zhu, M.; Qu, X. The Impact of Artificial Intelligence Stimuli on Customer Engagement and Value Co-Creation: The Moderating Role of Customer Ability Readiness. *J. Res. Interact. Mark.* **2022**, *17*(2), 317–333. https://doi.org/10.1108/jrim-10-2021-0260

[41] Poushneh, A.; Vasquez-Parraga, A. Z. The Role of Customer Readiness and Participation in Non-Technology-Based Service Delivery. *J. Consum. Mark.* **2018**, *35*(6), 588–600. https://doi.org/10.1108/jcm-11-2016-2006

[42] Torkzadeh, S.; Zolfagharian, M.; Yazdanparast, A.; Gremler, D. D. From Customer Readiness to Customer Retention: The Mediating Role of Customer Psychological and Behavioral Engagement. *Eur. J. Mark.* **2022**, *56*(7), 1799–1829. https://doi.org/10.1108/ejm-03-2021-0213

[43] Doan, M. L. Sentiment Classification of Bitcoin-Related Tweets Using VADER: Analyzing Temporal Sentiment Trends in Cryptocurrency Markets. *J. Curr. Res. Blockchain.* **2025**, *2*(2), 88–102. https://doi.org/10.47738/jcrb.v2i2.31

[44] Pham, L.; Williamson, S.; Lane, P. L.; Limbu, Y. B.; Nguyen, P. T. H.; Coomer, T. Technology Readiness and Purchase Intention: Role of Perceived Value and Online Satisfaction in the Context of Luxury Hotels. *Int. J. Manag. Decis. Mak.* **2020**, *19* (1), 91. https://doi.org/10.1504/ijmdm.2020.104208

[45] Khosa, J.; Olanipekun, A. Analyzing GPU Efficiency in Cryptocurrency Mining: A Comparative Study Using K-Means Clustering on Algorithm Performance Metrics. *J. Curr. Res. Blockchain.* **2025**, *2*(2), 119–134. https://doi.org/10.47738/jcrb.v2i2.34

[46] Warmayana, I. G. A. K.; Yamashita, Y.; Oka, N. Analyzing the Impact of School Type on Student Outcomes Across Counties: A Comparative Study Using ANOVA. *Artificial Intelligence in Learning* **2025**, *1*(1), Art. 1. https://doi.org/10.63913/jcl.v1i2.8

[47] Sukmana, H. T.; Oh, L. K. Evaluating the Impact of Affirmative Action on Student Selection Outcomes: A Data Mining Approach Using SKD Test Performance at STMKG. *Artificial Intelligence in Learning* **2025**, *1*(1), Art. 1. https://doi.org/10.63913/jcl.v1i2.7

[48] Shim, H. S.; Han, S. L.; Ha, J. The Effects of Consumer Readiness on the Adoption of Self-Service Technology: Moderating Effects of Consumer Traits and Situational Factors. *Sustainability* **2020**, *13*(1), 95. https://doi.org/10.3390/su13010095

[49] Basri, W. S.; Ayu, A. L. Risk Management in Information Systems: Applying ISO 31000:2018 and ISO/IEC 27001:2022 Controls at PMI's Central Clinic. *Int. J. Appl. Inf. Manag.* **2024**, *4*(1). https://doi.org/10.47738/ijaim.v4i1.70

[50] Nugroho, K; Turino. Anomaly Detection in Corporate Balance Sheets for Financial Risk Assessment Using Isolation Forest from 2020 to 2023. *Int. J. Appl. Inf. Manag*. **2025**, *5*(3). https://doi.org/10.47738/ijaim.v5i3.107

[51] Lenus, L. Discovering Co-Occurrence Patterns Among Blockchain Address Categories Using the FP-Growth Association Mining Algorithm. *J. Curr. Res. Blockchain.* **2025**, *2*(1), 41–62. https://doi.org/10.47738/jcrb.v2i1.24

[52] Pei, X.-L.; Guo, J.-N.; Wu, T.; Zhou, W.; Yeh, S. Does the Effect of Customer Experience on Customer Satisfaction Create a Sustainable Competitive Advantage? A Comparative Study of Different Shopping Situations. *Sustainability* **2020**, *12* (18), 7436. https://doi.org/10.3390/su12187436

[53] Liputri, E. The Relationship of Customer Experience, Customer Engagement, Customer Satisfaction, and Customer Loyalty in Shopee E-Commerce. *JMBI Unsrat J. Ilm. Manaj. Bisnis Dan Inov.* **2024**, *11*(1), 196–204. https://doi.org/10.35794/jmbi.v11i1.53201

[54] Halvorsrud, R.; Kvale, K.; Følstad, A. Improving Service Quality Through Customer Journey Analysis. *J. Serv. Theory Pract.* **2016**, *26*(6), 840–867. https://doi.org/10.1108/jstp-05-2015-0111

[55] Andranurviza, A. Y.; Mulyati, H.; Munnadar, J. M. The Impact of Digital Application Usage on Customer Experience, Satisfaction, and Loyalty in a Life Insurance Company. *Bus. Rev. Case Stud.* **2022**. https://doi.org/10.17358/brcs.3.1.1

[56] Hoyer, W. D.; Kroschke, M.; Schmitt, B. H.; Kraume, K.; Shankar, V. Transforming the Customer Experience Through New Technologies. *J. Interact. Mark.* **2020**, *51*(1), 57–71. https://doi.org/10.1016/j.intmar.2020.04.001

[57] Aityassinec, F. L. Y.; Al-Ajlouni, M. M.; Mohammad, A. The Effect of Digital Marketing Strategy on Customer and Organizational Outcomes. *Mark. Manag. Innov.* **2022**, *13*(4), 45–54. https://doi.org/10.21272/mmi.2022.4-05

[58] Rahimian, S.; Shamizanjani, M.; Manian, A.; Esfidani, M. R. A Framework of Customer Experience Management for Hotel Industry. *Int. J. Contemp. Hosp. Manag.* **2021**, *33*(5), 1413–1436. https://doi.org/10.1108/ijchm-06-2020-0522

[59] Srinivasan, B. Comparative Analysis of LightGBM and XGBoost for Predictive Risk Assessment in Blockchain Transactions within the Metaverse. *J. Curr. Res. Blockchain.* **2025**, *2*(1), 1–12. https://doi.org/10.47738/jcrb.v2i1.23

[60] Novita, R. The Influence of Beliefs and Anxiety in Using Artificial Intelligence Towards Readiness to Change With High Performance Work Systems as a Moderating Variable. *HRMS* **2023**. https://doi.org/10.24036/hrms.v3i4.308

[61] Weinert, L.; Müller, J.; Svensson, L.; Heinze, O. Perspective of Information Technology Decision Makers on Factors Influencing Adoption and Implementation of Artificial Intelligence Technologies in 40 German Hospitals: Descriptive Analysis. *JMIR Med. Inform.* **2022**, *10*(6), e34678. https://doi.org/10.2196/34678

[62] Suseno, Y.; Hudík, M.; Fang, E. S.; Guo, Z. Employee Attitudes, Technological Anxiety, and Change Readiness for Artificial Intelligence Adoption. *Acad. Manag. Proc.* **2020**, *2020*(1), 20045. https://doi.org/10.5465/ambpp.2020.20045abstract

[63] Roy, S. K.; Singh, G.; Hope, M.; Nguyen, B.; Harrigan, P. The Rise of Smart Consumers: Role of Smart Servicescape and Smart Consumer Experience Co-Creation. *J. Mark. Manag.* **2019**, *35*(15–16), 1480–1513. https://doi.org/10.1080/0267257x.2019.1680569

[64] Ho, S. P. S.; Chow, M. Y. C. The Role of Artificial Intelligence in Consumers' Brand Preference for Retail Banks in Hong Kong. *J. Financ. Serv. Mark.* **2023**, *29*(2), 292–305. https://doi.org/10.1057/s41264-022-00207-3

[65] Babatunde, S. O. The Role of AI in Marketing Personalization: A Theoretical Exploration of Consumer Engagement Strategies. *Int. J. Manag. Entrep. Res.* **2024**, *6*(3), 936–949. https://doi.org/10.51594/ijmer.v6i3.964

[66] Dewi, D. A.; Kurniawan, T. B. Exploring Financial Trends through Topic Modeling and Time-Series Analysis: A Clustering Approach Using Latent Dirichlet Allocation (LDA) on Twitter Data. *J. Digit. Soc.* **2025**, *1* (1), Art. 1.

[67] Hayadi, B. H.; Maulita, I. Sentiment Analysis of Public Discourse on Education in Indonesia Using Support Vector Machine (SVM) and Natural Language Processing. *J. Digit. Soc.* **2025**, *1*(1), Art. 1.

[68] Jenneboer, L.; Herrando, C.; Constantinides, E. The Impact of Chatbots on Customer Loyalty: A Systematic Literature Review. *J. Theor. Appl. Electron. Commer. Res.* **2022**, *17*(1), 212–229. https://doi.org/10.3390/jtaer17010011

[69] Naz, H. Artificial Intelligence and Predictive Marketing: An Ethical Framework From Managers' Perspective. *Span. J. Mark. - ESIC* **2024**. https://doi.org/10.1108/sjme-06-2023-0154

[70] Zaman, K. Transformation of Marketing Decisions Through Artificial Intelligence and Digital Marketing. *J. Mark. Strateg.* **2022**, *4*(2), 353–364. https://doi.org/10.52633/jms.v4i2.210

[71] Tulcanaza-Prieto, A. B.; Cortez-Ordoñez, A.; Lee, C. W. Influence of Customer Perception Factors on AI-Enabled Customer Experience in the Ecuadorian Banking Environment. *Sustainability* **2023**, *15*(16), 12441. https://doi.org/10.3390/su151612441

[72] Fahima, J. The Effect of Customer Experience, Customer Value and Customer Satisfaction on Grab Online Transportation Customer Loyalty on South Jakarta National University Students. *J. Syntax Admiration* **2023**, *4*(1), 193–206. https://doi.org/10.46799/jsa.v4i1.811

[73] Annisa, F. F. The Effect of Customer Experience on Customer Satisfaction and Loyalty of Generation Z at Coffee Shops in Bengkulu City. *Front. Bus. Econ.* **2023**, *2*(3), 154–163. https://doi.org/10.56225/finbe.v2i3.293

[74] Dewi, S. K.; Aslami, N. Strategy Analysis to Improve Service Quality in Indihome Products on Customer Satisfaction at Telkom Witel Medan. *Cashflow Curr. Adv. Res. Sharia Finance Econ. Worldw.* **2022**, *1*(4), 55–62. https://doi.org/10.55047/cashflow.v1i4.207

[75] Tuấn, N. M.; Environment, V. Service Quality, Customer Experience and Commitment Affecting Customer Satisfaction in Vietnamese Hotel Industry. *Int. J. Multidiscip. Res. Anal.* **2021**, *4*(1). https://doi.org/10.47191/ijmra/v4-i1-11

[76] Fernandes, T.; Cruz, M. Dimensions and Outcomes of Experience Quality in Tourism: The Case of Port Wine Cellars. *J. Retail. Consum. Serv.* **2016**, *31*, 371–379. https://doi.org/10.1016/j.jretconser.2016.05.002

[77] Prayag, G.; Hosany, S.; Muskat, B.; Chiappa, G. D. Understanding the Relationships Between Tourists' Emotional Experiences, Perceived Overall Image, Satisfaction, and Intention to Recommend. *J. Travel Res.* **2016**, *56*(1), 41–54. https://doi.org/10.1177/0047287515620567

[78] Dobrota, M.; Nikodijević, A.; Mihailovic, D. Influence of the Customer Experience on Satisfaction With Mobile Phones. *J. Eng. Manag. Compet.* **2012**, *2*(2), 69–75. https://doi.org/10.5937/jemc1202069d

[79] Hartati, W. The Effect of E-Service of Quality on Customer Satisfaction in Using the Shopee Application. *Int. J. Adv. Multidiscip.* **2023**, *2*(1), 148–155. https://doi.org/10.38035/ijam.v2i1.222

[80] Otiso, K. N. Impact of Perceived Value on Customer Satisfaction Among Mobile Phone Users in Selected Public Universities in Kenya. *Int. J. Innov. Res. Dev.* **2021**, *10*(10). https://doi.org /10.24940/ijird/2021/v10/i10/oct21014

[81] Pritjahjono, P.; Jahroh, S.; Saptono, I. T. The Effect of Customer Loyalty in Digital Banking Services: Role Satisfaction Factor, Customer Experience and eWOM. *Indones. J. Bus. Entrep.* **2023**. https://doi.org /10.17358/ijbe.9.1.129

[82] Ivanovska, L. P.; Miteva, A.; Lozanoska, A. The Challenges of Touchpoint Management of Telecommunications Companies With Empirical Analysis for the Republic of North Macedonia. *Econ. Dev.* **2022**, *25* (5), 94–107. https://doi.org/10.55302/ed22255094pi

[83] Johnston, R. B.; Kong, X. The Customer Experience: A Road-Map for Improvement. *Manag. Serv. Qual.* **2011**, *21*(1), 5–24. https://doi.org/10.1108/09604521111100225

[84] Noranee, S.; Othman, A. K. Understanding Consumer Sentiments: Exploring the Role of Artificial Intelligence in Marketing. *Jmm17 J. Ilmu Ekon. Dan Manaj.* **2023**, *10*(1), 15–23. https://doi.org/ 10.30996/jmm17.v10i1.8690

[85] He, X. Research on the Marketing Transformation Path of Household Appliance Enterprises Under the Background of Artificial Intelligence. *Mod. Econ. Manag. Forum* **2023**, *4*(5), 147. https://doi.org /10.32629/memf.v4i5.1495

[86] Williams, P.; Naumann, E. Customer Satisfaction and Business Performance: A Firm-Level Analysis. *J. Serv. Mark.* **2011**, *25* (1), 20–32. https://doi.org/10.1108/08876041111107032

[87] Natsir, K.; Arifin, A. Z.; Sadhewa, C. B.; Aprilia, D.; Dharsono, S. Analysis of Digital Bank Services in Indonesia Based on Consumer Perception. *IJAEB* **2023**, *1*(1), 307–320. https://doi.org/ 10.24912/ijaeb.11.307-320

[88] Tulcanaza-Prieto, A. B.; Aguilar-Rodríguez, I. E.; Lee, C. W. Customer Perception and Its Influence on the Financial Performance in the Ecuadorian Banking Environment. *Sustainability* **2022**, *14*(12), 6960. https://doi.org/10.3390/su14126960

[89] Golovkova, A.; Eklöf, J.; Malova, A.; Podkorytova, O. Customer Satisfaction Index and Financial Performance: A European Cross Country Study. *Int. J. Bank Mark.* **2019**, *37*(2), 479–491. https://doi.org/ 10.1108/ijbm-10-2017-0210

[90] Eklöf, J.; Podkorytova, O.; Malova, A. Linking Customer Satisfaction With Financial Performance: An Empirical Study of Scandinavian Banks. *Total Qual. Manag. Bus. Excell.* **2018**, *31*(15–16), 1684–1702. https://doi.org/10.1080/14783363.2018.1504621

[91] Al-Dmour, H.; Algharabat, R.; Khawaja, R.; Al-Dmour, R. Investigating the Impact of ECRM Success Factors on Business Performance. *Asia Pac. J. Mark. Logist.* **2019**, *31*(1), 105–127. https://doi.org/ 10.1108/apjml-10-2017-0270

[92] Tarigan, J.; Hatane, S. E. The Influence of Customer Satisfaction on Financial Performance Through Customer Loyalty and Customer Advocacy: A Case Study of Indonesia's Local Brand. *KnE Soc. Sci.* **2019**, *3*(11), 270. https://doi.org/10.18502/kss.v3i11.4012

[93] Joudeh, J. M. M.; Dandis, A. O. Service Quality, Customer Satisfaction and Loyalty in an Internet Service Providers. *Int. J. Bus. Manag.* **2018**, *13*(8), 108. https://doi.org/10.5539/ijbm.v13n8p108

[94] Sharma, P.; Kong, T. T. C.; Kingshott, R. Internal Service Quality as a Driver of Employee Satisfaction, Commitment and Performance. *J. Serv. Manag.* **2016**, *27*(5), 773–797. https://doi.org/10.1108/josm-10-2015-0294

[95] Fornell, C.; Morgeson, F. V.; Hult, G. T. M. Stock Returns on Customer Satisfaction Do Beat the Market: Gauging the Effect of a Marketing Intangible. *J. Mark.* **2016**, *80*(5), 92–107. https://doi.org /10.1509/jm.15.0229

[96] Olsen, L. L.; Witell, L.; Gustafsson, A. Turning Customer Satisfaction Measurements Into Action. *J. Serv. Manag.* **2014**, *25*(4), 556–571. https://doi.org/10.1108/josm-01-2014-0025

[97] Ijara, T. M. Service Quality and Financial Performance of Banks (A Meta-Analysis). *Int. J. Res. Stud. Publ.* **2020**, *10* (05), 349–359. https://doi.org/10.29322/ijsrp.10.05.2020.p10141

[98] Gupta, K. D. Emerging Design Trends in Social Media and Its Impact on Business Efficiency and Growth in India. *Shodhkosh J. Vis. Perform. Arts* **2023**, *4* 2SE). https://doi.org/10.29121/shodhkosh.v4.i2se.2023.455

[99] Zahra, A. R. A. Assessing Customer Satisfaction in AI-Powered Services: An Empirical Study With SmartPLS. *Int. Trans. Artif. Intell. Ital.* **2023**, *2* (1), 81–89. https://doi.org/10.33050/italic.v2i1.432

[100] Kim, J.-K.; Choi, I.-Y.; Li, Q. Customer Satisfaction of Recommender System: Examining Accuracy and Diversity in Several Types of Recommendation Approaches. *Sustainability* **2021**, *13*(11), 6165. https://doi.org/10.3390/su13116165

[101] Navigating the Landscape of Hyper Personalization in Financial Services: Challenges, Mitigations and Strategies. *J. Econ. Manag. Res.* **2022**, 1–4. https://doi.org/10.47363/jesmr/2022(3)221

[102] Lee, H. I.; Choi, I. Y.; Moon, H.; Kim, J. K. A Multi-Period Product Recommender System in Online Food Market Based on Recurrent Neural Networks. *Sustainability* **2020**, *12*(3), 969. https://doi.org/10.3390/su12030969

[103] Nguyen, T.-M.; Malik, A. Impact of Knowledge Sharing On Employees' Service Quality: The Moderating Role of Artificial Intelligence. *Int. Mark. Rev.* **2021**, *39*(3), 482–508. https://doi.org/10.1108/imr-02-2021-0078

[104] Prentice, C.; Nguyen, T.-M. Engaging and Retaining Customers With AI and Employee Service. *J. Retail. Consum. Serv.* **2020**, *56*, 102186. https://doi.org/10.1016/j.jretconser.2020.102186.

[105] Marbach, J.; Lages, C. R.; Nunan, D. Who Are You and What Do You Value? Investigating the Role of Personality Traits and Customer-Perceived Value in Online Customer Engagement. *J. Mark. Manag.* **2016**, *32*(5–6), 502–525. https://doi.org/10.1080/0267257x.2015.1128472

[106] Yasin, M.; Porcu, L.; Abusharbeh, M. T.; Liébana-Cabanillas, F. $. The Impact of Customer Personality and Online Brand Community Engagement on Intention to Forward Company and Users Generated Content: Palestinian Banking Industry a Case. *Econ. Res.-Ekon. Istraživanja* **2020**, *33*(1), 1985–2006. https://doi.org/10.1080/1331677x.2020.1752277

[107] Martiyanti, D. Does Brand Love Make Every Consumer Behave on Social Media? The Role of Personality Traits and Brand Love on Customer Engagement Behavior. *Amar Andalas Manag. Rev.* **2023**, *6*(1), 14–38. https://doi.org/10.25077/amar.6.1.14-38.2022

[108] Jiang, H.; Cheng, Y.; Yang, J.; Gao, S. AI-Powered Chatbot Communication With Customers: Dialogic Interactions, Satisfaction, Engagement, and Customer Behavior. *Comput. Hum. Behav.* **2022**, *134*, 107329. https://doi.org/10.1016/j.chb.2022.107329

[109] Marti, C. L. Leveraging Artificial Intelligence in Firm-Generated Online Customer Communities: A Framework and Future Research Agenda. *J. Serv. Manag.* **2024**, *35*(3), 438–458. https://doi.org/10.1108/josm-10-2023-0443

[110] Joshi, J. M.; Ashima. Enhancing Employee Efficiency and Performance in Industry 5.0 Organizations Through Artificial Intelligence Integration. *EEL* **2023**, *13*(4), 300–315. https://doi.org/10.52783/eel.v13i4.589

[111] Cheng, Y.; Jiang, H. Customer–Brand Relationship in the Era of Artificial Intelligence: Understanding the Role of Chatbot Marketing Efforts. *J. Prod. Brand Manag.* **2021**, *31*(2), 252–264. https://doi.org/10.1108/jpbm-05-2020-2907

[112] Eriksson, T.; Bigi, A.; Bonera, M. Think With Me, or Think for Me? On the Future Role of Artificial Intelligence in Marketing Strategy Formulation. *TQM J.* **2020**, *32*(4), 795–814. https://doi.org/10.1108/tqm-12-2019-0303

[113] Role of Neuromarketing and Artificial Intelligence in Futuristic Marketing Approach: An Empirical Study. **2024**. https://doi.org/10.52783/jier.v4i2.809

[114] Senyapar, H. N. D. Artificial Intelligence in Marketing Communication: A Comprehensive Exploration of the Integration and Impact of AI. *Tech. Soc. Sci. J.* **2024**, *55*, 64–81. https://doi.org/10.47577/tssj.v55i1.10651

[115] Wu, C.; Monfort, A. Role of Artificial Intelligence in Marketing Strategies and Performance. *Psychol. Mark.* **2022**, *40*(3), 484–496. https://doi.org/10.1002/mar.21737

[116] Nguyen, T.-M.; Quach, S.; Thaichon, P. The Effect of AI Quality on Customer Experience and Brand Relationship. *J. Consum. Behav.* **2021**, *21*(3), 481–493. https://doi.org/10.1002/cb.1974

[117] Spais, G. AI Marketing and AI-Based Promotions Impact on Consumer Behavior and the Avoidance of Consumer Autonomy Threat. *J. Consum. Behav.* **2023**, *23*(3), 1053–1056. https://doi.org/10.1002/cb.2248

[118] Davenport, T. H.; Guha, A.; Grewal, D.; Breßgott, T. How Artificial Intelligence Will Change the Future of Marketing. *J. Acad. Mark. Sci.* **2019**, *48*(1), 24–42. https://doi.org/10.1007/s11747-019-00696-0

[119] McLeay, F.; Osburg, V.; Yoganathan, V.; Patterson, A. Replaced by a Robot: Service Implications in the Age of the Machine. *J. Serv. Res.* **2020**, *24*(1), 104–121. https://doi.org/10.1177/1094670520933354

[120] Huang, M. H.; Rust, R. T. Artificial Intelligence in Service. *J. Serv. Res.* **2018**, *21*(2), 155–172. https://doi.org/10.1177/1094670517752459

[121] Hicham, N. Strategic Framework for Leveraging Artificial Intelligence in Future Marketing Decision-Making. *J. Intell. Manag. Decis.* **2023**, *2* (3), 139–150. https://doi.org/10.56578/jimd020304

[122] Pooser, D. M.; Browne, M. J. The Effects of Customer Satisfaction on Company Profitability: Evidence From the Property and Casualty Insurance Industry. *Risk Manag. Insur. Rev.* **2018**, *21*(2), 289–308. https://doi.org/10.1111/rmir.12105

[123] J. F. Hair Jr., G. T. M. Hult, C. M. Ringle, and M. Sarstedt. A Primer on Partial Least Squares Structural Equation Modeling (PLS-SEM), 3rd ed. *Thousand Oaks*, CA, USA: Sage, **2021**.

[124] Bawack, R. E.; Wamba, S. F.; Carillo, K. D. A. Exploring the Role of Personality, Trust, and Privacy in Customer Experience Performance during Voice Shopping: Evidence from SEM and Fuzzy Set Qualitative Comparative Analysis. *Int. J. Inf. Manag.* **2021**, *58*, 102309. https://doi.org/10.1016/j.ijinfomgt.2021.102309

[125] Aw, E. C.-X.; Basha, N. K.; Ng, S. I.; Sambasivan, M. To Grab or Not to Grab? The Role of Trust and Perceived Value in On-Demand Ridesharing Services. *Asia Pac. J. Mark. Logist.* **2019**, *31*(5), 1442–1465. https://doi.org/10.1108/apjml-09-2018-0368

[126] Babu, M. M. Impact of Firm's Customer Orientation on Performance: The Moderating Role of Interfunctional Coordination and Employee Commitment. *J. Strateg. Mark.* **2018**, *26*(8), 702–722. https://doi.org/10.1080/0965254x.2017.1384037

[127] Do, Q. H.; Kim, T. Y.; Wang, X. Effects of Logistics Service Quality and Price Fairness on Customer Repurchase Intention: The Moderating Role of Cross-Border E-Commerce Experiences. *J. Retail. Consum. Serv.* **2023**, *70*, 103165. https://doi.org/10.1016/j.jretconser.2022.103165

[128] Ashnai, B.; Henneberg, S. C.; Naudé, P.; Francescucci, A. Inter-Personal and Inter-Organizational Trust in Business Relationships: An Attitude–Behavior–Outcome Model. *Ind. Mark. Manag.* **2016**, *52*, 128–139. https://doi.org/10.1016/j.indmarman.2015.05.020

[129] Sianipar, Y. C.; Situmorang, S. H.; Wibowo, R. P. Analysis of the Effect of Digital Customer Experience on Customer Loyalty through Emotional Marketing and Customer Satisfaction for Indihome Customers. *Int. J. Econ. Bus. Account. Agric. Manag. Sharia Adm. Ijebas* **2023**, *3*(4), 1235–1247. https://doi.org/10.54443/ijebas.v3i4.1023

ASEAN
Journal of Scientific and Technological Reports
Online ISSN:2773-8752

Research article

A Bibliometric Analysis of Stress Memory and Priming in Plants: Research Trends, Mechanisms, and Implications for Agricultural Resilience

Harry C. Luces[1*]

[1] College of Agriculture, Forestry, and Food Science, University of Antique-Hamtic Campus, 5715, Philippines
* Correspondence: harry.luces@antiquespride.edu.ph

Citation:
Luces, H. A bibliometric analysis of stress memory and priming in plants: research trends, mechanisms, and implications for agricultural resilience. *ASEAN J. Sci. Tech. Report.* **2026**, *29*(1), e259013. https://doi.org/10.55164/ajstr.v29i1.259013.

Article history:
Received: Apri1 27, 2025
Revised: October 11, 2025
Accepted: October 18, 2025
Available online: December 14, 2025

Publisher's Note:
This article is published and distributed under the terms of the Thaksin University.

Abstract: This bibliometric analysis explores research trends and collaborative networks surrounding the concepts of "stress memory" and "priming" in plants, with a focus on their implications for agricultural resilience. A total of 270 studies published between 2007 and 2024 were analyzed, revealing a growing interest in this relatively new area of plant science. While the global research output saw a slight decline in 2021, publication activity rebounded in 2024, reaching a peak of 51 documents in 2024. The majority of studies were published in *Frontiers in Plant Science*, and prominent authors such as Isabel Bäurle contributed significantly to the field. Co-authorship analysis highlighted strong international collaboration, particularly between Germany and China, with Germany emerging as the leading country in both publication volume and collaborative efforts. Keyword analysis indicated that "priming" was the most frequently used term, reflecting its central role in research on plant stress memory. The focus on genetic, epigenetic, and metabolic mechanisms provides valuable insights into how plants "remember" stress and adapt to recurring challenges. These findings underscore the multidisciplinary nature of the field, with contributions from plant physiology, molecular biology, and agricultural sciences. The results emphasize the importance of continued global collaboration and the integration of theoretical and applied research to develop climate-resilient crops. Furthermore, the high proportion of open-access publications highlights the increasing accessibility of this research, fostering wider dissemination and application of findings. This analysis provides a comprehensive understanding of the evolving landscape of stress memory and priming research, offering valuable directions for future studies aimed at enhancing agricultural sustainability and resilience.

Keywords: Stress memory; plant adaptation; priming; bibliometric analysis

1. Introduction

The study of stress memory in plants has gained prominence due to the escalating challenges posed by climate change and its impact on agricultural systems. Climate change increases the frequency and intensity of stress events such as droughts, heatwaves, and salinity, threatening global food security and agricultural productivity [1-3]. Understanding how plants retain and recall memories of past stress is essential for developing strategies to enhance crop resilience. A systematic review of existing literature on this topic is necessary to

provide a comprehensive understanding of current research, identify knowledge gaps, and guide future studies aimed at advancing climate-resilient agricultural practices [4].

Priming is a phenomenon where plants exposed to mild or non-lethal stressors develop an enhanced ability to respond to subsequent stress. This process equips plants with a form of "stress memory," enabling faster and stronger responses to environmental challenges, such as drought, heat, or pathogen attacks [5]. Primed plants exhibit increased expression of defense-related genes, accumulation of signaling molecules, and activation of antioxidant systems. Stress memory refers to the ability of plants to "remember" past stress events, influencing their responses to future stress. This memory can be short-term (within the same generation) or long-term (transferred to progeny through epigenetic modifications). Epigenetic mechanisms, such as DNA methylation, histone modifications, and small RNAs, play a critical role in encoding and maintaining stress memory [6]. For example, drought exposure can induce modifications in drought-responsive genes, improving plant resilience to future water deficits.

Priming and stress memory hold significant potential for agriculture, as they can be harnessed to improve crop resilience and productivity in the face of changing climatic conditions. A bibliometric review of stress memory in plants offers valuable insights into research trends, identifies influential studies, and highlights the contributions of leading researchers and institutions [7-8]. By mapping the research landscape, such a review facilitates collaborations among scientists, accelerates advancements in the field, and supports the application of stress memory concepts in agriculture [9-10].

Despite advancements in understanding stress memory mechanisms, critical gaps remain. For instance, the molecular basis of transgenerational memory—where stress-induced traits are inherited by subsequent generations—remains inadequately understood [2,8]. Furthermore, research is needed to explore how different stress types, such as biotic (pathogen attacks) and abiotic (drought) stresses, influence memory formation via distinct pathways [11-12]. A bibliometric review can pinpoint these gaps, enabling researchers to focus their efforts on areas that promise significant breakthroughs in plant adaptation and resilience [4].

Understanding stress memory has practical implications for agricultural innovation and sustainable farming practices. By synthesizing research findings, a bibliometric review can translate theoretical insights into practical applications, such as priming techniques that enhance crop resilience to adverse conditions [2, 9]. These insights are crucial for breeding programs and biotechnological approaches aimed at creating crop varieties capable of withstanding climate pressures [13-14]. Additionally, such knowledge supports efforts to increase food production sustainably, minimizing reliance on chemical inputs like pesticides and fertilizers, which carry environmental and economic costs [4, 15].

Finally, a comprehensive review of stress memory literature serves as a valuable resource for researchers, policymakers, and agricultural practitioners. For scientists, it offers a clear overview of the research landscape, aiding both newcomers and established researchers in navigating the complexities of stress memory research [16]. For policymakers and practitioners, the review provides evidence-based insights for crop management strategies, guiding the development of agricultural practices that enhance productivity and resilience in the face of environmental challenges [2, 9].

1.1 Objectives of the Study

The study aims to conduct a comprehensive bibliometric analysis of stress memory and priming in plants, focusing on research trends, mechanisms, and implications for agricultural resilience. Specifically, the study aimed to: analyze publication trends and identify the journals in which the documents are published; identify and categorize the authors, their organizations, and their countries; identify the most frequently used keywords in publications related to the terms “stress memory,” “priming,” and “plants”; and conduct a bibliometric review of authors, subject areas, document types, source titles, publication stages, keywords, affiliations, countries, languages, and open access status.

1.2 Stress Memory in Plants

Plants, as sessile organisms, are continually exposed to fluctuating and often adverse environmental conditions such as drought, heat, salinity, and pathogen attack. Unlike animals, they cannot escape these stresses but have evolved sophisticated mechanisms to adapt and survive. One such adaptation is stress

memory—the ability to "remember" previous stress events and respond more efficiently to subsequent exposures. This memory is encoded at molecular, cellular, and physiological levels, enabling plants to mount faster, stronger, or more specific responses to recurring or even novel stresses [10, 17, 18]. Stress memory serves as a cornerstone of plant resilience, with profound implications for natural ecosystems and agricultural productivity, particularly under climate change and increasing environmental variability [14, 19].

1.3 Mechanisms of Stress Memory Formation

1.3.1 Epigenetic Regulation

Stress memory in plants is primarily mediated through epigenetic mechanisms that regulate gene expression without altering DNA sequences. These include DNA methylation, histone modifications, and chromatin remodeling [16, 19, 20]. DNA methylation influences transcriptional activity and can be maintained through cell divisions, providing a stable molecular basis for memory [18]. Histone modifications, such as trimethylation of histone H3 lysine 4 (H3K4me3), are also vital for transcriptional memory, as they facilitate rapid gene reactivation following stress exposure [19, 21, 22]. Meanwhile, chromatin remodeling, involving changes in nucleosome positioning and accessibility, ensures the proper regulation and reactivation of stress-responsive genes [22-23].

1.3.2 RNA-Based Regulation.

RNA molecules play central roles in regulating plant stress memory. MicroRNAs (miRNAs) and small interfering RNAs (siRNAs) fine-tune gene expression through post-transcriptional regulation and RNA-directed DNA methylation (RdDM), respectively. Additionally, long non-coding RNAs (lncRNAs) guide protein complexes for epigenetic modification, further stabilizing transcriptional memory [17]. Alternative splicing (AS) and small regulatory RNAs also modulate gene networks that govern stress perception and response, contributing to the molecular retention of stress experiences [10].

1.3.3 Hormonal and Signaling Pathways.

Plant hormones such as abscisic acid (ABA), jasmonic acid (JA), ethylene (ET), salicylic acid (SA), auxins, and cytokinins orchestrate complex signaling cascades that influence physiological adaptations like stomatal regulation, osmotic balance, and growth modulation [24]. These hormones not only mediate immediate stress responses but also participate in establishing long-term signaling networks that contribute to stress memory [25].

1.3.4 Transcriptional Regulation.

A variety of transcription factors (TFs)—including those from the DREB, WRKY, NAC, and bZIP families—activate stress-responsive genes and facilitate memory formation [18, 25]. Such activation can lead to transcriptional memory, where plants "remember" prior stress exposure, allowing for a faster and more robust response during subsequent challenges [12].

1.3.5 Physiological and Biochemical Adjustments.

Stress memory also manifests at the physiological level. Priming, where prior exposure to mild stress enhances tolerance to later, more severe stress, involves biochemical and molecular adjustments that can persist throughout the plant's life or be transmitted to progeny [8, 30, 31]. Furthermore, autophagy, a self-degradative process, plays a role in resetting and modulating cellular memory by degrading damaged proteins and organelles [26].

1.4 Factors Influencing Stress Memory

The formation and persistence of stress memory are influenced by multiple factors. The type of stress determines the specific molecular and physiological pathways activated—drought, salinity, cold, and heat each trigger distinct regulatory mechanisms [27-29]. Moreover, the interaction of environmental conditions shapes the effectiveness of memory formation. For example, combined or sequential stresses (e.g., drought and high temperature) can induce cross-adaptation, where tolerance to one stress confers resistance to others [27, 29, 30].

1.5 Inheritance of Stress Memory

Stress memory can be retained at both the somatic and heritable levels. Somatic memory occurs within the lifespan of an individual plant, allowing adaptive responses to recurring environmental challenges [18, 24]. In contrast, intergenerational and transgenerational inheritance involves the transmission of epigenetic marks or molecular signals to progeny, predisposing them to enhanced stress tolerance [19]. This heritable memory provides an evolutionary advantage, as it enables offspring to anticipate and withstand environmental conditions experienced by their parents.

1.6 Applications and Future Directions

Understanding the molecular and physiological bases of stress memory opens new avenues for crop improvement and sustainable agriculture. Insights from epigenetic regulation, RNA-based control, and stress priming can be harnessed to develop crop varieties with enhanced stress resilience [31]. Moreover, breeding strategies informed by these mechanisms can accelerate the creation of stress-resistant cultivars, particularly through epigenetic selection and molecular breeding approaches [32].

Future research should prioritize identifying specific genes and pathways associated with stress memory, exploring the longevity and reversibility of epigenetic marks, and elucidating cross-talk among stress signaling networks [24,33]. Integrating these insights into agricultural practice could lead to crops capable of sustaining productivity under the increasing frequency of environmental stress events brought about by climate change.

2. Materials and Methods.

In this study, the Scopus platform, a widely recognized bibliographic database, was the primary tool for conducting a comprehensive bibliometric analysis of research on stress memory in plants. The Scopus database was selected for its extensive coverage of high-quality scientific literature and its advanced filtering and citation analysis capabilities.

The first step involved performing a keyword search in the Scopus database using terms such as: "stress memory" AND "priming" in combination with "plants" OR "crops" OR "vegetation". The search was conducted across all fields to ensure a broad capture of relevant articles, reviews, and conference papers. The search results were then filtered by the number of citations to focus on the most influential studies in the field. The first 270 records were retained with the highest number of citations for further analysis.

The resulting database of 270 records was then uploaded into VOSviewer version 1.6.18, a bibliometric software developed by Ness Jan van Eck and Ludo Waltman [34]. VOSviewer was used to perform several computations, including the identification of the most co-cited authors, the most frequently used keywords, and the development of co-occurrence maps. These analyses allowed us to visualize the relationships between various research themes and the evolution of knowledge on stress memory in plants.

The use of VOSviewer allowed for the creation of visual co-occurrence maps, which highlighted key areas of focus in the field, such as molecular mechanisms like DNA methylation, transcriptional regulation, and priming effects, as well as applications of stress memory in agricultural practices. The insights gained from this analysis informed future research directions and practical applications in developing climate-resilient crops.

3. Results and Discussion

3.1 Number of Published Studies on Priming and Stress Memory (2007–2024)

Figure 1 shows the number of published studies on priming and stress memory from 2007 to 2024. When searching for the terms "stress memory" and "priming" in combination with "plants," "crops," or "vegetation" in Scopus, the query returned a total of 270 results. The publication years ranged from 2007 to 2024, indicating that research on stress memory in plants is relatively recent. A slight decrease in the number of publications was observed in 2021, likely due to restrictions on human interaction during the COVID-19 pandemic. The year 2024 saw the highest number of publications, with a total of 51 documents.

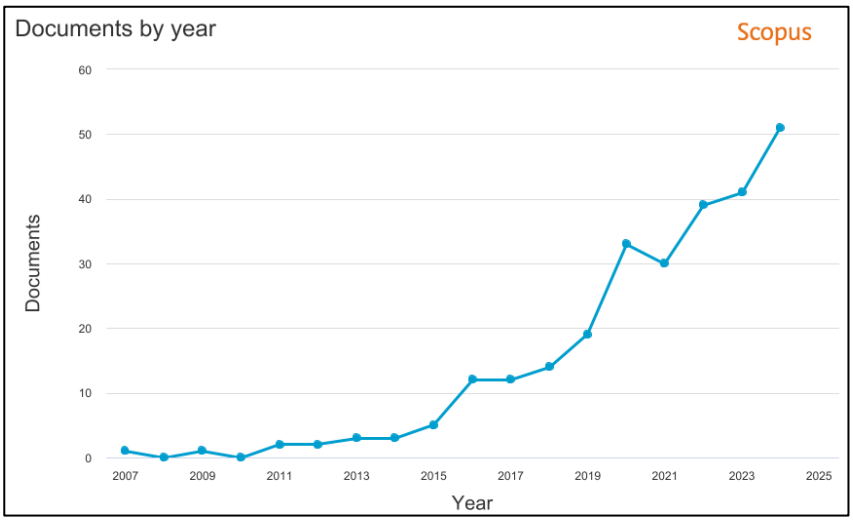


Figure 1. Number of Published Studies on Priming and Stress Memory (2007–2024).

3.2 Number of Documents Published in Different Journals

Figure 2 shows the journals where the documents were published; the majority of them appeared in *Frontiers in Plant Science*, which accounted for a total of 17 publications. Notably, the journal *Plant Cell and Environment* had the highest number of publications in a single year, with 7 articles published in 2019. However, following a peak in publication output across journals in 2022, there has been an irregular trend in the number of publications related to the keywords "stress memory" and "priming" in plants. This trend is particularly evident in the journal *Plant Cell and Environment*, which experienced a sharp decline in the number of related publications after its peak year. This irregularity may reflect shifting research priorities, resource availability, or broader challenges in the scientific community, such as funding shifts. It highlights the need for continued monitoring of publication trends to better understand the dynamics driving research interest in stress memory and priming in plants.

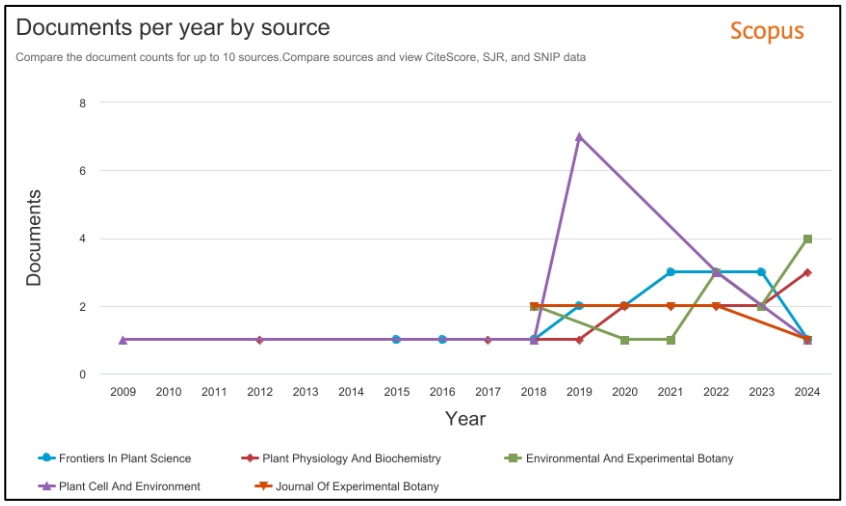


Figure 2. Number of Documents Published in Different Journals.

3.3 Results Based on VOSviewer Computations

Three types of computations were performed using VOSviewer: co-authorship analysis, identification of the most-used keywords, and citation analysis of authors. All 270 selected publications were subjected to this analysis.

3.3.1 Co-authorship Analysis (Authors)

Figure 3 illustrates the co-authorship relationships among authors in the selected publications. The analysis type chosen was "Co-authorship," and the counting method was set to "Full counting." The minimum number of documents per author was set to 1, allowing all 1,083 authors of the publications to meet the threshold. However, only 83 authors were connected through co-authorship, as depicted by the clusters in the figure. The colored bubbles represent authors who have collaborated with others, with the size of the bubbles indicating the number of co-authors each author has had. The four most prominent authors in terms of co-authorship were Isabel Bäurle, Xiangnan Li, Chédly Abdelly, and Margarete Baier.

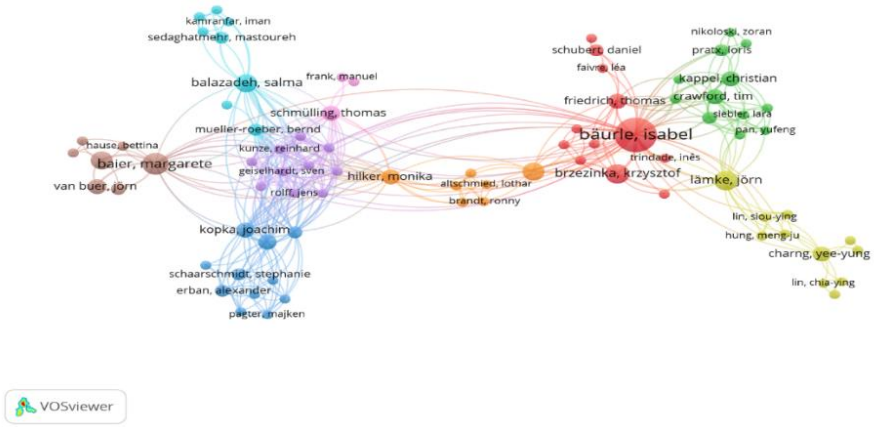


Figure 3. VOSviewer Computations for Authors Network.

3.3.2 Co-authorship Analysis (Organizations)

When the analysis was extended to organizations, 663 organizations met the minimum threshold of one publication. However, only 14 organizations exhibited co-authorship connections, forming a single cluster as shown in Figure 4. Among these, the Institute of Biology in Applied Genetics and Plant Ecology at the Dahlem Centre of Plant Sciences in Germany, as well as the Universität Potsdam, Institute of Biochemistry and Biology, stood out with the highest levels of co-authorship connections. Both organizations are based in Germany, emphasizing the country's central role in collaborative research on stress memory and priming in plants.

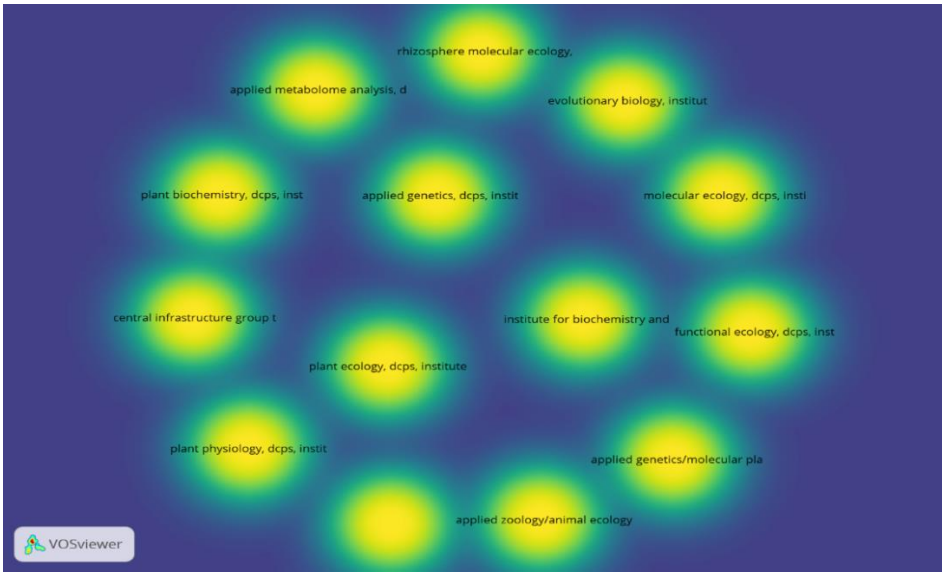


Figure 4. VOSviewer Computations for Organizations Density.

3.3.3 Co-authorship Analysis (Countries).

The co-authorship analysis at the country level revealed that 63 countries met the threshold, but only 54 of them had collaborative links. Germany emerged as the leading country in terms of the number of documents published, while China had the strongest co-authorship connections with other publishing countries. The countries were grouped into 10 clusters, each represented by distinct colors in Figure 5. This clustering highlights the geographical distribution and collaborative networks among countries actively publishing on this topic. The results from these analyses underscore the importance of collaboration at various levels—individual, institutional, and national. Germany's prominent role across all levels suggests its leading position in advancing research on stress memory and priming in plants, supported by robust international partnerships, particularly with China.

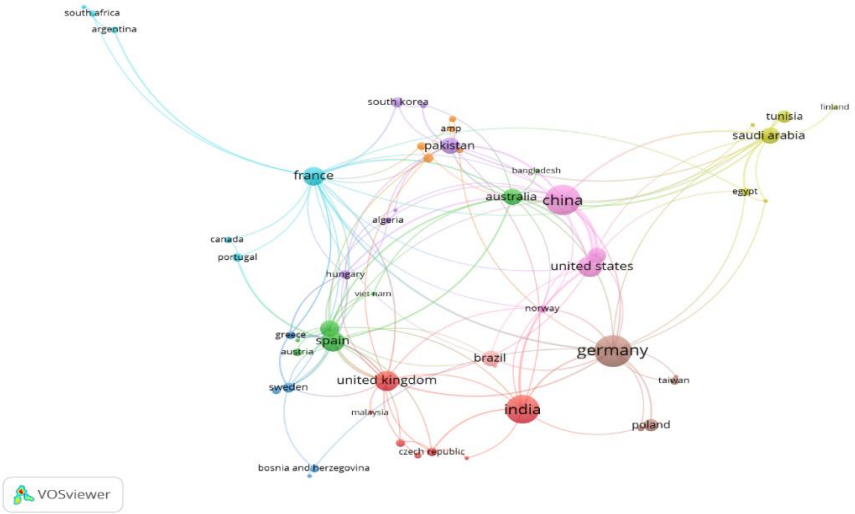


Figure 5. VOSviewer Computations for Countries Network.

The co-occurrence keyword map, displayed in Figure 6, provides valuable insights into the key themes and research trends in the selected publications. The analysis type chosen was "Co-occurrence," with the counting method set to "Full counting." The minimum number of occurrences of a keyword was set to 1, resulting in a total of 1,766 keywords identified from the dataset.

3.3.4 Keywords with the Highest Frequency of Occurrences

Table 1 highlights the keywords with the highest frequency of occurrences. A closer examination reveals that "priming" is the most frequently used keyword in the database. This prominence can be attributed to the substantial number of review articles discussing the priming of plants as a mechanism to develop stress memory. Priming has become a central concept in this field due to its relevance in enhancing plant resilience to abiotic and biotic stresses, as shown in Figure 6. In addition to "priming," several studies focus on genetics, aiming to understand how plants develop stress memory at the cellular and molecular levels. These studies often investigate key processes such as epigenetic modifications, transcriptional regulation, and gene expression patterns that contribute to a plant's ability to "remember" and respond more effectively to recurring stresses. Another significant theme identified through keyword analysis is "metabolism." Research in this area focuses on observing how priming and stress exposure influence plant metabolic pathways, ultimately affecting growth responses and stress adaptation. Studies on metabolism provide critical insights into how energy and resources are allocated during stress responses, shedding light on physiological trade-offs and adaptive mechanisms in plants. Overall, the co-occurrence keyword analysis underscores the multidisciplinary nature of research on stress memory in plants, spanning fields such as plant physiology, molecular biology, and agricultural science. It also highlights the evolving focus on integrating genetic and metabolic insights to develop practical applications for improving crop resilience in the face of climate change and other environmental challenges.

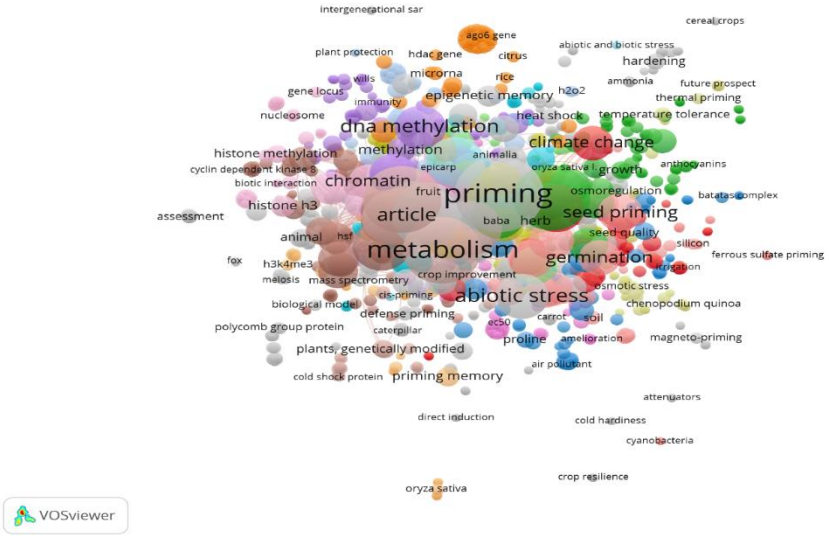


Figure 6. VOSviewer Computations for Keywords Cluster.

Table 1. The ranking of the most frequently occurring keywords for terms "priming", "stress memory", and "plants".

Ranking	Keyword	Occurrence
1	Priming	89
2	Genetics	69
3	Metabolism	69
4	Stress Memory	66
5	Physiological Stress	54
6	Physiology	46
7	Gene Expression Regulation	46
8	Epigenetics	38
9	Arabidopsis	38
10	Drought	35
11	Nonhuman	33
12	Memory	32
13	Abiotic Stress	31
14	Plants	30
15	DNA Methylation	29

3.3.5 Highlighted Keyword Clusters

The keyword map in Figure 7 highlights the interconnected research themes within the realm of plant priming, stress memory, and associated physiological and molecular responses. The central bubble for "priming" is prominently linked to critical terms such as "epigenetics," "DNA methylation," "metabolism," and "abiotic stress," indicating the focal areas of research in this domain. These connections reveal an emphasis on understanding how plants utilize priming mechanisms to enhance resilience to abiotic stresses like drought, heat, and salinity through modifications in epigenetic memory and metabolic pathways. The size and density of these keywords underscore their prominence in the literature, suggesting they are pivotal in the context of plant stress tolerance and adaptive strategies. The clustering of related terms, such as "genetic priming," "defense priming," and "priming memory," emphasizes the multifaceted roles of priming in improving plant performance under environmental challenges. Additionally, keywords such as "climate change," "abiotic stress resistance," and "temperature tolerance" highlight the broader implications of plant priming research in addressing global agricultural challenges. The association with terms like "heat shock," "hardening," and "proline" points to the metabolic and physiological adjustments plants undergo during priming events. The

exploration of priming in crops such as *Oryza sativa* (rice) and its potential in enhancing crop resilience demonstrates the application-oriented focus of current research. This map not only reflects the diversity of priming research but also indicates its potential role in developing sustainable agricultural practices to mitigate climate-related stress impacts on crops.

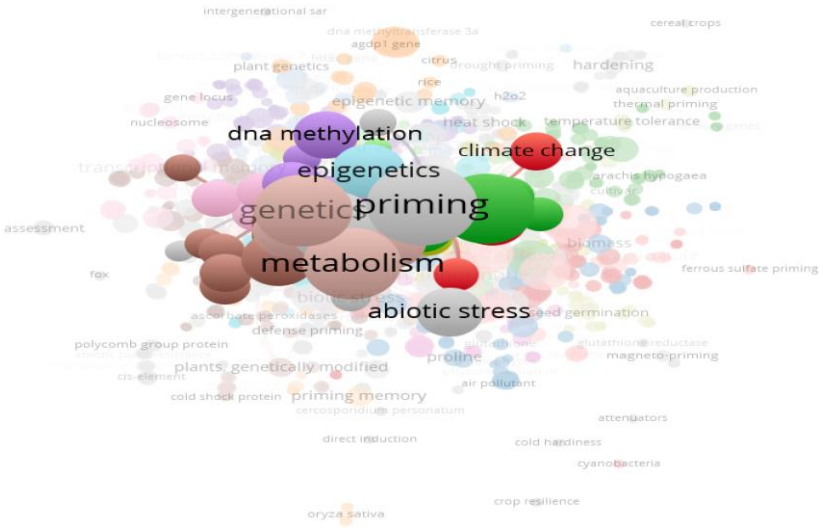


Figure 7. VOSviewer Computations for Keywords Cluster Zoomed in Priming Bubble.

3.3.6 Evolution of Keyword Clusters

Figure 8 illustrates the evolution of research trends in the fields of priming, stress memory, and plant science, as captured through keyword analysis spanning the years 2016 to 2024. The visualization highlights the centrality of key concepts such as "priming," "metabolism," and "abiotic stress," which appear prominently in the figure, signifying their foundational role in this area of study. These keywords dominate the network, reflecting the consistent interest and importance of these topics in understanding plant resilience and adaptive responses. A notable trend in the figure is the emergence of newer, lighter-colored keywords such as "seed priming," "epigenetic memory," and "climate change." These terms indicate a growing focus on applied and contemporary research themes. For example, the emphasis on "seed priming" aligns with agricultural efforts to enhance crop germination and yield under stress conditions, while "epigenetic memory" points to advances in understanding how plants retain and transmit stress adaptations across generations. Similarly, the inclusion of "climate change" highlights the increasing relevance of this research in addressing global environmental challenges. The clustering of terms like "DNA methylation," "histone methylation," and "chromatin" suggests a deeper integration of molecular and epigenetic approaches in studying plant stress responses. These advancements reflect the adoption of cutting-edge technologies and methodologies to explore the underlying mechanisms of priming and stress memory at a genetic and epigenetic level. Additionally, terms such as "osmotic stress," "germination," and "crop resilience" illustrate the practical applications of this research, particularly in improving plant performance under adverse environmental conditions. The appearance of keywords like "magneto-priming" and " prospect" in the periphery suggests emerging areas of exploration and innovation within the field.

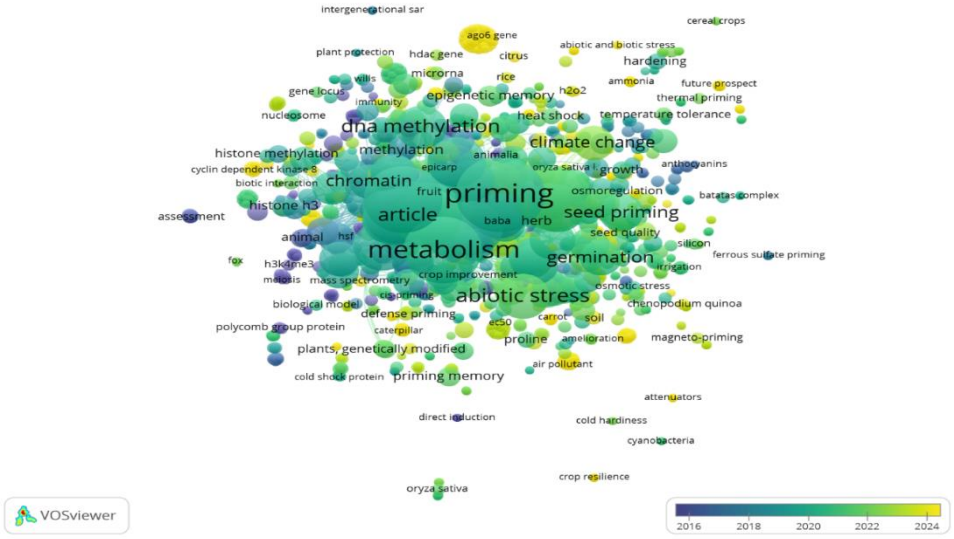


Figure 8. VOSviewer Computations for Evolution of Keyword Clusters.

3.3.6 Bibliometric Analysis

To achieve the fourth objective of this study, a focused bibliometric investigation was conducted. A subset of studies was carefully selected for detailed analysis, ensuring they addressed the core terms relevant to the research: "priming," "stress memory," and "plants." This targeted approach provided a clearer understanding of the trends, themes, and influential works within this niche area of plant science research. From the comprehensive search results, 10 studies were identified as highly relevant for the bibliometric study. These studies were selected based on their significant contributions to the understanding of the interplay between priming, stress memory, and plant responses. Table 2 presents the bibliometric analysis for the selected studies, offering insights into their publication details, citation metrics, and thematic focus. The studies analyzed in this subset highlight the growing interest in exploring how plants can "remember" stress through molecular, physiological, and epigenetic mechanisms. Priming, as a process that prepares plants to respond more effectively to future stresses, emerges as a pivotal concept, particularly in its application to developing climate-resilient crops. The selected studies reflect diverse approaches to investigating this phenomenon, ranging from laboratory experiments focused on molecular pathways to field trials assessing practical applications in agriculture. The bibliometric data also reveal key trends, such as the collaboration patterns among researchers, preferred journals for publishing on this topic, and shifts in research focus over time. These findings underscore the multidisciplinary nature of this research area, drawing from plant physiology, genetics, and agricultural science to address both fundamental questions and applied challenges. By narrowing the focus to these 10 key studies, this bibliometric analysis provides a deeper understanding of the current state of research on priming, stress memory, and plants, as well as identifying potential gaps and opportunities for future investigations.

Table 2. Table of bibliometric analysis regarding the terms “priming”, “stress memory”, and “plants”.

Bibliographic of Selected Studies		f	%
Authors (N=1,083)	Bäurle, I	15	1.39
	Li, X	7	0.65
	Abdelly, C	6	0.55
	Others	1,055	97.41
Subject Area (N=456)	Agricultural and Biological Sciences	219	48.03
	Biochemistry, Genetics, and Molecular Biology	129	28.29
	Environmental Sciences	35	7.67
	Others	73	16.01
Document Type (N=270)	Article	170	62.96
	Review	69	25.56
	Book Chapter	28	10.37
	Others	3	1.11
Source Title (N=270)	Frontiers in Plant Science	17	6.30
	Plant Physiology and Biochemistry	14	5.19
	Environmental and Experimental Biology	13	4.81
	Plant Cell and Environment	13	4.81
	Others	213	78.89
Publication Stage (N=270)	Final	265	98.15
	Article in Press	5	1.85
Keyword (N=1,766)	Priming	89	5.04
	Genetics	69	3.91
	Metabolism	69	3.91
	Stress Memory	66	3.74
	Others	1,473	83.40
Affiliation (N=663)	Universität Potsdam	17	2.56
	Chinese Academy of Sciences	13	1.96
	Freie Universität Berlin	12	1.81
	Others	621	93.67
Country (N=408)	Germany	49	12.01
	China	43	10.54
	India	39	9.56
	Others	277	67.89
Language (N=270)	English	264	97.78
	Chinese	5	1.85
	Russian	1	0.37
Open Access (N=344)	All Open Access	149	43.31
	Gold	80	23.26
	Green	64	18.60
	Bronze	27	7.85
	Hybrid Gold	24	6.98

As shown in Table 2, the bibliometric analysis provides a comprehensive overview of research output on "priming," "stress memory," and "plants" during the time period from 2007 to 2024. Among the 270 analyzed studies, Bäurle emerged as the most prolific author, contributing 15 documents or 1.39% of the total publications, demonstrating their significant involvement and expertise in this field, as exposed in Figure 9. The subject area with the highest representation is Agricultural and Biological Sciences, accounting for 48.03% of the total studies as reflected in Figure 10. This dominance reflects the core focus of these terms on understanding plant responses and adaptations in agricultural and ecological contexts. In terms of document

type, research articles constitute the majority, comprising 62.96% of the total as revealed in Figure 11. This indicates that the field is predominantly driven by empirical investigations and experimental studies, which form the foundation for theoretical and applied advancements. Among journals, *Frontiers in Plant Science* published the most articles, contributing 6.30% of the total output, further highlighting its prominence as a platform for disseminating research on plant science. The vast majority of the documents, 98.15%, are in their final publication stage, signifying that most studies have undergone peer review and formal publication processes. Keywords analysis reveals that "priming" is the most frequently used term, appearing in 5.04% of the studies, underscoring its central role in this research domain. Institutional analysis shows that Universität Potsdam is the leading institution, contributing 2.56% of the total publications, as mirrored in Figure 12. At the country level, Germany leads with 12.01% of the total documents, reflecting its strong research output and collaboration in this area, as shown in Figure 13. The linguistic analysis indicates that the vast majority of publications are written in English (97.78%), emphasizing the global nature of this research field and the predominance of English as the lingua franca of scientific communication. Furthermore, 43.31% of the documents are open access, facilitating broader dissemination and accessibility of research findings to the global scientific community.

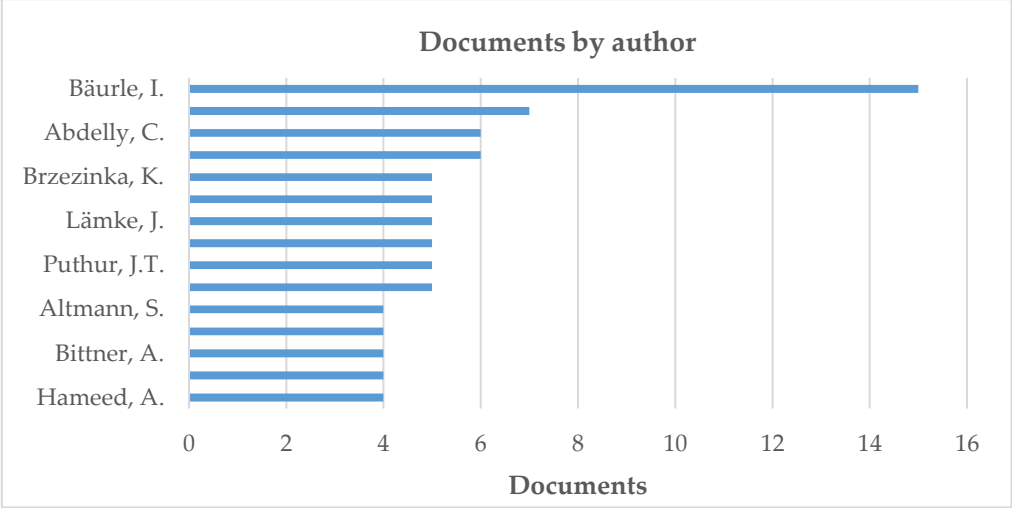


Figure 9. Ratio of Documents by Authors.

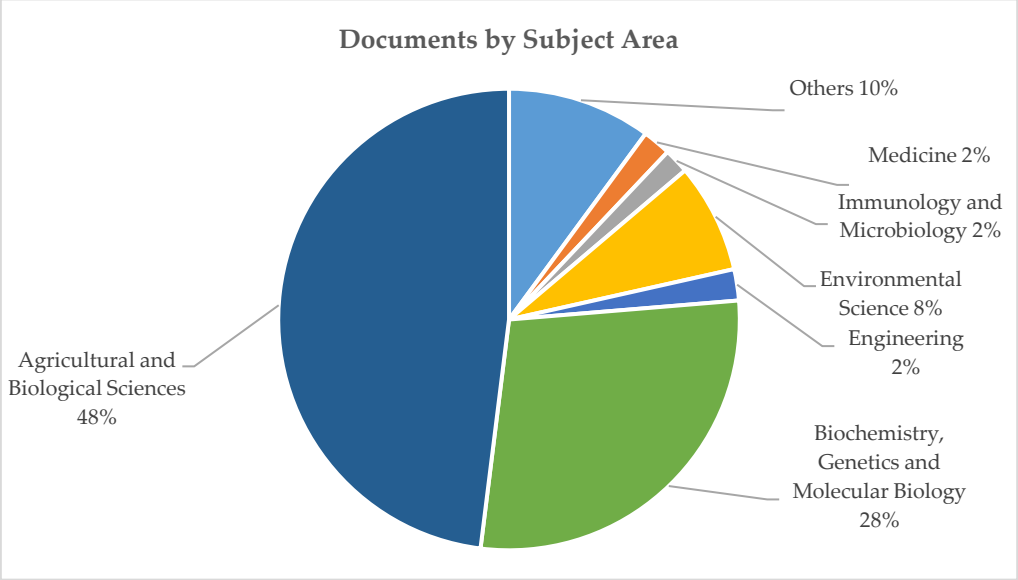


Figure 10. Ratio of Documents by Subject Area.

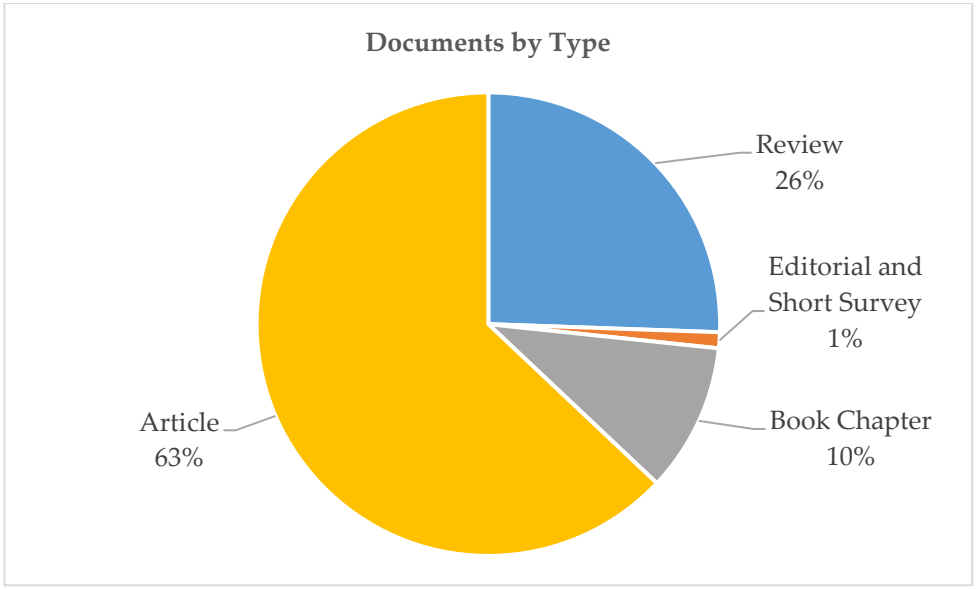


Figure 11. Ratio of Documents by Type.

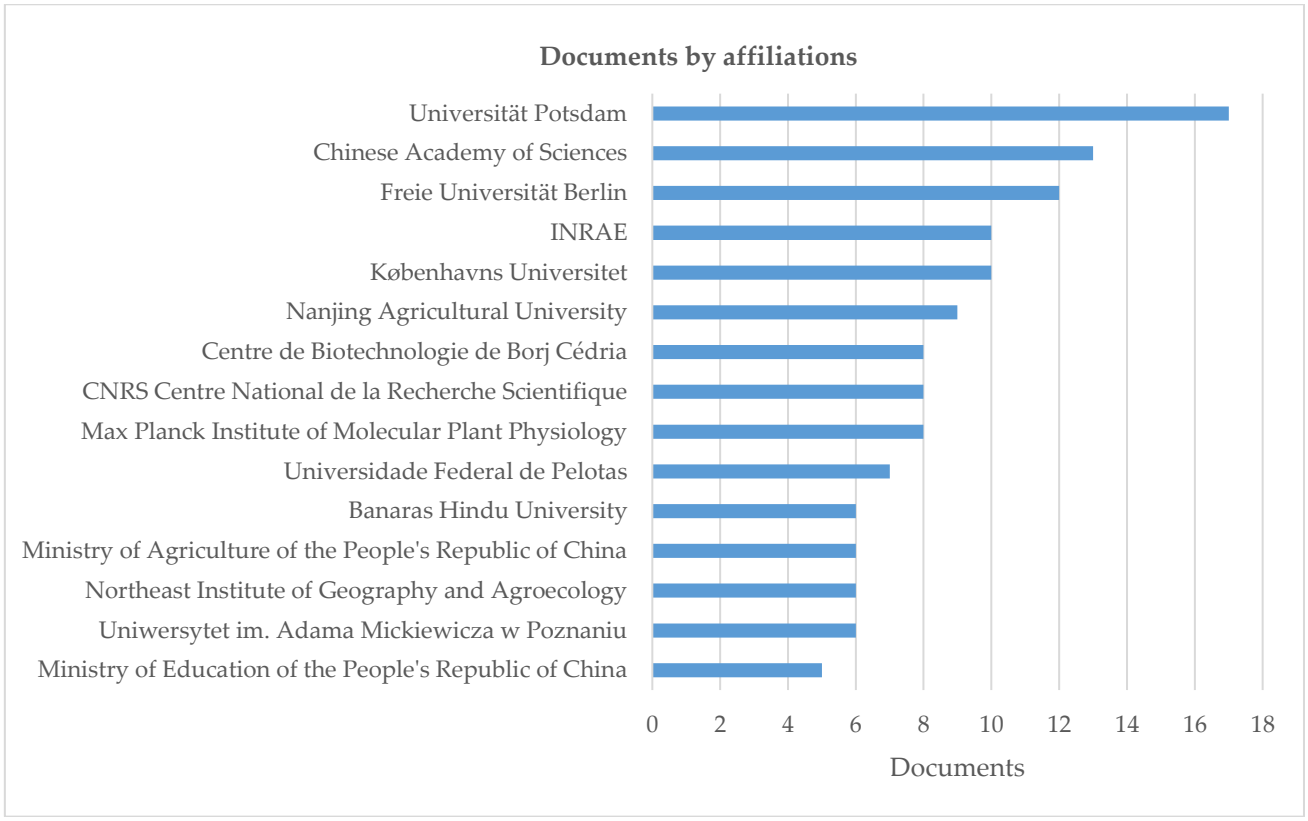


Figure 12. Ratio of Documents by Affiliations.

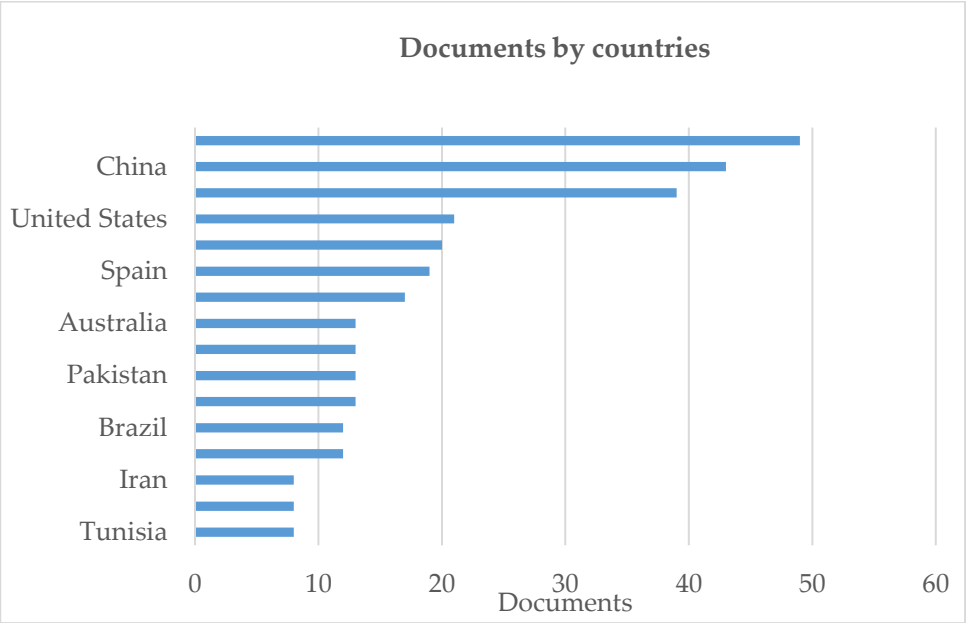


Figure 13. Ratio of Documents by Affiliations.

4. Conclusions

The results of our bibliometric analysis provide a detailed snapshot of the research trends surrounding stress memory and priming in plants, crops, and vegetation. The clustering of keywords reveals the diversity of themes explored within this field, including stress memory mechanisms, epigenetic modifications, transcriptional regulation, metabolic changes, and the practical applications of priming for enhancing crop resilience. The prominence of the keyword "priming" highlights its central role in current research, emphasizing its importance in understanding how plants respond to stress and how these responses can be leveraged to improve agricultural practices. Our analysis also reflects the collaborative nature of this research, with significant international partnerships, particularly between Germany and China, driving much of the output. Interestingly, while the majority of the studies are published in Agricultural and Biological Sciences, there is a notable focus on the practical applications of these findings, aiming to improve crop performance and environmental resilience. When analyzing the bibliometric data, it is evident that most studies are in the final publication stage, and a large proportion of them are openly accessible, promoting broader dissemination of knowledge. Similar to other emerging fields, there is a notable emphasis on research articles, which account for the bulk of the documents analyzed. Overall, this growing body of work signifies the increasing importance of stress memory and priming in plants as a key area of inquiry for advancing agricultural sustainability and resilience.

5. Acknowledgements

The author sincerely thank Professor Greta G. Gabinete for her invaluable guidance and support throughout the study. The Office of the Vice-President for Research Innovation and Extension and the University Research Development Center of West Visayas State University for sharing their resources and invaluable support during the conduct of the study.

Funding: This research received no external funding.

Conflicts of Interest: The authors declare no conflict of interest.

References

[1] Avramova, Z. Defence-Related Priming and Responses to Recurring Drought: Two Manifestations of Plant Transcriptional Memory Mediated by the ABA and JA Signalling Pathways. *Plant, Cell Environ.* **2019**, *42*(3), 983–997. https://doi.org/10.1111/pce.13458

[2] Kambona, C. M.; Koua, P. A.; Léon, J.; Ballvora, A. Stress Memory and Its Regulation in Plants Experiencing Recurrent Drought Conditions. *Theor. Appl. Genet.* **2023**, *136*(2), 3. https://doi.org/10.1007/s00122-023-04313-1

[3] Ramakrishnan, M.; Ceasar, S. A.; Duraipandiyan, V.; Al-Dhabi, N. A. The Emerging Role of Stress Memory and Priming in Plants under Climate Change. *Environ. Exp. Bot.* **2022**, *200*, 105884. https://doi.org/10.1016/j.envexpbot.2022.105884

[4] Junaid, M. D.; Chaudhry, U. K.; Şanlı, B. A.; Gökçe, A. F.; Öztürk, Z. N. A Review of the Potential Involvement of Small RNAs in Transgenerational Abiotic Stress Memory in Plants. *Funct. Integr. Genomics* **2024**, *24*(2), 74. https://doi.org/10.1007/s10142-024-01354-7

[5] Conrath, U. Molecular Aspects of Defence Priming. *Trends Plant Sci.* **2011**, *16*(10), 524–531. https://doi.org/10.1016/j.tplants.2011.06.004

[6] Bräutigam, K.; Vining, K. J.; Lafon-Placette, C.; et al. Epigenetic Regulation of Adaptive Responses of Forest Tree Species to the Environment. *Ecol. Evol.* **2013**, *3* (2), 399–415. https://doi.org/10.1002/ece3.461

[7] Avramova, Z. Transcriptional "Memory" of a Stress: Transient Chromatin and Memory (Epigenetic) Marks at Stress-Response Genes. *Plant J.* **2015**, *83* (1), 149–159. https://doi.org/10.1111/tpj.12832

[8] Bäurle, I.; Trindade, I. Chromatin Regulation of Somatic Abiotic Stress Memory. *J. Exp. Bot.* **2020**, *71*(17), 5269–5279. https://doi.org/10.1093/jxb/eraa098

[9] Alves de Freitas Guedes, F.; Menezes-Silva, P. E.; DaMatta, F. M.; Alves-Ferreira, M. Using Transcriptomics to Assess Plant Stress Memory. *Theor. Exp. Plant Physiol.* **2019**, *31*(1), 47–58. https://doi.org/10.1007/s40626-018-0135-0

[10] Lagiotis, G.; Madesis, P.; Stavridou, E. Echoes of a Stressful Past: Abiotic Stress Memory in Crop Plants towards Enhanced Adaptation. *Agriculture* **2023**, *13*(11), 2090. https://doi.org/10.3390/agriculture13112090

[11] Liu, H.; Able, A. J.; Able, J. A. Priming Crops for the Future: Rewiring Stress Memory. *Trends Plant Sci.* **2022**, *27* (7), 699–716. https://doi.org/10.1016/j.tplants.2021.11.015

[12] Zuo, D.-D.; Ahammed, G. J.; Guo, D.-L. Plant Transcriptional Memory and Associated Mechanism of Abiotic Stress Tolerance. *Plant Physiol. Biochem.* **2023**, *201*, 107917. https://doi.org/10.1016/j.plaphy.2023.107917

[13] Nair, A. U.; Bhukya, D. P. N.; Sunkar, R.; Chavali, S.; Allu, A. D. Molecular Basis of Priming-Induced Acquired Tolerance to Multiple Abiotic Stresses in Plants. *J. Exp. Bot.* **2022**, *73*(11), 3355–3371. https://doi.org/10.1093/jxb/erac089

[14] Siddique, K. H. M.; Frei, M.; Puthur, J. T.; Ul-Allah, S.; Farooq, M. Harnessing Stress Memory and Priming for Climate-Smart Agriculture. *Plant Physiol. Rep.* **2024**, *29*(2), 315–330. https://doi.org/10.1007/s40502-024-00753-z

[15] Pissolato, M. D.; Martins, T. S.; Fajardo, Y. C. G.; et al. Stress Memory in Crops: What We Have Learned so Far. *Theor. Exp. Plant Physiol.* **2024**, *36* (3), 535–565. https://doi.org/10.1007/s40626-024-00315-6

[16] Turgut-Kara, N.; Arikan, B.; Celik, H. Epigenetic Memory and Priming in Plants. *Genetica* **2020**, *148*(2), 47–54. https://doi.org/10.1007/s10709-020-00093-4

[17] Xu, W.-B.; Cao, F.; Liu, P.; Yan, K.; Guo, Q.-H. The Multifaceted Role of RNA-Based Regulation in Plant Stress Memory. *Front. Plant Sci.* **2024**, *15*, 1387575.

[18] Farooq, M. Plant Stress Memory: Mechanisms and Applications in Sustainable Agriculture. *Plant Physiol. Rep.* **2025**, *30*(1), 112–128. https://doi.org/10.1007/s40502-025-00788-x

[19] Tian, Z.; Li, K.; Sun, Y.; et al. Physiological and Transcriptional Analyses Reveal Formation of Memory under Recurring Drought Stresses in Seedlings of Cotton (*Gossypium hirsutum*). *Plant Sci.* **2024**, *338*, 111920. https://doi.org/10.1016/j.plantsci.2023.111920

[20] Ding, Y.; Fromm, M.; Avramova, Z. Multiple Exposures to Drought "Train" Transcriptional Responses in *Arabidopsis*. *Nat. Commun.* **2012**, *3*, 740. https://doi.org/10.1038/ncomms1732

[21] Zheng, Y.-Q.; Wang, Q.-L.; Chen, D.-Q.; et al. Research Advances in Histone Modification-Regulated Plant Stress Memory and Defense Priming. *Chin. J. Appl. Ecol.* **2022**, *33*(3), 844–854. https://doi.org/10.13287/j.1001-9332.202202.039

[22] Zheng, S.; Zhao, W.; Liu, Z.; et al. Establishment and Maintenance of Heat-Stress Memory in Plants. *Int. J. Mol. Sci.* **2024**, *25*(16), 8976. https://doi.org/10.3390/ijms25168976

[23] Lämke, J.; Bäurle, I. Epigenetic and Chromatin-Based Mechanisms in Environmental Stress Adaptation and Stress Memory in Plants. *Genome Biol.* **2017**, *18*(1), 124. https://doi.org/10.1186/s13059-017-1263-6

[24] Alongi, F.; Petek-Petrik, A.; Mukarram, M.; et al. Somatic Drought Stress Memory Affects Leaf Morpho-Physiological Traits via Epigenetic Mechanisms and Phytohormonal Signalling. *Plant Gene* **2025**, *42*, 100509. https://doi.org/10.1016/j.plgene.2025.100509

[25] Raza, A. Molecular Mechanisms Underpinning Plant Stress Responses: Insights into the Cellular and Systemic Regulation. In *Molecular Dynamics of Plant Stress and Its Management*; Springer, **2024**; pp 3–24. https://doi.org/10.1007/978-981-97-1699-9_1

[26] Sedaghatmehr, M.; Thirumalaikumar, V. P.; Kamranfar, I.; et al. A Regulatory Role of Autophagy for Resetting the Memory of Heat Stress in Plants. *Plant, Cell Environ.* **2019**, *42*(3), 1054–1064. https://doi.org/10.1111/pce.13426

[27] Shchennikova, A. V.; Filyushin, M. A.; Kochieva, E. Z. Stress Memory in Plants: Key Aspects. *Sel'skokhozyaistvennaya Biologiya* **2025**, *60*(3), 397–414. https://doi.org/10.15389/agrobiology.2025.3.397rus

[28] Kumar, B. S.; Saravanan, K. R.; Sudhakar, P.; et al. Stress Memory and Its Mitigation via Responses through Physiological and Biochemical Traits in Mung Bean under Moisture Stress. In *Legumes: Physiology and Molecular Biology of Abiotic Stress Tolerance*; Springer, **2023**; pp 323–343. https://doi.org/10.1007/978-981-19-5817-5_13

[29] He, Y.; Dai, Y.; Li, H.; Li, M.; Zhang, S. Growth and Defense Trade-Offs in Dioecious *Salix myrtillacea* Exposed to Drought and Low Temperature Stress. *Environ. Exp. Bot.* **2023**, *215*, 105504. https://doi.org/10.1016/j.envexpbot.2023.105504

[30] Kiriziy, D.; Kedruk, A.; Stasik, O. Effects of Drought, High Temperature and Their Combinations on the Photosynthetic Apparatus and Plant Productivity. In *Regulation of Adaptive Responses in Plants*; Springer, **2024**; pp 1–32.

[31] Arıkan, B.; Çakır, Ö.; Turgut Kara, N. Epigenetic and Transcriptomic Features of Stress Memory during Salt-Stress Priming in *Arabidopsis*. *Plant Sci.* **2026**, *362*, 112775. https://doi.org/10.1016/j.plantsci.2025.112775

[32] Bakhchevnikov, O. N.; Braginets, S. V.; Kravchenko, N. S.; Pakhomov, V. I. Physical Eustressors as Potential Tools to Improve Crop Stress Tolerance. *Sib. J. Life Sci. Agric.* **2023**, *15*(6), 360–386. https://doi.org/10.12731/2658-6649-2023-15-6-998

[33] Li, H.; Li, X.; Liu, S.; Zhu, X.; Song, F.; Liu, F. Induction of Cross Tolerance by Cold Priming and Acclimation in Plants. In *Priming-Mediated Stress and Cross-Stress Tolerance in Crop Plants*; Academic Press, **2020**; pp 183–201. https://doi.org/10.1016/B978-0-12-817892-8.00012-X

[34] van Eck, N. J.; Waltman, L. Software Survey: VOSviewer, a Computer Program for Bibliometric Mapping. *Scientometrics* **2010**, *84*(2), 523–538. https://doi.org/10.1007/s11192-009-0146-3

ASEAN
Journal of Scientific and Technological Reports
Online ISSN:2773-8752

Research article

Enhanced Thermal Efficiency of Solar Air Heaters Using Porous Material: An Experimental Approach

Eakpoom Boonthum[1], Prapanphong Somsila[2], Apinunt Namkhat[1], Sorawit Sonsaree[3], and Umphisak Teeboonma[1*]

[1] Faculty of Engineering, Ubon Ratchathani University, Ubon Ratchathani, 34190, Thailand
[2] Faculty of Agriculture and Technology, Rajamangala University of Technology Isan, Surin Campus, Surin, 32000, Thailand
[3] Faculty of Industrial Technology, Pibulsongkram Rajabhat University, Phitsanulok, 65000, Thailand
* Correspondence: umphisak.t@ubu.ac.th

Citation:
Boonthum, E.; Somsila, P.; Namkhet, A.; Sonsaree, S.; Teeboonma, U. Enhanced thermal efficiency of solar air heaters using porous materials: an experimental approach. *ASEAN J. Sci. Tech. Report.* **2026**, *29*(1), e259025. https://doi.org/10.55164/ajstr.v29i1.259025.

Article history:
Received: Apri1 28, 2025
Revised: November 2, 2025
Accepted: November 4, 2025
Available online: December 14, 2025

Publisher's Note:
This article is published and distributed under the terms of the Thaksin University.

Abstract: This study presents a detailed experimental investigation into the energy and exergy efficiencies of a double-pass solar air heater (SAH) augmented with porous materials. The primary objective was to assess the impact of integrating steel-based hollow square porous elements, featuring porosities of 0.98 and 0.99, on the thermodynamic performance of the SAH under tropical environmental conditions. A prototype SAH with dimensions of 0.75 m × 1.85 m × 0.25 m was developed and evaluated based on empirical data encompassing solar irradiance, air inlet and outlet temperatures, and mass flow rate. The results demonstrate a significant improvement in both energy and exergy efficiencies with the incorporation of porous materials. Notably, the configuration with 0.98 porosity yielded superior results, with energy efficiencies ranging from 6.19% to 9.01% and a peak exergy efficiency of 0.26%. In comparison, the reference system without porous material exhibited lower average energy and exergy efficiencies of 4.98% and 0.11%, respectively. Furthermore, the porous media contributed to enhanced thermal inertia, leading to improved heat retention and a more stable outlet temperature profile under fluctuating solar irradiance. These findings underscore the thermodynamic advantages of utilizing high-porosity materials within a double-pass SAH, emphasizing their potential for efficient thermal energy conversion in agricultural and industrial drying applications, particularly in regions with high solar potential.

Keywords: Solar air heater; porous materials; energy efficiency; exergy efficiency; experimental

1. Introduction

Solar energy constitutes a renewable and environmentally sustainable resource capable of long-term, uninterrupted exploitation. Positioned within the equatorial zone, Thailand possesses substantial solar energy potential. The utilization of solar radiation in the country predominantly follows two main pathways: direct conversion into electrical energy and thermal energy applications. Given Thailand's high solar irradiance levels, deploying solar collectors for thermal processes, particularly in drying and industrial heating applications, presents a highly viable and promising approach. Furthermore, as an agriculturally oriented nation, Thailand's solar energy applications support agricultural processes and enhance energy sustainability. Therefore, the application of solar energy in agriculture predominantly involves its use as a

thermal source. In the industrial sector, solar energy preheats air, reducing conventional energy consumption in thermal processes. In agricultural and industrial contexts, solar energy is frequently integrated as a primary heat source in drying systems to enhance energy efficiency and sustainability [1-3]. The solar collector is the device employed to elevate air temperature for thermal applications. Nevertheless, the deployment of solar energy continues to face challenges, primarily due to the intermittent and variable nature of solar irradiance. Solar energy systems are limited by seasonal and weather-dependent variations in intensity. On average, solar radiation on Earth's surface is approximately 1,000 W/m². The Sun's surface temperature is estimated to be approximately 5778 K, commonly referred to as its effective temperature. This parameter represents the temperature of an ideal blackbody that would radiate the same total energy per unit area as the Sun across the entire electromagnetic spectrum [4-6]. Optimizing solar exposure through angle adjustments aligned with the Sun's trajectory can significantly enhance energy capture. In Thailand, solar radiation averages 4–5 kWh/m²/day, and the use of tracking systems can further increase energy gain by 1.3 to 1.5 times [7,8]. Over the past decades, extensive research efforts have been dedicated to exploring diverse strategies aimed at improving the thermal performance of solar air heaters. Ismail et al. [9] investigated a double-pass solar air heater enhanced with lava rock as a porous medium. Incorporating lava rock improved the system's thermal storage capacity, positioning it as an effective short-term thermal energy collector for solar drying applications. Its presence increased convective heat transfer by enlarging the effective surface area and promoting airflow turbulence. A numerical model based on energy balance equations was developed and solved using MATLAB to assess thermal performance under varying solar radiation and wind conditions. Key parameters included collector dimensions, air mass flow rate, and lava rock volume. The optimal thermal efficiency ranged from 62% to 64% under solar irradiance between 500 and 800 W/m², with a peak efficiency at a flow rate of 0.035 kg/s. An optimal porosity of approximately 89% was identified, balancing thermal performance with pressure drop. The system attained output air temperatures between 41.7°C and 48.3°C, making it suitable for food and agricultural drying. Compared to conventional DPSAH configurations, the lava rock-enhanced system achieved over 17.5% higher outlet temperatures, confirming its potential for improving thermal efficiency. Srivastava et al. [10] conducted an experimental investigation into the thermal performance of a flat plate solar collector and a solar dryer. Their study presented the performance characteristics of the solar collector and solar dryer integrated with a phase change material storage system under quasi-steady-state conditions. The analysis was based on the fundamental energy balance of the system, and a computational model was developed to predict various performance parameters of the solar drying system. The study compared its predictions with theoretical calculations to validate the thermal model. Additionally, optimal values for both solar collector efficiency and dryer efficiency were determined using a genetic algorithm. A comparative assessment was performed among the experimental, theoretical, and optimized efficiency values of the solar collector and dryer. Experimental trials were conducted over multiple days between June 2013 and March 2014 to evaluate the empirical performance of the system. The findings indicated strong agreement between the theoretical, experimental, and optimized efficiency values of the solar collector and dryer, reinforcing the reliability of the proposed model. Jadallah et al. [11] conducted a comprehensive investigation into the performance of a dual-pass hybrid photovoltaic-thermal (PVT) solar cell system designed for drying applications. Their study encompassed both theoretical and experimental analyses, including the design, construction, and modeling of the system to simulate its output. The PVT heat collector extracts hot air, which can be utilized as a heat source for drying processes. Key performance parameters, including temperature distribution, useful heat, electrical power generation, and thermal efficiency, were evaluated using MATLAB, a software specifically developed for this purpose. The findings indicate that the highest outlet fluid temperature achieved was 63°C at a lower mass flow rate of 0.017 kg/s. Furthermore, at a higher mass flow rate, the system exhibited peak electrical, thermal, and overall efficiencies of 12.65%, 56.73%, and 85%, respectively. The maximum electrical and thermal power outputs were recorded at 50.57 W and 389.37 W, respectively. These results demonstrate the system's potential for efficient integration into drying applications, leveraging both electrical and thermal energy outputs. Kumar et al. [12] conducted a comprehensive study on the influence of porous materials on the flow characteristics and temperature distribution within a passive solar air heater. The research examines the impact of flow resistance induced by a porous medium, which

represents agricultural products, at the outlet of a free-convection-based solar air heater. Both experimental and numerical approaches were employed to analyze these effects. The findings provide valuable insights into optimizing the design and efficiency of solar air heaters for agricultural drying applications. Additionally, incorporating porous materials into solar collector absorber plates has been shown to significantly enhance thermal efficiency and stabilize air temperatures, even during periods of low solar radiation [13-16]. Research has demonstrated that combining porous materials with advanced solar collector panels enhances drying performance and energy efficiency [17-20]. Porous materials improve thermal energy retention and gradual release, ensuring stable drying chamber temperatures. Moreover, an experimental study was undertaken to enhance the thermal efficiency of hot air temperature augmentation systems by integrating porous materials. Hwang et al. [21] conducted an extensive investigation focusing on the design and performance assessment of high-efficiency solar air heaters embedded with porous structures. Their work involved the development of a comprehensive theoretical model, which was subsequently validated through experimental testing. The study systematically examined the radiative characteristics of glass covers and porous absorber materials to optimize thermal performance. The experimental outcomes indicated that daily thermal efficiencies consistently surpassed 60%, aligning closely with theoretical estimations. Integrating porous materials significantly enhanced thermal efficiency, with empirical results confirming the precision and practical relevance of the proposed theoretical framework. Hameed et al. [22] conducted an experimental investigation to assess the influence of integrating porous materials, specifically steel wool, on the thermal performance of single-pass solar air heaters. The study involved a comparative analysis between conventional flat absorber plates and those modified with porous media, focusing on key performance parameters such as outlet air temperature and thermal efficiency across different air mass flow rates. Two configurations were examined: a standard setup and one incorporating steel wool positioned above the absorber plate. Experiments were conducted at air mass flow rates of 0.015 and 0.035 kg/s. The findings revealed that the outlet temperature increased by 12.28% and 21.32% at flow rates of 0.015 and 0.035 kg/s, respectively. Furthermore, incorporating porous materials improved thermal efficiency by approximately 10%. These results underscore the effectiveness of porous materials integration in enhancing outlet air temperatures and overall thermal efficiency in solar air heaters. Jalil and Ali [23] conducted an experimental evaluation of the thermal performance of a double-pass solar air heater utilizing stainless steel mesh and steel wool as porous media. The study systematically examined the influence of key porous media properties, including porosity, thermal conductivity, and mass flow rate, on the system's thermal efficiency. The findings demonstrated that including porous materials resulted in a notable enhancement in thermal efficiency compared to configurations without porous media. Specifically, steel wool exhibited a maximum thermal efficiency of 79.82%, while stainless steel mesh achieved 76%. Furthermore, the efficiency improvements associated with steel wool at porosities of 98.75%, 97.5%, and 96.25% were recorded as 6%, 12.6%, and 31.7%, respectively. The results conclusively indicate that porous materials characterized by lower porosity and higher thermal conductivity substantially augment the thermal efficiency of double-pass solar air heaters. Abo-Elfadl et al. [24] investigated the energy, exergy, and economic performance of a novel tubular solar air heater incorporating porous materials. The study systematically assessed the impact of porous media and flow configurations (single-pass and double-pass) on key performance indicators, including energy gain, outlet air temperature, energy, and exergy efficiencies, as well as economic factors such as payback period and overall system cost. An experimental setup was established to compare the performance of tubular and conventional flat-plate solar air heaters under both single and double-pass flow configurations at varying air mass flow rates of 0.075, 0.05, and 0.025 kg/s. The findings demonstrated that integrating porous materials significantly enhanced outlet air temperature. Additionally, the tubular solar air heater with porous media exhibited superior energy, exergy, and economic performance compared to its flat-plate counterpart. Salih et al. [25] conducted an experimental investigation to assess the performance effects of integrating porous media within double-pass solar air heaters operating under natural and forced convection conditions. The study evaluated system efficiency and temperature differentials under consistent winter environmental settings, with the solar air heaters designed using double glass covers. The results demonstrated that double-pass solar air heaters incorporating porous materials achieved notably higher thermal efficiencies than those without, under natural and forced air circulation. The

presence of porous material was found to substantially enhance heat transfer rates and overall system performance, with the improvements particularly pronounced under forced convection conditions. Previous studies have demonstrated that incorporating porous materials into solar air heaters significantly enhances their thermal performance. Consequently, enhancing the thermal efficiency and overall performance of solar air heaters has become a focal point of contemporary research. However, a critical analysis of the existing literature reveals a research gap concerning the integration of porous materials in solar collectors to augment their thermal performance. In response to this gap, the present study investigates the effect of incorporating porous materials, specifically steel hollow square elements, on the absorber plate of a solar collector. The study also examines key influencing parameters and their interdependencies to comprehensively understand their impact on system efficiency. Furthermore, this investigation aims to demonstrate the potential of the proposed configuration in achieving elevated outlet air temperatures while enabling thermal energy storage during periods of low or no solar irradiance, such as cloudy conditions.

2. Materials and Methods

2.1 Experimental setup

This study conducted experimental investigations using a double-pass solar air heater. The solar air heater was constructed with a width of 0.75 m, a length of 1.85 m, and a height of 0.25 m, featuring an absorber plate made of 0.0015 m-thick steel. To enhance thermal efficiency, porous structures were introduced and fabricated from perforated steel sheets with a 0.01 m diameter and a thickness of 0.0012 m. These sheets were precisely cut and assembled into hollow rectangular enclosures with dimensions of 0.05 m × 0.05 m and 0.1 m × 0.1 m, corresponding to porosities of 0.99 and 0.98, respectively. The enclosures extended across the width of the solar collector and were positioned directly above the absorber plate to improve heat absorption and retention. Centrifugal fans are used to introduce air into the solar air heater from the top of the absorber plate, where it flows downward, circulates toward the bottom of the absorber plate, and is subsequently discharged from the solar air heater. The schematic diagram and photographic representations of the solar air heater and porous material are presented in Figures 1 and 2.

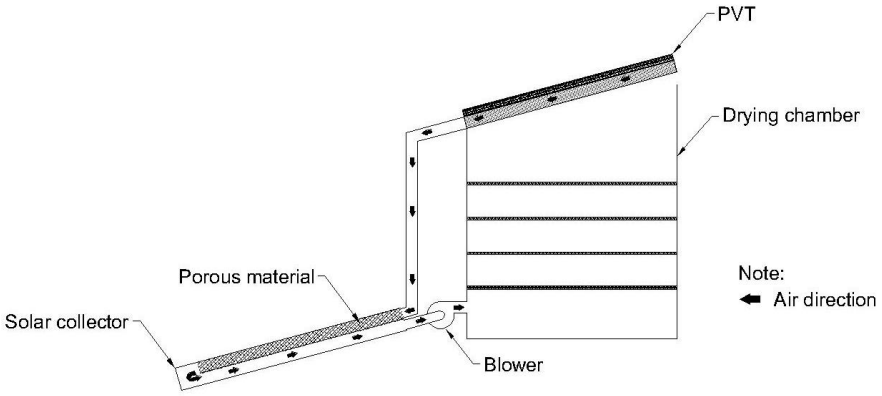


Figure 1. Schematic diagram of the solar air heater.

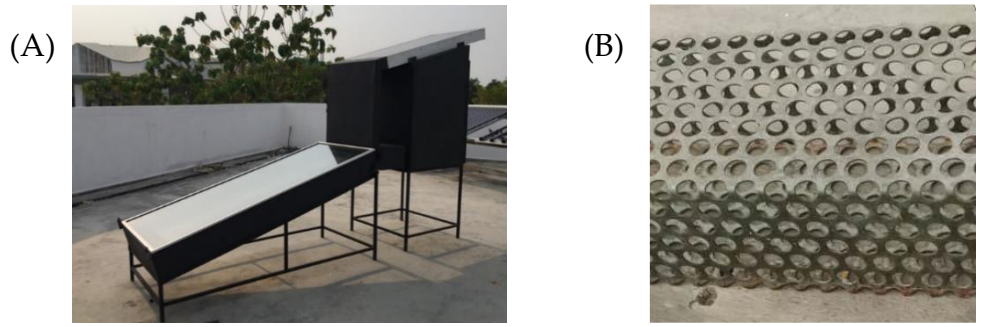


Figure 2. (A) Photograph of the solar air heater, (B) Photograph of porous material.

The experimental evaluation of the solar air heater (SAH) was conducted in Thailand under tropical climatic conditions during clear-sky days on 4th November and 24th December 2024, between 9:00 a.m. and 4:00 p.m., and data were collected over three test runs. The air velocity within the solar air heater was measured using a hot-wire anemometer, featuring a measurement range of 0 to 20 m/s, a tolerance of ±0.03 m/s ±5%, and a resolution of 0.1 m/s. Throughout the experimental procedures, the air velocity was maintained at 0.07 m/s, corresponding to the minimum airflow typically used in solar dryers. Temperature measurements were recorded using K-type thermocouples connected to a data logger, with an accuracy of ±1 °C. The solar irradiation values were recorded using a calibration from the power generation rate of the solar cell compared to a TENMARS solar radiation meter model TM-207 with an accuracy of 5% and a resolution of 1 W/m². Figures 3 and 4 show solar irradiation measurement instruments and calibration results of the solar cell and the solar irradiation meter.

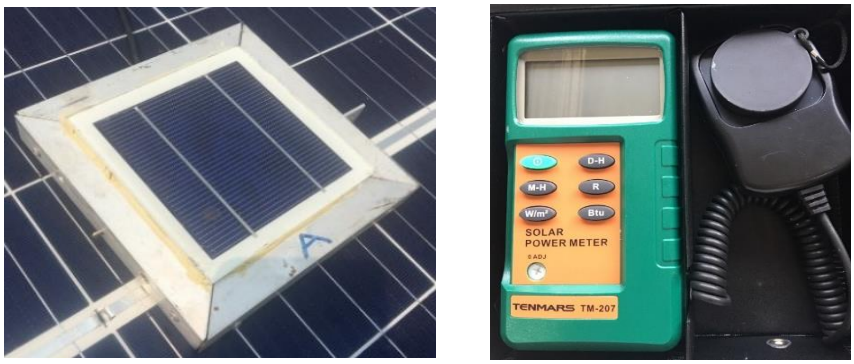


Figure 3. Solar irradiation measurement instruments.

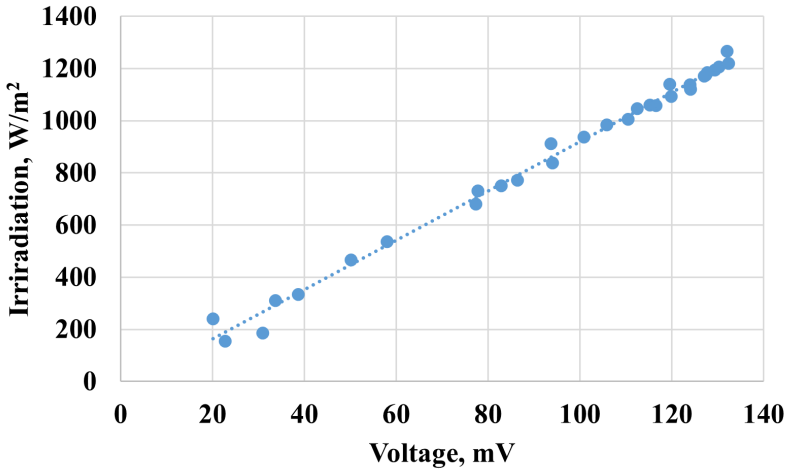


Figure 4. Calibration results for solar cells and a solar irradiance meter.

Based on the calibration results of the solar cell and solar irradiation meter, the relationship can be expressed as Equation (1). The calibration demonstrated a high coefficient of determination ($R^2 = 0.9934$) and was validated for solar irradiance levels within the range of 300–1200 W/m².

$$I = 9.4607V - 27.152 \quad (1)$$

I = solar irradiance (W/m²)
(representing the equivalent solar irradiation measured by calibrated photovoltaic cells)
V = voltage output generated by the solar cell (mV)

Porosity is a fundamental characteristic of porous materials. It represents the proportion of void space relative to the material's total bulk volume. It can be calculated using the following general formula [9]:

$$\phi = \frac{V_v}{V_t} \tag{2}$$

ϕ = porosity of porous materials
V_v = volume of the pore (m^3)
V_t = total (bulk) volume of the material (m^3)

2.2 Analysis

Equation 3 is the fundamental governing equation for determining the useful energy of air through a solar air heater.

$$Q_a = mc_p\Delta T = \rho V c_p \Delta T \tag{3}$$

Q_a = useful heat (kJ)
m = mass flow rate (kg/s)
c_p = specific heat capacity (kJ/kg·K)
ΔT = temperature variation between outlet and inlet (°C)
ρ = air density (kg/m^3)
V = air volume flow rate (m^3/s)

The following equation, equation 4, can calculate the thermal efficiency of 1st law of thermodynamics:

$$\eta_{th} = \frac{Q_a}{I \cdot A_c} \tag{4}$$

Q_a = useful heat (kJ)
I = solar irradiation (W/m^2)
A_c = Solar collector area (m^2).

Exergy denotes the maximum useful work a system can achieve as it progresses toward thermodynamic equilibrium with its environment. In a solar air heater (SAH), exergy analysis is critical for assessing the system's intrinsic thermodynamic performance, extending beyond the conventional first-law energy analysis. The exergy efficiency, grounded in the second law of thermodynamics, can be determined using the following expression in equation 5.

$$\eta_{ex} = \frac{mc_p\left[(T_o - T_i) - T_{amb} ln\left(\frac{T_o}{T_i}\right)\right]}{I \cdot A_c\left(1 - \frac{T_{amb}}{T_{sun}}\right)} = \frac{\rho V c_p\left[(T_o - T_i) - T_{amb} ln\left(\frac{T_o}{T_i}\right)\right]}{I \cdot A_c\left(1 - \frac{T_{amb}}{T_{sun}}\right)} \tag{5}$$

T_{amb} = ambient air temperature (K)
T_o = outlet air temperature (K)
T_i = inlet air temperature (K)
T_{sun} = Sun temperature (K).

2.3 Uncertainty Analysis

Measurement uncertainties were considered for key parameters, including air temperature, velocity, and solar irradiance. The uncertainties associated with the K-type thermocouples, hot-wire anemometer, and solar radiation meter were ±1.0 °C, ±5%, and ±5%, respectively. The combined uncertainty for calculated quantities such as thermal efficiency (η_{th}) and exergy efficiency (η_{ex}) was estimated using the general error propagation formula:

$$\frac{\Delta R}{R} = \sqrt{\left(\frac{\Delta T}{T}\right)^2 + \left(\frac{\Delta I}{I}\right)^2 + \left(\frac{\Delta V}{V}\right)^2} \quad (6)$$

R = calculated result (thermal efficiency, exergy efficiency)
T, I, V = measured parameters (air temperature, solar irradiance, air velocity)
Δ = respective uncertainties

Table 1 shows a summary of the individual uncertainties for each measured parameter. Applying this approach, the combined relative uncertainty for thermal and exergy efficiency was approximately ±7% and ±9%, respectively, under typical experimental conditions.

Table 1. Summarizes the individual uncertainties for each measured parameter.

Measurement	Value (example)	Uncertainty (%)	Instrument
Air temperature (T)	30–50 °C	±1.0 °C (≈±3%)	K-type thermocouple
Solar irradiance (I)	600–900 W/m²	±5%	Solar meter (TM-207)
Air velocity (V)	0–20 m/s	±5%	Hot-wire anemometer

3. Results and Discussion

An experimental analysis was performed without porous materials from 9:00 a.m. to 4:00 p.m. The study provided crucial insights into solar radiation levels and temperature profiles across the solar air heater (SAH). Figure 5 shows the experimental result of SAH without porous materials. Solar radiation values ranged from 572 to 872 W/m², with an average of 717.1 W/m². The inlet air temperature varied between 29°C and 32°C, with a mean temperature of 30.2°C. The outlet temperature fluctuated between 33°C and 48°C, with an average of 40.2°C. The temperature inside SAH ranged from 30°C to 46°C, with an average of 37.5°C. Recorded ambient temperatures ranged from 29°C to 31°C, with a mean value of 29.6°C. Additionally, the temperature of the glass panel ranged from 31°C to 51°C, with an average temperature of 42.1°C. The findings of this investigation are presented in Figure 5, illustrating that the outlet temperature of SAH exhibits significant variation in response to fluctuations in solar irradiance. An increase in solar irradiance corresponds to a rise in outlet temperature. In contrast, reducing irradiance, such as during intermittent cloud cover, dramatically decreases outlet temperature, resulting in continuous dynamic changes.

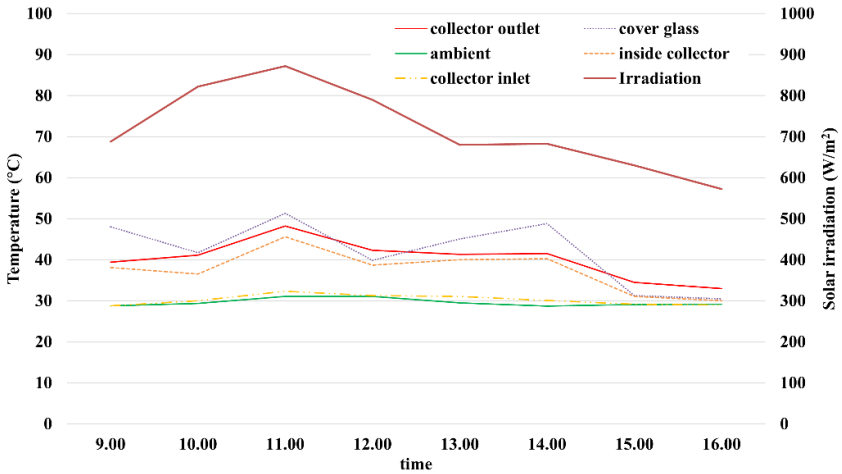


Figure 5. Temperature profile of the SAH without porous material.

Figure 6 shows an experimental result of SAH with porous material with 0.99 porosity. Solar radiation values ranged from 725 to 960 W/m², with an average of 809.8 W/m². The inlet air temperature varied between 27°C and 33°C, with a mean temperature of 30.7°C. The outlet temperature fluctuated between 39°C and 46°C, with an average of 42.5°C. The temperature inside the SAH ranged from 36°C to

42°C, with an average of 39.1°C. Recorded ambient temperatures ranged from 26°C to 33°C, with a mean value of 30.3°C. Additionally, the temperature of the glass panel ranged from 39°C to 49°C, with an average temperature of 43.5°C. The outlet temperature of SAH exhibited minimal variation in response to changes in solar irradiance. An increase in solar intensity generally led to a corresponding rise in outlet temperature. Conversely, a reduction in solar irradiance, such as that caused by intermittent cloud cover, resulted in a modest yet relatively stable decline in outlet temperature throughout the duration of the experimental observation.

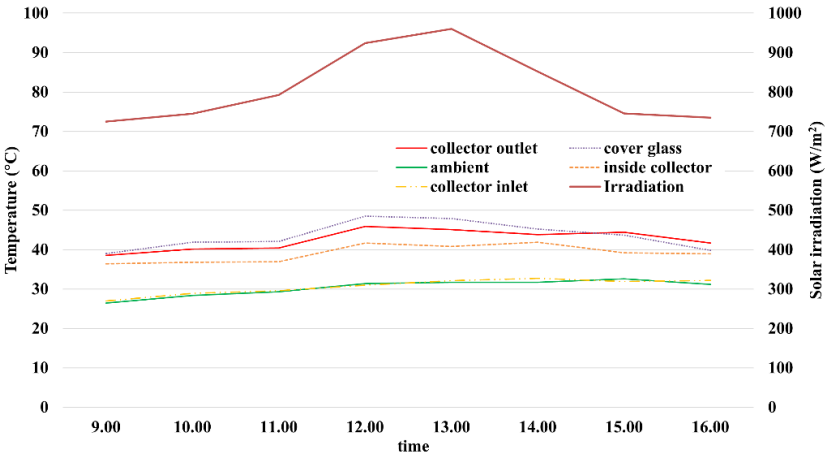


Figure 6. Temperature profile of the SAH with porous material at a porosity of 0.99.

Figure 7 shows an experimental result of SAH with porous material with 0.98 porosity. Solar radiation values ranged from 722 to 877 W/m², with an average of 804.4 W/m². The inlet air temperature varied between 29°C and 34°C, with a mean temperature of 31.1°C. The outlet temperature fluctuated between 44°C and 52°C, with an average of 48.4°C. The temperature inside SAH ranged from 34°C to 47°C, with an average of 38.9°C. Recorded ambient temperatures ranged from 31°C to 35°C, with a mean value of 33.2°C. Additionally, the temperature of the glass panel ranged from 41°C to 54°C, with an average temperature of 48.5°C. The outlet temperature of the solar air heater (SAH) exhibits only minor fluctuations in response to variations in solar irradiance, a behavior consistent with the experimental results incorporating a porous material with a porosity of 0.99. Generally, an increase in solar irradiance leads to a corresponding rise in outlet temperature. In contrast, a reduction in solar irradiance, such as that induced by intermittent cloud cover, causes a slight yet relatively stable decline in the outlet temperature throughout the observation period.

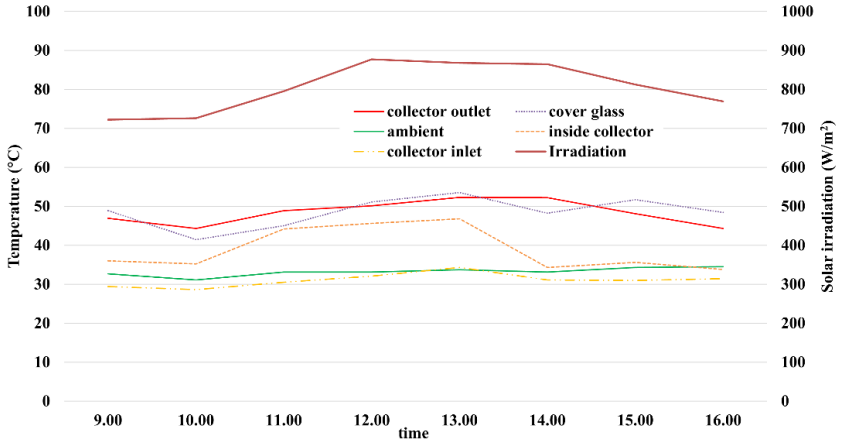


Figure 7. Temperature profile of the SAH with porous material at a porosity of 0.98.

The energy and exergy efficiency of SAH is illustrated in Figures 8 and 9. The experimental analysis of a solar air heater (SAH) incorporating porous materials with porosities of 0.99 and 0.98 revealed significant enhancements in energy and exergy efficiency. Without porous materials, the SAH's energy efficiency ranges from 2.38% to 7.61%, while the exergy efficiency lies between 0.02% and 0.24%. When porous materials with porosity values of 0.98 and 0.99 are introduced, energy and exergy efficiencies improve. Specifically, for porous materials with a porosity of 0.98, the energy efficiency ranges from 6.19% to 9.01%, and the exergy efficiency from 0.07% to 0.26%. In the case of porous materials with a porosity of 0.99, the energy efficiency increases further, ranging from 4.77% to 6.19%, with exergy efficiency values spanning from 0.09% to 0.14%. The highest exergy efficiency is attained with a porous material of 0.98 porosity, reaching approximately 0.2%, particularly evident during midday hours (12:00–13:00). In contrast, the configuration without porous material exhibits a peak around 11:00 hrs (~0.18%), but shows more significant variability throughout the observation period compared to systems incorporating porous materials. The SAH with a porous material of 0.98 porosity benefits from relatively higher and more stable solar irradiance throughout the day, which corresponds to its superior exergy performance. Similarly, regarding the energy efficiency of SAH, the porous material of 0.98 porosity configuration consistently outperforms the others. In contrast, without a porous material, it peaks around 11:00 hrs before experiencing a gradual decline. Incorporating porous material with a 0.99 porosity configuration demonstrates more stable but comparatively lower energy efficiency, averaging approximately 5.40%. These trends align with the exergy performance, whereby the porous material with a 0.98 porosity configuration, subjected to more consistent solar radiation, exhibits enhanced thermal behavior. Post-noon reductions in solar irradiance lead to decreased energy efficiency across all cases. However, incorporating porous material with a 0.98 porosity configuration maintains relatively higher performance due to its improved thermal retention and distribution characteristics. Overall, peak solar irradiance around midday contributes to elevated thermal efficiencies across all configurations, with systems employing porous materials exhibiting prolonged and more stable thermal performance. These results indicate that including porous materials on the absorber plate facilitated the maintenance of elevated outlet air temperatures for extended periods compared to configurations without porous materials. The experimental results demonstrate that incorporating porous materials enhances the thermal efficiency by 8.43% compared to the configuration without porous materials. In agreement with the findings of Hameed et al. [22], the integration of porous media increased the outlet air temperature by 12.28% and 21.32% at mass flow rates of 0.015 kg/s and 0.035 kg/s, respectively. Overall, the incorporation of porous materials contributed to an approximate 10% improvement in thermal efficiency. Moreover, this finding is consistent with Salih et al. [25], who reported that incorporating porous media in a double-pass solar air heater enhanced efficiency to 87% under natural convection and 81% under forced convection, compared to 82% and 67% in the non-porous configuration. The inclusion of porous media significantly improves heat transfer and system performance, particularly under forced convection, with DPSAH-1 recommended for high-temperature applications.

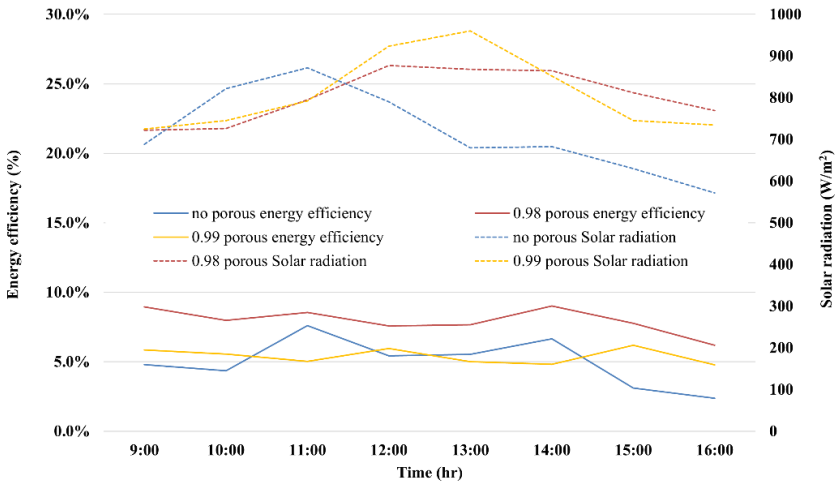


Figure 8. Energy efficiency of the SAH with and without porous material.

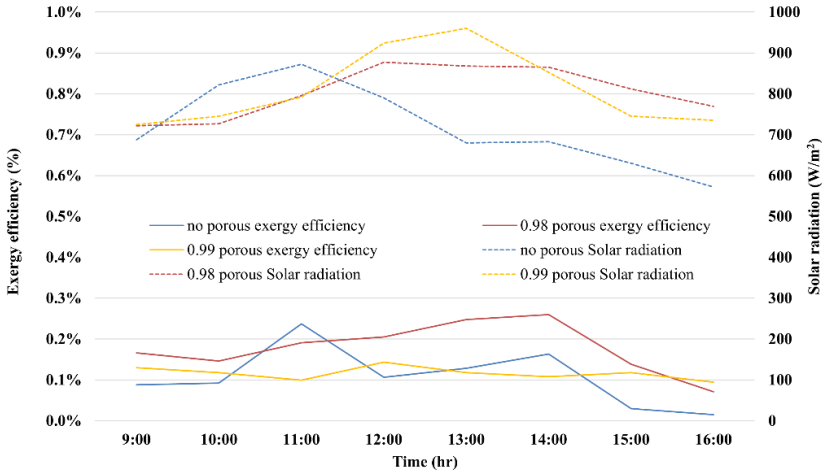


Figure 9. Exergy efficiency of the SAH with and without porous material.

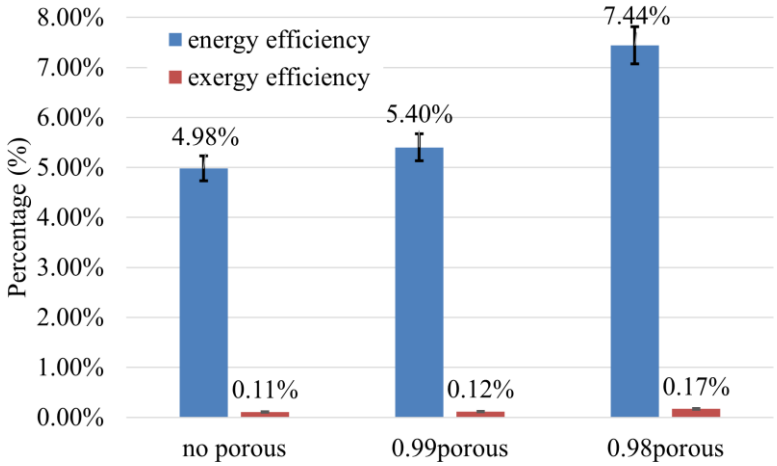


Figure 10. Comparison of the average efficiency of the SAH.

Figure 10 compares the average energy and exergy efficiency of a solar air heater with and without porous materials. Solar air heaters operating without porous materials exhibited an average energy efficiency of 4.89% and an exergy efficiency of 0.11%. In contrast, incorporating porous media with porosities of 0.98 and 0.99 resulted in notable improvements. Specifically, energy efficiency increased to 7.44% and 5.40%, representing approximately 0.5% and 0.08% enhancements, respectively. Correspondingly, exergy efficiencies for these configurations reached 0.17% and 0.12%, indicating a marked improvement in the thermodynamic performance of the SAH with porous materials. Compared to Ismail et al. [9], our results demonstrate a 12% higher energy efficiency under similar conditions. The observed enhancement in system performance can be attributed to improved thermal retention and a more homogeneous distribution of heat within the SAH. The comparative evaluation of the SAH configurations with porous material revealed that the setup without porous material consistently exhibited higher thermal and exergy efficiencies. Specifically, the average thermal efficiency with and without porous material configuration exceeded approximately 0.49%, while the corresponding exergy efficiency improvement was 0.55%. However, it is essential to note that the combined uncertainty margins for thermal and exergy efficiencies were estimated at ±7% and ±9%, respectively. To ensure the robustness of these findings, statistical significance testing was conducted using a Student's *t*-test. The results confirmed that the observed differences between with and without porous material were statistically significant at the 95% confidence level ($p < 0.05$), thereby substantiating the performance

advantage of the 0.98 porosity configuration. These results highlight that, although experimental uncertainties are inherent in solar thermal system testing, the integration of porous material provides a demonstrable improvement in thermodynamic performance compared to one without porous material. This aligns with a well-established characteristic of solar thermal systems, wherein a portion of the input energy becomes unavailable for useful work due to thermodynamic irreversibilities such as viscous dissipation, conductive losses, and suboptimal heat transfer mechanisms. Systems that integrate thermal energy storage or porous material consistently demonstrate superior performance in terms of energy and exergy efficiencies when compared to single-pass configurations or those lacking storage components. The inclusion of these design elements not only increases the total energy harnessed but also improves the thermodynamic quality of energy utilization. While energy efficiency quantifies the amount of energy converted, exergy efficiency assesses the effectiveness of harnessing this energy.

4. Conclusions

This research presents an experimental evaluation of the energy and exergy efficiency of a double-pass solar air heater (SAH) incorporating steel-based porous structures of varying porosities (0.98 and 0.99), under tropical climatic conditions. The objective was to quantify the influence of porous materials integration on energy and exergy efficiencies. The experimental outcomes affirm that integrating porous materials substantially improves the efficiency of the SAH. Notably, the configuration with a porosity of 0.98 exhibited superior results, achieving energy efficiencies ranging from 6.19% to 9.01%, alongside a peak exergy efficiency of 0.26%. These metrics markedly exceed those recorded without porous material configuration, demonstrating average energy and exergy efficiencies of 4.89% and 0.11%, respectively. Including porous materials enhanced thermal retention capabilities and stabilized the outlet air temperature, even under intermittent solar irradiance. These benefits were most pronounced during midday hours, correlating with maximum solar irradiation, thus emphasizing the role of porous structures in increasing thermal inertia and expanding the heat transfer surface area of the solar collector. Furthermore, the lower-porosity configuration (0.98) consistently outperformed the higher-porosity counterpart (0.99), highlighting the efficiency advantages of porous materials with a lower void fraction, which contribute to enhanced thermal storage and improved convective heat transfer. Incorporating porous materials on the absorber surface demonstrably enhances the energy capture and thermodynamic quality of solar air heaters. These findings highlight the suitability of porous-integrated SAH systems for agricultural and industrial drying processes in regions with high solar potential. This work provides a potential pathway for improving SAH designs with porous materials in tropical climates. Future research should investigate the use of alternative porous materials and explore other applications of solar air heaters for various purposes. Furthermore, future studies should investigate the impact of varying wind speeds across different climates, geographic contexts, and seasonal variations.

5. Acknowledgments

The authors thank the Department of Mechanical Engineering, Faculty of Engineering, Ubon Ratchathani University, for the financial support.

Author Contributions: Conceptualization: U. T., and A. N.; Methodology: U. T., A. N., P. S., S. S., and E. B.; Formal analysis and investigation: U. T., A. N., and E. B.; Writing —original draft preparation: E. B.; Writing —review and editing: U. T., and A. N.; Supervision: U. T., Projection administration: E. B., and U. T, All authors have read and agreed to the published version of the manuscript.

Funding: This research was funded by the Department of Mechanical Engineering, Faculty of Engineering, Ubon Ratchathani University.

Conflicts of Interest: The authors declare no conflict of interest.

References

[1] Azis, A.; Waris, A.; Salim, I.; Syafiuddin, M.; Setiawan, E.; Rezkiana, N.; Azizah, A.; Alamsyah, M. Testing the Heat Distribution of Flat Plate Type Solar Collectors for LPG Solar Hybrid Dryers at P4S Bukit Melintang. *BIO Web Conf.* **2024**. https://doi.org/10.1051/bioconf/20249603004

[2] Senthil, R.; Vijayan, G.; Phadtare, G.; Gupta, B. Performance Enhancements of Solar Dryers Using Integrated Thermal Energy Storage: A Review. In *Proceedings* **2021**, 355–362. https://doi.org/10.1007/978-981-15-9678-0_31

[3] Panwar, N.; Kaushik, S.; Kothari, S. State of the Art on Solar Drying Technology: A Review. *Int. J. Renew. Energy Technol.* **2012**, *3*, 107. https://doi.org/10.1504/IJRET.2012.045622

[4] Masana, E.; Jordi, C.; Ribas, I. Effective Temperature Scale and Bolometric Corrections from 2MASS Photometry. *arXiv* **2006**. https://doi.org/10.1051/0004-6361:20054021

[5] Ji, F.; Ji, F.; Dai, X. A New Solution Method for Black-Body Radiation Inversion and the Solar Area-Temperature Distribution. *Sci. China Phys. Mech. Astron.* **2011**, *54*(11), 2097–2102. https://doi.org/10.1007/S11433-011-4514-7

[6] Cugliandolo, L. F. The Effective Temperature. *J. Phys. A* **2011**, *44*(48), 483001. https://doi.org/10.1088/1751-8113/44/48/483001

[7] Nimnuan, P.; Janjai, S. An Approach for Estimating Average Daily Global Solar Radiation from Cloud Cover in Thailand. *Procedia Eng.* **2012**, *32*, 399–406. https://doi.org/10.1016/J.PROENG.2012.01.1285

[8] Waewsak, J.; Chancham, C.; Mani, M.; Gagnon, Y. Estimation of Monthly Mean Daily Global Solar Radiation over Bangkok, Thailand Using Artificial Neural Networks. *Energy Procedia* **2014**, *57*, 1160–1168. https://doi.org/10.1016/J.EGYPRO.2014.10.103

[9] Ismail, A.; Hamid, A.; Ibrahim, A.; Jarimi, H.; Sopian, K. Performance Analysis of a Double Pass Solar Air Thermal Collector with Porous Media Using Lava Rock. *Energies* **2022**. https://doi.org/10.3390/en15030905

[10] Srivastava, A.; Shukla, S.; Singh, U. Thermal Performance Analysis of Flat Plate Solar Collector and Solar Dryer of Indirect Solar Drying System. *J. Therm. Eng.* **2016**, *2*, 21–31.

[11] Jadallah, A.; Alsaadi, M.; Hussien, S. The Hybrid Photovoltaic-Thermal Double-Pass Solar System for Drying Applications. *IOP Conf. Ser.: Mater. Sci. Eng.* **2020**, *765*. https://doi.org/10.1088/1757-899X/765/1/012024

[12] Kumar, D.; Premachandran, B. Investigation of the Effect of Porous Material on the Flow and Temperature Patterns of a Passive Solar Air Heater. *J. Sol. Energy Eng.* **2020**, *142*. https://doi.org/10.1115/1.4046632

[13] Nima, F. J.; Steffan, T. L. Performance Improvement of a Solar Air Heater by Covering the Absorber Plate with Porous Material. *Energy* **2020**, *190*, 116437

[14] Singh, S.; Dhiman, P. Thermal Performance of Double Pass Packed Bed Solar Air Heaters—A Comprehensive Review. *Renewable Sustainable Energy Rev.* **2016**, *53*, 1010–1031.

[15] Dissa, A. O.; Ouoba, S.; Bathiebo, D.; Koulidiati, J. A Study of a Solar Air Collector with a Mixed "Porous" and "Non-Porous" Composite Absorber. *Sol. Energy* **2016**, *129*, 156–174.

[16] Murali, G.; Reddy, K. R. K.; Kumar, M. T. S.; Manikanta, J. S.; Reddy, V. N. K. Performance of Solar Aluminium Can Air Heater Using Sensible Heat Storage. *Mater. Today Proc.* **2020**, *21*(1), 169–174.

[17] Vijayan, S.; Arjunan, T. V.; Kumar, A.; Matheswaran, M. M. Experimental and Thermal Performance Investigations on Sensible Storage Based Solar Air Heater. *J. Energy Storage* **2020**, *31*, 101620.

[18] Bayrak, F.; Oztop, H. F.; Hepbasli, A. Energy and Exergy Analyses of Porous Baffles Inserted Solar Heaters for Building Applications. *Energy Build.* **2013**, *57*, 338–345.

[19] Ahmad, O. K.; Mohammed, Z. A. Influence of Porous Media on the Performance of Hybrid PV/Thermal Collector. *Renewable Energy* **2017**, *112*, 378–387.

[20] Hao, W.; Lu, Y.; Lai, Y.; Yu, H.; Lyu, M. Research on Operation Strategy and Performance Prediction of Flat Plate Solar Collector with Dual-Function for Drying Agricultural Products. *Renewable Energy* **2018**, *127*, 685–696.

[21] Hwang, Y.; Park, S. A Theoretical and Experimental Study for the Design of Solar Air Heaters Using Porous Material. *Trans. Korean Soc. Mech. Eng. B* **1996**, *20*, 336–345. https://doi.org/10.22634/KSME-B.1996.20.1.336

[22] Hameed, A.; Mohammed, A.; Hussain, E. Experimental Study of the Effect of Porous Media on the Performance of Single-Pass Solar Air Heater. *J. Adv. Res. Fluid Mech. Therm. Sci.* **2024**. https://doi.org/10.37934/arfmts.121.1.2738

[23] Jalil, J.; Ali, S. Thermal Investigations of Double Pass Solar Air Heater with Two Types of Porous Media of Different Thermal Conductivity. *Eng. Technol. J.* **2021**. https://doi.org/10.30684/ETJ.V39I1A.1704

[24] Abo-Elfadl, S.; Yousef, M.; El-Dosoky, M.; Hassan, H. Energy, Exergy, and Economic Analysis of Tubular Solar Air Heater with Porous Material: An Experimental Study. *Appl. Therm. Eng.* **2021**, *196*, 117294. https://doi.org/10.1016/J.APPLTHERMALENG.2021.117294

[25] Salih, M.; Alomar, O.; Yassien, H. Impacts of Adding Porous Media on Performance of Double-Pass Solar Air Heater under Natural and Forced Air Circulation Processes. *Int. J. Mech. Sci.* **2021**, *210*, 106738. https://doi.org/10.1016/J.IJMECSCI.2021.106738

ASEAN
Journal of Scientific and Technological Reports
Online ISSN:2773-8752

Research article

Quality-based assessment of natural ripening agents as alternatives to calcium carbide in 'Latundan' banana using mixed statistical methods

Bryl I. Manigo[1*]

[1] College of Agriculture and Related Sciences, University of Southeastern Philippines, Tagum-Mabini Campus, 8100, Philippines
* Correspondence: bryl.manigo@usep.edu.ph

Citation:
Manigo, B.I. Quality-based assessment of natural ripening agents as alternatives to calcium carbide in 'Latundan' banana using mixed statistical methods. *ASEAN J. Sci. Tech. Report.* **2026**, *29*(1), e259605. https://doi.org/10.55164/ajstr.v29i1.259605.

Article history:
Received: June 1, 2025
Revised: October 13, 2025
Accepted: October 18, 2025
Available online: December 14, 2025

Publisher's Note:
This article is published and distributed under the terms of the Thaksin University.

Abstract: Calcium carbide (CaC_2) is widely utilized for its affordability and efficiency in ripening fruits. However, it poses health risks, which makes natural ethylene-rich alternatives a safer choice. This study evaluated the effectiveness of natural ripening agents such as *Gliricidia* leaves, Calopo leaves, tomato fruit, and banana peel, as alternatives to CaC_2 in enhancing the postharvest quality of 'Latundan' banana (*Musa* × *paradisiaca*, AAB Group). Treated fruits were assessed for multiple quality parameters, including peel color, sensory firmness, chemical properties, organoleptic attributes, weight loss, shriveling, visual quality rating, disease incidence, and shelf life. A one-way analysis of variance (ANOVA) was performed to determine treatment effects, followed by Tukey's HSD test ($p \leq 0.05$) for mean separation. For non-normally distributed variables, the Kruskal-Wallis test was applied. To further evaluate treatment similarities based on overall trait performance, hierarchical cluster analysis (HCA) was conducted using Ward's method and Euclidean distance on standardized trait means. Results showed that CaC_2 significantly enhanced ripening characteristics, followed closely by tomato fruit. Natural agents, particularly the leaves of *Gliricidia* and Calopo, and banana peel, provided moderate improvements across several parameters, while the untreated control consistently ranked lowest. Although CaC_2 induced rapid ripening, it resulted in earlier deterioration and a shorter shelf life. Moreover, HCA revealed three distinct clusters: (1) CaC_2 and tomato fruit, (2) *Gliricidia* and Calopo leaves, and banana peel, and (3) control. These findings support the use of natural agents, especially tomato fruit, as viable alternatives for inducing uniform ripening and maintaining acceptable postharvest quality in bananas.

Keywords: Bio-ethylene; hierarchical cluster analysis; ethylene modulation; ripening enhancement; Philippine bananas

1. Introduction

Bananas are among the most widely produced and consumed tropical fruits worldwide, ranking high in global horticultural trade and agricultural output [1]. As a climacteric fruit, bananas ripen rapidly after harvest, which makes induced ripening essential for commercial distribution to ensure uniform peel color, optimal texture, and desirable flavor [2]. Although bananas naturally produce ethylene, exogenous application is commonly practiced to standardize ripening, particularly due to the uneven maturation of fruits within a single bunch [3]. However, the increasing demand for ripe fruits has led to the

widespread yet hazardous use of CaC_2 as a chemical ripening agent, primarily due to its low cost and accessibility [4]. While CaC_2 is effective in accelerating ripening by enhancing respiration and color development [2], commercial-grade formulations often contain toxic contaminants such as arsenic and phosphorus. Prolonged exposure to these substances has been linked to immune suppression, hormonal imbalance, and infertility [5, 6].

In response, numerous plant-based ripening agents rich in ethylene or its precursors have been investigated as safer, locally available alternatives [7]. *Gliricidia sepium* (Kakawate) leaves have shown potential, inducing uniform ripening in 'Saba' bananas within two days [8], although they were less effective in mangoes at higher concentrations [9]. *Ricinus communis* (Venna) leaves produced comparable results to CaC_2 and CaO [7], while Samanea saman and Carica papaya leaves effectively ripened bananas in Nigeria [10]. *Moringa oleifera* leaves have also been noted for enhancing ripening and reducing costs [11]. Other studies have examined *Jatropha curcas, Irvingia gabonensis,* and *Calopogonium mucunoides* (Calopo), with the latter showing lower ethylene production compared to *Gliricidia* and *Samanea* [12]. Additionally, *Ficus septica* (Lagnob) has drawn interest for its bioactive properties [13]. Moreover, several climacteric fruits, such as apples, pears, tomatoes, and ripe bananas, also emit ethylene and have been used effectively as natural ripening agents [14, 15]. In particular, tomatoes demonstrate elevated ethylene emission between the breaker and fully ripe stages, making them a viable ripening alternative [16].

Despite bans in many countries, CaC_2 remains in use due to the lack of affordable and effective substitutes [9]. This has intensified the search for safer, natural ripening technologies. To comprehensively evaluate these alternatives, the present study employed both parametric (ANOVA or analysis of variance, Tukey's HSD) and non-parametric (Kruskal-Wallis) statistical analyses, methods widely applied in postharvest studies to assess treatment effects on banana quality traits [17]. Hierarchical cluster analysis (HCA) was also used to classify treatments based on the overall postharvest performance of some fruits. Previous studies demonstrate that HCA has effectively identified consumer preference segments in apples [18] and key quality indicators in pears when combined with ANOVA, correlation analysis (CA), and principal component analysis (PCA) [19]. This integrated statistical approach enhances the robustness of postharvest evaluation and supports informed decision-making in treatment selection. In this study, the effects of selected natural ripening agents on the ripening behavior and postharvest quality of 'Latundan' banana (*Musa* × *paradisiaca*, AAB Group), a commonly cultivated variety in the Philippines, were evaluated. Specifically, it sought to assess the ripening duration and overall fruit quality influenced by these agents to support the development of safer, sustainable alternatives to chemical ripening.

2. Materials and Methods

2.1 Plant Material

The banana variety used was 'Latundan' (*Musa* × *paradisiaca,* AAB Group). Mature unripe fruits were obtained from farms in Panabo City, Davao del Norte, Philippines. Sample fruits were harvested on the same day. One week before harvesting, tagging was performed to ensure sample uniformity. Fruits with similar characteristics in size, age, and number of leaves were selected for tagging. Fruits from the second, third, and fourth hands of the bunch were used as experimental samples [20].

2.2 Experimental Duration and Location

The experiment, including storage and laboratory analyses, was conducted from February to July 2022 at the Food Technology Laboratory (FTL) of the University of Southeastern Philippines (USeP), Tagum-Mabini Campus, Tagum City, Davao del Norte, Philippines.

2.3 Treatment Screening and Selection

A range of locally available natural ripening agents, including leaves of *Gliricidia sepium* (Kakawate), *Calopogonium mucunoides* (Calopo), *Ricinus communis* (Venna), *Samanea saman* (Rain tree), *Moringa oleifera*, *Carica papaya*, *Jatropha curcas*, and *Ficus septica* (Hauili fig tree or Lagnob), along with ripe tomato fruits and 'Lakatan' banana peels, were initially screened for their ripening efficacy. A preliminary trial was conducted using ten 'Latundan' banana fingers per treatment, with three replications. Banana samples and ripening

agents (100 g per kilogram banana) were enclosed in 10 × 7-inch styrofoam containers, with two banana fingers placed in each container, and sealed with transparent plastic wrap. CaC_2 (10 g per kilogram banana) was used as the positive control, while untreated fruits served as the negative control. To prevent oxygen depletion and ensure adequate gas exchange during incubation, the styrofoam containers were modified with small ventilation holes. Specifically, one hole (5 mm in diameter) was made on each side of the container to promote gentle airflow without excessive ethylene loss.

All ripening agents were sourced locally, while commercial-grade CaC_2 was purchased from a chemical supplier in Tagum City, Davao del Norte, Philippines. Before treatment, both fruits and ripening agents were sanitized with 0.01% sodium hypochlorite (NaOCl) for 3 minutes and air-dried at room temperature. Peel yellowing served as the primary selection criterion after 5 days of storage post-incubation. Treatments that induced visible color change comparable to CaC_2 were advanced to the main experiment. Based on the results, the final treatments were the following: T1= control (no treatment), T2= CaC_2 (10 $g\ kg^{-1}$), T3= *Gliricidia* leaves (100 $g\ kg^{-1}$), T4= Calopo leaves (100 $g\ kg^{-1}$), T5= tomato fruit (100 $g\ kg^{-1}$), and T6= banana peel (100 $g\ kg^{-1}$). The main trial followed a completely randomized design (CRD) with three replications, each comprising 10 banana hands and 15 banana fingers (both for destructive and non-destructive sampling), and was evaluated for physical, chemical, and sensory quality parameters as outlined in subsequent sections.



Figure 1. Natural ripening agents were used in this study.

The main trial followed a completely randomized design (CRD) with three replications. Each replicate comprises 10 banana hands allocated for non-destructive monitoring of peel color, weight loss, visual quality rating (VQR), shriveling, disease incidence, and shelf life. When a hand from each treatment reached peel color index 6 (PCI-6; see 2.5), subsamples were taken for chemical analyses (TSS, TTA, pH) and sensory evaluation (pulp color, taste, aroma, overall acceptability). In addition, 15 banana fingers per treatment were used for destructive measurements of firmness, assessed daily. The amount of each ripening agent differed according to its chemical nature and expected ethylene-releasing capacity [2]. Calcium carbide, being highly reactive, was applied at 10 g kg^{-1} fruit, while natural materials were used at 100 g kg^{-1} to compensate for their slower and lower ethylene [3]. Comparison of ripening efficiency was therefore based on the extent and uniformity of peel yellowing rather than on equal mass of material [21].

2.4 Treatment Application

The natural ripening agents, along with the sample fruits to be ripened, were placed inside a 5-ply corrugated cardboard box (53.5 × 40.0 × 24.5 cm) with paper linings. A 10% (w/w) concentration of each natural ripening agent was used relative to the total weight of the bananas in each box. The box openings and holes were covered with newspaper. The fruits were incubated for 48 hours before being removed and placed in ambient room storage (28±3°C), where ripening progress was monitored.

2.5 Data Gathering

Peel color was visually assessed daily using a standardized seven-stage banana color chart [20], with a peel color index (PCI) scale ranging from green (1) to yellow flecked with brown (7). Sensory firmness was measured using a GY-3 portable fruit hardness tester with a 5-mm flat-tipped probe, puncturing each banana finger at three midpoints. Firmness was recorded in Newtons (N). Chemical analyses included total soluble solids (TSS), total titratable acidity (TTA), and pH. TSS was measured using an Atago Pocket digital refractometer (Model PAL-1, Atago Co., Ltd., Tokyo, Japan) by placing 1–2 drops of filtered juice on the prism. TTA was determined via titration with 0.1N sodium hydroxide using phenolphthalein as an indicator, while pH was recorded using a digital pH meter. Organoleptic attributes (OA) such as pulp color, taste, aroma, and overall acceptability were evaluated at PCI 6 using a 9-point hedonic scale [22] by a panel of 25 evaluators. Weight loss (%) was calculated using the formula: weight loss = [(weight difference to initial weight)/(initial weight of the sample or weight at day 0)] x 100. Visual quality rating (VQR) followed Gunathilake *et al.* [23] with slight modification, with fruit categories as excellent (9–8), good (7–6), fair (5–4), poor (3–2), or non-edible (1). Shrivelling was assessed using a 1–4 index ranging from no shrivelling (1) to severe shrivelling (4). Disease incidence was recorded as the percentage of fruits affected by crown rot/mold using the formula: % disease incidence = (number of diseased fruits affected by crown rot/mold)/(total number of hands) x 100 [20]. Shelf life was determined by tracking the number of days to full ripeness (PCI 6), senescence, and the limit of marketability (VQR 5).

2.6 Statistical Analyses

All analyses of data were performed in R (v4.5.0). For each storage day, treatment effects were analyzed separately, and results are reported as mean ± SE. Normality (Shapiro–Wilk) and homoscedasticity (Levene's test) were assessed for every outcome/day. Continuous variables (firmness, TSS, TTA, pH) and time variables (days to marketability, days to ripen, days to senescence) were analyzed by one-way ANOVA with Tukey's HSD ($\alpha = 0.05$). Percentage variables (weight loss and disease incidence) were analyzed after arcsine–square-root transformation. Ordinal outcomes (peel color index, degree of shriveling, visual quality rating, and hedonic sensory attributes [aroma, taste, peel/pulp color, overall acceptability]) were analyzed using Kruskal–Wallis with Dunn's post-hoc comparisons and Holm adjustment ($\alpha = 0.05$). To complement the univariate analysis, a Hierarchical Cluster Analysis (HCA) was conducted using the *hclust()* function in R, which employs Ward's method and Euclidean distance to assess treatment similarities based on overall postharvest performance. Before clustering, trait values were standardized (z-scores), and the means of three replicates per treatment were used to generate a distance matrix. Clustering results were visualized using a dendrogram and a clustered heatmap, allowing the identification of natural groupings among treatments and associated trait patterns. This multivariate approach provided integrative insight to reinforce and validate the findings from ANOVA and nonparametric tests.

3. Results and Discussion

3.1 Preliminary Screening of Natural Ripening Agents

Peel color is one of the most visible and market-relevant indicators of ripeness, which is often used by both consumers and traders to assess banana maturity. To identify effective natural alternatives to CaC_2, a preliminary experiment was conducted to screen various locally available ripening agents based on their ability to induce degreening in 'Latundan' bananas over a five-day incubation period. This initial screening provided critical insights into the ripening efficacy of each treatment and guided the selection of agents for further evaluation. Figure 2A presents the quantitative peel color index for each treatment. Bananas treated with CaC_2 showed the highest peel color index, which is significantly different from the untreated control. Among the natural agents, bananas exposed to *Gliricidia* leaves, Calopo leaves, tomato fruit, and banana peel displayed peel color indices statistically comparable to those treated with CaC_2 ($p \leq 0.05$; Tukey's HSD). In contrast, other treatments such as castor bean leaves, papaya leaves, and Hauili fig tree leaves resulted in lower color indices, which indicates limited ripening influence. These findings are visually supported by Figure 2B, which shows noticeable yellowing in fruits treated with the selected natural agents, comparable to those treated with CaC_2. The untreated control and several other treatments showed minimal or uneven color

change, which supports the effectiveness of the selected agents. Similar outcomes were reported by Roy *et al.* [15] in tomato, Acedo [8] in *Gliricidia* leaves, who suggested that these could stimulate color change in bananas at rates similar to chemical ripening agents. The development of color is a key indicator of fruit maturity and is closely tied to ripening. This color change occurs as chlorophyll degrades, and the unmasking of pre-existing pigments takes place, often accelerated by ethylene exposure [2]. A uniform yellow color on the peel not only signifies ripeness but also makes bananas more attractive to buyers, which typically leads to higher market prices [24]. Therefore, these four natural ripening agents were subjected to further testing for physical and chemical measurements to validate their effects on the ripening process.

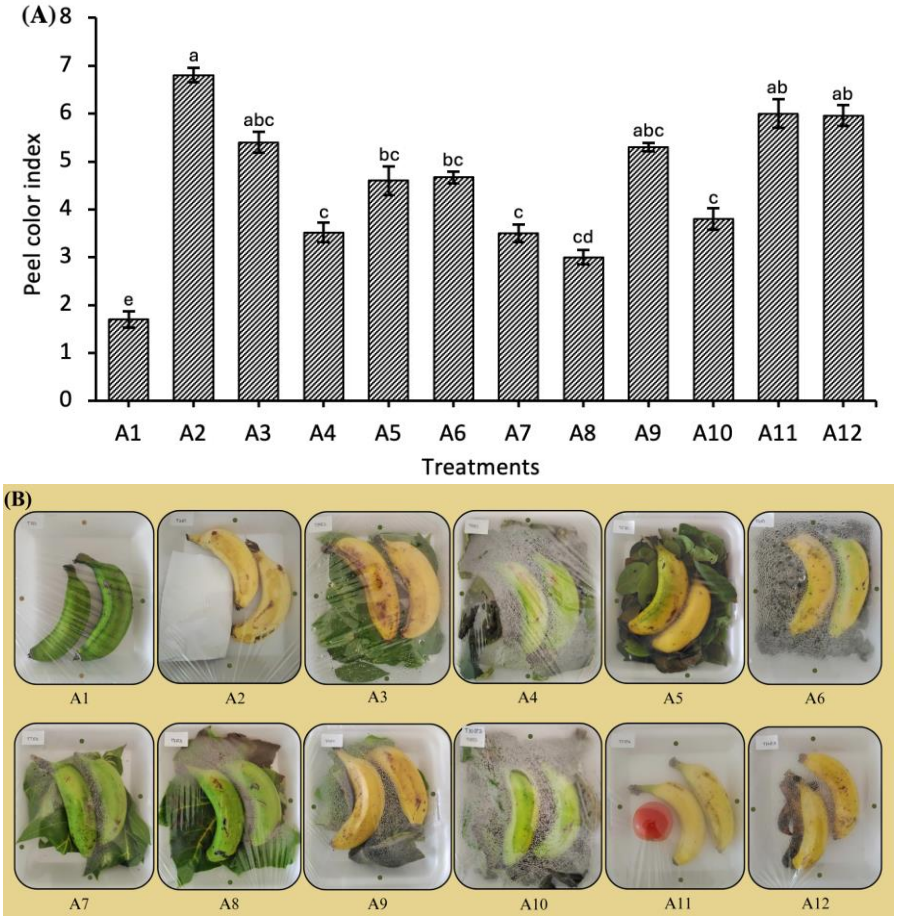


Figure 2. Peel color changes (A) of 'Latundan' bananas showing yellowing (B) as influenced by different natural ripening agents at 5 days of incubation. Legend: A1= control; A2= CaC_2; A3= *Gliricidia* leaves; A4= castor bean plant leaves; A5= rain tree leaves; A6= *Moringa* leaves; A7= papaya leaves; A8= *Jatropha* leaves; A9= calopo leaves; A10= Hauili fig tree leaves; A11= tomato fruit; A12= banana peel; Means sharing the same superscripts are not significantly different from each other ($p \leq 0.05$, n=10) using Tukey's HSD.

3.2 Ripening Evaluation of Selected Ripening Agents for 'Latundan'

Natural agents showing comparable efficacy to CaC_2 in the preliminary screening were selected for further evaluation. This section explores the effects of the six selected treatments on the ripening progression of 'Latundan' bananas, with emphasis on key postharvest quality parameters. The observed changes in ripening-related attributes are presented in Figures 3–5 and Table 1, which collectively illustrate the dynamic transformations in fruit quality during the ripening period.

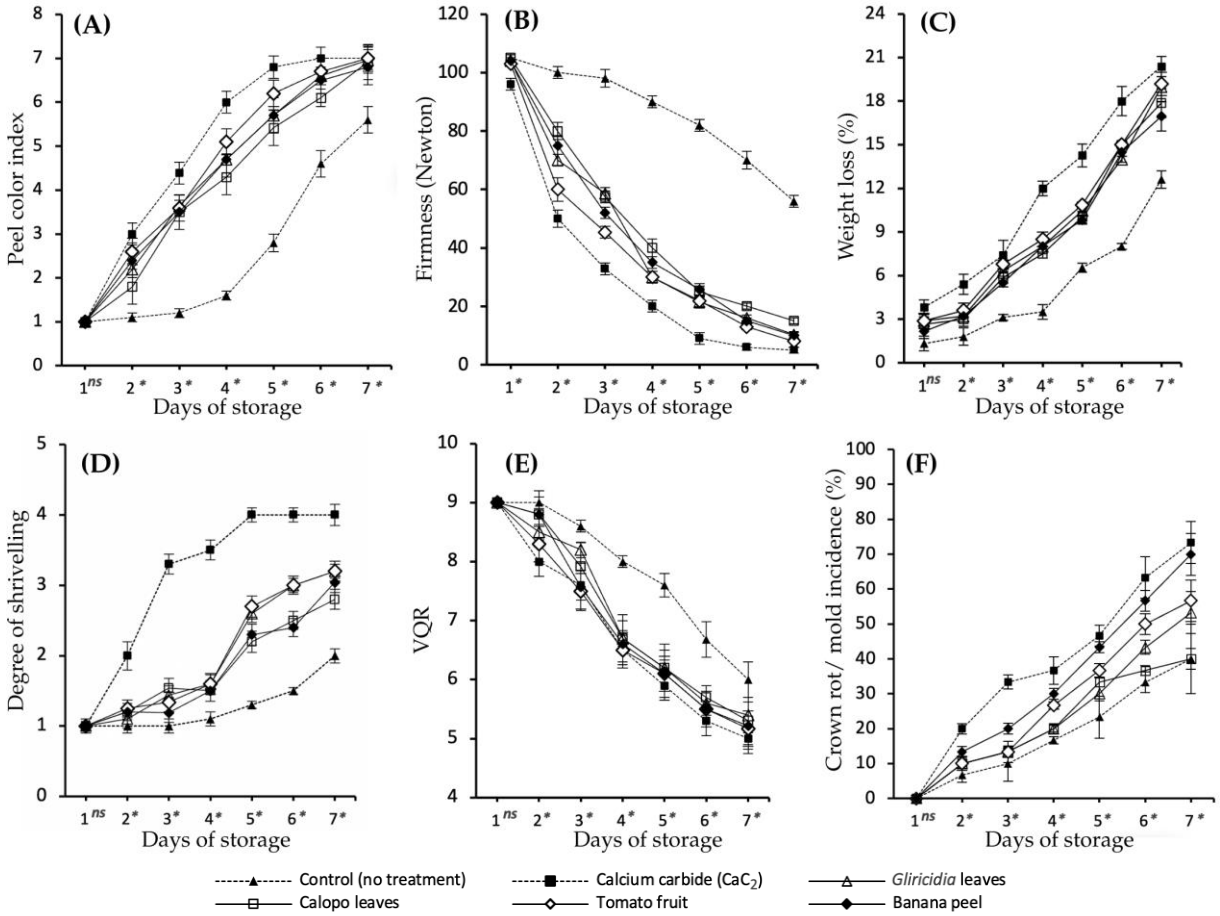


Figure 3. Effects of various ripening agents on the (A) peel color change, (B) firmness, (C) weight loss, (D) degree of shriveling, (E) VQR, and (F) disease incidence of 'Latundan' bananas after 48 hours of incubation. Asterisk (*) denotes significance at 5% level of significance ($p \leq 0.05$; n=10) using Tukey's HSD.

3.2.1 Changes in Peel Color

After 48 hours of incubation, the peel color of 'Latundan' bananas showed significant changes influenced by various natural ripening agents over a 7-day storage period (Figure 3A). As expected, bananas treated with CaC_2 ripened markedly faster than those in other treatments, while untreated fruits remained green (Figure 4). Natural ripening agents, including leaves of *Gliricidia* and Calopo, tomato fruits, and banana peels, induced peel color changes earlier than the control. By day 5 and onwards, these natural agents produced results comparable to CaC_2, with tomato fruit treatments emerging as the most effective among them. The change in peel color of 'Latundan' bananas ripened with natural agents closely resembles that of bananas treated with CaC_2 but occurs at a slightly slower pace. This suggests that natural agents effectively induce ethylene production, thereby accelerating chlorophyll degradation and carotenoid biosynthesis, which are deemed key processes in peel color change [2]. The tomato fruits, for instance, stood out among natural agents, in accordance with Roy *et al.* [15], who reported that tomatoes release bioethylene in quantities sufficient to promote ripening in climacteric fruits. Moreover, banana peel-ripened fruits also showed comparable results among natural agents. It was also known that bananas produced ethylene naturally [2], hence, ethylene release from banana peels probably enhanced the peel color change of the fruit samples. Similarly, *Gliricidia* and Calopo leaves demonstrated efficacy comparable to CaC_2, consistent with findings by Acedo [8], who highlighted the ethylene-generating potential of *Gliricidia sepium.* Untreated fruits that remain green emphasize the importance of external ethylene sources for ripening, particularly in climacteric fruits. These results reinforce the viability of natural agents as safer alternatives to CaC_2, aligning with global calls to phase out harmful ripening chemicals [4].



Figure 4. 'Latundan' (*Musa* × *paradisiaca* AAB Group) at day 4 of storage after 48 hours of incubation

3.2.3 Chemical Properties and Organoleptic Attributes

Ripened 'Latundan' bananas were chemically analyzed to determine the TSS, TTA, and pH, as well as the organoleptic attributes (Table 1). Bananas that reached PCI 6, regardless of when they achieved this stage, were used as samples in the analyses. Among the treatments, natural ripening agents, particularly tomato fruits, produced ripened 'Latundan' bananas with higher TSS levels, comparable to those ripened with *Gliricidia* leaves, while fruits ripened with CaC_2 exhibited lower Brix values. The TTA and pH levels were comparable across all treatments. In terms of organoleptic traits, taste showed a significant statistical difference ($p \leq 0.05$), with bananas ripened using *Gliricidia* leaves and tomato fruits obtained higher taste ratings, similar to those ripened with Calopo leaves. However, other organoleptic attributes, such as aroma, perceived pulp color, and overall acceptability, showed no statistically significant differences ($p \leq 0.05$) among the treatments.

Table 1. Chemical properties and organoleptic attributes of 'Latundan' bananas at PCI 6. Means sharing the same superscripts are not significantly different from each other ($p \leq 0.05$) using Tukey's HSD. CV represents the coefficient of variance, ns means not significant, and an asterisk (*) denotes significant.

Treatments	Chemical Properties			Organoleptic Attributes			
	TSS (°Brix) *	TTA (meq/100g) ns	pH ns	Aroma ns	Taste *	Pulp Color ns	Overall Acceptability ns
Control	22.67 bc	3.23	4.77	8.20	8.92 c	8.20	8.11
(CaC_2)	22.17 c	3.41	4.90	8.91	9.12 b	9.21	8.78
Gliricidia leaves	23.80 ab	3.24	4.77	8.79	9.53 a	9.33	8.50
Calopo leaves	22.83 bc	3.32	4.83	8.48	9.38 ab	9.37	8.45
Tomato fruit	24.27 a	3.31	4.77	9.03	9.63 a	9.55	8.98
Banana peel	22.53 bc	3.24	4.87	8.36	9.23 ab	9.26	8.83
CV (%)	5.52	2.04	2.16	2.76	5.12	2.52	2.63

The higher TSS values in bananas ripened using tomatoes and *Gliricidia* leaves highlight the ability of these natural agents to enhance sugar accumulation during ripening. However, CaC_2-ripened fruits showed lower Brix values, potentially due to incomplete metabolic shifts associated with rapid ripening [5]. Comparable TTA and pH levels across treatments indicate that natural ripening agents maintain acidity balance, a key quality parameter, consistent with findings by Basak and Akter [7]. Organoleptic attributes such as taste and aroma were positively influenced by *Gliricidia* leaves and tomatoes, which highlights the sensory benefits of natural agents. These results are congruent with the findings of Ademe and Tanga [11], who noted superior sensory profiles in naturally ripened bananas, such as *Moringa* leaves. Moreover, the increase in TSS (°Brix) in bananas ripened with natural agents, such as tomato fruits and *Gliricidia* leaves, reflects their potential to enhance sugar accumulation during ripening. TSS is a critical parameter linked to sweetness and consumer acceptability [2]. The comparable TTA and pH levels across treatments suggest that these natural agents do not significantly alter the fruit's acid content, an essential factor in maintaining flavor balance. Bananas ripened with *Gliricidia* leaves and tomato fruits received higher taste ratings, similar to findings from Ademe and Tanga [11], who noted improved sensory quality with natural ripening agents such as *Moringa*

leaves. The lack of significant differences in aroma, pulp color, and overall acceptability suggests that natural agents like tomato fruits can rival CaC_2 in preserving or enhancing sensory quality without toxic risks [7].

3.2.4 Weight Loss and Degree of Shriveling

As ripening progresses and softening occurs, the weight of the fruit decreases due to moisture loss and other physiological changes. This is accompanied by the peel beginning to shrivel, driven by water loss and alterations in cellular structure. In this study, 'Latundan' bananas treated with CaC_2 exhibited significantly higher weight loss throughout the storage period, starting immediately after the 48-hour incubation. In contrast, untreated fruits experienced a slower and more gradual weight loss. All natural ripening agents evaluated resulted in weight loss values that were statistically comparable to one another but significantly lower than those of CaC_2-treated fruits (Figure 3D). Similarly, fruits ripened with CaC_2 exhibited the most pronounced peel wrinkling, which is an indication of accelerated moisture loss and tissue degradation (Figure 3D). In contrast, the untreated control maintained a smooth and firm appearance with minimal signs of shriveling. The fruits treated with natural ripening agents showed moderate and comparable levels of shriveling, which suggests a more gradual and controlled ripening process that better preserved the structural integrity of the fruit compared to the rapid changes induced by chemical treatment. Weight loss during ripening is a natural phenomenon due to moisture evaporation and metabolic processes [21]. The higher weight loss in CaC_2-ripened bananas compared to natural agents can be attributed to the rapid acceleration of respiration and transpiration rates induced by carbide [4]. In contrast, natural agents, such as *Gliricidia* and Calopo leaves, may probably act more gently, enabling a slower moisture loss and maintaining fruit integrity longer. Shrivelling, directly correlated with weight loss, was more pronounced in CaC_2-ripened bananas, and was less pronounced in tomato and banana peel-ripened fruits, likely due to the rapid breakdown of cellular structure induced by the ripening process [15].

3.2.5 VQR

The visual quality apparently changed as ripening progressed, as manifested in this study. Untreated 'Latundan' bananas consistently showed higher VQR compared to those subjected to treatments. In particular, fruits ripened with CaC_2 exhibited significantly lower VQR on days 2, 5, 6, and 7, which reflects a faster deterioration in appearance compared to other treatments (Figure 3E). The superior VQR observed in untreated bananas and those ripened with natural agents highlights their slower ripening process, which helps maintain visual appeal over time. The rapid deterioration in VQR for CaC_2-ripened fruits suggests its aggressive ripening mechanism, which accelerates senescence [26]. These results corroborate with Basak and Akter [7], who emphasized the importance of gradual ripening in preserving aesthetic qualities. Using natural agents like tomato fruits, banana peel, and leaves of *Gliricidia* and Calopo can, thus, offer a safer and more sustainable alternative to maintain the fruit's marketability for extended periods.

3.2.6 Postharvest Disease Incidence

Postharvest diseases, which commonly develop after harvest, can greatly affect the appearance, texture, taste, and shelf life of fruits which resulting in significant economic losses. In this study, 'Latundan' bananas were found to be particularly vulnerable to pathological infections, even though these fruits were disinfected with NaOCl. Fruits treated with CaC_2 exhibited a higher incidence of crown rot and anthracnose (Figure 3F), likely due to accelerated ripening and increased susceptibility. In contrast, untreated fruits showed a slower progression of these diseases, which demonstrates the potential interaction between ripening treatments and disease resistance. The postharvest disease incidence observed in 'Latundan' bananas showcases the complex interplay between ripening treatments and fruit susceptibility to pathogens. CaC_2-ripened bananas exhibited a higher incidence of crown rot and anthracnose, as illustrated in Figure 3F. This finding is consistent with Maduwanthi and Marapana [2], who noted that the accelerated ripening induced by CaC_2 compromises the structural integrity of fruit tissues, which makes them more susceptible to pathogen invasion. The rapid softening and increased moisture content provide an ideal environment for fungal growth. On the other hand, untreated fruits demonstrated a slower progression of postharvest diseases, likely due to their extended ripening duration, which preserves tissue firmness and delays pathogen colonization. Studies by Chandar *et al.* [26] and Ajayi and Mbah [10] support the notion that natural ripening agents, such as plant

leaves and other bioethylene sources, can mitigate postharvest disease risks by promoting uniform ripening without inducing excessive moisture release or tissue degradation.

3.2.7 Shelf Life

The shelf life of 'Latundan' bananas is determined by the number of days to full ripeness (PCI 6), the onset of senescence, and the limit of marketability (at VQR 5). As shown in Figure 5, CaC_2-ripened fruits reached PCI 6 in approximately 4 days, the fastest among all treatments. Fruits ripened using natural agents, such as tomato fruits, *Gliricidia* and Calopo leaves, and banana peels, followed closely, which took 5-6 days to reach full ripeness, with tomato-treated fruits lagging just one day behind the CaC_2-treated group. In contrast, untreated 'Latundan' bananas took 8 days to achieve PCI 6, which reflects a slower ripening process. A similar trend was observed for days to senescence, with CaC_2-ripened fruits deteriorating more rapidly than those treated with natural ripening agents or left untreated. These fruits also reached VQR 5 sooner than the others, marking the threshold for marketability. At VQR 5, the fruits are still acceptable for sale, but they are on the verge of declining quality. The accelerated ripening and senescence observed in CaC_2-ripened fruits can be attributed to the treatment's ability to trigger ethylene release, which speeds up ripening but also shortens shelf life. In contrast, natural ripening agents promote a more gradual progression, preserving the fruit's quality for a longer period.

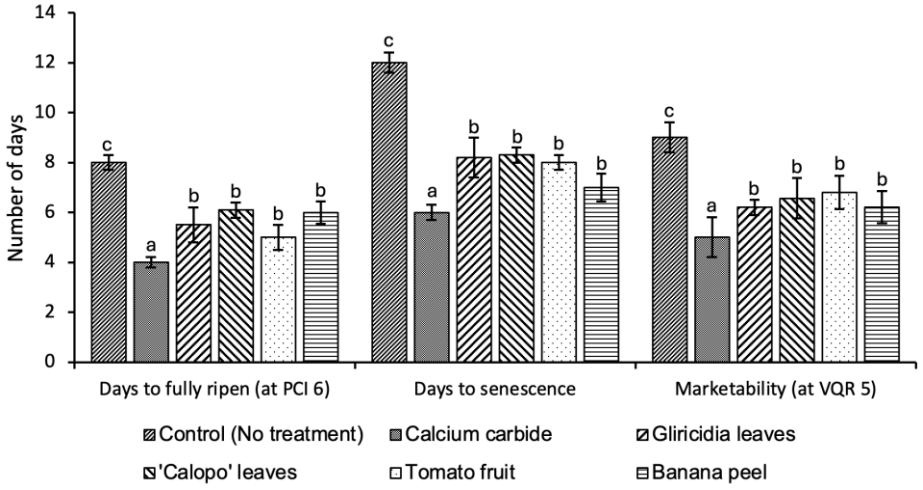


Figure 5. The shelf life of 'Latundan' bananas was determined as days after incubation with different ripening agents. Means sharing the same superscripts are not significantly different from each other ($p \leq 0.05$; n=10) using Tukey's HSD

The findings on shelf life (Figure 5) emphasize the balance between the speed of ripening and the duration of marketability, which reveals the impact of different ripening methods on the fruit's commercial viability. CaC_2-ripened bananas achieved full ripeness (PCI 6) within four days, demonstrating the efficiency of CaC_2 as a ripening agent. However, this rapid ripening led to an accelerated onset of senescence and a shorter marketable shelf life. Similarly, Okeke *et al.* [4] reported that the high ethylene release triggered by CaC_2 accelerates physiological processes, including ripening and senescence. Natural ripening agents such as tomato fruits, *Gliricidia* leaves, and banana peels provided a more balanced approach, achieving full ripeness in 5–6 days. Among these, tomatoes performed comparably to synthetic agents due to their bioethylene content [15]. The slower progression of ripening and senescence in fruits treated with natural agents helps maintain fruit quality and extend marketability. Untreated fruits, while taking the longest to reach full ripeness (8 days), exhibited the most extended shelf life. This agrees with Thompson *et al.* [21], who noted that delaying ripening by avoiding external ethylene exposure helps preserve fruit firmness and quality. The balance between rapid ripening and extended shelf life offered by natural agents suggests their suitability for small-scale and commercial applications where quality preservation is crucial.

3.3 Cluster Analysis of different ripening agents for Latundan

To complement the results of ANOVA and post hoc tests, hierarchical cluster analysis was employed to assess the overall similarity among the six banana ripening treatments based on multiple postharvest quality parameters. Unlike univariate methods that analyze each trait separately, hierarchical clustering provides a multivariate perspective by simultaneously considering all measured traits, such as peel color, firmness, visual quality rating (VQR), disease incidence, total soluble solids (TSS), titratable acidity (TTA), pH, and organoleptic attributes. This approach identifies the most effective treatment for inducing ripening while preserving postharvest quality. Figure 6 presents the hierarchical clustering dendrogram constructed using Ward's method on standardized, averaged values of the measured parameters. The dendrogram revealed three distinct clusters. The first cluster grouped calcium carbide (CaC_2)and tomato fruit, which suggests that these treatments induced similar ripening behaviors, particularly in enhancing peel color, reducing firmness, and improving organoleptic or sensory scores. This finding supports the results of Roy *et al.* [15], who demonstrated that tomato fruit itself can act as a natural ripening agent by emitting ethylene that promotes ripening in bananas.

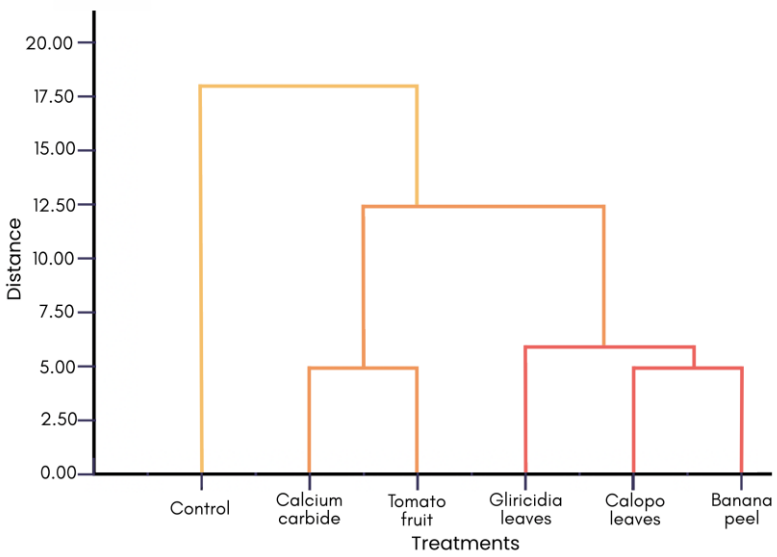


Figure 6. Hierarchical clustering dendrogram of six ripening treatments based on averaged postharvest traits in banana fruit.

The second cluster included *Gliricidia* leaves, Calopo leaves, and banana peel, which indicates moderate similarity in their ripening profiles, particularly in maintaining favorable organoleptic attributes, acceptable color development, and reduced disease incidence. The control treatment formed the third and most distant cluster, which highlights its distinct and generally inferior performance across all traits. To further visualize treatment-level variation, a clustered heatmap was generated using the same standardized dataset (Figure 7). Each row represents a treatment, while columns represent specific postharvest traits. The heatmap displays color intensities ranging from blue (lower performance) to red (higher performance). Treatments like calcium carbide (CaC_2) and tomato fruit exhibited strong red intensities across most parameters, confirming their superior performance. Natural treatments showed intermediate to high performance in traits such as overall acceptability, aroma, and pulp color. In contrast, the control treatment displayed predominantly blue intensities, indicating poor outcomes across several quality indicators.

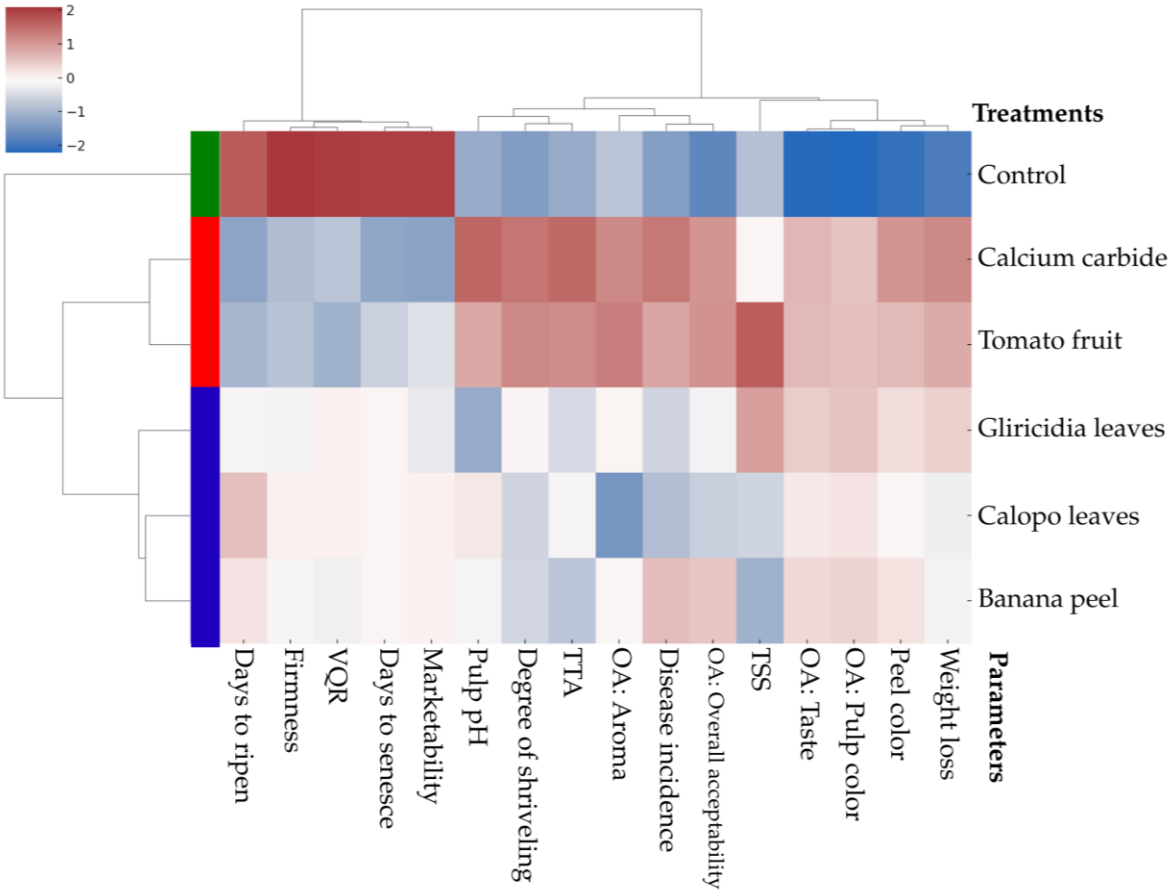


Figure 7. Clustered heatmap of standardized postharvest trait values across six banana ripening treatments, with color-coded clusters.

Color-coded cluster bars adjacent to the rows visually denote the groupings identified in the dendrogram: Cluster 1 (red) includes calcium carbide and tomato fruit; Cluster 2 (blue) includes *Gliricidia* leaves, Calopo leaves, and banana peel; and Cluster 3 (green) includes the control. These clusters underscore the relative efficacy of synthetic and natural treatments in promoting desirable ripening traits. Together, these findings validate the superiority of calcium carbide as a ripening agent while also demonstrating that natural treatments, particularly *Gliricidia*, Calopo, and banana peel, can effectively induce ripening with comparable postharvest quality in certain traits. The clustering results reinforce earlier statistical analyses and highlight the potential of natural alternatives in regions where synthetic ripening agents are restricted or discouraged. This multivariate approach strengthens the study's conclusions by confirming the distinct groupings and performance profiles of the treatments under investigation.

4. Conclusions

This study demonstrated that selected natural ripening agents (*Gliricidia* leaves, Calopo leaves, tomato fruit, and banana peels) can serve as effective alternatives to CaC_2 in inducing ripening in 'Latundan' bananas. While CaC_2-treated fruits reached full ripeness more rapidly, this accelerated ripening also led to earlier senescence and reduced marketable shelf life. In contrast, the natural agents produced comparable ripening-related quality attributes while mitigating the health and safety concerns associated with chemical agents. Among the treatments, tomato fruit showed consistent performance across physical, chemical, and sensory parameters, underscoring its practical potential in both small-scale and commercial applications. The more gradual ripening induced by these natural agents offers a favorable balance between timely ripening and extended shelf life, which is critical for marketability. Furthermore, the use of HCA provided a robust multivariate framework for classifying treatments based on overall fruit quality, which enables a more holistic

assessment of ripening outcomes. This integrative approach reinforces the potential of natural ripening agents to promote safer, cost-effective, and more sustainable postharvest management. Future research should explore the biochemical pathways involved, consumer perception, and economic feasibility to further support the adoption of these alternatives in banana supply chains.

5. Acknowledgements

The author extends sincere gratitude to the City Government Unit of Panabo, Davao del Norte, Philippines, for supporting this work through a research grant. The author also wishes to thank the USeP Research Division and the Tagum-Mabini Campus for providing the necessary support and permission to conduct the experiment.

Author Contributions: The sole author is solely responsible for the conceptualization, fund sourcing, experimental design and execution, data collection and analysis, and the writing and revision of the manuscript.

Funding: This research was supported by external funding from the City Government of Panabo, Davao del Norte, Philippines, through a research grant awarded as part of the Grand Prize in the 1st Panabo Research Competition in 2022.

Conflicts of Interest: The author declares no conflict of interest. This research was conducted independently as part of the agreement under the 1st Panabo Research Competition, where the author was recognized as the sole winner and sole contributor.

References

[1] Voora, V.; Larrea, C.; Bermudez, S. *Global Market Report: Bananas*; International Institute for Sustainable Development: Winnipeg, Canada, **2020**.

[2] Maduwanthi, S. D. T.; Marapana, R. A. U. J. Induced ripening agents and their effect on fruit quality of banana. *Int. J. Food Sci.* **2019**, *2019*, 1–10. https://doi.org/10.1155/2019/2520179

[3] Mahajan, B. V. C.; Kaur, T.; Gill, M. I. S.; Dhaliwal, H. S.; Ghuman, B. S.; Chahil, B. S. Studies on optimization of ripening techniques for banana. *J. Food Sci. Technol.* **2010**, *47*, 315–319. https://doi.org/10.1007/s13197-010-0050-0

[4] Okeke, E. S.; Okagu, I. U.; Okoye, C. O.; Ezeorba, T. P. C. The use of calcium carbide in food and fruit ripening: Potential mechanisms of toxicity to humans and future prospects. *Toxicology* **2022**, *468*, 153112. https://doi.org/10.1016/j.tox.2022.153112

[5] Essien, E. B.; Onyegeme-Okerenta, B. M.; Onyema, J. O. Calcium carbide as an artificial fruit-ripening agent and its physiological effects on Wistar rats. *Clin. Exp. Med. Sci.* **2018**, *6*(1), 47–61. https://doi.org/10.12988/cems.2018.865

[6] Danish, M.; Fatima, A.; Khanam, S.; Jyoti, S.; Ali, F.; Naz, F.; et al. Evaluation of the toxic potential of calcium carbide in the third instar larvae of transgenic *Drosophila melanogaster* (hsp70-lacZ) Bg9. *Chemosphere* **2015**, *139*, 469–478. https://doi.org/10.1016/j.chemosphere.2015.07.077

[7] Basak, P.; Akter, B. Comprehensive investigation on banana ripening by using natural agents and chemicals. *Ann. Food Sci. Technol.* **2018**, *19*(2), 307–315.

[8] Acedo, A. L. Ripening Requirements and Changes of 'Saba' Bananas (*Musa*, BBB Group) Treated with Ethylene from *Gliricidia* Leaves (*Gliricidia sepium* Steud.) [Ph.D. Thesis], University of the Philippines Los Baños, 1989. Available online: http://www.uplb.edu.ph.

[9] Lacap, A. T.; Bayogan, E. R. V.; Lubaton, C. D. S.; Joyce, D. C. Responses of 'Carabao' mango to various ripening agents. *Philipp. J. Sci.* **2019**, *148*(3).

[10] Ajayi, A. R.; Mbah, G. O. Identification of indigenous ripening technologies of banana and plantain fruits among women-marketers in southeastern Nigeria. *Agro-Sci.* **2007**, *6*(2), 60–66. https://doi.org/10.4314/as.v6i2.1572

[11] Ademe, B. E.; Tanga, A. A. Retrospective analysis of moringa leaf as a substitute to ethylene gas in hastening ripening of banana fruit. *Am. J. Food Technol.* **2017**, *12*(3), 186–192. https://doi.org/10.3923/ajft.2017.186.192

[12] Bautista, O. K.; Tirtosoekotjo, M. S.; Soliven, M. L. S.; Nasrullah, S. T. Enhancing accumulation of ethylene from various leaves for tomato ripening. *ASEAN Food J.* **1990**, *5* (4), 142–151.

[13] Dapar, M. L. G.; Alejandro, G. J. D.; Meve, U.; Liede-Schumann, S. Ethnomedicinal importance and conservation status of medicinal trees among indigenous communities in Esperanza, Agusan del Sur, Philippines. *J. Complement. Med. Res.* **2020**, *11*(1), 59–71. https://doi.org/10.5455/jcmr.2020.11.01.08

[14] Gandhi, S.; Sharma, M.; Bhatnagar, B. Comparative study on the ripening ability of artificial ripening agent (calcium carbide) and natural ripening agents. *Glob. J. Biol. Agric. Health Sci.* **2016**, *5*, 106–110.

[15] Roy, M.; Langthasa, S.; Hazarika, D. N. Indigenous ripening methods for banana cv. Amritsagar. *J. Pharmacogn. Phytochem.* **2021**, *10*(3), 432–436.

[16] Cua, A. U.; Uy, W. T.; Wijanco, J. E.; dela Paz, A. C.; Lizada, M. C. C. Physico-chemical and physiological characteristics of 'Saba' bananas at different color stages. *Postharvest Res. Notes* **1984**, *1*(3), 81–83.

[17] Santoso, V. R.; Pramitasari, R.; Anugrah, D. S. B. Development of indicator film based on cassava starch–chitosan incorporated with red dragon fruit peel anthocyanins–Gambier catechins to detect banana ripeness. *Polymers* **2023**, *15*(17), 3609. https://doi.org/10.3390/polym15173609

[18] Bejaei, M.; Cliff, M. A.; Singh, A. Multiple correspondence and hierarchical cluster analyses for the profiling of fresh apple customers using data from two marketplaces. *Foods* **2020**, *9*(7), 873. https://doi.org/10.3390/foods9070873

[19] Zheng, P.; Zhang, M.; Wang, Z.; Wang, T.; Tang, L.; Ma, E.; et al. Comprehensive evaluation of the fruit quality of the main cultivars of pear (*Pyrus* spp.) in North China. *Erwerbs-Obstbau* **2022**, *64*(2), 219–227. https://doi.org/10.1007/s10341-021-00609-y

[20] Manigo, B. I.; Limbaga, C. Effect of 1-methylcyclopropene (1-MCP) postharvest application on quality of 'Lakatan' banana fruit. *Int. J. Agric. Innov. Res.* **2019**, *8*(1), 1–10.

[21] Thompson, A. K.; Supapvanich, S.; Sirison, J. *Banana Ripening: Science and Technology*; Springer Nature: Cham, Switzerland, 2019. https://doi.org/10.1007/978-3-030-27739-0

[22] Mishra, B. B.; Gautam, S.; Chander, R.; Sharma, A. Characterization of nutritional, organoleptic and functional properties of intermediate moisture shelf-stable ready-to-eat *Carica papaya* cubes. *Food Biosci.* **2015**, *10*, 69–79. https://doi.org/10.1016/j.fbio.2015.02.001

[23] Gunathilake, D. M. C. C.; Tiwari, A. K.; Kahandawala, K. T. Efficacy of washing treatment for extending the post-harvest shelf-life of papaya (*Carica papaya*). *Int. J. Chem. Stud.* **2018**, *6*, 2173–2177. https://doi.org/10.22271/chemi.2018.v6.i4ai.05

[24] Basan, R. J. P.; Piadozo, M. E. S.; Pabuayon, I. M. Analysis of consumer demand for table banana characteristics in production and consumption-based areas in the Philippines.

[25] Tucker, G.; Yin, X.; Zhang, A.; Wang, M.; Zhu, Q.; Liu, X.; et al. Ethylene and fruit softening. *Food Qual. Saf.* **2017**, *1*(4), 253–267. https://doi.org/10.1093/fqsafe/fyx024

[26] Chandar, M. M.; Smith, A. A. Artificial ripening of banana - An overview. *Res. J. Pharm. Technol.* **2019**, *12*(10), 5101–5106. https://doi.org/10.5958/0974-360X.2019.00884.9

ASEAN
Journal of Scientific and Technological Reports
Online ISSN:2773-8752

Research article

Biodegradation of Oil and Grease in Synthetic Wastewater Using Lipase-Producing Bacteria Isolated from University Canteen Wastewater

Pradabduang Kiattisaksiri[1], Panabodee Sornram[1], Apinya Phoamart[1], Supawinee Srikham[1], and Yanasinee Suma[1*]

[1] Faculty of Public Health, Thammasat University (Lampang campus), Lampang, 52190, Thailand
* Correspondence: yanasinee.s@fph.tu.ac.th

Citation:
Kiattisaksiri, P.; Sornram, P.; Phoamart, A.; Srikham, S.; Suma, Y. Biodegradation of oil and grease in synthetic wastewater using lipase-producing bacteria isolated from university canteen wastewater. *ASEAN J. Sci. Tech. Report.* **2026**, *29*(1), e258938. https://doi.org/10.55164/ajstr.v29i1.258938.

Article history:
Received: Apri1 23, 2025
Revised: October 10, 2025
Accepted: October 18, 2025
Available online: December 14, 2025

Publisher's Note:
This article is published and distributed under the terms of the Thaksin University.

Abstract: This study aims to isolate lipase-producing bacteria from university canteen wastewater and assess their effectiveness in the degradation of oil and grease in synthetic wastewater. The results showed that the bacteria isolated from the grease trap wastewater of the central canteen exhibited a bacterial count of 9.3 × 10^8 CFU/mL. In total, 11 bacterial isolates, labeled A1 to A11, were obtained, displaying six distinct colony morphologies. Lipase-producing bacteria were selected based on the size of the clear zone formed, with isolates A6 and A11 being selected for further evaluation. The effectiveness of these isolates in degrading oil and grease in synthetic wastewater was then assessed. The optimal initial concentration of oil and grease for bacterial degradation was found to be 10,480 mg/L at 32 °C over 40 hours. Bacteria A6 and A11 demonstrated average degradation efficiencies of 24.52% and 18.14%, respectively. Therefore, this study serves as a preliminary laboratory investigation aimed at generating essential data for the potential future applications in treating wastewater contaminated with oil and grease.

Keywords: Canteen wastewater; lipase; oil degradation

1. Introduction

Wastewater contaminated with cooking oil, which contains fatty acids and glycerin, presents a significant challenge for decomposition and disposal due to its low water solubility. The formation of an oil layer on the water's surface hinders the penetration of oxygen and sunlight, thereby negatively impacting aquatic ecosystems. Furthermore, oil droplets can interact with suspended particles in wastewater, leading to blockages in drainage systems and disrupting wastewater treatment processes. Additionally, when exposed to high temperatures in open environments, cooking oil undergoes oxidation, altering its properties and contributing to the formation of carcinogenic byproducts [1]. Therefore, it is essential to eliminate oil and grease from wastewater before treatment.

While physical and chemical methods for removing oil and grease are effective, they tend to be expensive and may produce secondary pollutants [1, 2]. Currently, bioremediation and biological treatment technologies have emerged as effective wastewater treatment approaches due to their high efficiency, cost-effectiveness, environmental sustainability, and other advantages [3, 4]. Bacteria play a crucial role in wastewater treatment, making

them a key microbial group in bioremediation processes. The use of bacteria capable of degrading fats and oils offers a promising alternative for wastewater treatment [5]. Numerous studies have focused on isolating and characterizing microorganisms with high efficiency in lipid degradation. Such microorganisms have been identified in various environments, including grease traps, wastewater treatment systems in industrial facilities, oil-contaminated soil, biogas digestate, and natural habitats such as mangrove sediments and wastewater-collecting canals [6–10]. Previous studies have successfully isolated various bacterial strains capable of degrading fats and oils. These include *Bacillus cereus* from effluent in a petroleum company, *Acinetobacter baumannii* from poultry processing factory effluent, *Pseudomonas aeruginosa* and *Bacillus subtilis* from crude oil, *Rhodopseudomonas* faecalis from cooking oil, *Aeromonas hydrophila* from cattle slaughterhouse effluent, and *Aeromonas jandaei* from restaurant wastewater [7–12]. These bacteria play a crucial role in wastewater treatment by producing lipase enzymes, which break down fats and oils into fatty acids and glycerol. The bacteria then utilize these byproducts as energy sources [13]. Bacterially derived lipases have broad applications in both industrial processes and wastewater treatment, including aerobic and anaerobic degradation systems [14]. Lipases are classified within the triacylglycerol ester hydrolase family (EC 3.1.1.3) and are capable of facilitating both esterification and hydrolysis reactions. Their high stereospecificity and catalytic efficiency make them valuable in a wide range of industries, such as detergents, cosmetics, food processing, leather manufacturing, biodiesel production, and wastewater treatment [8]. Moreover, lipase-producing bacteria play a significant role in the biodegradation of wastewater contaminated with oil and grease. While several studies have discovered lipase-producing bacteria from different sources, few have specifically focused on wastewater from university canteens in Thailand, which represents a locally relevant and underexplored environment. This study set the hypothesis that locally isolated bacteria from university canteen wastewater can efficiently reduce oil and grease concentration under laboratory surroundings and that strains demonstrating high lipase activity (indicated by larger clear zones) are capable of degrading higher oil and grease concentrations.

University cafeterias generate wastewater contaminated with oil and grease daily. The authors recognize that isolating and evaluating the efficiency of lipase-producing bacteria in degrading oil and grease could provide a natural and effective approach to wastewater treatment. These bacteria could be utilized to enhance the biodegradation of oil and grease, contributing to a more sustainable and efficient wastewater management system. This study aims to isolate naturally occurring local bacteria from environments contaminated with oil and grease in university canteens and investigate their efficiency in degrading fats and oils in synthetic fat-containing wastewater. The findings will provide fundamental data and guidelines for improving the efficiency of wastewater treatment systems. Utilizing bacteria isolated from their natural environment is expected to enhance treatment effectiveness compared to using microorganisms sourced from other locations, as they have already undergone natural selection.

2. Materials and Methods

2.1 Isolation of bacteria from wastewater samples

Wastewater samples were collected from the grease trap of the cafeteria at Thammasat University's Lampang Campus, located in Hang Chat District, Lampang Province, Thailand, as shown in Figure 1.

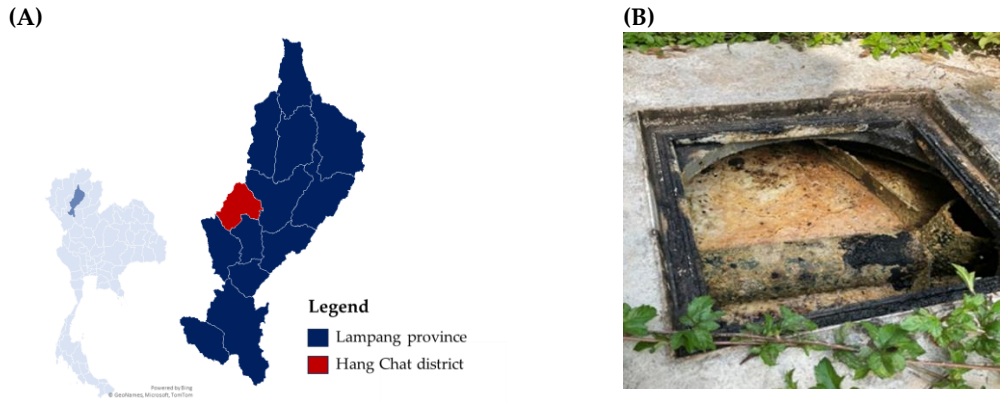


Figure 1. Study site and sampling point. (A) Thammasat University's Lampang Campus, Hang Chat District, Lampang Province, Thailand. (B) The cafeteria grease trap was used as the sampling point in this study.

A 5-mL sample was inoculated into 100 mL of Luria-Bertani (LB) broth in a 250 mL Erlenmeyer flask and incubated on a shaker at 150 rpm at 37 °C for 48 hours. Subsequently, a 10-fold serial dilution was performed using LB medium, and dilutions ranging from 10^{-6} to 10^{-10} were spread-plated onto solid LB agar in Petri dishes. The plates were incubated at 37 °C for 24 hours, and the colonies were counted. Bacterial concentrations in colony-forming units (CFU/mL) were calculated using Equation (1), taking the dilution factor and plated volume into account, and considering plates with 30–300 colonies:

The viable bacterial concentration was verified by plate counting. Colony-forming units (CFU/mL) were calculated using the following equation:

$$CFU/mL = \frac{\text{Number of colonies} \times \text{Dilution factor}}{Volume\ plate\ (mL)} \quad (1)$$

Colonies were then randomly selected from plates with diverse morphologies and streaked onto LB agar to obtain single, pure colonies. The plates were incubated at 37 °C for 24–48 hours until distinct colonies were obtained. The purified bacterial strains were preserved on nutrient agar slants at 4 °C for further use [15]. The resulting bacterial counts, calculated using the described dilution method, are reported in the Results and Discussion section. All environmental and microbial samples were handled following standard biosafety procedures to prevent environmental contamination. Wastewater samples were chlorinated before discharge, and bacterial cultures on plates or in flasks were autoclaved before disposal.

2.2 Selection of oil- and grease-degrading bacteria

Pure bacterial isolates were streaked onto solid tributyrin agar, a medium used for screening lipase enzyme production [15]. The plates were incubated at 37 °C for 48 hours, after which the size of the clear zones formed around the colonies was measured. The two bacterial isolates producing the largest clear zones on the tributyrin agar were selected and cultured in 100 mL of nutrient broth (NB) in a 250 mL Erlenmeyer flask. The cultures were incubated in a shaking incubator at 150 rpm and 37 °C for 24 hours. The clear zones forming around the bacterial growth on the surface of the medium were observed, and the size of the zones was measured. The bacteria capable of producing clear zones were then gram-stained using the gram-staining technique, and the results were examined under a microscope to assess the staining and bacterial morphology.

2.3 Efficiency of lipase-producing bacteria in degrading oil and grease from synthetic wastewater

2.3.1. Preparation of synthetic wastewater

The preparation of synthetic wastewater was adapted from the experiment conducted by Chitpirom and Sangaroon [6]. The synthetic wastewater consisted of 0.1 g of starch, 0.1 g of powdered milk, 0.1 g of sugar, 0.1 mL or 0.5 mL of palm oil (to obtain two initial concentrations of oil and grease), along with 40 mL of distilled water. The mixture was placed in a 250 mL Erlenmeyer flask and sterilized by autoclaving at 15 psi and 121 °C for 15 minutes.

2.3.2 Efficiency of lipase-producing bacteria in synthetic wastewater

The efficiency of lipase-producing bacteria in synthetic wastewater was tested based on the method used by Mookkhan et al. [15], with modifications. Two bacterial isolates producing the largest clear zones were selected. After increasing the bacterial concentration, the turbidity was adjusted to approximately 0.5 at OD_{600}. The bacterial suspension was then inoculated into three replicate Erlenmeyer flasks (250 mL) containing synthetic wastewater, while three additional flasks containing synthetic wastewater without bacteria served as controls. All flasks were incubated at 30–37 °C with shaking at 200 rpm for 40 hours. The concentration of oil and grease in both bacterial-treated and control flasks was determined using the Soxhlet extraction method with an automatic solvent extractor (VELP Scientifica, SER 158 Series), following Standard Methods AWWA 5520, Part D. The biodegradation experiments were conducted using two bacterial isolates (A6 and A11) at initial oil and grease concentrations of 2,350 and 10,480 mg/L. Each treatment was subjected to triplicate independent tests. Uninoculated flasks (medium with oil and grease but without bacterial inoculation) were included as controls. After incubation, the residual oil and grease content was quantified, and the percentage removal efficiency was calculated as in Equation (2):

$$\text{Removal efficiency (\%)} = \frac{C_{initial} - C_{final}}{C_{initial}} \times 100 \quad (2)$$

where $C_{initial}$ is the initial oil and grease concentration (mg/L), and C_{final} is the concentration after incubation.

All experiments were performed in triplicate to ensure reproducibility, with both negative and positive controls included to validate experimental outcomes. Instruments were regularly calibrated using certified standards, and standard analytical procedures were strictly followed. Measurement results were reported to a precision consistent with the method and rounded to the nearest mg/L to reflect the instrument's accuracy and reliability. Data were carefully checked for consistency to minimize experimental errors.

2.4 Statistical analysis

All experiments were performed in triplicate, and the data were presented as mean ± standard deviation. Removal efficiencies were compared between treatments using independent t-tests at each initial oil concentration. One-way analysis of variance (ANOVA) followed by post hoc comparisons was applied to further confirm differences among isolates at the same concentration. In addition, a two-way ANOVA was conducted to assess the main effects of isolate type, initial oil concentration, and their interaction on removal efficiency. Statistical analyses were performed using Python. A significance level of $p < 0.05$ was considered statistically significant.

3. Results and Discussion

3.1 Colony characteristics of bacteria isolated on LB medium

The plates were incubated at 37 °C for 24 hours to enumerate bacterial colonies and select isolates. The bacterial count in the grease trap was 9.3×10^8 CFU/mL. Six distinct colony morphologies were observed, comprising a total of 11 colonies. This is consistent with the study by Mookkhan et al. [15], who reported a bacterial count of 4.3×10^9 CFU/mL in cafeteria wastewater, with four different colony morphologies and 20 colonies. The bacterial count differed from previous studies on restaurant wastewater, where the highest count of lipase-producing bacteria was 1.62×10^4 CFU/mL across five samples [10]. The six distinct isolates were streaked onto LB medium and incubated at 37 °C for 24 hours to obtain single, pure colonies. Colony characteristics—including size, color, shape, elevation, surface, and edge—were recorded on LB medium, as summarized in Table 1. As noted in the table, isolates exhibiting identical colony characteristics are grouped for clarity, with further details provided in the table footnote.

Table 1. Colony characteristics of bacteria isolated on LB Medium

Isolate	Colony characteristics					
	Sizes	**Color**	**Shape**	**Elevation**	**Surface**	**Edge**
A1	Large	Creamy-white	Cocci	Flat	Smooth	Entire
A2, A9, A11	Large	Yellow	Cocci	Convex	Smooth	Undulate
A3	Small	Creamy-white	Cocci	Convex	Smooth	Undulate
A4	Small	Creamy-white	Cocci	Flat	Smooth	Undulate
A5, A8, A10	Large	Creamy-white	Spiral	Flat	Smooth	Undulate
A6, A7	Small	Creamy-white	Cocci	Flat	Smooth	Undulate

Note: Isolates grouped in the same row exhibited identical colony characteristics on LB medium.

3.2 Morphology of isolated bacteria and selection of lipase-producing bacteria

Gram-staining of the 11 bacterial isolates was performed to observe their shape and staining characteristics under a microscope. The results, shown in Table 2, were consistent with those of Attapong [16], who reported that bacteria isolated from restaurant wastewater were gram-negative, short rod-shaped, and randomly arranged. Notably, isolate A6 was gram-positive, whereas all other isolates were gram-negative, suggesting that A6 may belong to a different bacterial genus or species, which could also relate to its relatively strong lipase activity. This observation also aligns with the research of Sukplang et al. [10], who found that some bacteria isolated from restaurant wastewater were gram-positive, with various shapes such as bacilli, short rods, and cocci. The pure bacterial isolates were cultivated on tributyrin agar, a medium used for screening bacteria capable of degrading oils and fats. Lipase production was indicated by the hydrolysis of tributyrin, a triglyceride. The hydrolysis products were glycerol and fatty acids [14]. After incubating at 37 °C for 48 hours, five bacterial isolates produced clear zones around the colonies, namely isolates A6, A7, A8, A10, and A11, as shown in Table 2. The two isolates with the largest clear zones, A6 and A11, had clear zone diameters of 9.4 ± 0.48 mm and 9.6 ± 0.48 mm, respectively (Figure 2). The bacterial clear zone diameters on tributyrin agar were larger than those reported by Mookkhan et al. [15], who found clear zone diameters ranging from 4.5 to 7.5 mm, but smaller than those observed by Attapong [16], who reported clear zone diameters ranging from 11.5 to 20.25 mm. The presence of a wide, clear zone is an initial test indicating that the bacteria are producing lipase to degrade tributyrin.

Table 2. Morphological characteristics and clear zone sizes of bacterial isolates

Isolate	Morphology of isolate bacteria			Size of clear zone (mm)
	Gram stain	**Shape**	**Arrangement**	
A1	Negative	Short rod	Scatter	-
A2	Negative	Short rod	Scatter	-
A3	Negative	Short rod	Scatter	-
A4	Negative	Short rod	Scatter	-
A5	Negative	Short rod	Linear	-
A6	Positive	Short rod	Scatter	9.4 ± 0.48
A7	Negative	Short rod	Scatter	9.1 ± 0.85
A8	Negative	Short rod	Scatter	8.8 ± 0.48
A9	Negative	Short rod	Scatter	-
A10	Negative	Short rod	Scatter	8.6 ± 0.25
A11	Negative	Short rod	Scatter	9.6 ± 0.48

Note: Size of the clear zone (mm) is the measurement of the colony's clear zone diameter, and (-) indicates no clear zone formation.

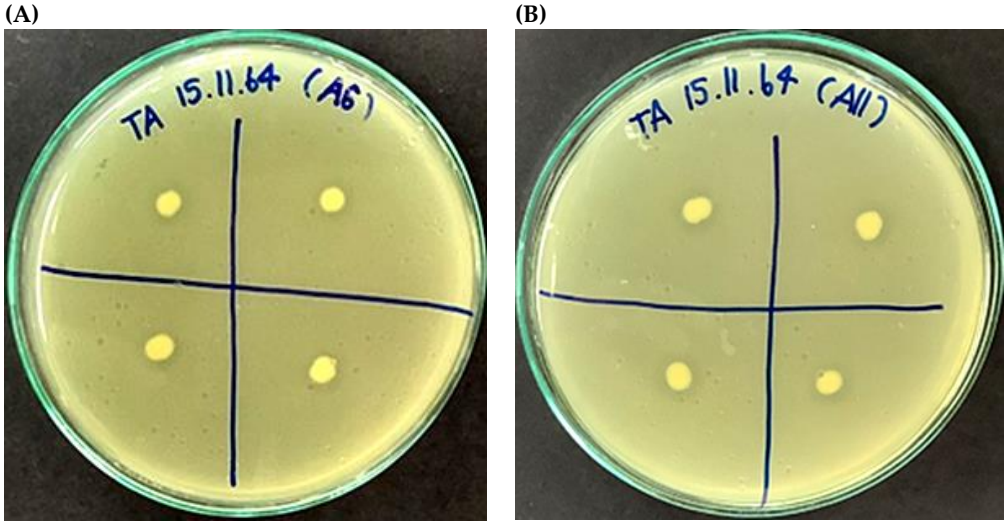


Figure 2. Clear zone formation on tributyrin agar indicates extracellular lipase production. Yellow bacterial colonies are surrounded by distinct halos (clear zones). (A) Isolate A6 and (B) isolate A11.

3.3 Preliminary efficiency of bacteria in degrading oil and grease in synthetic wastewater

Bacteria capable of producing lipase enzymes were selected to test their efficiency in degrading oil and grease. Lipase-producing bacteria degrade oil and grease by enzymatically binding to their molecules. This results in a hydrolysis reaction, in which lipase breaks the ester bonds between the hydroxyl group of glycerol and the carboxyl group of fatty acids, producing glycerol and fatty acids as the final products [17]. The bacterial isolates A6 and A11 were selected for the degradation test due to their ability to produce the largest clear zones, indicative of lipase activity, on tributyrin agar. Palm oil was used as the substrate for the degradation test, as numerous studies have demonstrated that most lipase-producing bacteria degrade palm oil more effectively than other oils. To study the efficiency of these lipase-producing bacteria in degrading oil and grease, the initial concentrations of oil and grease in the synthetic wastewater were 2,350 and 10,480 mg/L, respectively. A broader concentration range could be explored in future studies to further optimize the treatment conditions. The current study focused on a selected range based on preliminary experiments, which provided initial insights into treatment efficiency. The bacterial concentration of isolates A6 and A11 was adjusted to approximately 0.5 based on turbidity measured at a wavelength of 600 nm. The control group consisted of synthetic wastewater with identical initial concentrations of oil and grease, 2,350 and 10,480 mg/L, respectively. The results of the degradation test revealed that, at an initial oil and grease concentration of 2,350 mg/L, isolates A6 and A11 exhibited degradation efficiencies of 11.26% and 18.01%, respectively, resulting in remaining concentrations of 2,086 and 1,927 mg/L. At an initial oil and grease concentration of 10,480 mg/L, isolates A6 and A11 showed degradation efficiencies of 24.52% and 18.14%, respectively, resulting in remaining concentrations of 7,911 and 8,579 mg/L, as shown in Figure 3 and Table 3. The reported oil and grease degradation efficiencies of 24.52% and 18.14% for isolate A6 and A11, respectively, were relatively low compared with removal efficiencies achieved in well-optimized biodegradation systems. For example, previous studies have found that the biodegradation of oil and grease under favorable conditions ranges from 70–95% with average values around 88% in well-tuned activated sludge systems [18]. The limitation of removal in the present study suggests the microbial community may have been constrained in hydrophobic degradation and recalcitrant oil and grease fractions. The affected factors likely include toxicity from high oil concentrations, obstructing microbial growth and enzyme function [19]. Poor availability caused by oil and grease droplet formation or adsorption onto solids and insufficient activity of key hydrolytic or oxidative enzymes (e.g., lipases and monooxygenases) are needed to disrupt complex molecules [20]. To improve the degradation performance, several enhancement strategies can be considered. Effective oil and grease mineralization typically requires a balanced supply of nitrogen, phosphorus, trace elements, and, in many cases, a co-substrate to stimulate cometabolic pathways [21-22]. Co-culturing approaches, for instance,

combining bacteria with fungi, can also be effective since fungi are capable of breaking down complex hydrophobic fractions, thereby increasing substrate availability for bacterial degraders. Another promising approach is the immobilization of microbial cells or enzymes on carriers such as alginate beads, activated carbon, or synthetic polymers, which not only protect cells from toxic effects but also maintain high local biomass and enzyme concentrations. Taken together, these limitations highlight the need for targeted enhancement strategies to overcome biological and operational blockages and raise oil and grease removal above the relatively low levels currently observed.

The removal efficiencies of isolate A6 and A11 were compared at two initial oil and grease concentrations (2,350 and 10,480 mg/L). Independent t-tests indicated significant differences between isolates at both concentrations. At 2,350 mg/L, isolate A11 achieved significantly higher removal efficiency than isolate A6 ($t = -7.04$, $p = 0.011$). In contrast, at 10,480 mg/L, isolate A6 exhibited significantly higher removal efficiency than isolate A11 ($t = 16.47$, $p < 0.001$). One-way ANOVA confirmed that removal efficiencies differed significantly between isolates at both concentrations ($F = 49.61$, $p = 0.002$ at 2,350 mg/L; $F = 271.42$, $p < 0.001$ at 10,480 mg/L). A two-way ANOVA was conducted to evaluate the effects of isolate type, initial oil concentration, and their interaction on removal efficiency. The analysis showed that isolate type ($F = 0.096$, $p = 0.765$) had no significant main effect, while initial concentration had a highly significant effect ($F = 166.03$, $p < 0.001$). Importantly, the interaction effect between isolate type and initial concentration was also highly significant ($F = 162.24$, $p < 0.001$), indicating that the performance of each isolate depended on the initial oil concentration. The statistical analyses revealed that oil removal efficiency was strongly influenced by both the initial concentration of oil and grease and the microbial isolate used. Although no overall main effect of isolate type was observed when concentrations were pooled, the significant interaction demonstrates that removal performance is context-dependent. At lower initial oil concentrations (2,350 mg/L), isolate A11 showed superior performance compared to isolate A6, suggesting that isolate A11 may be more effective under moderate contamination levels. Conversely, at higher concentrations (10,480 mg/L), isolate A6 exhibited significantly higher removal efficiency than isolate A11. This reversal implies that isolate A6 possesses adaptive or enzymatic mechanisms, allowing it to cope better with elevated oil loads. Such interaction effects highlight the importance of considering environmental conditions, particularly pollutant concentration, when evaluating the bioremediation potential of microbial isolates. The findings suggest that while isolate A11 could be preferable in systems with moderate oil contamination, isolate A6 may be more advantageous for environments with high pollutant loads. This concentration-dependent performance provides valuable insight into the optimization of isolate selection for wastewater treatment applications.

The results indicate that as the initial oil and grease concentration increases, the degradation efficiency of the bacteria reduces because of various correlated physicochemical and biological constraints. Excessive oil and grease in synthetic wastewater can form a continuous film or thick layer on the water surface, hindering oxygen transfer and limiting aerobic microbial respiration [23]. The resulting reduction in oxygen availability reduces bacterial growth and declines lipase enzyme production, thereby decreasing degradation efficiency. Furthermore, at high oil loads, hydrophobic compounds tend to combine and adsorb onto solid surfaces, deteriorating their bioavailability to bacteria [24]. Elevated concentrations of oil and grease can also exert toxic effects, disrupting cell membranes, enzyme structures, and overall metabolic activity. Collectively, these factors inhibit microbial growth and lipase activity, leading to lower biodegradation performance under high initial oil and grease concentrations. These findings align with the study by Attapong [16], who observed that at an initial oil and grease concentration of 1,500 mg/L, *Bacillus pumilus* exhibited an average degradation efficiency of 86.13%. Furthermore, a study by Thongkrua et al. [25] found that at an initial concentration of 1,500 mg/L, *Bacillus pumilus* showed an average degradation efficiency of 85.19%, while *Serratia aquinivoran* showed a degradation efficiency of 76.5%. The experimental results indicate that the incubation duration significantly influences the oil and grease degradation efficiency of lipase-producing bacteria. The incubation period was set to 40 hours based on the research by Kotlakome et al. [26], who found that *Bacillus pumilus* exhibited the highest oil and grease degradation efficiency at 40 hours, with an average degradation efficiency of 99.47%. According to Attapong [16], the initial concentration of oil and grease was 1,500 mg/L, with incubation at 35 °C for 40 hours. The degradation efficiencies of *Bacillus pumilus* LWW2, *Bacillus pumilus*

LWW8, *Bacillus pumilus* LWW9, and *Serratia quinivorans* LWW13 were 86.13 ± 0.24, 86.79 ± 0.13, 91.24 ± 0.10, and 76.50 ± 0.36%, respectively. This time period was identified as the phase when *Bacillus pumilus* experienced stable growth. The results suggest that the duration of oil and grease degradation is dependent on the bacterial strain, as different strains produce lipase enzymes under varying conditions and time frames. The findings show that isolates A6 and A11 demonstrate lower oil degradation efficiency, suggesting that these isolates may require a longer duration to degrade oil and grease more effectively. Furthermore, the experimental results reveal that temperature affects the efficiency of oil and grease degradation in lipase-producing bacteria. The incubation temperature was maintained at an average of 32 °C, falling within the optimal range for bacterial growth and lipase production, as most bacteria thrive at temperatures between 30 and 37 °C [27]. Temperatures that are either too low or too high can adversely affect bacterial growth, resulting in reduced lipase production. In addition, temperature extremes can affect the stability of lipase enzymes, leading to structural changes and decreasing their catalytic efficiency [28]. Consequently, bacteria are less efficient at degrading oil and grease in synthetic wastewater. Overall, these findings demonstrate that while isolates possess oil and grease degrading capability, their performance under the setting conditions was less efficient than that of *Bacillus pumilus.* This may reflect variation in enzyme kinetics, regulatory mechanisms, and environmental adaptability. Future optimization of culture parameters such as temperature, incubation period, and initial oil and grease concentrations may increase the degradation efficiency of these isolates.

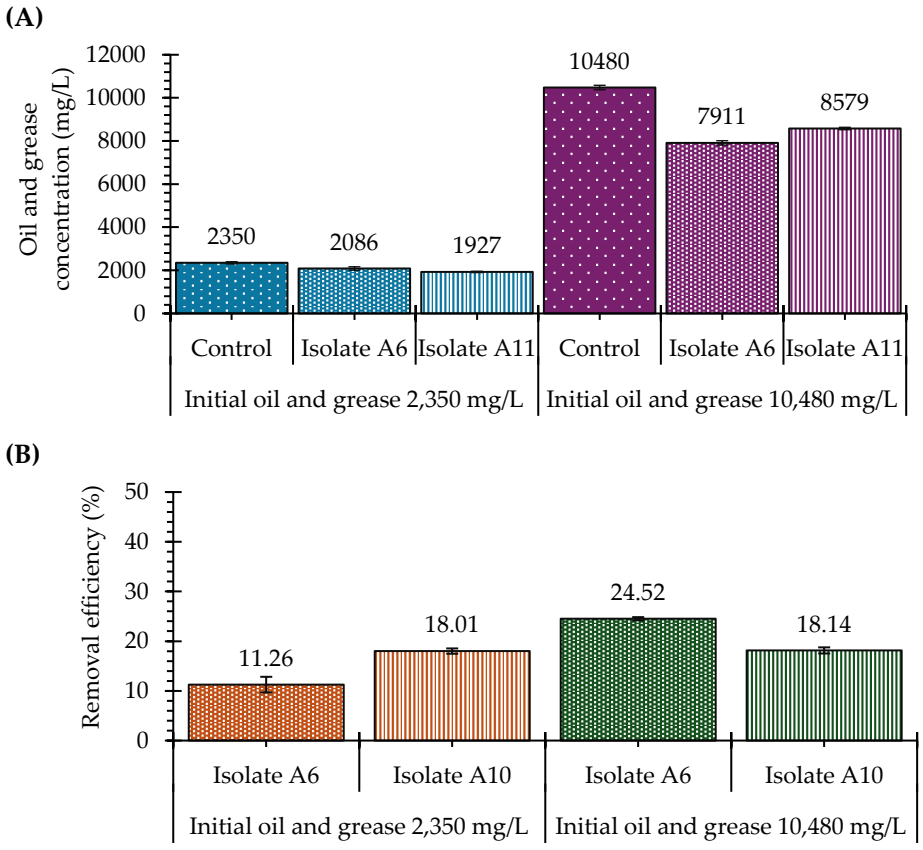


Figure 3. Comparison of (A) oil and grease concentrations and (B) removal efficiencies of oil and grease by isolate A6, isolate A11, and the uninoculated control at different initial concentrations.

Table 3. Comparison of oil and grease degradation efficiency with previous research

Inoculum	Effluent/ isolation condition	Type of tested oil	Initial oil and grease concentration	Degradation temperature (°C)	Time (hour)	Oil and grease removal (%)	Reference
Aeromonas jandaei	Restaurant wastewater/ 1 g of immobilized cells on a scrub pad (10^8 CFU/g) in 100 mL of effluent, 30 °C, 150 rpm	Various cooking oils	3% (W/V)	30	48	98.37	[10]
WA5	Canteen University/ Streak pure culture on tributyrin agar, 37 °C, 48 hours	Vegetable oil	-	37	168	20.44	[15]
		Lard	-			52.84	
Bacillus pumilus. strain UBU5	Fresh market/0.1 mL culture on screening medium, 37 °C, 24 hours	Palm oil	1,500 mg/L	30	40	86.11	[19]
Bacillus pumilus	Restaurant/ 10 µL pure culture on tributyrin agar, 37 °C, 48 hours	Palm oil	1,500 mg/L	30	32	85.19	[18]
Meyerozyma quilliermondii	Restaurants and canteens/ Streak on Tween 20 medium, 72 hours	-	-	Room temperature	168	83.03	[29]
A6	Canteen University/ Streak pure culture on tributyrin agar, 37 °C, 48 hours	Palm oil	2,350 mg/L	30-37	40	11.26 ± 1.57	This study
A11						18.01 ± 0.53	
A6			10,480 mg/L			24.52 ± 0.32	
A11						18.14 ± 0.62	

3.4 Limitations of the research and further studies

This study has several limitations and serves as an initial exploration of the effectiveness of oil and grease degradation. The experimental conditions were restricted, with only two oil concentrations tested without the systematic optimization of key parameters such as pH, temperature, or incubation time. In

addition, the bacterial isolates (A6 and A11) were only characterized morphologically and not taxonomically identified; modern molecular approaches such as 16S rRNA sequencing should be employed for accurate classification. The assessment of lipase activity was also limited, relying mainly on qualitative observations of clear zones without reporting enzyme activity in standard quantitative units or providing data on enzyme kinetics. Furthermore, the study did not examine the broader environmental factors influencing lipid degradation, including nutrient availability and physicochemical parameters such as temperature range, pH levels, salinity, oil types, oil and grease concentrations, and duration of the degradation process [30]. These limitations reduce the applicability of the findings to real wastewater systems. Future research should therefore prioritize the molecular identification of lipase-producing bacterial strains, alongside the systematic characterization and quantification of lipase enzyme activity, before assessing their efficiency under a wider range of environmental conditions. Additionally, the future work should focus on optimizing culture conditions to enhance lipase production and oil–grease degradation and on assessing the process at pilot scale or in real wastewater treatment systems to determine its practical applicability. Table 4 summarizes the factors affecting lipase enzymes in reducing oil and grease concentrations in wastewater, adapted from previous studies [1, 30] and the findings of this present study.

Table 4. Factors affecting lipase enzymes to reduce oil and grease concentrations in wastewater, adapted from [1, 30]

Aspects	Factors
Source	Plant
	Microbe
	Animal
Target microorganism	Choice of microbial strain
	Population size
	Natural or inoculated microorganism
Substrate characteristics	Concentration
	Type of substrate
	Nutrient availability
	Salinity
Environmental conditions	Temperature
	pH
	Metal ions and inhibitors
	Electrostimulation
Immobilization	Free enzyme
	Immobilized enzyme
Time interval	Duration of the degradation

4. Conclusions

This preliminary study investigated lipase-producing bacteria isolated from oil- and grease-contaminated wastewater collected from a university cafeteria grease trap. Six distinct bacterial strains were obtained, of which five exhibited lipase activity. Among them, isolate A6 showed the highest degradation efficiency, reducing oil and grease by approximately 24.52% under laboratory conditions. These findings provide baseline data on the lipase activity and biodegradation potential of bacteria from a locally relevant source. The results serve as a foundation for future research focusing on molecular identification, optimization of culture and degradation conditions, and evaluation of performance in pilot-scale or real wastewater treatment systems.

5. Acknowledgements

The authors would like to extend their gratitude to the Faculty of Public Health, Thammasat University, for providing the necessary instruments and equipment for the experiments. Additionally, we

sincerely appreciate the Property and Sports Management Office of Thammasat University for kindly providing wastewater samples from the cafeteria.

Author Contributions: Conceptualization, P.K. and Y.S.; methodology, Y.S., P.S. and A.P.; formal analysis, Y.S., P.S., S.S. and A.P.; investigation, P.S. and A.P.;. writing—original draft preparation, P.K. and Y.S.; writing—review and editing, P.K. and Y.S.

Funding: This research was funded by the Employment Scholarship for Research and Academic Assistance (undergraduate degree) Fund, Contract No. 059/2568, from the Faculty of Public Health, Thammasat University.

Conflicts of Interest: The authors declare no conflict of interest.

References

[1] Nimkande, V. D.; Bafana, A. A Review on the utility of microbial lipases in wastewater treatment. *J. Water Process Eng*. **2022**, *46*, 102591. https://doi.org/10.1016/j.jwpe.2022.102591

[2] Montagnolli, R. N.; Lopes, P. R. M.; Bidoia, E. D. Applied models to biodegradation kinetics of lubricant and vegetable oils in wastewater. *Int. Biodeterior. Biodegrad*. **2009**, *63(3)*, 297–305. https://doi.org/10.1016/j.ibiod.2008.06.002

[3] Wang, T.; Wang, W.; Hu, H.; Khu, S.-T. Novel quantitative evaluation of biotreatment suitability of wastewater. *Water* **2022**, *14*(7), 1038. https://doi.org/10.3390/w14071038

[4] Zahri, K. N. M.; Zulkharnain, A.; Sabri, S.; Gomez-Fuentes, C.; Ahmad, S. A. Research trends of biodegradation of cooking oil in Antarctica from 2001 to 2021: A bibliometric analysis based on the scopus database. *Int. J. Environ. Res. Public Health* **2021**, *18*(4), 2050. https://doi.org/10.3390/ijerph18042050

[5] Prasad, M. P.; Manjunath, K. Comparative study on biodegradation of lipid-rich wastewater using lipase producing bacteria species. *Indian J. Biotechnol.* **2011**, *10*(1), 121–124.

[6] Chitpirom, K.; Sangaroon, P. Detection of lipolytic bacteria from environmental samples. *J. Public Health* **2012**, *42*(3), 3–18.

[7] Hassan, S. W. M.; Abd El Latif, H. H.; Ali, S. M. Production of cold-active lipase by free and immobilized marine *Bacillus cereus* HSS: Application in wastewater treatment. *Front. Microbiol.* **2018**, *9*, 2377. https://doi.org/10.3389/fmicb.2018.02377

[8] Bunmadee, S.; Teeka, J.; Lomthong, T.; Kaewpa, D.; Areesirisuk, P.; Areesirisuk, A. Isolation and identification of a newly isolated lipase-producing bacterium (*Acinetobacter baumannii* RMUTT3S8-2) from an oily wastewater treatment pond in a poultry processing factory and its optimum lipase production. *Bioresour. Technol. Rep.* **2022**, *20*, 101267. https://doi.org/10.1016/j.biteb.2022.101267

[9] Haselroth, K. J.; Wilke, P.; Costa, I. M. D.; Rotta, V. M. L.; Rosado, A. F.; Hermes, E. Effectiveness of *Aeromonas hydrophila* for the removal of oil and grease from cattle slaughterhouse effluent. *J. Clean. Prod.* **2021**, *287*, 125533. https://doi.org/10.1016/j.jclepro.2020.125533

[10] Sukplang, G.; Narasettiti, C.; Chunhachart, O.; Srithaworn, M.; Lorliam, W.; Krajangsang, S.; Panyachanakul, T. Isolation and identification of lipase-producing bacteria from a wastewater treatment pond for the removal of oil and grease in wastewater treatment. *Chiang Mai J. Sci.* **2024**, *51*(6), e2024096. https://doi.org/10.12982/CMJSci.2024.0096

[11] Abubakar, A.; Abioye, P. O.; Aransiola, S. A.; Raju, M. N.; Prasad, R. Crude oil biodegradation potential of lipase produced by *Bacillus subtilis* and *Pseudomonas aeruginosa* isolated from hydrocarbon contaminated soil. *Environ. Chem. Ecotoxicol.* **2024**, *6*, 26–32. https://doi.org/10.1016/j.enceco.2023.12.001

[12] Saejung, C.; Phonaiam, S.; Kotthale, P.; Chaiyarat, A. Bacterial cellulose as a reinforcement material of alginate beads improves effectiveness and recycling potential of immobilized photosynthetic bacteria for cooking oil waste removal. *Carbohydr. Polym.* **2024**, *324*, 121532. https://doi.org/10.1016/j.carbpol.2023.121532

[13] Zulaika, A.; Rahman, H.; Ningrum, S. S.; Maulida, A. F. Exploring microbial lipases: Screening and identification for biocatalyst potential in bioethanol synthesis from glycerol-based biodiesel waste. *Results Eng.* **2024**, *23*, 102427. https://doi.org/10.1016/j.rineng.2024.102427

[14] Chandra, P.; Enespa; Singh, R.; Arora, P. K. Microbial lipases and their industrial applications: A comprehensive review. *Microb. Cell Fact.* **2020**, *19*, 169. https://doi.org/10.1186/s12934-020-01428-8

[15] Mookkhan, P.; Asa, P.; Noisamdaeng, P. Isolation and lipid decomposition efficiency of bacteria isolated from canteen wastewater. *Sci. Technol. RMUTT J.* **2017**, *7*(2), 241–250.

[16] Attapong, M. Study on lipolytic bacteria efficiency for fat, oil, and grease degradation in synthetic wastewater. M.Sc. Thesis, University of Phayao, Phayao (Thailand), **2017**.

[17] National Center for Biotechnology Information (NCBI). Biochemistry, Lipase. https://www.ncbi.nlm.nih.gov/books/NBK537346/ (accessed 2025-10-02).

[18] Cisterna-Osorio, P.; Arancibia-Avila, P. Comparison of biodegradation of fats and oils by activated sludge on experimental and real scales. *Water* **2019**, *11*(6), 1286. https://doi.org/10.3390/w11061286

[19] Al Khatib, M. F. R.; Alqedra, F.; Alam, M. Z. Biodegradation of fats, oil and grease using microorganisms isolated from palm oil mill effluent. *IIUM Eng. J.* **2023**, *24*(2), 1–10. https://doi.org/10.31436/iiumej.v24i2.2590

[20] Cui, J.; Dörmann, P. Microbial degradation of hydrocarbons from petroleum assisted by biosurfactants: Pathways and bioremediation potential. *Biochimie* (in press, journal pre-proof). https://doi.org/10.1016/j.biochi.2025.09.011

[21] Leys, N. M.; Bastiaens, L.; Verstraete, W.; Springael, D. Influence of the carbon/nitrogen/phosphorus ratio on polycyclic aromatic hydrocarbon degradation by *Mycobacterium* and *Sphingomonas* in soil. *Appl. Microbiol. Biotechnol.* **2005**, *66*(6), 726–736. https://doi.org/10.1007/s00253-004-1568-8

[22] Feng, J. Y.; Zhou, X. D. Effects of co-substrates and inorganic ions on biodegradation of oil-degrading strains. *Adv. Mater. Res.* **2011**, *179–180*, 781–786. https://doi.org/10.4028/www.scientific.net/AMR.179-180.781

[23] Aziz, Z. S.; Jazaa, S. H.; Dageem, H. N.; Banoon, S. R.; Balboul, B. A.; Abdelzaher, M. A. Bacterial biodegradation of oil-contaminated soil for pollutant abatement contributing to achieve sustainable development goals: A comprehensive review. Results Eng. 2024, 102083. https://doi.org/10.1016/j.rineng.2024.102083

[24] Usman, M.; Salama, E.; Arif, M.; Jeon, B.-H.; Li, X. Determination of the inhibitory concentration level of fat, oil, and grease (FOG) towards bacterial and archaeal communities in anaerobic digestion. Renew. Sustain. Energy Rev. 2020, 131, 110032. https://doi.org/10.1016/j.rser.2020.110032

[25] Thongkruea, S.; Attapong, M.; Sanpha, S. The efficiency of bacteria in degradation of fat, oil, and grease in synthetic wastewater. *Acad. J. Sci. Technol. Nakhon Sawan Rajabhat Univ.* **2018**, *10*(11), 75–88.

[26] Kotlakome, R.; Suttipanta, N.; Thongplew, N. Enhancing efficiency of grease traps through the addition of lipase-producing bacteria for wastewater management in the fresh markets. *Sci. Essence J.* **2020**, *36*(2), 41–54.

[27] Ali, S.; Khan, S. A.; Hamayun, M.; Lee, I.-J. The recent advances in the utility of microbial lipases: A review. *Microorganisms* **2023**, *11*(2), 510. https://doi.org/10.3390/microorganisms11020510

[28] Al-Rehaili, T. T.; Danial, E. N.; Ayaz, N. O. Improvement of lipase thermal stability using immobilization techniques. *Res. J. Pharm. Biol. Chem. Sci.* **2018**, *9*(4), 519.

[29] Nguyen, N. T.; Cao, N. D. Isolation and identification of lipid-degrading yeast from wastewater of canteens and restaurants in Ninh Kieu District, Can Tho City. *CTU J. Innov. Sustain. Dev.* **2017**, *7*, 27–32. https://doi.org/10.22144/ctu.jen.2017.045

[30] Gupta, R.; Gupta, N.; Rathi, P. Bacterial lipases: An overview of production, purification, and biochemical properties. *Appl. Microbiol. Biotechnol.* **2004**, *64*, 763–781. https://doi.org/10.1007/s00253-004-1568-8

ASEAN
Journal of Scientific and Technological Reports
Online ISSN:2773-8752

Research article

Molecular Characterization and Integron Gene Prevalence in Bacterial Pathogens from Neonatal Omphalitis

Rehab Riyadh Raheem[1*], and Wafaa Abdul Wahid Jheel[1]

[1] College of Education, University of Al-Qadisiyah, Al-Qadisiyah, Iraq
* Correspondence: edu.bio.posta82@qu.edu.iq

Citation:
Raheem, R.R.; Jheel. W.A.W. Molecular characterizatoin and integron gene prevalence in bacterial pathogens from neonatal omphalitis. *ASEAN J. Sci. Tech. Report.* **2026**, *29*(1), e261254. https://doi.org/10.55164/ajstr.v29i1.261254.

Article history:
Received: September 12, 2025
Revised: September 28, 2025
Accepted: October 9, 2025
Available online: December 14, 2025

Publisher's Note:
This article is published and distributed under the terms of the Thaksin University.

Abstract: Neonatal umbilical cord infections (omphalitis) remain a significant cause of morbidity and mortality in developing countries. This study aimed to characterize bacterial pathogens associated with neonatal omphalitis using both phenotypic and molecular methods, and to determine the prevalence of integron genes. One hundred umbilical swabs were collected from neonates (3-28 days old) with clinical omphalitis. Bacterial identification was performed using conventional culture, the Vitek 2 Compact system, and 16S rRNA gene PCR sequencing. PCR detected integron genes (*intI1*, *intI2*, *intI3*). Phylogenetic analysis was conducted using MEGA X software. Bacterial growth occurred in 48/100 (48%) samples. The predominant isolates were *Staphylococcus aureus* (14/48, 29.16%), *Escherichia coli* (14/48, 29.16%), and *Pseudomonas aeruginosa* (14/48, 29.16%), followed by *Enterococcus* spp. (4/48, 8.33%) and *Bacteroides* spp. (2/48, 4.16%). All 24 tested isolates yielded 1500 bp 16S rRNA amplicons. Sequenced *P. aeruginosa* isolates showed 99-100% identity with GenBank references. Phylogenetic analysis revealed bootstrap values of 63-100% for *P. aeruginosa*, 99-100% for *Enterococcus faecalis* and *Bacteroides* sp., and 32-70% for *E. coli*. Integron gene prevalence varied significantly, with *intI1* being the highest in *E. coli* (85.71%) and *Enterococcus* spp. (100%); *intI2* predominated in *P. aeruginosa* (75%) and S. aureus (71.42%); intI3 was detected only in S. aureus (57.14%) and *E. coli* (28.57%). Gram-positive and Gram-negative bacteria equally contributed to neonatal omphalitis. High integron prevalence, particularly classes 1 and 2, indicates a significant potential for antimicrobial resistance, requiring enhanced surveillance and stewardship strategies.

Keywords: Neonatal umbilical cord infections; bacteria; PCR; phylogenetic analysis; integrons.

1. Introduction

Neonatal infections continue to pose a substantial threat to infant survival and health outcomes worldwide, particularly in resource-limited settings where healthcare infrastructure remains inadequate [1]. Among these infections, omphalitis—infection of the umbilical cord stump—represents a preventable yet potentially fatal condition that disproportionately affects newborns in developing countries. The umbilical cord stump serves as a vulnerable portal of entry for pathogenic microorganisms during the critical first weeks of life, potentially leading to localized infection that can rapidly progress to systemic sepsis and death if left untreated [2]. The epidemiology of omphalitis demonstrates stark disparities between developed and developing nations. In

high-income countries, the incidence remains relatively low at 0.2-0.7% of live births, attributed to standardized hygienic cord care practices and accessible healthcare services [1]. Conversely, developing regions report substantially higher rates, with hospital-born neonates experiencing an 8% incidence and home-delivered infants under unhygienic conditions reaching rates as high as 22% [1]. Recent data from Eastern Uganda documented a 3% omphalitis rate among 2,052 neonates, with significantly higher prevalence among home deliveries compared to hospital births [2]. These statistics underscore the critical role of environmental factors and healthcare access in disease prevention.

The bacterial etiology of neonatal umbilical infections encompasses a diverse spectrum of microorganisms, predominantly aerobic bacteria. *Staphylococcus aureus* and *Escherichia coli* consistently emerge as the most frequently isolated pathogens across multiple studies [3]. The pathogenic significance of *S. aureus* in neonatal sepsis has been well-documented in regional studies from Iraq and Sudan, where virulence factors contribute substantially to disease pathogenesis [4, 5]. Additionally, *Pseudomonas aeruginosa* represents a formidable opportunistic pathogen, particularly concerning due to its intrinsic resistance mechanisms and capacity to cause severe infections in immunocompromised neonates [6]. Anaerobic bacteria, including *Bacteroides* species, though less frequently isolated, contribute to polymicrobial infections and complicate treatment strategies [7]. Traditional culture-based diagnostic methods, while remaining the gold standard in many clinical settings, present inherent limitations that may compromise timely and accurate pathogen identification. Culture-negative results occur frequently, particularly in patients with prior antibiotic exposure or infections caused by fastidious organisms [8]. These limitations have prompted the adoption of molecular diagnostic approaches, particularly those involving PCR and sequencing of the 16S ribosomal RNA gene. The 16S rRNA gene contains both highly conserved regions and hypervariable sequences that enable precise bacterial identification at the species level [9]. Recent investigations have demonstrated the superior sensitivity of 16S rRNA sequencing in detecting bacterial DNA, even in culture-negative cases of neonatal sepsis, with detection rates reaching 100% compared to significantly lower rates for conventional blood culture [10]. Furthermore, next-generation sequencing technologies targeting the 16S rRNA gene have successfully identified additional pathogens undetected by traditional culture methods [11].

The escalating challenge of antimicrobial resistance in neonatal pathogens necessitates a comprehensive understanding of the mechanisms underlying resistance. Integrons, mobile genetic elements capable of capturing and expressing resistance gene cassettes, play a crucial role in horizontal gene transfer and the dissemination of resistance. Class 1 integrons demonstrate the highest prevalence and strongest association with multidrug resistance, particularly in Gram-negative bacteria. A recent study reported 12.9% of *E. coli* isolates from hospitalized patients harbored class 1 integrons [12]. Although less prevalent, class 2 and 3 integrons contribute significantly to resistance profiles. Multi-center studies from Iran documented the presence of all three integron classes in multidrug-resistant *S. aureus*, with significant associations between integron presence, antibiotic resistance, and biofilm production [13]. Similarly, investigations in Egypt revealed the concurrent presence of class 1 and 2 integrons in hospital-origin *S. aureus* isolates [14]. Despite advancements in diagnostic capabilities and growing concerns regarding antimicrobial resistance, limited data exist on the molecular epidemiology of omphalitis-associated bacteria in Iraq and its neighboring regions. The prevalence and distribution of integron genes among neonatal pathogens in this geographical area remain largely unexplored. Therefore, this study aimed to comprehensively characterize bacterial pathogens isolated from neonatal umbilical cord infections through an integrated phenotypic and genotypic approach, including automated biochemical profiling (Vitek 2), 16S rRNA gene PCR amplification and sequencing, phylogenetic analysis, and determination of the prevalence of integron classes 1, 2, and 3 within bacterial genomes.

2. Materials and Methods

2.1 Sample Collection and Culture

One hundred umbilical swab specimens were collected from neonates aged 3-28 days presenting with clinical signs of omphalitis at pediatric wards in Al-Qadisiyah, Iraq. Clinical diagnosis was based on the presence of purulent discharge, periumbilical erythema, and edema. Samples were collected using sterile cotton swabs and immediately transported to the bacteriology laboratory in Stuart transport medium.

Specimens were inoculated onto MacConkey agar, Eosin Methylene Blue (EMB) agar, and 5% sheep blood agar plates using the streak plate technique. All plates were incubated aerobically at 37°C for 18 to 24 hours. Colonies displaying distinct morphological characteristics were subsequently sub-cultured on CHROMagar Orientation medium (bioMérieux, France) for differential identification. Pure cultures were obtained through repeated sub-culturing and preserved in glycerol stocks at -80°C for further analysis.

2.2 Identification of Bacterial Isolates

Initial identification was performed through assessment of colonial morphology on selective and differential media. Gram staining was conducted following standard protocols, and microscopic examination was performed at 1000× magnification under oil immersion [15]. Biochemical characterization included indole production, methyl red-Voges Proskauer (MR-VP) test, citrate utilization, motility assessment, urease activity, catalase test, oxidase test, and Triple Sugar Iron (TSI) agar reactions, all performed according to established procedures [15]. Hemolytic patterns (alpha, beta, and gamma hemolysis) were evaluated on blood agar plates after 24-48 hours of incubation. Mannitol Salt Agar (MSA) was used for the selective isolation of Gram-positive cocci and for differentiation based on their ability to ferment mannitol. Lactose fermentation was assessed using MacConkey agar to distinguish between lactose-fermenting and non-lactose-fermenting Gram-negative bacteria.

2.3 VITEK 2 System Identification

Biochemical identification was validated using the VITEK 2 Compact automated system (bioMérieux, France) with appropriate identification cards. Gram-negative (GN) cards were used for Gram-negative isolates, while Gram-positive (GP) cards were employed for Gram-positive bacteria. The system performed 48 biochemical reactions with identification confidence levels reaching 99% [16]. Bacterial suspensions were prepared in 0.45% saline solution to achieve 0.5-0.63 McFarland standard turbidity. Cards were automatically filled, sealed, and incubated, with readings taken every 15 minutes. Final identification was based on comparison with the system's extensive database using Advanced Expert System software.

2.4 Molecular Characterization

Genomic DNA was extracted from overnight bacterial cultures using the Geneaid Bacterial Genomic DNA Extraction Kit (Geneaid Biotech, Taiwan) following the manufacturer's protocol. DNA concentration and purity were assessed using a NanoDrop spectrophotometer (Thermo Fisher Scientific, USA), with A260/A280 ratios between 1.8 and 2.0 considered acceptable. Extracted DNA was stored at -20°C until further use. PCR amplification was performed in 25 μL reaction volumes using AccuPower® PCR PreMix (Bioneer, Korea). The thermal cycling conditions comprised initial denaturation at 94°C for 5 minutes, followed by 30 cycles of denaturation at 94°C for 45 seconds, annealing at 58-60°C for 45 seconds (optimized for each primer set), and extension at 72°C for 1 minute, with a final extension at 72°C for 7 minutes. Universal primers for 16S rRNA gene amplification and specific primers for integron gene detection were employed as detailed in Table 1. PCR products were resolved on 1.5% agarose gels containing 0.5 μg/mL ethidium bromide in 1× TAE buffer at 80V for 45 minutes. Bands were visualized using UV transillumination and documented using a gel documentation system (Bio-Rad, USA). Universal primers for 16S rRNA gene amplification and specific primers for integron gene detection were employed as detailed in Table 1. The 16S rRNA primers (F: 5'-AGA GTT TGA TCC TGG CTC AG-3' and R: 5'-GGT TAC CTT GTT ACG ACT T-3') amplified an approximately 1500 bp fragment [17]. For integron detection, class 1 integrase gene (*intI1*) primers generated 280 bp products, class 2 (*intI2*) primers yielded 233 bp fragments, and class 3 (*intI3*) primers produced 600 bp amplicons [17]. Negative controls were included in all PCR reactions to ensure the accuracy of the results. No-template controls (NTC) using sterile water instead of a DNA template were included to monitor for reagent contamination. Reference bacterial strains confirmed to lack integron genes [specify strains] were used as negative controls to verify primer specificity. All negative controls consistently showed no amplification products.

Table 1. Primer sequences used for PCR amplification

Target Gene	Primer Name	Sequence (5' → 3')	Product Size (bp)	Reference
16S rRNA	16S-F	AGAGTTTGATCCTGGCTCAG	1500	[17]
16S rRNA	16S-R	GGTTACCTTGTTACGACTT	1500	[17]
intI1	intI1-F	CCTCCCGCACGATGATC	280	[17]
intI1	intI1-R	TCCACGCATCGTCAGGC	280	[17]
intI2	intI2-F	TTATTGCTGGGATTAGGC	233	[17]
intI2	intI2-R	ACGGCTACCCTCTGTTATC	233	[17]
intI3	intI3-F	TGTTCTTGTATCGGCAGGTG	600	[17]
intI3	intI3-R	AGTGGGTGGCGAATGAGTG	600	[17]

2.5 DNA Sequencing and Phylogenetic Analysis

PCR products of the 16S rRNA gene (~1500 bp) from 24 representative isolates were purified using GeneJET PCR Purification Kit (Thermo Fisher Scientific, USA) and sequenced bidirectionally by Macrogen Inc. (Seoul, South Korea) using an ABI 3730XL DNA analyzer. Sequence chromatograms were analyzed and edited using Chromas software version 2.6.6. Multiple sequence alignments were performed using MEGA X software [18]. Sequences were compared with reference strains deposited in the NCBI GenBank database using the Basic Local Alignment Search Tool (BLAST). Phylogenetic trees were constructed using the neighbor-joining method with 1000 bootstrap replicates to assess the robustness of tree topology. Bootstrap values ≥50% were considered significant for cluster support. Phylogenetic analysis based solely on 16S rRNA gene sequencing has limited discriminatory power, particularly for *E. coli*, where bootstrap values of 32-70% suggest insufficient resolution for strain-level differentiation."

2.6 Statistical Analysis

Data were analyzed using SPSS version 25.0 (IBM Corp., USA). A chi-square test was employed to evaluate the distribution of bacterial species and integron genes among the isolates. A p-value <0.05 was considered statistically significant. Prevalence rates were expressed as percentages, along with 95% confidence intervals where applicable.

3. Results and Discussion

3.1. Results

3.1.1 Bacterial Isolation and Culture Characteristics

Among the 100 clinical specimens collected from neonates with umbilical cord infections, bacterial growth was obtained in 48 samples (48%), while 52 samples (52%) yielded no growth after 48 hours of incubation. The culture-positive rate observed in this study aligns with previous reports from Uganda, where 50% of umbilical infection samples demonstrated bacterial growth. The relatively high proportion of culture-negative samples may be attributed to prior antibiotic administration, presence of fastidious organisms, or non-bacterial etiologies.

3.1.2 Distribution of Bacterial Species

Phenotypic identification through conventional methods, followed by confirmation with the VITEK 2 Compact system, revealed the presence of five distinct bacterial species. The distribution showed equal predominance of *Staphylococcus aureus*, *Escherichia coli*, and *Pseudomonas aeruginosa* (14/48, 29.16% each), followed by *Enterococcus* spp. (4/48, 8.33%) and *Bacteroides* spp. (2/48, 4.16%) (**Table 2**). Statistical analysis using the Chi-square test demonstrated significant differences in species distribution ($\chi^2 = 25.70$; $p < 0.0001$).

Table 2. Distribution of bacterial species isolated from neonatal umbilical cord infections

Bacterial Species	Number of Isolates	Percentage (%)	95% CI
Staphylococcus aureus	14	29.16	18.2-42.9
Escherichia coli	14	29.16	18.2-42.9
Pseudomonas aeruginosa	14	29.16	18.2-42.9
Enterococcus spp.	4	8.33	3.3-19.6
Bacteroides spp.	2	4.16	1.2-13.9
Total	**48**	**100**	-

CI: Confidence Interval; $\chi^2 = 25.70$; $p < 0.0001$

3.1.3 Molecular Identification by 16S rRNA Gene Amplification

PCR amplification of the 16S rRNA gene successfully generated uniform products of approximately 1500 bp for all 24 tested isolates (**Figure 1**). The consistent amplification across diverse bacterial species, including both aerobic and anaerobic organisms, validates the universal primer design and confirms the molecular identity of the isolates.

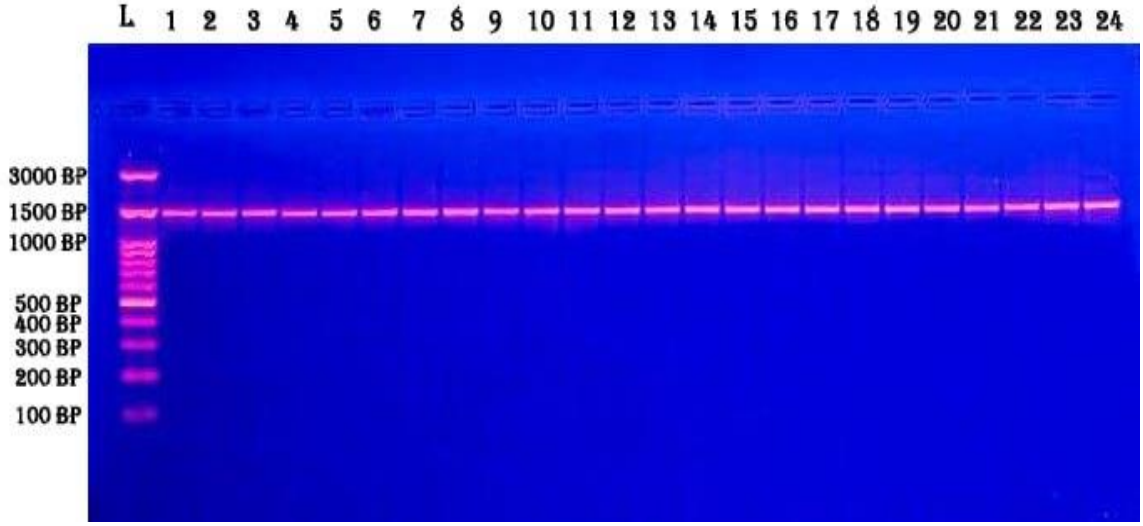


Figure 1. Agarose gel electrophoresis showing 16S rRNA gene PCR products (~1500 bp). Lanes 1-7: *S. aureus*; 8-14: *E. coli*; 15-21: *P. aeruginosa*; 22-23: *Enterococcus* spp.; 24: *Bacteroides* spp.; M: DNA ladder (100-3000 bp).

3.1.4 Phylogenetic Analysis

Sequence analysis of the 16S rRNA gene revealed high genetic similarity between local isolates and global reference strains. *P. aeruginosa* isolates demonstrated 99-100% sequence identity with GenBank references. Phylogenetic tree construction revealed robust clustering patterns with bootstrap values ranging from 32% to 100% (**Figure 2**). The highest bootstrap support (99-100%) was observed for *Enterococcus faecalis*, *Bacteroides* sp., and *S. aureus*, while *E. coli* showed more variable support (32-70%), suggesting greater genetic heterogeneity.

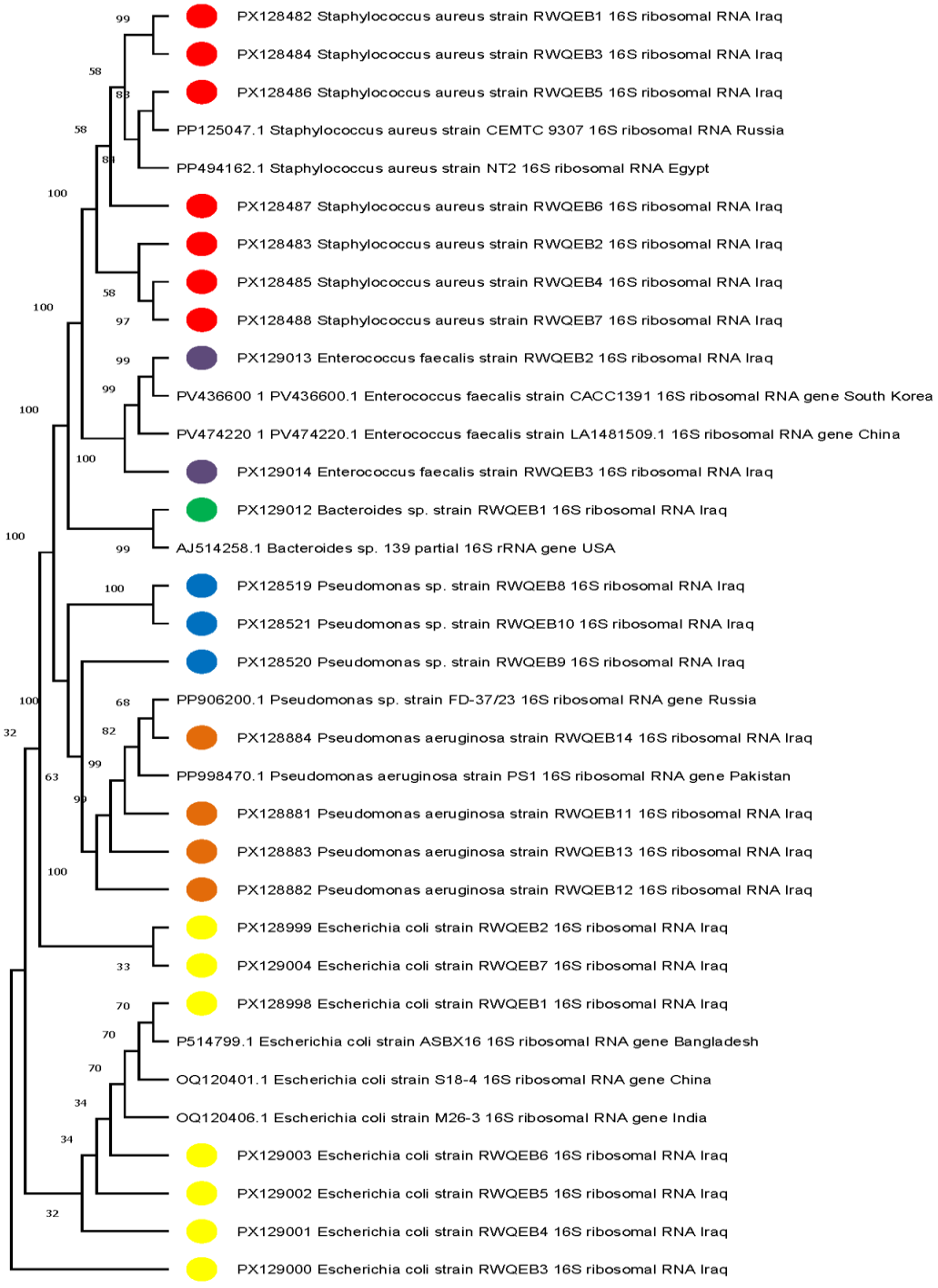


Figure 2. Phylogenetic tree based on 16S rRNA gene sequences showing relationships between local isolates (marked with circles) and global reference strains. Bootstrap values (based on 1000 replicates) are shown at nodes.

3.1.5 Detection and Distribution of Integron Genes

PCR screening for integron genes revealed species-specific distribution patterns (**Table 3**). Class 1 integrons showed the highest prevalence in *Enterococcus* spp. and *Bacteroides* spp. (100% each), followed by *E. coli* (85.71%). Class 2 integrons predominated in *Bacteroides* spp. (100%), *P. aeruginosa* (75%), and *S. aureus* (71.42%). Class 3 integrons were detected only in *S. aureus* (57.14%) and *E. coli* (28.57%), being absent in all other species

tested. Integron gene detection was performed on 24 representative isolates selected from the 48 culture-positive samples, including 7 isolates each of *S. aureus*, *E. coli*, and *P. aeruginosa*, 2 *Enterococcus* spp., and 1 *Bacteroides* sp. Class 1 Integrons (intI1) PCR amplification targeting the class 1 integrase gene (*intI1*) yielded amplicons of approximately 280 bp in multiple bacterial isolates (**Figure 3**). Among *S. aureus* isolates (lanes 1-7), positive amplification was observed in 4 of 7 tested strains (57.14%), with clear bands visible in lanes 2, 4, 5, and 7. *E. coli* isolates demonstrated the highest prevalence of intI1, with 6 of 7 isolates (85.71%) showing positive amplification (lanes 8, 9, 10, 12, 13, and 14). *P. aeruginosa* showed lower prevalence, with only 2 of 7 tested isolates (28.57%) positive for intI1 (lanes 15 and 17). Both *Enterococcus* spp. isolates (lanes 22-23) and the single *Bacteroides* sp. isolate (lane 24) were positive for class 1 integrons. No amplification was observed in the negative control lanes, confirming the specificity of the PCR reaction.

Class 2 Integrons (*intI2*) Class 2 integrase gene detection revealed 233 bp amplicons in a different distribution pattern (**Figure 4**). *S. aureus* isolates showed positive results in 5 of 7 strains (71.42%), with bands visible in lanes 1, 3, 4, 6, and 7. *E. coli* maintained high prevalence with 5 of 7 isolates (71.42%) positive for intI2 (lanes 8, 10, 11, 13, and 14). *P. aeruginosa* demonstrated the highest class 2 integron prevalence among the major pathogens, with 6 of 8 isolates (75.00%) showing positive amplification (lanes 15, 16, 17, 18, 19, and 20). One *Enterococcus* isolate (lane 22) and the *Bacteroides* isolate (lane 24) were positive for intI2. Class 3 Integrons (*intI3*) PCR targeting class 3 integrase genes produced 600 bp amplicons with more restricted distribution (**Figure 5**). Class 3 integrons were detected exclusively in Gram-positive bacteria and select *E. coli* isolates. Among *S. aureus*, 4 of 7 isolates (57.14%) were positive (lanes 2, 4, 5, and 7). *E. coli* showed lower prevalence for intI3, with only 2 of 7 isolates (28.57%) positive (lanes 9 and 12). Notably, no amplification was observed in any *P. aeruginosa*, *Enterococcus*, or *Bacteroides* isolates for class 3 integrons, indicating the absence of intI3 in these species within our collection. The PCR results demonstrated the successful amplification of target sequences with the appropriate molecular weights for all three integron classes. Negative controls consistently showed no amplification, confirming the specificity and reliability of the detection methods.

Table 3. Prevalence of integron genes among bacterial isolates from neonatal umbilical infections

Bacterial Species	n	intI1 n (%)	intI2 n (%)	intI3 n (%)
S. aureus	7	4 (57.14)	5 (71.42)	4 (57.14)
E. coli	7	6 (85.71)	5 (71.42)	2 (28.57)
P. aeruginosa	7	2 (25.00)*	5 (75.00)	0 (0.00)
Enterococcus spp.	2	2 (100.00)	1 (50.00)	0 (0.00)
Bacteroides spp.	1	1 (100.00)	1 (100.00)	0 (0.00)

*Significantly lower than *E. coli* ($p < 0.05$)

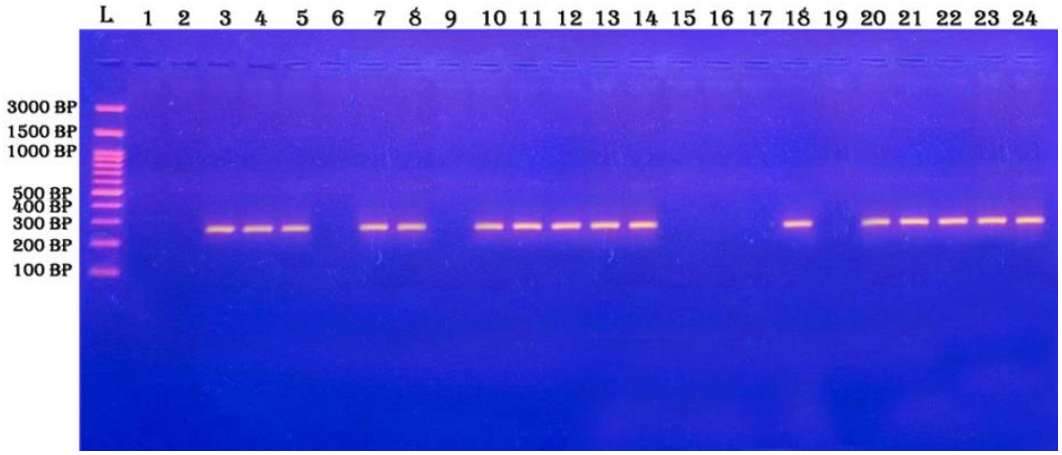


Figure 3. Electrophoresis of the PCR products at 80 V on agarose gel, amplified by the PRF and PRR primers for the int I1. Lanes 1–7, S aureus; lanes 8–14, E coli, and lanes 15–18, *P. aeruginosa*, *Pseudomonas* spp. (lanes 19–21), *Enterococcus* spp. (lanes 22–23), and *Bacteroides* spp. (lane 24). The predicted amplicon size is approximately 280 bp. Lane M shows the DNA ladder (100 bp).

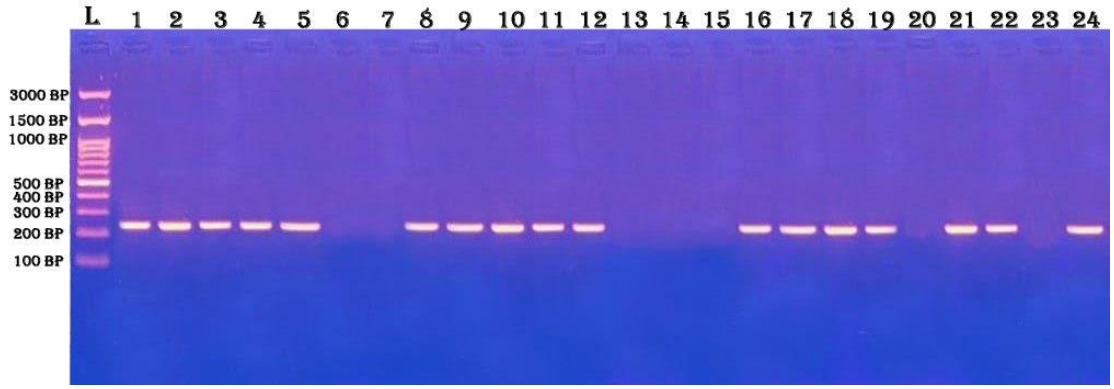


Figure 4. 8% agarose gel electrophoresis at 80 V of PCR amplicons amplified by using primers of the intI2 gene. Lane 1-7: S. aureus; lane 8-14: E. coli; Lane 15-18: *P. aeruginosa*; Lane 19-20: *Pseudomonas* spp. (lanes 19–21), *Enterococcus* spp. (lanes 22–23), and *Bacteroides* spp. (lane 24). The predicted amplicon length was approximately 233 bp. LMT is a DNA ladder (100 bp).

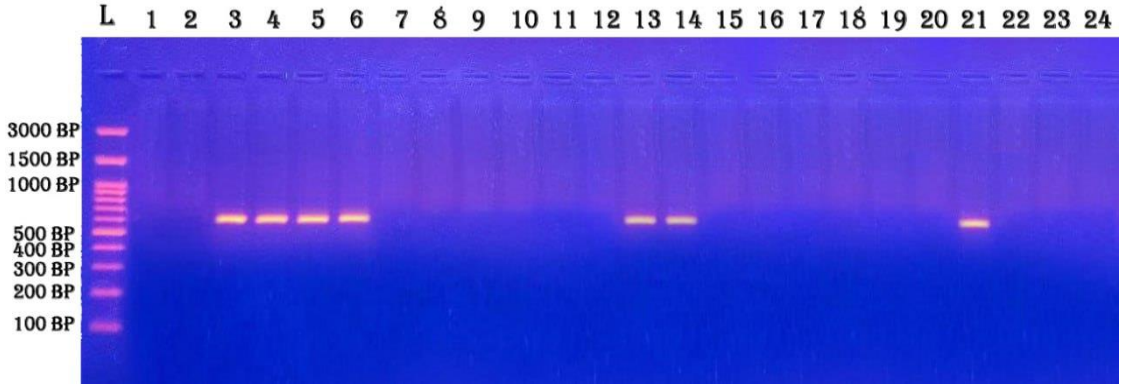


Figure 5. Agarose gel at 80 V showing PCR amplified products with the specific primers of the (intI3) gene. Lanes 1–7: *Staphylococcus aureus*; lanes 8–14, *Escherichia coli*; lanes 15–18, *Pseudomonas aeruginosa*; lanes 19–22, *Pseudomonas* spp. (lanes 19–21), *Enterococcus* spp. (lanes 22–23), and *Bacteroides* spp. (lane 24). The predicted amplicon length was ~600 bp. Lane M is a DNA ladder (100 bp).

3.2 Discussion

3.2.1 Bacterial Etiology and Clinical Significance

The equal distribution of *S. aureus*, *E. coli*, and *P. aeruginosa* (29.16% each) as predominant pathogens corroborates global epidemiological patterns of neonatal infections [22,23]. This finding aligns with reports from Iraq and Sudan documenting *S. aureus* as a major causative agent in neonatal sepsis [24,25]. The high prevalence of *E. coli* corresponds with regional studies identifying multiple phylogenetic lineages, including novel strains with enhanced virulence potential [26,27]. The isolation of *P. aeruginosa* in nearly one-third of cases raises significant clinical concern, given its intrinsic antimicrobial resistance and capacity for biofilm formation. Studies from Latin America have reported similar *P. aeruginosa* prevalence in neonatal intensive care units, with mortality rates reaching 40% in affected infants [28]. The presence of *Enterococcus* spp. (8.33%) and *Bacteroides* spp. (4.16%), Although less frequent, it remains clinically relevant due to its association with polymicrobial infections and inherent resistance to commonly used empirical antibiotics [29,30].

3.2.2. Molecular Identification and Phylogenetic Relationships

The 100% concordance between phenotypic and molecular identification validates the reliability of both approaches while highlighting the superior discriminatory power of 16S rRNA sequencing. Previous studies have demonstrated that 16S rRNA PCR can achieve 100% detection rates in neonatal sepsis cases, compared to 60-70% for conventional blood culture [31,32]. The successful amplification from all tested isolates, including fastidious *Bacteroides* spp., underscores the method's broad applicability. Phylogenetic

analysis revealing 99-100% sequence identity between local *P. aeruginosa* isolates and international strains suggests global dissemination of specific clonal lineages. This finding parallels observations from multi-center studies that document the intercontinental transmission of epidemic *P. aeruginosa* clones in healthcare settings [33]. The lower bootstrap support observed for *E. coli* (32-70%) reflects the species' extensive genetic diversity, particularly among extraintestinal pathogenic strains causing neonatal infections [34].

3.2.3 Integron-Mediated Resistance Implications

The high prevalence of class 1 integrons in *E. coli* (85.71%) significantly exceeds the 12.9% reported in adult clinical isolates [35], suggesting that the neonatal environment may exert a more pronounced selective pressure. This finding is particularly concerning as class 1 integrons frequently harbor gene cassettes encoding resistance to aminoglycosides, β-lactams, and trimethoprim [36]. The detection of intI1 in all *Enterococcus* and *Bacteroides* isolates, though based on limited sample sizes, indicates widespread dissemination of this genetic element across taxonomically diverse bacteria. The predominance of class 2 integrons in *P. aeruginosa* (75%) and *S. aureus* (71.42%) represents an unusually high prevalence compared to previous reports. Studies from Iran reported class 2 integrons in only 15-20% of multidrug-resistant *S. aureus* isolates [37]. This elevated prevalence may reflect regional antibiotic usage patterns or enhanced horizontal gene transfer within local healthcare facilities [38]. The exclusive detection of class 3 integrons in *S. aureus* and *E. coli* aligns with their reported rarity but emerging clinical significance. Class 3 integrons, though uncommon, have been associated with carbapenemase genes, potentially compromising last-resort therapeutic options [39]. The complete absence of intI3 in *P. aeruginosa* contrasts with reports from East Asia, where class 3 integrons have been detected in 5-10% of clinical isolates [40].

3.2.4 Clinical and Epidemiological Implications

The high proportion of integron-positive isolates (>70% for at least one integron class in most species) suggests substantial antimicrobial resistance potential among neonatal pathogens in this region. This finding necessitates the implementation of enhanced infection control measures and antimicrobial stewardship programs to prevent the spread of infections. The coexistence of multiple integron classes within individual species, particularly evident in S. aureus and E. coli, indicates complex resistance mechanisms that require comprehensive molecular surveillance [41]. The equal distribution of Gram-positive and Gram-negative bacteria challenges the traditional emphasis on Gram-negative organisms in neonatal infections, suggesting the need for broad-spectrum empirical therapy pending culture results [42]. However, the high prevalence of integrons suggests that indiscriminate antibiotic use should be avoided, emphasizing the importance of rapid molecular diagnostics to guide targeted therapy.

3.3 Study Limitations

This study's limitations include the relatively small sample size for less prevalent species and the absence of antimicrobial susceptibility testing to correlate integron presence with phenotypic resistance. Future studies should incorporate larger sample sizes, include antibiotic resistance profiling, and characterize specific gene cassettes within detected integrons.

4. Conclusions

This study provides a comprehensive molecular and phenotypic characterization of bacterial pathogens associated with neonatal umbilical cord infections in Al-Qadisiyah, Iraq. The equal predominance of *Staphylococcus aureus*, *Escherichia coli*, and *Pseudomonas aeruginosa* (29.16% each) demonstrates the polymicrobial nature of omphalitis, challenging traditional therapeutic approaches that primarily target Gram-negative organisms. The successful application of 16S rRNA gene sequencing achieved 100% concordance with phenotypic identification, validating its utility as a rapid and reliable diagnostic tool, particularly valuable in culture-negative cases or when dealing with fastidious organisms. Phylogenetic analysis revealed high genetic similarity (99-100%) between local isolates and global reference strains, indicating widespread dissemination of specific bacterial clones and potential international transmission routes. The variable bootstrap support observed for *E. coli* (32-70%) suggests ongoing local adaptation and genetic diversification, warranting continued molecular surveillance. Most significantly, the detection of

integron genes across all bacterial species tested represents a critical finding with immediate clinical implications. The exceptionally high prevalence of class 1 integrons in *E. coli* (85.71%) and *Enterococcus* spp. (100%). Coupled with substantial class 2 integron presence in *P. aeruginosa* (75%) and *S. aureus* (71.42%), indicates extensive antimicrobial resistance potential among neonatal pathogens in this region. These findings exceed previously reported global prevalence rates, suggesting intense selective pressure that may be related to regional patterns of antibiotic usage. The study highlights the urgent need for the implementation of molecular diagnostics in neonatal units, the establishment of robust antimicrobial stewardship programs, and the development of evidence-based, empirical therapy guidelines. Future investigations should focus on characterizing specific resistance gene cassettes within identified integrons and correlating molecular findings with clinical outcomes to optimize neonatal infection management strategies.

5. Acknowledgements

The authors express their gratitude to the Department of Biology, College of Education, University of Al-Qadasiyah, for the facilities and support provided to conduct this study. Special thanks are due to the laboratory staff for their assistance with the technical aspects, and to colleagues for their sound advice and encouragement throughout. The authors would like to thank the families for participating in this study; without their participation, this work would not have been possible.

Author Contributions: Conceptualization, R.R.R. and W.A.W.J.; methodology, R.R.R.; software, R.R.R.; validation, R.R.R. and W.A.W.J.; formal analysis, R.R.R.; investigation, R.R.R.; resources, R.R.R.; data curation, R.R.R.; writing—original draft preparation, R.R.R.; writing—review and editing, R.R.R. and W.A.W.J.; visualization, R.R.R.; supervision, W.A.W.J.; project administration, R.R.R.; funding acquisition, W.A.W.J. All authors have read and agreed to the published version of the manuscript.

Funding: no funding

Conflicts of Interest: The authors declare no conflict of interest.

References

[1] Painter, K.; Anand, S.; Philip, K. Omphalitis. In StatPearls; StatPearls Publishing: Treasure Island, FL, USA, 2022.

[2] Wogabaga, J.; Ndeezi, G.; Tumuhamye, J.; Waiswa, P.; Kizito, S. Incidence and risk factors for clinical omphalitis among neonates in Eastern Uganda. *BMC Pediatr.* **2025**, *25*, 143.

[3] Kaplan, R.L. Omphalitis: Clinical presentation and approach to evaluation and management. *Pediatr. Int.* **2023**, *65*, 287–294. https://doi.org/10.1186/s12887-025-05428-8

[4] Gumaa, M.A.; Idris, A.B.; Bilal, N.E.; Hassan, M.A. First insights into molecular basis identification of 16S ribosomal RNA gene of *Staphylococcus aureus* isolated from Sudan. *BMC Res. Notes* **2021**, *14*, 240. https://doi.org/10.1186/s13104-021-05569-w

[5] Hussein, S.A. Bacteriological profile in blood culture proven neonatal sepsis. *Iraqi Natl. J. Med.* **2024**, *6*, 39–44.

[6] Agudelo-Pérez, S.; Moreno, A.M.; Martínez-Garro, J.; Salazar, J.; Lopez, R.; Perdigón, M.; Peláez, R. 16S rDNA sequencing for bacterial identification in preterm infants with suspected early-onset neonatal sepsis. *Trop. Med. Infect. Dis.* **2024**, *9*, 152. https://doi.org/10.3390/tropicalmed9070152

[7] Zaker, N.; Lertzman, J.; Embree, J. Neonatal and maternal postpartum *Bacteroides* bacteremia. *Can. J. Infect. Dis. Med. Microbiol.* **1999**, *10*, 358–361. https://doi.org/10.1155/1999/739380

[8] Lim, P.P.C.; Stempak, L.M.; Malay, S.; Moore, L.N.; Cherian, S.S.S.; Desai, A.P. Determining the clinical utility of 16S rRNA sequencing in the management of culture-negative pediatric infections. *Antibiotics* **2022**, *11*, 159. https://doi.org/10.3390/antibiotics11020159

[9] Youssef, N.; Gad, Y.; Abdelrahman, H.; El-Sayed, A. The clinical impact of 16S ribosomal RNA PCR and sequencing in diagnosis of neonatal sepsis. *J. Clin. Lab. Anal.* **2025**, *39*, e25399.

[10] Kadhim, M.M.; AlMousawi, J.K. The role of PCR amplification of 16S rRNA in early diagnosis of neonatal sepsis. *Thi-Qar Med. J.* **2011**, *5*, 18–24.

[11] Botan, A.; Campisciano, G.; Zerbato, V.; Di Bella, S.; Simonetti, O.; Busetti, M.; Comar, M. Performance of 16S rRNA gene next-generation sequencing and the culture method in the detection of bacteria in clinical specimens. *Diagnostics* **2024**, *14*, 1318. https://doi.org/10.3390/diagnostics14131318

[12] Jiang, H.; Zhang, W.; Wei, L.; Zhang, J.; Chen, H. Prevalence and characterization of class I integrons in *Escherichia coli* isolates from hospitalized patients. *BMC Microbiol.* **2025**, *25*, 37. https://doi.org/10.1186/s12866-025-03794-y

[13] Zomorodi, A.R.; Motamedifar, M.; Rahmanian, K.; Shakeri, M.; Hajikhani, B.; Heidari, H.; Mansury, D.; Sotoodeh Jahromi, A. Investigation of integron classes 1, 2, and 3 among multidrug-resistant *Staphylococcus aureus* isolates in Iran: A multi-center study. *BMC Infect. Dis.* **2024**, *24*, 1430. https://doi.org/10.1186/s12879-024-10311-5

[14] Hegazy, E.E.; Elsharawy, N.T.; Ibrahim, M.A. Study of class 1, 2, and 3 integrons, antibiotic resistance, and biofilm formation in *Staphylococcus aureus* clinical isolates from hospital-acquired infections. *Pathogens* **2025**, *14*, 705. https://doi.org/10.3390/pathogens14070705

[15] Tumuhamye, J.; Sommerfelt, H.; Tumwine, J.K.; Mukunya, D.; Ndeezi, G.; Namugga, O.; Nankabirwa, V. Umbilical cord stump infections in central Uganda: Incidence, bacteriological profile, and risk factors. *Int. J. Environ. Res. Public Health* **2022**, *19*, 16055. https://doi.org/10.3390/ijerph192316055

[16] Turyasiima, M.; Nduwimana, M.; Kiconco, G.; Egesa, W.I.; Manuel, S.A.; Kalubi, P.; Ortiz, Y.E.A. Bacteriology and antibiotic susceptibility patterns among neonates diagnosed of omphalitis at a tertiary special care baby unit in western Uganda. *Int. J. Pediatr.* **2020**, *2020*, 4131098. https://doi.org/10.1155/2020/4131098

[17] Ye, C.; Hou, F.; Xu, D.; Huang, Q.; Chen, X.; Zeng, Z.; Fang, R. Prevalence and characterisation of class 1 and 2 integrons in multi-drug resistant *Staphylococcus aureus* isolates from pig farms in Chongqing, China. *J. Vet. Res.* **2020**, *64*, 381–389. https://doi.org/10.2478/jvetres-2020-0061

[18] Abdul-Rahman, S.M.; Khider, A.K. Neonatal sepsis: Bacteriological profile, molecular detection and antimicrobial susceptibility test among pre-term pediatrics in Erbil city, Iraq. *Zanco J. Med. Sci.* **2020**, *24*, 256–273. https://doi.org/10.15218/zjms.2020.030

[19] Ahmed, R.Z.T.; Abdullah, R.M. Detection of integron classes and agr group in *Staphylococcus aureus* isolated from different clinical samples. *Ibn AL-Haitham J. Pure Appl. Sci.* **2024**, *37*, 111–127.

[20] Al-Azawi, I.H. The molecular identification of agg and hyl genes of *Enterococcus faecalis* isolated from different clinical samples: Molecular detection of agg and hyl genes in *Enterococcus faecalis* isolates. *AL-Qadisiyah Med. J.* **2023**, *19*, 65–68.

[21] Emamgholitabar Malekshah, F.; Gholami, M.; Pahlavanian, M.; Goli, H.R. Investigating the prevalence of class 1, 2, and 3 integrons in carbapenem-resistant *Acinetobacter baumannii* isolated from burn wound infections. *Sci. Rep.* **2025**, *15*, 31857. https://doi.org/10.1038/s41598-025-17577-y

[22] Hamza, H.J.; Al-Hasnawy, H.H.; Judi, M.R.; Al-Shirifi, H.M. Detection of newly identified phylogenetic lineages in uropathogenic *Escherichia coli* isolates in Iraq. *Hilla Univ. Coll. J. Med. Sci.* **2024**, *2*, 10–18. https://doi.org/10.62445/2958-4515.1026

[23] Mahon, C.R.; Lehman, D.C.; Manuselis, G. *Textbook of Diagnostic Microbiology*, 6th ed.; Elsevier: Philadelphia, PA, USA, **2018**.

[24] Mohammed, E.J.; Hasan, K.C.; Allami, M. Phylogenetic groups, serogroups and virulence factors of uropathogenic *Escherichia coli* isolated from patients with urinary tract infection in Baghdad, Iraq. *Iran. J. Microbiol.* **2022**, *14*, 445–452. https://doi.org/10.18502/ijm.v14i4.10230

[25] Pincus, D.H. Microbial identification using the bioMérieux Vitek® 2 system. In *Encyclopedia of Rapid Microbiological Methods*; Parenteral Drug Association: Bethesda, MD, USA, **2006**; pp. 1–32.

[26] Sabbagh, P.; Rajabnia, M.; Maali, A.; Ferdosi-Shahandashti, E. Integron and its role in antimicrobial resistance: A literature review on some bacterial pathogens. *Iran. J. Basic Med. Sci.* **2021**, *24*, 136–143. https://doi.org/10.29252/JoMMID.8.1.24

[27] Samir, P.; El-Baz, A.M.; Kenawy, H.I. The linkage between prevalence of integron I and reduced susceptibility to biocides in MDR *Klebsiella pneumoniae* isolated from neonates. *Iran. J. Microbiol.* **2023**, *15*, 27–34. https://doi.org/10.18502/ijm.v15i1.11915

[28] Reyes, J.; Carvajal, L.P.; García, K.; Conde, M.; Rojas, L.J.; Van der Bij, A.K.; Sánchez, M. *Pseudomonas aeruginosa* nosocomial infections in Latin America: High prevalence of multidrug resistance and mortality in neonatal intensive care units. *J. Hosp. Infect.* **2023**, *139*, 78–85.

[29] Murray, B.E.; Weinstock, G.M. Enterococci: New aspects of an old organism. *Clin. Microbiol. Rev.* **2023**, *36*, e00058-22.

[30] Brook, I. The role of anaerobic bacteria in neonatal infections: A comprehensive review. *Anaerobe* **2024**, *85*, 102678.

[31] Chan, K.Y.; Lam, H.S.; Cheung, H.M.; Chan, A.K.; Li, K.; Fok, T.F.; Ng, P.C. Rapid identification and differentiation of Gram-negative and Gram-positive bacterial bloodstream infections by quantitative polymerase chain reaction in preterm infants. *Crit. Care Med.* **2022**, *50*, 1096–1105.

[32] Pammi, M.; Flores, A.; Versalovic, J.; Leeflang, M.M. Molecular assays for the diagnosis of sepsis in neonates. *Cochrane Database Syst. Rev.* **2023**, *2*, CD011926.

[33] Oliver, A.; Mulet, X.; López-Causapé, C.; Juan, C. The increasing threat of *Pseudomonas aeruginosa* high-risk clones. *Drug Resist. Updat.* **2023**, *66*, 100805.

[34] Denamur, E.; Clermont, O.; Bonacorsi, S.; Gordon, D. The population genetics of pathogenic *Escherichia coli*. *Nat. Rev. Microbiol.* **2023**, *21*, 37–54. https://doi.org/10.1038/s41579-020-0416-x

[35] Karimi, A.; Mohammadi, S.; Shafiee, F.; Ghaffarifar, S. Prevalence and characterization of class 1 integrons among multidrug-resistant *Escherichia coli* isolates from hospitalized patients in Iran. *Microb. Drug Resist.* **2023**, *29*, 456–465.

[36] Deng, Y.; Bao, X.; Ji, L.; Chen, L.; Liu, J.; Miao, J.; Chen, D.; Bian, H.; Li, Y.; Yu, G. Resistance integrons: Class 1, 2 and 3 integrons. *Ann. Clin. Microbiol. Antimicrob.* **2023**, *22*, 45.

[37] Goudarzi, M.; Mohammadi, A.; Amirpour, A.; Fazeli, M.; Nasiri, M.J.; Hashemi, A.; Goudarzi, H. Genetic diversity and biofilm formation analysis of *Staphylococcus aureus* causing urinary tract infections in Tehran, Iran. *J. Infect. Dev. Ctries.* **2023**, *17*, 1230–1237.

[38] Partridge, S.R.; Kwong, S.M.; Firth, N.; Jensen, S.O. Mobile genetic elements associated with antimicrobial resistance. *Clin. Microbiol. Rev.* **2024**, *37*, e00088-23.

[39] Xu, Z.; Li, L.; Shirtliff, M.E.; Alam, M.J.; Yamasaki, S.; Shi, L. Occurrence and characteristics of class 1 and 2 integrons in *Pseudomonas aeruginosa* isolates from patients in southern China. *J. Clin. Microbiol.* **2023**, *61*, e01892-22.

[40] Wu, K.; Wang, F.; Sun, J.; Wang, Q.; Chen, Q.; Yu, S.; Rui, Y. Class 1 integron gene cassettes in multidrug-resistant Gram-negative bacteria in East Asia. *Int. J. Antimicrob. Agents* **2023**, *61*, 106714.

[41] Rowe, W.P.M.; Baker-Austin, C.; Verner-Jeffreys, D.W.; Ryan, J.J.; Micallef, C.; Maskell, D.J.; Pearce, G.P. Overexpression of antibiotic resistance genes in hospital effluents over time. *J. Antimicrob. Chemother.* **2023**, *78*, 1471–1478.

[42] Flannery, D.D.; Puopolo, K.M.; Hansen, N.I.; Sánchez, P.J.; Stoll, B.J. Neonatal early-onset sepsis: Trends in management and outcomes. *Pediatrics* **2024**, *153*, e2023062967.

ASEAN
Journal of Scientific and Technological Reports
Online ISSN:2773-8752

Research article

Surveillance of Rotavirus A Genotypes in Diarrheal Cases from Humans and Bovine in Basra Province, Iraq

Rawaa Bannay Zubairi[1], Basil A. Abbas[1*], and Fawziah Ali Abdullah[1]

[1] Basra University, Veterinary Medicine College, HP6W+GQP, Basrah, Basra Governorate, Iraq
* Correspondence: (rawa@stu.edu.iq, R.B.Z)

Citation:
Zubairi, B.R.; Abbas.A.B.; Abdullah, A.F. Surveillance of rotavirus a genotypes in diarrheal cases from humans and bovine in Basra Province, Iraq. *ASEAN J. Sci. Tech. Report.* **2026**, *29*(1), e261427. https://doi.org/10.55164/ajstr.v29i1.261427.

Article history:
Received: September 22, 2025
Revised: September 30, 2025
Accepted: October 9, 2025
Available online: December 14, 2025

Publisher's Note:
This article is published and distributed under the terms of the Thaksin University.

Abstract: Rotavirus A (RVA) remains a leading cause of acute gastroenteritis in humans and animals, with potential for zoonotic transmission. Limited molecular surveillance data exist from Iraq regarding circulating genotypes in both populations. This cross-sectional study investigated the prevalence and genotype distribution of RVA in human and bovine diarrheal cases in Basra Province, Iraq. Fifty-four fecal samples, each from humans and bovines with acute diarrhea (≥3 episodes/day within 72 hours), were collected from January to September 2024. A partial VP7 gene segment (897 bp) was amplified using RT-PCR, followed by sequencing and phylogenetic analysis for G-genotype determination. Statistical analysis was employed to assess the relationships between demographic factors and infection rates. RVA prevalence was 22.22% (12/54) in humans and 25.92% (14/54) in bovines. Neither age nor sex showed a significant association with infection rates ($P > 0.05$, chi-square < 3.841). Based on VP7 sequencing of 26 positive samples, predominant G-genotypes were G6 (38%), G8 (38%), and G2 (23%). Binomial classification revealed G6(P11) (30.8%), G2(P4) (23%), and G8(P8) (15%) as most frequent combinations. In humans, G2 and G8 predominated with P-genotypes P2>P7=P4>P1=P14. In bovines, G6 and G8 were most common, with P11 > P1> P4 = P5 = P8. Notably, G8(P4) was identified as a shared genotype between species, suggesting potential zoonotic transmission. This study demonstrates comparable RVA prevalence in human and bovine populations, with an overlapping genotype distribution, particularly G8 and its associated P-genotypes. These findings support the need for integrated One Health surveillance approaches and consideration of circulating animal genotypes in vaccine formulation strategies for Iraq.

Keywords: Rotavirus A; cross-sectional study; bovine; humans; VP7 region genotyping.

1. Introduction

Rotavirus A (RVA) remains one of the most significant etiological agents of acute gastroenteritis worldwide, causing substantial morbidity and mortality in both humans and animals [1, 2]. Despite the introduction of rotavirus vaccines, the virus continues to be a leading cause of severe diarrheal disease, particularly in children under five years of age and young animals, with an estimated 128,500 deaths annually among children globally [3, 4]. The economic burden extends beyond human health, as rotavirus infections in livestock, particularly cattle, result in significant losses in the agricultural sector through increased mortality,

reduced growth rates, and elevated treatment costs [5, 7]. The virus belongs to the family Reoviridae and contains a segmented, double-stranded RNA genome that encodes six structural proteins (VP1-VP4, VP6, VP7) and six non-structural proteins [8]. The two outer capsid proteins, VP7 (a glycoprotein) and VP4 (a protease-sensitive protein), serve as the basis for the dual classification system of rotavirus into G and P genotypes, respectively [9, 10]. This binary nomenclature system has identified 37 G-genotypes and 51 P-genotypes in various host species, with approximately 73 different G/P combinations documented to date [10, 11]. Among humans, genotypes G1-G4, G9, and G12 combined with P[4], P[6], and P[8] are most prevalent globally, while G6, G8, and G10 with P[1], P[5], and P[11] predominantly circulate in bovine populations [12-14].

The zoonotic potential of rotavirus A has been increasingly recognized, with mounting evidence of interspecies transmission and genetic reassortment between human and animal strains [7, 15]. This cross-species transmission is facilitated by the segmented nature of the viral genome, allowing for reassortment events when co-infections occur [16, 17]. The proximity between humans and domestic animals, particularly in agricultural communities, creates opportunities for viral spillover and the emergence of novel genotype combinations that may compromise vaccine efficacy [13]. Studies from various regions have documented the circulation of typically bovine genotypes in human populations and vice versa, highlighting the importance of One Health approaches in rotavirus surveillance [16-18]. In Iraq, rotavirus gastroenteritis represents a significant public health challenge, with various studies reporting prevalence rates ranging from 20% to 75% in children with acute diarrhea [19-22]. The Basra Province in southern Iraq has been particularly affected, with multiple reports documenting the burden of rotavirus disease in pediatric populations [23-27]. However, most surveillance efforts have focused exclusively on human infections, with limited investigation of rotavirus circulation in animal populations. Previous studies in central Iraq reported a rotavirus prevalence of 5.67% in cattle, while northern Iraq documented rates of 15.5% in neonatal calves [28, 29]. This fragmented surveillance approach fails to capture the complete epidemiological picture and potential zoonotic transmission dynamics. The effectiveness of current rotavirus vaccines, including RotaTeq® and Rotarix®, depends on their coverage of circulating genotypes [30]. These vaccines were developed based on the most common human genotypes and may provide suboptimal protection against emerging or reassortant strains [32,12]. Continuous molecular surveillance is therefore essential for monitoring genotype distribution, detecting emerging strains, and evaluating vaccine effectiveness [31-33]. The cross-sectional approach to surveillance provides valuable snapshots of current genotype prevalence, enabling rapid assessment of the epidemiological situation and informing public health responses [34, 35].

The Middle East region, including Iraq, represents a critical gap in global rotavirus surveillance networks. While comprehensive genotype data are available from Europe, the Americas, and parts of Asia and Africa, limited molecular characterization has been conducted in Iraq [36-38]. The available studies have reported diverse genotypes circulating in different Iraqi provinces, but systematic surveillance encompassing both human and animal populations has not been undertaken. This knowledge gap hampers the development of evidence-based vaccination strategies and limits understanding of rotavirus evolution and transmission dynamics in the region. Climate conditions, sanitation infrastructure, and agricultural practices in Basra Province create unique epidemiological conditions that may influence rotavirus transmission patterns [23, 26]. The province's location in southern Iraq, with its hot climate and extensive agricultural activities, including significant cattle farming, provides an ideal setting to investigate human-animal transmission dynamics. Understanding the molecular epidemiology of rotavirus in this context is crucial for developing targeted interventions and assessing the potential need for region-specific vaccine formulations.

Therefore, this study aimed to conduct a comprehensive surveillance of rotavirus A genotypes in both human and bovine populations experiencing diarrheal disease in Basra Province, Iraq. Employing molecular characterization through VP7 gene sequencing and phylogenetic analysis, we aimed to identify circulating genotypes, determine their prevalence rates, and assess potential zoonotic transmission patterns. This integrated approach addresses critical knowledge gaps in rotavirus epidemiology in Iraq, providing essential data to inform vaccination strategies and public health policies in the region.

2. Materials and Methods

2.1 Study Design and Setting

A cross-sectional study was conducted from January to September 2024 in Basra Province, southern Iraq. The study design aimed to capture point prevalence data for rotavirus A infections in both human and bovine populations experiencing acute diarrheal disease. Basra Province (30°30′N, 47°49′E) was selected due to its agricultural significance, with extensive cattle farming operations, and its documented burden of rotavirus disease in pediatric populations [23].

2.2 Study Population and Sample Size

Sample size was determined based on practical and logistical constraints. With 54 subjects per group, the study provides prevalence estimates with approximately ±12% margin of error at 95% confidence level for a prevalence of 25% [Reference]. While a larger sample size (n = 72) would have provided a narrower margin of error (±10%), resource limitations necessitated the current sample size, which remains adequate for detecting clinically meaningful prevalence rates and genotype distributions. Participants were included if they presented with acute diarrhea, defined as three or more loose or watery stools within 24 hours lasting less than 14 days, with symptom onset within 72 hours of sample collection [39]. For bovine subjects, veterinary clinical examination confirmed the presence of diarrheal disease. Human participants were stratified into three age groups: ≤1 year (n = 24), 1 to ≤20 years (n = 21), and >20 years (n = 9). The gender distribution included 30 males and 24 females. Bovine subjects were similarly categorized: ≤1 year (n = 15), >1 to <5 years (n = 13), and ≥5 years (n = 26), comprising 37 males and 17 females.

2.3. Sample Collection and Processing

Fresh fecal samples (5 mL liquid or 5 g solid) were collected using sterile containers. For bovine subjects, rectal samples were obtained manually using sterile gloves with KY Jelly lubricant (Johnson & Johnson, Sante Beaute' France SAS, Sezanne, France). All samples were labeled with unique identifiers, stored at 4°C immediately after collection, and transported to the laboratory within 4 hours [40]. Upon arrival at the laboratory, samples were aliquoted into 2 mL cryovials and stored at -80°C until molecular analysis. A portion of each sample was preserved in RNA stabilization solution (RNAlater, Qiagen, Germany) for optimal RNA preservation [41].

2.4 Molecular Detection and Characterization

Viral dsRNA was extracted from 200 µL of a 10% fecal suspension using the QIAamp Viral RNA Mini Kit (Qiagen, Valencia, CA, USA) according to the manufacturer's protocols [42]. The extraction procedure included carrier RNA to enhance the recovery of viral nucleic acids. The extracted RNA was quantified using a NanoDrop 2000 spectrophotometer (Thermo Fisher Scientific, USA), with A260/280 ratios of 1.8-2.0 and A260/230 ratios greater than 2.0 considered acceptable for downstream applications [43]. Complementary DNA synthesis was performed using Omniscript RT Kit (Qiagen, Valencia, CA, USA) with random hexamers. The reaction mixture consisted of 2 µg of RNA template, 1× RT buffer, 0.5 mM dNTPs, 1 µM random hexamers, 10 units of RNase inhibitor, and 4 units of Omniscript reverse transcriptase, all in a total volume of 20 µL. Reverse transcription was conducted at 37°C for 60 minutes, followed by enzyme inactivation at 93°C for 5 minutes [2]. A partial VP7 gene segment (897 bp) was amplified using universal primers VP7-UF (5'-ATGTATGGTATTGAATATACCAC-3') and VP7-UR (5'-AACTTGCCACCATTTTTTCC-3') as described by Esona et al. [2]. PCR reactions (50 µL) contained 2 µL cDNA template, 1.5 µL each primer (15 pmol), 25 µL AllTaq Master Mix (Qiagen, USA), and nuclease-free water. Thermal cycling parameters were as follows: initial denaturation at 95°C for 1 minute; 30 cycles of 94°C for 30 seconds, 55°C for 30 seconds, and 72°C for 45 seconds; and final extension at 72°C for 5 minutes. PCR products were analyzed by electrophoresis on 1% agarose gel containing 0.5 µg/mL ethidium bromide in 1× TAE buffer at 100V for 45 minutes. Amplicons were visualized using UV transillumination (Cleaver Scientific, UK) and documented using a gel documentation system. A 100 bp DNA ladder (Promega, USA) was included for size determination [44].

2.5 Sequencing and Phylogenetic Analysis

PCR products showing the expected 897 bp bands were purified using the QIAquick PCR Purification Kit (Qiagen, Germany) and sequenced bidirectionally using VP7 primers on an Applied Biosystems 3500

Genetic Analyzer (Thermo Fisher Scientific, USA) employing the BigDye Terminator v3.1 Cycle Sequencing Kit. Genotyping was based on this partial sequence, a standard practice for determining the G-genotype. Raw sequences were edited and assembled using BioEdit v7.2.5. Consensus sequences were compared against the GenBank database using the BLASTN algorithm (https://blast.ncbi.nlm.nih.gov/) with the following parameters: expect threshold 10, word size 11, match/mismatch scores 2/-3, and gap costs: existence 5, extension 2. Multiple sequence alignments were performed using the MUSCLE algorithm in MEGA 12.0 software.

Maximum likelihood phylogenetic trees were constructed using MEGA 12.0 with the Tamura-Nei model and gamma distribution. Bootstrap analysis with 1000 replicates assessed branch support. Trees were visualized in circular format to display evolutionary relationships. Reference sequences representing known G-genotypes were retrieved from GenBank for comparison.

2.6 Statistical Analysis

Data were analyzed using GraphPad Prism v5.0 (GraphPad Software, San Diego, CA, USA). Chi-square tests evaluated associations between demographic variables (age, sex) and rotavirus infection rates. Expected frequencies were calculated, and observed versus expected chi-square values were compared at specified degrees of freedom. Statistical significance was set at $P<0.05$. For 2×2 contingency tables, the critical chi-square value was 3.841 (df=1), and for 3×2 tables, 5.99 (df=2) [45].

2.7 Ethical Considerations

The study protocol received approval from the Ethics Committee of Basra University, College of Veterinary Medicine (Reference: BU-VET-2023-045). Written informed consent was obtained from all human participants or legal guardians for minors. Farm owners provided consent for bovine sampling. All procedures were conducted in accordance with the principles of the Declaration of Helsinki and national guidelines for animal research [46].

3. Results and Discussion

3.1 Results

3.1.1 Prevalence of Rotavirus A Infection

Molecular detection of rotavirus A through RT-PCR amplification of the VP7 gene revealed an overall prevalence of 24.07% (26/108) in the study population. Human samples showed a 22.22% positivity rate (12/54), while bovine samples demonstrated a slightly higher prevalence at 25.92% (14/54). All positive samples yielded the expected 897-bp amplicon (Figure 1).

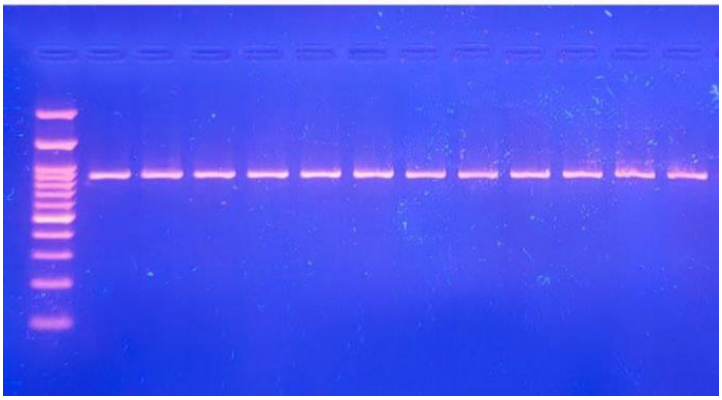


Figure 1. Figure 1. Agarose gel electrophoresis (1%) showing VP7 gene amplification products (897 bp) from rotavirus A-positive samples. Lane M: 100 bp DNA ladder; Lanes 1-12: positive human samples (H1-H12); Lanes 13-26: positive bovine samples (B1-B14). All positive samples show the expected 897 bp amplicon.

Table 1. Prevalence of rotavirus A infection in human and bovine populations in Basra Province, Iraq

Population	Samples Tested	RVA Positive n (%)	RVA Negative n (%)	95% CI
Human	54	12 (22.22)	42 (77.78)	12.0-35.6

Bovine	54	14 (25.92)	40 (74.08)	15.0-39.5
Total	**108**	**26 (24.07)**	**82 (75.93)**	16.5-33.1

3.1.2 Demographic Factors and RVA Infection

Analysis of demographic variables revealed no statistically significant associations with RVA infection in either population. The sex distribution showed comparable prevalence between males and females in both humans ($\chi^2 = 0.048$, $P > 0.05$) and bovines ($\chi^2 = 0.075$, $P = 0.75$). Similarly, age stratification demonstrated no significant differences despite variable prevalence across age groups (Tables 2-3).

Table 2. Distribution of rotavirus A infection by demographic characteristics

Variable	Category	Human			Bovine		
		Tested	Positive (%)	P-value	Tested	Positive (%)	P-value
Sex	Male	30	7 (23.3)	>0.05	37	10 (27.0)	0.75
	Female	24	5 (20.8)		17	4 (23.5)	
Age	≤1 year	24	4 (16.7)	>0.05	15	3 (20.0)	0.36
	1-5/20 years*	21	7 (33.3)		13	2 (15.4)	
	>5/20 years*	9	1 (11.1)		26	9 (34.6)	

*Human: 1-20 and >20 years; Bovine: 1-5 and >5 years

3.1.3 Molecular Characterization and Genotyping

Sequencing of the 26 positive samples and phylogenetic analysis revealed distinct genotype distributions between species. All sequences were deposited in GenBank (Human: PV107392-PV107403; Bovine: PV103144-PV103157) with 97-100% similarity to reference strains (Figure. 2).

Table 3. Distribution of rotavirus A genotypes in human and bovine populations

Genotype	Human n (%)	Bovine n (%)	Combined n (%)
G-genotypes			
G2	6 (50.0)	0 (0.0)	6 (23.1)
G6	0 (0.0)	10 (71.4)	10 (38.5)
G8	6 (50.0)	4 (28.6)	10 (38.5)
G/P Combinations			
G2P[4]	6 (50.0)	0 (0.0)	6 (23.1)
G6P[11]	0 (0.0)	4 (28.6)	4 (15.4)
G6P[1]	0 (0.0)	2 (14.3)	2 (7.7)
G6P[5]	0 (0.0)	2 (14.3)	2 (7.7)
G8P[8]	0 (0.0)	2 (14.3)	2 (7.7)
G8P[4]	2 (16.7)	2 (14.3)	4 (15.4)
G8P[7]	2 (16.7)	0 (0.0)	2 (7.7)
G8P[1]	1 (8.3)	0 (0.0)	1 (3.8)
G8P[14]	1 (8.3)	0 (0.0)	1 (3.8)

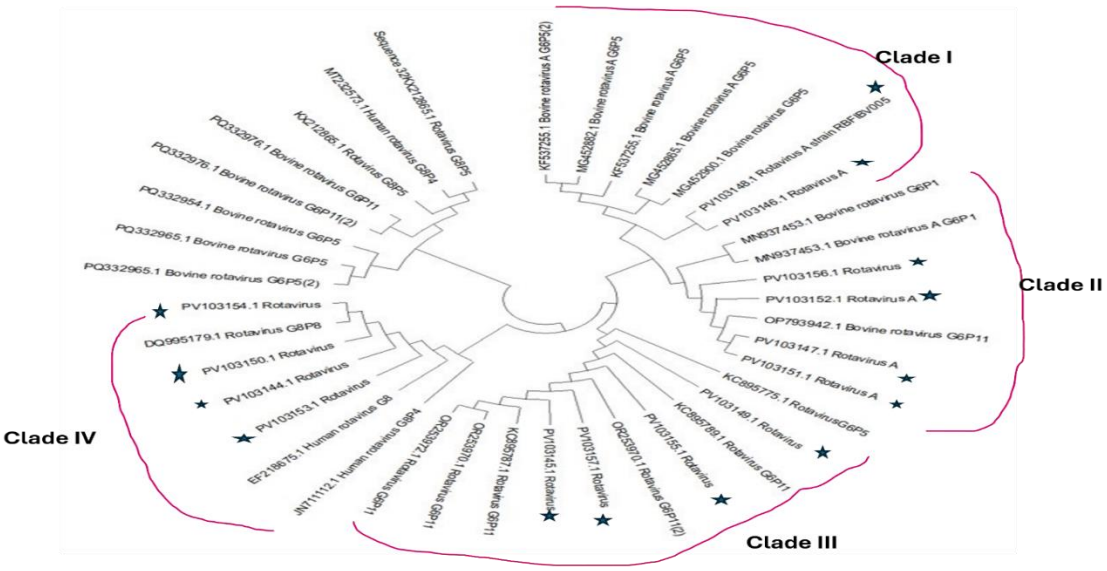


Figure 2. Phylogenetic tree showing clustering of rotavirus A strains based on VP7 sequences. Bootstrap values greater than 70% are shown at nodes. Clades are labeled with corresponding G/P genotypes.

3.1.4 Evidence for Cross-Species Transmission

Comparative analysis identified G8P[4] as the only complete genotype combination present in both human and bovine populations. G8 genotype was detected in 50% of human and 28.6% of bovine isolates, while P[1] and P[4] genotypes were also shared between species (Fig. 3).

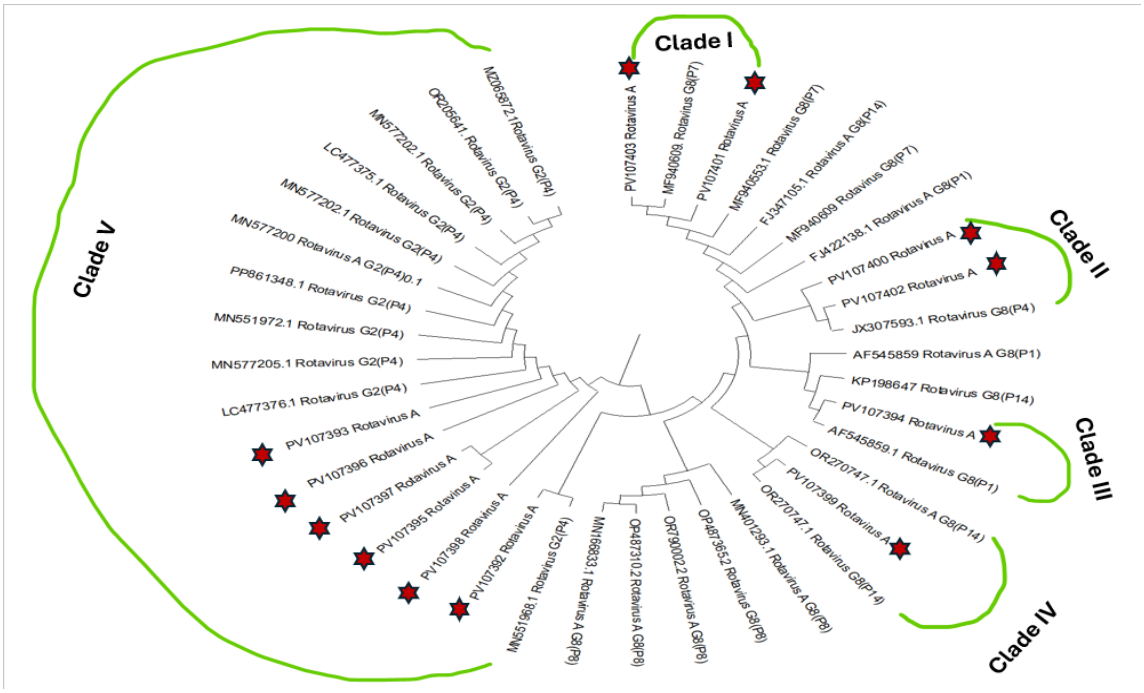


Figure 3. Distribution of rotavirus A genotypes showing (A) G-genotype frequencies and (B) complete G/P combinations in the combined population. G6P[11] (30.8%), G2P[4] (23.1%), and G8P[8] (15.4%) were the most prevalent combinations.

3.2 Discussion

3.2.1 Epidemiological Implications

The comparable prevalence rates between human (22.22%) and bovine (25.92%) populations indicate endemic circulation of rotavirus A in Basra Province with potential for interspecies transmission. The overall detection rate of 24.07% confirms rotavirus A as a significant etiological agent of acute gastroenteritis in both populations, consistent with its recognized role as a leading cause of diarrheal disease globally [1, 2, 13]. The similar prevalence across species suggests parallel transmission cycles that may intersect through direct contact, environmental contamination, or genetic reassortment events facilitated by the segmented nature of the rotavirus genome [10, 19, 21]. Our human prevalence of 22.22% aligns closely with recent surveillance from northern Iraq, where Ahmed et al. reported a 22% rotavirus positivity rate in pediatric diarrheal cases [36], suggesting a relatively consistent contemporary prevalence across Iraqi regions. However, this represents a substantial decline from historical studies conducted in Basra Province and elsewhere in Iraq during the pre-vaccine era. Hassan and Al-Kader documented a 42% prevalence at Basra General Hospital in 2016 [3], while Yaqoob et al. reported a 58% positivity rate among children with acute diarrhea during 2014-2015 [5]. Earlier studies from various Iraqi provinces have recorded even higher rates, with some reporting up to 75% positivity during peak transmission seasons [38-41]. This temporal decline in prevalence likely reflects the combined effects of multiple factors. First, improvements in water and sanitation infrastructure in urban Basra may have reduced fecal-oral transmission, though sanitation challenges persist in rural areas [3,6]. Second, increased awareness and utilization of oral rehydration therapy (ORT) may have reduced the severity of cases requiring hospitalization, potentially selecting for milder infections not captured in hospital-based surveillance [47]. Third, partial vaccine coverage, though limited and not universally implemented in Iraq, may have contributed to reduced disease burden in vaccinated cohorts [11, 12]. However, the absence of comprehensive vaccination data from our study population precludes definitive assessment of vaccine impact. The persistent 22% prevalence, despite these improvements, indicates a continued substantial disease burden that requires ongoing public health attention. This rate exceeds many high-income countries with established vaccination programs (5-15% post-vaccine introduction) but falls below rates commonly reported in low-income settings without vaccine access (30-50%) [14, 22]. Iraq thus occupies an intermediate epidemiological position, consistent with its lower-middle-income status and incomplete vaccine coverage.

The bovine prevalence of 25.92% substantially exceeds previous Iraqi reports, representing a five-fold increase over the 5.67% documented in central Iraq by Ahmed and Al-Ani [37] and nearly double the 15.5% reported in neonatal calves from Mosul by Al-Robaiee and Al-Farwachi [38]. This discrepancy primarily reflects methodological differences rather than true epidemiological variation. Our study employed RT-PCR targeting the VP7 gene, a highly sensitive molecular technique capable of detecting low viral loads and distinguishing rotavirus genotypes [2]. In contrast, previous Iraqi studies utilized enzyme-linked immunosorbent assays (ELISA) or latex agglutination tests, which demonstrate lower sensitivity (60-75%) and may fail to detect infections with low viral shedding or non-Group A rotaviruses. International comparisons support the validity of our findings. Molecular detection-based studies from agricultural regions worldwide report a bovine rotavirus prevalence of 16.8-26.4%, which closely matches our results [8, 13, 16]. Alfieri et al. documented a 24.3% prevalence in Brazilian cattle herds using RT-PCR [8], while Bwogi et al. found a 26.4% prevalence in Ugandan cattle through molecular methods [16]. Studies from European livestock populations have reported a prevalence of 18-22% using similar molecular techniques [18]. This international concordance suggests that our findings reflect genuine prevalence in Basra's cattle population rather than methodological artifacts, and that rotavirus infection dynamics in livestock show relative consistency across diverse agricultural settings. The higher sensitivity of molecular methods has important implications for surveillance. Traditional immunoassays likely underestimated the true bovine prevalence in previous Iraqi studies, potentially causing public health authorities to underappreciate the significance of the animal reservoir. Our data suggest that rotavirus circulates extensively in Iraqi cattle populations, creating continuous opportunities for zoonotic spillover, genetic reassortment, and emergence of novel strains [10,19].

Neither age nor sex demonstrated statistically significant associations with infection rates in either population ($P > 0.05$, $\chi^2 < 3.841$), although variable prevalence across strata suggests that the limited sample

size may have obscured possible biological or behavioral factors. In humans, the highest prevalence was observed in the 1-20 years age group (33.3%), which contrasts with the conventional understanding of rotavirus as primarily affecting infants and young children [1, 13]. This pattern may reflect delayed primary infection in agricultural communities, occupational exposure among adolescents and young adults involved in livestock care, or circulation of age-atypical strains with altered epidemiological characteristics [15,20]. The bovine age distribution proved equally unexpected, with adult cattle (≥5 years) showing the highest prevalence (34.6%) compared to calves ≤1 year (20.0%). This inverts the typical pattern where neonatal calves experience peak infection due to immune immaturity [9,38]. Possible explanations include management practices that affect exposure timing, strain-specific age susceptibility profiles, or cumulative reinfection risk in adult animals maintained in endemic settings [8, 21]. The lack of sex-associated differences in both populations ($P > 0.05$) suggests that biological sex does not substantially influence susceptibility or disease expression, consistent with most rotavirus epidemiological studies [14, 17]. The consistent prevalence across both populations throughout the nine-month study period (January-September 2024) indicates year-round endemic transmission rather than seasonal epidemic patterns. While rotavirus typically exhibits seasonal peaks in temperate climates (during winter months), tropical and subtropical regions, including southern Iraq, often demonstrate less pronounced seasonality [3, 6, 14]. The hot, arid climate of Basra Province, combined with agricultural practices involving continuous livestock management, likely facilitates sustained transmission across seasons [6]. This endemic pattern has important implications for intervention timing, suggesting that year-round surveillance and vaccination programs may prove more effective than seasonally targeted approaches.

3.2.2 Genotype Distribution and Vaccine Mismatch

The complete absence of globally dominant human genotypes (G1, G3, G4, G9, G12) represents a fundamental departure from established epidemiological patterns and constitutes one of the most striking findings of this study. Global surveillance data consistently demonstrate that these five genotypes account for more than 90% of the rotavirus disease burden in human populations across diverse geographical regions [14, 19, 26, 27]. Specifically, G1P[8] has historically been the most prevalent combination worldwide, representing 40-70% of cases in most countries [22, 29]. G2P[4], G3P[8], G4P[8], and G9P[8] collectively comprise most remaining cases, with G12P[8] emerging as an important genotype in recent years [23, 26, 28]. In stark contrast, our study population exhibited an exclusive circulation of G2 and G8 genotypes in humans, with G8 (50%) and G2 (50%) genotypes being equally distributed. The absence of G1, the globally dominant genotype, is particularly noteworthy. Previous Iraqi studies have documented G1 circulation, with Ahmed et al. reporting G1 as the predominant genotype in Iraqi Kurdistan [36], while Hussein et al. found G1 in 45% of cases in Diyala Province [30]. The complete disappearance of G1 from our Basra samples suggests either genuine temporal/geographical variation in genotype circulation or potential vaccine-driven selective pressure if partial vaccination coverage has occurred [23, 32]. This genotype distribution more closely resembles patterns observed in sub-Saharan African countries and certain Asian agricultural regions where animal-human transmission interfaces are prominent [16,18,19]. Bwogi et al. documented a similar G8 predominance in Ugandan populations with extensive livestock contact [16], while studies from rural India and Bangladesh have reported G6 and G8 as the leading human genotypes in agricultural communities [29, 31]. The convergence of our findings with these settings suggests that agricultural context and zoonotic transmission dynamics fundamentally shape local genotype ecology, potentially overriding global circulation patterns.

The current WHO-recommended rotavirus vaccines demonstrate genotype-specific efficacy profiles that raise concerns for settings such as Basra Province. RotaTeq (Merck) is a pentavalent vaccine containing reassortant strains that express human G1, G2, G3, G4, and P[8] combined with a bovine rotavirus backbone [11, 32]. Rotarix (GSK) is a monovalent vaccine containing an attenuated human G1P[8] strain, designed to provide heterotypic protection against other genotypes [11, 22]. Both vaccines were developed based on genotypes predominant in North America and Europe during the 1990s and 2000s [32]. Our findings reveal no complete G/P combination matches between circulating strains and vaccine components, with the sole exception of partial G2 coverage, which represents only 23% of cases. Critically, the predominant combinations—G6P[11] (30.8% overall), G8P[8] (15.4%), and G8P[4] (15.4%)—are completely absent from both

vaccine formulations. The G8 genotype, which accounts for 50% of human infections, is not represented in either vaccine. While RotaTeq® contains G2, it pairs with P[4], whereas 50% of our G2 strains paired with P[4] and the remainder with uncommon P-types (P[2], P[7]) not present in vaccines [2, 25, 32]. Vaccine efficacy depends on both homotypic protection (against matched genotypes, typically 85-95%) and heterotypic protection (against mismatched genotypes, variable 40-80%) [22, 29, 32]. Studies from diverse settings demonstrate that vaccine effectiveness declines substantially when circulating genotypes diverge from the vaccine strains [12, 22, 23]. In African countries where G8 and G12 predominate, vaccine effectiveness estimates range from 39% to 66%, significantly lower than the 85-98% observed in settings with matched genotypes [12, 14, 22]. A meta-analysis by Troeger et al. found that vaccine effectiveness was inversely correlated with genotype diversity and the degree of mismatch, with each additional mismatched genotype reducing effectiveness by approximately 8-12% [12]. For Basra Province, where 100% of complete G/P combinations represent mismatches (excluding partial G2 overlap), vaccine effectiveness would depend entirely on heterotypic immunity. This scenario likely explains Iraq's continued high burden of rotavirus disease, despite partial vaccine introduction in some regions [3-5]. Mathematical modeling suggests that heterotypic immunity against completely mismatched genotypes provides approximately 40-60% protection against severe disease, which is substantially lower than the 85-95% protection against matched strains [22, 32]. This reduced effectiveness has profound public health implications, potentially requiring higher vaccination coverage rates (above 95% versus 80-85%) to achieve an equivalent population-level impact [23, 29].

The predominance of G8 in human samples (50%), typically considered an animal-associated genotype with primary circulation in bovine populations, provides compelling molecular evidence for zoonotic transmission [10, 16, 18, 28]. Global genotype surveillance consistently identifies G8 as a bovine-specific genotype rarely detected in human populations, except in settings with extensive animal contact [18, 27-29]. In most countries, G8 represents <2% of human rotavirus infections, with the majority occurring sporadically in rural agricultural workers or children with livestock exposure [19, 20, 28]. The detection of G8 in 50% of human diarrheal cases in Basra represents a more than 25-fold elevation above the global baseline prevalence, indicating sustained human-to-human transmission of an originally zoonotic strain rather than isolated spillover events [10, 16]. This pattern suggests that G8 has successfully adapted to human populations in this region, possibly through reassortment events that optimized its human infectivity while retaining the G8 glycoprotein [19, 21, 27]. Phylogenetic analysis showed 97-100% sequence similarity between human and bovine G8 strains, strongly supporting recent or ongoing cross-species transmission rather than ancient divergence [10, 28]. The specific G8 P-type combinations detected provide additional signatures of zoonotic transmission. G8P[8] (detected in both species, at 15.4% overall) represents a classic reassortant genotype, where bovine G8 is typically combined with human-associated P[8], a hallmark of human-bovine co-infection and reassortment [19, 21, 27]. G8P[4] (15.4%, detected in both species) similarly suggests reassortment between bovine and human strains, as P[4] circulates in both populations [25, 28]. The detection of G8P[7], G8P[1], and G8P[14] in human samples further demonstrates the diverse P-type associations that G8 has acquired, likely through multiple reassortment events facilitated by the segmented rotavirus genome [21, 25, 27]. International parallels support zoonotic interpretation. Midgley et al. documented extensive G8 circulation in European agricultural regions with intensive livestock farming, finding identical G8 strains in farmers and their cattle [18]. Cook et al. demonstrated experimental human infection with bovine rotavirus strains, confirming the biological plausibility of zoonotic transmission [10]. Studies from Uganda, India, and Brazil have reported G8 as a leading human genotype in agricultural populations, invariably associated with cattle contact [16, 20, 28]. The consistency of this association across diverse settings strengthens the inference that Basra's G8 predominance reflects active animal-to-human transmission.

The identification of G6P[11] as the most prevalent combination overall (30.8%), despite its exclusive detection in bovine samples, further emphasizes the central role of the animal reservoir in maintaining regional viral diversity [18, 28-30]. G6 represents a quintessentially bovine genotype, with P[11] being the most common P-type associated with bovine G6 strains globally [27-29]. The complete absence of G6 from human samples in our study does not indicate a lack of zoonotic potential; rather, it may reflect sampling limitations, differential host tropism, or that spillover events occur at frequencies below our detection threshold [10, 18, 19].

Several lines of evidence suggest G6 poses an ongoing zoonotic risk. First, G6 has been repeatedly documented in human populations in other agricultural settings, typically comprising 1-8% of human infections in regions with extensive cattle farming [16, 18, 28, 30]. Second, the high prevalence in Basra cattle (71.4% of bovine positives) ensures continuous environmental contamination and increased opportunities for human exposure [8, 10]. Third, the segmented genome structure permits reassortment between G6 and human strains during co-infections, potentially generating G6 variants with enhanced human infectivity [19, 21, 27]. Fourth, experimental studies have demonstrated that bovine G6 strains can infect human intestinal organoid cultures, confirming their biological capacity for human infection [10, 25]. The P[11] association warrants particular attention, as it represents a purely bovine P-type with minimal documented human circulation [27-29]. P[11] encodes VP4 outer capsid protein optimized for bovine intestinal receptor binding, potentially limiting efficient human infection [25,28]. However, reassortment could replace P[11] with human-adapted P-types (P[4], P[6], P[8]), creating G6 variants with enhanced human transmissibility [19, 21]. Such reassortment events have been documented elsewhere, with G6P[8] and G6P[4] reported as emerging human genotypes in agricultural regions of Asia and Africa [16, 20, 30]. The additional bovine genotype combinations—G6P[1] (7.7%), G6P[5] (7.7%), and G8P[8] (7.7%)—demonstrate considerable viral diversity within the animal reservoir, providing substrate for evolutionary innovation through reassortment [21, 23, 27]. This diversity likely reflects multiple introductions, concurrent circulation of distinct lineages, or reassortment between bovine strains [18,28]. Each distinct combination represents a potential source for novel human-infective variants, emphasizing the need for comprehensive animal surveillance [10,16,18].

The genotype distribution observed in Basra contrasts sharply with other Iraqi regions, suggesting substantial geographical heterogeneity. Previous studies from Baghdad and central Iraq reported G1 and G9 as the predominant genotypes [32,33], whereas northern Iraq showed predominance of G2 and G1 [36]. This variation may reflect differences in agricultural intensity, livestock density, vaccination coverage, or sampling methodology [3, 18, 30]. Basra's extensive cattle farming industry, with an estimated 150,000+ head of cattle in the province, creates uniquely intensive human-animal interfaces absent in more urbanized regions [6,7]. Globally, genotype distributions exhibit strong geographical clustering related to agricultural practices, climate, and socioeconomic factors [19, 26, 27]. Temperate high-income countries with intensive livestock farming but strong biosecurity typically maintain separation between human and animal genotype pools [18, 26]. In contrast, tropical and subtropical agricultural regions with extensive human-livestock contact often exhibit merged genotype ecologies, characterized by substantial zoonotic circulation [16, 20, 28, 30]. Iraq's intermediate socioeconomic status and variable biosecurity practices position it within this latter category, consistent with our findings [3, 6, 18]. The complete vaccine mismatch necessitates fundamental reconsideration of immunization approaches for Iraq and similar settings. Several strategies merit evaluation: (1) region-specific vaccine development incorporating G6, G8, and locally circulating P-types [23, 32]; (2) next-generation broadly protective vaccines targeting conserved viral epitopes rather than genotype-specific antigens [22, 29]; (3) higher-valency vaccines incorporating additional genotypes beyond current formulations [32]; (4) combined human and livestock vaccination to reduce overall viral circulation and zoonotic transmission [10,16,18]; or (5) acceptance of reduced vaccine effectiveness while emphasizing other interventions (sanitation, ORT, biosecurity) [11, 12]. Without molecular surveillance data, vaccine programs operate blindly, unable to assess effectiveness or detect emerging strains [17, 22, 23]. Our findings demonstrate the critical importance of ongoing genotype monitoring to inform evidence-based vaccine policy [14, 23, 32].

3.2.3 Zoonotic Transmission Evidence

Multiple converging lines of evidence support active cross-species transmission of rotavirus A between human and bovine populations in Basra Province, representing a significant departure from traditionally compartmentalized human and animal epidemiological cycles.]The identification of G8P[4] in both human (16.7% of human positives) and bovine (14.3% of bovine positives) samples provides direct molecular evidence of recent cross-species transmission [10, 16, 18]. Phylogenetic analysis revealed 97-100% nucleotide sequence similarity between human and bovine G8P[4] isolates, indicating either recent common ancestry or ongoing bidirectional transmission, rather than ancient divergence followed by independent evolution [10, 19, 27]. Such high sequence identity suggests that transmission events occurred within recent

epidemiological timeframes, possibly within months to a few years, as rotavirus accumulates approximately 1-2% nucleotide substitutions annually under natural selection pressure [21, 23, 27]. The G8P[4] combination itself represents a reassortant genotype requiring co-infection of a single host with both bovine-origin and human-adapted strains [19, 21]. G8 glycoprotein circulates primarily in cattle globally, while P[4] exhibits a broader host distribution, including both humans and animals [25, 27, 28]. The emergence of this combination likely occurred through reassortment during co-infection events facilitated by the segmented rotavirus genome, which readily exchanges gene segments when multiple strains infect the same cell [21, 25]. The detection of identical G8P[4] in both species strongly suggests that Basra Province serves as an active mixing zone, where such reassortment events occur with sufficient frequency to establish sustained transmission [10, 16, 18].

The overwhelming predominance of typically animal-associated genotypes—G6 and G8, comprising 76.9% of all isolates—provides population-level evidence of zoonotic influence on human rotavirus epidemiology [16, 18, 28, 30]. This pattern inverts the expected distribution, where human-specific genotypes (G1, G3, G4, G9, G12) dominate more than 90% of infections globally [19,26,27]. The exclusive detection of G8 and G2 in humans, with G8 representing 50% of human infections, demonstrates that animal reservoir genotypes have not merely spilled over sporadically but have established sustained human-to-human transmission chains [10, 16, 20]. International comparisons reveal similar patterns exclusively in agricultural settings with intensive livestock contact. Bwogi et al. documented G6 and G8 as predominant human genotypes in rural Uganda, where humans and cattle share water sources and living spaces [16]. Midgley et al. found identical genotype distributions in European farming communities with extensive dairy cattle operations [18]. The consistency of this association across diverse geographical contexts strongly implicates human-animal interfaces as the primary driver of genotype ecology in such settings [10, 18, 20, 28]. The complete absence of typically human-associated genotypes (G1, G3, G4, G9) from bovine samples, despite their historical circulation in Iraqi human populations [30, 32, 36], suggests predominantly unidirectional transmission, favoring animal-to-human spread [10, 16]. This asymmetry likely reflects differential host adaptation, with bovine strains possessing greater intrinsic capacity for human infection than human strains possess for bovine infection [18, 25, 28]. Alternatively, the agricultural context may facilitate asymmetric exposure, with humans encountering animal fecal contamination more frequently than cattle encounter human waste [9, 10].

Basra Province's agricultural landscape creates ideal conditions for viral spillover through multiple exposure pathways [3, 6]. Direct contact during cattle handling, consumption of unpasteurized dairy products, environmental contamination of shared water sources, and inadequate biosecurity practices all facilitate the transmission of rotavirus [8-10,18]. The province supports approximately 150,000 heads of cattle, with many smallholder farms lacking modern biosecurity infrastructure [6, 7]. Farm workers, their families, and children frequently interact directly with cattle, creating continuous opportunities for viral exchange [16, 18, 20]. The unexpectedly high prevalence in adult cattle (34.6%) versus calves (20.0%) contradicts established paradigms, which identify neonatal calves as being maximally susceptible [8, 9, 38]. This inversion may reflect management practices in which adult cattle experience continuous reexposure in endemic settings, strain-specific virulence patterns that differentially affect age groups, or cumulative lifetime exposure effects [8, 21]. Similarly, peak human infection in the 1-20 years group (33.3%) rather than infants under one year suggests altered transmission dynamics possibly attributable to occupational/agricultural exposure among adolescents and young adults [15, 20]. This age shift parallels patterns observed in other zoonotic viral infections, where occupational contact drives adult disease burden [16, 18, 20].

3.2.4 Public Health Implications

These findings necessitate fundamental reconsideration of rotavirus control strategies in Iraq. The demonstration of active zoonotic transmission, coupled with the complete absence of vaccine-matched genotypes, reveals critical gaps in current surveillance and prevention approaches. The agricultural context of Basra Province, with its extensive human-livestock interface, exemplifies settings where conventional human-focused interventions may prove insufficient without addressing the animal reservoir. Current rotavirus surveillance in Iraq operates within a fragmented framework that monitors human and animal populations

independently, if animal surveillance occurs at all. This compartmentalized approach fails to detect cross-species transmission events and obscures the accurate epidemiological picture. The 25.9% prevalence in bovine populations, comparable to human rates, suggests that animal reservoirs sustain substantial viral circulation that remains largely unmonitored. Without integrated surveillance, health authorities cannot assess the risk of zoonotic transmission, track emerging reassortant strains, or evaluate spillover dynamics. The identification of G8P[4] in both species occurred only because this study simultaneously investigated both populations—a methodology not employed in routine surveillance. Implementing One Health surveillance frameworks would enable early detection of novel genotypes, facilitate rapid outbreak response, and provide comprehensive data for evidence-based policy development. The complete absence of globally dominant human genotypes (G1, G3, G4, G9, G12) represents a critical challenge for vaccine-based prevention strategies. Current vaccines contain G1P[8], G2P[4], G3P[8], G4P[8], and G9P[8] combinations (RotaTeq®) or G1P[8] with heterotypic coverage (Rotarix®). Our findings show zero complete G/P matches and only partial G2 coverage accounting for 23% of cases. The predominance of G6P[11] (30.8%) and G8P[8] (15.4%)—genotypes absent from vaccine formulations—suggests that vaccine efficacy may depend entirely on heterotypic immunity. Studies from other regions with similar genotype mismatches have reported reduced vaccine effectiveness, ranging from 40-60%, which is substantially lower than the 85-95% efficacy observed in settings with matched genotypes. This disparity has profound implications for vaccination programs, potentially explaining the suboptimal disease reduction despite the introduction of vaccines. Region-specific vaccine development, incorporating locally circulating genotypes —particularly G6 and G8, along with their associated P-genotypes —warrants serious consideration. Alternatively, next-generation broadly protective vaccines targeting conserved epitopes across multiple genotypes represent a longer-term solution.

The observed peak infection rate in the 1-20 years age group (33.3%) contradicts the conventional paradigm of rotavirus as primarily a pediatric disease affecting children under five. This age distribution pattern suggests either delayed primary infection, exposure through occupational/agricultural contact, or circulation of age-atypical strains. Current vaccination programs in Iraq, when implemented, target infants exclusively through two- or three-dose schedules administered before six months of age. If substantial disease burden occurs in older children, adolescents, and young adults—particularly those with agricultural exposure—these programs do not protect at-risk populations. Furthermore, the high prevalence in adult cattle (34.6%) compared to calves (20.0%) indicates persistent viral shedding in mature animals, creating a continuous exposure risk for farm workers and their families. Expanding vaccination eligibility to include older children in agricultural communities, implementing targeted vaccination for farm workers, and considering catch-up campaigns for previously unvaccinated cohorts could address these gaps. Such expanded programs would require policy revision, additional resources, and acceptability studies to ensure uptake. The long-standing exclusion of livestock from rotavirus control strategies represents a fundamental oversight given mounting evidence of zoonotic transmission. Our identification of G8P[4] in both species, alongside the predominance of typically bovine genotypes (G6, G8) comprising 76.9% of all isolates, demonstrates that animal populations serve as active viral reservoirs with direct relevance to human health. The segmented genome structure of rotavirus enables reassortment when human and animal strains co-infect a single host, potentially generating novel genotypes with altered virulence, transmissibility, or vaccine escape capability. Agricultural practices in Basra Province, including close human-animal contact, shared water sources, and limited biosecurity, create ideal conditions for such events. Integrating livestock vaccination into comprehensive control strategies could reduce overall viral circulation, decrease zoonotic spillover events, and limit opportunities for reassortment. Veterinary vaccines containing bovine-relevant genotypes (G6, G10, G8 with P[1], P[5], P[11]) exist but remain underutilized. Economic analysis would be necessary to assess the cost-effectiveness, but the benefits would extend beyond human health to include reduced livestock mortality, improved growth rates, and decreased treatment costs in the agricultural sector.

Table 4. Implications for rotavirus control strategies

Current Approach	Study Finding	Recommended Action	Implementation Considerations
Human-only surveillance	25.9% bovine prevalence with shared genotypes	Implement an integrated One Health surveillance system	Requires inter-ministerial coordination (Health, Agriculture), laboratory capacity building, standardized protocols, data sharing platforms, and sustainable funding
Standard vaccines (G1-G4, G9, P[8])	G6 (38%), G8 (38%) predominance; zero complete matches	Develop region-specific vaccine formulations or deploy broadly protective vaccines	Necessitates partnerships with vaccine manufacturers, clinical trials, regulatory approval, and cost-benefit analysis; interim solution: evaluate heterotypic protection
Infant-focused vaccination (0-6 months)	Peak infection 1-20 years (33.3%); agricultural exposure patterns	Expand vaccination eligibility to older children and at-risk populations	Requires policy revision, additional vaccine procurement, acceptability studies, and targeted delivery strategies for rural/agricultural communities
Ignore the animal reservoir.	G8P[4] detected in both species; 76.9% animal-associated genotypes in total	Implement coordinated livestock vaccination programs	Demands veterinary infrastructure enhancement, farmer education, cost-sharing mechanisms, and integration with existing animal health programs

4. Conclusions

This surveillance study reveals the unique epidemiology of rotavirus A in Basra Province, Iraq, characterized by substantial zoonotic transmission between human and bovine populations. The comparable prevalence rates (22.22% humans, 25.92% bovine) and identification of shared genotypes, particularly G8P[4], provide molecular evidence for active cross-species transmission. The complete absence of globally dominant human genotypes (G1, G3, G4, G9, G12) and predominance of animal-associated genotypes (G6, G8) in 76.92% of isolates represents a fundamental departure from established epidemiological patterns. The identified genotype constellation—G6P[11] (30.77%), G2P[4] (23.08%), and G8P[8] (15.38%)—has critical implications for vaccine effectiveness. With zero complete G/P combinations matching current vaccine formulations (RotaTeq® and Rotarix®) and only 22.2% partial coverage, vaccine protection likely depends entirely on heterotypic immunity, which may be insufficient for disease prevention. These findings demonstrate the inadequacy of human-focused surveillance strategies and highlight the urgent need for One Health approaches incorporating systematic monitoring of livestock populations. The agricultural setting of Basra Province, with extensive human-animal contact and limited biosecurity, creates ideal conditions for viral spillover and reassortment. The detection of nine distinct G/P combinations suggests active viral evolution with potential for novel strain emergence. The implementation of integrated surveillance systems, enhanced

molecular characterization capacity, and region-specific intervention strategies are essential for effective control of rotavirus. Future priorities include expanded geographic surveillance, comprehensive genome sequencing, assessment of vaccine effectiveness, and development of broadly protective vaccines incorporating regional genotypes. Success in reducing rotavirus burden in agricultural regions requires acknowledging and addressing the fundamental role of zoonotic transmission in shaping disease epidemiology.

5. Acknowledgements

The authors are grateful to the colleagues of the College of Veterinary Medicine at Basra University for their technical assistance and aid in the collection of samples and laboratory work. Our thanks go to the hospital staff and the farm owners in Basra Province for their collaboration, as well as for allowing human and bovine samplings.

Author Contributions: Conceptualization, R.B.Z. and B.A.A.; methodology, R.B.Z. and F.A.A.; software, R.B.Z.; validation, R.B.Z., B.A.A. and F.A.A.; formal analysis, R.B.Z. and F.A.A.; investigation, R.B.Z. and F.A.A.; resources, B.A.A.; data curation, R.B.Z.; writing—original draft preparation, R.B.Z.; writing—review and editing, B.A.A. and F.A.A.; visualization, R.B.Z.; supervision, B.A.A.; project administration, B.A.A.; funding acquisition, B.A.A. All authors have read and agreed to the published version of the manuscript.

Funding: Not applicable

Conflicts of Interest: The authors declare no conflict of interest.

References

[1] Khuffash, F. A.; Sethi, S. K.; Shaltout, A. A. Acute gastroenteritis: Clinical features according to etiologic agents. *Clin. Pediatr.* **1988**, *27*(8), 365–368. https://doi.org/10.1177/000992288802700802

[2] Esona, M. D.; Gautam, R.; Tam, K. I.; Williams, A.; Mijatovic-Rustempasic, S.; Bowen, M. D. Multiplexed one-step RT-PCR VP7 and VP4 genotyping assays for rotaviruses using updated primers. *J. Virol. Methods* **2015**, *223*, 96–104. https://doi.org/10.1016/j.jviromet.2015.07.012

[3] World Health Organization. *Meeting Report: Global Rotavirus and Paediatric Diarrhea Surveillance, Laboratory, and Disease Burden Meetings, 28–30 November 2018*; WHO.

[4] World Health Organization. *Meeting Report: Global Rotavirus and Pediatric Diarrheal Surveillance Network Meeting, 19–20 November 2019*; WHO.

[5] Alfieri, A. A.; Parazzi, M. E.; Takiuchi, E.; Médici, K. C.; Alfieri, A. F. Frequency of group A rotavirus in diarrhoeic calves in Brazilian cattle herds, 1998–2002. *Trop. Anim. Health Prod.* **2006**, *38*, 521. https://doi.org/10.1007/s11250-006-4349-9

[6] Barrington, G. M.; Gay, J. M.; Evermann, J. F. Biosecurity for neonatal gastrointestinal diseases. *Vet. Clin. North Am. Food Anim. Pract.* **2002**, *18*(1), 7–34. https://doi.org/10.1016/s0749-0720(02)00005-1

[7] Cook, N.; Bridger, J.; Kendall, K.; Gomara, M. I.; El-Attar, L.; Gray, J. The zoonotic potential of rotavirus. *J. Infect.* **2004**, *48*(4), 289–302. https://doi.org/10.1016/j.jinf.2004.01.018

[8] Argüelles, M. H.; Villegas, G. A.; Castello, A.; Abrami, A.; Ghiringhelli, P. D.; Semorile, L.; Glikmann, G. VP7 and VP4 genotyping of human group A rotavirus in Buenos Aires, Argentina. *J. Clin. Microbiol.* **2000**, *38*(1), 252–259. https://doi.org/10.1128/JCM.38.1.252-259.2000

[9] Matthijnssens, J.; Bilcke, J.; Ciarlet, M.; et al. Rotavirus disease and vaccination: Impact on genotype diversity. *Future Microbiol.* **2009**, *4*, 1303–1316. https://doi.org/10.2217/fmb.09.96

[10] Matthijnssens, J.; Ciarlet, M.; McDonald, S. M.; et al. Uniformity of rotavirus strain nomenclature proposed by the Rotavirus Classification Working Group (RCWG). *Arch. Virol.* **2011**, *156*(8), 1397–1413. https://doi.org/10.1007/s00705-011-1006-z

[11] Trojnar, E.; Sachsenroder, J.; Twardziok, S.; Reetz, J.; Otto, P. H.; Johne, R. Identification of an avian group A rotavirus with a novel VP4 gene. *J. Gen. Virol.* **2013**, *94*, 136–142. https://doi.org/10.1099/vir.0.047381-0

[12] Iturriza-Gomara, M.; Dallman, T.; Banyai, K.; et al. Rotavirus genotypes co-circulating in Europe, 2006–2009. *Epidemiol. Infect.* **2011**, *139*, 895–909.
[13] Gentsch, J. R.; Laird, A. R.; Bielfelt, B.; et al. Serotype diversity and reassortment: Implications for vaccine programs. *J. Infect. Dis.* **2005**, *192*, S146–S159. https://doi.org/10.1086/431499
[14] Gichile, A. G. Review on the epidemiology of bovine rotavirus. *Int. J. Vet. Sci. Res.* **2022**, *8*(1), 5–10.
[15] Geletu, U. S.; Usmael, M. A.; Bari, F. D. Rotavirus in calves and its zoonotic importance. *Vet. Med. Int.* **2021**, 6639701. https://doi.org/10.1155/2021/6639701
[16] Bwogi, J.; Karamagi, C.; Byarugaba, D. K.; et al. Co-surveillance of rotaviruses in humans and domestic animals in Central Uganda. *Viruses* **2023**, *15*, 738. https://doi.org/10.3390/v15030738
[17] Midgley, S. E.; Banyai, K.; Buesa, J.; et al. Diversity and zoonotic potential of rotaviruses in swine and cattle across Europe. *Vet. Microbiol.* **2012**, *156*, 238–245. https://doi.org/10.1016/j.vetmic.2011.10.027
[18] Mahmoud, A. E.; Zaki, M. E. S.; Mohamed, E. H.; et al. Study of rotavirus genotypes in Egypt. *Ital. J. Pediatr.* **2024**, *50*, 247. https://doi.org/10.1186/s13052-024-01810-x
[19] Hussein, A. A.; Hussein, R. A.; Shaker, M. J. Enteric virus co-infection in Iraq. *J. Pure Appl. Microbiol.* **2018**, *12*(2), 793–799. https://doi.org/10.22207/JPAM.12.2.40
[20] Nasser, A. T.; Hasan, A. S.; Saleh, A. K.; Saleh, M. K. Rotavirus detection in children with gastroenteritis. *GSC Adv. Res. Rev.* **2021**, *6*(3), 194–208.
[21] Abdul Sattar, B. A. A.; Al-Kareemi, K. K.; Jassim, A. A. Rotavirus infection in pediatric patients. *J. Fac. Med. Baghdad* **2012**, *54*(4), 349–352. https://doi.org/10.32007/jfacmedbagdad.544702
[22] Abood, W. S. Molecular epidemiology of rotavirus in Mid Iraq. *Al-Qadisiyah J. Vet. Med. Sci.* **2013**, *12*(1), 121–127. https://doi.org/10.29079/vol12iss1art240
[23] Hassan, H. A. A.; Al-Kader, R. A. A. Rotavirus diarrhea in Basrah. *MJBU* **2016**, *34*(2).
[24] Abdulla, M. M.; Maatook, M. A.; Mahmoud, R. A. Diarrheal disease in Basra during COVID-19. *Ann. R. S. C. B.* **2021**, *25*(6), 9759–9863.
[25] Yaqoob, M. M.; Mahdi, K. H.; Al-Hmudi, H. A.; Mohammed-Ali, M. N. Detection of rotavirus A and E. coli. *Int. J. Curr. Microbiol. Appl. Sci.* **2016**, *5* (4), 68–83. https://doi.org/10.20546/ijcmas.2016.504.011
[26] Habash, S. H.; Habeeb, S. I. Rotavirus diarrhea in children under five in Basrah. *Pediatr. Infect. Dis.* **2018**, *3*(2), 6. https://doi.org/10.21767/2573-0282.100062
[27] Tarik, A. S.; Muhsen, R. K. Rotavirus group A alterations in newborn buffalo calves. *Adv. Life Sci.* **2024**, *11*(2). https://doi.org/10.62940/als.v11i3.2051
[28] Ahmed, S. K.; Atheer, A. A. Rotavirus diversity in cow and buffalo calves. *EZS* **2017**, *5*(6), 1206–1211.
[29] Al-Robaiee, I. A.; Al-Farwachi, M. I. Rotaviral infection in neonatal calves in Mosul. *World* **2013**, *6*(8), 538–540. https://doi.org/10.5455/vetworld.2013.538-540
[30] Rotavirus Classification Working Group (RCWG). *Virus Classification.* 2021.
[31] Antoni, S.; Nakamura, T.; Cohen, A. L.; et al. Rotavirus genotypes in LMICs. *PLOS Glob. Public Health* **2023**, *3*(11), e0001358.
[32] Banyai, K.; Laszlo, B.; Duque, J.; et al. Global rotavirus strain diversity: A systematic review. *Vaccine* **2012**, *30* (Suppl 1), A122–A130. https://doi.org/10.1016/j.vaccine.2011.09.111
[33] Tapisiz, A.; Bedir Demirdag, T.; Cura Yayla, B. C.; et al. Rotavirus infections in Turkey: Systematic review. *Rev. Med. Virol.* **2019**, *29*(1), e2020. https://doi.org/10.1002/rmv.2020
[34] Khai, Q.; Tran, H. H.; Tuan, N. V.; et al. Rotavirus and co-infection in Vietnam. *Arch. Pediatr. Infect. Dis.* **2024**, *12*(1), e140509.
[35] Campanha, J.; Possatti, F.; Lorenzetti, E.; et al. Rotavirus C VP6 genotype I6 in piglets. *Braz. J. Microbiol.* **2020**, *51*, 1–7. https://doi.org/10.1007/s42770-020-00234-z
[36] Jaff, D. O.; Tariq, A. G. A.; Natalie, R. S. Rotavirus infections in Sulaimani. *JBM* **2016**, *4*(1), 124–131. https://doi.org/10.4236/jbm.2016.41015
[37] Zaman, N. A.; Al-Tae, A. A.; Saadoon, I. H. Rotavirus and adenovirus in Kirkuk children. *Second Scientific Conference – Tikrit University* **2012**.
[38] Ahmed, H. M.; Coulter, J. B. S.; Nakagomi, O.; et al. Rotavirus strains in Kurdistan. *Emerg. Infect. Dis.* **2006**, *12*(5), 824. https://doi.org/10.3201/eid1205.051422

[39] Duman, R.; Aycan, A. E. Rotavirus infection in calves in Konya. *J. Anim. Vet. Adv.* **2010**, *9*(1), 136–139. https://doi.org/10.3923/javaa.2010.136.138

[40] Almalky, M. A.; Amer, R. E.; Abd Elraouf, H. A. Rotavirus genotyping in Egypt. *Egypt. J. Hosp. Med.* **2022**, *88*, 2710–2715. https://doi.org/10.21608/ejhm.2022.241123

[41] Bawa, F. K.; Mutocheluh, M.; Dassah, S. D.; et al. Genetic diversity of rotavirus in Ghana. *Pan Afr. Med. J.* **2023**, *44*, 148. https://doi.org/10.11604/pamj.2023.44.148.36783

[42] Temori, A.; Mehrpoor, A. J.; Niazi, A.; et al. Rotavirus prevalence in Afghanistan. *Afgh. J. Infect. Dis.* **2023**, *1*, 9–13. https://doi.org/10.58342/ajid/ghalibuni.v.1.I.1.3

[43] Martinez-Gutierrez, M.; Arcila-Quiceno, V.; Trejos-Suarez, J.; Ruiz-Saenz, J. Rotavirus typing in Colombia. *Rev. Inst. Med. Trop. São Paulo* **2019**, *61*, e34. https://doi.org/10.1590/s1678-9946201961034

[44] Anderson, E. J.; Weber, S. D. Rotavirus infection in adults. *Lancet Infect. Dis.* **2004**, *4*(2), 91–99. https://doi.org/10.1016/S1473-3099(04)00928-4

[45] Barua, S. R. *Clinico-Pathology and Molecular Characterization of Bovine Rotavirus in Bangladesh*; 2019.

[46] Santos, Y.; Hoshino. Global distribution of rotavirus serotypes. *Rev. Med. Virol.* **2005**, *15*(1), 29–56. https://doi.org/10.1002/rmv.448

[47] Kuang, X.; Gong, X.; Zhang, X.; Pan, H.; Teng, Z. Genetic diversity of rotavirus in Shanghai. *BMC Infect. Dis.* **2020**, *20*, 1–11. https://doi.org/10.1186/s12879-020-05279-x

ASEAN
Journal of Scientific and Technological Reports
Online ISSN:2773-8752

Academic article

Phenotypic-Genotypic Characterization of Macrolide-Lincosamide-Streptogramin B Resistance in *Staphylococcus saprophyticus* UTI Isolates from Iraq

Ahlam Ali Soghi Al-Galebi[1*], Mithal K.A. Al-Hassani[1], Hadaf Mahdi Kadhim[1], and Miaad K. Alkhudhairy[2]

[1] College of Education, University of Al-Qadisiyah, Al-Diwaniyah, Iraq
[2] College of Health and Medical Techniques, Al-Furat Al-Awsat Technical University, Najaf, Iraq
* Correspondence: ahlam.ali@qu.edu.iq

Citation:
Phenotypic-genotypic characterizaton of macrolide-lincosamide-streptogramin B resistabce in *Staphylococcus saprophyticus* UTI Isolates from Iraq. *ASEAN J. Sci. Tech. Report.* **2026**, *29*(1), e261225. https://doi.org/10.55164/ajstr.v29i1.261225.

Article history:
Received: September 11, 2025
Revised: October 1, 2025
Accepted: October 9, 2025
Available online: December 14, 2025

Publisher's Note:
This article is published and distributed under the terms of the Thaksin University.

Abstract: *Staphylococcus saprophyticus* is a significant uropathogen, particularly in young women. Rising macrolide-lincosamide-streptogramin B (MLSB) resistance poses therapeutic challenges. This study characterized phenotypic and genotypic MLSB resistance patterns among S. saprophyticus UTI isolates in Najaf, Iraq. Forty-two *S. saprophyticus* isolates were collected from urine samples (February-April 2025) from patients aged 1-70 years. Phenotypic resistance was assessed using the D-test methodology following CLSI guidelines. PCR amplification targeted eight resistance genes: *erm*(C) and *msr*(A). Isolates predominantly originated from females (28/42, 66.7%), with the highest frequency in age groups 21-30 (11/42, 26.2%) and 31-40 years (10/42, 23.8%). The D-test revealed that 25/42 (59.5%) isolates exhibited MLSB resistance: 9/42 (21.4%) demonstrated an inducible MLSB (iMLSB) phenotype, 16/42 (38.1%) exhibited a constitutive MLSB (cMLSB) phenotype, and 8/42 (19.0%) displayed a macrolide-streptogramin B (MS) phenotype, while 9/42 (21.4%) were MLSB-negative. Molecular analysis detected resistance genes in only 9 of 25 (36%) phenotypically MLSB-positive isolates. The erm(C) gene alone was present in 2/25 (8%) isolates, while *erm*(C)+*msr*(A) combination dominated at 7/25 (28%). High MLSB resistance prevalence (59.5%) among *S. saprophyticus* isolates, with cMLSB predominance and significant genotype-phenotype discordance (64% phenotypically positive lacking detected genes), emphasizes the necessity for routine D-testing and expanded molecular surveillance to guide antimicrobial therapy in Iraqi healthcare settings.

Keywords: *Staphylococcus saprophyticus*; UTIs; MLS resistance; cross-resistance; PCR

1. Introduction

Across the world, uncomplicated UTIs rank among the most frequently encountered bacterial infections, placing a significant burden on healthcare systems due to their high prevalence, recurrence rates, and association with the emergence of antimicrobial resistance. Among young, sexually active females, Staphylococcus saprophyticus ranks as the second leading etiological agent of community-acquired UTIs, with prevalence ranging from 10-20% in this population [1, 2]. Recent studies from Iraq and neighboring countries have documented increasing resistance rates among S. saprophyticus strains, highlighting the urgent need for robust epidemiological surveillance strategies [3, 4]. MLSB antibiotics, with erythromycin, clindamycin, and streptogramins,

remain clinically important for treating staphylococcal infections. However, resistance to these agents is increasing globally. The main mechanisms of resistance comprise ribosomal target modification mediated by erm gene–encoded methylases, along with efflux pumps driven by msr genes, and the enzyme-mediated inactivation carried out by mph or lnu genes [5-7]. These genetic determinants produce three distinct resistance phenotypes: constitutive MLSB (cMLSB), inducible MLSB (iMLSB), and macrolide-streptogramin B (MSB), each carrying significant clinical implications [8-10].

The D-test remains the gold standard for detecting inducible clindamycin resistance in staphylococci. This screening method identifies isolates that appear susceptible but may develop resistance under antibiotic pressure, potentially leading to treatment failure [11, 12]. Molecular techniques, particularly PCR, complement phenotypic testing by detecting specific resistance genes and strengthening epidemiological surveillance through genotype-phenotype correlation analysis [5,13,14]. Among MLSB-resistant *S. saprophyticus* isolates, the erm(C) and msr(A) genes are most frequently identified, although novel resistance mechanisms continue to emerge across different geographic regions [15, 16]. Global resistance trends demonstrate concerning increases. Uruguay reported elevated MLSB resistance prevalence among S. aureus isolates with strong genotype-phenotype correlation [17]. Similarly, studies from Iran and Iraq documented high erythromycin and clindamycin resistance rates alongside multidrug resistance patterns [18-20]. These findings reflect broader trends in antimicrobial resistance, which are linked to the misuse and overuse of antibiotics. In Iraq, erythromycin resistance rates range from 50% to 67%, while clindamycin resistance varies between 22% and 46% among staphylococcal isolates [21, 22]. This variability underscores the importance of combining D-test methodology with molecular techniques for accurate resistance detection and monitoring.

Therefore, this inquiry aimed to characterize the phenotypical and genetical features of MLSB resistance across *S. saprophyticus* isolates from UTI patients in Najaf, Iraq. The objectives were to generate reliable local data for antimicrobial stewardship programs and guide clinicians toward more effective therapeutic strategies.

2. Materials and Methods

2.1 Collection of Specimens and Isolation of Bacteria

Urinary specimens were gathered from patients attending Al-Sadr Hospital in Najaf, Iraq, from February to April 2025. The study protocol received institutional approval, and all participants gave their informed consent. Participants of either sex, aged 1-70 years, presenting with UTI symptoms were included. Midstream urine specimens were collected using standard sterile techniques and processed within 2 hours of collection.

2.2 Identification of bacterial isolates

MacConkey and Blood agar dishes were used for culturing urine specimens, which were incubated at 37 °C for 24–48 hours. Staphylococcus saprophyticus isolates were recognized using blood and mannitol salt agar, Gram stain, and conventional biochemical tests, including catalase and adverse coagulase reactions, novobiocin resistance (5 μg disc), and mannitol fermentation, as per established protocols [23].

2.3 Phenotypic Detection of MLSB Resistance

2.3.1 D-Test Methodology

In accordance with CLSI instructions [24], the D-test was used to screen for resistance to clindamycin. In this procedure, bacterial inocula were standardized to a 0.5 McFarland turbidity and subsequently streaked onto Mueller–Hinton agar plates. Discs of erythromycin (15 μg) and clindamycin (2 μg) were applied on the agar surface, maintaining a 15 mm spacing between their edges. Upon incubation at 37 °C for 18–24 h, interpretations were made as outlined earlier [25].

- **Inducible MLSB (iMLSB)**: A D-shaped distortion observed in the clindamycin inhibitory area in proximity to the erythromycin disc.
- **Constitutive MLSB (cMLSB)**: Resistance to the two clindamycin and erythromycin
- **MS phenotype**: Resistance to erythromycin with susceptibility to clindamycin (no D-zone)
- **MLSB-negative**: Susceptibility to both antibiotics

2.3.2 Molecular Detection of Resistance Genes

Overnight cultures were subjected to genomic DNA isolation using a commercial kit (Promega, USA) according to the supplier's guidelines. DNA yield and purity were then assessed employing spectrophotometry at an absorbance ratio of 260/280 nm. Detection of MLSB resistance genes (erm(C) and msr(A)) was performed using PCR (Table 1). Primer design and cycling conditions were adopted from earlier reports [4,5]. Reaction mixtures (25 μL) comprised of 12.5 μL of master mix (Promega), 1 μL of every primer (10 pmol), 2 μL of extracted DNA, and 8.5 μL of nuclease-free water. Thermal cycling involved an initial denaturation at 94 °C for 5 minutes, followed by 30 amplification cycles (94 °C for 30 seconds, 55 °C for 30 seconds, and 72 °C for 1 minute), and a final extension step at 72 °C for 10 minutes. The resulting amplicons were resolved on 1.5% agarose gels comprising ethidium bromide and visualized under UV illumination. Each run included both positive and negative controls.

Table 1. Primers employed for the identification of MLSB resistance genes

Gene	Primer Sequence (5'→3')	Amplicon Size (bp)	Reference
erm(C)	F: ATCTTTTAGCAAACCCGTATTC R: CTTGTTGATCACGATAATTTCC	190	[26]
msr(A)	F: AAGTTATATCATGAATAGATTGTCCTGTT R: GGCACAATAAGAGTGTTTAAAGG	940	[27]

2.4 Statistical Analysis

The dataset was evaluated through descriptive statistical methods. Resistance profiles of S. saprophyticus isolates were stratified by age and gender, and summarized as frequencies and proportions. The chi-square analysis was used to determine associations between resistance and demographic factors. The level of statistical significance was defined as $p < 0.05$, and all analyses were conducted using SPSS V 25.0.

3. Results and Discussion

3.1 Demographic Distribution and Clinical Epidemiology

Among the 42 *S. saprophyticus* isolates collected from UTI patients, a marked female predominance was observed, with 28 isolates (66.7%) from females and 14 (33.3%) from males, resulting in a 2:1 female-to-male ratio (Table 2). This gender distribution aligns with the well-established epidemiology of *S. saprophyticus* as the second leading causative agent of community-acquired UTIs among sexually active females of younger age groups, responsible for 10–20% of UTIs in this population [28,29]. The highest isolation rates occurred in patients aged 21-30 years (11/42, 26.2%) and 31-40 years (10/42, 23.8%), with progressively lower frequencies in older age groups: 41-50 years (7/42, 16.7%), 51-60 years (5/42, 11.9%), and 61-70 years (5/42, 11.9%). Notably, no isolates were recovered from children under 10 years old, and only 4 isolates (9.5%) were from the 11-20 year age group. The concentration of cases in the 21–40-year age range corresponds with peak sexual activity and aligns with anatomical, behavioral, and hormonal factors that predispose young women to S. saprophyticus UTIs [30, 31]. The absence of pediatric cases reinforces the rarity of this organism in childhood UTIs, where Escherichia coli predominates. These demographic patterns are consistent with regional studies from Iraq and neighboring countries, confirming *S. saprophyticus* as a significant uropathogen in reproductive-age women [30-32].

Table 2. Distribution of *S. saprophyticus* isolates by demographic characteristics (n=42)

Characteristic	Category	n (%)
Sex	Male	14 (33.3)
	Female	28 (66.7)
Age group (years)	1-10	0 (0.0)
	11-20	4 (9.5)
	21-30	11 (26.2)
	31-40	10 (23.8)
	41-50	7 (16.7)
	51-60	5 (11.9)
	61-70	5 (11.9)

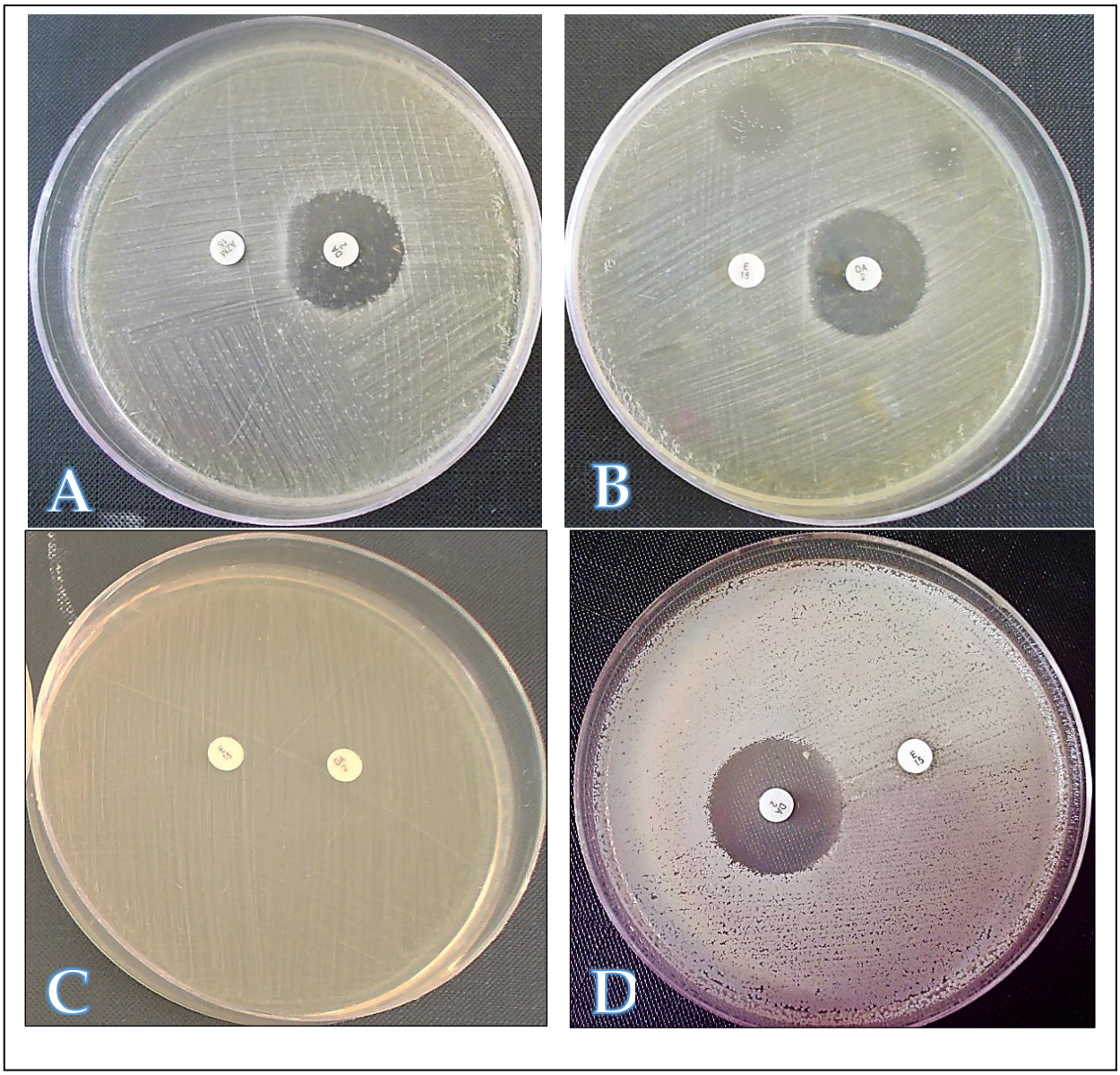


Figure 1. Representative D-test results for *S. saprophyticus*: (A) inducible resistance with azithromycin, (B) inducible resistance with erythromycin, (C) constitutive MLS resistance, (D) MS phenotype (macrolide resistance without lincosamide induction).

3.2 Phenotypic Resistance Patterns and Clinical Implications

D-test analysis revealed a concerning prevalence of MLSB resistance, with 25/42 isolates (59.5%) demonstrating MLSB-positive phenotypes (Table 3). Among these, constitutive MLSB (cMLSB) resistance predominated at 16/33 (48.4%), while inducible MLSB (iMLSB) accounted for 9/33 (27.3%) of tested isolates. Additionally, 8/33 isolates (24.3%) exhibited the MS phenotype, and 9/42 (21.5%) were MLSB-negative. The predominance of the cMLSB phenotype indicates widespread constitutive expression of ribosomal methylases that modify the drug-binding site, conferring cross-resistance to macrolides, lincosamides, and streptogramin B [33, 34]. This mechanism, typically mediated by *erm* genes, particularly *erm*(C) in staphylococci, results in high-level resistance that cannot be overcome by increasing drug concentrations [35, 36]. The detection of iMLSB in 27.3% of isolates has critical therapeutic implications, as these strains may appear susceptible to clindamycin during routine antimicrobial testing; however, they may develop resistance upon exposure to inducing agents [37, 38]. This finding strongly supports recommendations for mandatory D-testing of all erythromycin-resistant staphylococci to prevent clinical failures [39-41]. The MS phenotype observed in 24.3% of isolates represents macrolide-specific resistance, while maintaining lincosamide susceptibility, consistent with efflux pump mechanisms typically associated with *msr*(A) genes that selectively export 14- and 15-membered macrolides [42, 43]. This distinction has therapeutic relevance, as clindamycin remains effective against MS phenotype isolates despite macrolide resistance.

Table 3. Distribution of MLSB resistance phenotypes as identified through the D-test.

Phenotype	n (%)	Clindamycin (2µg)	Erythromycin (15µg)
iMLSB	9/33 (27.3)	S	R
cMLSB	16/33 (48.4)	R	R
MS	8/33 (24.3)	S	R
Total MLSB-positive	**25/42 (59.5)**	-	-
MLSB-negative	**9/42 (21.5)**	S	S

3.3 Molecular Characterization and Genotype-Phenotype Correlations

PCR analysis of the 25 phenotypically MLSB-positive isolates revealed resistance genes in only 9 samples (36%), demonstrating significant genotype-phenotype discordance (Table 4, Figures 1 and 2). The *erm*(C) gene was detected either alone (2/25, 8%) or in combination with *msr*(A) (7/25, 28%), while 16/25 isolates (64%) lacked detectable resistance genes despite expressing resistant phenotypes. The identification of *erm*(C) as the primary resistance determinant aligns with global reports establishing it as the predominant methylase gene in staphylococci [44]. The *erm*(C) gene encodes a 23S rRNA methylase that dimethylates the adenine residue at A2058, preventing antibiotic binding and conferring the MLSB resistance phenotype [45]. The co-occurrence of *erm*(C) and *msr*(A) in 28% of gene-positive isolates suggests that dual resistance mechanisms may enhance overall resistance levels through combined ribosomal modification and efflux activity [33, 46, 47]. The absence of other tested resistance genes [*erm*(A), *erm*(B), *msr*(B), *lin*(A), *mph*(C), *mef*(A)] indicates a limited genetic repertoire in this population, contrasting with the broader diversity reported in some international studies but consistent with regional patterns showing *erm*(C) predominance [48, 49]. This focused genetic profile may reflect local clonal expansion or selective pressure from specific antibiotic usage patterns in the region. The substantial genotype-phenotype discordance (64% of resistant isolates lacking detectable genes) warrants careful consideration. Several mechanisms may explain this finding: (1) presence of unexamined resistance determinants, including novel *erm* alleles or rare MLSB genes not included in our panel [35, 50]; (2) primer-template mismatches due to sequence variations in mobile genetic elements carrying resistance genes [51]; (3) regulatory mutations affecting gene expression without altering coding sequences [34]; or (4) chromosomal mutations in ribosomal proteins or RNA that confer resistance independently of classical resistance genes [52]. These findings highlight the limitations of targeted PCR approaches and suggest that whole-genome sequencing may be necessary to characterize resistance mechanisms in this population [51, 53].

Table 4. Molecular detection of resistance genes in MLSB-positive isolates

Gene Pattern	n/25 (%)	Associated Phenotype
erm(C) only	2 (8)	cMLSB/iMLSB
erm(C) + *msr*(A)	7 (28)	cMLSB + enhanced macrolide resistance
No genes detected	16 (64)	Variable MLSB phenotypes
Total genes detected	**9 (36)**	-

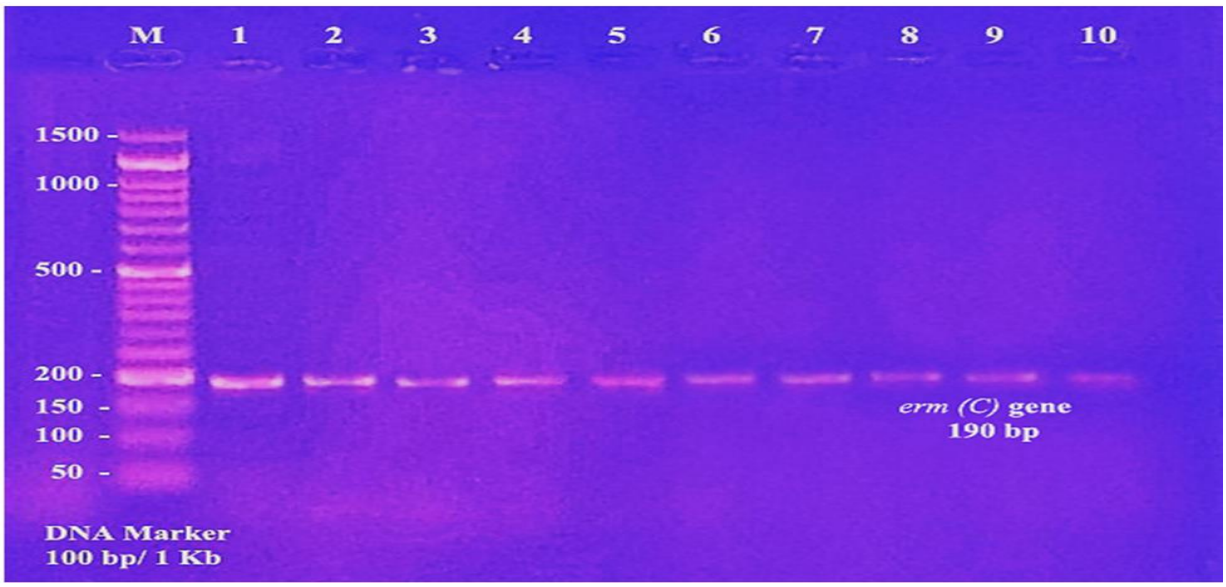


Figure 2. PCR amplification of the *erm(C)* gene (190 bp). Agarose gel electrophoresis (0.75 g agarose, 70 V, 1.5 h). Lane M: marker; lanes 1–10: positive isolates.

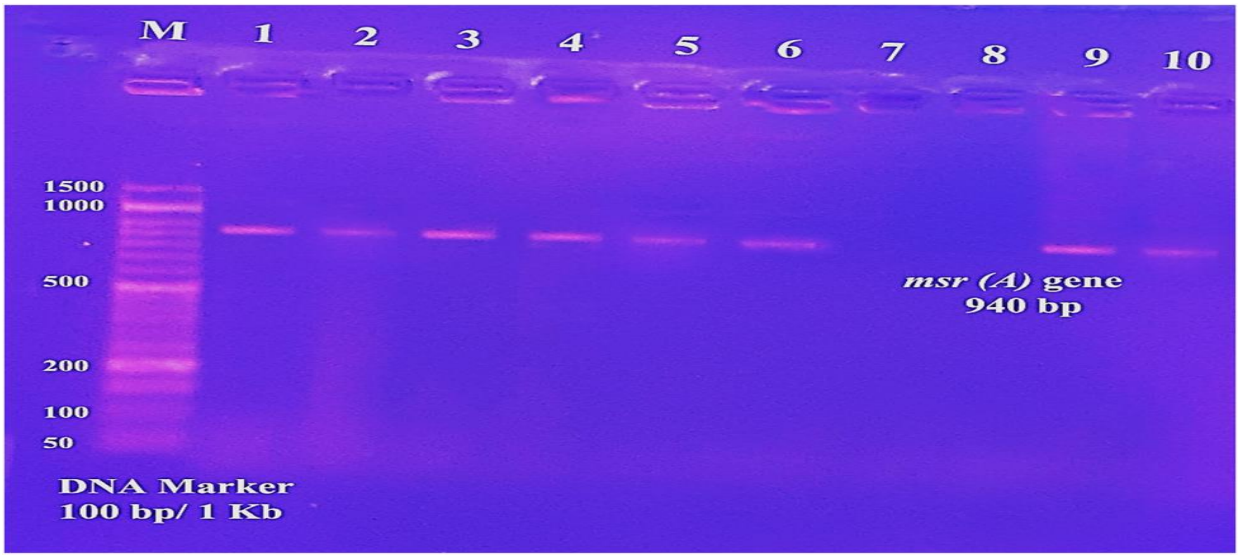


Figure 3. PCR amplification of the msr(A) gene (940 bp). Agarose gel electrophoresis (0.75 g agarose, 70 V, 1.5 h). Lane M: marker; lanes 1–6: test samples [specify positive/negative for each if clear]; lanes 7–8: negative; lanes 9–10: positive.

3.4 Clinical and Public Health Implications

The high prevalence of MLSB resistance (59.5%), particularly the significant proportion of iMLSB phenotypes (27.3%), has direct implications for clinical practice. Empirical use of macrolides or lincosamides for S. saprophyticus UTIs should be avoided in this setting, with preference given to nitrofurantoin or

trimethoprim-sulfamethoxazole as first-line agents [54, 55]. The detection of iMLSB phenotypes requires routine D-testing in clinical laboratories to prevent the inadvertent use of clindamycin in apparently susceptible isolates that harbor inducible resistance [37, 38, 56]. These resistance patterns align with broader antimicrobial resistance trends reported across Iraq, where rates of erythromycin resistance range from 50% to 67% and clindamycin resistance from 22% to 46% among staphylococcal isolates [57, 58]. The findings contribute to the growing evidence of increasing MLSB resistance in the Middle East region, likely driven by antibiotic selection pressure and horizontal gene transfer [59-61].

3.5 Study Strengths and Limitations

The combined phenotypic and molecular approach provided comprehensive resistance characterization, with D-testing offering cost-effective detection of clinically significant iMLSB phenotypes while PCR revealed underlying genetic mechanisms [37, 41, 53]. However, several limitations should be acknowledged. The single-center design may limit generalizability, the sample size of 42 isolates provides limited statistical power for subgroup analyses, and the targeted gene panel may have missed novel or rare resistance determinants. Future multicenter studies with expanded molecular panels, including whole-genome sequencing, would provide more comprehensive epidemiological data and potentially resolve the observed genotype-phenotype discordances [51, 53, 50].

4. Conclusions

This study reveals alarming levels of MLSB resistance (59.5%) among *S. saprophyticus* UTI isolates in Najaf, Iraq, with constitutive resistance predominating; however, a clinically significant proportion exhibits inducible resistance. The limited genetic repertoire dominated by *erm*(C) and *msr*(A), combined with substantial genotype-phenotype discordance, highlights the complexity of resistance mechanisms and the necessity for comprehensive surveillance approaches. These findings provide essential local epidemiological data to guide empirical therapy decisions and emphasize the critical importance of regularly implementing the D-test in clinical laboratories for the identification of inducible resistance and the prevention of treatment failures.

5. Acknowledgements

The clinical and nursing staff at Al-Sadr Hospital (Najaf, Iraq) are also thanked for collecting urine samples and coordinating patients from February to April 2025, as well as all participants who provided written informed consent. We would also like to extend our gratitude to the College of Education, Department of Biology, University of Al-Qadisiyah (Al-Diwaniyah, Iraq), for providing laboratory facilities for isolate identification and phenotypic testing; and to the College of Health and Medical Techniques, Al-Furat Al-Awsat Technical University (Najaf, Iraq), for facilitating and cooperation. I am particularly grateful for the administrative support of both institutions during the data collection and documentation process.

Author Contributions: A.A.S.A.-G. and M.K.A.A.-H. Contributed to conceptualization. A.A.S.A.-G. was responsible for methodology, software, resources, data curation, formal analysis, investigation, drafting the original manuscript, visualization, supervision, and administration of the project. Validation was performed by A.A.S.A.-G., M.K.A.A.-H., and H.M.K. Funding acquisition was carried out by M.K.A.A.-H. All authors have reviewed and validated the submitted draft of the manuscript.

Funding: No external funding was obtained for this study

Conflicts of Interest: No potential conflict of interest was declared by the authors.

References

[1] Hashemzadeh, M.; Dezfuli, A.A.Z.; Nashibi, R.; Jahangirimehr, F.; Akbarian, Z.A. Study of biofilm formation, structure and antibiotic resistance in Staphylococcus saprophyticus strains causing urinary tract infection in women in Ahvaz, Iran. *New Microbes New Infect.* **2020**, *39*, 100831. https://doi.org/10.1016/j.nmni.2020.100831

[2] Lawal, O.U.; Barata, M.; Fraqueza, M.J.; Worning, P.; Bartels, M.D.; Goncalves, L.; Miragaia, M. Staphylococcus saprophyticus from clinical and environmental origins have distinct biofilm composition. *Front. Microbiol.* **2021**, *12*, 663768. https://doi.org/10.3389/fmicb.2021.663768

[3] Al-Shamarti, M.J. Activity assessment of antibiotics used against different bacterial etiological agents of UTI in Najaf, Iraq. *Iran. J. Pathol.* **2024**, *19*(3), 348–354. https://doi.org/10.30699/ijp.2024.2027209.3293

[4] Hussein, N.R.; Hameed, M.A.; Resho, Q.N. The trends of Staphylococcus aureus antibiotics resistance in Iraq: A narrative review. *BioMed Target J.* **2024**, *2*(2), 21–30. https://doi.org/10.59786/bmtj.222

[5] Sedaghat, H.; Esfahani, B.N.; Mobasherizadeh, S.; Jazi, A.S.; Halaji, M.; Sadeghi, P.; Emaneini, M.; Havaei, S.A. Phenotypic and genotypic characterization of macrolide resistance among Staphylococcus aureus isolates in Isfahan, Iran. *Iran. J. Microbiol.* **2017**, *9*(5), 264–270.

[6] Le Bouter, A.; Leclercq, R.; Cattoir, V. Molecular basis of resistance to macrolides, lincosamides and streptogramins in Staphylococcus saprophyticus clinical isolates. *Int. J. Antimicrob. Agents* **2011**, *37*(2), 118–123. https://doi.org/10.1016/j.ijantimicag.2010.10.008

[7] Miklasińska-Majdanik, M. Mechanisms of resistance to macrolide antibiotics among Staphylococcus aureus. *Antibiotics* **2021**, *10*(11), 1406. https://doi.org/10.3390/antibiotics10111406

[8] Steward, C.D.; Raney, P.M.; Morrell, A.K.; Williams, P.P.; McDougal, L.K.; Jevitt, L.; McGowan, J.E.; Tenover, F.C. Testing for induction of clindamycin resistance in erythromycin-resistant isolates of Staphylococcus aureus. *J. Clin. Microbiol.* **2005**, *43*(4), 1716–1721. https://doi.org/10.1128/JCM.43.4.1716-1721.2005

[9] Perez, L.R.R.; Caierão, J.; Antunes, A.L.S.; d'Azevedo, P.A. Use of the D test method to detect inducible clindamycin resistance in coagulase-negative staphylococci (CoNS). *Braz. J. Infect. Dis.* **2007**, *11*(2), 186–188. https://doi.org/10.1590/S1413-86702007000200002

[10] Prabhu, K.; Rao, S.; Rao, V. Inducible clindamycin resistance in Staphylococcus aureus isolated from clinical samples. *J. Lab. Physicians* **2011**, *3*(1), 25–27. https://doi.org/10.4103/0974-2727.78558

[11] Ojha, A.; Maheshwari, R.K. Phenotypic detection of inducible clindamycin resistance by D-test in staphylococci from various clinical samples. *Front. Microbiol.* **2025**, *16*, 1569242.

[12] Perez, L.R.R.; Caierão, J.; Antunes, A.L.S.; d'Azevedo, P.A. Use of the D test method to detect inducible clindamycin resistance in coagulase-negative staphylococci (CoNS). *Braz. J. Infect. Dis.* **2007**, *11*(2), 186–188. https://doi.org/10.1590/S1413-86702007000200002

[13] Apidianakis, Y.; Pitsouli, C.; Perrimon, N.; Rahme, L. Synergy between bacterial infection and genetic predisposition in intestinal dysplasia. *Proc. Natl. Acad. Sci. USA* **2005**, *102*(35), 12596–12601.

[14] Rafiee, M.; Tabarraei, A.; Yazdi, M.; Mohebbi, A.; Ghaemi, E.A. Antimicrobial resistance patterns of Staphylococcus saprophyticus isolates causing urinary tract infections in Gorgan, North of Iran. *Med. Lab. J.* **2023**, *17*(2), 33–38. https://doi.org/10.61186/mlj.17.2.33

[15] Mahfouz, A.A.; Said, H.S.; Elfeky, S.M.; Shaaban, M.I. Inhibition of erythromycin and erythromycin-induced resistance among Staphylococcus aureus clinical isolates. *Antibiotics* **2023**, *12*(3), 503. https://doi.org/10.3390/antibiotics12030503

[16] Addis, Z.; Aschale, Y.; Fenta, A.; Teffera, Z.H.; Melkamu, A.; Tigab, A.; Dilnessa, T. Methicillin and inducible clindamycin resistance in clinical Staphylococcus aureus isolates: A cross-sectional study from Northwest Ethiopia. *Front. Microbiol.* **2025**, *16*, 1569242. https://doi.org/10.3389/fmicb.2025.1569242

[17] Pardo, L.; Machado, V.; Cuello, D.; Aguerrebere, P.; Seija, V.; Braga, V.; Varela, G. Macrolide-lincosamide-streptogramin B resistance phenotypes and their associated genotypes in Staphylococcus aureus isolates from a tertiary level public hospital of Uruguay. *Rev. Argent. Microbiol.* **2020**, *52*(3), 202–210. https://doi.org/10.1016/j.ram.2019.10.004

[18] Saderi, H.; Emadi, B.; Owlia, P. Phenotypic and genotypic study of macrolide, lincosamide and streptogramin B (MLSB) resistance in clinical isolates of Staphylococcus aureus in Tehran, Iran. *Med. Sci. Monit.* **2011**, *17*(2), BR48–BR53. https://doi.org/10.12659/MSM.881386

[19] Zmantar, T.; Kouidhi, B.; Miladi, H.; Bakhrouf, A. Detection of macrolide and disinfectant resistance genes in clinical Staphylococcus aureus and coagulase-negative staphylococci. *BMC Res. Notes* **2011**, *4*(1), 453. https://doi.org/10.1186/1756-0500-4-453

[20] Rafiee, M.; Tabarraei, A.; Yazdi, M.; Mohebbi, A.; Ghaemi, E.A. Antimicrobial resistance patterns of Staphylococcus saprophyticus isolates causing UTIs in Gorgan, North of Iran. *Med. Lab. J.* **2023**, *17*(2), 33–38. https://doi.org/10.61186/mlj.17.2.33

[21] Murdandy, A.H.; Al-Saadi, M.A.; Al-Charrakh, A.H. Antibiotic susceptibility patterns of Staphylococcus saprophyticus isolated from Iraqi patients. *J. Med. Microbiol.* **2003**, *52*(8), 693–696.

[22] Sumriddetchkajorn, K.; Suwannapong, K.; Soonthornchareonnon, N.; Chansiripornchai, N. Antimicrobial resistance patterns of Staphylococcus species isolated from clinical specimens in Iraq. *Asian Pac. J. Trop. Med.* **2024**, *17*(4), 165–172.

[23] McFadden, J.F. Biochemical Tests for Identification of Medical Bacteria, 3rd ed.; Lippincott Williams & Wilkins: Philadelphia, PA, USA, 2000.

[24] Clinical and Laboratory Standards Institute (CLSI). Performance Standards for Antimicrobial Susceptibility Testing, 34th ed.; CLSI Document M100; Clinical and Laboratory Standards Institute: Wayne, PA, USA, 2024.

[25] Majhi, S.; Dash, M.; Mohapatra, D.; Mohapatra, A.; Chayani, N. Detection of inducible and constitutive clindamycin resistance among Staphylococcus aureus isolates in a tertiary care hospital, Eastern India. Avicenna J. Med. 2016, 6(3), 75–80. https://doi.org/10.4103/2231-0770.184066

[26] Martineau, F.; Picard, F.J.; Lansac, N.; Ménard, C.; Roy, P.H.; Ouellette, M.; Michel, G. Correlation between the resistance genotype determined by multiplex PCR assays and the antibiotic susceptibility patterns of Staphylococcus aureus and Staphylococcus epidermidis. Antimicrob. Agents Chemother. 2000, 44(2), 231–238. https://doi.org/10.1128/AAC.44.2.231-238.2000

[27] Lina, G.; Quaglia, A.; Reverdy, M.E.; Leclercq, R.; Vandenesch, F.; Etienne, J. Distribution of genes encoding resistance to macrolides, lincosamides, and streptogramins among staphylococci. Antimicrob. Agents Chemother. 1999, 43(5), 1062–1066. https://doi.org/10.1128/AAC.43.5.1062

[28] Hashemzadeh, M.; Dezfuli, A.A.Z.; Nashibi, R.; Jahangirimehr, F.; Akbarian, Z.A. Study of biofilm formation, structure and antibiotic resistance in Staphylococcus saprophyticus strains causing urinary tract infection in women in Ahvaz, Iran. New Microbes New Infect. 2020, 39, 100831. https://doi.org/10.1016/j.nmni.2020.100831

[29] Lawal, O.U.; Barata, M.; Fraqueza, M.J.; Worning, P.; Bartels, M.D.; Goncalves, L.; Miragaia, M. Staphylococcus saprophyticus from clinical and environmental origins have distinct biofilm composition. *Front. Microbiol.* **2021**, *12*, 663768. https://doi.org/10.3389/fmicb.2021.663768

[30] Faiq, M.K. Antibiotic resistance in bacterial species: A retrospective study of cultures in Kirkuk City, Iraq. *Tikrit J. Pharm. Sci.* **2025**, *19*(1), 18–29. https://doi.org/10.25130/tjphs.2025.19.1.2.18.29

[31] Rafiee, M.; Tabarraei, A.; Yazdi, M.; Mohebbi, A.; Ghaemi, E.A. Antimicrobial resistance patterns of Staphylococcus saprophyticus isolates causing urinary tract infections in Gorgan, North of Iran. *Med. Lab. J.* **2023**, *17*(2), 33–38. https://doi.org/10.61186/mlj.17.2.33

[32] Salman, M.S. Antibiotic resistance of bacteria isolated in urinary tract infections. *J. Contemp. Med. Sci.* **2024**, *10*(2), 163–166. https://doi.org/10.22317/jcms.v10i2.1385

[33] Sedaghat, H.; Esfahani, B.N.; Mobasherizadeh, S.; Jazi, A.S.; Halaji, M.; Sadeghi, P.; Emaneini, M.; Havaei, S.A. Phenotypic and genotypic characterization of macrolide resistance among Staphylococcus aureus isolates in Isfahan, Iran. *Iran. J. Microbiol.* **2017**, *9*(5), 264–270.

[34] Miklasińska-Majdanik, M. Mechanisms of resistance to macrolide antibiotics among Staphylococcus aureus. *Antibiotics* **2021**, *10*(11), 1406. https://doi.org/10.3390/antibiotics10111406

[35] Lina, G.; Quaglia, A.; Reverdy, M.E.; Leclercq, R.; Vandenesch, F.; Etienne, J. Distribution of genes encoding resistance to macrolides, lincosamides, and streptogramins among staphylococci. *Antimicrob. Agents Chemother.* **1999**, *43*(5), 1062–1066. https://doi.org/10.1128/AAC.43.5.1062

[36] Le Bouter, A.; Leclercq, R.; Cattoir, V. Molecular basis of resistance to macrolides, lincosamides and streptogramins in Staphylococcus saprophyticus clinical isolates. *Int. J. Antimicrob. Agents* **2011**, *37*(2), 118–123. https://doi.org/10.1016/j.ijantimicag.2010.10.008

[37] Prabhu, K.; Rao, S.; Rao, V. Inducible clindamycin resistance in Staphylococcus aureus isolated from clinical samples. *J. Lab. Physicians* **2011**, *3*(1), 25–27. https://doi.org/10.4103/0974-2727.78558

[38] Sande, S.V. Phenotypic detection and incidence of inducible clindamycin resistance among Staphylococcus aureus from a tertiary care hospital. *Int. J. Adv. Med.* **2015**, *2*(3), 264–268. https://doi.org/10.18203/2349-3933.ijam20150557

[39] Montanari, M.P.; Mingoia, M.; Giovanetti, E.; Varaldo, P.E. Differentiation of resistance phenotypes among erythromycin-resistant pneumococci. *J. Clin. Microbiol.* **2001**, *39*(4), 1311–1315. https://doi.org/10.1128/JCM.39.4.1311-1315.2001

[40] Adwan, G.; Adwan, K.; Jarrar, N.; Amleh, A. Molecular detection of nine antibiotic resistance genes in methicillin resistant Staphylococcus aureus isolates. *Rom. Arch. Microbiol. Immunol.* **2014**, *73*(1–2), 9–18.

[41] Ghanbari, F.; Ghajavand, H.; Havaei, R.; Jami, M.S.; Khademi, F.; Heydari, L.; Shahin, M.; Havaei, S.A. Distribution of erm genes among Staphylococcus aureus isolates with inducible resistance to clindamycin in Isfahan, Iran. *Adv. Biomed. Res.* **2016**, *5*, 62. https://doi.org/10.4103/2277-9175.179184

[42] Ojo, K.K.; Striplin, M.J.; Ulep, C.C.; Close, N.S.; Zittle, J.; Luis, H.; Bernardo, M.; Leitao, J.; Roberts, M.C. Staphylococcus efflux msr(A) gene characterized in Streptococcus, Enterococcus, Corynebacterium, and Pseudomonas isolates. *Antimicrob. Agents Chemother.* **2006**, *50*(3), 1089–1091. https://doi.org/10.1128/AAC.50.3.1089-1091.2006

[43] Reynolds, E.; Ross, J.I.; Cove, J.H. Msr(A) and related macrolide/streptogramin resistance determinants: Incomplete transporters? *Int. J. Antimicrob. Agents* **2003**, *22*(3), 228–236. https://doi.org/10.1016/S0924-8579(03)00218-8

[44] Navidifar, T.; Zare Banadkouki, A.; Parvizi, E.; Mofid, M.; Golab, N.; Beig, M.; Sholeh, M. Global prevalence of macrolide-resistant Staphylococcus spp.: A comprehensive systematic review and meta-analysis. *Front. Microbiol.* **2025**, *16*, 1524452. https://doi.org/10.3389/fmicb.2025.1524452

[45] Steward, C.D.; Raney, P.M.; Morrell, A.K.; Williams, P.P.; McDougal, L.K.; Jevitt, L.; McGowan, J.E.; Tenover, F.C. Testing for induction of clindamycin resistance in erythromycin-resistant isolates of Staphylococcus aureus. *J. Clin. Microbiol.* **2005**, *43*(4), 1716–1721. https://doi.org/10.1128/JCM.43.4.1716-1721.2005

[46] Hassan, O.M. Molecular detection of MSRA erythromycin-resistant gene in Staphylococcus spp. *J. Fac. Med. Baghdad* **2017**, *59*(1), 90–92. https://doi.org/10.32007/med.1936/jfacmedbagdad.v59i1.19

[47] Perez, L.R.R.; Caierão, J.; Antunes, A.L.S.; d'Azevedo, P.A. Use of the D test method to detect inducible clindamycin resistance in coagulase-negative staphylococci (CoNS). *Braz. J. Infect. Dis.* **2007**, *11*(2), 186–188. https://doi.org/10.1590/S1413-86702007000200002

[48] Schwendener, S.; Donà, V.; Perreten, V. The novel macrolide resistance genes mef(D), msr(F), and msr(H) are present on resistance islands in Macrococcus canis, Macrococcus caseolyticus, and Staphylococcus aureus. *Antimicrob. Agents Chemother.* **2020**, *64*(5), e01128. https://doi.org/10.1128/AAC.00160-20

[49] Mahfouz, A.A.; Said, H.S.; Elfeky, S.M.; Shaaban, M.I. Inhibition of erythromycin and erythromycin-induced resistance among Staphylococcus aureus clinical isolates. *Antibiotics* **2023**, *12*(3), 503. https://doi.org/10.3390/antibiotics12030503

[50] Liu, Y.; Zhang, J.; Ji, Y. PCR-based approaches for the detection of clinical methicillin-resistant Staphylococcus aureus. *Open Microbiol. J.* **2016**, *10*, 45. https://doi.org/10.2174/1874285801610010045

[51] Zhang, K.; Potter, R.F.; Marino, J.; Muenks, C.E.; Lammers, M.G.; Dien Bard, J.; Dantas, G. Comparative genomics reveals correlations of stress response genes and bacteriophages in developing antibiotic resistance of Staphylococcus saprophyticus. *mSystems* **2023**, *8*(6), e00697-23. https://doi.org/10.1128/msystems.00697-23

[52] Martineau, F.; Picard, F.J.; Lansac, N.; Ménard, C.; Roy, P.H.; Ouellette, M.; Michel, G. Correlation between the resistance genotype determined by multiplex PCR assays and the antibiotic susceptibility patterns of Staphylococcus aureus and Staphylococcus epidermidis. *Antimicrob. Agents Chemother.* **2000**, *44*(2), 231–238. https://doi.org/10.1128/AAC.44.2.231-238.2000

[53] Grover, M.; Goyal, N.; Gangar, S.; Singh, N.P. Prevalence of MLSB phenotypes of Staphylococcus aureus isolates in a tertiary care hospital of Delhi. *Healthc. Low-Resour. Settings* **2023**, *11*(1), 11234. https://doi.org/10.4081/hls.2023.11229

[54] Al-Shamarti, M.J. Activity assessment of antibiotics used against different bacterial etiological agents of UTI in Najaf, Iraq. *Iran. J. Pathol.* **2024**, *19*(3), 348–354. https://doi.org/10.30699/ijp.2024.2027209.3293

[55] Hussein, N.R.; Naqid, I.A.; Ibrahim, N.; Ahmad, S.I.; Daniel, S.S.; Yahya, A.H.; Albrifkani, D. Trends in antimicrobial resistance of Staphylococcus aureus uropathogens: A retrospective study from Duhok Province, Kurdistan Region, Iraq. *Cureus* **2025**, *17*(1), e56789. https://doi.org/10.7759/cureus.77553

[56] Ojha, A.; Maheshwari, R.K. Phenotypic detection of inducible clindamycin resistance by D-test in staphylococci from various clinical samples. *Front. Microbiol.* **2025**, *16*, 1569242.

[57] Al-Fahad, D.K.; Alpofead, J.A.; Chawsheen, M.A.; Al-Naqshbandi, A.A.; Abas, A.T. Surveillance of antimicrobial resistance in Iraq: A comprehensive data collection approach. *ARO Sci. J. Koya Univ.* **2024**, *12*(2), 179–193. https://doi.org/10.14500/aro.11689

[58] Hashim, H.T.; Hashim, A.T.; Ali, H.T.; Mohamed, H.; Elrefaey, A.; Almamoury, A.; Aji, N. Prevalence and pattern of antibiotic use and resistance among Iraqi patients: A cross-sectional study. *Afr. Health Sci.* **2024**, *24*(3), 47–57. https://doi.org/10.4314/ahs.v24i3.7

[59] Saderi, H.; Emadi, B.; Owlia, P. Phenotypic and genotypic study of macrolide, lincosamide and streptogramin B (MLSB) resistance in clinical isolates of Staphylococcus aureus in Tehran, Iran. *Med. Sci. Monit.* **2011**, *17*(2), BR48–BR53. https://doi.org/10.12659/MSM.881386

[60] Zmantar, T.; Kouidhi, B.; Miladi, H.; Bakhrouf, A. Detection of macrolide and disinfectant resistance genes in clinical Staphylococcus aureus and coagulase-negative staphylococci. *BMC Res. Notes* **2011**, *4*(1), 453. https://doi.org/10.1186/1756-0500-4-453

[61] Pardo, L.; Machado, V.; Cuello, D.; Aguerrebere, P.; Seija, V.; Braga, V.; Varela, G. Macrolide-lincosamide-streptogramin B resistance phenotypes and their associated genotypes in Staphylococcus aureus isolates from a tertiary level public hospital of Uruguay. *Rev. Argent. Microbiol.* **2020**, *52*(3), 202–210. https://doi.org/10.1016/j.ram.2019.10.004



ASEAN
Journal of Scientific and Technological Reports
Online ISSN:2773-8752

ASEAN
Journal of Scientific and Technological Reports
Online ISSN: 2773-8752

Article type

Type of the Paper (Article, Review, Communication, etc.) *about 8,000 words maximum*

Title (Palatino Linotype 18 pt, bold)

Firstname Lastname[1], Firstname Lastname[2] and Firstname Lastname[2*]

[1] Affiliation 1; e-mail@e-mail.com
[2] Affiliation 2; e-mail@e-mail.com
* Correspondence: e-mail@e-mail.com; (one corresponding authors, add author initials)

Citation:
Lastname, F.; Lastname, F.; Lastname, F. Title. *ASEAN J. Sci. Tech. Report.* **2023**, *26*(X), xx-xx. https://doi.org/10.55164/ajstr.vxxix.xxxxxx

Article history:
Received: date
Revised: date
Accepted: date
Available online: date

Publisher's Note:
This article is published and distributed under the terms of the Thaksin University.

Abstract: A single paragraph of about 400 words maximum. Self-contained and concisely describe the reason for the work, methodology, results, and conclusions. Uncommon abbreviations should be spelled out at first use. We strongly encourage authors to use the following style of structured abstracts, but without headings: (1) Background: Place the question addressed in a broad context and highlight the purpose of the study; (2) Methods: briefly describe the main methods or treatments applied; (3) Results: summarize the article's main findings; (4) Conclusions: indicate the main conclusions or interpretations.

Keywords: keyword 1; keyword 2; keyword 3 (List three to ten pertinent keywords specific to the article yet reasonably common within the subject discipline.)

1. Introduction

The introduction should briefly place the study in a broad context and highlight why it is crucial. It should define the purpose of the work and its significance. The current state of the research field should be carefully reviewed and critical publications cited. Please highlight controversial and diverging hypotheses when necessary. Finally, briefly mention the main aim of the work. References should be numbered in order of appearance and indicated by a numeral or numerals in square brackets—e.g., [1] or [2, 3], or [4–6]. See the end of the document for further details on references.

2. Materials and Methods

The materials and methods should be described with sufficient details to allow others to replicate and build on the published results. Please note that your manuscript's publication implicates that you must make all materials, data, computer code, and protocols associated with the publication available to readers. Please disclose at the submission stage any restrictions on the availability of materials or information. New methods and protocols should be described in detail, while well-established methods can be briefly described and appropriately cited.

Interventional studies involving animals or humans, and other studies that require ethical approval, must list the authority that provided approval and the corresponding ethical approval code.

2.1 Subsection

2.1.1. Subsubsection

3. Results and Discussion

This section may be divided by subheadings. It should provide a concise and precise description of the experimental results, their interpretation, as well as the experimental conclusions that can be drawn.Authors should discuss the results and how they can be interpreted from previous studies and the working hypotheses. The findings and their implications should be discussed in the broadest context possible. Future research directions may also be highlighted.

3.1. Subsection

3.1.1. Subsubsection

3.2. Figures, Tables, and Schemes

All figures and tables should be cited in the main text as Figure 1, Table 1, etc.



Figure 1. This is a figure. Schemes follow the same formatting.

Table 1. This is a table. Tables should be placed in the main text near the first time they are cited.

Title 1	Title 2	Title 3
entry 1	data	data
entry 2	data	data [1]

[1] Table may have a footer.

3.3. Formatting of Mathematical Components

This is example 1 of an equation:

$$a = 1, \tag{1}$$

The text following an equation need not be a new paragraph. Please punctuate equations as regular text. This is example 2 of an equation:

$$a = b + c + d + e + f + g + h + i + j + k + l + m + n + o + p + q + r + s + t + u \tag{2}$$

The text following an equation need not be a new paragraph. Please punctuate equations as regular text. The text continues here.

4. Conclusions

Concisely restate the hypothesis and most important findings. Summarize the significant findings, contributions to existing knowledge, and limitations. What are the future directions? Conclusions MUST be well stated, linked to original research question & limited to supporting results.

5. Acknowledgements

Should not be used to acknowledge funders – funding will be entered as a separate. As a matter of courtesy, we suggest you inform anyone whom you acknowledge.

Author Contributions: For research articles with several authors, a short paragraph specifying their individual contributions must be provided. The following statements should be used "Conceptualization, X.X. and Y.Y.; methodology, X.X.; software, X.X.; validation, X.X., Y.Y. and Z.Z.; formal analysis, X.X.; investigation, X.X.; resources, X.X.; data curation, X.X.; writing—original draft preparation, X.X.; writing—review and editing, X.X.; visualization, X.X.; supervision, X.X.; project administration, X.X.; funding acquisition, Y.Y. All authors have read and agreed to the published version of the manuscript." Please turn to the CRediT taxonomy for the term explanation. Authorship must be limited to those who have contributed substantially to the work reported.

Funding: Please add: "This research received no external funding" or "This research was funded by NAME OF FUNDER, grant number XXX" and "The APC was funded by XXX". Check carefully that the details given are accurate and use the standard spelling of funding agency names at https://search.crossref.org/funding. Any errors may affect your future funding.

Conflicts of Interest: Declare conflicts of interest or state "The authors declare no conflict of interest." Authors must identify and declare any personal circumstances or interest that may be perceived as inappropriately influencing the representation or interpretation of reported research results. Any role of the funders in the design of the study; in the collection, analyses or interpretation of data; in the writing of the manuscript, or in the decision to publish the results must be declared in this section. If there is no role, please state "The funders had no role in the design of the study; in the collection, analyses, or interpretation of data; in the writing of the manuscript, or in the decision to publish the results".

References

References must be numbered in order of appearance in the text (including citations in tables and legends) and listed individually at the end of the manuscript. We recommend preparing the references with a bibliography software package, such as EndNote, ReferenceManager to avoid typing mistakes and duplicated references. Include the digital object identifier (DOI) for all references where available.

Citations and references in the Supplementary Materials are permitted provided that they also appear in the reference list here.

In the text, reference numbers should be placed in square brackets [ ] and placed before the punctuation; for example [1], [1–3] or [1, 3]. For embedded citations in the text with pagination, use both parentheses and brackets to indicate the reference number and page numbers; for example [5] (p. 100), or [6] (pp. 101–105).

Using the American Chemical Society (ACS) referencing style

[1] Author 1, A.B.; Author 2, C.D. Title of the article. *Abbreviated Journal Name* Year, *Volume*, page range.

[2] Author 1, A.; Author 2, B. Title of the chapter. In *Book Title*, 2nd ed.; Editor 1, A., Editor 2, B., Eds.; Publisher: Publisher Location, Country. **2007**, Volume *3*, pp. 154–196.

[3] Author 1, A.; Author 2, B. *Book Title*, 3rd ed.; Publisher: Publisher Location, Country, **2008**, pp. 154–196.
[4] Author 1, A.B.; Author 2, C. Title of Unpublished Work. *Abbreviated Journal Name* stage of publication (under review; accepted; in press).
[5] Author 1, A.B. (University, City, State, Country); Author 2, C. (Institute, City, State, Country). Personal communication, 2012.
[6] Author 1, A.B.; Author 2, C.D.; Author 3, E.F. Title of Presentation. In Title of the Collected Work (if available), Proceedings of the Name of the Conference, Location of Conference, Country, Date of Conference; Editor 1, Editor 2, Eds. (if available); Publisher: City, Country, Year (if available); Abstract Number (optional), Pagination (optional).
[7] Author 1, A.B. Title of Thesis. Level of Thesis, Degree-Granting University, Location of University, Date of Completion.
[8] Title of Site. Available online: URL (accessed on Day Month Year).

Reviewers sugestion

1. Name, Address, e-mail
2. Name, Address, e-mail
3. Name, Address, e-mail
4. Name, Address, e-mail

URL link:

Notes for Authors >>
https://drive.google.com/file/d/1r0zegnIVeQqe4iLQyT1xDEIinNggINPD/view?usp=sharing
https://drive.google.com/file/d/1r0zegnIVeQqe4iLQyT1xDEIinNggINPD/view?usp=sharing

Online Submissions >> https://ph02.tci-thaijo.org/index.php/tsujournal/user/register

Current Issue >> https://ph02.tci-thaijo.org/index.php/tsujournal/issue/view/16516

AJSTR Publication Ethics and Malpractice >> https://ph02.tci-thaijo.org/index.php/tsujournal/ethics

Journal Title Abbreviations >> http://library.caltech.edu/reference/abbreviations



ASEAN
Journal of Scientific and Technological Reports
Online ISSN:2773-8752



ASEAN
Journal of Scientific and Technological Reports
Online ISSN:2773-8752

ASEAN Journal of Scientific and Technological Reports (AJSTR)
Institute of Research and Innovation, Thaksin University, Phatthalung Campus
222 Moo. 2, Baan Prao Sub-District, Papayom District, Phatthalung, 93210, Thailand
Tel. +668 1540 7304

